

INTERNATIONAL COUNCIL FOR RESEARCH AND INNOVATION  
IN BUILDING AND CONSTRUCTION

WORKING COMMISSION W18 - TIMBER STRUCTURES

# **CIB - W18**

MEETING THIRTY-TWO

GRAZ

AUSTRIA

AUGUST 1999

Lehrstuhl für Ingenieurholzbau und Baukonstruktionen  
Universität Karlsruhe  
Germany  
Compiled by Rainer Görlacher  
1999

ISSN 0945-6996

## CONTENTS

- 0 List of Participants
- 1 Chairman's Introduction
- 2 Co-operation With Other Organisations
- 3 Limit State Design
- 4 Stress Grading
- 5 Stresses for Solid Timber
- 6 Timber Joints and Fasteners
- 7 Duration of Load
- 8 Laminated Members
- 9 Trussed Rafters
- 10 Structural Stability
- 11 Serviceability
- 12 Other Business
- 13 Venue for Next Meeting
- 14 Close
- 15 List of CIB W18 Papers/Graz, Austria 1999
- 16 Current List of CIB-W18 Papers

CIB-W18 Papers 32-1-1 up to 32-20-1



**0 List of Participants**

INTERNATIONAL COUNCIL FOR RESEARCH AND INNOVATION  
IN BUILDING AND CONSTRUCTION  
WORKING COMMISSION W18 - TIMBER STRUCTURES

MEETING THIRTY-TWO  
GRAZ, AUSTRIA 23-25 AUGUST 1999

LIST OF PARTICIPANTS

**AUSTRIA**

M Augustin	Lignum Research, Graz
K Frühwald	Joanneum Research, HDI, Judenburg
B Hasewend	Lignum Research, Graz
B Obermayr	Lignum Research, Graz
G Oswald	Techn. University of Graz
R Pischl	Techn. University of Graz
G Schickhofer	Techn. University of Graz
A Trummer	Techn. University of Graz
M Wallner	Techn. University of Graz

**CAMEROON**

C Nguedjio Fouepe	National School of Engineering, Yaounde
-------------------	---

**CANADA**

E Karacabeyli	Forintek, Vancouver
F Lam	Department of Civil Eng. UBC, Vancouver
P Quenneville	Royal Military College of Canada, Kingston

**DENMARK**

C O Clorius	Technical University of Denmark, Lyngby
H J Larsen	Danish Building Research Institute, Hørsholm
J Nielsen	Aalborg University, Aalborg
M U Pedersen	Technical University of Denmark, Lyngby

**FINLAND**

A Ranta-Maunus	VTT Building Technology, Espoo
J Vesa	Helsinki University of Technology

**FRANCE**

P Racher	C.U.S.T. Aubiere Cedex
F Rouger	CTBA, Bordeaux

**GERMANY**

P Becker	Bauhaus University, Weimar
A Bernasconi	BFH Hamburg
H J Blaß	University of Karlsruhe
J Ehlbeck	University of Karlsruhe

R Görlacher	University of Karlsruhe
V Krämer	University of Karlsruhe
B Laskewitz	University of Karlsruhe
B Mohr	Ingenieurbüro Dr.-Ing. Schütz
K Rautenstrauch	Bauhaus University, Weimar
M Schmid	University of Karlsruhe
T Wolf	University of Darmstadt

### **ITALY**

M Ballerini	University of Trento
A Ceccotti	University of Florence

### **JAPAN**

N Kawai	Building Research Institute, Tsukuba
K Komatsu	Kyoto University, Kyoto
M Yasumura	Shizuoka University, Shizuoka

### **NETHERLANDS**

A Jorissen	TU Delft
A D Leijten	TU Delft

### **SWEDEN**

S Andreasson	Lund University
T Isaksson	Lund University
B Källsner	Swedish Institute for Wood Technology Research, Stockholm
J König	Swedish Institute for Wood Technology Research, Stockholm
L Stehn	Lulea University of Technology, Lulea
S Svensson	Lund University
S Thelandersson	Lund University

### **SWITZERLAND**

A Mischler	ETH Zürich
V Schrepfer	ETH Zürich

### **UK**

M P Ansell	University of Bath
R Bainbridge	TRADA Technology LTD, Buckinghamshire
T D G Canisius	Building Research Establishment, Garston
V Enjily	Building Research Establishment, Garston
R Grantham	Building Research Establishment, Garston
C J Mettem	TRADA Technology LTD, Buckinghamshire
T Reynolds	Building Research Establishment, Garston

### **USA**

P Mazikins	American Forest & Paper Association
B Yeh	American Plywood Association

1. **Chairman's Introduction**
2. **Co-operation With Other Organisations**
3. **Limit State Design**
4. **Stress Grading**
5. **Stresses for Solid Timber**
6. **Timber Joints and Fasteners**
7. **Duration of Load**
8. **Laminated Members**
9. **Trussed Rafters**
10. **Structural Stability**
11. **Serviceability**
12. **Other Business**
13. **Venue for Next Meeting**
14. **Close**



INTERNATIONAL COUNCIL FOR RESEARCH AND INNOVATION  
IN BUILDING AND CONSTRUCTION

WORKING COMMISSION W18 - TIMBER STRUCTURES

MEETING THIRTY-TWO

GRAZ, AUSTRIA 23-25 AUGUST 1999

MINUTES

(F Lam)

**1. CHAIRMAN'S INTRODUCTION**

H.J.Blass opened the meeting and welcomed the participants. He noted the name change of CIB to International Council for Research and Innovation in Building and Construction.

Prof. Riesberger, Dean of Faculty of Civil Engineering, Technical University of Graz (TU), welcomed the participants and gave an introduction to the history of TU Graz.

Prof. Pischl, Head of Timber Structures Department Technical University of Graz, welcomed the participants and presented a brief history of forestry and timber engineering in Austria.

G.Schickhofer dealt with meeting organization matters.

H.J.Blass stated that a CIBW18 meeting in Austria was held in Vienna 1979. The current 1999 meeting is the 2nd CIBW18 venue in Austria. Papers 32-12-1 and 32-13-1 are canceled because the authors cannot attend the meeting. These papers will not appear in the proceedings. Papers brought directly to the meeting will not be accepted. Three late submissions, 32-5-1, 32-7-8, and 32-9-2 will be fitted into the agenda. The presentations are limited to 15 minutes with 10 minutes discussion period. Presenters are reminded that they should conclude presentation with statements concerning impact of research to code applications. There are 9 topics covered originally in this meeting: limit state design, stress grading, stresses for solid timber, timber joints and fasteners, duration of load, laminated members, trussed rafters, structural stability, and serviceability. Meeting proceedings are targeted to be available by Christmas 1999.

**2. CO-OPERATION WITH OTHER ORGANISATIONS**

**(a) RILEM**

S.Thelandersson gave a brief discussion of RILEM timber related activities. He reported that there are currently two timber groups in RILEM. A RILEM meeting in Timber Engineering will be held in Stockholm Sept. 1999. Expecting 120 participants.

**(b) CEN TC 124 and TC 250**

CEN - Activities in CEN on TC 124 Standards for Timber Structures and TC 250 Subcommittee 5 have been discussed.

H.J.Larsen presented activities in TC 124: Seismic work has been included, two new standards related to glued in rods and machine grading are under development and will be included when ready. Revision of standards on measurement of Bending Strength and Stiffness is also under discussion. A.Leijten is the convener for working group 1 "Test Method" and the Fastener and Joint work group is looking for a new convener.

H.J.Blass will retire from chairing TC 250 Subcommittee 5 by the end of the year and J.König will take over the chairmanship. J.König gave a brief presentation of TC 250 subcommittee 5 activities and presented a timetable for conversion to EN standard.

**(c) IUFRO S5.02**

IUFRO S5.02 - F.Rouger replaced P.Hoffmeyer as the new convener for IUFRO S5.02. He reported that IUFRO 5.02 meeting was intended for a small group of 40 to 50 people to present and discuss basic timber engineering and scientific issues. The last IUFRO 5.02 meeting was held 2 years ago. F.Rouger also discussed the relationship between CIBW18 and IUFRO S5.02 and looks forward to improve the collaboration between the two groups and reduce overlap. H.J.Blass raised the question of the possibility of holding CIBW18 and IUFRO S5.02 meetings in alternating years. Based on past record, it was rationalized that the annual CIBW18 meeting format should be kept. And the group will attempt to find a way to promote IUFRO S5.02 activities. F.Rouger suggested establishing a common paper review committee to steer the papers to appropriate forum.

**3. LIMIT STATE DESIGN**

*Paper 32-1-1 Determination of Partial Coefficients and Modification factors - H.J.Larsen, S.Svensson, S.Thelandersson*

Presenter: H.J.Larsen

- H.J.Blass asked whether wind loads were considered in the analysis.
- H.J.Larsen answered that wind loads were not considered and it would be useful to do the analysis.
- A.Ranta-Maunus asked why a different DOL model was needed for panel material.
- H.J.Larsen responded that the Foschi model did not work for  $\sigma_0 < 0.2$  which is needed for panel material.
- E.Karacabeyli asked why was the DOL model calibrated to Madison curve.
- H.J.Larsen responded that data with full size material were not available.
- F.Lam commented that although the shape of stress ratio versus log time curve from the fitted DOL model looks correct, such curves based on N. American DOL data on full size timber would intersect with the Madison curve at a time  $\ll 100$  years.
- H.J.Larsen said that the comments would be taken into consideration.

- S.Svensson said that the model was fitted to Madison curve and checked against some available data from literature.
- E.Karacabeyli commented that the use of two models might impact on result consistency.
- S.Thelandersson commented that exact shape of the curve might not matter as results represented the behaviour well.
- A.Ranta-Maunus asked why the mean values were compared.
- S.Thelandersson responded that comparison of ratios of short- and long-term 5<sup>th</sup> %tile strengths approximately equaled similar ratios of mean strengths; therefore, mean strength was used.

*Paper 32-1-2 Design by testing Structural Timber Components - V.Enjily and L.Whale*

Presenter: V.Enjily

- H.J.Blass questioned that if the procedure was based on timber component having CV<8%, what would be needed for other timber components that might have CV>8%.
- V.Enjily responded that the procedure would not be not valid for cases with CV>8%.
- H.J.Larsen stated that the EC5 does not require sample size of 30. Also one might have difficulties promoting the concept.
- V.Enjily responded that when timber properties could be considered as component would be an important issue for this procedure.
- H.J.Larsen further questioned that whether CV<8% would be correct based on the limited sample size.

#### 4. STRESS GRADING

*Paper 32-5-1 Actual Possibilities of the machine grading of timber - K.Frühwald and A.Bernasconi*

Presenter: K.Frühwald.

- H.J.Larsen pointed out that the detection of failure location would not be critical in machine stress grading. He also questioned whether the machine performance or machine settings in the different machines were responsible for the poor performance.
- K.Frühwald responded that the machine manufacturers would need to provide the answer.
- R.Görlacher pointed out that some of the machine used has settings for glulam laminates not structural timber. The issue of edgewise and flatwise application was not considered with these machines.
- G.Schickhofer responded that tensile tests were also performed.
- F.Rouger pointed out that the new version of CEN519 is better than the old version and output of machine is important.

*Paper 32-5-2 Detection of severe timber defects by machine grading - A.Bernasconi, L.Boström, B.Schacht*

Presenter: A.Bernasconi.

- F.Rouger discussed the intent to create distribution of grades.
- A.Bernasconi stated that it would be a possible safety concern if severe defects were

missed.

- P.Quenneville questioned whether any of the defects were more problematic.
- A.Bernasconi responded prebroken specimen.
- S.Thelandersson pointed out that this study clearly confirmed the general misconception that the tails of MSR timber strength distributions were truncated.
- M.Ansell stated that image analysis might be used for grain deviation detection.

## 5. STRESSES FOR SOLID TIMBER

*Paper 32-6-1 Development of high-resistance glued Robinia products and an attempt to assign such products to the European system of strength classes - G.Schickhofer, B.Obermayr*

Presenter: G.Schickhofer

- H.J.Blass pointed out that the procedure to set characteristic bending strength to  $1/0.6$  of characteristic tensile strength might not be conservative because the 0.6 factor was intended to be used to conservatively convert characteristic tensile strength to characteristic bending strength and not the other way around.
- C.Mettem discussed the use of hardwood.
- A.Jorissen questioned how the quality of test material was selected.
- G.Schickhofer responded that the quality of test material was determined by the supplier.
- B.J.Yeh commented the COV seemed high.
- G.Schickhofer responded that most beams failed in the finger joints.
- A.Ceccotti informed that hardwood such as Chestnut would also be used in Italy.

*Paper 32-6-2 Length and load configuration effects in the code format - T.Isaksson*

Presenter: T.Isaksson

- T.D.G.Canisius discussed the general application of the method in design such as 2 and 3 spans situations.
- T.Isaksson responded that theory was statistical effect based and could be applied to complicated loading.
- A.Jorissen questioned how the strength of reference length determined.
- T.Isaksson responded that bending tests with 2 loading points were used.

*Paper 32-6-3 Length effect on the tensile strength of truss chord members - F.Lam*

Presenter: F.Lam

- B.J.Yeh asked whether the reduction in COV of series system was considered.
- F.Lam responded that the simulation procedures directly took it into account.
- T.D.G.Canisius requested the presenter to comment on the difference in safety level and snow load return period between EU and N. America.
- F.Lam responded that different regions/countries should set their own safety level and the loading return period. In Canada the timber code adopted a safety level equivalent to the steel code and the return period for snow was 30 years.
- S.Thelandersson asked how was the k factor determined .
- F.Lam discussed the use of Equation 10 to establish k from a minimization of error

procedure.

- A.Ranta-Maunus questioned whether the conclusion from this paper that length effect was most important for long span cases contradicted with the conclusion from paper 32-6-4 that length effect was most important for short span cases.
- F.Lam responded that there was no contradiction because the conclusion from current paper was based on the decrease in strength with increase in length (point of view of safety) and the conclusion from paper 32-6-4 was based on the increase in strength with decrease in length (point of view of utilization).

*Paper 32-6-4 Tensile strength perpendicular to grain of glued laminated timber - H.J.Blass, M.Schmid*

Presenter: M.Schmid

- S.Svensson questioned whether climatic treatment was considered as tension strength perpendicular to grain would be very sensitive to climatic changes.
- M.Schmid responded that the climatic condition was under normal laboratory condition and it was almost constant. The material was left in the lab for a long time.
- G.Schickhofer commented on the code applications.
- M.Schmid responded that the tension strength perpendicular to grain is strength class independent
- H.J.Blass added that the tension strength perpendicular to grain is very low and one should detail structures so that it would not depend on tension strength perpendicular to grain.
- P.Quenneville asked for an explanation of why the previous findings that tensile strength perpendicular to grain was dependent on density differ from current findings.
- H.J.Blass responded that solid database were not available before.
- A.Jorissen asked whether fracture mechanics approach was used.
- M.Schmid responded that it was not tried.
- A.Ranta-Maunus added that the past database that showed tensile strength perpendicular to grain was dependent on density was based on clear wood data.

*Paper 32-6-5 On the reliability-based strength adjustment factors for timber design - T.D.G.Canisius*

Presenter: T.D.G.Canisius

- No discussions.

## 6. TIMBER JOINTS AND FASTENERS

*Paper 32-7-1 Behaviour of wood-steel-wood bolted glulam connections - M.Mohammad, J.H.P.Quenneville*

Presenter: J.H.P.Quenneville

- H.J.Larsen commented that with 6 mm displacement the failure mode should be considered as bearing (B) rather than row shear (RS) failures.
- P.Quenneville agreed that Table 2 group 2 should be identified as B/RS failures. Capacities based on RS predictions should be close to those based on B predictions. The predicted capacities of Group 2 might be increased.

- A.Jorissen questioned whether RS as a group was observed in cases with close row spacing of 5d.
- P.Quenneville responded that RS as a group was not observed in those cases as specimen thickness also would have an impact.
- A.Jorissen discussed the single fastener connection strength and the redistribution of load.
- P.Quenneville responded that some localized ductility was possible.
- H.J.Larsen cautioned that the theory and recommendations were based on test results mean values with sample size of 10 only.
- E.Karacabeyli asked whether the findings could be extrapolated to large bolt diameter cases.
- P.Quenneville responded that it would depend on the ductility or localized breaking.
- A.Jorissen pointed out that one of the equations could lead to negative shear capacity.
- P.Quenneville agreed that the equation did not have a lower bound and would look into it.
- C.Mettem discussed the issue of tension strength perpendicular to grain.
- A.Mischler questioned whether the strength of the bolts was measured.
- P.Quenneville responded that the strength of the bolts was not measured. They were Grade 2 bolts.
- A.Mischler pointed out that without measuring the strength of the bolts might lead to dangerous situation if different grades of steel were used.
- M.Ansell commented that the choice of yield stress for steel would have an impact.
- P.Quenneville responded that only mild steel would be permitted in the Canadian Code.

*Paper 32-7-2 A new set of experimental tests on beams loaded perpendicular-to-grain by dowel-type joints - M.Ballerini*

Presenter: M.Ballerini

- A.Leijten questioned whether the failure was governed by compression perpendicular to grain rather than tension perpendicular to grain. If so the Van der Put model for compression perpendicular to grain would fit the data well.
- M.Ballerini responded that the forms of the Van der Put formulae for compression and tension perpendicular to grain failures were similar. The only difference was the use of either compression or tension perpendicular to grain strength values in the respective equation.
- C.Mettem commented that modification factors for perpendicular to grain applications would also be available from TRADA.
- P.Quenneville asked where was the location of the split with respect to the bolt.
- M.Ballerini responded that the splits generally were located from mid diameter of the bolt to the compression side of the bolt.

*Paper 32-7-3 Design and analysis of bolted timber joints under lateral force perpendicular to grain - M.Yasumura, L.Daudeville*

Presenter: M.Yasumura

- Brief discussion took place on the yield strength of the connection and embedment strength of the bolt.

*Paper 32-7-4 Predicting capacities of joints with laterally loaded nails - I.Smith, J.H.P.Quenneville*

Presenter: J.H.P.Quenneville

- C.N.Fouepe asked the applicability of the results to tropical hard wood.
- H.J.Blass commented that for high-density tropical hardwood pre-drilling would be needed before nailing. Also embedment strength data for high-density tropical hardwood would be needed. Otherwise the equations should still be valid.
- E.Karacabeyli asked about the applicability of the results to plywood to wood connections.
- J.H.P.Quenneville responded that the results would be valid for timber to timber connections only.

*Paper 32-7-5 Strength reduction rules for multiple fastener joints - A.Mischler, E.Gehri*

Presenter: A.Mischler

- H.J.Blass asked for clarification of the title of the paper in relation to the conclusions.
- A.Mischler responded that the dowel slenderness ratio has a major influence on strength capacity of dowel.
- P.Quenneville asked which cases listed in Table 3 were ductile.
- A.Mischler responded that 10d/10d and 10d/7d cases were very ductile.
- A.Jorissen discussed and clarified that timber to timber joints were previously studied which differed from the current steel to timber connections. Timber to timber joints would tend to have higher ductility than steel to timber joints. In the past study sample size of 140 were used and only 2 cases were brittle failures.
- A.Jorissen asked whether the values reported in Table 1 were test results.
- A.Mischler responded that they were test results but Johansen theory fitted the results well.
- Detailed discussion took place on the difference in results between timber to timber connection and steel to timber connection with respect to the influence of the side members.
- A.Leijten questioned whether embedment tests could replace connection tests.
- H.J.Blass said that it would be end distance dependent. He also questioned whether the same level of confidence can be expected in the cases of 1 dowel in line (N=25) and 3 dowels in line (N=5).
- A.Mischler responded that this was considered by density matching of the test specimens in the single and multiple specimen groups.
- P.Quenneville asked about the use of same tolerance in the parallel and perpendicular directions
- A.Mischler clarified that in slender dowels one could balance the tolerance in the parallel and perpendicular directions. This was not the case for non-slender dowels.

*Paper 32-7-6 The stiffness of multiple bolted connections - A.Jorissen*

Presenter: A.Jorissen

- A.Ceccotti asked which density value was used in EC5 predictions and test result comparisons.
- A.Jorissen responded that an equation in EC5 was used for density adjustments.

- A.Leijten discussed the issue of serviceability versus ultimate limit state issues in bolted joints.
- A.Jorissen responded that there was no additional friction from washers.

*Paper 32-7-7 Concentric loading tests on girder truss components - T.N.Reynolds, A.Refford, V.Enjily, L.Whale*

Presented by T.N.Reynolds

- A.Leijten raised a question on the relatively short span of 60 cm with respect to the 40 cm long metal plate and pointed out that the sample size was limited. He also questioned the use of a 2.5 factor to obtain characteristic values, which were not based on material test properties.
- T.N.Reynolds and V.Enjily responded that the study allowed the design formula to be evaluated. Furthermore additional test results on 16 girder trusses were conducted but not included in the present paper and the 2.5 factor was used to convert the girder truss results to be used in the current study.
- S.Thelandersson stated that the span influence should be addressed.
- T.N.Reynolds and V.Enjily responded that the observed failure mode in this study was representative in truss applications. They tried spans of 1.6 to 1.8 m but the failure modes were found to be dominated by bending and shear failures.
- C.N.Fouepe suggested that FEM approach could be used to analyze the system.
- P.Quenneville suggested the use of Ehlbeck formula for dowel.
- T.N.Reynolds responded that the metal plate situation differ from the dowel application which would have stress concentration.
- S.Svensson stated that all test results should be shown and information on the variation of data should be provided.
- M.Ansell suggested the nail plate could be made full depth to eliminate the problem.
- T.N.Reynolds responded that similar recommendations were made to the industry.
- H.J.Blass asked why the reinforcement plate were not moved closer together in view of the failure mode of the unreinforced cases.
- T.N.Reynolds responded that the failure mode of the unreinforced cases was not known apriori and the placement of the reinforcement plates was based on industry recommendations which provided only temporary arrest of the failure.
- H.J.Blass stated that the reinforcement plates could be used in other situation such as notched beams and split area. However, design formula would be required.
- V.Enjily agreed and added that in Australia reinforcement plates were used in shear applications. The suggestion of using large plate was rejected because large presses were not available.

*Paper 32-7-8 Dowel type connections with slotted-in steel plates - M.U.Pedersen, C.O.Clorius, L.Damkilde, P.Hoffmeyer, L.Esklidsen*

Presenter: M.U.Pedersen

- H.J.Blass asked how were the  $M_y$  values obtained.
- M.U.Pedersen responded that they were measured by 3 point bending of the dowel upto 35 degree.
- H.J.Blass commented that since the connection test did not reach the same level of rotation, one should consider using smaller  $M_y$  values in the model.
- A.Jorissen asked and received clarification that Johansen theory was used.
- H.J.Blass asked about the procedures used to consider oversize holes.



- M.U.Pedersen responded that the stresses in one of the direction were removed in the analysis to account for the oversized hole.

*Paper 32-7-9 Creep of nail plate reinforced bolt joints - J.Vesa, A.Kevarinmaki*

Presenter: J.Vesa

- H.J.Blass commented that both the metal nail plate and the timber joint carried the loads. He asked whether the load sharing between the metal nail plate and the timber joint would change over time in a creep test.
- J.Vesa responded that it was not likely as the metal nail plate was much stiffer than the timber joint.

*Paper 32-7-10 The behaviour of timber joints with ring connectors - E.Gehri, A.Mischler*

Presenter: A.Mischler

- H.J.Blass commented that the paper content has severe deficiencies as previous work by other researchers were ignored and in some cases the interpretation of past results were incorrect. The paper in its present form would need major revisions before it would be allowed to appear in the proceedings.
- A.Mischler responded that he will discuss the issue with the first author.
- J.H.P.Quenneville also suggested that the author should examine some of the past research in UK and Canada.

*Paper 32-7-11 Non-metallic, adhesiveless joints for timber structures - R.D.Drake, M.P.Ansell, C.J.Mettem, R.Bainbridge*

Presenter: M.P.Ansell

- H.J.Blass asked how were the dowels installed.
- M.P.Ansell responded that the dowels were installed using a press.
- H.J.Larsen commented that this was an interesting test material and asked about the bending properties of the dowel.
- M.P.Ansell responded that the dowels were tested in shear mode to obtain their "bending" properties. It was felt that this mode of testing was appropriate after observing the failure mode of the dowels in a joint.
- H.J.Larsen commented that the use of Johansen theory based on shear failure might not be appropriate
- F.Lam asked whether there were plans to conduct cyclic tests.
- M.P.Ansell responded that at the moment no cyclic tests of the connection were available but there were fatigue test results in other applications.
- H.J.Blass asked about the cost of the dowels.
- M.P.Ansell responded that the cost were similar to steel.
- H.J.Blass asked about the reserved capacity in relation to the observed shear failure.
- M.P.Ansell responded that the dowel is irreversible at high loads.
- A.Jorissen asked about the post peak load response and failure mechanism.
- M.P.Ansell responded that the connection would absorb significant amount of energy at high loads based on its failure mechanism.
- E.Karacabeyli asked whether this dowel could be made into a bolt.
- M.P.Ansell responded that it would be possible.

*Paper 32-7-12 Effect of spacing and edge distance on the axial strength of glued-in-rods - H.J.Blass, B.Laskewitz*

Presenter: B.Laskewitz

- C.N.Fouepe commented that the findings of distance  $> 5d$  would fit with theoretical results of orthotropic material.
- A.Jorissen asked how to obtain characteristic values based on regression equation.
- B.Laskewitz responded that the number of test was small but regression analysis was appropriate.
- H.J.Blass added that more test results will be available later from the European Project.
- A.Jorissen commented that  $r^2$  values were low.
- B.Laskewitz responded that density information could also be used to perform multiple regression to improve  $r^2$ .
- B.J.Yeh asked whether environmental conditions were considered.
- B.Laskewitz responded that yes there are test results.
- C.N.Fouepe asked what are the failure modes.
- B.Laskewitz responded that mixed adhesive and wood failures were observed in each failed specimen with mostly wood failure.
- E.Karacabeyli commented that improving  $r^2$  in equation would be needed.
- A.Jorissen commented that splitting of wood might be due to tension perpendicular to grain stresses.
- H.J.Blass responded that high strength steel was used to get the failure mode. Mild steel could be used to get more ductile connection.

*Paper 32-7-13 Evaluation of material combinations for bonded in rods to achieve improved timber connections - C.J.Metten, R.Bainbridge, K.Harvey, M.P.Ansell, J.G.Broughton, A.R.Hutchinson*

Presenter: C.J.Metten

- S.Svensson received clarification from C.J.Metten on the HDT\* values in Table 8.

## 7. DURATION OF LOAD

*Paper 32-9-1 Bending-stress-redistribution caused by different creep in tension and compression and resulting DOL-effect - P.Becker, K.Rautenstrauch*

Presenter: P.Becker

- H.J.Larsen severely questioned the basic assumptions made in the paper.
- S.Thelandersson agreed with H.J.Larsen that the principle of linear viscoelasticity theory would not be appropriate in this case.
- H.J.Larsen stated that the results may be acceptable only if limitations were put on the approach based on the assumed stress strain relationship and not generalised to application to timber.
- A.Ranta-Maunus commented that non-linear creep model was used in VTT. Results were presented a few years ago in Copenhagen. The results also showed minor influence on DOL.
- M.Ansell agreed with the point that initial damage was compression and ultimate failure was in tension.

· F.Rouger also pointed out that since the influence on DOL was insignificant; therefore, the title of the paper was inappropriate.

*Paper 32-9-2 The long term performance of ply-web beams - R.Grantham, V.Enjily*

Presenter: R.Grantham

- P.Becker commented that the creep recovery period was too short.
- R.Grantham agreed but pointed out that there were funding limitations.
- H.J.Larsen stated that comments and reference to EC5 should be revised to reflect design values issue.
- S.Svensson questioned about the influence on climatic data to results.
- R.Grantham and V.Enjily responded that there was insufficient detailed climatic data to allow comparisons; therefore, the formula only accounted for time effects and did not account for climate.
- S.Svensson commented that the results would be highly dependent on climatic conditions.
- V.Enjily responded that additional results were available from a different study.
- A.Ranta-Maunus stated that shear creep is much more significant than bending creep in panel material; therefore, I-beam would be especially susceptible to creep under permanent loads.
- V.Enjily stated that creep in I-beam rather than creep of individual elements was measured.
- M.U.Pedersen commented that the change in deformation resulted from drying shrinkage on the compression side.
- C.Mettem discussed issues on web buckling and depth of web member. He also commented that report on component-based properties rather than material properties might cause difficulties for application to design.
- R.Grantham responded that lateral web buckling was not observed.
- F.Rouger asked and received clarification on the calculation of design load.

## 8. LAMINATED MEMBERS

*Paper 32-12-1 The bending stiffness of nail-laminated timber elements in transverse direction - T.Wolf, O.Schafer*

Presenter: T.Wolf

- H.J.Blass asked and received clarification that the withdrawal information of nails was based on measurements conducted in another institution.
- H.J.Blass commented that the deformation of 2 to 3 mm was high and head side deformation should also be considered.
- P.Quenneville asked and received clarification that repeated loading was not considered.
- G.Schickhofer disagreed with the use of concrete model analogy.
- B.Mohr stated permanent load should not be applied to nails.
- H.J.Blass clarified that permanent load should not be applied to smooth shank nail only.
- G.Schickhofer further stated that these members should be considered as one span elements without plate action.

## 9. TRUSSED RAFTERS

*Paper 32-14-1 Analysis of timber reinforced with punched metal plate fasteners - J.Nielsen*

Presented by J. Nielsen

- H.J.Blass asked whether the installation of nail plates would have a weakening effect from the nails cutting the wood fibers.
- J.Nielsen stated that this would be an issue with thick nail plates.
- S.Thelandersson asked about the use of grading method.
- J.Nielsen responded that the material was visually graded
- S.Thelandersson further commented that machine grading could be used to develop matched sample group.
- J.Nielsen responded that the material was density/weight matched.
- F.Lam asked about the compression failure mode and stated that reinforcement on the tension side would not help the situation.
- P.Quenneville stated that 4 point bending should be used to eliminate the compression problem.
- J.Nielsen agreed.
- S.Svensson questioned and received clarification on load deformation curves.
- P.Quenneville suggested that characteristic strength might be increased by reinforcing defects rather the entire section.
- E.Karacabeyli asked if the use of a bigger plate would affect results.
- J.Nielsen responded that moment capacity would be different.
- A.Jorissen stated that the linear model could not predict large deformation due to compression failure.
- J.Nielsen agreed and this would be a research topic in the future.

## 10. STRUCTURAL STABILITY

*Paper 32-15-1 Three-dimensional interaction in stabilization of multi-storey timber frame buildings - S.Andreasson*

Presenter: S.Andreasson

- B.Källsner questioned the procedure that calibrated the model directly to full scale wall tests rather than fastener load slip information. He pointed out that the calibrated model would be specific to the full scale wall tests because the stiffness of the structure is sensitive to the location and distribution of fasteners within a system and the application of dead load during testing.
- A.Andreasson responded that the smear action of fastener was considered and single fastener based model calibration was difficult.
- F.Lam agreed that although single fastener based model calibration procedures were more difficult, past work at UBC are successful examples.

*Paper 32-15-2 Application of capacity spectrum method to timber houses - N.Kawai*

Presenter: N.Kawai

- M.Yasumura asked and received clarification of the procedures used to establish heq

values and suggested that higher cycles rather than the first cycle in the load deformation curves of cyclic tests could be used to establish heq values.

*Paper 32-15-3 Design methods for shear walls with openings - C.Ni, E.Karacabeyli, A.Ceccotti*

Presenter: E.Karacabeyli

- V.Enjily received clarification of the term vd.
- M.Yasamura asked about the applicability of the procedures to multi-story systems.
- E.Karacabeyli responded that the design procedures could be applied to multi-story system based on a story to story approach.
- H.J.Larsen received clarification of the formula J with respect to both loading directions.
- S.Thelandersson asked about the applicability of the procedures to serviceability rather than capacity.
- E.Karacabeyli and A.Ceccotti responded that stiffness and displacement work was not considered here. More analyses would be needed.

*Paper 32-15-4 Static cyclic lateral loading tests on nailed plywood shear walls - K.Komatsu, K.H.Hwang, Y.Itou*

Presenter: K.Komatsu

- A.Ceccotti asked about the procedures to get ductility-based force reduction factor based on a static analysis.
- K.Komatsu responded that the Japanese system would only require static cyclic results and would not need ductility-based force reduction factor.
- F.Lam asked and received clarification that only envelope curves from static cyclic test results were shown.

## 11. SERVICEABILITY

*Paper 32-20-1 Floor vibrations - B.Mohr*

Presenter: B.Mohr

- T.D.G.Canisius asked whether experiment data were used to calibrate simplified model.
- B.Mohr responded that the simplified model was compared to FEM results.

## 12. OTHER BUSINESS

V.Enjily asked and received clarification from J.Ehlbeck that there is no connection between CIBW18 and RILEM activities on metal hardware fasteners.

H.J.Blass reminded the participants to send in the corrected final version of the paper within 4 weeks as a printed master copy. The title page should reflect the new name change of CIB W18. H.J.Blass also suggested that for participants who are not currently a member of CIBW18 to consider becoming official members.

### **13. VENUE AND PROGRAM FOR NEXT MEETING**

TU Delft Netherlands will be the venue for the 33<sup>rd</sup> CIBW18 meeting during the week of August 28, 2000 to September 1, 2000. It will again be a 3 day meeting with 2.5 days of technical session and half day for technical excursion.

The venue for the 34<sup>th</sup> CIBW18 meeting is provisionally set in the 1st week of September 2001 in Venice Italy.

The venue for the 35<sup>th</sup> CIBW18 meeting is provisionally set in the 1<sup>st</sup> week of September 2002 in Japan.

H.J.Blass thanked Prof. Pischl, Prof. Schickhofer, and the staff of TU Graz for successfully hosting the 33<sup>rd</sup> CIBW18 meeting and will be looking forward to future cooperation.

The 33<sup>rd</sup> CIBW18 meeting was closed (1500).

### **14. CLOSE**

**15. List of CIB-W18 Papers,  
Graz, Austria 1999**

## List of CIB-W18 Papers, Graz, Austria 1999

- 32-1-1 Determination of Partial Coefficients and Modification Factors- H J Larsen, S Svensson, S Thelandersson
- 32-1-2 Design by Testing of Structural Timber Components - V Enjily, L Whale
- 32-5-1 Actual Possibilities of the Machine Grading of Timber - K Frühwald and A Bernasconi
- 32-5-2 Detection of Severe Timber Defects by Machine Grading - A Bernasconi, L Boström and B Schacht
- 32-6-1 Development of High-Resistance Glued Robinia Products and an Attempt to Assign Such Products to the European System of Strength Classes - G Schickhofer and B Obermayr
- 32-6-2 Length and Load Configuration Effects in the Code Format - T Isaksson
- 32-6-3 Length Effect on the Tensile Strength of Truss Chord Members - F Lam
- 32-6-4 Tensile Strength Perpendicular to Grain of Glued Laminated Timber - H J Blaß and M Schmid
- 32-6-5 On the Reliability-based Strength Adjustment Factors for Timber Design - T D G Canisius
- 32-7-1 Behaviour of Wood-Steel-Wood Bolted Glulam Connections - M Mohammad and J H P Quenneville
- 32-7-2 A new set of experimental tests on beams loaded perpendicular-to-grain by dowel-type joints - M Ballerini
- 32-7-3 Design and Analysis of Bolted Timber Joints under Lateral Force Perpendicular to Grain - M Yasumura and L Daudeville
- 32-7-4 Predicting Capacities of Joints with Laterally Loaded Nails - I Smith and P Quenneville
- 32-7-5 Strength Reduction Rules for Multiple Fastener Joints - A Mischler and E Gehri
- 32-7-6 The Stiffness of Multiple Bolted Connections - A Jorissen



- 32-7-7 Concentric Loading Tests on Girder Truss Components - T N Reynolds, A Reffold, V Enjily and L Whale
- 32-7-8 Dowel Type Connections with Slotted-In Steel Plates - M U Pedersen, C O Clorius, L Damkilde, P Hoffmeyer and L Esklidsen
- 32-7-9 Creep of Nail Plate Reinforced Bolt Joints - J Vesa and A Kevarinmäki
- 32-7-10 The Behaviour of Timber Joints with Ring Connectors - E Gehri and A Mischler
- 32-7-11 Non-Metallic, Adhesiveless Joints for Timber Structures - R D Drake, M P Ansell, C J Mettem and R Bainbridge
- 32-7-12 Effect of Spacing and Edge Distance on the Axial Strength of Glued-in Rods - H J Blaß and B Laskewitz
- 32-7-13 Evaluation of Material Combinations for Bonded in Rods to Achieve Improved Timber Connections - C J Mettem, R J Bainbridge, K Harvey, M P Ansell, J G Broughton and A R Hutchinson
- 32-9-1 Bending-Stress-Redistribution Caused by Different Creep in Tension and Compression and Resulting DOL-Effect - P Becker and K Rautenstrauch
- 32-9-2 The Long Term Performance of Ply-Web Beams - R Grantham and V Enjily
- 32-12-1 The bending stiffness of nail-laminated timber elements in transverse direction - T Wolf and O Schäfer
- 32-14-1 Analysis of Timber Reinforced with Punched Metal Plate Fasteners- J Nielsen
- 32-15-1 Three-Dimensional Interaction in Stabilisation of Multi-Storey Timber Frame Buildings - S Andreasson
- 32-15-2 Application of Capacity Spectrum Method to Timber Houses - N Kawai
- 32-15-3 Design Methods for Shear Walls with Openings - C Ni, E Karacabeyli and A Ceccotti
- 32-15-4 Static Cyclic Lateral Loading Tests on Nailed Plywood Shear Walls - K Komatsu, K H Hwang and Y Itou
- 32-20-1 Floor Vibrations - B Mohr

**16. Current List of CIB-W18(A) Papers**

## CURRENT LIST OF CIB-W18(A) PAPERS

Technical papers presented to CIB-W18(A) are identified by a code CIB-W18(A)/a-b-c, where:

- a denotes the meeting at which the paper was presented.  
Meetings are classified in chronological order:

- 1 Princes Risborough, England; March 1973
- 2 Copenhagen, Denmark; October 1973
- 3 Delft, Netherlands; June 1974
- 4 Paris, France; February 1975
- 5 Karlsruhe, Federal Republic of Germany; October 1975
- 6 Aalborg, Denmark; June 1976
- 7 Stockholm, Sweden; February/March 1977
- 8 Brussels, Belgium; October 1977
- 9 Perth, Scotland; June 1978
- 10 Vancouver, Canada; August 1978
- 11 Vienna, Austria; March 1979
- 12 Bordeaux, France; October 1979
- 13 Otaniemi, Finland; June 1980
- 14 Warsaw, Poland; May 1981
- 15 Karlsruhe, Federal Republic of Germany; June 1982
- 16 Lillehammer, Norway; May/June 1983
- 17 Rapperswil, Switzerland; May 1984
- 18 Beit Oren, Israel; June 1985
- 19 Florence, Italy; September 1986
- 20 Dublin, Ireland; September 1987
- 21 Parksville, Canada; September 1988
- 22 Berlin, German Democratic Republic; September 1989
- 23 Lisbon, Portugal; September 1990
- 24 Oxford, United Kingdom; September 1991
- 25 Åhus, Sweden; August 1992
- 26 Athens, USA; August 1993
- 27 Sydney, Australia; July 1994
- 28 Copenhagen, Denmark, April 1995
- 29 Bordeaux, France, August 1996
- 30 Vancouver, Canada, August 1997
- 31 Savonlinna, Finland, August 1998
- 32 Graz, Austria, August 1999

b denotes the subject:

- 1 Limit State Design
- 2 Timber Columns
- 3 Symbols
- 4 Plywood
- 5 Stress Grading
- 6 Stresses for Solid Timber
- 7 Timber Joints and Fasteners
- 8 Load Sharing
- 9 Duration of Load
- 10 Timber Beams
- 11 Environmental Conditions
- 12 Laminated Members
- 13 Particle and Fibre Building Boards
- 14 Trussed Rafters
- 15 Structural Stability
- 16 Fire
- 17 Statistics and Data Analysis
- 18 Glued Joints
- 19 Fracture Mechanics
- 20 Serviceability
- 21 Test Methods
- 100 CIB Timber Code
- 101 Loading Codes
- 102 Structural Design Codes
- 103 International Standards Organisation
- 104 Joint Committee on Structural Safety
- 105 CIB Programme, Policy and Meetings
- 106 International Union of Forestry Research Organisations

c is simply a number given to the papers in the order in which they appear:

Example: CIB-W18/4-102-5 refers to paper 5 on subject 102 presented at the fourth meeting of W18.

Listed below, by subjects, are all papers that have to date been presented to W18. When appropriate some papers are listed under more than one subject heading.

## LIMIT STATE DESIGN

- 1-1-1 Limit State Design - H J Larsen
- 1-1-2 The Use of Partial Safety Factors in the New Norwegian Design Code for Timber Structures - O Brynildsen
- 1-1-3 Swedish Code Revision Concerning Timber Structures - B Noren
- 1-1-4 Working Stresses Report to British Standards Institution Committee BLC/17/2
- 6-1-1 On the Application of the Uncertainty Theoretical Methods for the Definition of the Fundamental Concepts of Structural Safety - K Skov and O Ditlevsen
- 11-1-1 Safety Design of Timber Structures - H J Larsen
- 18-1-1 Notes on the Development of a UK Limit States Design Code for Timber - A R Fewell and C B Pierce
- 18-1-2 Eurocode 5, Timber Structures - H J Larsen
- 19-1-1 Duration of Load Effects and Reliability Based Design (Single Member) - R O Foschi and Z C Yao
- 21-102-1 Research Activities Towards a New GDR Timber Design Code Based on Limit States Design - W Rug and M Badstube
- 22-1-1 Reliability-Theoretical Investigation into Timber Components Proposal for a Supplement of the Design Concept - M Badstube, W Rug and R Plessow
- 23-1-1 Some Remarks about the Safety of Timber Structures - J Kuipers
- 23-1-2 Reliability of Wood Structural Elements: A Probabilistic Method to Eurocode 5 Calibration - F Rouger, N Lheritier, P Racher and M Fogli
- 31-1-1 A Limit States Design Approach to Timber Framed Walls - C J Mettem, R Bainbridge and J A Gordon
- 32 -1-1 Determination of Partial Coefficients and Modification Factors- H J Larsen, S Svensson and S Thelandersson
- 32 -1-2 Design by Testing of Structural Timber Components - V Enjily and L Whale

## TIMBER COLUMNS

- 2-2-1 The Design of Solid Timber Columns - H J Larsen
- 3-2-1 The Design of Built-Up Timber Columns - H J Larsen
- 4-2-1 Tests with Centrally Loaded Timber Columns - H J Larsen and S S Pedersen
- 4-2-2 Lateral-Torsional Buckling of Eccentrically Loaded Timber Columns- B Johansson
- 5-9-1 Strength of a Wood Column in Combined Compression and Bending with Respect to Creep - B Källsner and B Norén
- 5-100-1 Design of Solid Timber Columns (First Draft) - H J Larsen
- 6-100-1 Comments on Document 5-100-1, Design of Solid Timber Columns - H J Larsen and E Theilgaard
- 6-2-1 Lattice Columns - H J Larsen
- 6-2-2 A Mathematical Basis for Design Aids for Timber Columns - H J Burgess
- 6-2-3 Comparison of Larsen and Perry Formulas for Solid Timber Columns- H J Burgess
- 7-2-1 Lateral Bracing of Timber Struts - J A Simon

- 8-15-1 Laterally Loaded Timber Columns: Tests and Theory - H J Larsen
- 17-2-1 Model for Timber Strength under Axial Load and Moment - T Poutanen
- 18-2-1 Column Design Methods for Timber Engineering - A H Buchanan, K C Johns, B Madsen
- 19-2-1 Creep Buckling Strength of Timber Beams and Columns - R H Leicester
- 19-12-2 Strength Model for Glulam Columns - H J Blaß
- 20-2-1 Lateral Buckling Theory for Rectangular Section Deep Beam-Columns- H J Burgess
- 20-2-2 Design of Timber Columns - H J Blaß
- 21-2-1 Format for Buckling Strength - R H Leicester
- 21-2-2 Beam-Column Formulae for Design Codes - R H Leicester
- 21-15-1 Rectangular Section Deep Beam - Columns with Continuous Lateral Restraint - H J Burgess
- 21-15-2 Buckling Modes and Permissible Axial Loads for Continuously Braced Columns - H J Burgess
- 21-15-3 Simple Approaches for Column Bracing Calculations - H J Burgess
- 21-15-4 Calculations for Discrete Column Restraints - H J Burgess
- 22-2-1 Buckling and Reliability Checking of Timber Columns - S Huang, P M Yu and J Y Hong
- 22-2-2 Proposal for the Design of Compressed Timber Members by Adopting the Second-Order Stress Theory - P Kaiser
- 30-2-1 Beam-Column Formula for Specific Truss Applications - W Lau, F Lam and J D Barrett
- 31-2-1 Deformation and Stability of Columns of Viscoelastic Material Wood - P Becker and K Rautenstrauch

## SYMBOLS

- 3-3-1 Symbols for Structural Timber Design - J Kuipers and B Norén
- 4-3-1 Symbols for Timber Structure Design - J Kuipers and B Norén
- 28-3-1 Symbols for Timber and Wood-Based Materials - J Kuipers and B Noren
- 1 Symbols for Use in Structural Timber Design

## PLYWOOD

- 2-4-1 The Presentation of Structural Design Data for Plywood - L G Booth
- 3-4-1 Standard Methods of Testing for the Determination of Mechanical Properties of Plywood - J Kuipers
- 3-4-2 Bending Strength and Stiffness of Multiple Species Plywood - C K A Stieda
- 4-4-4 Standard Methods of Testing for the Determination of Mechanical Properties of Plywood - Council of Forest Industries, B.C.
- 5-4-1 The Determination of Design Stresses for Plywood in the Revision of CP 112 - L G Booth
- 5-4-2 Veneer Plywood for Construction - Quality Specifications - ISO/TC 139. Plywood, Working Group 6

- 6-4-1 The Determination of the Mechanical Properties of Plywood Containing Defects - L G Booth
- 6-4-2 Comparison of the Size and Type of Specimen and Type of Test on Plywood Bending Strength and Stiffness - C R Wilson and P Eng
- 6-4-3 Buckling Strength of Plywood: Results of Tests and Recommendations for Calculations - J Kuipers and H Ploos van Amstel
- 7-4-1 Methods of Test for the Determination of Mechanical Properties of Plywood - L G Booth, J Kuipers, B Norén, C R Wilson
- 7-4-2 Comments Received on Paper 7-4-1
- 7-4-3 The Effect of Rate of Testing Speed on the Ultimate Tensile Stress of Plywood - C R Wilson and A V Parasin
- 7-4-4 Comparison of the Effect of Specimen Size on the Flexural Properties of Plywood Using the Pure Moment Test - C R Wilson and A V Parasin
- 8-4-1 Sampling Plywood and the Evaluation of Test Results - B Norén
- 9-4-1 Shear and Torsional Rigidity of Plywood - H J Larsen
- 9-4-2 The Evaluation of Test Data on the Strength Properties of Plywood - L G Booth
- 9-4-3 The Sampling of Plywood and the Derivation of Strength Values (Second Draft) - B Norén
- 9-4-4 On the Use of the CIB/RILEM Plywood Plate Twisting Test: a progress report - L G Booth
- 10-4-1 Buckling Strength of Plywood - J Dekker, J Kuipers and H Ploos van Amstel
- 11-4-1 Analysis of Plywood Stressed Skin Panels with Rigid or Semi-Rigid Connections - I Smith
- 11-4-2 A Comparison of Plywood Modulus of Rigidity Determined by the ASTM and RILEM CIB/3-TT Test Methods - C R Wilson and A V Parasin
- 11-4-3 Sampling of Plywood for Testing Strength - B Norén
- 12-4-1 Procedures for Analysis of Plywood Test Data and Determination of Characteristic Values Suitable for Code Presentation - C R Wilson
- 14-4-1 An Introduction to Performance Standards for Wood-base Panel Products - D H Brown
- 14-4-2 Proposal for Presenting Data on the Properties of Structural Panels - T Schmidt
- 16-4-1 Planar Shear Capacity of Plywood in Bending - C K A Stieda
- 17-4-1 Determination of Panel Shear Strength and Panel Shear Modulus of Beech-Plywood in Structural Sizes - J Ehlbeck and F Colling
- 17-4-2 Ultimate Strength of Plywood Webs - R H Leicester and L Pham
- 20-4-1 Considerations of Reliability - Based Design for Structural Composite Products - M R O'Halloran, J A Johnson, E G Elias and T P Cunningham
- 21-4-1 Modelling for Prediction of Strength of Veneer Having Knots - Y Hirashima
- 22-4-1 Scientific Research into Plywood and Plywood Building Constructions the Results and Findings of which are Incorporated into Construction Standard Specifications of the USSR - I M Guskov
- 22-4-2 Evaluation of Characteristic values for Wood-Based Sheet Materials - E G Elias
- 24-4-1 APA Structural-Use Design Values: An Update to Panel Design Capacities - A L Kuchar, E G Elias, B Yeh and M R O'Halloran

## STRESS GRADING

- 1-5-1 Quality Specifications for Sawn Timber and Precision Timber - Norwegian Standard NS 3080
- 1-5-2 Specification for Timber Grades for Structural Use - British Standard BS 4978
- 4-5-1 Draft Proposal for an International Standard for Stress Grading Coniferous Sawn Softwood - ECE Timber Committee
- 16-5-1 Grading Errors in Practice - B Thunell
- 16-5-2 On the Effect of Measurement Errors when Grading Structural Timber - L Nordberg and B Thunell
- 19-5-1 Stress-Grading by ECE Standards of Italian-Grown Douglas-Fir Dimension Lumber from Young Thinnings - L Uzielli
- 19-5-2 Structural Softwood from Afforestation Regions in Western Norway - R Lackner
- 21-5-1 Non-Destructive Test by Frequency of Full Size Timber for Grading - T Nakai
- 22-5-1 Fundamental Vibration Frequency as a Parameter for Grading Sawn Timber - T Nakai, T Tanaka and H Nagao
- 24-5-1 Influence of Stress Grading System on Length Effect Factors for Lumber Loaded in Compression - A Campos and I Smith
- 26-5-1 Structural Properties of French Grown Timber According to Various Grading Methods - F Rouger, C De Lafond and A El Quadrani
- 28-5-1 Grading Methods for Structural Timber - Principles for Approval - S Ohlsson
- 28-5-2 Relationship of Moduli of Elasticity in Tension and in Bending of Solid Timber - N Burger and P Glos
- 29-5-1 The Effect of Edge Knots on the Strength of SPF MSR Lumber - T Courchene, F Lam and J D Barrett
- 29-5-2 Determination of Moment Configuration Factors using Grading Machine Readings - T D G Canisius and T Isaksson
- 31-5-1 Influence of Varying Growth Characteristics on Stiffness Grading of Structural Timber - S Ormarsson, H Petersson, O Dahlblom and K Persson
- 31-5-2 A Comparison of In-Grade Test Procedures - R H Leicester, H Breitingner and H Fordham
- 32-5-1 Actual Possibilities of the Machine Grading of Timber - K Frühwald and A Bernasconi
- 32-5-2 Detection of Severe Timber Defects by Machine Grading - A Bernasconi, L Boström and B Schacht

## STRESSES FOR SOLID TIMBER

- 4-6-1 Derivation of Grade Stresses for Timber in the UK - W T Curry
- 5-6-1 Standard Methods of Test for Determining some Physical and Mechanical Properties of Timber in Structural Sizes - W T Curry
- 5-6-2 The Description of Timber Strength Data - J R Tory
- 5-6-3 Stresses for EC1 and EC2 Stress Grades - J R Tory
- 6-6-1 Standard Methods of Test for the Determination of some Physical and Mechanical Properties of Timber in Structural Sizes (third draft) - W T Curry



- 7-6-1 Strength and Long-term Behaviour of Lumber and Glued Laminated Timber under Torsion Loads - K Möhler
- 9-6-1 Classification of Structural Timber - H J Larsen
- 9-6-2 Code Rules for Tension Perpendicular to Grain - H J Larsen
- 9-6-3 Tension at an Angle to the Grain - K Möhler
- 9-6-4 Consideration of Combined Stresses for Lumber and Glued Laminated Timber - K Möhler
- 11-6-1 Evaluation of Lumber Properties in the United States - W L Galligan and J H Haskell
- 11-6-2 Stresses Perpendicular to Grain - K Möhler
- 11-6-3 Consideration of Combined Stresses for Lumber and Glued Laminated Timber (addition to Paper CIB-W18/9-6-4) - K Möhler
- 12-6-1 Strength Classifications for Timber Engineering Codes - R H Leicester and W G Keating
- 12-6-2 Strength Classes for British Standard BS 5268 - J R Tory
- 13-6-1 Strength Classes for the CIB Code - J R Tory
- 13-6-2 Consideration of Size Effects and Longitudinal Shear Strength for Uncracked Beams - R O Foschi and J D Barrett
- 13-6-3 Consideration of Shear Strength on End-Cracked Beams - J D Barrett and R O Foschi
- 15-6-1 Characteristic Strength Values for the ECE Standard for Timber - J G Sunley
- 16-6-1 Size Factors for Timber Bending and Tension Stresses - A R Fewell
- 16-6-2 Strength Classes for International Codes - A R Fewell and J G Sunley
- 17-6-1 The Determination of Grade Stresses from Characteristic Stresses for BS 5268: Part 2 - A R Fewell
- 17-6-2 The Determination of Softwood Strength Properties for Grades, Strength Classes and Laminated Timber for BS 5268: Part 2 - A R Fewell
- 18-6-1 Comment on Papers: 18-6-2 and 18-6-3 - R H Leicester
- 18-6-2 Configuration Factors for the Bending Strength of Timber - R H Leicester
- 18-6-3 Notes on Sampling Factors for Characteristic Values - R H Leicester
- 18-6-4 Size Effects in Timber Explained by a Modified Weakest Link Theory- B Madsen and A H Buchanan
- 18-6-5 Placement and Selection of Growth Defects in Test Specimens - H Riberholt
- 18-6-6 Partial Safety-Coefficients for the Load-Carrying Capacity of Timber Structures - B Norén and J-O Nylander
- 19-6-1 Effect of Age and/or Load on Timber Strength - J Kuipers
- 19-6-2 Confidence in Estimates of Characteristic Values - R H Leicester
- 19-6-3 Fracture Toughness of Wood - Mode I - K Wright and M Fonselius
- 19-6-4 Fracture Toughness of Pine - Mode II - K Wright
- 19-6-5 Drying Stresses in Round Timber - A Ranta-Maunus
- 19-6-6 A Dynamic Method for Determining Elastic Properties of Wood - R Görlacher
- 20-6-1 A Comparative Investigation of the Engineering Properties of "Whitewoods" Imported to Israel from Various Origins - U Korin

- 20-6-2 Effects of Yield Class, Tree Section, Forest and Size on Strength of Home Grown Sitka Spruce - V Picardo
- 20-6-3 Determination of Shear Strength and Strength Perpendicular to Grain - H J Larsen
- 21-6-1 Draft Australian Standard: Methods for Evaluation of Strength and Stiffness of Graded Timber - R H Leicester
- 21-6-2 The Determination of Characteristic Strength Values for Stress Grades of Structural Timber. Part 1 - A R Fewell and P Glos
- 21-6-3 Shear Strength in Bending of Timber - U Korin
- 22-6-1 Size Effects and Property Relationships for Canadian 2-inch Dimension Lumber - J D Barrett and H Griffin
- 22-6-2 Moisture Content Adjustments for In-Grade Data - J D Barrett and W Lau
- 22-6-3 A Discussion of Lumber Property Relationships in Eurocode 5 - D W Green and D E Kretschmann
- 22-6-4 Effect of Wood Preservatives on the Strength Properties of Wood - F Ronai
- 23-6-1 Timber in Compression Perpendicular to Grain - U Korin
- 24-6-1 Discussion of the Failure Criterion for Combined Bending and Compression - T A C M van der Put
- 24-6-3 Effect of Within Member Variability on Bending Strength of Structural Timber - I Czmochn, S Thelandersson and H J Larsen
- 24-6-4 Protection of Structural Timber Against Fungal Attack Requirements and Testing- K Jaworska, M Rylko and W Nozynski
- 24-6-5 Derivation of the Characteristic Bending Strength of Solid Timber According to CEN-Document prEN 384 - A J M Leijten
- 25-6-1 Moment Configuration Factors for Simple Beams- T D G Canisius
- 25-6-3 Bearing Capacity of Timber - U Korin
- 25-6-4 On Design Criteria for Tension Perpendicular to Grain - H Petersson
- 25-6-5 Size Effects in Visually Graded Softwood Structural Lumber - J D Barrett, F Lam and W Lau
- 26-6-1 Discussion and Proposal of a General Failure Criterion for Wood - T A C M van der Put
- 27-6-1 Development of the "Critical Bearing": Design Clause in CSA-086.1 - C Lum and E Karacabeyli
- 27-6-2 Size Effects in Timber: Novelty Never Ends - F Rouger and T Fewell
- 27-6-3 Comparison of Full-Size Sugi (*Cryptomeria japonica* D. Don) Structural Performance in Bending of Round Timber, Two Surfaces Sawn Timber and Square Sawn Timber - T Nakai, H Nagao and T Tanaka
- 28-6-1 Shear Strength of Canadian Softwood Structural Lumber - F Lam, H Yee and J D Barrett
- 28-6-2 Shear Strength of Douglas Fir Timbers - B Madsen
- 28-6-3 On the Influence of the Loading Head Profiles on Determined Bending Strength - L Muszyński and R Szukala
- 28-6-4 Effect of Test Standard, Length and Load Configuration on Bending Strength of Structural Timber- T Isaksson and S Thelandersson
- 28-6-5 Grading Machine Readings and their Use in the Calculation of Moment Configuration Factors - T Canisius, T Isaksson and S Thelandersson

- 28-6-6 End Conditions for Tension Testing of Solid Timber Perpendicular to Grain - T Canisius
- 29-6-1 Effect of Size on Tensile Strength of Timber - N Burger and P Glos
- 29-6-2 Equivalence of In-Grade Testing Standards - R H Leicester, H O Breitingner and H F Fordham
- 30-6-1 Strength Relationships in Structural Timber Subjected to Bending and Tension - N Burger and P Glos
- 30-6-2 Characteristic Design Stresses in Tension for Radiata Pine Grown in Canterbury - A Tsehaye, J C F Walker and A H Buchanan
- 30-6-3 Timber as a Natural Composite: Explanation of Some Peculiarities in the Mechanical Behaviour - E Gehri
- 31-6-1 Length and Moment Configuration Factors - T Isaksson
- 31-6-2 Tensile Strength Perpendicular to Grain According to EN 1193 - H J Blaß and M Schmid
- 31-6-3 Strength of Small Diameter Round Timber - A Ranta-Maunus, U Saarelainen and H Boren
- 31-6-4 Compression Strength Perpendicular to Grain of Structural Timber and Glulam - L Damkilde, P Hoffmeyer and T N Pedersen
- 31-6-5 Bearing Strength of Timber Beams - R H Leicester, H Fordham and H Breitingner
- 32-6-1 Development of High-Resistance Glued Robinia Products and an Attempt to Assign Such Products to the European System of Strength Classes - G Schickhofer and B Obermayr
- 32-6-2 Length and Load Configuration Effects in the Code Format - T Isaksson
- 32-6-3 Length Effect on the Tensile Strength of Truss Chord Members - F Lam
- 32-6-4 Tensile Strength Perpendicular to Grain of Glued Laminated Timber - H J Blaß and M Schmid
- 32-6-5 On the Reliability-based Strength Adjustment Factors for Timber Design - T D G Canisius

#### TIMBER JOINTS AND FASTENERS

- 1-7-1 Mechanical Fasteners and Fastenings in Timber Structures - E G Stern
- 4-7-1 Proposal for a Basic Test Method for the Evaluation of Structural Timber Joints with Mechanical Fasteners and Connectors - RILEM 3TT Committee
- 4-7-2 Test Methods for Wood Fasteners - K Möhler
- 5-7-1 Influence of Loading Procedure on Strength and Slip-Behaviour in Testing Timber Joints - K Möhler
- 5-7-2 Recommendations for Testing Methods for Joints with Mechanical Fasteners and Connectors in Load-Bearing Timber Structures - RILEM 3 TT Committee
- 5-7-3 CIB-Recommendations for the Evaluation of Results of Tests on Joints with Mechanical Fasteners and Connectors used in Load-Bearing Timber Structures - J Kuipers
- 6-7-1 Recommendations for Testing Methods for Joints with Mechanical Fasteners and Connectors in Load-Bearing Timber Structures (seventh draft) - RILEM 3 TT Committee
- 6-7-2 Proposal for Testing Integral Nail Plates as Timber Joints - K Möhler

- 6-7-3 Rules for Evaluation of Values of Strength and Deformation from Test Results - Mechanical Timber Joints - M Johansen, J Kuipers, B Norén
- 6-7-4 Comments to Rules for Testing Timber Joints and Derivation of Characteristic Values for Rigidity and Strength - B Norén
- 7-7-1 Testing of Integral Nail Plates as Timber Joints - K Möhler
- 7-7-2 Long Duration Tests on Timber Joints - J Kuipers
- 7-7-3 Tests with Mechanically Jointed Beams with a Varying Spacing of Fasteners - K Möhler
- 7-100-1 CIB-Timber Code Chapter 5.3 Mechanical Fasteners; CIB-Timber Standard 06 and 07 - H J Larsen
- 9-7-1 Design of Truss Plate Joints - F J Keenan
- 9-7-2 Staples - K Möhler
- 11-7-1 A Draft Proposal for International Standard: ISO Document ISO/TC 165N 38E
- 12-7-1 Load-Carrying Capacity and Deformation Characteristics of Nailed Joints - J Ehlbeck
- 12-7-2 Design of Bolted Joints - H J Larsen
- 12-7-3 Design of Joints with Nail Plates - B Norén
- 13-7-1 Polish Standard BN-80/7159-04: Parts 00-01-02-03-04-05. "Structures from Wood and Wood-based Materials. Methods of Test and Strength Criteria for Joints with Mechanical Fasteners"
- 13-7-2 Investigation of the Effect of Number of Nails in a Joint on its Load Carrying Ability - W Nozynski
- 13-7-3 International Acceptance of Manufacture, Marking and Control of Finger-jointed Structural Timber - B Norén
- 13-7-4 Design of Joints with Nail Plates - Calculation of Slip - B Norén
- 13-7-5 Design of Joints with Nail Plates - The Heel Joint - B Källsner
- 13-7-6 Nail Deflection Data for Design - H J Burgess
- 13-7-7 Test on Bolted Joints - P Vermeyden
- 13-7-8 Comments to paper CIB-W18/12-7-3 "Design of Joints with Nail Plates"- B Norén
- 13-7-9 Strength of Finger Joints - H J Larsen
- 13-100-4 CIB Structural Timber Design Code. Proposal for Section 6.1.5 Nail Plates - N I Bovim
- 14-7-1 Design of Joints with Nail Plates (second edition) - B Norén
- 14-7-2 Method of Testing Nails in Wood (second draft, August 1980) - B Norén
- 14-7-3 Load-Slip Relationship of Nailed Joints - J Ehlbeck and H J Larsen
- 14-7-4 Wood Failure in Joints with Nail Plates - B Norén
- 14-7-5 The Effect of Support Eccentricity on the Design of W- and WW-Trussed with Nail Plate Connectors - B Källsner
- 14-7-6 Derivation of the Allowable Load in Case of Nail Plate Joints Perpendicular to Grain - K Möhler
- 14-7-7 Comments on CIB-W18/14-7-1 - T A C M van der Put

- 15-7-1 Final Recommendation TT-1A: Testing Methods for Joints with Mechanical Fasteners in Load-Bearing Timber Structures. Annex A Punched Metal Plate Fasteners - Joint Committee RILEM/CIB-3TT
- 16-7-1 Load Carrying Capacity of Dowels - E Gehri
- 16-7-2 Bolted Timber Joints: A Literature Survey - N Harding
- 16-7-3 Bolted Timber Joints: Practical Aspects of Construction and Design; a Survey - N Harding
- 16-7-4 Bolted Timber Joints: Draft Experimental Work Plan - Building Research Association of New Zealand
- 17-7-1 Mechanical Properties of Nails and their Influence on Mechanical Properties of Nailed Timber Joints Subjected to Lateral Loads - I Smith, L R J Whale, C Anderson and L Held
- 17-7-2 Notes on the Effective Number of Dowels and Nails in Timber Joints - G Steck
- 18-7-1 Model Specification for Driven Fasteners for Assembly of Pallets and Related Structures - E G Stern and W B Wallin
- 18-7-2 The Influence of the Orientation of Mechanical Joints on their Mechanical Properties - I Smith and L R J Whale
- 18-7-3 Influence of Number of Rows of Fasteners or Connectors upon the Ultimate Capacity of Axially Loaded Timber Joints - I Smith and G Steck
- 18-7-4 A Detailed Testing Method for Nailplate Joints - J Kangas
- 18-7-5 Principles for Design Values of Nailplates in Finland - J Kangas
- 18-7-6 The Strength of Nailplates - N I Bovim and E Aasheim
- 19-7-1 Behaviour of Nailed and Bolted Joints under Short-Term Lateral Load - Conclusions from Some Recent Research - L R J Whale, I Smith and B O Hilson
- 19-7-2 Glued Bolts in Glulam - H Riberholt
- 19-7-3 Effectiveness of Multiple Fastener Joints According to National Codes and Eurocode 5 (Draft) - G Steck
- 19-7-4 The Prediction of the Long-Term Load Carrying Capacity of Joints in Wood Structures - Y M Ivanov and Y Y Slavic
- 19-7-5 Slip in Joints under Long-Term Loading - T Feldborg and M Johansen
- 19-7-6 The Derivation of Design Clauses for Nailed and Bolted Joints in Eurocode 5 - L R J Whale and I Smith
- 19-7-7 Design of Joints with Nail Plates - Principles - B Norén
- 19-7-8 Shear Tests for Nail Plates - B Norén
- 19-7-9 Advances in Technology of Joints for Laminated Timber - Analyses of the Structural Behaviour - M Piazza and G Turrini
- 19-15-1 Connections Deformability in Timber Structures: A Theoretical Evaluation of its Influence on Seismic Effects - A Ceccotti and A Vignoli
- 20-7-1 Design of Nailed and Bolted Joints-Proposals for the Revision of Existing Formulae in Draft Eurocode 5 and the CIB Code - L R J Whale, I Smith and H J Larsen
- 20-7-2 Slip in Joints under Long Term Loading - T Feldborg and M Johansen
- 20-7-3 Ultimate Properties of Bolted Joints in Glued-Laminated Timber - M Yasumura, T Murota and H Sakai

- 20-7-4 Modelling the Load-Deformation Behaviour of Connections with Pin-Type Fasteners under Combined Moment, Thrust and Shear Forces - I Smith
- 21-7-1 Nails under Long-Term Withdrawal Loading - T Feldborg and M Johansen
- 21-7-2 Glued Bolts in Glulam-Proposals for CIB Code - H Riberholt
- 21-7-3 Nail Plate Joint Behaviour under Shear Loading - T Poutanen
- 21-7-4 Design of Joints with Laterally Loaded Dowels. Proposals for Improving the Design Rules in the CIB Code and the Draft Eurocode 5 - J Ehlbeck and H Werner
- 21-7-5 Axially Loaded Nails: Proposals for a Supplement to the CIB Code - J Ehlbeck and W Siebert
- 22-7-1 End Grain Connections with Laterally Loaded Steel Bolts A draft proposal for design rules in the CIB Code - J Ehlbeck and M Gerold
- 22-7-2 Determination of Perpendicular-to-Grain Tensile Stresses in Joints with Dowel-Type Fasteners - A draft proposal for design rules - J Ehlbeck, R Görlacher and H Werner
- 22-7-3 Design of Double-Shear Joints with Non-Metallic Dowels A proposal for a supplement of the design concept - J Ehlbeck and O Eberhart
- 22-7-4 The Effect of Load on Strength of Timber Joints at high Working Load Level - A J M Leijten
- 22-7-5 Plasticity Requirements for Portal Frame Corners - R Gunnewijk and A J M Leijten
- 22-7-6 Background Information on Design of Glulam Rivet Connections in CSA/CAN3-086.1-M89 - A proposal for a supplement of the design concept - E Karacabeyli and D P Janssens
- 22-7-7 Mechanical Properties of Joints in Glued-Laminated Beams under Reversed Cyclic Loading - M Yasumura
- 22-7-8 Strength of Glued Lap Timber Joints - P Glos and H Horstmann
- 22-7-9 Toothed Rings Type Bistyp 075 at the Joints of Fir Wood - J Kerste
- 22-7-10 Calculation of Joints and Fastenings as Compared with the International State - K Zimmer and K Lissner
- 22-7-11 Joints on Glued-in Steel Bars Present Relatively New and Progressive Solution in Terms of Timber Structure Design - G N Zubarev, F A Boitemirov and V M Golovina
- 22-7-12 The Development of Design Codes for Timber Structures made of Composite Bars with Plate Joints based on Cylindrical Nails - Y V Piskunov
- 22-7-13 Designing of Glued Wood Structures Joints on Glued-in Bars - S B Turkovsky
- 23-7-1 Proposal for a Design Code for Nail Plates - E Aasheim and K H Solli
- 23-7-2 Load Distribution in Nailed Joints - H J Blass
- 24-7-1 Theoretical and Experimental Tension and Shear Capacity of Nail Plate Connections - B Källsner and J Kangas
- 24-7-2 Testing Method and Determination of Basic Working Loads for Timber Joints with Mechanical Fasteners - Y Hirashima and F Kamiya
- 24-7-3 Anchorage Capacity of Nail Plate - J Kangas
- 25-7-2 Softwood and Hardwood Embedding Strength for Dowel type Fasteners - J Ehlbeck and H Werner

- 25-7-4 A Guide for Application of Quality Indexes for Driven Fasteners Used in Connections in Wood Structures - E G Stern
- 25-7-5 35 Years of Experience with Certain Types of Connectors and Connector Plates Used for the Assembly of Wood Structures and their Components- E G Stern
- 25-7-6 Characteristic Strength of Split-ring and Shear-plate Connections - H J Blass, J Ehlbeck and M Schlager
- 25-7-7 Characteristic Strength of Tooth-plate Connector Joints - H J Blass, J Ehlbeck and M Schlager
- 25-7-8 Extending Yield Theory to Screw Connections - T E McLain
- 25-7-9 Determination of  $k_{def}$  for Nailed Joints - J W G van de Kuilen
- 25-7-10 Characteristic Strength of UK Timber Connectors - A V Page and C J Mettem
- 25-7-11 Multiple-fastener Dowel-type Joints, a Selected Review of Research and Codes - C J Mettem and A V Page
- 25-7-12 Load Distributions in Multiple-fastener Bolted Joints in European Whitewood Glulam, with Steel Side Plates - C J Mettem and A V Page
- 26-7-1 Proposed Test Method for Dynamic Properties of Connections Assembled with Mechanical Fasteners - J D Dolan
- 26-7-2 Validatory Tests and Proposed Design Formulae for the Load-Carrying Capacity of Toothed-Plate Connected Joints - C J Mettem, A V Page and G Davis
- 26-7-3 Definitions of Terms and Multi-Language Terminology Pertaining to Metal Connector Plates - E G Stern
- 26-7-4 Design of Joints Based on in V-Shape Glued-in Rods - J Kangas
- 26-7-5 Tests on Timber Concrete Composite Structural Elements (TCCs) - A U Meierhofer
- 27-7-1 Glulam Arch Bridge and Design of it's Moment-Resisting Joints - K Komatsu and S Usuku
- 27-7-2 Characteristic Load - Carrying Capacity of Joints with Dowel - type Fasteners in Regard to the System Properties - H Werner
- 27-7-3 Steel Failure Design in Truss Plate Joints - T Poutanen
- 28-7-1 Expanded Tube Joint in Locally DP Reinforced Timber - A J M Leijten, P Ragupathy and K S Viridi
- 28-7-2 A Strength and Stiffness Model for the Expanded Tube Joint - A J M Leijten
- 28-7-3 Load-carrying Capacity of Steel-to Timber Joints with Annular Ring Shanked Nails. A Comparison with the EC5 Design Method - R Görlacher
- 28-7-4 Dynamic Effects on Metal-Plate Connected Wood Truss Joints - S Kent, R Gupta and T Miller
- 28-7-5 Failure of the Timber Bolted Joints Subjected to Lateral Load Perpendicular to Grain - M Yasumura and L Daudeville
- 28-7-6 Design Procedure for Locally Reinforced Joints with Dowel-type Fasteners - H Werner
- 28-7-7 Variability and Effects of Moisture Content on the Withdrawal Characteristics for Lumber as Opposed to Clear Wood - J D Dolan and J W Stelmokas
- 28-7-8 Nail Plate Capacity in Joint Line - A Kevarinmäki and J Kangas

- 28-7-9 Axial Strength of Glued-In Bolts - Calculation Model Based on Non-Linear Fracture Mechanics - A Preliminary Study - C J Johansson, E Serrano, P J Gustafsson and B Enquist
- 28-7-10 Cyclic Lateral Dowel Connection Tests for seismic and Wind Evaluation - J D Dolan
- 29-7-1 A Simple Method for Lateral Load-Carrying Capacity of Dowel-Type Fasteners - J Kangas and J Kurkela
- 29-7-2 Nail Plate Joint Behaviour at Low Versus High Load Level - T Poutanen
- 29-7-3 The Moment Resistance of Tee and Butt - Joint Nail Plate Test Specimens - A Comparison with Current Design Methods - A Reffold, L R J Whale and B S Choo
- 29-7-4 A Critical Review of the Moment Rotation Test Method Proposed in prEN 1075 - M Bettison, B S Choo and L R J Whale
- 29-7-5 Explanation of the Translation and Rotation Behaviour of Prestressed Moment Timber Joints - A J M Leijten
- 29-7-6 Design of Joints and Frame Corners using Dowel-Type Fasteners - E Gehri
- 29-7-7 Quasi-Static Reversed-Cyclic Testing of Nailed Joints - E Karacabeyli and A Ceccotti
- 29-7-8 Failure of Bolted Joints Loaded Parallel to the Grain: Experiment and Simulation - L Davenne, L Daudeville and M Yasumura
- 30-7-1 Flexural Behaviour of GLT Beams End-Jointed by Glued-in Hardwood Dowels - K Komatsu, A Koizumi, J Jensen, T Sasaki and Y Iijima
- 30-7-2 Modelling of the Block Tearing Failure in Nailed Steel-to-Timber Joints - J Kangas, K Aalto and A Kevarinmäki
- 30-7-3 Cyclic Testing of Joints with Dowels and Slotted-in Steel Plates - E Aasheim
- 30-7-4 A Steel-to-Timber Dowelled Joint of High Performance in Combination with a High Strength Wood Composite (Parallam) - E Gehri
- 30-7-5 Multiple Fastener Timber Connections with Dowel Type Fasteners - A Jorissen
- 30-7-6 Influence of Ductility on Load-Carrying Capacity of Joints with Dowel-Type Fasteners - A Mischler
- 31-7-1 Mechanical Properties of Dowel Type Joints under Reversed Cyclic Lateral Loading - M Yasumura
- 31-7-2 Design of Joints with Laterally Loaded Dowels - A Mischler
- 31-7-3 Flexural Behaviour of Glulam Beams Edge-Jointed by Lagscrews with Steel Splice Plates - K Komatsu
- 31-7-4 Design on Timber Capacity in Nailed Steel-to-Timber Joints - J Kangas and J Vesa
- 31-7-5 Timber Contact in Chord Splices of Nail Plate Structures - A Kevarinmäki
- 31-7-6 The Fastener Yield Strength in Bending - A Jorissen and H J Blaß
- 31-7-7 A Proposal for Simplification of Johansen's Formulae, Dealing With the Design of Dowelled-Type Fasteners - F Rouger
- 31-7-8 Simplified Design of Connections with Dowel-type fasteners - H J Blaß and J Ehlbeck
- 32-7-1 Behaviour of Wood-Steel-Wood Bolted Glulam Connections - M Mohammad and J H P Quenneville



- 32-7-2 A new set of experimental tests on beams loaded perpendicular-to-grain by dowel-type joints- M Ballerini
- 32-7-3 Design and Analysis of Bolted Timber Joints under Lateral Force Perpendicular to Grain - M Yasumura and L Daudeville
- 32-7-4 Predicting Capacities of Joints with Laterally Loaded Nails - I Smith and P Quenneville
- 32-7-5 Strength Reduction Rules for Multiple Fastener Joints - A Mischler and E Gehri
- 32-7-6 The Stiffness of Multiple Bolted Connections - A Jorissen
- 32-7-7 Concentric Loading Tests on Girder Truss Components - T N Reynolds, A Reffold, V Enjily and L Whale
- 32-7-8 Dowel Type Connections with Slotted-In Steel Plates - M U Pedersen, C O Clorius, L Damkilde, P Hoffmeyer and L Esklidsen
- 32-7-9 Creep of Nail Plate Reinforced Bolt Joints - J Vesa and A Kevarinmäki
- 32-7-10 The Behaviour of Timber Joints with Ring Connectors - E Gehri and A Mischler
- 32-7-11 Non-Metallic, Adhesiveless Joints for Timber Structures - R D Drake, M P Ansell, C J Mettem and R Bainbridge
- 32-7-12 Effect of Spacing and Edge Distance on the Axial Strength of Glued-in Rods - H J Blaß and B Laskewitz
- 32-7-13 Evaluation of Material Combinations for Bonded in Rods to Achieve Improved Timber Connections - C J Mettem, R J Bainbridge, K Harvey, M P Ansell, J G Broughton and A R Hutchinson

#### LOAD SHARING

- 3-8-1 Load Sharing - An Investigation on the State of Research and Development of Design Criteria - E Levin
- 4-8-1 A Review of Load-Sharing in Theory and Practice - E Levin
- 4-8-2 Load Sharing - B Norén
- 19-8-1 Predicting the Natural Frequencies of Light-Weight Wooden Floors - I Smith and Y H Chui
- 20-8-1 Proposed Code Requirements for Vibrational Serviceability of Timber Floors - Y H Chui and I Smith
- 21-8-1 An Addendum to Paper 20-8-1 - Proposed Code Requirements for Vibrational Serviceability of Timber Floors - Y H Chui and I Smith
- 21-8-2 Floor Vibrational Serviceability and the CIB Model Code - S Ohlsson
- 22-8-1 Reliability Analysis of Viscoelastic Floors - F Rouger, J D Barrett and R O Foschi
- 24-8-1 On the Possibility of Applying Neutral Vibrational Serviceability Criteria to Joisted Wood Floors - I Smith and Y H Chui
- 25-8-1 Analysis of Glulam Semi-rigid Portal Frames under Long-term Load - K Komatsu and N Kawamoto

#### DURATION OF LOAD

- 3-9-1 Definitions of Long Term Loading for the Code of Practice - B Norén
- 4-9-1 Long Term Loading of Trussed Rafters with Different Connection Systems - T Feldborg and M Johansen

- 5-9-1 Strength of a Wood Column in Combined Compression and Bending with Respect to Creep - B Källsner and B Norén
- 6-9-1 Long Term Loading for the Code of Practice (Part 2) - B Norén
- 6-9-2 Long Term Loading - K Möhler
- 6-9-3 Deflection of Trussed Rafters under Alternating Loading during a Year - T Feldborg and M Johansen
- 7-6-1 Strength and Long Term Behaviour of Lumber and Glued-Laminated Timber under Torsion Loads - K Möhler
- 7-9-1 Code Rules Concerning Strength and Loading Time - H J Larsen and E Theilgaard
- 17-9-1 On the Long-Term Carrying Capacity of Wood Structures - Y M Ivanov and Y Y Slavic
- 18-9-1 Prediction of Creep Deformations of Joints - J Kuipers
- 19-9-1 Another Look at Three Duration of Load Models - R O Foschi and Z C Yao
- 19-9-2 Duration of Load Effects for Spruce Timber with Special Reference to Moisture Influence - A Status Report - P Hoffmeyer
- 19-9-3 A Model of Deformation and Damage Processes Based on the Reaction Kinetics of Bond Exchange - T A C M van der Put
- 19-9-4 Non-Linear Creep Superposition - U Korin
- 19-9-5 Determination of Creep Data for the Component Parts of Stressed-Skin Panels - R Kliger
- 19-9-6 Creep an Lifetime of Timber Loaded in Tension and Compression - P Glos
- 19-1-1 Duration of Load Effects and Reliability Based Design (Single Member) - R O Foschi and Z C Yao
- 19-6-1 Effect of Age and/or Load on Timber Strength - J Kuipers
- 19-7-4 The Prediction of the Long-Term Load Carrying Capacity of Joints in Wood Structures - Y M Ivanov and Y Y Slavic
- 19-7-5 Slip in Joints under Long-Term Loading - T Feldborg and M Johansen
- 20-7-2 Slip in Joints under Long-Term Loading - T Feldborg and M Johansen
- 22-9-1 Long-Term Tests with Glued Laminated Timber Girders - M Badstube, W Rug and W Schöne
- 22-9-2 Strength of One-Layer solid and Lengthways Glued Elements of Wood Structures and its Alteration from Sustained Load - L M Kovaltchuk, I N Boitemirova and G B Uspenskaya
- 24-9-1 Long Term Bending Creep of Wood - T Toratti
- 24-9-2 Collection of Creep Data of Timber - A Ranta-Maunus
- 24-9-3 Deformation Modification Factors for Calculating Built-up Wood-Based Structures - I R Kliger
- 25-9-2 DVM Analysis of Wood. Lifetime, Residual Strength and Quality - L F Nielsen
- 26-9-1 Long Term Deformations in Wood Based Panels under Natural Climate Conditions. A Comparative Study - S Thelandersson, J Nordh, T Nordh and S Sandahl
- 28-9-1 Evaluation of Creep Behavior of Structural Lumber in Natural Environment - R Gupta and R Shen

- 30-9-1 DOL Effect in Tension Perpendicular to the Grain of Glulam Depending on Service Classes and Volume - S Aicher and G Dill-Langer
- 30-9-2 Damage Modelling of Glulam in Tension Perpendicular to Grain in Variable Climate - G Dill-Langer and S Aicher
- 31-9-1 Duration of Load Effect in Tension Perpendicular to Grain in Curved Glulam - A Ranta-Maunus
- 32-9-1 Bending-Stress-Redistribution Caused by Different Creep in Tension and Compression and Resulting DOL-Effect - P Becker and K Rautenstrauch
- 32-9-2 The Long Term Performance of Ply-Web Beams - R Grantham and V Enjily

#### TIMBER BEAMS

- 4-10-1 The Design of Simple Beams - H J Burgess
- 4-10-2 Calculation of Timber Beams Subjected to Bending and Normal Force - H J Larsen
- 5-10-1 The Design of Timber Beams - H J Larsen
- 9-10-1 The Distribution of Shear Stresses in Timber Beams - F J Keenan
- 9-10-2 Beams Notched at the Ends - K Möhler
- 11-10-1 Tapered Timber Beams - H Riberholt
- 13-6-2 Consideration of Size Effects in Longitudinal Shear Strength for Uncracked Beams - R O Foschi and J D Barrett
- 13-6-3 Consideration of Shear Strength on End-Cracked Beams - J D Barrett and R O Foschi
- 18-10-1 Submission to the CIB-W18 Committee on the Design of Ply Web Beams by Consideration of the Type of Stress in the Flanges - J A Baird
- 18-10-2 Longitudinal Shear Design of Glued Laminated Beams - R O Foschi
- 19-10-1 Possible Code Approaches to Lateral Buckling in Beams - H J Burgess
- 19-2-1 Creep Buckling Strength of Timber Beams and Columns - R H Leicester
- 20-2-1 Lateral Buckling Theory for Rectangular Section Deep Beam-Columns - H J Burgess
- 20-10-1 Draft Clause for CIB Code for Beams with Initial Imperfections - H J Burgess
- 20-10-2 Space Joists in Irish Timber - W J Robinson
- 20-10-3 Composite Structure of Timber Joists and Concrete Slab - T Poutanen
- 21-10-1 A Study of Strength of Notched Beams - P J Gustafsson
- 22-10-1 Design of Endnotched Beams - H J Larsen and P J Gustafsson
- 22-10-2 Dimensions of Wooden Flexural Members under Constant Loads - A Pozgai
- 22-10-3 Thin-Walled Wood-Based Flanges in Composite Beams - J König
- 22-10-4 The Calculation of Wooden Bars with flexible Joints in Accordance with the Polish Standart Code and Strict Theoretical Methods - Z Mieleczarek
- 23-10-1 Tension Perpendicular to the Grain at Notches and Joints - T A C M van der Put
- 23-10-2 Dimensioning of Beams with Cracks, Notches and Holes. An Application of Fracture Mechanics - K Riipola
- 23-10-3 Size Factors for the Bending and Tension Strength of Structural Timber - J D Barret and A R Fewell

- 23-12-1 Bending Strength of Glulam Beams, a Design Proposal - J Ehlbeck and F Colling
- 23-12-3 Glulam Beams, Bending Strength in Relation to the Bending Strength of the Finger Joints - H Riberholt
- 24-10-1 Shear Strength of Continuous Beams - R H Leicester and F G Young
- 25-10-1 The Strength of Norwegian Glued Laminated Beams - K Solli, E Aasheim and R H Falk
- 25-10-2 The Influence of the Elastic Modulus on the Simulated Bending Strength of Hyperstatic Timber Beams - T D G Canisius
- 27-10-1 Determination of Shear Modulus - R Görlacher and J Kürth
- 29-10-1 Time Dependent Lateral Buckling of Timber Beams - F Rouger
- 29-10-2 Determination of Modulus of Elasticity in Bending According to EN 408 - K H Solli
- 29-10-3 On Determination of Modulus of Elasticity in Bending - L Boström, S Ormarsson and O Dahlblom
- 29-10-4 Relation of Moduli of Elasticity in Flatwise and Edgewise Bending of Solid Timber - C J Johansson, A Steffen and E W Wormuth
- 30-10-1 Nondestructive Evaluation of Wood-based Members and Structures with the Help of Modal Analysis - P Kuklik
- 30-10-2 Measurement of Modulus of Elasticity in Bending - L Boström
- 30-10-3 A Weak Zone Model for Timber in Bending - B Källsner, K Salmela and O Ditlevsen
- 30-10-4 Load Carrying Capacity of Timber Beams with Narrow Moment Peaks - T Isaksson and J Freysoldt

#### ENVIRONMENTAL CONDITIONS

- 5-11-1 Climate Grading for the Code of Practice - B Norén
- 6-11-1 Climate Grading (2) - B Norén
- 9-11-1 Climate Classes for Timber Design - F J Keenan
- 19-11-1 Experimental Analysis on Ancient Downgraded Timber Structures - B Leggeri and L Paolini
- 19-6-5 Drying Stresses in Round Timber - A Ranta-Maunus
- 22-11-1 Corrosion and Adaptation Factors for Chemically Aggressive Media with Timber Structures - K Erler
- 29-11-1 Load Duration Effect on Structural Beams under Varying Climate Influence of Size and Shape - P Galimard and P Morlier
- 30-11-1 Probabilistic Design Models for the Durability of Timber Constructions - R H Leicester

#### LAMINATED MEMBERS

- 6-12-1 Directives for the Fabrication of Load-Bearing Structures of Glued Timber - A van der Velden and J Kuipers
- 8-12-1 Testing of Big Glulam Timber Beams - H Kolb and P Frech
- 8-12-2 Instruction for the Reinforcement of Apertures in Glulam Beams - H Kolb and P Frech

- 8-12-3 Glulam Standard Part 1: Glued Timber Structures; Requirements for Timber (Second Draft)
- 9-12-1 Experiments to Provide for Elevated Forces at the Supports of Wooden Beams with Particular Regard to Shearing Stresses and Long-Term Loadings - F Wassipaul and R Lackner
- 9-12-2 Two Laminated Timber Arch Railway Bridges Built in Perth in 1849 - L G Booth
- 9-6-4 Consideration of Combined Stresses for Lumber and Glued Laminated Timber - K Möhler
- 11-6-3 Consideration of Combined Stresses for Lumber and Glued Laminated Timber (addition to Paper CIB-W18/9-6-4) - K Möhler
- 12-12-1 Glulam Standard Part 2: Glued Timber Structures; Rating (3rd draft)
- 12-12-2 Glulam Standard Part 3: Glued Timber Structures; Performance (3 rd draft)
- 13-12-1 Glulam Standard Part 3: Glued Timber Structures; Performance (4th draft)
- 14-12-1 Proposals for CEI-Bois/CIB-W18 Glulam Standards - H J Larsen
- 14-12-2 Guidelines for the Manufacturing of Glued Load-Bearing Timber Structures - Stevin Laboratory
- 14-12-3 Double Tapered Curved Glulam Beams - H Riberholt
- 14-12-4 Comment on CIB-W18/14-12-3 - E Gehri
- 18-12-1 Report on European Glulam Control and Production Standard - H Riberholt
- 18-10-2 Longitudinal Shear Design of Glued Laminated Beams - R O Foschi
- 19-12-1 Strength of Glued Laminated Timber - J Ehlbeck and F Colling
- 19-12-2 Strength Model for Glulam Columns - H J Blaß
- 19-12-3 Influence of Volume and Stress Distribution on the Shear Strength and Tensile Strength Perpendicular to Grain - F Colling
- 19-12-4 Time-Dependent Behaviour of Glued-Laminated Beams - F Zaupa
- 21-12-1 Modulus of Rupture of Glulam Beam Composed of Arbitrary Laminae - K Komatsu and N Kawamoto
- 21-12-2 An Appraisal of the Young's Modulus Values Specified for Glulam in Eurocode 5- L R J Whale, B O Hilson and P D Rodd
- 21-12-3 The Strength of Glued Laminated Timber (Glulam): Influence of Lamination Qualities and Strength of Finger Joints - J Ehlbeck and F Colling
- 21-12-4 Comparison of a Shear Strength Design Method in Eurocode 5 and a More Traditional One - H Riberholt
- 22-12-1 The Dependence of the Bending Strength on the Glued Laminated Timber Girder Depth - M Badstube, W Rug and W Schöne
- 22-12-2 Acid Deterioration of Glulam Beams in Buildings from the Early Half of the 1960s - Preliminary summary of the research project; Overhead pictures - B A Hedlund
- 22-12-3 Experimental Investigation of normal Stress Distribution in Glue Laminated Wooden Arches - Z Mielczarek and W Chanaj
- 22-12-4 Ultimate Strength of Wooden Beams with Tension Reinforcement as a Function of Random Material Properties - R Candowicz and T Dziuba
- 23-12-1 Bending Strength of Glulam Beams, a Design Proposal - J Ehlbeck and F Colling
- 23-12-2 Probability Based Design Method for Glued Laminated Timber - M F Stone

- 23-12-3 Glulam Beams, Bending Strength in Relation to the Bending Strength of the Finger Joints - H Riberholt
- 23-12-4 Glued Laminated Timber - Strength Classes and Determination of Characteristic Properties - H Riberholt, J Ehlbeck and A Fewell
- 24-12-1 Contribution to the Determination of the Bending Strength of Glulam Beams - F Colling, J Ehlbeck and R Görlacher
- 24-12-2 Influence of Perpendicular-to-Grain Stressed Volume on the Load-Carrying Capacity of Curved and Tapered Glulam Beams - J Ehlbeck and J Kürth
- 25-12-1 Determination of Characteristic Bending Values of Glued Laminated Timber. EN-Approach and Reality - E Gehri
- 26-12-1 Norwegian Bending Tests with Glued Laminated Beams-Comparative Calculations with the "Karlsruhe Calculation Model" - E Aasheim, K Solli, F Colling, R H Falk, J Ehlbeck and R Görlacher
- 26-12-2 Simulation Analysis of Norwegian Spruce Glued-Laminated Timber - R Hernandez and R H Falk
- 26-12-3 Investigation of Laminating Effects in Glued-Laminated Timber - F Colling and R H Falk
- 26-12-4 Comparing Design Results for Glulam Beams According to Eurocode 5 and to the French Working Stress Design Code (CB71) - F Rouger
- 27-12-1 State of the Art Report: Glulam Timber Bridge Design in the U.S. - M A Ritter and T G Williamson
- 27-12-2 Common Design Practice for Timber Bridges in the United Kingdom - C J Mettem, J P Marcroft and G Davis
- 27-12-3 Influence of Weak Zones on Stress Distribution in Glulam Beams - E Serrano and H J Larsen
- 28-12-1 Determination of Characteristic Bending Strength of Glued Laminated Timber - E Gehri
- 28-12-2 Size Factor of Norwegian Glued Laminated Beams - E Aasheim and K H Solli
- 28-12-3 Design of Glulam Beams with Holes - K Riipola
- 28-12-4 Compression Resistance of Glued Laminated Timber Short Columns- U Korin
- 29-12-1 Development of Efficient Glued Laminated Timber - G Schickhofer
- 30-12-1 Experimental Investigation and Analysis of Reinforced Glulam Beams - K Oiger
- 31-12-1 Depth Factor for Glued Laminated Timber-Discussion of the Eurocode 5 Approach - B Källsner, O Carling and C J Johansson
- 32-12-1 The bending stiffness of nail-laminated timber elements in transverse direction- T Wolf and O Schäfer

#### PARTICLE AND FIBRE BUILDING BOARDS

- 7-13-1 Fibre Building Boards for CIB Timber Code (First Draft)- O Brynildsen
- 9-13-1 Determination of the Bearing Strength and the Load-Deformation Characteristics of Particleboard - K Möhler, T Budianto and J Ehlbeck
- 9-13-2 The Structural Use of Tempered Hardboard - W W L Chan
- 11-13-1 Tests on Laminated Beams from Hardboard under Short- and Longterm Load - W Nozynski

- 11-13-2 Determination of Deformation of Special Densified Hardboard under Long-term Load and Varying Temperature and Humidity Conditions - W Halfar
- 11-13-3 Determination of Deformation of Hardboard under Long-term Load in Changing Climate - W Halfar
- 14-4-1 An Introduction to Performance Standards for Wood-Base Panel Products - D H Brown
- 14-4-2 Proposal for Presenting Data on the Properties of Structural Panels - T Schmidt
- 16-13-1 Effect of Test Piece Size on Panel Bending Properties - P W Post
- 20-4-1 Considerations of Reliability - Based Design for Structural Composite Products - M R O'Halloran, J A Johnson, E G Elias and T P Cunningham
- 20-13-1 Classification Systems for Structural Wood-Based Sheet Materials - V C Kearley and A R Abbott
- 21-13-1 Design Values for Nailed Chipboard - Timber Joints - A R Abbott
- 25-13-1 Bending Strength and Stiffness of Izopanel Plates - Z Mielczarek
- 28-13-1 Background Information for "Design Rated Oriented Strand Board (OSB)" in CSA Standards - Summary of Short-term Test Results - E Karacabeyli, P Lau, C R Henderson, F V Meakes and W Deacon
- 28-13-2 Torsional Stiffness of Wood-Hardboard Composed I-Beam - P Olejniczak

#### TRUSSED RAFTERS

- 4-9-1 Long-term Loading of Trussed Rafters with Different Connection Systems - T Feldborg and M Johansen
- 6-9-3 Deflection of Trussed Rafters under Alternating Loading During a Year - T Feldborg and M Johansen
- 7-2-1 Lateral Bracing of Timber Struts - J A Simon
- 9-14-1 Timber Trusses - Code Related Problems - T F Williams
- 9-7-1 Design of Truss Plate Joints - F J Keenan
- 10-14-1 Design of Roof Bracing - The State of the Art in South Africa - P A V Bryant and J A Simon
- 11-14-1 Design of Metal Plate Connected Wood Trusses - A R Egerup
- 12-14-1 A Simple Design Method for Standard Trusses - A R Egerup
- 13-14-1 Truss Design Method for CIB Timber Code - A R Egerup
- 13-14-2 Trussed Rafters, Static Models - H Riberholt
- 13-14-3 Comparison of 3 Truss Models Designed by Different Assumptions for Slip and E-Modulus - K Möhler
- 14-14-1 Wood Trussed Rafter Design - T Feldborg and M Johansen
- 14-14-2 Truss-Plate Modelling in the Analysis of Trusses - R O Foschi
- 14-14-3 Cantilevered Timber Trusses - A R Egerup
- 14-7-5 The Effect of Support Eccentricity on the Design of W- and WW-Trusses with Nail Plate Connectors - B Källsner
- 15-14-1 Guidelines for Static Models of Trussed Rafters - H Riberholt
- 15-14-2 The Influence of Various Factors on the Accuracy of the Structural Analysis of Timber Roof Trusses - F R P Pienaar

- 15-14-3 Bracing Calculations for Trussed Rafter Roofs - H J Burgess
- 15-14-4 The Design of Continuous Members in Timber Trussed Rafters with Punched Metal Connector Plates - P O Reece
- 15-14-5 A Rafter Design Method Matching U.K. Test Results for Trussed Rafters - H J Burgess
- 16-14-1 Full-Scale Tests on Timber Fink Trusses Made from Irish Grown Sitka Spruce - V Picardo
- 17-14-1 Data from Full Scale Tests on Prefabricated Trussed Rafters - V Picardo
- 17-14-2 Simplified Static Analysis and Dimensioning of Trussed Rafters - H Riberholt
- 17-14-3 Simplified Calculation Method for W-Trusses - B Källsner
- 18-14-1 Simplified Calculation Method for W-Trusses (Part 2) - B Källsner
- 18-14-2 Model for Trussed Rafter Design - T Poutanen
- 19-14-1 Annex on Simplified Design of W-Trusses - H J Larsen
- 19-14-2 Simplified Static Analysis and Dimensioning of Trussed Rafters - Part 2 - H Riberholt
- 19-14-3 Joint Eccentricity in Trussed Rafters - T Poutanen
- 20-14-1 Some Notes about Testing Nail Plates Subjected to Moment Load - T Poutanen
- 20-14-2 Moment Distribution in Trussed Rafters - T Poutanen
- 20-14-3 Practical Design Methods for Trussed Rafters - A R Egerup
- 22-14-1 Guidelines for Design of Timber Trussed Rafters - H Riberholt
- 23-14-1 Analyses of Timber Trussed Rafters of the W-Type - H Riberholt
- 23-14-2 Proposal for Eurocode 5 Text on Timber Trussed Rafters - H Riberholt
- 24-14-1 Capacity of Support Areas Reinforced with Nail Plates in Trussed Rafters - A Kevarinmäki
- 25-14-1 Moment Anchorage Capacity of Nail Plates in Shear Tests - A Kevarinmaki and J. Kangas
- 25-14-2 Design Values of Anchorage Strength of Nail Plate Joints by 2-curve Method and Interpolation - J Kangas and A Kevarinmaki
- 26-14-1 Test of Nail Plates Subjected to Moment - E Aasheim
- 26-14-2 Moment Anchorage Capacity of Nail Plates - A Kevarinmäki and J Kangas
- 26-14-3 Rotational Stiffness of Nail Plates in Moment Anchorage - A Kevarinmäki and J Kangas
- 26-14-4 Solution of Plastic Moment Anchorage Stress in Nail Plates - A Kevarinmäki
- 26-14-5 Testing of Metal-Plate-Connected Wood-Truss Joints - R Gupta
- 26-14-6 Simulated Accidental Events on a Trussed Rafter Roofed Building - C J Mettem and J P Marcroft
- 30-14-1 The Stability Behaviour of Timber Trussed Rafter Roofs - Studies Based on Eurocode 5 and Full Scale Testing - R J Bainbridge, C J Mettern, A Reffold and T Studer
- 32-14-1 Analysis of Timber Reinforced with Punched Metal Plate Fasteners- J Nielsen



## STRUCTURAL STABILITY

- 8-15-1 Laterally Loaded Timber Columns: Tests and Theory - H J Larsen
- 13-15-1 Timber and Wood-Based Products Structures. Panels for Roof Coverings. Methods of Testing and Strength Assessment Criteria. Polish Standard BN-78/7159-03
- 16-15-1 Determination of Bracing Structures for Compression Members and Beams - H Brüninghoff
- 17-15-1 Proposal for Chapter 7.4 Bracing - H Brüninghoff
- 17-15-2 Seismic Design of Small Wood Framed Houses - K F Hansen
- 18-15-1 Full-Scale Structures in Glued Laminated Timber, Dynamic Tests: Theoretical and Experimental Studies - A Ceccotti and A Vignoli
- 18-15-2 Stabilizing Bracings - H Brüninghoff
- 19-15-1 Connections Deformability in Timber Structures: a Theoretical Evaluation of its Influence on Seismic Effects - A Ceccotti and A Vignoli
- 19-15-2 The Bracing of Trussed Beams - M H Kessel and J Natterer
- 19-15-3 Racking Resistance of Wooden Frame Walls with Various Openings - M Yasumura
- 19-15-4 Some Experiences of Restoration of Timber Structures for Country Buildings - G Cardinale and P Spinelli
- 19-15-5 Non-Destructive Vibration Tests on Existing Wooden Dwellings - Y Hirashima
- 20-15-1 Behaviour Factor of Timber Structures in Seismic Zones. - A Ceccotti and A Vignoli
- 21-15-1 Rectangular Section Deep Beam - Columns with Continuous Lateral Restraint - H J Burgess
- 21-15-2 Buckling Modes and Permissible Axial Loads for Continuously Braced Columns- H J Burgess
- 21-15-3 Simple Approaches for Column Bracing Calculations - H J Burgess
- 21-15-4 Calculations for Discrete Column Restraints - H J Burgess
- 21-15-5 Behaviour Factor of Timber Structures in Seismic Zones (Part Two) - A Ceccotti and A Vignoli
- 22-15-1 Suggested Changes in Code Bracing Recommendations for Beams and Columns - H J Burgess
- 22-15-2 Research and Development of Timber Frame Structures for Agriculture in Poland- S Kus and J Kerste
- 22-15-3 Ensuring of Three-Dimensional Stiffness of Buildings with Wood Structures - A K Shenghelia
- 22-15-5 Seismic Behavior of Arched Frames in Timber Construction - M Yasumura
- 22-15-6 The Robustness of Timber Structures - C J Mettem and J P Marcroft
- 22-15-7 Influence of Geometrical and Structural Imperfections on the Limit Load of Wood Columns - P Dutko
- 23-15-1 Calculation of a Wind Girder Loaded also by Discretely Spaced Braces for Roof Members - H J Burgess
- 23-15-2 Stability Design and Code Rules for Straight Timber Beams - T A C M van der Put

- 23-15-3 A Brief Description of Formula of Beam-Columns in China Code - S Y Huang
- 23-15-4 Seismic Behavior of Braced Frames in Timber Construction - M Yasumura
- 23-15-5 On a Better Evaluation of the Seismic Behavior Factor of Low-Dissipative Timber Structures - A Ceccotti and A Vignoli
- 23-15-6 Disproportionate Collapse of Timber Structures - C J Mettem and J P Marcroft
- 23-15-7 Performance of Timber Frame Structures During the Loma Prieta California Earthquake - M R O'Halloran and E G Elias
- 24-15-2 Discussion About the Description of Timber Beam-Column Formula - S Y Huang
- 24-15-3 Seismic Behavior of Wood-Framed Shear Walls - M Yasumura
- 25-15-1 Structural Assessment of Timber Framed Building Systems - U Korin
- 25-15-3 Mechanical Properties of Wood-framed Shear Walls Subjected to Reversed Cyclic Lateral Loading - M Yasumura
- 26-15-1 Bracing Requirements to Prevent Lateral Buckling in Trussed Rafters - C J Mettem and P J Moss
- 26-15-2 Eurocode 8 - Part 1.3 - Chapter 5 - Specific Rules for Timber Buildings in Seismic Regions - K Becker, A Ceccotti, H Charlier, E Katsaragakis, H J Larsen and H Zeitter
- 26-15-3 Hurricane Andrew - Structural Performance of Buildings in South Florida - M R O'Halloran, E L Keith, J D Rose and T P Cunningham
- 29-15-1 Lateral Resistance of Wood Based Shear Walls with Oversized Sheathing Panels - F Lam, H G L Prion and M He
- 29-15-2 Damage of Wooden Buildings Caused by the 1995 Hyogo-Ken Nanbu Earthquake - M Yasumura, N Kawai, N Yamaguchi and S Nakajima
- 29-15-3 The Racking Resistance of Timber Frame Walls: Design by Test and Calculation - D R Griffiths, C J Mettem, V Enjily, P J Steer
- 29-15-4 Current Developments in Medium-Rise Timber Frame Buildings in the UK - C J Mettem, G C Pitts, P J Steer, V Enjily
- 29-15-5 Natural Frequency Prediction for Timber Floors - R J Bainbridge, and C J Mettem
- 30-15-1 Cyclic Performance of Perforated Wood Shear Walls with Oversize Oriented Strand Board Panels - Ming He, H Magnusson, F Lam, and H G L Prion
- 30-15-2 A Numerical Analysis of Shear Walls Structural Performances - L Davenne, L Daudeville, N Kawai and M Yasumura
- 30-15-3 Seismic Force Modification Factors for the Design of Multi-Storey Wood-Frame Platform Construction - E Karacabeyli and A Ceccotti
- 30-15-4 Evaluation of Wood Framed Shear Walls Subjected to Lateral Load - M Yasumura and N Kawai
- 31-15-1 Seismic Performance Testing On Wood-Framed Shear Wall - N Kawai
- 31-15-2 Robustness Principles in the Design of Medium-Rise Timber-Framed Buildings - C J Mettem, M W Milner, R J Bainbridge and V. Enjily
- 31-15-3 Numerical Simulation of Pseudo-Dynamic Tests Performed to Shear Walls - L Daudeville, L Davenne, N Richard, N Kawai and M Yasumura
- 31-15-4 Force Modification Factors for Braced Timber Frames - H G L Prion, M Popovski and E Karacabeyli
- 32-15-1 Three-Dimensional Interaction in Stabilisation of Multi-Storey Timber Frame Buildings - S Andreasson

- 32-15-2 Application of Capacity Spectrum Method to Timber Houses - N Kawai  
 32-15-3 Design Methods for Shear Walls with Openings - C Ni, E Karacabeyli and A Ceccotti  
 32-15-4 Static Cyclic Lateral Loading Tests on Nailed Plywood Shear Walls - K Komatsu, K H Hwang and Y Itou

## FIRE

- 12-16-1 British Standard BS 5268 the Structural Use of Timber: Part 4 Fire Resistance of Timber Structures  
 13-100-2 CIB Structural Timber Design Code. Chapter 9. Performance in Fire  
 19-16-1 Simulation of Fire in Tests of Axially Loaded Wood Wall Studs - J König  
 24-16-1 Modelling the Effective Cross Section of Timber Frame Members Exposed to Fire - J König  
 25-16-1 The Effect of Density on Charring and Loss of Bending Strength in Fire - J König  
 25-16-2 Tests on Glued-Laminated Beams in Bending Exposed to Natural Fires - F Bolonius Olesen and J König  
 26-16-1 Structural Fire Design According to Eurocode 5, Part 1.2 - J König  
 31-16-1 Revision of ENV 1995-1-2: Charring and Degradation of Strength and Stiffness - J König

## STATISTICS AND DATA ANALYSIS

- 13-17-1 On Testing Whether a Prescribed Exclusion Limit is Attained - W G Warren  
 16-17-1 Notes on Sampling and Strength Prediction of Stress Graded Structural Timber - P Glos  
 16-17-2 Sampling to Predict by Testing the Capacity of Joints, Components and Structures - B Norén  
 16-17-3 Discussion of Sampling and Analysis Procedures - P W Post  
 17-17-1 Sampling of Wood for Joint Tests on the Basis of Density - I Smith, L R J Whale  
 17-17-2 Sampling Strategy for Physical and Mechanical Properties of Irish Grown Sitka Spruce - V Picardo  
 18-17-1 Sampling of Timber in Structural Sizes - P Glos  
 18-6-3 Notes on Sampling Factors for Characteristic Values - R H Leicester  
 19-17-1 Load Factors for Proof and Prototype Testing - R H Leicester  
 19-6-2 Confidence in Estimates of Characteristic Values - R H Leicester  
 21-6-1 Draft Australian Standard: Methods for Evaluation of Strength and Stiffness of Graded Timber - R H Leicester  
 21-6-2 The Determination of Characteristic Strength Values for Stress Grades of Structural Timber. Part 1 - A R Fewell and P Glos  
 22-17-1 Comment on the Strength Classes in Eurocode 5 by an Analysis of a Stochastic Model of Grading - A proposal for a supplement of the design concept - M Kiesel  
 24-17-1 Use of Small Samples for In-Service Strength Measurement - R H Leicester and F G Young  
 24-17-2 Equivalence of Characteristic Values - R H Leicester and F G Young

- 24-17-3 Effect of Sampling Size on Accuracy of Characteristic Values of Machine Grades - Y H Chui, R Turner and I Smith
- 24-17-4 Harmonisation of LSD Codes - R H Leicester
- 25-17-2 A Body for Confirming the Declaration of Characteristic Values - J Sunley
- 25-17-3 Moisture Content Adjustment Procedures for Engineering Standards - D W Green and J W Evans
- 27-17-1 Statistical Control of Timber Strength - R H Leicester and H O Breitingger
- 30-17-1 A New Statistical Method for the Establishment of Machine Settings - F Rouger

#### GLUED JOINTS

- 20-18-1 Wood Materials under Combined Mechanical and Hygral Loading - A Martensson and S Thelandersson
- 20-18-2 Analysis of Generalized Volkersen - Joints in Terms of Linear Fracture Mechanics - P J Gustafsson
- 20-18-3 The Complete Stress-Slip Curve of Wood-Adhesives in Pure Shear - H Wernersson and P J Gustafsson
- 22-18-1 Perspective Adhesives and Protective Coatings for Wood Structures - A S Freidin

#### FRACTURE MECHANICS

- 21-10-1 A Study of Strength of Notched Beams - P J Gustafsson
- 22-10-1 Design of Endnotched Beams - H J Larsen and P J Gustafsson
- 23-10-1 Tension Perpendicular to the Grain at Notches and Joints - T A C M van der Put
- 23-10-2 Dimensioning of Beams with Cracks, Notches and Holes. An Application of Fracture Mechanics - K Riipola
- 23-19-1 Determination of the Fracture Energie of Wood for Tension Perpendicular to the Grain - W Rug, M Badstube and W Schöne
- 23-19-2 The Fracture Energy of Wood in Tension Perpendicular to the Grain. Results from a Joint Testing Project - H J Larsen and P J Gustafsson
- 23-19-3 Application of Fracture Mechanics to Timber Structures - A Ranta-Maunus
- 24-19-1 The Fracture Energy of Wood in Tension Perpendicular to the Grain - H J Larsen and P J Gustafsson
- 28-19-1 Fracture of Wood in Tension Perpendicular to the Grain: Experiment and Numerical Simulation by Damage Mechanics - L Daudeville, M Yasumura and J D Lanvin
- 28-19-2 A New Method of Determining Fracture Energy in Forward Shear along the Grain - H D Mansfield-Williams
- 28-19-3 Fracture Design Analysis of Wooden Beams with Holes and Notches. Finite Element Analysis based on Energy Release Rate Approach - H Petersson
- 28-19-4 Design of Timber Beams with Holes by Means of Fracture Mechanics - S Aicher, J Schmidt and S Brunold
- 30-19-1 Failure Analysis of Single-Bolt Joints - L Daudeville, L Davenne and M Yasumura

## SERVICEABILITY

- 27-20-1 Codification of Serviceability Criteria - R H Leicester
- 27-20-2 On the Experimental Determination of Factor  $k_{def}$  and Slip Modulus  $k_{ser}$  from Short- and Long-Term Tests on a Timber-Concrete Composite (TCC) Beam - S Capretti and A Ceccotti
- 27-20-3 Serviceability Limit States: A Proposal for Updating Eurocode 5 with Respect to Eurocode 1 - P Racher and F Rouger
- 27-20-4 Creep Behavior of Timber under External Conditions - C Le Govic, F Rouger, T Toratti and P Morlier
- 30-20-1 Design Principles for Timber in Compression Perpendicular to Grain - S Thelandersson and A Mårtensson
- 30-20-2 Serviceability Performance of Timber Floors - Eurocode 5 and Full Scale Testing - R J Bainbridge and C J Mettem
- 32-20-1 Floor Vibrations - B Mohr

## TEST METHODS

- 31-21-1 Development of an Optimised Test Configuration to Determine Shear Strength of Glued Laminated Timber - G Schickhofer and B Obermayr
- 31-21-2 An Impact Strength Test Method for Structural Timber. The Theory and a Preliminary Study - T D G Canisius

## CIB TIMBER CODE

- 2-100-1 A Framework for the Production of an International Code of Practice for the Structural Use of Timber - W T Curry
- 5-100-1 Design of Solid Timber Columns (First Draft) - H J Larsen
- 5-100-2 A Draft Outline of a Code for Timber Structures - L G Booth
- 6-100-1 Comments on Document 5-100-1; Design of Solid Timber Columns - H J Larsen and E Theilgaard
- 6-100-2 CIB Timber Code: CIB Timber Standards - H J Larsen and E Theilgaard
- 7-100-1 CIB Timber Code Chapter 5.3 Mechanical Fasteners; CIB Timber Standard 06 and 07 - H J Larsen
- 8-100-1 CIB Timber Code - List of Contents (Second Draft) - H J Larsen
- 9-100-1 The CIB Timber Code (Second Draft)
- 11-100-1 CIB Structural Timber Design Code (Third Draft)
- 11-100-2 Comments Received on the CIB Code
- a U Saarelainen
  - b Y M Ivanov
  - c R H Leicester
  - d W Nozynski
  - e W R A Meyer
  - f P Beckmann; R Marsh
  - g W R A Meyer
  - h W R A Meyer
- 11-100-3 CIB Structural Timber Design Code; Chapter 3 - H J Larsen
- 12-100-1 Comment on the CIB Code - Sous-Commission Glulam

- 12-100-2 Comment on the CIB Code - R H Leicester
- 12-100-3 CIB Structural Timber Design Code (Fourth Draft)
- 13-100-1 Agreed Changes to CIB Structural Timber Design Code
- 13-100-2 CIB Structural Timber Design Code. Chapter 9: Performance in Fire
- 13-100-3a Comments on CIB Structural Timber Design Code
- 13-100-3b Comments on CIB Structural Timber Design Code - W R A Meyer
- 13-100-3c Comments on CIB Structural Timber Design Code - British Standards Institution
- 13-100-4 CIB Structural Timber Design Code. Proposal for Section 6.1.5 Nail Plates - N I Bovim
- 14-103-2 Comments on the CIB Structural Timber Design Code - R H Leicester
- 15-103-1 Resolutions of TC 165-meeting in Athens 1981-10-12/13
- 21-100-1 CIB Structural Timber Design Code. Proposed Changes of Sections on Lateral Instability, Columns and Nails - H J Larsen
- 22-100-1 Proposal for Including an Updated Design Method for Bearing Stresses in CIB W18 - Structural Timber Design Code - B Madsen
- 22-100-2 Proposal for Including Size Effects in CIB W18A Timber Design Code - B Madsen
- 22-100-3 CIB Structural Timber Design Code - Proposed Changes of Section on Thin-Flanged Beams - J König
- 22-100-4 Modification Factor for "Aggressive Media" - a Proposal for a Supplement to the CIB Model Code - K Erler and W Rug
- 22-100-5 Timber Design Code in Czechoslovakia and Comparison with CIB Model Code - P Dutko and B Kozelouh

#### LOADING CODES

- 4-101-1 Loading Regulations - Nordic Committee for Building Regulations
- 4-101-2 Comments on the Loading Regulations - Nordic Committee for Building Regulations

#### STRUCTURAL DESIGN CODES

- 1-102-1 Survey of Status of Building Codes, Specifications etc., in USA - E G Stern
- 1-102-2 Australian Codes for Use of Timber in Structures - R H Leicester
- 1-102-3 Contemporary Concepts for Structural Timber Codes - R H Leicester
- 1-102-4 Revision of CP 112 - First Draft, July 1972 - British Standards Institution
- 4-102-1 Comparison of Codes and Safety Requirements for Timber Structures in EEC Countries - Timber Research and Development Association
- 4-102-2 Nordic Proposals for Safety Code for Structures and Loading Code for Design of Structures - O A Brynildsen
- 4-102-3 Proposal for Safety Codes for Load-Carrying Structures - Nordic Committee for Building Regulations
- 4-102-4 Comments to Proposal for Safety Codes for Load-Carrying Structures - Nordic Committee for Building Regulations
- 4-102-5 Extract from Norwegian Standard NS 3470 "Timber Structures"

- 4-102-6 Draft for Revision of CP 112 "The Structural Use of Timber" - W T Curry
- 8-102-1 Polish Standard PN-73/B-03150: Timber Structures; Statistical Calculations and Designing
- 8-102-2 The Russian Timber Code: Summary of Contents
- 9-102-1 Svensk Byggnorm 1975 (2nd Edition); Chapter 27: Timber Construction
- 11-102-1 Eurocodes - H J Larsen
- 13-102-1 Program of Standardisation Work Involving Timber Structures and Wood-Based Products in Poland
- 17-102-1 Safety Principles - H J Larsen and H Riberholt
- 17-102-2 Partial Coefficients Limit States Design Codes for Structural Timberwork - I Smith
- 18-102-1 Antiseismic Rules for Timber Structures: an Italian Proposal - G Augusti and A Ceccotti
- 18-1-2 Eurocode 5, Timber Structures - H J Larsen
- 19-102-1 Eurocode 5 - Requirements to Timber - Drafting Panel Eurocode 5
- 19-102-2 Eurocode 5 and CIB Structural Timber Design Code - H J Larsen
- 19-102-3 Comments on the Format of Eurocode 5 - A R Fewell
- 19-102-4 New Developments of Limit States Design for the New GDR Timber Design Code - W Rug and M Badstube
- 19-7-3 Effectiveness of Multiple Fastener Joints According to National Codes and Eurocode 5 (Draft) - G Steck
- 19-7-6 The Derivation of Design Clauses for Nailed and Bolted Joints in Eurocode5 - L R J Whale and I Smith
- 19-14-1 Annex on Simplified Design of W-Trusses - H J Larsen
- 20-102-1 Development of a GDR Limit States Design Code for Timber Structures - W Rug and M Badstube
- 21-102-1 Research Activities Towards a New GDR Timber Design Code Based on Limit States Design - W Rug and M Badstube
- 22-102-1 New GDR Timber Design Code, State and Development - W Rug, M Badstube and W Kofent
- 22-102-2 Timber Strength Parameters for the New USSR Design Code and its Comparison with International Code - Y Y Slavik, N D Denesh and E B Ryumina
- 22-102-3 Norwegian Timber Design Code - Extract from a New Version - E Aasheim and K H Solli
- 23-7-1 Proposal for a Design Code for Nail Plates - E Aasheim and K H Solli
- 24-102-2 Timber Footbridges: A Comparison Between Static and Dynamic Design Criteria - A Ceccotti and N de Robertis
- 25-102-1 Latest Development of Eurocode 5 - H J Larsen
- 25-102-1A Annex to Paper CIB-W18/25-102-1. Eurocode 5 - Design of Notched Beams - H J Larsen, H Riberholt and P J Gustafsson
- 25-102-2 Control of Deflections in Timber Structures with Reference to Eurocode 5 - A Martensson and S Thelandersson
- 28-102-1 Eurocode 5 - Design of Timber Structures - Part 2: Bridges - D Bajolet, E Gehri, J König, H Kreuzinger, H J Larsen, R Mäkipuro and C Mettem

- 28-102-2 Racking Strength of Wall Diaphragms - Discussion of the Eurocode 5 Approach - B Källsner
- 29-102-1 Model Code for the Probabilistic Design of Timber Structures - H J Larsen, T Isaksson and S Thelandersson
- 30-102-1 Concepts for Drafting International Codes and Standards for Timber Constructions - R H Leicester

#### INTERNATIONAL STANDARDS ORGANISATION

- 3-103-1 Method for the Preparation of Standards Concerning the Safety of Structures (ISO/DIS 3250) - International Standards Organisation ISO/TC98
- 4-103-1 A Proposal for Undertaking the Preparation of an International Standard on Timber Structures - International Standards Organisation
- 5-103-1 Comments on the Report of the Consultation with Member Bodies Concerning ISO/TC/P129 - Timber Structures - Dansk Ingeniorforening
- 7-103-1 ISO Technical Committees and Membership of ISO/TC 165
- 8-103-1 Draft Resolutions of ISO/TC 165
- 12-103-1 ISO/TC 165 Ottawa, September 1979
- 13-103-1 Report from ISO/TC 165 - A Sorensen
- 14-103-1 Comments on ISO/TC 165 N52 "Timber Structures; Solid Timber in Structural Sizes; Determination of Some Physical and Mechanical Properties"
- 14-103-2 Comments on the CIB Structural Timber Design Code - R H Leicester
- 21-103-1 Concept of a Complete Set of Standards - R H Leicester

#### JOINT COMMITTEE ON STRUCTURAL SAFETY

- 3-104-1 International System on Unified Standard Codes of Practice for Structures - Comité Européen du Béton (CEB)
- 7-104-1 Volume 1: Common Unified Rules for Different Types of Construction and Material - CEB

#### CIB PROGRAMME, POLICY AND MEETINGS

- 1-105-1 A Note on International Organisations Active in the Field of Utilisation of Timber - P Sonnemans
- 5-105-1 The Work and Objectives of CIB-W18-Timber Structures - J G Sunley
- 10-105-1 The Work of CIB-W18 Timber Structures - J G Sunley
- 15-105-1 Terms of Reference for Timber - Framed Housing Sub-Group of CIB-W18
- 19-105-1 Tropical and Hardwood Timbers Structures - R H Leicester
- 21-105-1 First Conference of CIB-W18B, Tropical and Hardwood Timber Structures Singapore, 26 - 28 October 1987 - R H Leicester

#### INTERNATIONAL UNION OF FORESTRY RESEARCH ORGANISATIONS

- 7-106-1 Time and Moisture Effects - CIB W18/IUFRO 55.02-03 Working Party



**INTERNATIONAL COUNCIL FOR RESEARCH AND INNOVATION  
IN BUILDING AND CONSTRUCTION**

**WORKING COMMISSION W18 - TIMBER STRUCTURES**

**DETERMINATION OF PARTIAL COEFFICIENTS AND MODIFICATION FACTORS**

H J Larsen

Danish Building Research Institute / Structural Mechanics, Lund Institute of Technology,

Hørsholm / Lund

DENMARK / SWEDEN

S Svensson

S Thelandersson

Structural Engineering, Lund Institute of Technology,

Lund

SWEDEN

**MEETING THIRTY-TWO**

**GRAZ**

**AUSTRIA**

**AUGUST 1999**

---

Presenter: H.J.Larsen

- H.J.Blass asked whether wind loads were considered in the analysis.
- H.J.Larsen answered that wind loads were not considered and it would be useful to do the analysis.
- A.Ranta-Maunus asked why a different DOL model was needed for panel material.
- H.J.Larsen responded that the Foschi model did not work for  $\sigma_o < 0.2$  which is needed for panel material.
- E.Karacabeyli asked why was the DOL model calibrated to Madison curve.
- H.J.Larsen responded that data with full size material were not available.
- F.Lam commented that although the shape of stress ratio versus log time curve from the fitted DOL model looks correct, such curves based on N. American DOL data on full size timber would intersect with the Madison curve at a time  $\ll 100$  years.
- H.J.Larsen said that the comments would be taken into consideration.
- S.Svensson said that the model was fitted to Madison curve and checked against some available data from literature.
- E.Karacabeyli commented that the use of two models might impact on result consistency.
- S.Thelandersson commented that exact shape of the curve might not matter as results represented the behaviour well.
- A.Ranta-Maunus asked why the mean values were compared.
- S.Thelandersson responded that comparison of ratios of short- and long-term 5<sup>th</sup> %tile strengths approximately equaled similar ratios of mean strengths; therefore, mean strength was used.

# Determination of Partial Coefficients and Modification Factors

H.J. Larsen

Danish Building Research Institute / Structural Mechanics, Lund Institute of Technology,  
Hørsholm / Lund  
Denmark / Sweden

S. Svensson

S. Thelandersson

Structural Engineering, Lund Institute of Technology,  
Lund  
Sweden

## 1 General

In most codes the safety requirements are expressed in symbolic form as

$$S(\gamma_G G_k + \gamma_{Q,1} Q_{k,1} + \gamma_{Q,2} Q_{k,2} \dots) \leq k_{mod} R_k / \gamma_m \quad (1)$$

where

$S$	Action effect
$G$	Permanent action
$Q_1, Q_2, \dots$	Variable actions
$R$	Capacity
$\gamma$	Partial coefficient (safety element) on $G$ , $Q$ and $R$
$k_{mod}$	Factor that takes into account the difference between the resistance in the structure under the actual conditions and the resistance determined in a standard test. For most materials other than wood, $k_{mod}$ is equal to unity. For wood, $k_{mod}$ depends on the moisture and load history.

Index  $k$  denotes characteristic value, i.e. a chosen or prescribed fractile in the distribution.

By setting  $\gamma_G = \gamma_{Q,1} = \gamma_{Q,2} = \dots = 1$ , expression (1) corresponds to the permissible stress system, the safety factor being  $\gamma_m / k_{mod}$ . In the now common partial safety system,  $\gamma_G$  is different from at least one  $\gamma_Q$ . It should be noted that a factor can be moved freely from the

action side to the resistance side, i.e. the safety level is described by  $\gamma_m \gamma_G$ ,  $\gamma_m \gamma_{Q,1}$ , .... Examples of  $\gamma$ -values are given in table 1.

Table 1 – Examples of  $\gamma$ -values.

		Eurocodes <sup>1)</sup>	Nordic recommendations <sup>2)</sup>	New Danish Code <sup>3)</sup>
$\gamma_G$		1.35	1.0	1.0
$\gamma_Q$	imposed actions <sup>4)</sup>	1.5	1.3	1.3
	natural actions <sup>5)</sup>	1.5	1.3	1.5
$\gamma_m$	timber	1.3	1.5	1.64
	glulam	1.3	1.35	1.50
$\gamma_Q \gamma_m$	(timber)	1.95	1.95	2.13 - 2.46

1) [ENV 1991-1, 1994] and [ENV 1995-1-1, 1993]. – 2) e.g. [DS 409, 1982] and [DS 413, 1982]. – 3) [DS 409, 1998] and [DS 413, 1998]. Until the end of 1998 the Danish values were identical to the Nordic ones. – 4) Floor loads etc. – 5) Wind and snow loads etc.

## 2 Danish code calibrations

In connection with a revision of the Danish structural codes (in force from 1st January 1999) a calibration study was carried out by S. O. Hansen and J. Dalgaard Sørensen. Its purpose was to ensure uniform reliability across structures and materials. The results are

Table 2 – Assumptions and old and optimised partial coefficients

	Fractile per cent	Coeff. of variation, per cent	Distribution	Partial coefficients	
				Old	Optimised
<i>Selfweight</i>	50		Normal	1.0 <sup>1)</sup>	1.0 (fixed)
concrete		6			
steel		4			
wood		6			
<i>Other permanent</i>	50	10	Normal	1.0	1.0 (fixed)
<i>Variable action</i>	98		Gumbel		
imposed		20		1.3	1.3
natural		40		1.3	1.5
<i>Concrete</i>	10/5 <sup>2)</sup>	15		1.58	1.49
reinforcement	0.1/5 <sup>2)</sup>	5	Log-normal	1.32	1.23
<i>Steel</i>	5	5		1.42	1.29
<i>Wood</i>					
structural	5	20		1.49	1.64
glulam	5	15		1.34	1.51
<i>Model uncertainty</i>	50		Normal		
concrete		5			
steel		3			
wood		5			

1)  $\gamma_G=1$  is a “holy” number for Danes due to the influence of geotechnical people in the code committees. – 2) Old codes/new codes.

published in [Sørensen, 1998]. The main load combination studied was permanent action and one variable, acting in the same direction, i.e. uplift was not studied. Two structures were investigated: a simply supported beam and an axially loaded column. The assumptions regarding distribution functions, existing (old) partial coefficients etc. are given in table 2.

The safety indices,  $\beta$ , were calculated according to the standard method proposed by Hashofer and Lind, see e.g. [Thoft-Christensen & Baker]. The results are given in table 3. The relation between safety index and formal probability of failure is given in table 4.

Table 3 – Calculated values of safety index  $\beta$

	Concrete		Steel		Glulam	
	beam	column	beam	column	beam	column
<i>Old</i>						
mean	5.39	4.64	5.06	5.10	4.58	4.58
standard deviation	0.62	0.26	0.64	0.66	0.27	0.27
<i>Optimised</i>						
mean	4.69	4.81	4.64	4.67	4.81	4.81
standard deviation	0.34	0.20	0.39	0.41	0.22	0.22

Table 4 – Relation between safety index and formal probability of failure

Safety index $\beta$	3.1	3.7	4.3	4.7	5.2
Annual probability of failure	$10^{-3}$	$10^{-4}$	$10^{-5}$	$10^{-6}$	$10^{-7}$

The variation between structures of one material and between materials is high and the scatter within a group is also high. An optimisation was therefore performed to make the  $\beta$ -values as uniform as possible. The resulting  $\gamma$ -values are given in table 3 (the optimum values for  $\gamma_Q$  are 1.28 and 1.52, respectively, but the values have been rounded off). As can be seen in the lower part of table 3, the  $\beta$ -values have become much more uniform.

An immediate result of this would be an increase of up to 25 per cent in the required geometrical parameters for timber structures (second moment of area for beams, area for tension members, etc.). Increasing the  $k_{mod}$ -values has to some extent counteracted this, see table 5, which also gives the Eurocode 5-values. Even so, the size of many structures will increase when the structures are designed according to the new Danish Timber Code.

One could argue that because of the greater uniformity the general safety level should have been reduced – the structures with very low  $\beta$ -values having been removed – but the majority of the members of the Danish code committee decided to maintain an average  $\beta$ -value of 4.8 on the grounds that, for many structures (other than timber), the new values had already resulted in reduced sizes and they dared not go further.

Out of kindness to the timber people, the effect of using other distributions - for instance, a Weibull distribution - was investigated. This distribution has a certain attraction because it is linked to the failure type often found in timber, namely brittle failure due to shear or tension perpendicular to the grain. The calculations simply demonstrated yet again that the formal probability of failure depends heavily on the assumed distribution and that if the distribution was really a Weibull distribution it would require even bigger partial

coefficients to obtain a required  $\beta$ -value. It should be stressed that the calculated probabilities of failure are formal values. Their purpose is to ensure uniform reliability (expressed by  $\beta$ -values) for comparable structures. Far too little is known about the tails of the distributions to calculate the true probabilities of failure. This is not an argument for not studying in greater detail the lower tails of the strength distribution. Wood is a graded natural product and the grading, whether visual or mechanical, has a great influence. This is, for example, demonstrated by [Foschi et al., 1989], see figure 2: it will often be better to use the distribution fitted to the lower 10-20 per cent strength values than to the complete data set. Of course, the mean values become lower but that is more than counteracted by the reduced coefficient of variation.

Table 5 –  $k_{mod}$  values according to old and new Danish Timber Design Code together with the values of Eurocode 5.

	Old Danish Code (Strength Class C24)	Eurocode 5	New Danish Code
Permanent	0.7	0.6	0.6
Storage	0.7	0.7	0.7
Imposed	0.7	0.8	0.8
Snow	0.8	0.9	0.9
Wind	1.0	0.9	1.10
Accidental	1.0	1.10	1.10

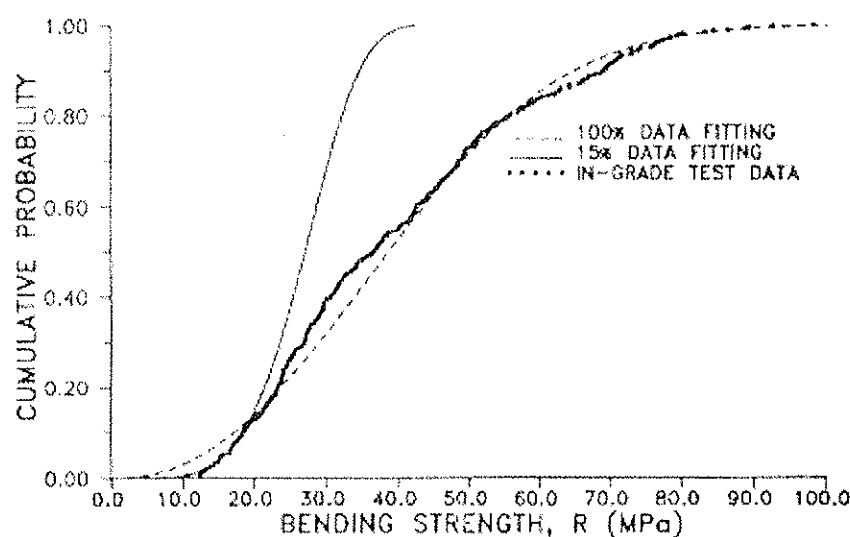


Figure 1 – 2-parameter Weibull fitted to test data. From [Foschi et al., 1989]

### 3 Damage models

The determination of partial coefficients as described above is based on the assumption that the strength at a given time is independent of the previous load history. This is not the case for timber and wood-based products. Load above a certain threshold stress (that may be zero) results in a weakening of the material. This means that a given high load is more dangerous if it occurs late in the load history than if it occurs early. This is taken into account by the factor  $k_{mod}$  in (1).

To determine  $k_{mod}$  it is necessary to have a model for the damage incurred by a load history. There are different models that try to explain the long-term behaviour of timber. The models use a variable  $\alpha(t)$  to describe the damage at time  $t$ . This variable increases with time (and moisture history), depending on the intensity and duration of applied stress from  $\alpha = 0$  in the undamaged state until failure occurs, at which time  $\alpha$  is unity.

One of the simplest damage models is the one proposed by Gerhards [Gerhards & Link, 1986]:

$$d\alpha/dt = \exp(A-B\sigma/f) \quad (2)$$

$A$  and  $B$  are constants,  $\sigma$  is the applied stress and  $f$  is the short-term strength. For Douglas fir  $A = 40$  (ln day) and  $B = 50$ . In this model – known as the U.S. Damage Accumulation Model – the threshold stress is zero.

The best known damage models are those proposed by Ricardo O. Foschi et al. They are not based on theoretical considerations, but a reasonable differential equation is proposed for the damage development and the parameters in the model are determined by curve fitting. The first model, proposed in [Barrett & Foschi, 1978], can be expressed as:

$$d\alpha/dt = A(\sigma - \sigma_0)^B + C\alpha \quad \text{for } \sigma > \sigma_0 \quad (3)$$

$\sigma_0$  is the threshold stress. A more complicated model is proposed in [Foschi & Yao, 1984] and this is the model normally referred to as Foschi's Model or the Canadian Damage Model:

$$d\alpha/dt = A(\sigma - \sigma_0)^B + C(\sigma - \sigma_0)^n \alpha \quad \text{for } \sigma > \sigma_0 \quad (4)$$

A model proposed by Nielsen, see for example the short presentation in [Madsen, 1992], is based on a fracture mechanics approach.

The models are discussed in [Foschi & Yao, 1986]. The following is quoted from the conclusions:

“...the fracture mechanics approach (Nielsen's) and the damage accumulation model (expression(4)) by Foschi were found suitable to represent accurately the experimental trends... The model by Gerhards was found to be lacking in the flexibility needed to follow the experimental trends. The fracture mechanics approach is not easy to use, since it requires numerical integration to obtain the time-to-failure in all cases when the applied stress varies with time...”

The models (3) and (4) are discussed in [Ellingwood & Rosowosky, 1991]. They conclude:

“...The damage rate models in (3) and (4) are nearly the same except at stress levels below about 0.65. Equation (4) is more difficult to implement because it cannot be non-dimensionalised...Accordingly, subsequent comparisons of the effect of the damage model... will be made using the models described by (3)...”

The models are used in [Ellingwood & Rosowosky, 1991] to calculate the effect of live load and snow load. They conclude:

“...Detailed examination of the simulated damage accumulation processes...revealed that for both light occupancy live and snow loads, damage usually accumulates only during one or two of the largest load pulses to occur during 50 years...This behaviour is a result of the highly non-linear nature of the damage-rate models...”

## 4 Determination of $k_{mod}$ for timber

At the Department of Structural Engineering in Lund, Sweden, a probabilistic analysis has been made to calibrate  $k_{mod}$  for timber under combinations of permanent action and snow. The analysis and the results are summarised in the following. For more details readers are referred to [Svensson et al., 1999] and [Thelandersson et al., 1999]. The steps in the procedure used to determine  $k_{mod}$  were:

### Step 1

The annual snow load was assumed to have a triangular variation as shown in figure 2 with a normally distributed maximum load with mean  $\mu_Q$  and coefficient of variation  $COV_Q$ . The annual snow period is also assumed to be normally distributed with mean  $\mu_T$  and coefficient of variation  $COV_T = COV_Q$ , i.e. it is assumed that the two variables are fully correlated. Two locations were investigated: Umeå in Northern Sweden (with a severe continental climate) and Lund in Southern Sweden (with a mild Atlantic climate), see [Forsler et al., 1971]. The values used are given in table 6. A load sequence covering 50 years is constructed by drawing the annual maximum load at random.

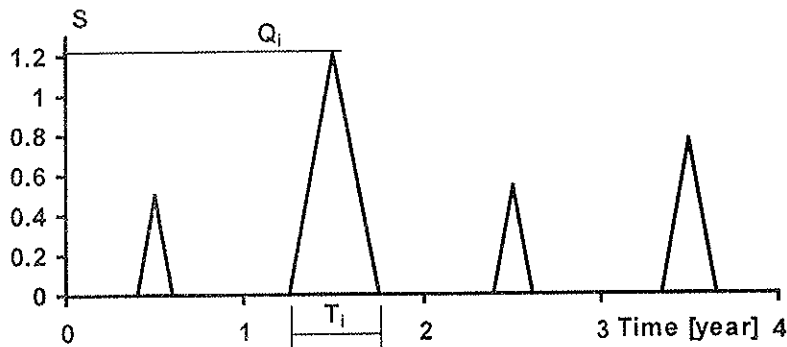


Figure 2 – Load sequence of snow load covering 4 years.

The method for determining the  $k_{mod}$ -factor is not limited to the simple triangular shapes of variable loads; any continuous function can be used to describe the variable loads. The triangular shaped annual snow variation with randomly selected amplitude and period, even though simple, has however the ability to simulate the mean snow amplitude and relative time period for continuous years of snow with good accuracy, see [Thelandersson et al., 1999].

Table 6 – Assumed values for the two locations: Umeå and Lund.

	Umeå	Lund
<i>Maximum annual snow load</i>		
Coefficient of variation $COV_Q$	0.35	0.66
<i>Annual snow period</i>		
Mean, $\mu_T$ , hours	3592	788
Coefficient of variation	0.35	0.66
<i>Required mean bending capacity <math>\mu_R/(\mu_G+\mu_Q)</math></i>		
$\mu_Q/(\mu_G+\mu_Q) = 1$ (only snow)	4.12	5.99
$\mu_Q/(\mu_G+\mu_Q) = 0.2$ (80 per cent permanent load)	2.77	2.88
$\mu_G + \mu_Q =$ mean total load		

### Step 2

The required bending capacity for the snow load described in Step 1 was determined as described in section 2, the only differences being that – in accordance with the Swedish requirements – a normal distribution was used for snow (instead of Gumbel's) and the required safety index was  $\beta = 4.3$ . The required mean bending capacity is shown in figure 3. Examples of the required mean bending capacity are given in table 7.

The analysis shows that a more variable action requires a higher load carrying capacity relative to the action than an action with lower variability. In reality, a structure in Lund does not require higher load carrying capacity than in Umeå. The required load carrying capacity in absolute terms is higher for Umeå because the average snow load is three times greater than in Lund.

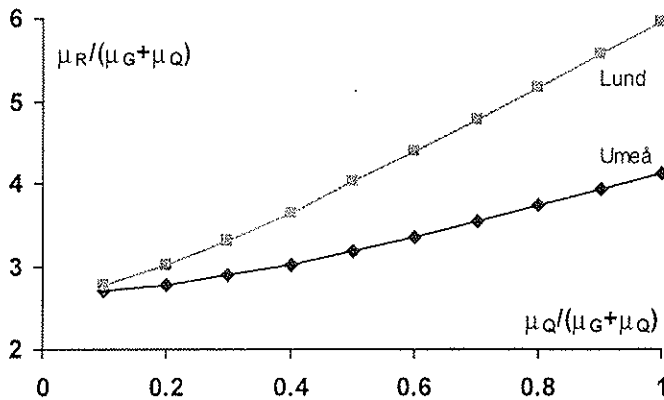


Figure 3 – Required mean bending capacity  $\mu_R$  for Umeå and Lund as function of the ratio between mean variable load and mean total load.

Table 7 – Examples of required bending capacity ( $\mu_R$ ) for short-term load, calculated equivalent load  $S_{equ}$ , required bending capacity for the equivalent loads  $\mu_{R,50}$  and  $k_{mod}$ . Mean total load is  $(\mu_G + \mu_Q)$ .

	Umeå		Lund	
$\mu_Q / (\mu_G + \mu_Q)$	0	0.20	0	0.20
$\mu_R / (\mu_G + \mu_Q)$	4.12	2.77	5.99	2.88
$S_{equ} / (\mu_G + \mu_Q)$				
mean	2.38	1.69	3.24	1.65
Coefficient of variation	0.096	0.022	0.134	0.070
$\mu_{R,50} / (\mu_G + \mu_Q)$	5.32	3.57	7.56	3.60
$k_{mod}$	0.78	0.78	0.79	0.80

### Step 3

As argued above, Foschi's simple damage model, expression (3), was used. The relative threshold stress was put at 0.5, and the parameters in the model were evaluated against the so-called Madison curve, [Wood, 1947] as modified by [Pearson, 1972], i.e. against a ramp load with a loading time  $t_r = 2$  minutes and then constant load until failure. To acquire an overall acceptable correlation between the model and the Madison curve the ramp load strength corresponding to 2 minutes ( $\log h = -1,5$ ) was underestimated. The result is shown in figure 4.



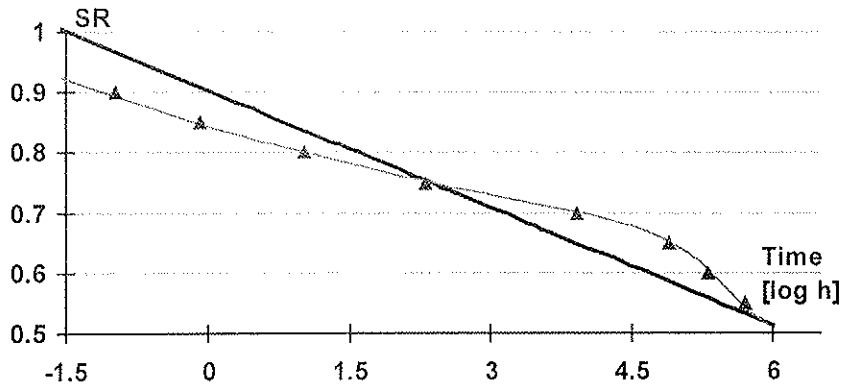


Figure 4 – Damage accumulation model (3) fitted to the Madison curve. The constants are  $A = 7.08 \cdot 10^7$ ,  $B = 17$  and  $C = 1/20000$ .

#### Step 4

With the damage accumulation model the minimum resistance,  $R_{min}$ , required to survive under a 50-year snow load sequence was calculated for 400 sequences for each location and for two load combinations of table 3: one with snow load only and one with 80 per cent permanent load. This resistance can be interpreted as an equivalent time-independent load  $S_{equ,i} = R_{min,i}$ . The equivalent load, see figure 4, can be approximated with good accuracy by normal distributions with the parameters given in table 7.

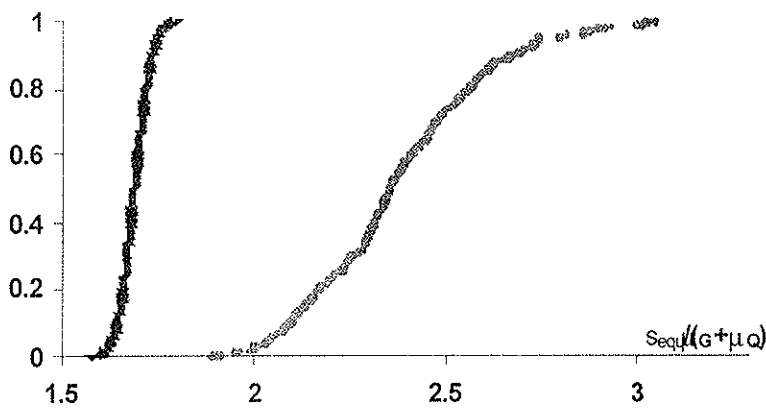


Figure 5 – Equivalent loads for Umeå with two load combinations. Right: only snow load. Left: 80 per cent permanent load.

#### Step 5

The required bending capacity  $\mu_{R,50}$  for the equivalent load was calculated as in Step 2, but the reference period was changed from 1 year to 50 years. This corresponds to changing the safety index from 4.3 to  $\beta = 3.3$ . The mean value  $\mu_{R,50}$  is given in table 7 for the two load combinations: snow load alone and 80 per cent permanent load.

#### Step 6

$k_{mod}$  is now calculated as  $\mu_R/\mu_{R,50}$ . The result is given in table 7.

It is interesting to note that  $k_{mod}$  is practically independent of the location; the differences are mainly reflected in the different requirement to the relative short-term strengths.

## 5 Determination of $k_{mod}$ for a panel material

The method described above was also used for a typical panel material with a relative threshold stress of 0.2, although without success: the fitting of the Foschi damage model to the corresponding “Madison”-curve became unstable. Instead, Gerhards’ damage model, expression (2) was used, see figure 6, with the following assumptions:

- The short-term strength corresponds to the two-minute loading case
- The threshold value is obtained for  $10^6$  hours (~100 years).

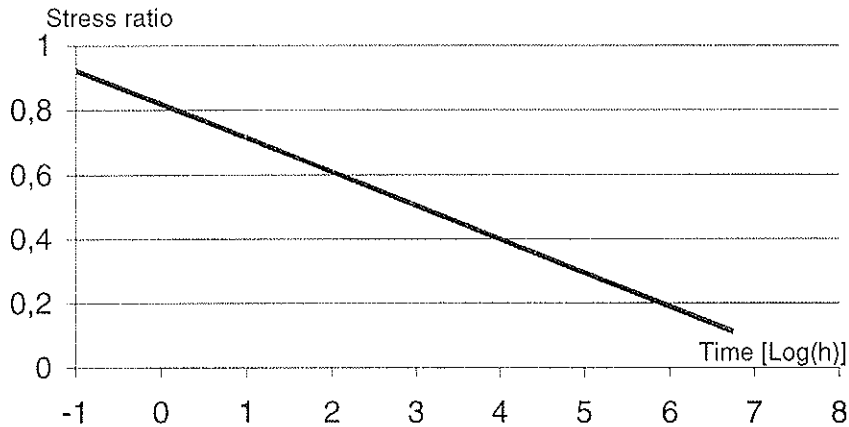


Figure 6 – Damage accumulation according to Gerhards’ model.  $A = 18$  and  $B = 22$ .

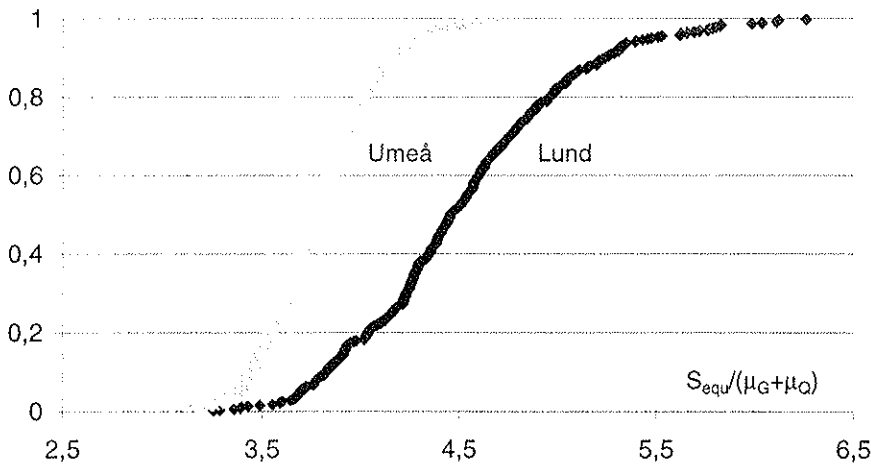


Figure 7 – Equivalent loads for Umeå and Lund for snow load alone.

The parameters are the same as in section 4 except that the coefficient of variation for the bending capacity is taken equal to 0.15 and the dimensional uncertainty is assumed to correspond to a coefficient of variation 0.05. The calculated equivalent loads are shown in figure 7. The results are summarised in table 8.

A value of  $k_{mod} = 0.5$  seems reasonable for snow loaded panel materials with  $k_{mod} = 0.2$  for permanent actions.

Table 8 – Results corresponding to table 7 for a panel material.

	Umeå		Lund	
	0	0.65	0	0.65
$\mu_Q/(\mu_Q+\mu_G)$				
$\mu_{S_{equ}}$	3.79	3.49	4.51	3.72
$COV_{S_{equ}}$	0.074	0.046	0.122	0.09
$\mu_R$	3.65	3.02	5.33	3.72
$\mu_{R,50}$	7.33	6.65	9.27	7.33
$k_{mod}$	0.50	0.45	0.58	0.56

## References

1. Barrett, J. D. and R. O. Foschi, Duration of load and probability of failure in wood, part I and II. *Canadian Journal of Civil Engineering*, 5(4), 1978, pp 505-532.
2. DS 409, Danish Standard, Code of Practice for the Safety of Structures, 1982 (Translation 1983).
3. DS 409, Danish Standard, Norm for Sikkerhedsbestemmelser for konstruktion (Code of Practice for the Safety of Structures - in Danish), 1982??
4. DS 413 Danish Standard, Code of Practice for the Structural Use of Timber, 1982 (Translation 1983).
5. DS 413 Danish Standard, Norm for Trækonstruktioner, (Code of Practice for the Use of Timber), 1998.
6. Ellingwood, B. and D. Rosowsky, Duration of Load Effects in LRFD for Wood Construction. *Journal of Structural Engineering*, 117(2), 1991.
7. ENV 1991-1, 1995, Eurocode 1, Part 1-1, Basis of Design General Rules and Rules for Buildings.
8. ENV 1995-1-1, 1994, Eurocode 5, Design of Timber Structures, Part 1-1.
9. Forsler, S., H. Jonasson, W. Landin, L. Schärnell and S. Åkerlund, Snödjup och vattenvärde. In Swedish. Rapport 24, Institutionen för Byggnadsteknik, Lunds Tekniska Högskola, 1971.
10. Foschi, R.O., B. R. Folz and F. J. Yao, Reliability Based Design of Wood Structures. Structural Research Series Report No. 34, University of British Columbia, Vancouver, Canada, 1989.
11. Foschi and Yao 1986, Another look at Three Duration of Load models Proceedings CIB-W18/19-9-1. Florence Italy.
12. Gerhards, C. and C. Link. Effects of loading rate on bending strength of Douglas-fir 2 by 4's. *Forest Prod. J.*, 36(2) 1986, pp 63-66.
13. Madsen, B., Structural behaviour of timber, Timber Engineering Ltd., Vancouver, Canada, 1992
14. Pearson, R. G., The Effects of Duration of Load on the Bending Strength of Wood. *Holz Forschung*, 26(4), 1972, pp. 153-158.
15. Svensson, S.,S. Thelandersson and H.J. Larsen, Reliability of Timber Structures under Long Term Loads. Proc. RILEM Symposium on Timber Engineering, Stockholm, Sweden, September 1999.
16. Sørensen, J. D., Probabilistic Calibration of Partial Safety Factors for Danish Codes. Aalborg University Centre, September 1997.
17. Thelandersson, S., H. J. Larsen, L. Östlund, T. Isaksson and S. Svensson. Säkerhetsnivåer för trä och träbaserade produkter (Safety Level for Timber and Wood-based Products). Report TVBK 3035, Div. of Structural Engineering, Lund University, Sweden, 1999.
18. Thoft-Christensen, P. and M. J. Baker, Structural Reliability Theory and its Applications. Springer-Verlag Berlin Heidelberg New York 1982.

**INTERNATIONAL COUNCIL FOR RESEARCH AND INNOVATION  
IN BUILDING AND CONSTRUCTION**

**WORKING COMMISSION W18 - TIMBER STRUCTURES**

**DESIGN BY TESTING OF STRUCTURAL TIMBER COMPONENTS**

V Enjily

Building Research Establishment (BRE),

CTTC - Timber Engineering

L Whale

TimberSolve Ltd

UNITED KINGDOM

**MEETING THIRTY-TWO**

**GRAZ**

**AUSTRIA**

**AUGUST 1999**

---

Presenter: V.Enjily

- H.J.Blass questioned that if the procedure was based on timber component having CV<8%, what would be needed for other timber components that might have CV>8%.
- V.Enjily responded that the procedure would not be not valid for cases with CV>8%.
- H.J.Larsen stated that the EC5 does not require sample size of 30. Also one might have difficulties promoting the concept.
- V.Enjily responded that when timber properties could be considered as component would be an important issue for this procedure.
- H.J.Larsen further questioned that whether CV<8% would be correct based on the limited sample size.

# DESIGN BY TESTING OF STRUCTURAL TIMBER COMPONENTS

Enjily V

Building Research Establishment (BRE), CTTC - Timber Engineering, UK

Whale L

TimberSolve Ltd, UK

## 1. ABSTRACT

This paper is concerned with the conversion of component test results such as trussed rafters, wall panels, ply-web beams, etc. to design values in accordance with DD ENV 1995-1-1<sup>(1)</sup>. Since the publication of DD ENV 1995-1-1: 1994<sup>(1)</sup>, the lack of guidance for converting component test results into design values and the importance of number of tests required for practical and economical reasons have been repeatedly highlighted.

Annex A of DD ENV 1995-1-1: 1994<sup>(1)</sup> (although informative) deals with the determination of 5-percentile characteristic values from test results and acceptance criteria for a sample. Although, this part of DD ENV 1995-1-1<sup>(1)</sup> may be adequate for determining the properties of materials or small component tests, such as joints, it is totally unacceptable for component tests by the industry, as the minimum number of tests given in this section of DD ENV 1995-1-1<sup>(1)</sup> is 30. This is not only uneconomical, it is also impractical for component tests such as trussed rafters, wall panels, ply-web beams, glulam beams, etc.

A method is proposed for converting component test results to design values using suggested modification factors and the acceptance of the results for consideration by CIB/W18, TC250/SC5 and its Project Teams for inclusion in DD ENV 1995-1-1<sup>(1)</sup>.

## 2- INTRODUCTION

There has been attempts in the past<sup>(2,3)</sup> to evolve methods to quantify the consequent risks of any decision process required to classify products (components) into design values on the basis of evidence from small samples based on the statistical theories. The minimum number of tests for which an acceptable statistical justification could be obtained was found to be 10<sup>(2)</sup>; this is still unacceptable and unrealistic for component tests for industry.

ENV 1991-1, Eurocode 1<sup>(4)</sup>, Section 8 deals with “Design assisted by testing” which provides guidance for planning and evaluating tests related to structural design, based on two principles:

“(1)P Where calculation rules or material properties given in ENVs 1991 to 1999 are not sufficient, or where economy may result from tests on prototypes, part of the design procedure may be performed on the basis of test. Note: Some of the clauses in this section may also be helpful in cases when the performance of an existing structure is to be investigated”.

“(2)P Tests shall be set up and evaluated in such a way that the structure has the same level of reliability with respect to all possible limit states and design situations as achieved by design based on calculation procedures specified in ENVs 1991 to 1999, including this part of ENV1991.”

ENV 1991-1<sup>(4)</sup> also gives guidance on “Derivation of design values” with a principle of “The determination of the design values for a material; property, a model parameter or resistance value from tests can be performed in either of the following two ways:

- (a)- by assessing a characteristic value, which is divided by a partial factor and possibly multiplied by an explicit conversion factor;
- (b)- by direct determination of the design value, implicit or explicit accounting for the conversion aspects and the total reliability required.

ENV 1991-1 then goes on to say that in general method (a) should be used.”. Annex D (informative) of ENV 1991-1<sup>(4)</sup> states that testing may be carried out if adequate calculation models are not available, if a large number of similar components will be used, and if their real behaviour is of special interest. The Annex also gives some guidance on the conversion of test results to design values, BUT admits that the guidance given is incomplete since it must also depend on the type of test and materials involved.

Annex A of DD ENV 1995-1-1: 1994<sup>(1)</sup> (although informative) deals with the determination of 5-percentile characteristic values from test results and acceptance criteria for a sample. Although, this part of DD ENV 1995-1-1 may be adequate for determining the properties of materials or small component tests, such as joints, it is totally unacceptable for component tests by the industry as the minimum number of tests given in this section of DD ENV 1995-1-1<sup>(1)</sup> is 30. This is not only uneconomical, it is also impractical for component tests such as trussed rafters, wall panels, ply-web beams, glulam beams, etc.

British Standards BS5268: Parts 2<sup>(5)</sup> (design of timber structures), 3<sup>(6)</sup> (Trussed rafter roofs) and 6<sup>(7)</sup> (wall panels) provide methods to convert the component test results into design values. Identical modification factors (although expressed in different formats) for reducing the component test results are also given in each standard as the number of tests reduces from 5 to 1. The modification factors given in these standards are based on the assumption that the coefficient of variation of the components tested is 8%. This is an important factor, as when the coefficient of variation increases so does the number of replicates to be tested. In BS5268: Parts 2<sup>(5)</sup> and 3<sup>(6)</sup>, the load-duration is considered while in Part 6<sup>(7)</sup> it is not (which is correct as the wind loading is assumed to be short-term, assuming that the duration of test is the same as that given for short-term loading).

### **3. DERIVATION METHODS OF DESIGN VALUES**

#### **3.1- ENV 1991-1<sup>(4)</sup> Method**

ENV 1991-1, Section 8 and Annex D, provide guidance for planning and evaluating experiments related to structural design, when the number of tests is sufficient for a statistical interpretation of their results.

ENV 1991-1<sup>(4)</sup> states that the derivation of the design values for a material property, a model parameter or a resistance value from tests can be performed in either of the following ways:

- a) by assessing a characteristic value, which is divided by a partial factor and possibly multiplied by an explicit conversion factor. That is :
 

$X_k \cdot \text{explicit conversion factor} / \text{partial factor}$
- b) by direct determination of the design value, implicit or explicitly accounting for the conversion aspects and the total reliability required.

ENV 1991-1 carries on stating that “In general method a) should be used.”.

### 3.1.1- Assessment of Design value by testing

Statistical evaluation of resistance / material tests is given in Clauses D.3.2.1, D.3.2.2 and D.3.2.3 of ENV 1991-1. They give operational formulae for deriving design values from tests for resistance and material testing where the characteristic value is determined from standardised or established distribution of the material properties. Bayesian procedure with vague prior distributions are used which leads to almost the same result as classical statistics with confidence levels equal to 0.75.

Two methods are distinguished namely; a) and b) stated above. The values and formulae used in these two methods are based on:

- the normal distribution;
- a complete lack of prior knowledge for the mean;
- a complete lack of prior knowledge for the coefficient of variation in the case “ $V_x$  unknown” or, on the other hand, full knowledge for the coefficient of variation in the case “ $V_x$  known”.

#### 3.1.1.1- Method a): Assessment via the characteristic value

Assume that a sample of  $n$  numerical test results is available. The design of a variable  $X$  is obtained from:

$$X_d = \eta_d X_{k(n)} / \gamma_M = \eta_d m_x (1 - K_n V_x) / \gamma_M \dots\dots\dots \text{Equation 1}$$

- Where:
- $\gamma_M$  = the partial factor for the design
  - $\eta_d$  = the design value of the conversion factor
  - $X_{k(n)}$  = the characteristic value including statistical uncertainty
  - $m_x$  = the mean of the sample results ( =  $\Sigma x_i / n$  )
  - $V_x$  = the coefficient of variation of  $X$
  - $K_n$  = the coefficient from Table 1

**Note:** ENV 1991-1 does not provide guidance for  $\eta_d$  and  $K_n$  values in Table 1 are based on 5% characteristic value and on the normal distribution.

Two cases are considered for  $V_x$ :

- i) The coefficient of variation of  $V_x$  is known from pre-knowledge (previous knowledge might be found from the evaluation of previous tests in comparable situations). In this case the



modification factors for “V<sub>x</sub> known” given in Table 1 should be used.

- ii) The coefficient of variation of V<sub>x</sub> is unknown from pre-knowledge but must be estimated from the sample by the following:

$$S_x = 1/(n - 1) \cdot \sqrt{\sum (x_i - m_x)^2} \dots\dots\dots \text{Equation 2}$$

$$V_x = S_x / m_x \dots\dots\dots \text{Equation 3}$$

In this case the modification factors for “V<sub>x</sub> unknown” given in Table 1 should be used.

n	1	2	3	4	5	6	8	10	20	30	∞
V <sub>x</sub> known	2.31	2.01	1.89	1.83	1.8	1.77	1.74	1.72	1.68	1.67	1.64
V <sub>x</sub> unknown	-	-	3.37	2.63	2.33	2.18	2.00	1.92	1.76	1.73	1.64

**Table 1: Values of K<sub>n</sub> for the 5% characteristic value**

**3.1.1.2- Method b): Direct Assessment of the design value**

The design value should be obtained from:

$$X_d = \eta_d X_{od} = \eta_d m_x (1 - K_n V_x) \dots\dots\dots \text{Equation 4}$$

Where the notations are the same as before except that η<sub>d</sub> should now cover all uncertainties not covered by the tests. The value of K<sub>n</sub> should be obtained from Tables 2 and 3.

n	1	2	3	4	5	6	8	10	20	30	∞
V <sub>x</sub> known	4.36	3.77	3.56	3.44	3.37	3.33	3.27	3.23	3.16	3.13	3.08
V <sub>x</sub> unknown	-	-	-	11.4	7.85	6.36	5.07	4.51	3.64	3.44	3.08

**Table 2: Values of K<sub>n</sub> for the ULS design value, if X is dominating**

n	1	2	3	4	5	6	8	10	20	30	∞
V <sub>x</sub> known	1.81	1.57	1.48	1.43	1.40	1.38	1.36	1.34	1.31	1.30	1.28
V <sub>x</sub> unknown	-	3.77	2.18	1.83	1.68	1.56	1.51	1.45	1.36	1.33	1.28

**Table 3: Values of K<sub>n</sub> for the ULS design value, if X is non-dominating**

**3.2- SIMPLIFIED PROPOSED METHOD FOR DD ENV 1995-1-1**

**3.2.1- Criterion for Testing**

All structures/components should be tested in accordance with relevant EN standards supporting DD ENV 1995-1-1<sup>(1)</sup>. These ENs are generally well established and no extra work is needed other than usual amendments (if necessary) during the course of their application. Design by Testing may be carried out where:

- a structure or part of a structure is not amenable to calculation, or where calculation is deemed impracticable;
- materials or design methods are used other than those of the relevant specification or code of practice;
- there is doubt or disagreement as to whether the structure or some part of it conforms to design rules, or as to whether the quality of the materials is of the required standard;

- a routine check of a structure is required by prior agreement between the client and the manufacturer.

Where possible, more than one structure of the same design should be tested to enable an assessment to be made of the likely variability in performance. Table 4 gives factors ( $K_n$ ) for the number of tests based on:

- the assumption that the coefficient of variation of the components tested is 8% (this is an important factor, as when the coefficient of variation increases, so does the number of replicates to be tested).
- experience of behaviour of components in service.
- proof of their safe use in the past few decades.

No of tests (n)	1	2	3	4	5
Modification factor $K_n$	0.80	0.87	0.93	0.97	1.00

**Table 4: Modification factors for number of tests**

### 3.2.2- Ultimate Limit State Design

The minimum ultimate load obtained from testing should be:

$$\text{Minimum Ultimate Test load} \geq F_d \times \gamma_m / (\eta \times K_{\text{mod}} \times K_n) \dots\dots\dots \text{Equation 5}$$

Where:

$F_d$  = Design load on the component based on ENV 1991-1<sup>(4)</sup>. The Design load ( $F_d$ ) should be based on ENV 1991-1<sup>(4)</sup> and be equal to  $\gamma_F F_{\text{rep}}$  where  $\gamma_F$  is the partial factor for the action considered and  $F_{\text{rep}}$  is the representative value of the action (ie design loads for different types of actions using relevant load factors).

$\gamma_m$  = Modification factor for primary structural material in the component given in DD ENV 1995-1-1<sup>(1)</sup>.

$K_{\text{mod}}$  = Modification factor for load duration given in DD ENV 1995-1-1<sup>(1)</sup>.

$K_n$  = Modification factor for the number of component tests (Table 4).

$\eta$  = 0.894 for timber, plywood and glulam timber components in Service Classes 1, 2 & 3.

$\eta$  = 0.93 for components with panel products other than plywood in Service Class 1.

$\eta$  = 1.182 for components with panel products other than plywood in Service Class 2.

Tables 5 to 8 in Annex A include factors of safety obtained using Equation 5 above for each category of materials, service classes and load-durations. The factors for permanent loading would not be used in practice as it is unlikely that a structure or component would have a design load consisting of permanent load only (ie self-weight). However, they are included in Tables 5 to 8.

### 3.2.3- Serviceability Limit State Design

The Serviceability Limit State is reached during testing if :

- (a)- a discontinuity, indicating irreversible damage, occurs on the load deflection curve even if cracks or other damage are not visible. OR

- (b)- when  $0.4F_{ult}$  load is reached whichever occurs first. The mean stiffness value  $R_{mean}$  is calculated from the individual R values from the prototype testing. The mean stiffness value shall fulfil the following requirement:

$$R_{mean} = > (\gamma_F F_k / \delta_{required}) (1+K_{def,x}) / [0.8 K_n (1+K_{def,y})] \dots\dots\dots\text{Equation 6}$$

Where:

- $R_{mean}$  = Mean stiffness of component in N/mm found by testing ( $F_{test}/\delta_{test}$ ).
- $F_k$  = the characteristic load, in kN, depending on load categories as specified in ENV 1991-2-1 at the requirement deflection  $\delta_{required}$ , in mm.
- $K_{def,x}$  = creep factor depending on the type of material, end-use and Service Class given in DD ENV 1995-1-1<sup>(1)</sup>.
- $K_{def,y}$  = creep factor for short-term duration given in DD ENV 1995-1-1<sup>(1)</sup>.
- $\delta_{required}$  = permissible deflection in design given in DD ENV 1995-1-1<sup>(1)</sup>.
- $\delta_{test}$  = deflection in test.
- $\gamma_F$  = load factor = 1.0
- $K_n$  = modification factor for number of tests given in Table 4 of this document.

## 4- CONCLUSIONS AND RECOMMENDATIONS

- The lack of guidance for converting component test results into design values and the importance of the number of tests required for practical and economical reasons have been highlighted.
- The assessment of the conversion factor from test to design is strongly dependent on the type of test and the type of material. No further guidance is given in DD ENV 1991-1: 1994. DD ENV 1991-1: 1994 admits that the guidance given for Design by Testing is incomplete since it must also depend on the type of test and materials involved.
- The current DD ENV 1995-1-1 and ENV 1991-1 methods of deriving design values by testing is not appropriate for timber structures / components.
- Although, Annex A of DD ENV 1995-1-1: 1994 may be adequate for determining the properties of materials or small component tests, such as joints, it is totally unacceptable for component tests by the industry, as the minimum number of tests given in this section of DD ENV 1995-1-1 is 30. This is not only cumbersome and uneconomical, it is also impractical for component tests such as trussed rafters, wall panels, ply-web beams, glulam beams, etc.
- It is recommended that the proposed simplified Design by Testing methods for Ultimate and Serviceability limit state designs given in this paper should be adopted for the revision of DD ENV 1995-1-1: 1994. The modification factors recommended for the number of component tests in this paper are based on:
  - the assumption that the coefficient of variation of the components tested is 8% (this is an important factor, as when the coefficient of variation increases, so does the number of replicates to be tested).
  - experience of behaviour of components in service.
  - proof of their safe use in the past few decades.
- The factor  $\eta$  used in Equation 5 has three values, one for timber, plywood and glulam timber (0.894) and another two for board materials other than plywood related to service classes 1 and 2 (0.93 and 1.182 respectively).

- Tables 5 to 8 in Annex A include factors of safety obtained using the proposed method. The factors for permanent loading would not be used in practice as it is unlikely that a structure or component would have a design load consisting of a permanent load only (ie self-weight).

## REFERENCES

- 1- British Standards Institution. DD ENV 1995-1-1;- Eurocode 5: Design of timber Structures. Part 1.1: General rules and rules for buildings (together with the UK National Application Document). DD ENV 1995-1-1, BSI, London, 1994.
- 2- C B Pierce. A method for quantifying the risks involved in small sample acceptance testing of building components. N93/77, BRE, 1977.
- 3- D G Beech. The concept of characteristic strength. The British Ceramic research Association, Technical Note No 265, September 1977.
- 4- European Committee for Standardisation (CEN). ENV 1991-1. Eurocode 1:- Basis of design and actions on structures. Part 1: Basis of Design. CEN/TC250, August 1994.
- 5- British Standards Institution. BS5268: Part 2:- Structural use of timber. Code of practice for permissible stress design, materials and workmanship. BS5268: Part 2. BSI, London, 1996.
- 6- British Standards Institution. BS5268: Part 3:- Structural use of timber. Code of practice for trussed rafter roofs. BS5268: Part 3. BSI, London, 1998.
- 7- British Standards Institution. BS5268: Part 6:- Structural use of timber. Code of practice for timber frame walls. Section 6.1: Dwellings not exceeding four storeys. BS5268: Part 6, Section 6.1. BSI, London, 1996.

## **ANNEX A**

**Factors of safety obtained using proposed method of  
Design by Testing (Equation 5)**

Load-durations		Solid timber, plywood & glulam																			
No of tests		Service Class 1					Service Class 2					Service Class 3									
Permanent	1	3.03	-	-	-	-	3.03	-	-	-	-	-	3.64	-	-	-	-	-			
	2	2.79	-	-	-	-	2.79	-	-	-	-	-	3.34	-	-	-	-	-			
	3	2.61	-	-	-	-	2.61	-	-	-	-	-	3.13	-	-	-	-	-			
	4	2.50	-	-	-	-	2.5	-	-	-	-	-	3.00	-	-	-	-	-			
	5	2.43	-	-	-	-	2.43	-	-	-	-	-	2.91	-	-	-	-	-			
Long-term	1	2.60	2.50	2.50	2.85	2.85	2.60	2.50	2.50	2.85	2.85	3.30	2.50	2.50	2.85	2.85	3.30	-	-		
	2	2.39	2.29	2.30	2.62	2.62	2.39	2.29	2.30	2.62	2.62	3.03	2.29	2.30	2.62	2.62	3.03	-	-		
	3	2.24	2.16	2.16	2.46	2.46	2.24	2.16	2.16	2.46	2.46	2.84	2.16	2.16	2.46	2.46	2.84	-	-		
	4	2.15	2.05	2.06	2.36	2.36	2.15	2.05	2.06	2.36	2.36	2.72	2.05	2.06	2.36	2.36	2.72	-	-		
	5	2.08	2.00	2.00	2.28	2.28	2.08	2.00	2.00	2.28	2.28	2.64	2.00	2.00	2.28	2.28	2.64	-	-		
Medium-term	1	2.28	2.18	2.24	2.28	2.28	2.28	2.18	2.24	2.28	2.28	2.80	2.18	2.24	2.28	2.28	2.80	-	-		
	2	2.10	2.01	2.06	2.09	2.09	2.10	2.01	2.06	2.09	2.09	2.57	2.01	2.06	2.09	2.09	2.57	-	-		
	3	1.96	1.89	1.93	1.97	1.97	1.96	1.89	1.93	1.97	1.97	2.41	1.89	1.93	1.97	1.97	2.41	-	-		
	4	1.88	1.80	1.84	1.87	1.87	1.88	1.80	1.84	1.87	1.87	2.31	1.80	1.84	1.87	1.87	2.31	-	-		
	5	1.82	1.74	1.79	1.82	1.82	1.82	1.74	1.79	1.82	1.82	2.24	1.74	1.79	1.82	1.82	2.24	-	-		
Short term	1	2.01	1.94	1.90	1.90	1.90	2.01	1.94	1.90	1.90	1.90	2.60	1.94	1.90	1.90	1.90	2.60	-	-		
	2	1.85	1.79	1.75	1.75	1.75	1.85	1.79	1.75	1.75	1.75	2.39	1.79	1.75	1.75	1.75	2.39	-	-		
	3	1.73	1.68	1.64	1.64	1.64	1.73	1.68	1.64	1.64	1.64	2.24	1.68	1.64	1.64	1.64	2.24	-	-		
	4	1.66	1.60	1.57	1.57	1.57	1.66	1.60	1.57	1.57	1.57	2.15	1.60	1.57	1.57	1.57	2.15	-	-		
	5	1.61	1.56	1.52	1.52	1.52	1.61	1.56	1.52	1.52	1.52	2.08	1.56	1.52	1.52	1.52	2.08	-	-		
		Proposed method (Equation 5)	NAD	BS5268: Part 2	BS5268: Part 3	Proposed method (Equation 5)	NAD	BS5268: Part 2	BS5268: Part 3	Proposed method (Equation 5)	NAD	BS5268: Part 2	BS5268: Part 3	Proposed method (Equation 5)	NAD	BS5268: Part 2	BS5268: Part 3	Proposed method (Equation 5)	NAD	BS5268: Part 2	BS5268: Part 3

Table 5: Comparison of safety factors of ‘Design by Testing’ with existing factors given in national standards for solid wood, plywood and glulam.

Load-durations		Particleboard (EN312-6 & -7) and OSB (EN300, Grades 3 & 4)																
No of tests		Service Class 1					Service Class 2					Service Class 3						
Permanent	1	4.37	-	-	-	4.58	-	-	-	-	-	-	-	-	-	-	-	-
	2	4.02	-	-	-	4.21	-	-	-	-	-	-	-	-	-	-	-	-
	3	3.76	-	-	-	3.94	-	-	-	-	-	-	-	-	-	-	-	-
	4	3.60	-	-	-	3.78	-	-	-	-	-	-	-	-	-	-	-	-
	5	3.50	-	-	-	3.67	-	-	-	-	-	-	-	-	-	-	-	-
Long-term	1	3.50	3.50	2.89	-	3.44	3.50	2.89	-	3.44	3.50	2.89	-	3.44	3.50	2.89	-	-
	2	3.21	3.21	2.65	-	3.16	3.21	2.65	-	3.16	3.21	2.65	-	3.16	3.21	2.65	-	-
	3	3.01	3.01	2.48	-	2.96	3.02	2.48	-	2.96	3.02	2.48	-	2.96	3.02	2.48	-	-
	4	2.88	2.88	2.37	-	2.84	2.87	2.37	-	2.84	2.87	2.37	-	2.84	2.87	2.37	-	-
	5	2.80	2.80	2.30	-	2.75	2.80	2.30	-	2.75	2.80	2.30	-	2.75	2.80	2.30	-	-
Medium-term	1	2.50	2.50	2.24	-	2.50	2.50	2.24	-	2.50	2.50	2.24	-	2.50	2.50	2.24	-	-
	2	2.30	2.29	2.06	-	2.30	2.29	2.06	-	2.30	2.29	2.06	-	2.30	2.29	2.06	-	-
	3	2.15	2.16	1.93	-	2.15	2.16	1.93	-	2.15	2.16	1.93	-	2.15	2.16	1.93	-	-
	4	2.06	2.05	1.84	-	2.06	2.05	1.84	-	2.06	2.05	1.84	-	2.06	2.05	1.84	-	-
	5	2.00	2.00	1.79	-	2.00	2.00	1.79	-	2.00	2.00	1.79	-	2.00	2.00	1.79	-	-
Short term	1	1.94	1.94	1.96	-	1.96	1.94	1.96	-	1.96	1.94	1.96	-	1.96	1.94	1.96	-	-
	2	1.79	1.79	1.81	-	1.81	1.79	1.81	-	1.81	1.79	1.81	-	1.81	1.79	1.81	-	-
	3	1.67	1.68	1.70	-	1.69	1.68	1.70	-	1.69	1.68	1.70	-	1.69	1.68	1.70	-	-
	4	1.60	1.60	1.62	-	1.62	1.60	1.62	-	1.62	1.60	1.62	-	1.62	1.60	1.62	-	-
	5	1.55	1.56	1.57	-	1.57	1.56	1.57	-	1.57	1.56	1.57	-	1.57	1.56	1.57	-	-
		Proposed method (Equation 5)	NAD	BS5268: Part 2	BS5268: Part 3	Proposed method (Equation 5)	NAD	BS5268: Part 2	BS5268: Part 3	Proposed method (Equation 5)	NAD	BS5268: Part 2	BS5268: Part 3	Proposed method (Equation 5)	NAD	BS5268: Part 2	BS5268: Part 3	Proposed method (Equation 5)

Table 6: Comparison of safety factors of ‘Design by Testing’ with existing factors given in national standards for particleboard (EN312-6 & -7) and OSB (EN300, Grades 3&4).

Load-durations	No of tests	Particleboard (EN312-4 & -5), OSB (EN300, Grade 2) and Fiberboards (EN622-5, hardboard)											
		Service Class 1			Service Class 2			Service Class 3					
Permanent	1	5.82	-	-	6.87	-	-	-	-	-	-	-	-
		2	5.36	-	-	6.32	-	-	-	-	-	-	-
Long-term	3	5.01	-	-	5.91	-	-	-	-	-	-	-	-
		4	4.80	-	-	5.67	-	-	-	-	-	-	-
Medium-term	5	4.66	-	-	5.50	-	-	-	-	-	-	-	-
		1	3.88	3.84	2.89	-	4.58	3.84	2.89	-	-	-	-
Short term	2 <td>3.57</td> <td>3.53</td> <td>2.65</td> <td>-</td> <td>4.21</td> <td>3.53</td> <td>2.65</td> <td>-</td> <td>-</td> <td>-</td> <td>-</td> <td>-</td>	3.57	3.53	2.65	-	4.21	3.53	2.65	-	-	-	-	-
		3	3.34	3.32	2.48	-	3.94	3.32	2.48	-	-	-	-
	4	3.20	3.17	2.37	-	3.78	3.17	2.37	-	-	-	-	-
		5 <td>3.11</td> <td>3.07</td> <td>2.30</td> <td>-</td> <td>3.67</td> <td>3.07</td> <td>2.30</td> <td>-</td> <td>-</td> <td>-</td> <td>-</td>	3.11	3.07	2.30	-	3.67	3.07	2.30	-	-	-	-
	1	2.69	2.66	2.24	-	3.06	2.66	2.24	-	-	-	-	-
		2	2.47	2.45	2.06	-	2.81	2.45	2.06	-	-	-	-
	3	2.31	2.30	1.93	-	2.63	2.30	1.93	-	-	-	-	-
		4 <td>2.22</td> <td>2.19</td> <td>1.84</td> <td>-</td> <td>2.52</td> <td>2.19</td> <td>1.84</td> <td>-</td> <td>-</td> <td>-</td> <td>-</td>	2.22	2.19	1.84	-	2.52	2.19	1.84	-	-	-	-
	5	2.15	2.13	1.79	-	2.44	2.13	1.79	-	-	-	-	-
		1 <td>2.06</td> <td>2.03</td> <td>1.96</td> <td>-</td> <td>2.29</td> <td>2.03</td> <td>1.96</td> <td>-</td> <td>-</td> <td>-</td> <td>-</td>	2.06	2.03	1.96	-	2.29	2.03	1.96	-	-	-	-
	2	1.89	1.88	1.81	-	2.11	1.88	1.81	-	-	-	-	-
		3 <td>1.77</td> <td>1.75</td> <td>1.70</td> <td>-</td> <td>1.97</td> <td>1.75</td> <td>1.70</td> <td>-</td> <td>-</td> <td>-</td> <td>-</td>	1.77	1.75	1.70	-	1.97	1.75	1.70	-	-	-	-
	4	1.70	1.68	1.62	-	1.89	1.68	1.62	-	-	-	-	-
		5 <td>1.65</td> <td>1.62</td> <td>1.57</td> <td>-</td> <td>1.83</td> <td>1.62</td> <td>1.57</td> <td>-</td> <td>-</td> <td>-</td> <td>-</td>	1.65	1.62	1.57	-	1.83	1.62	1.57	-	-	-	-
		Proposed method (Equation 5)	NAD	BSS268: Part 2	BSS268: Part 3	Proposed method (Equation 5)	NAD	BSS268: Part 2	BSS268: Part 3	Proposed method (Equation 5)	NAD	BSS268: Part 2	BSS268: Part 3

Table 7: Comparison of safety factors of “Design by Testing” with existing factors given in national standards for particleboard (EN312-4 & -5), OSB (EN300, Grades 2) and Fiberboard (EN622-5, hardboard).



Load-durations		No of tests		Fiberboards (EN622-3, medium boards and hardboards)																	
		Service Class 1					Service Class 2					Service Class 3									
Permanent	1	8.74	-	-	-	-	-	-	-	-	-	-	-	-	-	-	-	-	-	-	
	2	8.03	-	-	-	-	-	-	-	-	-	-	-	-	-	-	-	-	-	-	
	3	7.52	-	-	-	-	-	-	-	-	-	-	-	-	-	-	-	-	-	-	
	4	7.21	-	-	-	-	-	-	-	-	-	-	-	-	-	-	-	-	-	-	
	5	6.99	-	-	-	-	-	-	-	-	-	-	-	-	-	-	-	-	-	-	
Long-term	1	4.37	4.28	3.06	-	-	4.28	3.06	-	-	4.28	3.06	-	-	-	-	-	-	-	-	
	2	4.02	3.94	2.82	-	-	3.94	2.82	-	-	3.94	2.82	-	-	-	-	-	-	-	-	
	3	3.76	3.70	2.65	-	-	3.70	2.65	-	-	3.70	2.65	-	-	-	-	-	-	-	-	
	4	3.60	3.52	2.52	-	-	3.52	2.52	-	-	3.52	2.52	-	-	-	-	-	-	-	-	
	5	3.50	3.42	2.45	-	-	3.42	2.45	-	-	3.42	2.45	-	-	-	-	-	-	-	-	
Medium-term	1	2.91	2.58	2.33	-	-	2.58	2.33	-	-	2.58	2.33	-	-	-	-	-	-	-	-	
	2	2.68	2.62	2.14	-	-	2.62	2.14	-	-	2.62	2.14	-	-	-	-	-	-	-	-	
	3	2.51	2.47	2.01	-	-	2.47	2.01	-	-	2.47	2.01	-	-	-	-	-	-	-	-	
	4	2.40	2.35	1.92	-	-	2.35	1.92	-	-	2.35	1.92	-	-	-	-	-	-	-	-	
	5	2.33	2.28	1.86	-	-	2.28	1.86	-	-	2.28	1.86	-	-	-	-	-	-	-	-	
Short term	1	2.18	2.14	2.01	-	-	2.14	2.01	-	-	2.14	2.01	-	-	-	-	-	-	-	-	
	2	2.01	1.96	1.85	-	-	1.96	1.85	-	-	1.96	1.85	-	-	-	-	-	-	-	-	
	3	1.88	1.84	1.74	-	-	1.84	1.74	-	-	1.84	1.74	-	-	-	-	-	-	-	-	
	4	1.80	1.77	1.66	-	-	1.77	1.66	-	-	1.77	1.66	-	-	-	-	-	-	-	-	
	5	1.75	1.71	1.61	-	-	1.71	1.61	-	-	1.71	1.61	-	-	-	-	-	-	-	-	
		Proposed method (Equation 5)	NAD	BS5268: Part 2	BS5268: Part 3	Proposed method (Equation 5)	NAD	BS5268: Part 2	BS5268: Part 3	Proposed method (Equation 5)	NAD	BS5268: Part 2	BS5268: Part 3	Proposed method (Equation 5)	NAD	BS5268: Part 2	BS5268: Part 3	Proposed method (Equation 5)	NAD	BS5268: Part 2	BS5268: Part 3

Table 8: Comparison of safety factors of “Design by Testing” with existing factors given in national standards for Fiberboards (EN622-3, medium-boards and hardboards).

**INTERNATIONAL COUNCIL FOR RESEARCH AND INNOVATION  
IN BUILDING AND CONSTRUCTION**

**WORKING COMMISSION W18 - TIMBER STRUCTURES**

**ACTUAL POSSIBILITIES OF THE MACHINE GRADING OF TIMBER**

K Frühwald

Joanneum Research, Judenburg

AUSTRIA

A Bernasconi

BFH Hamburg

GERMANY

**MEETING THIRTY-TWO**

**GRAZ**

**AUSTRIA**

**AUGUST 1999**

---

Presenter: K.Frühwald

- H.J.Larsen pointed out that the detection of failure location would not be critical in machine stress grading. He also questioned whether the machine performance or machine settings in the different machines were responsible for the poor performance.
- K.Frühwald responded that the machine manufacturers would need to provide the answer.
- R.Görlacher pointed out that some of the machine used has settings for glulam laminates not structural timber. The issue of edgewise and flatwise application was not considered with these machines.
- G.Schickhofer responded that tensile tests were also performed.
- F.Rouger pointed out that the new version of CEN519 is better than the old version and output of machine is important.

# Actual possibilities of the machine grading of timber

K. Frühwald (Joanneum Research, Judenburg), Dr. A. Bernasconi (BFH Hamburg)

## 1 Introduction

In the Austrian and German sawmilling and wood construction industry structural timber is visually graded according to DIN 4074. But visual grading only allows a prediction of the very wide variation of mechanical properties within a piece of lumber or between several pieces. The dimensioning values including relative high safety factors have to be established to reach the lowest strength and stiffness values, which can not be realized by visual grading. Therefore of that only a limited utilisation of the potential timber properties is possible. Additionally visual grading only fulfils partly existing requirements of quality control. Generally the competition between wood and other material in the structural building sector puts structural lumber under high technical and economical pressure. This requires more efficient utilisation of the technical possibilities of timber which is only possible with a reliable prediction of the mechanical properties of timber. This is one reason why research and the industry have been engaged in the further development and practical utilisation of machine strength grading.

The aim of the study “Actual possibilities of machine grading of timber” is the comparison of the various technologies for strength grading for timber in Europe. The efficiency of grading is described as

- a) yield in each strength class and
- b) their mechanical properties which have to meet the requirements of the international EN- or national DIN-standards.

## 2 Material tested

For this study standard spruce timber in two dimensions was purchased from a big sawmill in Germany. The timber was planed and dried to 12 % m.c.:

- 223 lamellas for gluelam-production with 38x150x4000 mm<sup>3</sup> and
- 301 flexural beams for timber-frame construction with 46x114x3000 mm<sup>3</sup>.

## 3 Grading methods

All boards and beams were normally graded on six different grading machines according to the rules and requirements of the machines and the daily use in the timber industry:

- **Steinkamp** and **Sylvatest** determining the dynamic MOE from the speed of ultrasonic waves longitudinal through the piece of timber,
- **Grademaster** determining the dynamic MOE from the resonance frequency of the piece of timber and the density and visible knots by scanning technique,
- **Cook-Bolinder** and **Computermatic** as bending machines,
- **Eurogrecomat** as bending machine with x-ray detection of density and knots.

Finally a **visual grading** of all boards **according to DIN 4074** was performed.

## 4 Determination of the mechanical properties

The grading and classification of timber (c.f. the requirements of the EN 519 and DIN 4074) is based on the determination of the critical section of the board (where failure is expected to occur). The testing and determination of the mechanical properties – bending a tensile strength and stiffness (as MOE) – have to be done at this critical section of the board. Therefore the grading system must be able to determine the weakest section of the piece of timber (see chapter 5.1).

After the mechanical and visual grading the **mechanical properties** of each piece was tested according to DIN EN 408:

- Tensile MOR and MOE were determined for the gluelam-lamellas on the full length (free testing length of about 3 m), which allows an exact determination of the weakest section of the board (over the length of 3 m).
- Bending MOR and MOE were determined for the flexural beams in an universal testing machine (bending at four points according to EN 408 and EN 384<sup>1</sup>).

The **density** of the timber was determined from the mass and the volume of the whole piece of timber.

## 5 Results

In the following, the names of the various machine grading systems are not visibly linked with the results. For the various machines only A, B, C, D, E, F is used which reflects not the sequence described in chapter 3.

### 5.1 Critical section

The determination of the critical section is required in EN 384, EN 519 resp. DIN 4074.

Depending on the grading system different methods to determine this weakest section are used, such as lowest bending stiffness (Computermatic, Cook-Bolinder and Eurogrecomat) or knot dimension (Grademaster). Some grading systems – e.g. the grading based on speed of ultrasonic waves longitudinal through the timber piece – cannot predict the critical section and therefore do not meet the requirements of the EN or DIN standards for strength grading.

The predicted critical section of the board often differs with the different grading machines. The tension test for the gluelam-lamellas determines the critical section best, which means that this is the section of ultimate lowest strength in the board. A comparison can be made of the distance between the ultimate lowest (tension test) and the predicted critical section predicted by the various machines.

Generally, if the distance would be high in general terms, the requirement of prediction of the critical section can be questioned.

---

<sup>1</sup> The tested section was positioned, that most of the critical sections of the different grading machines lay between the inner load points (see chapter 5.1).

Fig. 1 shows the frequency of the distance between actual failure and predicted critical section for the four machines which can predict the critical section. Only 40-50 % of the results are within 500 mm and only 55-70 % are within 1000 mm.

**Fig. 1:** *Frequency curve: Distance of the machine determined critical section from the actual failure section of the glulam-lamellas*

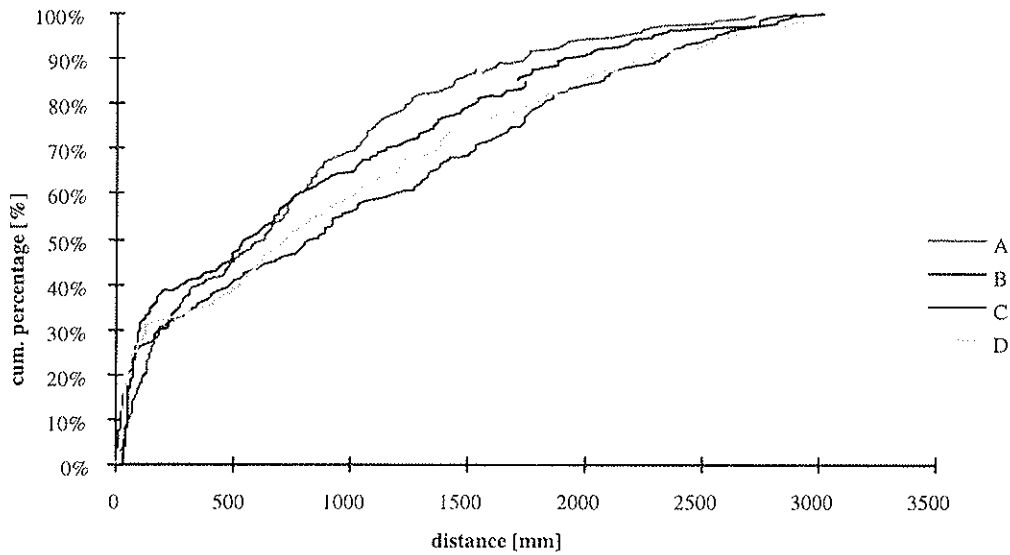
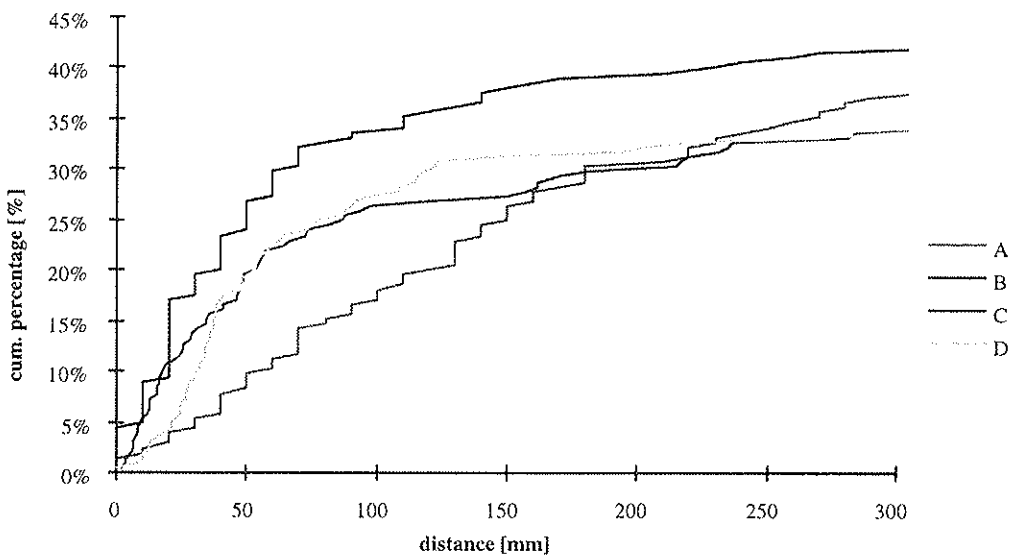


Fig. 2 shows more in detail the frequency for the first 300 mm. As it can be seen the machines show very different results. For 100 mm it varies between 17 and 34 %, for 200 mm between 30 and 39 %.

**Fig. 2:** *Detail of the frequency curve in Fig. 11: Max. 300 mm distance of the machine determined critical section from the actual failure section of the glulam-lamellas*



## 5.2 Yield in strength classes

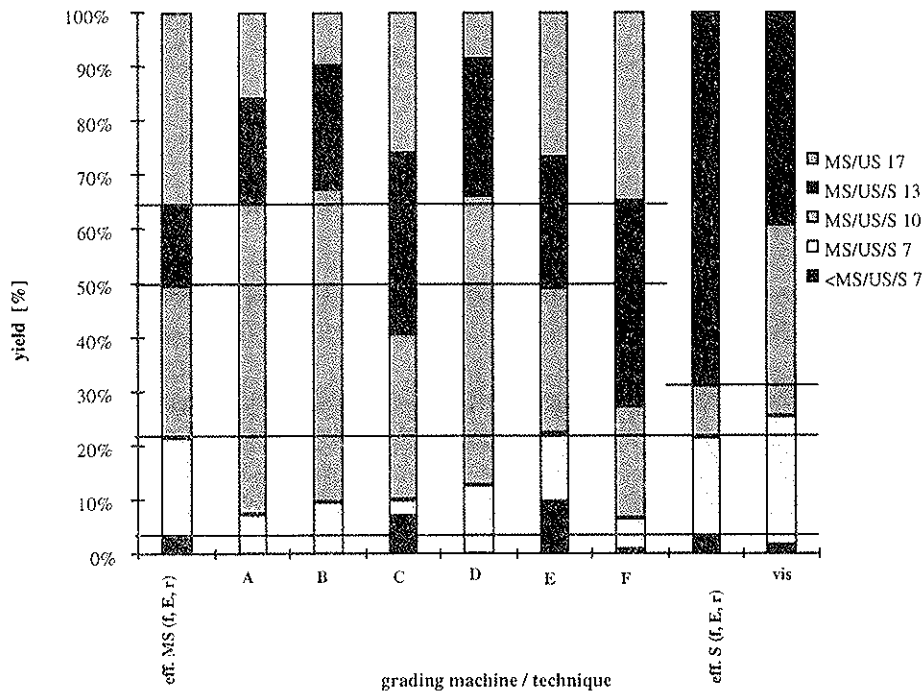
From the results of the tension test (tension MOR, MOE, density) the boards could be attributed to “strength classes”. The same could be obtained for the bending test. These strength classes are called “(pot.) MS” for the machine grading and “(pot.) S” for the visual grading respectively. The yield gained in the various classes (<MS7 – MS17), (<S7-S13) from the machines A-F and the visual grading can be compared with the pot. MS and pot. S results:

Tab. 1 shows this comparison for the gluelam-lamellas. Fig. 3 shows the result in an diagram. The pot. MS resp. the pot. S is quite different from the yield of the visual grading (“vis”) and the different grading machines (“A-F”):

*Tab. 1: Comparison of the machine resp. visual obtained yield with the potential yield for gluelam-lamellas*

strength class	pot. MS	A	B	C	D	E	F	pot. S	vis
<MS/US/S <sup>2</sup> 7	3%	0%	0%	7%	0%	10%	1%	3%	1%
MS/US/S 7	18%	7%	10%	3%	13%	13%	5%	18%	24%
MS/US/S 10	28%	58%	58%	31%	53%	27%	21%	10%	35%
MS/US/S 13	15%	19%	23%	33%	25%	24%	37%	69%	39%
MS/US 17	36%	16%	10%	26%	9%	27%	35%	-	-
MS/US/S 13 + MS/US 17	51%	35%	33%	59%	34%	51%	72%	69%	39%

*Fig. 3: Comparison of the machine resp. visual obtained yield with the potential yield for gluelam-lamellas (see also Tab. 1)*



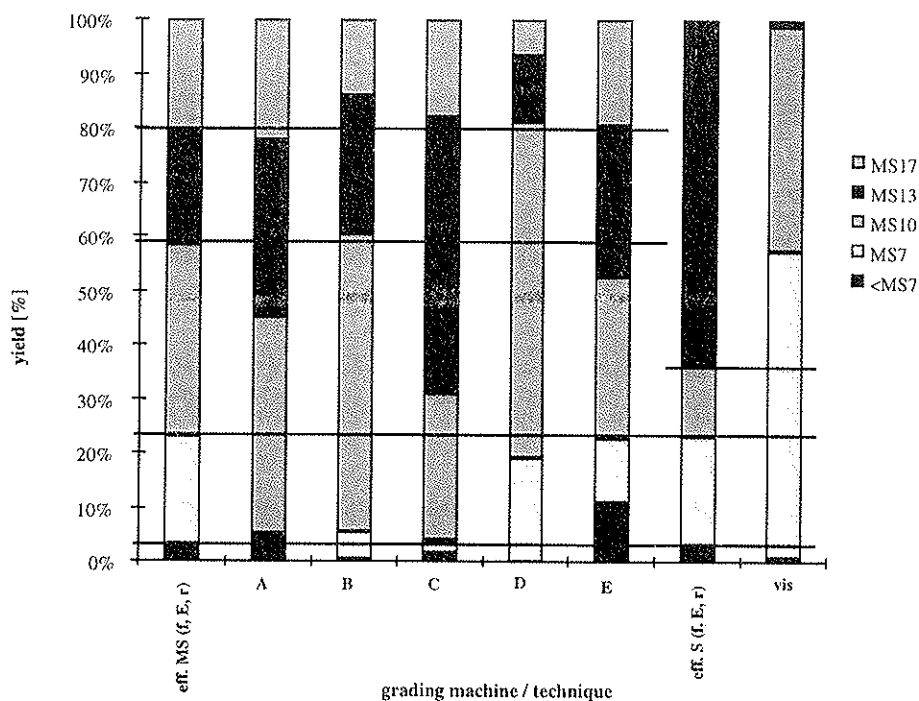
<sup>2</sup> In the following only the term „MS“ is used for a strength class: “MS” substitutes “US” resp. “S”.

Tab. 2 shows the comparison of the yield for the beams tested for bending strength. Fig. 4 gives the comparisons in a diagram.

**Tab. 2:** Comparison of the machine resp. visual obtained yield with the potential yield for construction timber for bending

strength class	pot. MS	A	B	C	D	E	pot. S	vis
<MS7	3%	0%	0%	2%	0%	11%	3%	1%
MS7	20%	5%	5%	2%	19%	12%	20%	57%
MS10	35%	40%	55%	27%	62%	30%	13%	42%
MS13	21%	33%	26%	51%	12%	28%	64%	1%
MS17	21%	22%	14%	18%	7%	20%	-	-
MS13 + MS17	42%	55%	40%	69%	19%	48%	64%	1%

**Fig. 4:** Comparison of the machine resp. visual obtained yield with the potential yield for construction timber for bending (see also Tab. 2)



The effective mechanical properties of each strength class were calculated for each grading machine:

- 5-percentile of the tensile- resp. bending-MOR and density and
- mean characteristic value of the tensile- resp. bending-MOE.

These were compared with the requirements of the EN and DIN standards.

The required values for strength, stiffness and density (EN 338) are mostly not achieved.

### 5.3 5-percentile of the MOR

Tab. 3 shows a comparison between achieved and required (EN 338) values for gluelam-lamellas, fig. 5 shows the absolute deviation. Tab. 4 and fig. 6 contains similar information for the beams bending tested.

Tab. 3: Deviation of the  $f_{t,0,05}$  of the gluelam-lamellas from the requirements of EN 338

$f_{t,0,05}$ [N/mm <sup>2</sup> ]									
strength class	EN 338	A	B	C	D	E	F	EN 338	vis
<MS 7				(10,1)		10,1			7,3
MS 7	10	(10,1)	10,1		10,2	11,5	9,9	10	10,4
MS 10	14	13,1	13,1	12,1	13,1	13,0	10,9	14	15,9
MS 13	21	20,6	22,2	17,1	21,4	18,1	13,9	18	19,0
MS 17	24	23,8	22,7	22,5	(21,6)	22,6	18,9		

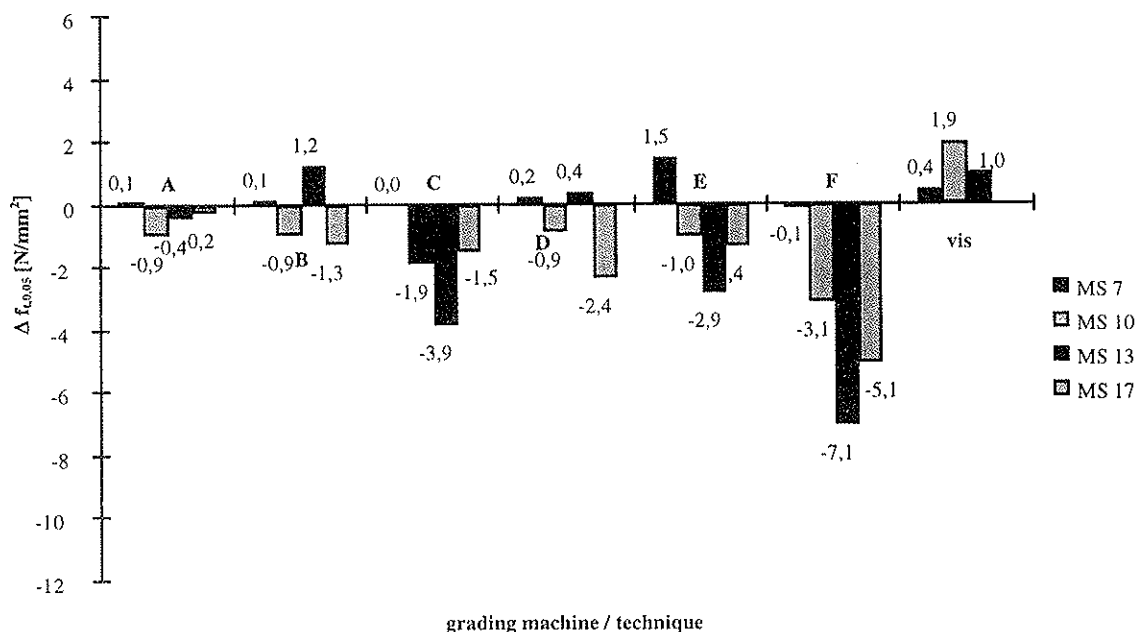
Absolute deviation [N/mm <sup>2</sup> ]								
strength class	A	B	C	D	E	F		vis
MS 7	(0,1)	0,1		0,2	1,5	-0,1		0,4
MS 10	-0,9	-0,9	-1,9	-0,9	-1,0	-3,1		1,9
MS 13	-0,4	1,2	-3,9	0,4	-2,9	-7,1		1,0
MS 17	-0,2	-1,3	-1,5	(-2,4)	-1,4	-5,1		

Relative deviation [%, basic is the required $f_{t,0,05}$ in EN 338]								
strength class	A	B	C	D	E	F		vis
MS 7	(1%)	1%		2%	15%	-1%		4%
MS 10	-7%	-7%	-14%	-6%	-7%	-22%		14%
MS 13	-2%	6%	-18%	2%	-14%	-34%		6%
MS 17	-1%	-5%	-6%	(-10%)	-6%	-21%		

(The values in brackets are based upon less than 20 boards in each strength class in contrary to the requirements in EN 338.)

Fig. 5: Absolute deviation of the  $f_{t,0,05}$  of the gluelam-lamellas from the required  $f_{t,0,05}$  in EN 338 [N/mm<sup>2</sup>]

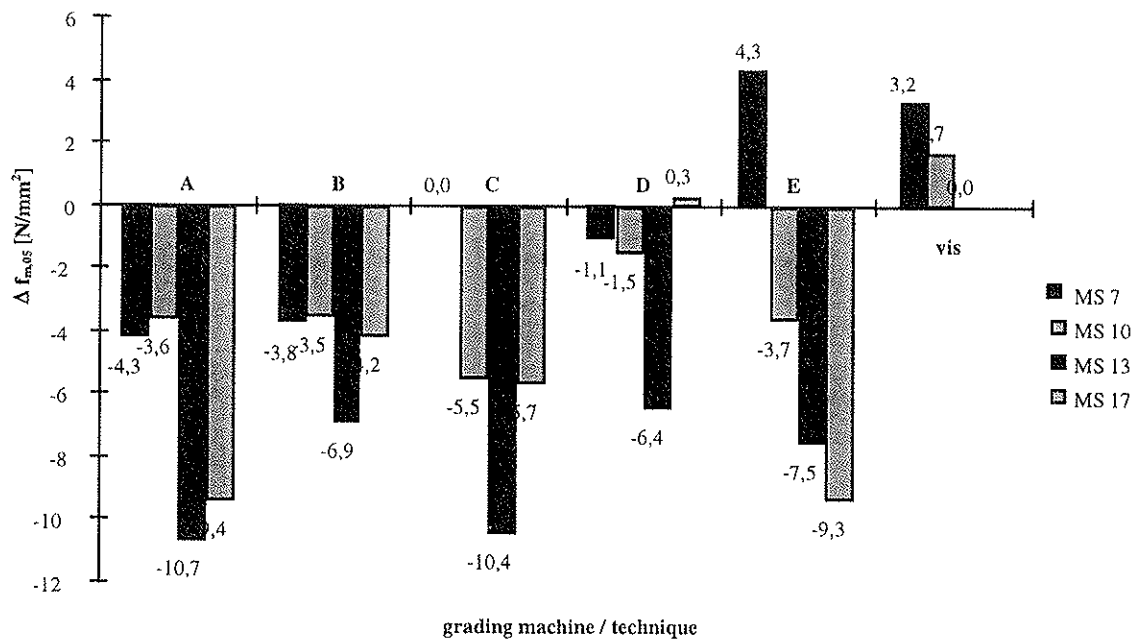




Tab. 4: Deviation of the  $f_{m,05}$  of the construction timber for bending from the requirements of EN 338

$f_{m,05}$ [N/mm <sup>2</sup> ]								
strength class	EN 338	A	B	C	D	E	EN 338	vis
<MS 7						12,2		
MS 7	16	(11,7)	(12,2)		14,9	20,3	16	19,2
MS 10	24	20,4	20,5	18,5	22,5	20,3	24	25,7
MS 13	35	24,3	28,1	24,6	28,6	27,5	30	
MS 17	40	30,6	35,8	34,3	40,3	30,7		
Absolute deviation [N/mm <sup>2</sup> ]								
strength class		A	B	C	D	E		vis
MS 7		(-4,3)	(-3,8)		-1,1	4,3		3,2
MS 10		-3,6	-3,5	-5,5	-1,5	-3,7		1,7
MS 13		-10,7	-6,9	-10,4	-6,4	-7,5		
MS 17		-9,4	-4,2	-5,7	0,3	-9,3		
Relative deviation [%, basic is the required $f_{m,05}$ in EN 338]								
strength class		A	B	C	D	E		vis
MS 7		(-27%)	(-24%)		-7%	27%		20%
MS 10		-15%	-15%	-23%	-6%	-15%		7%
MS 13		-31%	-20%	-30%	-18%	-21%		
MS 17		-24%	-11%	-14%	1%	-23%		

Fig. 6: Absolute deviation of the  $f_{m,05}$  of the construction timber for bending from the required  $f_{m,05}$  in EN 338 [N/mm<sup>2</sup>]



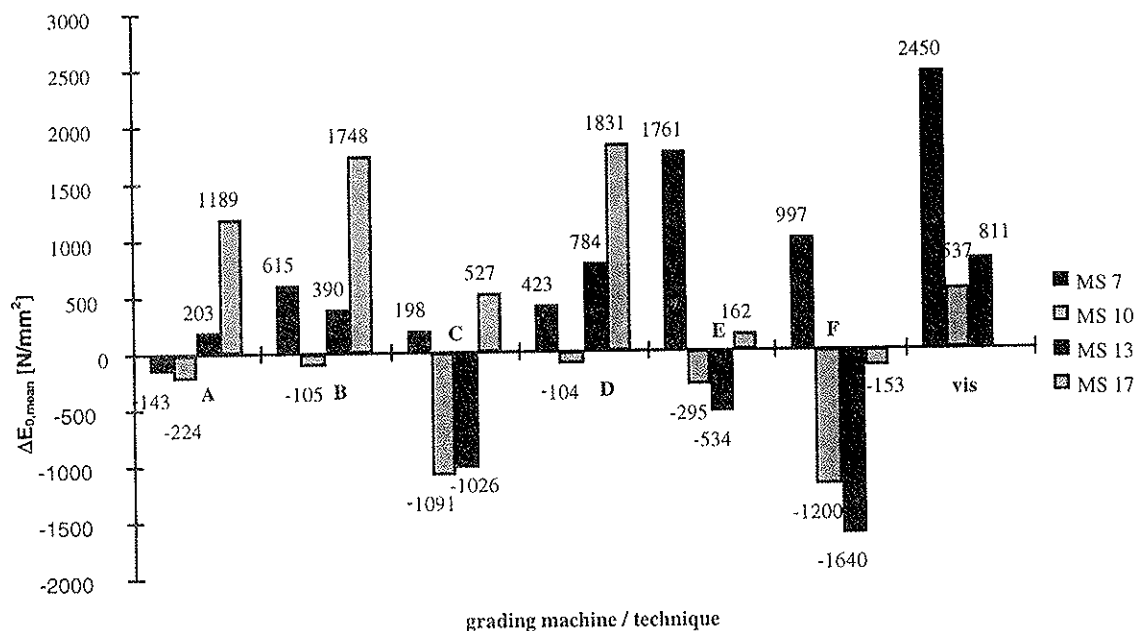
## 5.4 Mean characteristic value for MOE

EN 338 requires mean characteristic values for MOE. The results from destructive testing are attributed to the strength classes determined by the machines and visual grading. In Tab. 5 and fig. 7 and tab. 6 and fig. 8 the difference between requirement in EN 338 and the achievements are compared.

**Tab. 5:** Deviation of the  $E_{0, mean}$  of the gluelam-lamellas from the requirements of EN 338

$E_{0, mean}$ [ $N/mm^2$ ]								
strength class	EN 338	A	B	C	D	E	F	EN 338 vis
<MS 7				(9743)		8615	(6585)	(8549)
MS 7	8000	(7857)	8615	(8198)	8423	9761	(8997)	8000 10450
MS 10	11000	10776	10895	9909	10896	10705	9800	11000 11537
MS 13	13000	13203	13390	11974	13784	12466	11360	12000 12811
MS 17	14000	15189	15748	14527	(15831)	14162	13847	
Absolute deviation [ $N/mm^2$ ]								
strength class		A	B	C	D	E	F	vis
MS 7		(-143)	615	(198)	423	1761	(997)	2450
MS 10		-224	-105	-1091	-104	-295	-1200	537
MS 13		203	390	-1026	784	-534	-1640	811
MS 17		1189	1748	527	(1831)	162	-153	
Relative deviation [%, basic is the required $E_{0, mean}$ in EN 338]								
strength class		A	B	C	D	E	F	vis
MS 7		(-2%)	8%	2%	5%	22%	(12%)	31%
MS 10		-2%	-1%	-10%	-1%	-3%	-11%	5%
MS 13		2%	3%	-8%	6%	-4%	-13%	7%
MS 17		8%	12%	4%	(13%)	1%	-1%	

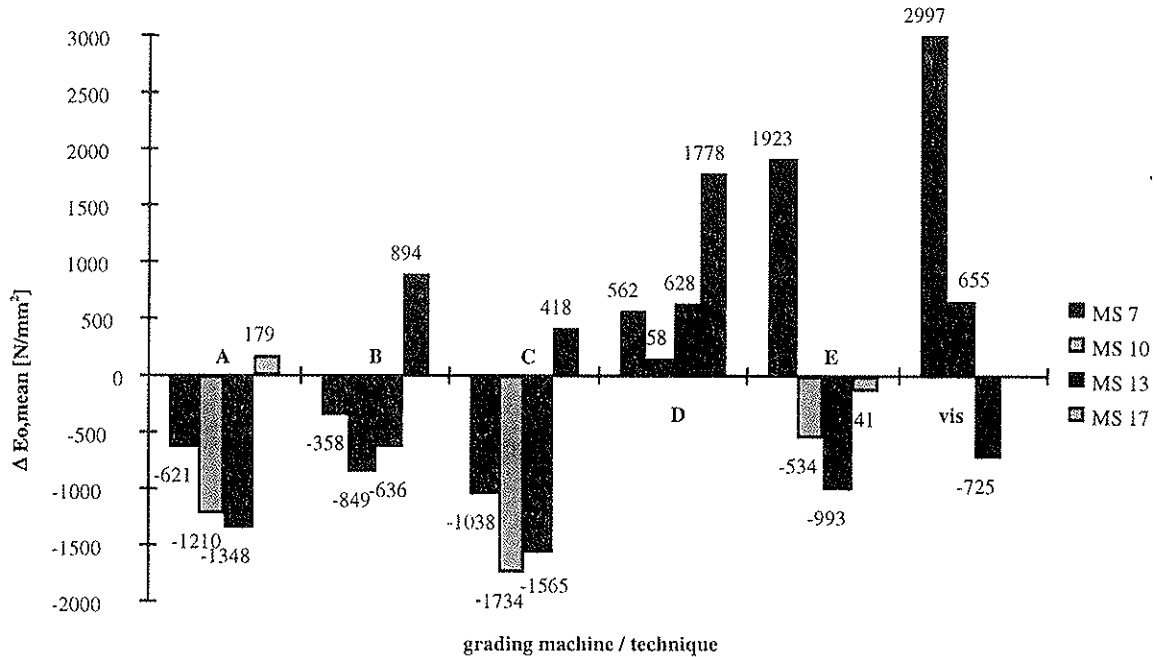
**Fig. 7:** Absolute deviation of the  $E_{0, mean}$  of the gluelam-lamellas from the required  $E_{0, mean}$  in EN 338 [ $N/mm^2$ ]



Tab. 6: Deviation of the  $E_{0,mean}$  of the construction timber for bending from the requirements of EN 338

$E_{0,mean}$ [N/mm <sup>2</sup> ]								
strength class	EN 338	A	B	C	D	E	EN 338	vis
<MS 7		**	**	(10652)		8351		(8933)
MS 7	8000	(7379)	(7642)	(6962)	8562	9923	8000	10997
MS 10	11000	9790	10151	9266	11158	10466	11000	11655
MS 13	13000	11652	12364	11435	13628	12007	12000	(11275)
MS 17	14000	14179	14894	14418	15778	13859		
Absolute deviation [N/mm <sup>2</sup> ]								
strength class		A	B	C	D	E		vis
MS 7		(-621)	(-358)	(-1038)	562	1923		2997
MS 10		-1210	-849	-1734	158	-534		655
MS 13		-1348	-636	-1565	628	-993		(-725)
MS 17		179	894	418	1778	-141		
Relative deviation [%, basic is the required $E_{0,mean}$ in EN 338]								
strength class		A	B	C	D	E		vis
MS 7		(-8%)	(-4%)	(-13%)	7%	24%		37%
MS 10		-11%	-8%	-16%	1%	-5%		6%
MS 13		-10%	-5%	-12%	5%	-8%		(-6%)
MS 17		1%	6%	3%	13%	-1%		

Fig. 8: Absolute deviation of the  $E_{0,mean}$  of the construction timber for bending from the required  $E_{0,mean}$  in EN 338 [N/mm<sup>2</sup>]



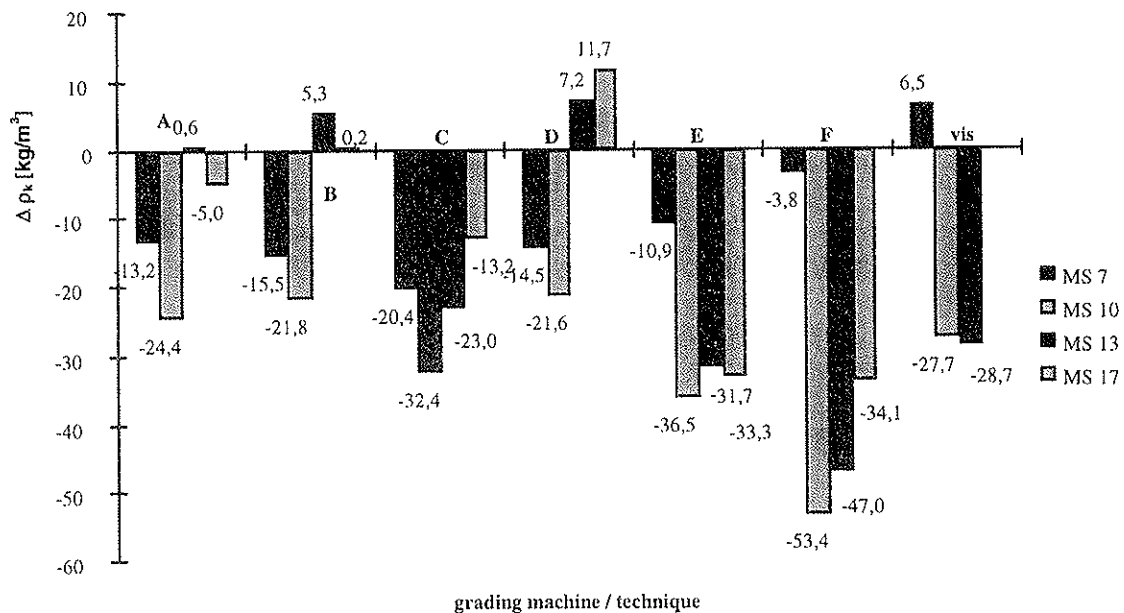
## 5.5 Characteristic value of the density

The importance of the density on the grading of timber has to be discussed:

Tab. 7: Deviation of the  $\rho_k$  of the gluelam-lamellas from the requirements of the German NAD

$\rho_k$ [kg/m <sup>3</sup> ]									
strength class	German NAD	A	B	C	D	E	F	German NAD	vis
<MS 7				(339,8)		333,9	(379,4)		(374,2)
MS 7	350	(336,8)	334,5	(329,6)	335,5	339,1	(346,2)	350	356,5
MS 10	380	355,6	358,2	347,6	358,4	343,5	326,6	380	352,3
MS 13	400	400,6	405,3	377,0	407,2	368,3	353,0	380	351,3
MS 17	420	415,0	420,2	406,8	(431,7)	386,7	385,9		
Absolute deviation [kg/m <sup>3</sup> ]									
strength class		A	B	C	D	E	F		vis
MS 7		(-13,2)	-15,5	(-20,4)	-14,5	-10,9	-3,8		6,5
MS 10		-24,4	-21,8	-32,4	-21,6	-36,5	-53,4		-27,7
MS 13		0,6	5,3	-23,0	7,2	-31,7	-47,0		-28,7
MS 17		-5,0	0,2	-13,2	(11,7)	-33,3	-34,1		
Relative deviation [%, basic is the required $\rho_k$ in the German NAD]									
strength class		A	B	C	D	E	F		vis
MS 7		(-4%)	-4%	(-6%)	-4%	-3%	-1%		2%
MS 10		-6%	-6%	-9%	-6%	-10%	-14%		-7%
MS 13		0%	1%	-6%	2%	-8%	-12%		-8%
MS 17		-1%	0%	-3%	(3%)	-8%	-8%		

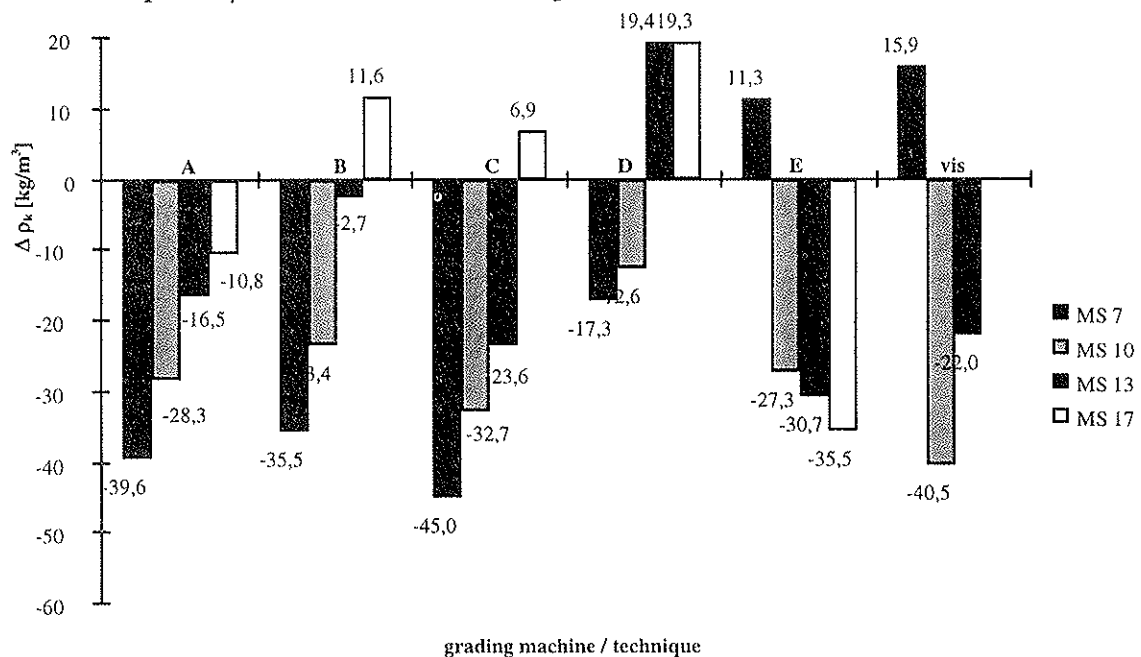
Fig. 9: Absolute deviation of the  $\rho_k$  of the gluelam-lamellas from the required  $\rho_k$  in the German NAD [kg/m<sup>3</sup>]



Tab. 8: Deviation of the  $\rho_k$  of the construction timber for bending from the requirements of the German NAD

$\rho_k$ [kg/m <sup>3</sup> ]								
strength class	German NAD	A	B	C	D	E	German NAD	vis
<MS 7		**	**	(373,8)		330,1		(425,0)
MS 7	350	(310,4)	(314,5)	(305,0)	332,7	361,3	350	365,9
MS 10	380	351,7	356,6	347,3	367,4	352,7	380	339,5
MS 13	400	383,5	397,3	376,4	419,4	369,3	380	(358,0)
MS 17	420	409,2	431,6	426,9	439,3	384,5		
Absolute deviation [kg/m <sup>3</sup> ]								
strength class	German NAD	A	B	C	D	E	German NAD	vis
MS 7		(-39,6)	(-35,5)	(-45,0)	-17,3	11,3		15,9
MS 10		-28,3	-23,4	-32,7	-12,6	-27,3		-40,5
MS 13		-16,5	-2,7	-23,6	19,4	-30,7		(-22,0)
MS 17		-10,8	11,6	6,9	19,3	-35,5		
Relative deviation [%, basic is the required $\rho_k$ in the German NAD]								
strength class	German NAD	A	B	C	D	E	German NAD	vis
MS 7		(-11%)	(-10%)	(-13%)	-5%	3%		5%
MS 10		-7%	-6%	-9%	-3%	-7%		-11%
MS 13		-4%	-1%	-6%	5%	-8%		(-6%)
MS 17		-3%	3%	2%	5%	-8%		

Fig. 10: Absolute deviation of the  $\rho_k$  of the construction timber for bending from the required  $\rho_k$  in the German NAD [kg/m<sup>3</sup>]



## 5.6 Comparison of the machine determined and the potential strength class

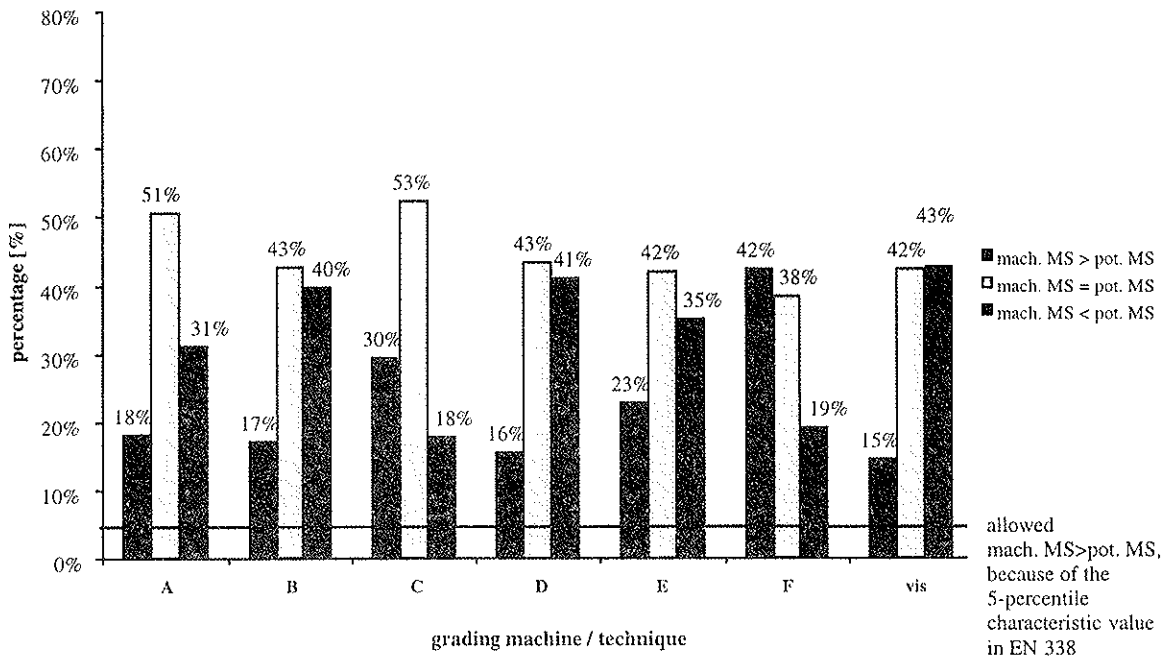
Tab. 9: Comparison of the machine resp. visual determined strength class and the potential strength class from the tension test of the gluelam-lamella

deviation by		quantity [boards]							percentage [%]						
		A	B	C	D	E	F	vis	A	B	C	D	E	F	vis
mach. > pot.	+3 classes	0	0	0	0	3	5	3	0	0	0	0	1	2	1
	+2 classes	4	3	4	3	11	27	15	2	1	2	1	5	12	7
	+1 class	36	35	61	31	36	61	14	16	16	28	14	16	28	6
mach. = pot.		111	94	115	95	92	84	93	51	43	53	43	42	38	42
mach. < pot.	-1 class	54	72	31	75	58	40	66	25	33	14	34	26	18	30
	-2 classes	14	15	4	14	15	2	27	6	7	2	6	7	1	12
	-3 classes	0	0	2	1	3	0	1	0	0	1	0	1	0	0
	-4 classes	0	0	2	0	1	0	0	0	0	1	0	0	0	0
total		219	219	219	219	219	219	219	100	100	100	100	100	100	100

deviation by		quantity [boards]							percentage [%]						
		A	B	C	D	E	F	vis	A	B	C	D	E	F	vis
mach. > pot.		40	38	65	34	50	93	32	18	17	30	16	23	42	15
mach. = pot.		111	94	115	95	92	84	93	51	43	53	43	42	38	42
mach. < pot.		68	87	39	90	77	42	94	31	40	18	41	35	19	43
total		219	219	219	219	219	219	219	100	100	100	100	100	100	100

Fig. 11: Comparison of the machine resp. visual determined strength class and the potential strength class from the tension test of the gluelam-lamella (cf. Tab 7.)

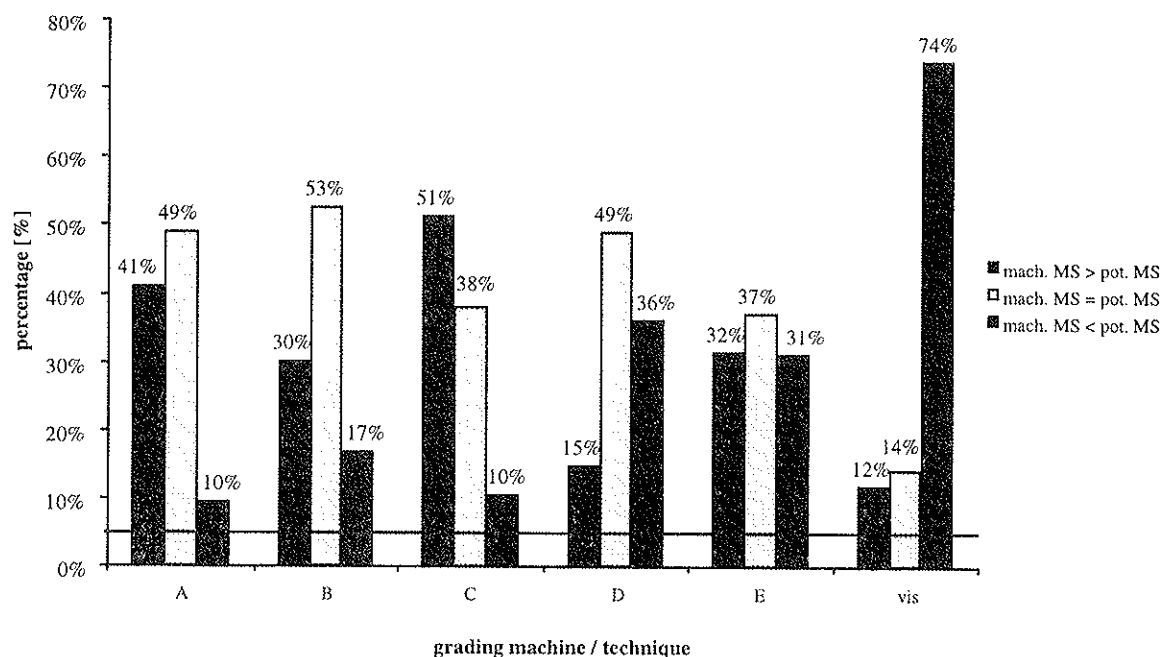


**Tab. 10:** Comparison of the machine resp. visual determined strength class and the potential strength class from the bending test of the construction timber for bending

deviation by		quantity [boards]						percentage [%]					
		A	B	C	D	E	vis	A	B	C	D	E	vis
mach. > pot.	+4 classes	0	0	0	0	1	0	0	0	0	0	0	0
	+3 classes	0	0	0	0	1	0	0	0	0	0	0	0
	+2 classes	17	4	20	0	16	5	6	1	7	0	5	2
	+1 class	105	86	132	44	76	30	35	29	45	15	26	10
mach. = pot.		146	157	113	145	110	42	49	53	38	49	37	14
mach. < pot.	-1 class	25	42	25	83	68	119	8	14	8	28	23	40
	-2 classes	4	8	4	23	19	101	1	3	1	8	6	34
	-3 classes	0	0	2	1	6	0	0	0	1	0	2	0
	-4 classes	0	0	0	0	0	0	0	0	0	0	0	0
total		297	297	296	296	297	297	100	100	100	100	100	100

deviation by		quantity [boards]						percentage [%]					
		A	B	C	D	E	vis	A	B	C	D	E	vis
mach. > pot.		122	90	152	44	94	35	41	30	51	15	32	12
mach. = pot.		146	157	113	145	110	42	49	53	38	49	37	14
mach. < pot.		29	50	31	107	93	220	10	17	10	36	31	74
total		297	297	296	296	297	297	100	100	100	100	100	100

**Fig. 12:** Comparison of the machine resp. visual determined strength class and the potential strength class from the bending test of the construction timber for bending (cf. Tab. 8)



## 5.7 Conclusions

The possibilities of visual and machine grading can not be estimated by the yield in the strength classes. That requires a correct grading in the different strength classes. Therefore according to EN 338 all “characteristic values of bending strength, density and mean modulus of elasticity (...) (have to be) greater or equal to the values” of the given strength class.

**Tab. 11:** Approximate limits of the different criteria's

	detection of the critical cross section with a maximum tolerance of 10 cm	achieved yield in MS13 + MS17 is	The achieved yield is compared to the potential yield in MS13+MS17
++ very good		very high >65 %	about the same about -9...+9 %
+ good		high 41...65 %	lower <sup>1)</sup> about -10...-29 %
o moderate	>30 % of the boards	moderate 31...40 %	much lower <sup>1)</sup> about ≥-30 %
- poor	20...30 % of the boards	poor 16...30 %	higher about +10...+29 %
-- very poor	<20 % of the boards	very poor ≤15 %	

	the determined characteristic values of the different grading systems are below the required characteristic values of EN 338 resp. the German NAD	machine derived strength class is higher than the potential strength class at
++ very good	extreme little ≤-2 %	
+ good	very little ≤-5 % (for ρ: ≤-6 %)	
o moderate	little ≤-10 %	≤20 % of the boards
- poor	big ≤-20 %	20...40 % of the boards
-- very poor	extreme big >-20 %	>40 % of the boards

<sup>1)</sup> The machine determined yield is lower than the effective yield. This is not “bad” in regard to the safety, but in regard to the profitability of the grading machine. For the potential strength of the timber is not fully used.

**Tab. 12:** Summary of the visual grading and machine grading (gluelam-lamellas)

	A	B	C	D	E	F	vis
<b>detection of the critical cross-section</b>	--	o	-	-	*1)	*1)	*2)
dispersion of the strength-values in one strength class	o	+	++	+	+	o	--
separation of the different strength classes in regard to strength	o	+	+	+	-	o	-
<b>yield in MS13+MS17</b>	<b>o</b>	<b>o</b>	<b>+</b>	<b>o</b>	<b>+</b>	<b>++</b>	<b>o</b>
achieved yield compared to the potential yield in MS13+MS17	+	+	++	+	++	-	o
<b>f<sub>t,0,05</sub></b>	<b>o</b>	<b>o</b>	-	<b>o</b>	-	--	<b>++</b>
E <sub>0,mean</sub>	++	++	-	++	+	-	++
ρ <sub>k</sub>	+	+	o	+	o	-	o
<b>machine derived strength class compared to the potential strength class</b>	<b>o</b>	<b>o</b>	-	<b>o</b>	-	--	<b>o</b>

<sup>1)</sup> The grading system can not detect the critical cross section.

<sup>2)</sup> The critical cross section can be detected by visual grading, but this was not done systematically in this project.



**Tab. 13:** Summary of the visual grading and machine (construction timber in bending)

	A	B	C	D	E	vis
dispersion of the strength-values in one strength class	o	o	o	-	-	--
separation of the different strength classes in regard to strength	o	o	o	o	-	--
<b>yield in MS13+MS17</b>	<b>+</b>	<b>+</b>	<b>++</b>	<b>-</b>	<b>+</b>	<b>--</b>
achieved yield compared to the potential yield in MS13+MS17	-	++	-	+	++	o
$f_{t,0,05}$	--	--	--	-	--	++
$E_{0,mean}$	-	o	-	++	o	o
$\rho_k$	-	o	-	+	o	-
<b>machine derived strength class compared to the potential strength class</b>	<b>--</b>	<b>-</b>	<b>--</b>	<b>o</b>	<b>-</b>	<b>o</b>

**None** of the tested grading systems **fulfils all** in EN 338 resp. the German NAD **required characteristic values**.

The **quality of the tested grading systems** (i.e. the fulfilment of the required characteristic values and a least possible classification of the boards in a higher strength class than the potential strength class) **depends less on the actual quality of the grading** (the quality of separation of the different strength classes and the dispersion of the single strength values in a strength class), **but it depends on the yield in the higher strength classes MS13 + MS17**.

**The higher the machine or visual determined yield in MS13 + MS17, the lower are the characteristic values (above all the strength), and the boards are graded in a higher strength class than the correct strength class according to the tensile resp. bending tests.**

The rules for grading and classification of timber should be discussed based on the results of the timber properties in the different strength classes and compared with the requirements of the standards (EN 338 + NAD, DIN 4074 and DIN 1052).

*What would have been the results, if all grading machines produced the same yield in the different strength classes?*

**INTERNATIONAL COUNCIL FOR RESEARCH AND INNOVATION  
IN BUILDING AND CONSTRUCTION**

**WORKING COMMISSION W18 - TIMBER STRUCTURES**

**DETECTION OF SEVERE TIMBER DEFECTS BY MACHINE GRADING**

A Bernasconi  
BFH Hamburg

B Schacht  
Universität Hamburg  
GERMANY

L Boström  
SP Borås  
SWEDEN

**MEETING THIRTY-TWO**

**GRAZ**

**AUSTRIA**

**AUGUST 1999**

---

Presenter: A. Bernasconi

- F. Rouger discussed the intent to create distribution of grades.
- A. Bernasconi stated that it would be a possible safety concern if severe defects were missed.
- P. Quenneville questioned whether any of the defects were more problematic.
- A. Bernasconi responded prebroken specimen.
- S. Thelandersson pointed out that this study clearly confirmed the general misconception that the tails of MSR timber strength distributions were truncated.
- M. Ansell stated that image analysis might be used for grain deviation detection.

# Detection of severe timber defects by machine grading

Dr. A. Bernasconi, BFH Hamburg, Germany

Dr. L. Boström, SP Borås, Sweden

Dipl.-Holzwirtin B. Schacht, Universität Hamburg, Germany

## 1. Introduction

The grading of timber in strength classes by machine-grading systems is influenced by the detection of different characteristics or defects of a piece of timber. Typical characteristics are knots, their position and dimension, fibre deviation, bending stiffness, density variation. The prediction of the strength of the timber - as the most important characteristic in grading - is mostly derived from measurements of other parameters, such as the determination of deflection, the determination of the bending force necessary to achieve a deflection, (ultrasonic) wave propagation time, x-ray technique or the determination of vibration frequency.

Different systems of grading machines supply reliable results for normal timber characteristics and are currently used. The setup of the grading system is the result of many experimental tests and is usually given by a correlation between directly measured parameters and the expected strength of each piece of timber. The basis of the determination of this correlation is the high variation of the wood characteristic, because the grading system should be able to grade each piece of timber by given conditions: for example spruce with defined dimension of the cross section and moisture content. But it is still unknown, whether the grading machines are able to detect severe defects and determine correctly the mechanical properties of the tested timber, in order to assure a proper classification of the timber.

The objective of this project was to test the ability of different grading machines to detect significant timber defects. For this three groups of spruce timber specimens with particular characteristics was first graded by different grading machines and later tested by loading to determine the effective strength and stiffness. The specimens were picked out of the regular production of a sawmill by visual means regarding that the defects were "well fitting". In fact the specimens were rejected in the sawmills by more or less accurate visual grading. Thus, it has to be stated that the total number of chosen samples are not representative and could not be compared with standard timber graded in a sawmill.

## **2. Timber specimens - investigated defects**

### **2.1 Principles**

It was first decided to use natural timber defects for testing and not man-made defects, as the influence of man-made defects on the strength of the timber does not give information about the ability to detect important natural defects by machine grading. Three different kinds of defects were tested. The common property was derived from the fact that each defect was not simple to detect and would have an important influence on the ultimate strength of the timber.

### **2.2 Grain deviation**

Grain deviations have a higher influence on the ultimate strength of timber. Grain deviations are caused e.g. by big knots or by growth that is not straight (e.g. juvenile wood). In this test, only severe grain deviation was considered. Specimens with severe grain deviation, rejected by first visual control in the sawmill, were picked out for grading and testing. The chosen samples were grown in the southern part of Sweden.

### **2.3 Slip planes**

Slip planes appear as compression failures in a part of the cross section and are mostly caused by high loads from storm, inadequate handling or transportation. The very small damaged area in the longitudinal direction and the fact that only a compression failure occurs make the detection of the damage very difficult. By planing the surfaces, it is possible to detect some slip planes by visual inspection, but only the bigger damages can be detected. Practically it is possible to detect some slip planes in logs, as reinforcements are built up by forming tissue in the concerned zone after a storm damage. If the damage is caused by the handling of the log, it is very hard to detect it visually before the surfaces are planed.

Slip plane damages are mechanically caused compression failures. In this way the timber is partially or completely broken in the damaged zone. This fracture reduces the tension strength of the timber in a particular section, but normally it does not affect the compression strength.

Timber with slip planes was selected from the rejected production of a sawmill in the region of Zurich, Switzerland. The sawmill uses a quality control system to detect timber with slip planes based on rigorous visual observation of each surface by optimized lighting. The detected timber with slip planes is rejected after the ultrasonic wave grading and before finger-jointing.

### **2.4 Pre-broken timber**

Pre-broken timber was tested only in one part of the project. The test elements were loaded in a bending testing equipment up to the first clearly "audible" crack. Immediately after unloading, it was not possible in most cases to determine the broken zone visually, because only a part of the cross section was broken and the timber pieces did not show plastic deformations.

Timber pieces were fractured in this way to be graded by the different machines and to be tested up to ultimate bending capacity later.

### **3. Machine-grading systems**

It was the intention of the present work to test the ability of common grading systems to detect severe timber defects, so that commonly used grading equipment was required for the grading procedure. The decision on the different grading machines was determined by the availability of the grading machines in mills or in research laboratories.

Due to the fact that the bending tests were carried out at the SP in Borås and in order to reduce shipping costs, grading was carried out with the following grading machines. The complete machine grading data for each piece of timber was stored on a personal computer for all of the grading machines.

#### **3.1 Cook-Bolinder**

The Cook-Bolinder is one of the oldest grading machines. The working principle is based on the determination of the bending stiffness by measuring the bending load required to achieve a predetermined deformation. The results of the machine measurements are based on flatwise bending stiffness of the timber. The measurements were carried out twice by rotating the test specimen at 180 degrees to prevent the influence of timber curvature. The average of the two measurements indicates the definitive values of the stiffness.

Based on a predetermined statistical regression between resistance and stiffness, it is possible to grade each specimen into a class of resistance; the weakest section being the lowest stiffness along the longitudinal axis.

Grading tests were carried out with the Cook-Bolinder machine at the laboratory of the SP in Borås.

#### **3.2 Computermatic**

The Computermatic grading machine is based on the same principle as the Cook-Bolinder, but it measures bending deflection with a given bending load. The curvature of the test specimens is determined by direct measurement, and it is considered when calculating the stiffness.

The determination of the resistance class of the specimens is also based on a predefined correlation between machine values and resistance.

These grading tests, as well, were carried out with the Computermatic machine at the laboratory of the SP in Borås.

### **3.3 Eurogrecomat**

The Eurogrecomat is a German grading machine based on continuous measurement of the bending stiffness along the longitudinal axis. Additional parameters for grading are density, knots position and knot size (diameter) by x-ray.

The machine is calibrated in order to grade timber in different classes and automatically determines the class for each piece of timber. The Eurogrecomat grading was done in a Swedish sawmill and ordered the timber in the resistance classes C18 and C30.

### **3.4 Dynagrade**

The grading by the Dynagrade equipment is based on the measurement of vibrations and determination of the vibration frequency of the timber. Vibration frequency of the timber was precisely determined by a microphone; specimen length was determined by a laser measurement system. The test result was the indicated property (IP) for the grading and the decision on rejection or acceptance, graded in class C18 or C24.

## **4. Tested material**

Planed spruce timber specimens (4000 x 150 x 45 mm) and planed surfaces were tested. Timber samples with grain deviations and slip planes were picked out from the rejected timber at two sawmills. The timber tested was kiln dried at a moisture content of 12 %.

In the total, 159 samples were graded and tested: 98 showed severe grain deviation, 22 sample were pre-broken and 39 were slip plane samples.

## **5. Determination of the mechanical properties**

After grading on the four different machine grading systems, the mechanical properties of each timber were determined by bending tests. Four point bending tests were carried out to EN 408. For each sample, maximum load and the curvature in the middle part of the beam were measured; finally MOR and MOE were calculated.

Exact dimension of each timber, density and moisture were determined, as well.

The bending tests, as well, were done at the testing laboratory of the SP in Borås.

Due to very low mechanical properties of some timber samples tested, some of the results from the bending test could not be used for the final discussion. In some tests, the bending failure was outside of the middle part of the bent beam (failure between load and support) so that the measured maximum force and the calculated bending strength were not considered in the discussion. In some cases, the timber sample could not be tested correctly, because the investigated defect was near to the end of the beam, and it was not possible to test the defect zone in the middle part of the element.

Therefore, in all cases of possible uncertainty the tested beam was eliminated. Thus, only a part of the results could be considered in the final discussion, as shown in the following table.

	Number of tested elements	Samples considered in the discussion
Timber with slip planes	39	27
Pre-broken timber	22	19
Grain deviation	98	75
Total	159	121

**Table 1:** Number of tested samples and of specimens considered in the discussion

## 6. Results

### 6.1. Grading into strength classes

The timber was graded by Dynagrade in the classes C18 and C24 and by Eurogrecomat in the classes C18 and C30. For a comparative discussion of the classification of the different grading systems, the results of each grading procedure were completed with the limits for all the three grading classes (C18, C24 and C30). For this, a linear distribution between the indicating property from the grading machine and the resistance class was assumed. This is not an impeccable method, but it allows a direct comparison of the different grading systems and gives some indications on the more or less accurate detection of the timber defects investigated.

### 6.2 Slip planes

In the most cases slip planes were not recognized by the grading systems. The failure occurs very brittle, and it seems that there is no correspondence between the dimensions of the slip planes and the measured MOE. The details of the results of the "misgraded" timber are summarized in the table 2.

Specimen	Bending strength	Cook-Bolinder	Computer-matic	Dynagrade	Euro-grecomat
Unit	N/mm <sup>2</sup>	Grading classes			
C03	29.3	C24	C24	C24	*C30
C04	25.5	C24	*C30	*C30	*C30
C06	19.0	*C30	*C30	*C30	*C30
C07	24.7	*C30	*C30	*C30	*C30
C09	21.9	*C30	*C30	*C30	*C30
C10	23.4	*C30	*C30	*C30	*C30
C12	12.2	*C24	*C24	*C30	*C30
C14	15.8	*C30	*C30	*C30	*C30
C16	17.2	*C24	*C24	*C30	*C30
C18	17.8	*C24	*C24	*C30	*C30

C20	29.4	*C30	*C30	*C30	*C30
C21	24.6	*C30	*C30	*C30	*C30
C25	13.6	*C30	*C30	*C24	*C30
C33	21.9	C18	C18	*C24	C18
C34	24.4	*C30	*C30	C24	C24
Number of "misgraded" elements		12	13	13	13
In % of 27 samples		44 %	48 %	48 %	48 %

**Table 2:** "Misgraded" timber samples with slip planes - results from each grading system and bending strength: asterised values (\*) did not meet the requirement

### 6.3. Grain deviation

The results of timber samples with grain deviations show considerable differences depending on the grading systems. "Misgraded" samples are summarized in table 3.

Specimen	Bending strength	Cook-Bolinder	Computer-matic	Dynagrade	Euro-grecomat
Unit	N/mm <sup>2</sup>	Grading classes			
S02	16.8	*C30	*C30	*C18	*C24
S03	18.0	*C24	C18	C18	
S10	21.7	*C30	*C24	R	*C24
S15	25.3	*C30	C24	C18	C24
S16	26.2	*C30	*C30	C18	C24
S24	23.9	*C30	*C24	C18	*C30
S25	19.2	*C24	*C24	R	C18
S26	11.6	*C18	R	R	R
S27	20.9	*C24	*C24	C18	C18
S28	22.8	*C30	*C30	*C24	*C30
S32	22.3	*C30	*C30	*C30	*C30
S38	15.4	*C30	*C30	R	R
S40	18.1	*C24	C18	R	R
S42	14.7	*C24	*C24	*C18	*C24
S44	16.1	*C24	*C18	R	*C18
S49	27.7	*C30	C24	R	*C30
S51	28.8	*C30	*C30	C18	C24
S54	13.2	*C30	*C30	*C18	*C30
S59	13.1	*C24	*C18	R	*C18
S62	28.7	*C30	*C30	C18	*C30
S66	21.2	*C24	*C24	C18	*C24
S76	28.3	*C30	*C30	C24	*C30
S82	23.7	*C24	C18	R	*C24
S86	28.6	*C30	*C30	C24	*C30
S87	17.2	*C24	*C18	R	*C18
S90	16.3	*C30	*C30	R	*C30



S92	29.2	*C30	*C30	C18	*C30
S98	29.1	*C30	*C30	C18	*C30
Number of misgraded elements		28	22	5	19
In % of 75		37 %	29 %	7 %	25 %

**Table 3:** "Misgraded" timber samples with grain deviation - results from each grading system and bending strength values

## 6.4 Pre-broken timber

The number of investigated samples in the group of "pre-broken timber" was very small; the results merely indicate the detection of the defect by the grading procedure. Grading was carried out only with the Cook-Bolinder and the Computermatic, as the timber samples were not finished at the time of the grading in the mills. But the low number of results, nevertheless, indicates some interesting observations, as shown in table 4.

Specimen	Bending strength	Cook-Bolinder	Computer-matic
Unit	N/mm <sup>2</sup>	Grading classes	
B01	1.6	*C30	*C30
B11	12.3	*C30	*C30
B12	8.5	*C24	*C30
B22	3.8	R	*C18
B28	22.7	*C30	*C30
Number of "misgraded" elements		4	5
In % of 22		21 %	26 %

**Table 4:** "Misgraded" pre-broken timber samples - results from two grading systems and bending strength values

The timber samples were pre-broken before machine-grading, and the ultimate bending resistance in the bending test - after grading - was very small, as summarized in table 4. It is interesting to notice that grading by measuring the flatwise bending stiffness classified some samples as C30, although the edgewise bending resistance was considerably low.

## 7. Conclusions and discussion

### 7.1 Global overview

An overview on the results of the different grading systems is given in table 5.

	Number of elements	Number of "misgraded" samples							
		Cook-Bolinder		Computer-matic		Dynagrade		Eurogrecomat	
		n	%	n	%	n	%	n	%
Slip planes	27	12	44	13	48	13	48	13	48
Broken timber	19	4	21	5	21	-	-	-	-
Grain deviation	75	28	37	22	37	5	7	19	25
Total	121 (102)	44	36	40	33	18	18	32	31

**Table 5:** "Misgraded" elements by defect and grading systems

It seems very difficult for the selected grading systems to recognize the types of severe timber defects indicated. Cook-Bolinder and Computermatic are working on the same principle (measurement of the bending stiffness) and show similar results and similar rates of "misgrading".

The grading was defined as "mistake", if the bending strength was smaller than the 5 % requirement (characteristic value according EN 338). Thus, it can be assumed that a successful grading was obtained if the ratio of mistakes was less than 5 %.

## 7.2. Slip planes

Detecting slip planes, the Eurogrecomat was not more advisable than the Cook-Bolinder and the Computermatic, although the Eurogrecomat disposes of a x-ray system to determine the position and the dimension of knots. It is possible that the slip planes are too small for being recognized by x-ray investigation. X-ray detects only variations of density and it seems that the variation of density caused by slip planes is too small to be detected, or probably the region of higher density is too small. A short additional investigation with the same timber material (not discussed in this paper) has confirmed that slip planes were not identified by x-ray systems like those used for luggage inspection on airports.

Grading by Dynagrade leads to the same results; probably the damage by slip planes is too small and does not influence the vibration frequency of the board.

## 7.3. Pre-broken timber

Pre-broken timber represents a very severe defect and should not appear in practical application of grading in mills. But broken timber as used by this investigation is very similar to the damage by slip planes. The extreme low values of ultimate bending resistance show that the timber was completely broken in some cases at the time it was graded as "good quality timber " (C30 for example). The small number of specimens in this investigation

does not allow representative conclusions. But it should not be forgotten that it was possible to grade broken timber as C30.

#### **7.4. Grain deviations**

Severe grain deviation is the most common timber defect in this investigation. The different grading results on the different testing systems are very important. Cook-Bolinder and Computermatic show more or less similar results. It is possible that the part of defected timber in the tested beam is shorter than the length of the measurement of the bending stiffness in the machine (support distance usually 700 to 900 mm) and for this reason, the influence on the MOE measured is too low to downgrade the sample. This leads to a number of upgrades and a high ratio of "mistakes" by the grading output.

The Eurogrecomat considers the distribution of the density and the information from the ray analysis as parameters to grade each timber sample. It is not clear if this caused better results with severe grain deviation by Eurogrecomat, but the rate of "mistakes" is smaller than for Cook-Bolinder and Computermatic (which was exclusively based on measurement of bending stiffness).

The grading by Dynagrade produces an interesting result: most defects were detected and the timber elements are correctly downgraded or rejected. It seems as if the grain deviation has a great influence on the vibration frequency. This consequently, is good to detect severe grain deviation in timber. The "mistake" rate of 7 % by the grading of 75 samples is a good result for a practical application. The requirements for resistance are normally given by 5 % values (characteristical value).

#### **7.5. Conclusions and questions**

The investigations carried out show clearly that machine-grading of timber with severe defects leads to some difficulties. Severe grain deviation is a frequent quality mark in common timber production. Severe grain deviation can be detected more or less easily by visual quality control. But machine grading should guarantee for the correct grading and should be used as substitute for the not always reliable judgement of the grading personnel. In case of the grading system investigated, only the measurement of the vibration frequency allows the detection of timber defects and gives good results for practical timber usage (required bending strength not fulfilled in up to 5 % of the samples).

Grading machines mostly work on the bending principle, so that the detection of severe grain deviation is not possible. Therefore, "mistakes" by grading seems possible.

Other investigated defects - pre-broken timber and slip planes - were very poorly detected and the result was a high percentage of "mistakes" by grading. The requirement for bending strength was not fulfilled in up to about 50 % of the investigated samples. Pre-broken timber normally should not be graded, but in case of grading pre-broken timber it should be expected that these samples will be automatically downgraded and rejected and not graded, as for example C30. Also slip planes are not so infrequently found in timber production. It was relatively simple to find sawmills, forestry agencies or timber companies offering defect timber. The reliable detection of slip planes does not seem to be possible for the investigated grading systems. Unfortunately, slip planes have an important influence on resistance values.

The chosen grading systems are practically used for the machine-grading of timber. But the use of timber with higher mechanical properties (C30 and higher) for structural purposes is possible since new codes appeared (EN 519, EN 338, EC 5, or the new DIN codes for grading and strength classes for timber). The difficulties to detect some of the timber defects can lead to a reduction of the safety of some buildings.

This work should not only end with the presentation of the results. Also questions should be asked on the requirement of grading systems, if the actual grading fulfilled the requirements on safety and if the non-detection of severe defects in timber can be accepted as normal characteristic of the grading machine. If so, it is necessary to mention the reasons related.

## 8. Bibliography

Schacht, B.: Überprüfung verschiedener Verfahren der maschinellen Schnittholzsortierung zur Erkennung ausgewählter Holzfehler. Diplomarbeit Fachbereich Biologie Universität Hamburg, 1998, 89 Seiten

Boström, L.: Machine strength grading. Swedish National Testing and Research Institute, Borås, 1994

Diebold, R.: Möglichkeiten der maschinellen Sortierung mit dem Euro-Grecomat. In: Vom Brett zum Brettschichtholz. Grazer Holzbau-Fachtagung: Sortierung und Festigkeit, 1997

Kisser, J.; Steininger, A.: Mikroskopische Veränderungen der Holzstruktur bei mechanischer Überbeanspruchung von Holz in der Faserrichtung. Holztagung 1949, Österreichische Gesellschaft für Holzforschung, Heft 2

Koch, G.; Bauch, J.; Dünisch, O.; Seehann, G.; Schmitt, U.: Sekundäre Veränderungen im Holz akut belasteter Fichten in Hochlagen des Osterzgebirges. Holz als Roh- und Werkstoff 54 (1996): 243-249

**INTERNATIONAL COUNCIL FOR RESEARCH AND INNOVATION  
IN BUILDING AND CONSTRUCTION**

**WORKING COMMISSION W18 - TIMBER STRUCTURES**

**DEVELOPMENT OF HIGH-RESISTANCE GLUED ROBINIA PRODUCTS AND  
AN ATTEMPT TO ASSIGN SUCH PRODUCTS TO THE EUROPEAN SYSTEM  
OF STRENGTH CLASSES**

G Schickhofer

Graz University of Technology

B Obermayr

Lignum Research Graz

AUSTRIA

**MEETING THIRTY-TWO**

**GRAZ**

**AUSTRIA**

**AUGUST 1999**

---

Presenter: G.Schickhofer

- H.J.Blass pointed out that the procedure to set characteristic bending strength to  $1/0.6$  of characteristic tensile strength might not be conservative because the 0.6 factor was intended to be used to conservatively convert characteristic tensile strength to characteristic bending strength and not the other way around.
- C.Mettern discussed the use of hardwood.
- A.Jorissen questioned how the quality of test material was selected.
- G.Schickhofer responded that the quality of test material was determined by the supplier.
- B.J.Yeh commented the COV seemed high.
- G.Schickhofer responded that most beams failed in the finger joints.
- A.Ceccotti informed that hardwood such as Chestnut would also be used in Italy.

## Abstract

Both national design codes and EN 338 list strength classes D30 to D70 for hardwood in addition to softwood classes C14 to C50 (according to CEN/TC124/WG2/N304). Many current papers analyse and discuss the correlations between a grading class and strength classes for softwood, generally used as structural timber - defined by wood species, origin and application. For hardwood these correlations are largely unclear. The question that arises is, what hardwoods are already used as structural timber and what hardwoods should be used to a greater extent in the construction industry? In order to find an answer it is essential that we are familiar with the performance of the relevant hardwood species such as oak, beech, ash, chestnut and robinia. Owing to the natural durability and classification of the robinia species as resistance class 1-2 according to EN 350-2, this wood species is above all very suitable for outdoor use - for example bridge building and facade elements. However, there is no knowledge concerning wood quality, grading features concerning strength and appearance, the specific determination of grading parameters and threshold values, and allocation to a suitable strength class. For this reason, the present project attempted to define applications and suitable products, based on the resistance of the robinia species, and to identify characteristic parameters for this purpose. In addition to tensile tests performed on 45 robinia boards with a cross-section of 20 / 115 mm and 46 finger joints, extensive bending tests were conducted on structural laminated timber and glued laminated timber (glulam). The tests comprised 8 series with 47 structural laminated timber beams (packs of 2, 3, 4 and 5), and 3 series with a total of 33 glulam beams (h = 160 mm and h = 300 mm). With the aid of the available material parameters, the aim is to attempt to assign the robinia wood species to a strength class and a grading range on the basis of EN 338. In addition, the application of the functional relationships of EN 1194 to robinia are examined. The results show that it is indeed conceivable - using further research results - to extend the scope of application of EN 1194 to hardwood.

## 1.0 Introduction

### Forestry aspects, scopes of use and application

The robinia originates from North America. It was introduced to Europe as an ornamental and avenue tree at the beginning of the 17th century. Today, there are a large number of regions where the species is known to grow in significant quantities. Of particular interest is Hungary, where robinia forests already account for 20% of the total forest area, representing a growing stock of about 35 million cubic metre stock. In Austria, robinia only accounts for 0.2% of the total stock, and can therefore be qualified as being insignificant for forestry purposes, and it is also for this reason that there is no forestry maintenance or the required qualities. The replacement time of the robinia tree is 31 years, but the following growth and timber defects can be observed as a result of defective care:

- arching
- forking
- irregular annual ring structure and annual ring width
- eccentric growth
- knottiness

The robinia is a ring-porous deciduous tree with a marked contrast in density between the annual rings (tendency towards tangential cracks and cutting cracks if dried quickly). The natural durability of robinia wood - durability class 1-2 (very resistant to resistant) -

guarantees that this wood is ideally suited for external applications – bridge building, facade elements. The present work will deal in particular with glued products.

## **2.0 Mechanical and physical parameter of bar-shaped robinia products for use in the building sector.**

### **2.1 Tests**

#### **2.1.1 General**

Bending and tensile tests on test specimens with dimensions appropriate to construction elements are used to determine the structurally relevant strength, rigidity and density values. The objective is to achieve an overview of the mechanical characteristics of possible robinia wood products. Given the relatively small scope of sampling, an allocation to a strength class in the European standards is only possible to a limited extent, and must be regarded with caution. On the contrary, the aim is rather to determine the strength class range for robinia and to develop possible products and to determine the scopes of application that result.

#### **2.1.2 Starting material**

Roughly 61 m<sup>3</sup> of round timber from various regions of Europe - Austria/Danube riverside meadows (21 m<sup>3</sup>), Poland, Czech Republic, Hungary (roughly 40 m<sup>3</sup>) were required for the manufacturer of bar-shaped and panel-shaped sample specimens. Cutting produced a quantity of 30.4 m<sup>3</sup> sawn timber (yield: roughly 50 %) in the form of posts, boards and veneer (6 mm).

Of this, 23 m<sup>3</sup> were required for the production of bar-shaped specimens - boards, finger joints, structural laminated timber (SLT) and glued laminated timber (glulam). The volume of the finished elements was roughly 6.5 m<sup>3</sup>. Accordingly, only roughly 28% of the sawn timber available could be used for the production of higher quality products such as SLT and glulam. The extremely high rejection rate must be ascribed to the lower quality of the round timber and the sawn timber.

The remaining quantity of sawn timber was used for the production of 3-layer and 5-layer panel elements. The investigations carried out on these elements are not the subject of the present contribution.

#### **2.1.3 Test schedule and scope of tests**

The main element of the tests on the robinia was the bending test on glued beams, both beams with vertical glued joints - structural laminated timber (SLT) - and other beams with horizontal glued joints - glued laminated timber (glulam) being investigated. In order to be able to determine the system factor (homogenisation through a number of adjoining lamellae) of the structural laminated timber, tests were made of beams in the form of packs of 2,3,4 and 5, consisting of 2 (DUO), 3 (TRIO), 4 (QUATTRO) and 5 (CINQUE) vertical lamellae. In the case of the glued laminated timber beams, 2 series of different depths (160 mm, 300 mm) were tested in order to determine the influence of different dimensions (volume influence) on the mechanical characteristics of robinia wood.

Fig. 2.1 shows an overview of the schedule and scope of the bending test.

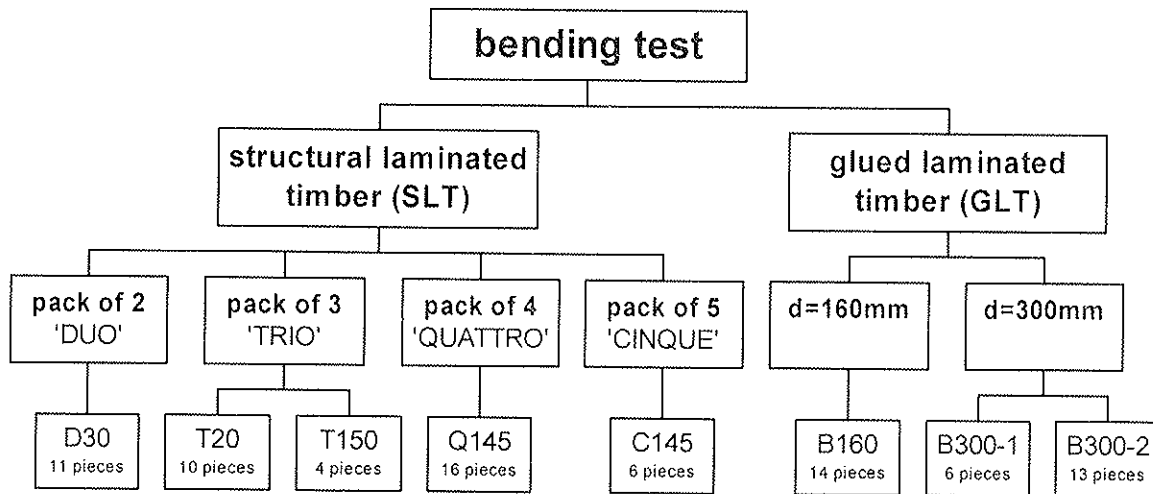


Fig. 2.1: Bending test, test schedule and scope of test

A further element of the investigations to determine the mechanical characteristics of robinia wood was the tensile test on lamellae and on finger joints.

Fig. 2.2 shows an overview of the schedule and scope of the tensile tests.

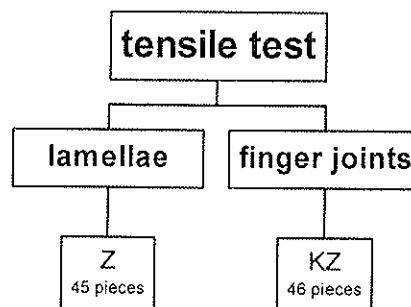


Fig. 2.2: Tensile test, test schedule and scope of test

#### 2.1.4 Test configuration and execution

The bending tests on the structural laminated timber and on the glued laminated timber beams with a depth of 160 mm were carried out at the Construction Test Institute at the Technical University of Graz under the direction of Prof. K. Kernbichler. The tensile tests on the boards and the finger joints, and the bending tests on glued laminated timber beams with a depth of 300 mm were carried out at the Institute for Wood Technology at the ETH Zurich.



## Structural laminated timber

The test configuration corresponds with the test procedure pursuant to ÖNORM EN 408, as shown in Fig. 2.3. The total length and the span  $l$  refer to a beam depth  $h$  of 150 mm. Since the actual beam depth of the test sample varied between 140 mm and 150 mm, the distance between support and application of load is not  $6h$  but  $[18 \times 150 \text{ (span)} - 6h \text{ (distance between the load application points)}]/2$ , with the values thus calculated lying within a variation range of  $\pm 1.5h$ , as specified and permitted in EN 408.

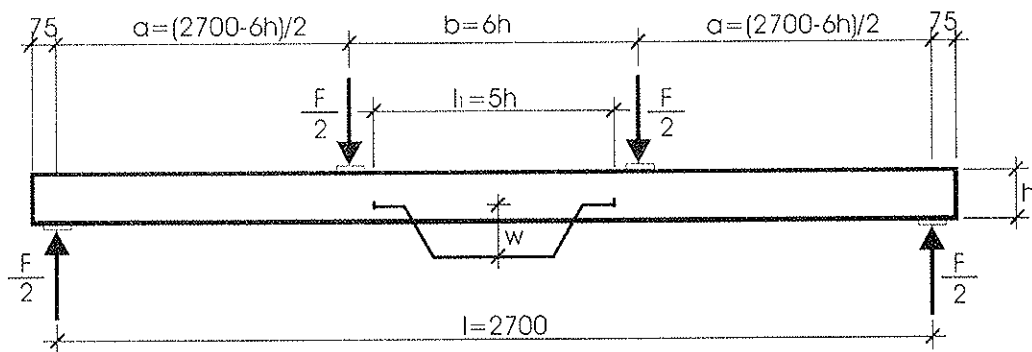


Fig. 2.3: Test procedure for bending test pursuant to ÖNORM EN 408

Table 2.1 lists the most important dimensions of the test samples for the different series.

			D30	T20	T150	Q145	C145
cross-section	b/d	[mm]	60/150	60/140	60/150	80/145	100/145
	b <sub>Lam</sub>	[mm]	30	20	20	20	20
test config.	l	[mm]	2700	2700	2700	2700	2700
	a	[mm]	900	930	900	915	915
	b	[mm]	900	840	900	870	870
	l <sub>1</sub>	[mm]	750	700	750	725	725


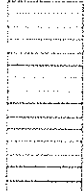

Table 2.1: Dimensions of the SLT test samples

In the course of the test, the static modulus of elasticity was measured according to ÖNORM EN 408. Having determined the modulus of elasticity, bending strength was then determined, with no interruption to the load process.

## Glued laminated timber (glulam)

As in the case of structural laminated timber, the test procedure was arranged pursuant to ÖNORM EN 408 (see Fig. 2.3).

Table 2.2 lists the most important dimensions of the test specimens for the different series.

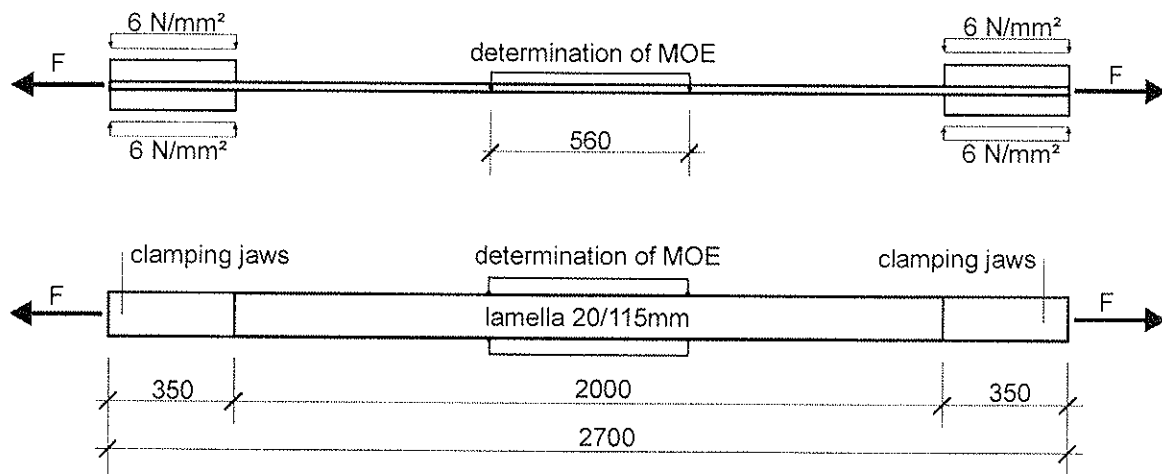
			B160	B300-1	B300-2
cross-section	b/d	[mm]	100/160	120/300	100/300
	b <sub>Lam</sub>	[mm]	20	20	20
					
test config.	l	[mm]	2880	5400	5400
	a	[mm]	960	1800	1800
	b	[mm]	960	1800	1800
	l <sub>1</sub>	[mm]	800	1500	1500

**Table 2.2:** Dimensions of the glulam test specimens

The actual course of the test - determination of the bending modulus of elasticity and determination of bending strength - is analogous to that for the structural laminated timber series.

#### Tensile tests on lamellae

Fig. 2.4 shows the test configuration for the tensile tests. The free test length is 2000 mm, corresponding to the minimum length in EN 1194 for which no length adjustment to the test result is necessary. The measurement range for the measurement of the static modulus of elasticity corresponds to 560 mm, a slight departure from the measurement length required by ÖNORM EN 408 of four times the width (575 mm). The scope of the test comprised 45 lamellae with a cross-section of 20 / 115 mm.



**Fig. 2.4:** Test procedure for the tensile tests on lamellae

In addition to dimensions, mass and timber moisture, ultrasonic speed was also recorded using the "Sylvatest" measurement instrument, in order to be able to determine the correlations to tensile strength and the static modulus of elasticity.

The test was carried out with the GEHZU 850 testing machine. Tensile strength was applied using clamping jaws in which the lamella were mounted with a pressing force of 6 N/mm<sup>2</sup>.

The static modulus of elasticity was determined by means of displacement transducers screwed onto both narrow edges of the lamella. The two measured stress-strain diagrams were used to calculate the modulus of elasticity values by means of a regression straight line for both narrow edges, and this was then used to calculate the static modulus of elasticity of the lamella as a whole as a mean value.

Once the modulus of elasticity had been determined, tensile strength was determined, without any release of the load during the two test procedures.

### **Tensile tests on finger joints**

The test procedure corresponds essentially with the test configuration for the tensile test on lamellae shown in Fig. 2.4. The differences are firstly the free test length of 200 mm and secondly the length of the clamping jaws of 300 mm. Pressing force is unchanged as compared with the tensile tests on lamellae.

The lamellae used for the finger joint investigation are identical with those used for determining tensile strength of robinia wood (cross-section 20 / 115 mm). The finger joint has a length of 15 mm (precise dimensions 15 / 3.8 / 0.3 / 0.11) and was glued with the phenol-resorcinol resin glue mixture Aerodux 185 and HRP 150 hardener.

The tests to determine tensile strength of the finger joints comprise 46 test specimens.

As with the tensile tests on lamellae, the test determined not only the dimensions, volume and wood moisture but also ultrasonic speed. The static modulus of elasticity was not determined.

The tests were carried with the GEHZU 600 tensile testing machine.

## **2.2 Test results**

### **2.2.1 General**

The test results were evaluated using the unadjusted values; this primarily means that the test results are not adjusted to the standard wood moisture content of 12%. The reason for this is that there are no known adjustment functions for robinia timber and that the application of functions for other wood types such as spruce may lead to a falsification of the test results that would be difficult to assess. By using the unadjusted measurement values for the evaluation, the influence of wood moisture content on the mechanical (strength, modulus of elasticity) and physical parameters (density) of robinia wood was not taken into account.

## 2.2.2 Tensile test on lamellae

Table 2.3 lists the results of the statistical evaluation

		scope of test	mean value	5%-fractile	COV	function
N	tensile strength [N/mm <sup>2</sup> ]	45	61,6	31,1	43,5	Lognormal
	tensile MOE [N/mm <sup>2</sup> ]	40	18380	14720	-	Weibull
	density [kg/m <sup>3</sup> ]	45	787	699	7,2	Lognormal

Comments:

In the measurement of the modulus of elasticity, a defect occurred in 5 test samples which led to unrealistic results. For this reason, these test samples are not taken into account in the statistical evaluation. This explains why the sample is smaller, 40 items instead of 45.

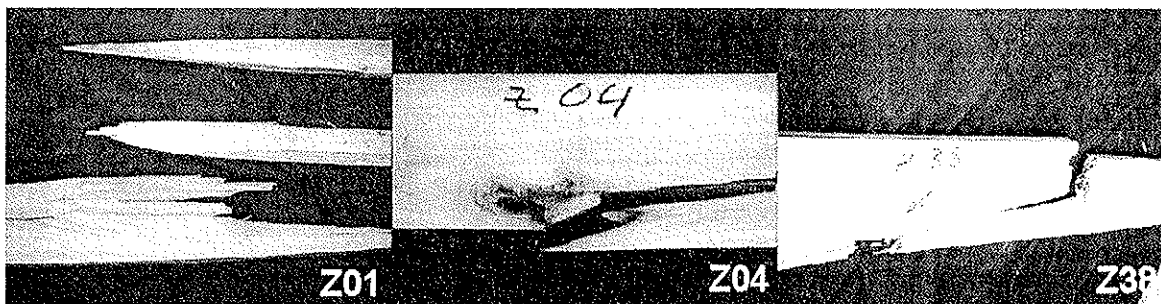
**Table 2.3:** Statistical evaluation of the tensile tests on lamellae

The evaluation reveals two points that must be particularly emphasised.

On the one hand, robinia wood has a very high tensile modulus of elasticity ( $E_{t,50} = 18380$  N/mm<sup>2</sup>) with little spread ( $COV_{Normal} = 10.1\%$ ).

Secondly, although the tensile strength achieved is considerable ( $f_{t,50} = 61.6$  N/mm<sup>2</sup>), nevertheless there is considerable spread in the test results ( $COV_{Lognormal} = 43.5\%$ ), for which reason the 5%-fractile value of 31.1 N/mm<sup>2</sup> must be regarded as rather low. The correlations also show that tensile strength only moderately correlates with other parameters such as modulus of elasticity, density or ultrasonic speed.

Both the considerable spread and the moderate correlation are due to local defects in the lamella which are the result of the non-existence of strength-relevant grading criteria for robinia wood. Fig. 2.5 shows three characteristic fractures of lamellae under tensile.



**Fig. 2.5:** Characteristic fractures of lamellae under tensile  
Angle grain/grain deviation - large individual knots - brittle fracture

The most frequent defect causing a fracture is angle grain, in many cases caused by a large branch. Knots themselves play a somewhat subordinate role, which may however be due to the fact that these were largely eliminated in the preliminary grading. Some of the lamellae suffered very brittle fracture, as shown in the fracture image of lamella Z38.

### 2.2.3 Tensile test, finger joints

Table 2.4 lists the results of the statistical evaluation.

		scope of test	mean value	5%-fractile	COV	function
KZ	tensile strength [N/mm <sup>2</sup> ]	46	53,3	27,7	29,3	Normal
	tensile MOE [N/mm <sup>2</sup> ]	46	-	-	-	-
	density [kg/m <sup>3</sup> ]	46	780	674	-	Weibull

**Table 2.4:** Statistical evaluation of the tensile tests on finger joints

Almost all test specimens failed when the finger joints were pulled apart (D-fracture). This leads to the conclusion that the joint geometry and/or the gluing quality and the production process are unsuitable for robinia wood. This also means that the tensile strength of the finger joints achieved is not satisfactory, since it is 11 % lower in comparison with that of the lamellae.

Since most of the finger joints failed through pulling apart, it is permissible to conclude that the wood quality of the series provided had no influence on the test results.

### 2.2.4 Structural laminated timber

Table 2.5 lists the results of the statistical evaluation.

		scope of test	mean value	5%-fractile	COV	function
D30	bending strength [N/mm <sup>2</sup> ]	11	44,4	34,4	13,6	Normal
	bending MOE [N/mm <sup>2</sup> ]	11	16970	14570	8,6	Normal
	density [kg/m <sup>3</sup> ]	11	750	702	4	Lognormal
T20	bending strength [N/mm <sup>2</sup> ]	10	63,1	39,5	29,1	Lognormal
	bending MOE [N/mm <sup>2</sup> ]	10	15370	13380	8,5	Lognormal
	density [kg/m <sup>3</sup> ]	10	767	740	-	Weibull
T150	bending strength [N/mm <sup>2</sup> ]	4	69,1	44,2	27,6	Lognormal
	bending MOE [N/mm <sup>2</sup> ]	4	17930	15960	7,1	Lognormal
	density [kg/m <sup>3</sup> ]	4	827	787	-	Weibull
Q145	bending strength [N/mm <sup>2</sup> ]	16	64,0	51,1	13,8	Lognormal
	bending MOE [N/mm <sup>2</sup> ]	16	17420	15770	-	Weibull
	density [kg/m <sup>3</sup> ]	16	802	750	-	Weibull
C145	bending strength [N/mm <sup>2</sup> ]	6	79,8	73,7	4,9	Lognormal
	bending MOE [N/mm <sup>2</sup> ]	6	17560	15990	5,7	Lognormal
	density [kg/m <sup>3</sup> ]	6	767	724	3,5	Lognormal

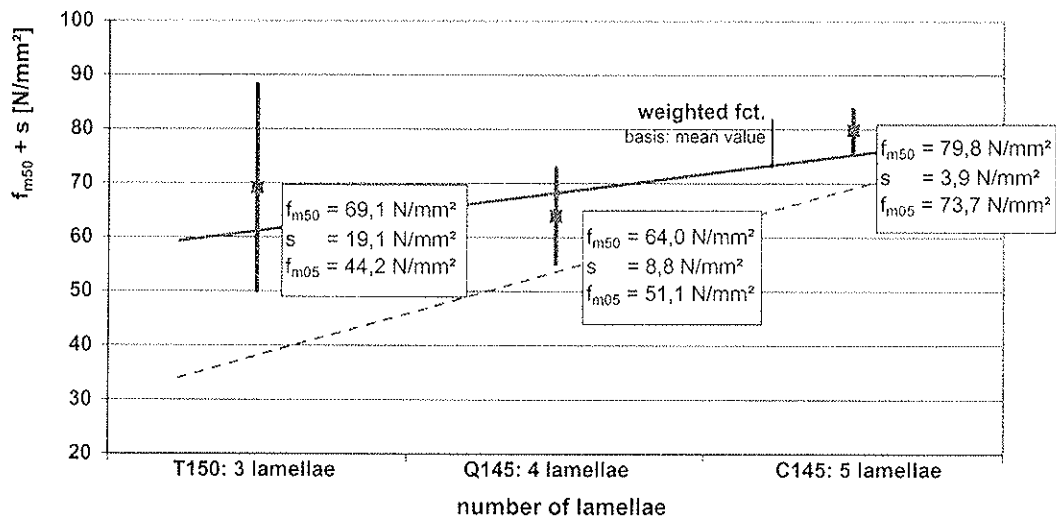
Comments:

The D30 and T20 test beams series were glued with resorcinol resin glue, which proved to be unsuitable for gluing the two series. However, production-related defects cannot be excluded. As a result of this, the test results concerning bending strength and the bending modulus of elasticity are of only limited representational character.

**Table 2.5:** Statistical evaluation of the bending tests on structural laminated timber

The structural laminated timber is marked by the fact that the vertical lamellae have a certain homogenising effect, which is greater the more lamellae are laid next to each other. This system factor can also be found in the present test series. However, thanks to the in part low size of the samples (T150 and C145), the results are of only limited informational value.

Fig. 2.6 sets out for comparison the parameters for bending strength (mean value, 5%-fractile value, standard deviation) against the number of lamellae. It shows that the spread falls strongly as the number of lamellae increases (homogenisation), while the 5%-fractile value increases. However, it should be pointed out that the values of the C145 series appear too optimistic, which may result from the small size of the sample.

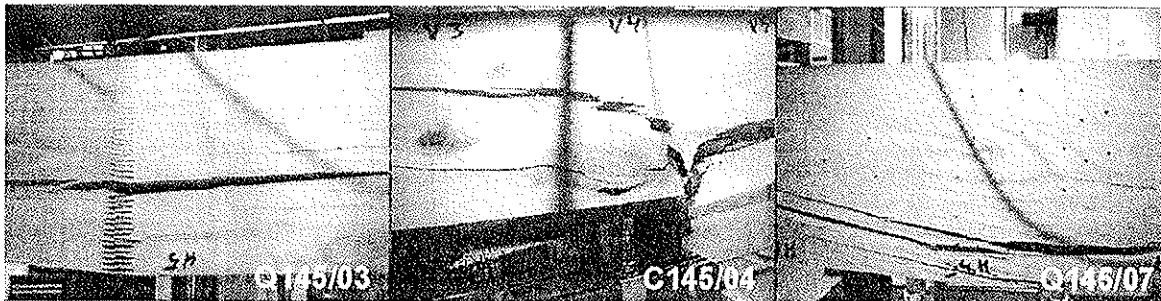


**Fig. 2.6:** Influence of the number of lamellae on bending strength of structural laminated timber

The bending tests on structural laminated timber confirm the findings from the tensile tests that the finger joints represent a significant weak point, for a large percentage of the test specimens failed when the finger joints came apart (D-fracture).

In addition to the finger joints, large knots and considerable grain deviations are the main causes of failure.

Fig. 2.7 shows examples of the three most important weak points (finger joints, large knot, grain deviation).



**Fig. 2.7:** Characteristic fractures of structural laminated timber

## 2.2.5 Glued laminated timber

In the evaluation of the bending tests on glued laminated timber beams, series B300-1 and B300-2 were also examined together as serie B300, thus allowing more precise statements concerning correlations as a result of the larger scope of the sample. The bending strength values were not adjusted on the basis of the different widths pursuant to EN 1194.

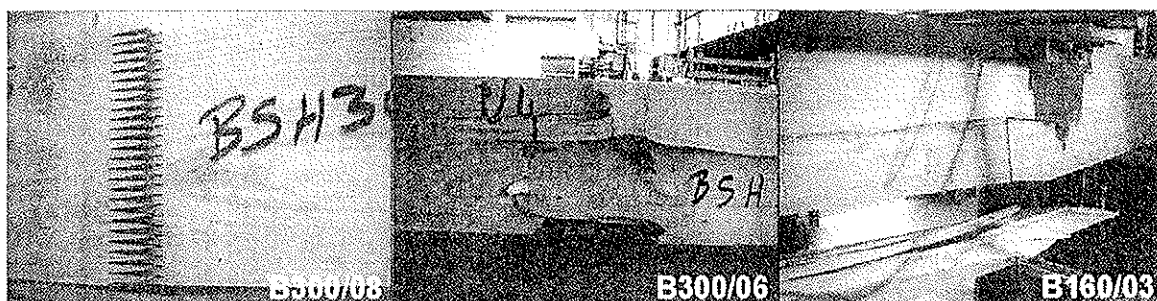
Table 2.6 lists the results of the statistical evaluation.

		scope of test	mean value	5%-fractile	COV	function
B160	bending strength [N/mm <sup>2</sup> ]	14	67,2	46,7	22,4	Lognormal
	bending MOE [N/mm <sup>2</sup> ]	14	17940	15200	-	Weibull
	density [kg/m <sup>3</sup> ]	14	783	767	1,2	Lognormal
B300-1	bending strength [N/mm <sup>2</sup> ]	6	50,2	42,9	9,7	Lognormal
	bending MOE [N/mm <sup>2</sup> ]	6	17490	16170	4,8	Lognormal
	density [kg/m <sup>3</sup> ]	6	747	732	1,2	Lognormal
B300-2	bending strength [N/mm <sup>2</sup> ]	13	60,0	38,1	-	Weibull
	bending MOE [N/mm <sup>2</sup> ]	13	18870	16750	-	Weibull
	density [kg/m <sup>3</sup> ]	13	779	761	1,5	Normal
B300	bending strength [N/mm <sup>2</sup> ]	19	55,4	40,0	20,0	Lognormal
	bending MOE [N/mm <sup>2</sup> ]	19	18490	16090	-	Weibull
	density [kg/m <sup>3</sup> ]	19	772	735	-	Weibull

**Table 2.6:** Statistical evaluation of the bending tests on glued laminated timber

The bending tests on glued laminated timber confirm the results of the tensile tests, according to which the finger joint tensile strength is too low in comparison with the tensile strength of the lamellae, for a large number of the test specimens failed in a finger joint. The fact that the majority of finger joints failed when the joint was pulled apart is a further indication that the joint geometry and the gluing require closer investigation. Additional causes for fracture are knots and angle grain, which frequently occur together. However, both are of secondary importance as compared with the failure of finger joints.

Fig. 2.8 shows three characteristic fractures of glued laminated timber beams.



**Fig. 2.8:** Characteristic fractures of glued laminated timber beams

The frequent occurrence of finger joint failure is probably also a reason why there is no relationship between bending strength and the bending modulus of elasticity.

On the basis of the different sample dimensions, it is possible to determine the influence of volume on bending strength. Thus the B160 series beams ( $d = 160$  mm) achieved a 22 % higher bending strength than the 300-2 series beams ( $d = 300$  mm). In both cases, the spread is very high (COV=20-22%), with the series B160 being marginally greater.

### 3.0 Examination of the results in the light of the standards

#### 3.1 General

In this chapter, an attempt is made to consider the test results in the light of the standards, specifically EN 338 (D-classes) and EN 1194 (glued laminated timber made of hardwood). Given the insufficient quantities within the series, it is a problem to classify robinia timber on the basis of strength based on the present results, and this issue should be regarded as a restriction of scope.

#### 3.2 EN 338: Allocation of robinia to a D-class

The bending tests on solid wood with a depth of 150 mm required for classification according to EN 338 could not be carried out, since the quality of the round timber was insufficient for the cutting of solid timber beams. Instead, structural laminated timber beams were glued.

Since the possible difference between solid timber and structural laminated timber (SLT) with respect to bending strength is not known, the bending strength of robinia wood was determined using the tensile tests and the relationship between tensile strength and bending strength specified in document CEN/TC124/WG2/N304 (EN 338) ( $f_{m,k} = f_{t,0,k}/0.6$ ).

In order to increase the information concerning the bending strength of robinia wood, it was determined using additional tensile tests on 11 lamellae with a cross-section 30 / 120 mm and a free test length of 1220 mm cited in the literature [3].

Table 3.1 lists the results of the statistical evaluation known from the literature [3].

		scope of test	mean value	5%-fractile	COV	function
<b>N</b>	tensile strength [N/mm <sup>2</sup> ]	11	83,1	36,8	34,0	-
	tensile MOE [N/mm <sup>2</sup> ]	11	18090	16090	7,0	-
	density [kg/m <sup>3</sup> ]	11	-	-	-	-

**Table 3.1:** Statistical evaluation of the tensile tests from the literature [3]

Concerning the tensile tests in [3], it should be noted that stricter grading criteria were applied, i.e. the lamellae were free of knots and relatively straight grained. Alongside the shorter test length, this is probably the main reason why the strength values are higher than those determined in the course of the present project. What is also remarkable is that the spread is very large (COV = 34%) despite the stricter classification criteria.



Given that the test dimensions differ from those in the standards, an adjustment of tensile strength values is necessary. The conversion is based on EN 1194, both with respect to the reference dimensions ( $d = 150 \text{ mm}$ ,  $l = 2000 \text{ mm}$ ) and with respect to the determination of the adjustment factor  $k_{\text{size}}$ . Table 3.2 sets out the adjustment according to EN 1194.

	number	dimensions			adjustment	tensile strength	
	n [-]	b [mm]	d [mm]	l [mm]	$k_{\text{size}}$ [-]	$f_{t,0,05,\text{unadjust}}$ [N/mm <sup>2</sup> ]	$f_{t,0,05,\text{adjust}}$ [N/mm <sup>2</sup> ]
TU Graz	45	20	115	2000	0,924	31,1	33,64
UNI Hamburg	11	30	120	1220	1,020	36,8	36,06

**Table 3.2:** Adjustment of tensile strength values to the reference dimensions in EN 1194

Using the adjusted tensile strength values, the tensile strength can be calculated backwards by means of the relationship  $f_{t,0,k} = 0.6 f_{m,k}$  to EN 338/Document CEN/TC124/WG2/N304, thus permitting allocation of robinia wood to a D-class to EN 338. Table 3.3 shows the parameters of bending strength, modulus of elasticity and density necessary for a classification, it being noted that these were determined from tensile tests, and the D-classes allocated to the parameters in question.

	bending strength $f_{m,05} = 1/0,6 * f_{t,0,05}$ [N/mm <sup>2</sup> ]	MOE $E_{0,1,50}$ [N/mm <sup>2</sup> ]	density $\rho_{1,05}$ [kg/m <sup>3</sup> ]
TU-Graz	50,47	18382	699
Uni Hamburg	57,08	18089	-
D-class	<b>D50</b>	<b>D60</b>	<b>D60</b>

**Table 3.3:** Allocation of robinia to a D-class pursuant to EN 338 based on tensile tests

Table 3.3 shows that robinia corresponds with class D60 with respect to modulus of elasticity and density. This is also confirmed by the tests on structural laminated timber (SLT), for both the modulus of elasticity and density are significantly above the limits for D60 to EN 338, namely 17000 N/mm<sup>2</sup> and 700 kg/m<sup>3</sup> respectively. Thus the values for the modulus of elasticity range between 17420 and 17930 N/mm<sup>2</sup> and the values for density between 724 and 787 kg/m<sup>3</sup>. Since the influence of the modified test configuration - structural laminated timber instead of solid timber - is probably of secondary importance for the modulus of elasticity and density, the test results can indeed be regarded as representative. The two test series D30 and T20 were ignored, since the results are uninformative as a result of defective gluing.

The bending strength values calculated backwards from the tensile tests correspond with class D50. However, table 3.3. shows that the values from the University of Hamburg are significantly higher than those of the Technical University Graz. A significant cause of this is probably, as already mentioned, the different grading and the scope of the samples. Thus angle grain was largely eliminated for the tests at the University of Hamburg, which was

not the case for the Technical University of Graz. The fact that angle grain was the main cause of fracture in the tests in this project, shows, on the other hand, the significant influence that grain angle has on the tensile strength of robinia wood. By determining grading criteria, in particular with respect to grain angle, it should therefore be possible to classify robinia wood as hardwood at least in strength class D50.

The tests on structural laminated timber (SLT), are of only limited representational value for allocation to a class, thanks to the system factors explained in chapter 2.2.4 between packs of 2 (DUO), 3 (TRIO), 4 (QUATTRO) and 5 (CINQUE). Nevertheless they show that a classification of robinia wood in hardwood class D50 is justified. Thus in series Q145, a bending strength  $f_{m,05}$  of 51.1 N/mm<sup>2</sup> was achieved. Although the actual characteristic bending strength  $f_{m,k}$  of robinia wood is probably below this value as a result of the system factor, since in many of the test bases a failure of a finger joint was the cause of the fracture, the influence of the system factor did not have an effect to the extent expected.

**In summary it can be said that robinia wood is in the range of hardwood classes D50 and D60 to EN 338. While the modulus of elasticity and density most probably satisfy the threshold values for D60, bending strength is probably in class D50. It is true that the determination of bending strength is somewhat uncertain, but the fact that D50 was achieved without detailed grading shows that D50 is realistic if corresponding grading criteria are determined, but D60 is probably not achievable in the light of the test results.**

### 3.3 EN 1194: Applicability of the functional relationships to the hardwood robinia

EN 1194 defines the parameters for glued laminated timber beams as functions of tensile strength, tensile modulus of elasticity and the density of lamellae. The subject matter of this chapter is the extent to which these functions can be applied to hardwoods, and in particular to robinia wood.

Since the cross-section values of the glued laminated timber beams deviate from the reference dimensions in EN 1194 ( $b = 150$  mm,  $d = 600$  mm), it is necessary to adjust the bending strength values. Since there is no adjustment function for hardwood, recourse is had to the formulas specified in EN 1194. Table 3.4 shows the adjustment of the bending strength values for the glulam bases.

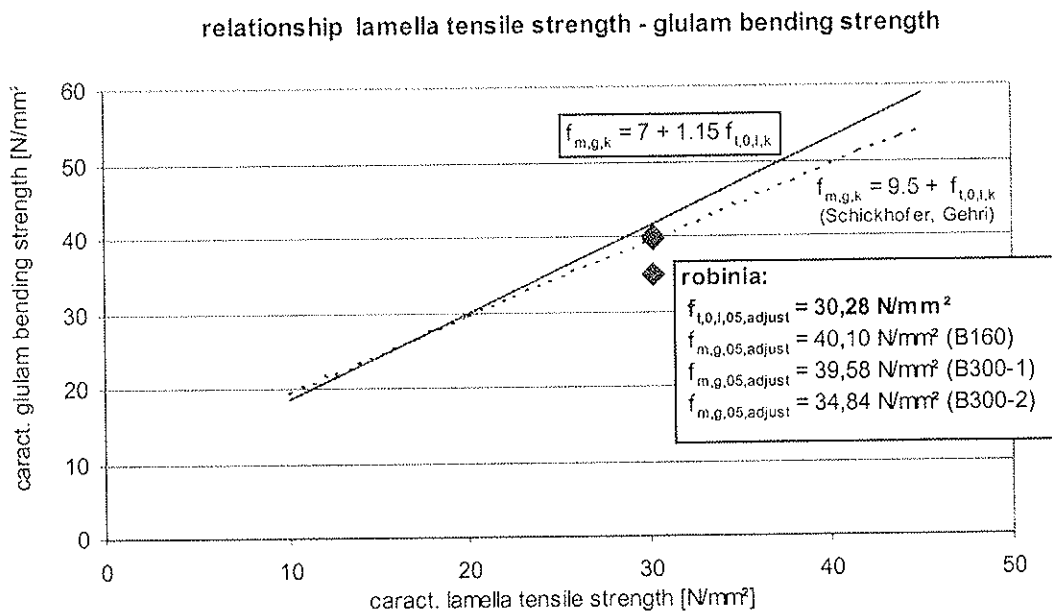
	number n [-]	dimensions			adjustment $k_{size}$ [-]	bending strength	
		b [mm]	d [mm]	l [mm]		$f_{m,q,05,unadjust}$ [N/mm <sup>2</sup> ]	$f_{m,q,05,adjust}$ [N/mm <sup>2</sup> ]
<b>B160</b>	14	100	160	2880	0,859	46,70	40,10
<b>B300-1</b>	6	120	300	5400	0,923	42,90	39,58
<b>B300-2</b>	13	100	300	5400	0,914	38,10	34,84

**Table 3.4:** Adjustment of the bending strength values to the reference dimensions in EN 1194

The adjustment of the tensile strength values to the reference dimensions in EN 1194 can be found in Table 3.2, it being noted that only the tensile tests carried out by the Technical University of Graz have been taken into account for the questions considered in this chapter.

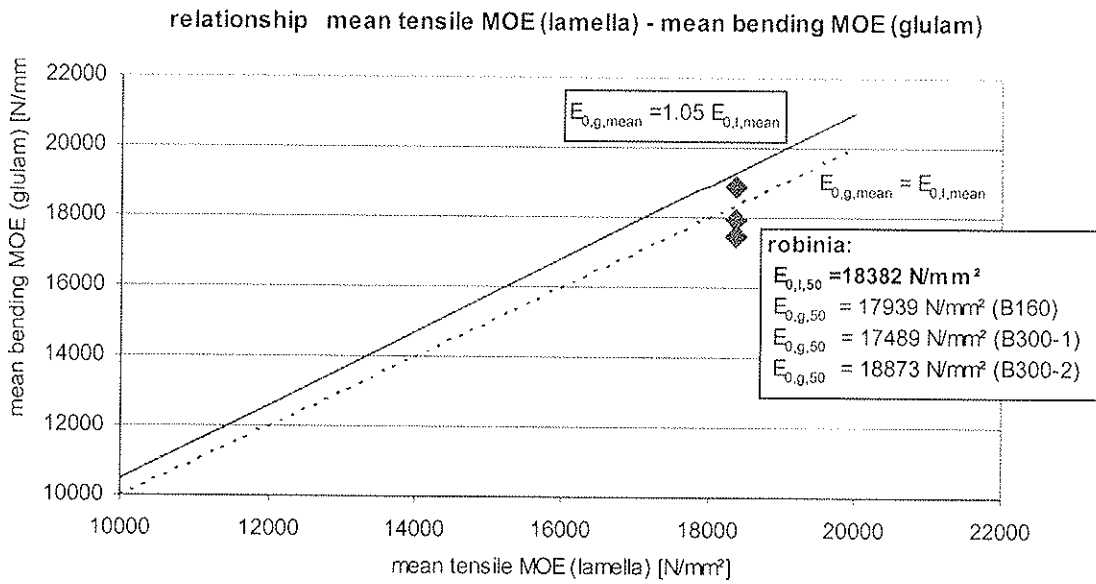
Figs. 3.1 to 3.4 set out the connection between the following parameters, on the one hand to EN 1194 and on the other hand on the basis of the test results:

- Lamella tensile strength  $f_{t,0,1,k}$  - glulam bending strength  $f_{m,g,k}$
- Lamella tensile modulus of elasticity  $E_{0,1,mean}$  - glulam bending modulus of elasticity  $E_{0,g,mean}$  (mean value)
- Lamella tensile modulus of elasticity  $E_{0,1,mean}$  - glulam bending modulus of elasticity  $E_{0,g,k}$  (characteristic value)
- Lamella density  $\rho_{l,k}$  - glulam density  $\rho_{g,k}$



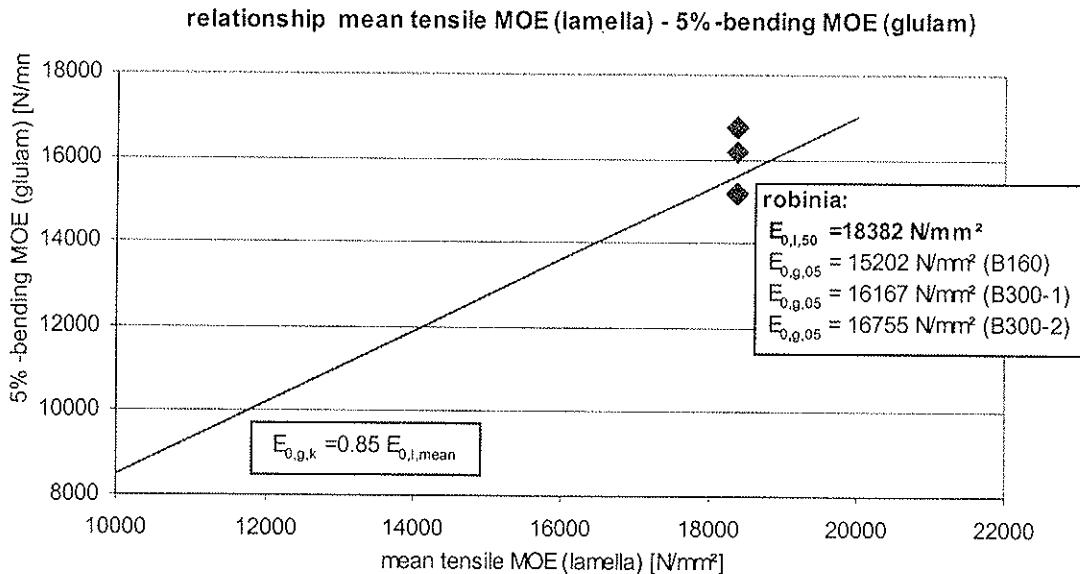
**Fig. 3.1:** Relationship between lamella tensile strength and glulam bending strength

Fig. 3.1 shows on the one hand that there is close agreement between the functional relationship lamella tensile strength to GLT bending strength pursuant to EN 1194 and the test results. On the other hand, the figure also shows that the function in EN 1194 appears too optimistic in the upper strength area, but fundamentally could also be confirmed for hardwood glued laminated timber (robinia) based on the present results.

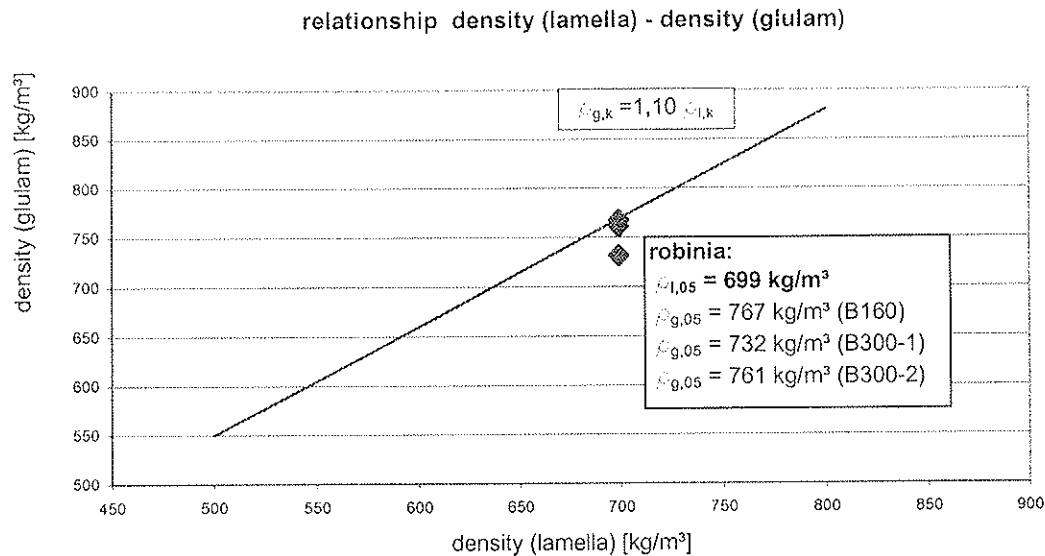


**Fig. 3.2:** Relationship between mean tensile MOE (lamella) and mean bending MOE (glulam)

Fig. 3.2 shows that the bending modulus of elasticity of robinia glued laminated timber is not greater than the tensile modulus of elasticity of lamellae. Hence the factor 1.05 in EN 1194 cannot be confirmed. On the contrary, the bending modulus of elasticity of glued laminated timber should be set at the same value as the tensile modulus of elasticity of the lamellae.



**Fig. 3.3:** Relationship between mean tensile MOE (lamella) and 5%-bending MOE (glulam)



**Fig. 3.4:** Relationship between density of lamella and density of glued laminated timber

Figs. 3.3 and 3.4 show that the functions in EN 1194 for the relationships between lamella tensile modulus of elasticity and bending modulus of elasticity (5%-fractile value) and lamella density and density of glued laminated timber - leaving aside a minimum overestimate of the density of the glulam - agrees very closely with the test results.

If the figures are examined, it is apparent that the functional relationships specified in EN 1194 correspond very closely with the relationships determined from the robinia tests. In particular the functions for glulam density and the 5%-fractile value of the glulam modulus of elasticity are confirmed. Slight deviations are on the one hand to be noted for the mean value of the glulam modulus of elasticity, where the factor of increase over the mean lamella tensile modulus of elasticity of 1.05 cannot be confirmed, and on the other hand for glulam bending strength, where the glulam bending strength calculated from lamella tensile strength according to EN 1194 is too high. However, tests on whitewood already showed that this function is slightly too optimistic in the upper strength area, and robinia wood is without doubt in this range.

### 3.4 EN 1194: Relationship between lamella tensile strength and finger joint tensile strength

EN 1194 regulates the quality requirements for finger joints. This can be checked either by tensile tests or by flat edge bending tests on finger joints. In this project, the finger joints were investigated using tensile tests. On this, EN 1194 lays down that finger joint strength must be 5 N/mm<sup>2</sup> higher than lamella tensile strength.

Table 3.5 sets out a comparison between finger joint tensile strength and lamella tensile strength on the basis of the tests at the University of Hamburg [3] and those in the present project at the Technical University of Graz.

	tensile strength values				
	lamellae		finger joint		finger joint
	range	$f_{t,0,05}$ from test	range	$f_{t,j,05}$ from test	$f_{t,j,05}$ as required by EN1194
	[-]	[N/mm <sup>2</sup> ]	[-]	[N/mm <sup>2</sup> ]	[N/mm <sup>2</sup> ]
TU Graz	45	31,1	46	27,7	36,1
Uni Hamburg	11	36,8	21	42,0-65,3	41,8

Comments:

At the University of Hamburg, the suitability of three different glues for robinia wood was examined (melamine, phenol-resorcinol and polyurethane). 21 finger joint tests were carried out for each type of glue. This led to the range of finger joint tensile strength set out in the table, with polyurethane glue achieving the lowest and phenol-resorcinol achieving the highest strength.

**Table 3.5:** Comparison of lamella tensile strength and finger joint tensile strength

The comparison in table 3.5 shows a considerable difference between finger joint tensile strength obtained at the Technical University of Graz and that obtained at the University of Hamburg. This difference is probably due to the different production processes, for on the one hand the joint geometry in both cases was identical (15 mm) and on the other hand the Hamburg tests achieved a significantly higher strength even with the least suitable glue.

While the finger joints at the Technical University of Graz were produced under industrial conditions, those for the University of Hamburg were made under laboratory conditions. This is reflected above all in pressing time, which was 2 seconds (usual for the production of glued laminated spruce timber) and 10 seconds respectively. However, the more careful manufacture in the laboratory probably also had a positive effect on the test results. While the finger joints of the University of Hamburg satisfy the criterion of EN 1194, the finger joints of the Technical University of Graz fell significantly short of this level. The finger joint strength is even significantly below lamella tensile strength. It is therefore necessary to rethink the finger joints of the Technical University of Graz, particularly since the tests on glued laminated timber beams show that the finger joints represent the most important weak point. In particular pressing time, joint geometry (joint length → larger glued area) and an ideal glue recipe adjusted to the characteristics of the type of wood should be the subject matter of further investigations.

## 4.0 Summary and final considerations

With respect to the starting material, it is found that given the low forestry significance of robinia as a wood species in Austria, the forestry maintenance and hence the quality of the round timber is not satisfactory. This is shown in the one hand on the low sawn timber yield and on the other hand in the high reject rate during the production of glued products. When examining the sawn wood, alongside the features of relevance to appearance - such as the marked colour differentiation within this type of wood - it is the strength-relevant and fracture-determining criteria such as

- angle grain and
- knottiness (large knots affecting cross-section),

that significantly determine the quality of this type of wood.

In the absence of grading criteria for hardwood in the national grading standard ÖN DIN 4074-1 - the application of grading rules for softwood appears inappropriate - it is seen as necessary to define grading criteria for hardwood taking into account strength and stress for hardwoods, if the latter are to be increasingly used in the construction sector in the future. This applies not only to the hardwood robinia examined as an example in the present project, but primarily to the hardwoods beech, oak, chestnut and ash, which are of greater forestry importance.

The suitability for use of hardwood in the construction sector also depends to a large extent on its gluing characteristics. It is thus important to define the suitable glue types for glued hardwood products in connection with the corresponding areas of use. In the case of robinia, relatively good results have been achieved with phenol-resorcinol resin glue Aerodux 185 + HRP 150 hardener.

A further problem area is revealed in the examination of factory-made finger joints. A pure failure of the wood only occurred with one single finger joint sample. In all the other finger joints, the feature causing the defect was the pulling apart of the joint. In this context, it should be noted that account should be taken of a

- finger joint geometry,
- finger joint manufacture (pressing time, pressing force, etc.)
- and a corresponding glue type and a glue recipe based on the ingredients of hardwood

that are suitable for hardwoods.

The tests show that robinia wood will lie in the range of hardwood classes D50 and D60 to EN 338. While the modulus of elasticity and density probably satisfy the threshold values for D60, bending strength probably falls in class D50. It is true that the determination of bending strength is somewhat uncertain, but the fact that D50 was achieved without detailed grading shows that D50 is realistic if corresponding grading criteria are determined, while D60 is probably not achievable in the light of the test results.

If Figs. 3.1 to 3.4 are examined, it is apparent that the functional relationships specified in EN 1194 correspond very closely with the relationships determined from the robinia tests. In particular the functions for glulam density and the 5%-fractile value of the glulam modulus of elasticity are confirmed. Slight deviations are on the one hand to be noted for the mean value of the glulam modulus of elasticity, where the factor of increase over the mean lamella tensile modulus of elasticity of 1.05 cannot be confirmed, and on the other hand for glulam bending strength, where the glulam bending strength calculated from lamella tensile strength according to EN 1194 is too high. However, tests on whitewood have already shown that this function is too optimistic in the upper strength area, and robinia wood is without doubt in this range.

If greater use is to be made of the hardwoods beech, oak, chestnut, ash and robinia in the construction sector, e.g. in the form of glued laminated timber, it is necessary to ensure that the timber construction engineer has access to the corresponding material characteristic values. Thus in the author's opinion, the following questions must in particular be answered:

What grading criteria for specifying strength should apply for hardwoods?  
Which D-classes of EN 338 are the relevant hardwood types to be ascribed to?  
Do the relationships specified in EN 1194 also apply to hardwoods?

The present project has been able to reveal the problems related to these questions and set them out using the hardwood robinia as an example, but they remain largely unanswered.

## **5.0 Acknowledgements**

At this point I would like to thank B. Hasewend of Lignum Research for the literature searches and analysis of the forestry problems concerning robinia. In addition I should like to thank A. Bernasconi and I. Jeremias of the University of Hamburg and M. Augustin of Lignum Research for their participation in the tests at the Technical University of Graz and the ETH Zurich. Finally I should like to express my thanks to E. Gehri, Professor of Wood Technology, ETH Zurich, and K. Kernbicher and J. Linder, KVA, Technical University of Graz, for the opportunity to carry out the tests. The funds for this project were kindly made available by the FFF, the Styrian Sawmills Industry and the Federal Ministry for Agriculture and Forestry.



## 6.0 References

### 6.1 Books, publications

- Chugg, W.A.; James, P.E.: „The Gluability of Hardwoods for Structural Proposes“ Timber Research and Development Association, Bucks, USA, 1965
- Schall, W.; Kraus, B.; Mayer, H.: „Tropenholzersatz bei Fensterkantel“ Österr. Holzforschungsinstitut ÖHFI, Vienna, 2/1994
- Gehri, E.; Kucera, L. J.; Molnár, S.; Lang, M.; Molnár-Posch, P.: „Das Holz der Robinie – Eigenschaften und Verwendungsmöglichkeiten“, Fortbildungskurs, Publication No. 93-1, ETH Zurich, 1993
- Dyno Industrier A.S.: „Surface Preparation and Gluing Techniques for Difficult Timbers“ Dyno Industrier A.S., Lilleström, Norway
- Göhre, K.; Erteld, W.; Krueel, W.; Liese, J.; Scamoni, A.: „Die Robinie (falsche Akazie) und ihr Holz“, Deutscher Bauernverlag, 1952

### 6.2 Standards, approvals, product guidelines

- CEN/TC124/WG2/N304 (EN 338): „Structural timber – Strength classes“, 12/1998
- CEN/TC124/WG2/N305 (EN 384): „Structural timber – Determination of characteristic values of mechanical properties and density“, 12/1998
- ÖNORM EN 385: „Keilzinkenverbindungen in Bauholz – Leistungs- und Mindestanforderungen an die Herstellung“, 5/1995
- ÖNORM EN 386: „Brettschichtholz – Leistungs- und Mindestanforderungen an die Herstellung“, 5/1995
- CEN/TC124/WG2/N306 (EN 408): „Timber structures – Structural timber and glued laminated timber -Determination of some physical and mechanical properties“, 12/1998
- ÖNORM EN 518: „Bauholz für tragende Zwecke – Sortierung – Anforderungen an Normen über visuelle Sortierung nach der Festigkeit“, 5/1995
- EN 1194: „Timber structures – Glued laminated timber – Strength classes and determination of characteristic values“, 9/1996
- Technical notice: „Dynomel L725 – pulverförmiger Melamin-Harnstoffharzleim für den Holzleimbau“, Dyno Industrier A.S., Lilleström, Norway, 1995
- Technical notice: „Aerodux 185 mit Härter HRP 150 oder HRP 155“  
Dyno Industrier A.S., Lilleström, Norway, 1995

### 6.3 Theses

- [1] Akman, H.: „Untersuchungen über die Verklebung von Robinie zur Herstellung von Fensterkanteln“ University of Hamburg, Department of Biology, 1994
- [2] Fink, S.: „Untersuchungen über die dynamische Belastbarkeit des Robinienholzes“, University of Hamburg, Department of Biology, 1994
- [3] Jauernig, H.: „Untersuchungen über die Verklebung von Robinie bei höheren Holzfeuchten“, University of Hamburg, Department of Biology, 1997

**INTERNATIONAL COUNCIL FOR RESEARCH AND INNOVATION  
IN BUILDING AND CONSTRUCTION**

**WORKING COMMISSION W18 - TIMBER STRUCTURES**

**LENGTH AND LOAD CONFIGURATION EFFECTS IN THE CODE FORMAT**

T Isaksson  
Department of Structural Engineering  
Lund University  
SWEDEN

**MEETING THIRTY-TWO**

**GRAZ**

**AUSTRIA**

**AUGUST 1999**

---

Presenter: T.Isaksson

- T.D.G.Canisius discussed the general application of the method in design such as 2 and 3 spans situations.
- T.Isaksson responded that theory was statistical effect based and could be applied to complicated loading.
- A.Jorissen questioned how the strength of reference length determined.
- T.Isaksson responded that bending tests with 2 loading points were used.

# Length and Load Configuration Effects in the Code Format

Tord Isaksson  
Department of Structural Engineering, Lund University

## Abstract

The effect of length and type of loading on the load carrying capacity of a timber member is the subject of this paper. The effects are evaluated using reliability methods and a calibration according to the code format is performed. Based on a model of the between and within member variability of bending strength, series of beams of different lengths are subjected to different load configurations. The results of simulated testing of beams of different lengths under different loads can be used to evaluate the effect of length and load.

Both the Swedish and European design code are based on using partial coefficients. When calibrating these coefficients, one of the parameters is connected to the uncertainty in the calculation model. This parameter takes into account the differences between the length and loading conditions of the beam in the structure and the length and load used for determining the strength of the beam, i.e. the third point loading according to EN 408. Using the simulated test results, the calculation model parameter can be evaluated. The parameter is divided into one stochastic part and one deterministic part. The latter describes known effects when changing length and load conditions compared to the reference conditions. The introduction of such a function, which is dependent on length and type of loading, results in a substantial increase in design strength for most lengths and load configurations.

## 1 Introduction

An investigation of the within member variability of structural timber has been presented in previous CIB papers, 28-6-4, 30-10-4 and 31-6-1. The purpose was to experimentally find data to derive a model of the variation of bending strength within and between timber beams. Knowledge about the variability makes it possible to investigate the length and load dependent strength of a beam.

The effect of length and load has often been explained by Weibull theory, e.g. Eurocode 5, or at least it has been calibrated against the Weibull theory. In this paper the length and load configuration effect is introduced when calibrating the code format. Based on simulated testing of beams of different lengths and loading conditions it is possible to introduce a deterministic function of length and type of loading. This function takes into account the difference between the standard test set-up and the beam to be designed, i.e. it improves the precision in the calculation model and thus in most cases giving a higher resistance of the beam.

## 2 Modelling the variability of bending strength

Based on experimental tests a model of the variability in bending strength between and within beams has been developed (see paper CIB W18/31-6-1). The model gives the distance between weak sections (knot clusters), the strength of weak sections and the strength of the wood connecting weak sections.

The strength  $f$  of section  $j$  in beam  $i$  is given by eq. (1). The strength is modelled using a log normal distribution. Figure 1 shows the strength model with its parameters.

$$\ln(f_{ij}) = \mu + \tau_i + \varepsilon_{ij} \quad (1)$$

where

$\mu$  is the logarithm mean of all weak sections in all beams.

$\tau_i$  is the difference between the logarithm mean of weak sections within a beam  $i$  and  $\mu$ . The mean equals zero and the standard deviation is  $\sigma_i$ .  
 $\varepsilon_{ij}$  is the difference between weak section  $j$  in beam  $i$  and the value  $\mu + \tau_i$ . The mean equals zero and the standard deviation is  $\sigma_j$ .

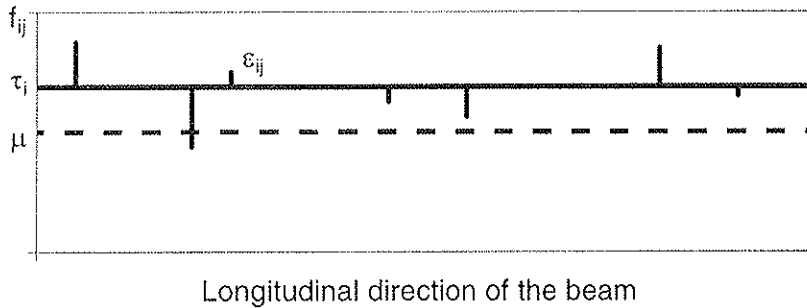


Figure 1. Model of the variation of strength along a beam.

The model described above is completed in two ways. One with strong sections connecting the weaker and one with only weak sections connected to each other, see Figure 2 and Figure 3 respectively. The strong section strength equals the strength of the strongest weak section. The reason for proposing the latter model is because the difference in strength between weak and strong sections was found to be in the same order as the difference between weak sections, Isaksson (1999). Also, the strength of weak sections was determined over a length of 400 mm which is close to the average distance between weak sections.

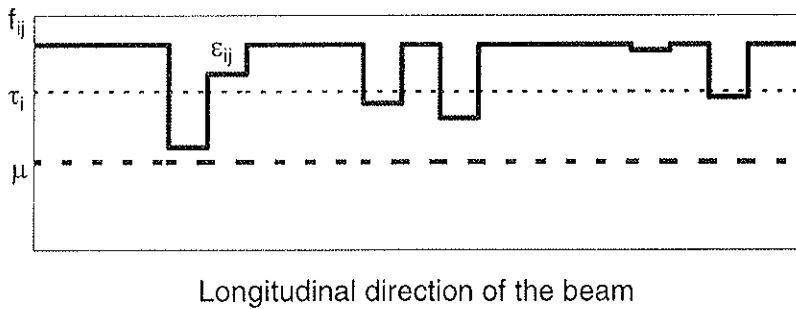


Figure 2. Model 1, lengthwise variation of bending strength with weak sections connected by stronger wood.

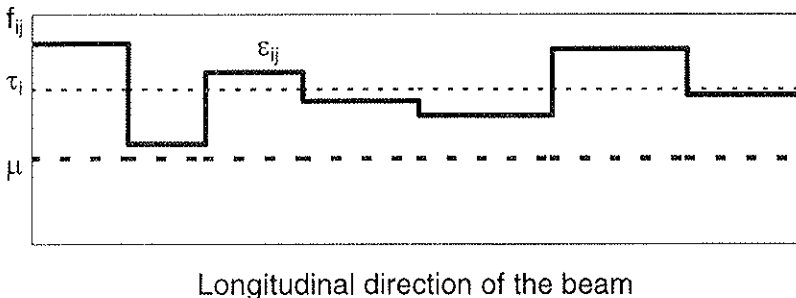


Figure 3. Model 2, lengthwise variation of bending strength with weak sections located after each other.

The correlation between strengths of different weak sections is independent of the distance between the sections. For the investigated material the correlation coefficient is around 0.56.

The experimental tests were performed on Norway spruce (*picea abies*). The variability in strength was low and the mean distance between weak sections was 490 mm resulting in a more or less homogeneous material. In order to investigate the effect of within member variability for a more variable material, Radiata pine was also used. The data about this material was found in Leicester et al (1996). The data was adjusted to fit to the model used in this study. Leicester found the correlation between strength of weak sections to be around 0.30. Several studies, Williamson (1994) and Riberholt et al (1979), have shown that the correlation is between 0.50 and 0.60 independent of the material. Thus the correlation for Radiata pine was set to 0.55.

Table 1 summarises the input to the models. For Model 1 and IRP a constant length of 150 mm is used for the weak sections.

Parameter	Model		
	1	2	IRP
Distance [mm]	Gamma (2.5445, 194.12 )	Gamma (2.5445, 194.12 )	Exp (1 ,1300 )
Length of weak section [mm]	150	-	150
Weak section strength [MPa]	LogN (4.01977, 0.247136 )	LogN (4.01977, 0.247136 )	LogN (3.75443, 0.38523 )
Coeff. of corr. between weak section strengths	0.565	0.565	0.55
Strong section strength [MPa]	greatest weak section strength	-	greatest weak section strength

Table 1. Summary of the input to the models. Model IRP is used for the Radiata pine material.

### 3 Simulating strength testing of beams

Using the model described above, beams of any length can be generated and subjected to various loads. In this study seven different load configurations are used, see Figure 4. For each load, the length of the beam is varied between 1.5 m and 5.5 m. All in all, 63 samples with 10 000 beams in each are generated for each model. Table 2 shows the results of Model 2. The mean,  $\mu_r$ , and standard deviation,  $\sigma_r$ , is based on 10 000 beams. The same table is generated for Model 1 and Model IRP.

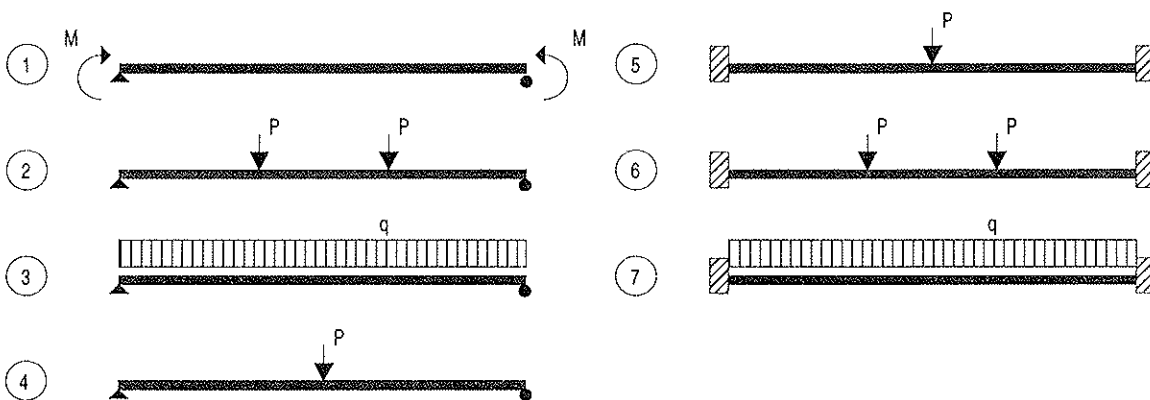


Figure 4. The seven load configurations used in this study.

Load configuration	Length (m)								
	1.5	2	2.5	3	3.5	4	4.5	5	5.5
1 $\mu_r$	48.658	47.615	46.774	46.119	45.593	45.160	44.759	44.382	44.079
$\sigma_r$	10.596	10.219	9.902	9.686	9.531	9.373	9.257	9.124	9.030
2 $\mu_r$	52.927	51.506	<b>50.579</b>	49.857	49.222	48.687	48.224	47.861	47.530
$\sigma_r$	12.303	11.658	<b>11.314</b>	10.995	10.713	10.530	10.363	10.218	10.025
3 $\mu_r$	54.868	53.310	52.245	51.460	50.784	50.223	49.763	49.374	49.034
$\sigma_r$	12.710	12.116	11.721	11.401	11.129	10.941	10.750	10.574	10.407
4 $\mu_r$	61.009	59.609	58.325	57.347	56.379	55.660	54.971	54.398	53.943
$\sigma_r$	14.158	13.860	13.420	13.273	12.965	12.648	12.366	12.130	11.979
5 $\mu_r$	51.811	51.480	51.069	50.820	50.621	50.369	50.152	49.852	49.739
$\sigma_r$	11.618	11.465	11.168	11.151	10.950	10.888	10.779	10.742	10.620
6 $\mu_r$	52.382	52.344	52.105	52.025	51.977	51.791	51.729	51.520	51.482
$\sigma_r$	11.889	11.763	11.563	11.617	11.518	11.455	11.452	11.450	11.316
7 $\mu_r$	52.447	52.442	52.237	52.185	52.178	51.995	51.969	51.789	51.778
$\sigma_r$	11.925	11.820	11.621	11.684	11.622	11.533	11.565	11.571	11.451

Table 2. Mean,  $\mu_r$ , and standard deviation,  $\sigma_r$ , of the resistance  $r$  for the 7 load configurations, and 9 lengths using the Model 2. The box shows the reference length and load configuration. This configuration is close to the test set-up according to EN408.

## 4 Probabilistic theories and the code format

### 4.1 The code format

Both the Swedish code BKR94 and the Eurocode use the partial coefficient method. In this study the Swedish code is considered but the results are representative for Eurocode as well. The design format according to BKR 94 is given in eq. (3).  $\gamma_m$ ,  $\gamma_n$  and  $\gamma_i$  are partial coefficients related to the material, safety class and action, respectively.

$$\frac{R_k}{\gamma_m \gamma_n} - \sum \gamma_i S_{ki} \geq 0 \quad (3)$$

The resistance  $R_k$  is a product of several parameters, eq. (4).

$$R_k = C_k \kappa f_k a \quad (4)$$

where

$C_k$  is the uncertainty in the model

$\kappa$  reflects climate and duration of load (not included in this study, set to 1)

$f_k$  is the characteristic strength

$a$  is a dimension variable

The uncertainty in the model ( $C$ ) includes the effect of length and load configuration. Let us now consider  $C_k$  as a product of two variables, namely  $\alpha$  and  $\Psi_k$ , eq. (5).  $\alpha$  represents a deterministic relation between different lengths and load configurations.  $\Psi_k$  is the characteristic value of the stochastic part of  $C$ .

$$C_k = \alpha \Psi_k \quad (5)$$

$\alpha$  is a function of the length,  $L$ , and a load configuration coefficient,  $\xi$ , defined according to eq. (6). Table 3 gives the coefficient for the seven load configurations used throughout this investigation, see Figure 4.

$$\xi = \frac{\int_0^L M(x) dx}{M_{max} L} \quad (6)$$

$M(x)$  is the moment distribution as a function of the distance  $x$  along the beam.  
 $M_{max}$  is the maximum bending moment in the beam and  $L$  is the length of the beam.

Load configuration (LC)	$\int_0^L M(x) dx$	$M_{max}$	$\xi$
1	$M$	$M$	1
2	$2PL^2/9$	$PL^2/3$	0.667
3	$qL^3/12$	$qL^2/8$	0.667
4	$PL^2/8$	$PL^2/4$	0.5
5	$PL^2/16$	$PL^2/8$	0.5
6	$8PL^2/81$	$2PL^2/9$	0.444
7	$qL^3/18\sqrt{3}$	$qL^2/12$	0.385

Table 3. Load configuration coefficient,  $\xi$ , for the different loading conditions studied.

The design strength, using an  $\alpha$  function, is now written as

$$R_d = \alpha \frac{\kappa \Psi_k f_k}{\gamma_m \gamma_n} \quad (7)$$

If  $\alpha=1$  the above equation is the same as the one given in the Swedish code, BKR 94. The design load is given by eq. (8). This is the governing load combination for a dominating variable load  $Q$ .

$$S_d = \gamma_G G_k + \gamma_Q Q_k \quad (8)$$

where

$$\gamma_G = 1$$

$$\gamma_Q = 1.3$$

$G_k$  is the characteristic permanent load equal to its mean.

$Q_k$  is the characteristic variable load equal to the upper 98th percentile.

## 4.2 The probabilistic format

In general the relation between the action  $S$  (load, stress) and the resistance  $R$  (load-carrying capacity, strength) can be given as a failure function  $g(R, S)$ , eq. (9).

$$g(R, S) = R - S \quad (9)$$

This function divides the two-dimensional space into a safe region,  $g(R, S) > 0$ , a failure region,  $g(R, S) < 0$ , and a failure surface (or limit state surface),  $g(R, S) = 0$ . The format used in this paper is based on the principles given in NKB (1987). The strength  $R$  is a function of several stochastic variables, eq. (10).

$$R = C a \rho f \quad (10)$$

where

$C$  is the uncertainty in the model

$a$  is a dimension variable

$\rho$  is a duration of load variable

$f$  is the strength

Duration of load is not included in this study which means that  $\rho = 1$ . The uncertainty in the model,  $C$ , is divided into one stochastic variable,  $\Psi$ , and one deterministic variable,  $\alpha$ . The deterministic variable aims at improving the calculation model by increasing its precision. This means that the variability is decreased. Eq. (10) can now be written as

$$R = \alpha \Psi a f \quad (11)$$

The ratio  $\frac{R}{a}$  is referred to as  $r$ . Including this in eq. (11) gives

$$\frac{R}{\alpha a} = \frac{r}{\alpha} = \Psi f \quad (12)$$

$r$  is the actual simulated test result from different lengths and load configurations, see Table 2. The strength,  $r$ , of a beam of a certain length under a certain type of loading is thus a product of the uncertainty in the calculation model,  $\Psi$ , and the "pure" strength  $f$ . If the length and loading of the beam coincides with the prescribed test method for determining the bending strength, the uncertainty in the calculation model is zero, which means  $r = f$ .

The mean of  $r$  is a product of the mean of  $f$  and the mean of  $\Psi$  according to eq. (13). This is a consequence of the variables being log-normally distributed.

$$\mu_r = \mu_\Psi \mu_f \quad (13)$$

The coefficients of variation are related according to eq. (14).

$$COV_r^2 = COV_\Psi^2 + COV_f^2 \quad (14)$$

The probabilistic format of the action,  $S$ , is based on the variable action,  $Q$ , and the permanent action,  $G$ , eq. (15). Both are assumed to be normally distributed.  $G_k$  and  $Q_k$  are characteristic values.

$$S = G + Q = Q_k \left( \frac{G}{Q_k} + \frac{Q}{Q_k} \right) = Q_k \left( \frac{G}{G_k} \eta + \frac{Q}{Q_k} \right) \quad (15)$$



$$\text{where } \eta = \frac{G_k}{Q_k}$$

The following two variables are also introduced, eqs. (16) and (17).

$$g = \frac{G}{G_k} \in N(1, \sigma_g); \text{COV}_g = \text{COV}_G \quad (16)$$

and

$$q = \frac{Q}{Q_k} \in N(\mu_q, \sigma_q); \text{COV}_q = \text{COV}_Q \quad (17)$$

$$\text{where } \mu_q = \frac{\mu_Q}{Q_k} = \frac{\mu_Q}{\mu_Q(1 + \Phi^{-1}(0.98)\text{COV}_Q)}$$

Substituting eqs. (16) and (17) into eq. (15) gives

$$S = Q_k(g\eta + q) \quad (18)$$

The probabilistic format given by the failure function is given by eq. (19).

$$g(R, S) = R - S = R - Q_k(g\eta + q) \quad (19)$$

where  $R$ ,  $S$ ,  $g$  and  $q$  are normalised stochastic variables.

The next step is to combine the code format and the probabilistic format. This is described in the next section.

### 4.3 Combination of code format and probabilistic format

Before attempting to calibrate the parameters in the code format, the probabilistic format and code format must be combined. The design criterion is  $R_d \geq S_d$ , where  $R_d$  and  $S_d$  are the designing resistance and action, respectively. Using eq. (8) and  $\eta$ ,  $S_d$  can be written:

$$S_d = Q_k(\gamma_G\eta + \gamma_Q) \quad (20)$$

The design criteria and eq. (20) give the following expression for  $Q_k$ :

$$Q_k = \frac{R_d}{\gamma_G\eta + \gamma_Q} \quad (21)$$

Inserting this into the failure function, eq. (19), gives

$$g(R, S) = R - \frac{R_d(g\eta + q)}{\gamma_G\eta + \gamma_Q} = 0 \quad (22)$$

The normalised variables  $R'$ ,  $g'$  and  $q'$  are now introduced into the failure function.

$$\mu_R \exp(-R' COV_R) = R_d \frac{(\mu_s (1 - g' COV_s) \eta + \mu_q (1 - q' COV_q))}{\gamma_G \eta + \gamma_Q} \quad (23)$$

$R'$ ,  $g'$  and  $q'$  are substituted by  $\alpha_R \beta$ ,  $\alpha_g \beta$  and  $\alpha_q \beta$  at the design point. Since there are four unknowns in eq. (23),  $\alpha_R$ ,  $\alpha_g$ ,  $\alpha_q$  and  $\mu_R$ , it must be solved iteratively.

Returning to eq. (12), we know that  $\Psi f = r/\alpha$  and consequently  $\mu_\Psi \mu_f = \mu_r/\alpha$ . Up till now, the dividing of  $COV_r$  into  $COV_f$  and  $COV_\Psi$  has not been explained but when the characteristic values of  $f$  and  $\Psi$  are determined, this is necessary. However, it is not known how much of  $COV_r$  is due to  $COV_f$  and how much is due to  $COV_\Psi$ . The way in which the variation is divided affects the calibration of the partial coefficient,  $\gamma_m$ , but not the final design value,  $R_d$ . Thus, it is only a matter of giving a suitable value of  $COV_f$ .

The characteristic values are given by eqs. (24) and (25).

$$f_k = \mu_f \exp(\Phi^{-1}(0.05) COV_f) \quad (24)$$

$$\Psi_k = \mu_\Psi \exp(\Phi^{-1}(0.05) COV_\Psi) \quad (25)$$

The partial coefficient connected to the material,  $\gamma_m$ , is given by eq. (26).

$$R_d = \frac{\Psi_k f_k}{\gamma_m \gamma_n} \Rightarrow \gamma_m = \frac{\Psi_k f_k}{R_d \gamma_n} \quad (26)$$

$R_d$  is equal to  $S_d$  and is given by eq. (20), and  $\gamma_n$  is the partial coefficient related to the safety class, i.e. the safety index  $\beta$ . The tools necessary to analyse the results of the simulations are now available.

## 5 Calibration of the code format

The procedure of calibrating the code format using the relations given in the previous sections is described for Model 2. For the other two models, 1 and 1RP, only the results are given.

Table 2 shows the results obtained from simulating beams using Model 2 input. The mean and standard deviations given in the table are valid for  $r$ . The third point loading of a beam with a length of 2.5 m is chosen as the reference configuration as this is close to the test arrangement specified in most codes for determining the bending strength, see for example EN408. For this reference beam,  $r$  should be equal to  $f$ , i.e. there is no uncertainty in the model since it coincides with the actual test arrangement.

The next step is to divide the values in Table 2 by the mean strength of the reference beam, see Table 4. The normalised values of  $r$  are represented by  $r'$ . This results in  $\mu_f = 1$  and gives a value of  $\Psi$  close to 1. The values in Table 4 are valid for  $\alpha = 1$ , i.e. no function is introduced to account for different lengths and load configurations. The mean of all  $\mu_{r'}$  is denoted  $\mu_{r'tot}$ .  $\Delta_{r'}$  in Table 4 is the difference between  $\mu_{r'}$  and  $\mu_{r'tot}$ . The standard deviation

for the whole population is given by eq. (27) where  $n$  is the total number of length and load configurations, i.e. 9 times 7.

$$\sigma_{r'tot} = \frac{\sum \sigma_{r'}^2}{n} + \frac{\sum \Delta_{r'}^2}{n} \quad (27)$$

All lengths and load configurations are given the same weight. For Model 2  $\mu_{r'tot}$  is 1.01193 and  $\sigma_{r'tot}$  is 0.23385, see also Table 6.

Load configuration	Length (m)								
	1.5	2	2.5	3	3.5	4	4.5	5	5.5
1 $\mu_{r'}$	0.9620	0.9414	0.9248	0.9118	0.9014	0.8929	0.8849	0.8775	0.8715
$\sigma_{r'}$	0.2095	0.2020	0.1958	0.1915	0.1884	0.1853	0.1830	0.1804	0.1785
$\Delta_{r'}$	-0.0499	-0.0706	-0.0872	-0.1001	-0.1105	-0.1191	-0.1270	-0.1345	-0.1405
2 $\mu_{r'}$	1.0464	1.0183	1	0.9857	0.9732	0.9626	0.9534	0.9463	0.9397
$\sigma_{r'}$	0.2433	0.2305	0.2237	0.2174	0.2118	0.2082	0.2049	0.2020	0.1982
$\Delta_{r'}$	0.0345	0.0064	-0.0119	-0.0262	-0.0388	-0.0493	-0.0585	-0.0657	-0.0722
3 $\mu_{r'}$	1.0848	1.0540	1.0329	1.0174	1.0041	0.9930	0.9839	0.9762	0.9695
$\sigma_{r'}$	0.2513	0.2395	0.2317	0.2254	0.2200	0.2163	0.2125	0.2091	0.2058
$\Delta_{r'}$	0.0729	0.0421	0.0210	0.0055	-0.0079	-0.0190	-0.0281	-0.0358	-0.0425
4 $\mu_{r'}$	1.2062	1.1785	1.1532	1.1338	1.1147	1.1005	1.0868	1.0755	1.0665
$\sigma_{r'}$	0.2799	0.2740	0.2653	0.2624	0.2563	0.2501	0.2445	0.2398	0.2368
$\Delta_{r'}$	0.1943	0.1667	0.1412	0.1219	0.1027	0.0885	0.0749	0.0636	0.0546
5 $\mu_{r'}$	1.0244	1.0178	1.0097	1.0048	1.0008	0.9958	0.9916	0.9856	0.9834
$\sigma_{r'}$	0.2297	0.2267	0.2208	0.2205	0.2165	0.2153	0.2131	0.2124	0.2100
$\Delta_{r'}$	0.0124	0.0059	-0.0023	-0.0072	-0.0111	-0.0161	-0.0204	-0.0263	-0.0286
6 $\mu_{r'}$	1.0356	1.0349	1.0302	1.0286	1.0276	1.0240	1.0227	1.0186	10.178
$\sigma_{r'}$	0.2351	0.2326	0.2286	0.2297	0.2277	0.2265	0.2264	0.2264	0.2237
$\Delta_{r'}$	0.0237	0.0230	0.0182	0.0167	0.0157	0.0120	0.0108	0.0067	0.0059
7 $\mu_{r'}$	1.0369	1.0368	1.0328	1.0317	1.0316	1.0280	1.0275	1.0239	1.0237
$\sigma_{r'}$	0.2358	0.2337	0.2298	0.2310	0.2298	0.2280	0.2287	0.2288	0.2264
$\Delta_{r'}$	0.0250	0.0249	0.0209	0.0198	0.197	0.0161	0.0156	0.0120	0.0118

Table 4. Adjusted mean and standard deviation of  $r'$  for the 7 load configurations and 9 lengths using Model 2. The box shows the reference length and load configuration.

It is now time to introduce  $\alpha$  into the analysis in order to improve the calculation model.  $\alpha$  is a deterministic function of the length,  $L$ , and a load configuration coefficient,  $\xi$ , see Section 5.1.

Theoretically, this function can be very complicated and of high order. Here, a more simple and code friendly function is used. A function of higher order does not improve the model significantly, see Isaksson 1999. The function is a first-order equation in both  $L$  and  $\xi$ , eq. (28).

$$\alpha = p + p_1 L + p_2 \xi \quad (28)$$

The evaluation of this function is performed on the complete set of load configurations and on a set only containing the simply supported beams, i.e. load configuration 1-4. Table 5 gives the function for the three input models and the coefficient of correlation. The

functions seem to give about the same relations between  $L$ ,  $\xi$  and  $\alpha$ , thus, a simplified relation, according to eq. (29) is introduced.

$$\alpha = 1.4 - 0.45\xi - 0.03L \quad (29)$$

Table 6 summarises the data on  $r'$  using  $\alpha$  according to eq. (29). Model 2 (LC 1-7) is not improved but changed for the worse when eq. (29) is chosen. The other models work well.

Model	$\alpha = f(L, \xi)$	$r$
2, LC 1-7	$\alpha = 1.2135 - 0.2317\xi - 0.0182L$	0.75
2, LC 1-4	$\alpha = 1.3854 - 0.3999\xi - 0.0272L$	0.93
1, LC 1-7	$\alpha = 1.4421 - 0.4812\xi - 0.0287L$	0.96
1, LC 1-4	$\alpha = 1.4285 - 0.4452\xi - 0.0327L$	0.95
IRP, LC 1-7	$\alpha = 1.4133 - 0.4956\xi - 0.0340L$	0.97
IRP, LC 1-4	$\alpha = 1.4916 - 0.5573\xi - 0.0411L$	0.99

Table 5. The  $\alpha$  function and coefficient of correlation for the three input models.

Model	$\alpha=1$			$\alpha = f(L, \xi)$		
	$\mu_{r' tot}$	$\sigma_{r' tot}$	$COV_{r' tot}$	$\mu_{r' tot}$	$\sigma_{r' tot}$	$COV_{r' tot}$
2, LC 1-7	1.011932	0.233846	0.2311	0.989548	0.241712	0.2443
2, LC 1-4	1.006248	0.239180	0.2377	1.033047	0.233302	0.2258
1, LC 1-7	1.054975	0.273867	0.2596	1.027192	0.245659	0.2392
1, LC 1-4	0.997974	0.248822	0.2493	1.023387	0.235772	0.2304
IRP, LC 1-7	0.998994	0.383400	0.3838	0.971420	0.358075	0.3686
IRP, LC 1-4	0.951868	0.370394	0.3891	1.000033	0.366978	0.3670

Table 6. Summary of data on  $r'$  for the different input models.  $\alpha = f(L, \xi)$  according to eq. (29).

$r'$  is a product of two log-normally distributed variables,  $f$  and  $\Psi$ . Consequently, the mean and coefficient of variation of these three variables are given by eqs. (30) and (31). The reduction in  $COV_{r' tot}$  due to the introduction of the  $\alpha$  function is seen when comparing the fourth and seventh columns in Table 6, Model 2 excluded.

$$\mu_{r'} = \mu_{\Psi} \mu_f \quad (30)$$

$$COV_{r'}^2 = COV_{\Psi}^2 + COV_f^2 \quad (31)$$

It is not possible to conclude how much of  $COV_{r'}$  is related to  $COV_f$  and how much to  $COV_{\Psi}$ , i.e. how much of the variability is due to the variation in the strength and how much is due to the uncertainty in the calculation model. The probabilistic part of the calibration is, however, independent of the proportions since the interesting number is  $COV_{r'}$ . The characteristic values of  $f$  and  $\Psi$  used in the partial coefficient method are, however, dependent on the values of  $COV_f$  and  $COV_{\Psi}$ , but not the final design value which is a product of the two.

A few more assumptions must be made before the calibration can be performed.

- A value of  $\beta$  must be chosen, in this case 4.3, which corresponds to safety class 2 according to the Swedish code, BKR 94.
- A coefficient of variation for the permanent action  $g$  is chosen. In this case  $COV_G = COV_g = 0.05$ .
- A coefficient of variation for the variable action  $q$  is chosen. In this case  $COV_Q = COV_q = 0.40$ .
- A coefficient of variation for the dimension variable  $a$  is chosen. In this case  $COV_a = 0.02$ .
- The sum of the means of the actions is set equal to 1,  $\mu_G + \mu_Q = 1$ .
- Based on the values of  $COV_r$  given in Table 6, it seems reasonable to set  $COV_f$  to 0.20, and assume that the remainder of the variation is due to  $\Psi$ .
- $\mu_G$  is varied between 0 and 0.90.

The three sensitivity parameters  $\alpha_i$  and  $\mu_R$  are solved iteratively. Once these are found,  $\mu_f$  can be determined as  $\mu_R / \mu_\Psi$ . Finally  $\gamma_m \gamma_n$  is given by  $f_k \Psi_k / R_d$ . For each combination of length and load configuration, and for several ratios between permanent and variable action these two steps are performed:

- $\mu_R$  is determined for  $\alpha = 1$ . The product  $\gamma_{m1} \gamma_n$  is calculated. The design strength is given as  $R_{d1} = \frac{\Psi_k f_k}{\gamma_{m1} \gamma_n}$ .
- $\mu_R$  is determined for  $\alpha = f(L, \xi)$ . The product  $\gamma_{m2} \gamma_n$  is calculated. The design strength is given as  $R_{d2} = \frac{\Psi_k f_k}{\gamma_{m2} \gamma_n}$ .

$\gamma_m \gamma_n$  should be calibrated at a representative proportion between permanent and variable action or at least so that common usage of a beam is not unsafe. For timber structures the permanent part of the total action is often low. If  $\mu_G = 0.8$  is chosen most combinations of actions are covered. This value of  $\mu_G$  corresponds to a value of 0.64 for the ratio  $G_d / (G_d + Q_d)$ .

The results show that the partial coefficient,  $\gamma_m$ , increases with increasing permanent action, see Table 7. However,  $\gamma_m$  is not significantly influenced by the introduction of the  $\alpha$  function. In Table 7  $\gamma_m$  is around 1.34 for  $\mu_G = 0.8$ . The corresponding value for Radiata pine is 1.67.

$\alpha R_{d1}$  for  $\alpha = 1$  is now compared with  $\alpha R_{d2}$  for  $\alpha = f(L, \xi)$  by determining the ratio between the two, see Figure 5. The ratio is independent of the level of  $\mu_G$ . In all cases except that for the constant bending moment (load configuration 1) and long simply supported beams, the  $\alpha$  function results in an increase in the design value. The increase is due to the lower coefficient of variation  $COV_r$ . The increase is independent of the ratio between permanent and variable action and decreases with length. The most significant increase in strength is achieved for beams with fixed supports. Compared with a simply supported beam an increase of 15 % is possible. Under the same conditions Radiata pine shows a slightly smaller increase of 12 %.

$\mu_G$	$\alpha=1$		$\alpha = f(L, \xi)$	
	$\gamma_n \gamma_{m1}$	$R_{d1}$	$\gamma_n \gamma_{m2}$	$R_{d2}$
0	1.1489	2.1527	1.1344	2.2461
0.05	1.1531	2.0905	1.1379	2.1823
0.1	1.1577	2.0283	1.1418	2.1185
0.2	1.1687	1.9040	1.1513	1.9910
0.3	1.1827	1.7796	1.1635	1.8635
0.4	1.2008	1.6552	1.1796	1.7359
0.5	1.2249	1.5309	1.2011	1.6083
0.6	1.2573	1.4065	1.2306	1.4803
0.7	1.3012	1.2822	1.2717	1.3516
0.8	1.3609	1.1578	1.3292	1.2212
0.9	1.4450	1.0334	1.4132	1.0886

Table 7.  $\gamma_m$  and  $R_d$  for  $\alpha=1$  and  $\alpha = f(L, \xi)$  according to eq. (29) at different levels of  $\mu_G$ . Model 1 input and load configurations 1 to 7.

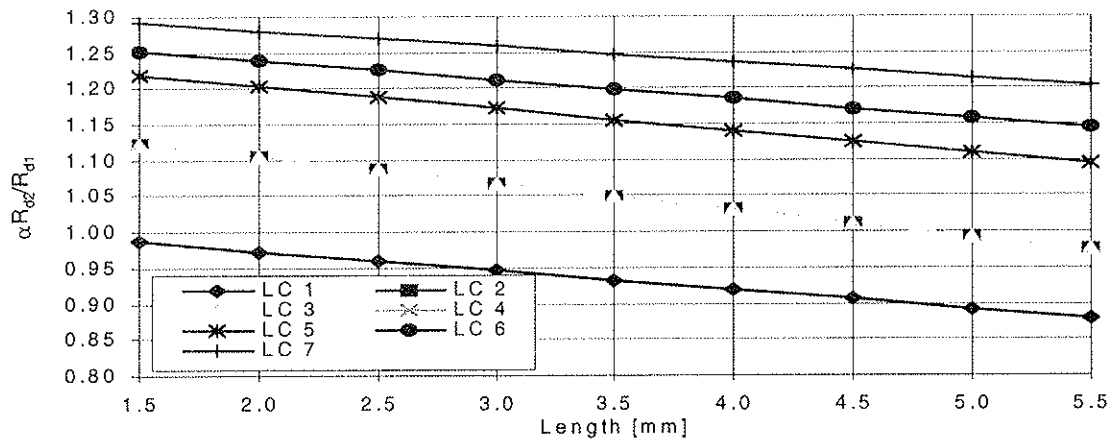


Figure 5. The ratio  $\alpha R_{d2}/R_{d1}$  as a function of length and load configuration,  $\mu_G = 0.8$ . Model 1 input and load configurations 1 to 7.  $\alpha = f(L, \xi)$  according to eq. (29).

## 6 Conclusions

Using a model of the within and between beam variation of bending strength, beams of different lengths were subjected to seven different load configurations. This enables new possibilities of evaluating length and load configuration effects.

In this study timber beams in the bending mode are represented by seven load configurations and lengths between 1.5 m and 5.5 m. A deterministic function  $\alpha$  is introduced to account for the difference between a specific length and load configuration, and the reference beam. The reference beam is identical with the EN408 test set-up for determining the bending strength. Introducing this function when calibrating the partial coefficients in the code format reduces the variability assigned to the resistance variable, i.e. the uncertainty in the calculation model is reduced.

For the material in this investigation, Norway spruce, the following function of length,  $L$ , and load configuration,  $\xi$ , was found:

$$\alpha = 1.4 - 0.45\xi - 0.03L$$

This function is added to the design format for the strength

$$R_d = \alpha \frac{Y_k f_k}{\gamma_m \gamma_n}$$

For a beam this means that halving the length results in around 7 % increase in load carrying capacity only because of  $\alpha$ . Including the  $\alpha$ -function in the calibration of the partial coefficients results in significant increase in the designing strength. Compared to using  $\alpha=1$  the increase is more than 10 % for most length and load combinations.

The results presented in this study are pure statistical effects. To be able to explain the complete behaviour of beams of different lengths under various loading conditions, other theories like fracture mechanics must be introduced into the model.

Whether length and load configurations should be included in a code is probably a "political" decision. On the one hand, one may want to encourage the use of timber and make it more competitive, but the other hand one would not want to discourage engineers from using timber by having too many coefficients and factors to take into account.

## 7 References

- BKR 94, (1994). *Boverkets konstruktionsregler* (Swedish code) (in Swedish). Boverket BFS 1993:58.
- EN 408. *Timber structures – Structural timber and glued laminated timber – Determination of some physical and mechanical properties*. Final draft March 1994.
- Eurocode 5, (1993). *Design of timber structures – Part 1-1: General rules and rules for buildings*. European Committee for Standardization, Bruxelles, Belgium.
- Isaksson T., (1999). *Modelling the variability of bending strength in structural timber – Length and load configuration effects*. Report TVBK-1015, Dept. of Structural Engineering, Lund University, Sweden.
- Leicester R.H, Breitinger H.O., Fordham H.F., (1996). *Equivalence of in-grade testing standards*. CIB/W18A – Timber structures. Paper 29-6-2. Bordeaux, France.
- NKB, (1987). *Retningslinjer for last- og sikkerhedsbestemmelser for baerende konstruktioner*. NKB skrift nr 55.
- Riberholt H., Madsen P.H., (1979). *Strength of timber structures, measured variation of the cross sectional strength of structural timber*. Struct. Research Lab., Technical University of Denmark. Report R114.
- Williamson J., (1994). *Statistical dependence of timber strength*. IUFRO Timber engineering. Sydney, Australia.

**INTERNATIONAL COUNCIL FOR RESEARCH AND INNOVATION  
IN BUILDING AND CONSTRUCTION**

**WORKING COMMISSION W18 - TIMBER STRUCTURES**

**LENGTH EFFECT ON THE TENSILE STRENGTH OF TRUSS CHORD MEMBERS**

F Lam

Department of Wood Science

University of British Columbia

CANADA

**MEETING THIRTY-TWO**

**GRAZ**

**AUSTRIA**

**AUGUST 1999**

---

Presenter: F.Lam

- B.J.Yeh asked whether the reduction in COV of series system was considered.
- F.Lam responded that the simulation procedures directly took it into account.
- T.D.G.Canisius requested the presenter to comment on the difference in safety level and snow load return period between EU and N. America.
- F.Lam responded that different regions/countries should set their own safety level and the loading return period. In Canada the timber code adopted a safety level equivalent to the steel code and the return period for snow was 30 years.
- S.Theandersson asked how was the k factor determined .
- F.Lam discussed the use of Equation 10 to establish k from a minimization of error procedure.
- A.Ranta-Maunus questioned whether the conclusion from this paper that length effect was most important for long span cases contradicted with the conclusion from paper 32-6-4 that length effect was most important for short span cases.
- F.Lam responded that there was no contradiction because the conclusion from current paper was based on the decrease in strength with increase in length (point of view of safety) and the conclusion from paper 32-6-4 was based on the increase in strength with decrease in length (point of view of utilization).



# Length Effect on the Tensile Strength of Truss Chord Members

Frank Lam  
Dept. of Wood Science  
University of B.C.  
Canada

## 1 Abstract

Length effect on the tensile strength of multiple member truss chords has been studied. Simulation and reliability studies have quantified the impact of length and multiple member effects on the target safety index for tensile failure of truss chord members. Weibull weakest link based length effect adjustment procedures have been established. Further simulation and reliability studies have demonstrated the robustness of the proposed length effect adjustment procedures to maintain target reliability index of long multiple tension chord members.

## 2 Introduction

In Canada, the specified strengths for tension parallel to grain of structural light framing members in the Code on Engineering Design in Wood CSA-086.1-94 are supported with test data from the Canadian Wood Council (CWC) Lumber Properties In-grade Testing Program (Barrett and Lau, 1995). The tensile strength database for selected species, size, and grade combinations of visually graded and machine stress rated (MSR) lumber are shown in Table 1. The test gauge lengths are shown in Table 2 for each specimen size. During testing, the instantaneous tensile load along the length of the test specimen is considered constant.

Madsen (1992) and Barrett *et al.* (1994) provided comprehensive reviews of length effect studies on the tensile strength of lumber. Past experimental studies (Lam and Varoglu 1990, Madsen 1990, Showalter *et al.* 1987) demonstrated that tensile strength of lumber was member length dependent. Madsen (1992) further suggested length and depth adjustment factors for tension members based on an assumed uniform loading along the member length.

Table 1. Species, size grade combinations of visually graded and MSR lumber from the CWC Lumber Properties In-grade Testing Program (Tensile Strength).

Material	Species	Size	Grade
Visually Graded	Douglas fir/ Larch (DF)	38 mm x 89 mm (2x4)	Select Structural (SS)
	Hem-Fir (HF)	38 mm x 184 mm (2x8)	Number 1 (No. 1)
	Spruce Pine Fir (SPF)	38 mm x 235 mm (2x10)	Number 2 (No. 2)
Machine Stress Rated	Spruce Pine Fir	38 mm x 89 mm	1450f-1.3E
			1650f-1.5E
			1800f-1.6E
			2100f-1.8E
			2400f-2.0E

Table 2. Specimen size and gauge length information from the CWC Lumber Properties In-grade Testing Program.

Specimen Size	Visually Graded Lumber		MSR Lumber	
	Specimen Length	Gauge Length	Specimen Length	Gauge Length
38 mm x 89 mm	3658 mm	2642 mm	4877 mm	3683 mm
38 mm x 184 mm	4877 mm	3683 mm	-	-
38 mm x 235 mm	4877 mm	3683 mm	-	-

In Canada, the Technical Committee on Engineering design in Wood, CSA086, adopted standardized/end-use lengths for presentation of design properties of visually graded material in the Canadian Code on Engineering Design in Wood (Canadian Standards Association, 1994). The standardized lengths for various design properties adopted in Canadian and US timber codes are shown in Table 3. The concept of end-use adjustments for member length is intended to provide design properties suitable for a broad range of applications permitted by the design code thereby avoiding the need to introduce length adjustments in the code itself. In the case of MSR material, there is no specific reference to standardized length; therefore, the test testing gauge length of 3.683 m used in the CWC In-grade test program can be considered.

Table 3. Standardized lengths (mm), for design property calculations adopted in US National Design Specification (NDS) and Canadian Standard CAN/CSA 086.1-M94 (CSA).

Width	NDS	CSA	
	Bending and Tension	Bending and Compression Length = 17 Width	Tension Length = 24 Width
89	3660	1520	2140
140	3660	2380	3360
184	4880	3130	4420
235	4880	4000	5640
286+	6100	4860	6864

In the Canadian code (Canadian Standards Association, 1994), a target reliability or safety index ( $\beta$ ) is implicitly associated with member design derived using the specified tensile strength ( $F_t$ ), the size factor ( $K_{zt}$ ), and performance factor ( $\phi$ ) provided in the code. These target  $\beta$  values for various modes of loading were established by Foschi *et al.* (1989) in an extensive study on the reliability-based design of wood structures which related the performance of the members in terms of an expected or target probability of failure to the code design equations. In the case of the design of tension members, a mean target  $\beta$  of 2.81 (with a range of 2.51 to 3.00) is associated with the performance of a 3.0-m long 38 x 184 mm member when the performance factor  $\phi$  equals 0.9.

Although the standardized length approach is acceptable in many single member applications, this approach may lead to “unsafe” designs in long span and multiple-member designs. The term “unsafe” is taken in the context that the actual safety level may be significantly lower than the target level of safety. The compromise on the target safety level may be even more severe in cases where lumber is used as a part of a complex structural system such as wood trusses. In these systems several issues need to be considered:

- 1) length effects - the lengths of individual tension members may be different from the standardized length for design property calculations;
- 2) multiple member effects - the entire bottom tension chord of a truss, composed of multiple members, may be considered as a single long series of individual members in tension because failure of any individual piece in the bottom chord will likely lead to collapse of the truss. The length of the bottom chord is generally significantly longer than the standardized length;
- 3) non-uniform stress effects –an added level of complexity is introduced due to the fact that the bottom tension chord member in trusses is commonly subjected to non-constant tensile load along its length. Therefore, its impact must also be considered to realistically reflect the member loading conditions.

Foschi *et al.* (1989) and Lam (1989, 1990) have investigated the reliability of truss systems. Foschi *et al.* (1989) examined the reliability of a parallel chord truss system comprised of pin-jointed sawn lumber. The study provided a methodology for studying the reliability of trusses. Specific code recommendations were not available from this study because of the lack of general treatment for different truss geometry and loading. Lam (1989, 1990) studied the baseline reliability of typical metal plate connected, pitched truss systems by combining simulation based non-linear finite element methods with reliability analyses. The results of these studies (Foschi *et al.* 1989 and Lam 1989, 1990) indicate that the probability of failure increases as the truss length increases. There is a need to address the length effects on truss chord members in the code to avoid “unsafe” designs for wood trusses.

In this paper a procedure is proposed and verified for the design of truss chord members under tension using a Weibull weakest link size effect model to account for length effects and non-uniform loading along the length of bottom chord truss members.

### 3 Weibull Weakest Link Theory

Assuming that the stress distribution in a member  $\sigma(x, y, z)$  can be normalized as

$$\sigma(x, y, z) = \hat{\tau} \lambda(x, y, z) \quad (1)$$

where  $\hat{\tau}$  is a scalar characteristic stress for the member and  $\lambda(x, y, z)$  is a dimensionless function describing the spatial variation of within-member stresses. According to the classical two parameter Weibull theory, the probability of failure  $p$ , for a volume  $v$  subjected to the stresses of Equation 1 is given by

$$p = 1 - \exp \left( - \int_v \left( \frac{\hat{\tau} \lambda}{m} \right)^k d v \right) \quad (2)$$

where  $m$  and  $k$  are the scale and shape parameters for the strength property distribution. For a member subjected to non-uniform tensile loading along the member length,  $\lambda(x,y,z) = \lambda(y)$ . In such cases, the member can be divided into  $n$  uniformly stressed elements with  $\lambda(y)$  given as:

$$\lambda(y) = \begin{matrix} \lambda_1 & 0 < y \leq L_1 \\ \lambda_2 & L_2 < y \leq L_3 \\ \lambda_3 & L_3 < y \leq L_4 \\ \vdots & \vdots \\ \lambda_n & L_{n-1} < y \leq L_n \end{matrix} \quad (3)$$

Here, the  $\lambda_i$  values can be taken as the ratio between the tensile stress in the  $i^{\text{th}}$  element to the maximum tensile stress in the series. The probability of failure of a member with cross sectional area  $A$  can therefore be expressed as

$$p=1-\exp\left[-A\left[\int_0^{L_1}\left(\frac{\hat{\tau}\lambda_1}{m}\right)^k dL + \int_{L_1}^{L_2}\left(\frac{\hat{\tau}\lambda_2}{m}\right)^k dL + \dots + \int_{L_{n-1}}^{L_n}\left(\frac{\hat{\tau}\lambda_n}{m}\right)^k dL\right]\right] \quad (4)$$

For members with the same cross section, comparing the strength of members with uniform and non-uniform tensile stresses along the member length at common probability of failure, Equation 4 yields the tensile length effect adjustment factor as follows:

$$\xi = \left[ \frac{\sum_{i=1}^n \lambda_i^k L_i}{L_{st}} \right]^{\frac{-1}{k}} \quad (5)$$

where  $L_{st}$  is the standard length of the member under uniform stress as implied in the code.

#### 4 Verification using Simulation and Reliability Analyses

Simulation and reliability studies were conducted to 1) evaluate the impact on “target” reliability indices if tensile length effect on multiple members was ignored and 2) validate the tensile strength adjustment factors for multiple members under non-uniform tensile stresses (Equation 5). Since there are many possible combinations of number of members ( $n$ ), member length ( $L_i$ ) and the relative load ratios for each members ( $\lambda_i$ ,  $i = 1, \dots, n$ ), it was not possible to evaluate every case. Therefore, only a baseline case (one member under uniform load) and 8 fairly representative cases (series of multiple equal length members) were chosen to elucidate the situation (see Table 4). Within a series of multiple members, the tensile stress in an individual member is uniform but the tensile stresses may be different between members. For example, case 1 represents 4 equal length members in a series under uniform stress. Case 8 represents a series of 6 non-uniformly stressed equal length members where 4 of the members are loaded at 60% of the peak stress in the series and the remaining 2 members are equally

loaded at the peak stress. Failure of any one member in a series corresponds to the failure of the system.

Table 4. Load conditions of various cases considered in this study.

Case	n	Load ratio, $\lambda_i$ $i=1, \dots, n$					
		$\lambda_1$	$\lambda_2$	$\lambda_3$	$\lambda_4$	$\lambda_5$	$\lambda_6$
Baseline	1	1.0					
1	4	1.0	1.0	1.0	1.0		
2	4	1.0	0.8	0.8	1.0		
3	4	1.0	0.6	0.6	1.0		
4	6	1.0	1.0	1.0	1.0	1.0	1.0
5	6	1.0	1.0	0.8	0.8	1.0	1.0
6	6	1.0	0.8	0.8	0.8	0.8	1.0
7	6	1.0	1.0	0.6	0.6	1.0	1.0
8	6	1.0	0.6	0.6	0.6	0.6	1.0

Simulation studies were conducted for each of the 8 representative cases using the published information on the statistical distributions on tensile strength properties of Canadian visually graded and MSR dimension lumber (Barrett and Lau 1994). In total, 18 cells/combinations of visually graded material were considered: 3 species (DF, HF, SPF); 3 sizes (2x4, 2x8, 2x10); and 2 grades (SS and No. 2). For MSR material, 5 grades (1450f-1.3E, 1650f-1.5E, 1800f-1.6E, 2100f-1.8E, and 2400f-2.0E) of 2x4 SPF lumber were also considered. Consistent with the reliability based design procedures developed by Foschi *et al.* (1989), the study used censored two parameter Weibull tensile strength distributions fitted to the lower 15% of the test data for the 23 test cells (Table 5).

In each simulated case, a sample size (nn) of 1000 series was used. The tensile strength of each individual member within a series was simulated first,  $s_{i,j}$  ( $i=1, \dots, n$  and  $j=1, \dots, nn$ ). For cases (Cases 1 to 8), the tensile strength of a series was taken as the minimum strength (adjusted for non-uniform stress) of the individual members within a series as:

$$S_j = \left\{ \text{minimum} \left[ \frac{s_{i,j}}{\lambda_i} \right] (i = 1, \dots, n), (j = 1, \dots, nn) \right\} \quad (6)$$

Censored two parameters Weibull probability distributions were fitted to the lower 15% of the various cases of the simulated series strengths  $S_j$  ( $j=1, \dots, nn$ ) and the resulting shape and scale parameters are shown in Table 6. It should be noted that the simulation studies were based on In-grade database where members were tested at specific gauge lengths (Table 2). Therefore, the total length of a series of simulated multiple members would be either 4 times (cases 1 to 3) or 6 times (cases 4 to 8) the specified test gauge lengths given in Table 2.

Next, reliability analyses were performed on the tensile performance of members under dead and snow load conditions for five Canadian cities (Arvida, Halifax, Ottawa, Saskatoon, and Vancouver) following the procedures outlined by Foschi *et al.* (1989). In the current study, the

length effect adjustment factor,  $\xi$  (Equation 5), was incorporated in the analyses to evaluate the impact of ignoring length effects and the robustness of the proposed model.

Table 5. Shape and scale parameters of the censored two parameter Weibull tensile strength distributions (Barrett and Lau 1994).

Size	Species	Grade	Ingrade database			UTS <sub>0.05,g</sub> (MPa)
			Scale (MPa)	Shape	R <sub>0.05</sub> (MPa)	
2x4	DF	SS	30.96	6.00	18.31	-
2x4	DF	No. 2	21.83	4.51	11.47	-
2x4	HF	SS	33.35	4.77	17.99	-
2x4	HF	No. 2	21.97	5.49	12.91	-
2x4	SPF	SS	26.76	5.88	16.34	-
2x4	SPF	No. 2	19.61	4.39	9.69	-
2x8	DF	SS	25.34	6.16	14.89	-
2x8	DF	No. 2	17.55	4.83	9.38	-
2x8	HF	SS	22.27	6.93	13.78	-
2x8	HF	No. 2	19.40	4.65	10.39	-
2x8	SPF	SS	21.46	5.20	12.02	-
2x8	SPF	No. 2	15.84	4.75	8.20	-
2x10	DF	SS	22.71	6.53	14.09	-
2x10	DF	No. 2	16.08	4.78	8.35	-
2x10	HF	SS	22.51	5.68	13.12	-
2x10	HF	No. 2	16.59	5.25	8.96	-
2x10	SPF	SS	21.85	5.24	11.73	-
2x10	SPF	No. 2	16.22	4.59	8.47	-
2x4	SPF	1450f-1.3E	23.19	9.08	15.86	11.60
2x4	SPF	1650f-1.5E	26.28	7.22	17.14	14.80
2x4	SPF	1800f-1.6E	32.49	7.66	19.96	17.00
2x4	SPF	2100f-1.8E	38.55	7.55	26.03	22.80
2x4	SPF	2400f-2.0E	40.44	9.62	29.50	27.90

Note:

- R<sub>0.05</sub> is the non-parametric estimate of the 5<sup>th</sup> percentile strength from the Ingrade data.
- UTS<sub>0.05,g</sub> is the 5<sup>th</sup> percentile tensile strength specified for the various MSR lumber grades in NLGA Special Product Standard for MSR lumber (SPS2).
- The shape and scale parameters correspond to censored two parameters Weibull tensile strength distributions fitted to the lower 15% of the Ingrade test data.

A limit state design equation for the tensile strength parallel to grain can be expressed as

$$\alpha_D G_D D_N + \alpha_L G_L L_N = \xi \phi F_t \quad (7)$$

where  $\alpha_D$  and  $\alpha_L$  are the load factors for dead (1.25) and live (1.5) loads, respectively;  $G_D$  and  $G_L$  are the dead and live load geometric factors which convert the applied loads to tensile stresses;  $D_N$  and  $L_N$  are the nominal design dead load and nominal design total roof snow and rain load, respectively;  $F_t$  is the characteristic tensile strength (typically taken as the 5<sup>th</sup> percentile strength); and  $\phi$  is the performance factor.

Table 6. Shape and scale parameters of the censored two parameter Weibull tensile strength distributions from simulation studies.

Size	Species	Grade	Simulation Studies															
			Case 1		Case 2		Case 3		Case 4		Case 5		Case 6		Case 7		Case 8	
			Scale (MPa)	Shape	Scale (MPa)	Shape	Scale (MPa)	Shape	Scale (MPa)	Shape	Scale (MPa)	Shape	Scale (MPa)	Shape	Scale (MPa)	Shape	Scale (MPa)	Shape
2x4	DF	SS	24.53	5.66	26.27	5.82	27.44	5.79	22.47	5.89	23.09	6.21	25.22	5.93	26.12	5.94	27.47	5.66
2x4	DF	No.2	16.01	4.25	17.32	4.32	17.82	4.54	14.25	4.43	14.58	4.68	15.95	4.52	16.75	4.51	18.19	4.27
2x4	HF	SS	24.88	4.50	26.63	4.64	27.99	4.70	22.28	4.68	22.89	4.92	25.10	4.73	26.18	4.76	28.20	4.51
2x4	HF	No.2	17.03	5.18	18.36	5.27	19.10	5.35	15.47	5.39	15.93	5.66	17.18	5.57	18.13	5.42	19.29	5.13
2x4	SPF	SS	21.10	5.55	22.68	5.66	23.47	5.76	19.29	5.77	19.87	6.07	21.64	5.83	22.55	5.77	23.65	5.55
2x4	SPF	No.2	14.27	4.14	15.51	4.18	15.94	4.40	12.65	4.31	12.91	4.58	14.05	4.46	14.56	4.55	16.32	4.11
2x8	DF	SS	20.20	5.81	21.55	6.02	22.56	5.94	18.54	6.05	19.02	6.41	20.93	6.01	21.40	6.16	22.61	5.80
2x8	DF	No.2	13.14	4.56	14.12	4.67	14.74	4.77	11.78	4.74	12.09	5.00	13.29	4.78	13.80	4.84	14.96	4.53
2x8	HF	SS	18.20	6.54	19.32	6.84	20.18	6.66	16.87	6.81	17.61	6.92	19.18	6.58	19.31	6.95	20.05	6.65
2x8	HF	No.2	14.37	4.39	15.45	4.49	15.96	4.68	12.83	4.57	13.16	4.81	14.34	4.67	15.02	4.67	16.29	4.40
2x8	SPF	SS	16.40	4.91	17.76	4.96	18.47	5.06	14.82	5.11	15.22	5.38	16.49	5.26	17.28	5.21	18.40	4.97
2x8	SPF	No.2	11.80	4.48	12.64	4.62	13.25	4.69	10.56	4.66	10.86	4.90	11.88	4.72	12.40	4.75	13.39	4.49
2x10	DF	SS	18.33	6.16	19.40	6.49	20.29	6.37	16.91	6.41	17.36	6.80	19.31	6.18	19.53	6.47	20.32	6.23
2x10	DF	No.2	12.00	4.51	12.86	4.65	13.50	4.71	10.75	4.69	11.04	4.94	12.12	4.74	12.63	4.77	13.60	4.53
2x10	HF	SS	17.60	5.36	19.01	5.43	19.69	5.53	16.04	5.58	16.57	5.82	17.89	5.71	18.79	5.58	19.87	5.32
2x10	HF	No.2	12.71	4.95	13.74	5.02	14.38	5.06	11.50	5.16	11.86	5.39	12.76	5.34	13.42	5.24	14.30	4.99
2x10	SPF	SS	16.74	4.94	18.10	5.01	18.93	5.05	15.13	5.15	15.60	5.39	16.80	5.32	17.66	5.24	18.79	5.00
2x10	SPF	No.2	11.96	4.33	12.89	4.42	13.32	4.61	10.67	4.51	10.95	4.74	11.95	4.60	12.47	4.63	13.53	4.37
2x4	SPF	1450F-1.3E	19.88	8.57	21.08	8.87	21.60	8.72	18.76	8.92	19.50	9.07	21.04	8.59	21.38	8.64	21.63	8.57
2x4	SPF	1650F-1.5E	21.66	6.81	22.95	7.14	23.87	6.98	20.13	7.09	21.02	7.19	22.72	6.94	23.11	7.12	23.71	6.98
2x4	SPF	1800F-1.6E	27.07	7.22	28.50	7.70	29.65	7.45	25.27	7.52	26.29	7.68	28.64	7.23	29.07	7.42	29.53	7.41
2x4	SPF	2100F-1.8E	32.04	7.13	33.78	7.56	35.11	7.36	29.88	7.42	31.12	7.56	33.81	7.18	34.34	7.36	35.01	7.29
2x4	SPF	2400F-2.0E	34.97	9.07	36.84	9.55	37.80	9.27	33.11	9.44	34.33	9.64	36.99	9.10	37.53	9.13	37.84	9.10

If  $\xi$  is taken as unity, Equation 7 converts to a form of the limit state design equation in the Canadian Code on Engineering Design in Wood (Canadian Standards Association, 1994) which ignores length effects. The failure function developed to relate the tensile resistance and the effect of loads for first-order second-moment reliability analyses is as follows:

$$G = R - (G_D D + G_L L) \quad (8)$$

$G = 0 \quad \Rightarrow$  Limit State

$G > 0 \quad \Rightarrow$  Safe

$G < 0 \quad \Rightarrow$  Failure

where  $R$ ,  $D$ , and  $L$  are random variables representing the tensile strength, dead load, and live snow load, respectively. Statistical distributions and parameters for the snow load for the five Canadian cities were described in detail in past studies (Foschi *et al.* 1989). The tensile strength  $R$  was represented by the censored 2 parameter Weibull distributions established for the various cells and load cases (Tables 4 and 5).

The failure function can be rewritten as:

$$G = R - \frac{(\varepsilon \delta \gamma + \iota) \xi \phi F_t}{\alpha_D \varepsilon \gamma + \alpha_L} \quad (9)$$

where  $\gamma = D_N/L_N$ ;  $\delta = D/D_N$ ;  $\iota = L/L_N$ ; and  $\varepsilon = G_D/G_L$ . The variables  $\varepsilon$  and  $\gamma$  were assumed to equal 1.0 and 0.25, respectively. The values of  $F_t$  for the various cells considered in this study were taken as the  $R_{0.05}$  and  $UTS_{0.05,g}$  values given in Table 4 for the visually graded and MSR material, respectively. The random variable  $\delta$  was assumed to be normal with mean of 1.0 and standard deviation of 0.1.

First-order second-moment reliability analyses were performed for all the data cells and the baseline and simulation cases, with  $\xi=1$ , to evaluate the impact of ignoring length effects. Summary results are shown in Table 7. Figure 1 shows example plots of  $\beta$  versus  $\phi$  relationships for SS, No. 2 and 2100f-1.8E SPF 2x4 material for Vancouver snow load. Clearly, if length effects were ignored, a range of  $\beta$  resulted for a given  $\phi$  value (which is set at 0.9 in the Canadian code). As expected, the range of  $\beta$  values for a given  $\phi$  depended on the variability in the lower tail of the strength distribution and hence the grade of material. The results show that MSR material has a narrower range of  $\beta$  compared to the SS material, which in turn has a smaller range in  $\beta$  compared to the No. 2 material. These results are consistent for all species, sizes, and locations for the various cases considered.

It can also be observed that the  $\beta$  versus  $\phi$  relationships for MSR SPF 2x4 material are higher than that for visually graded material; i.e., for a given  $\phi$  value the  $\beta$  values are higher. The reasons are that: 1) MSR material is less variable than visually graded material and 2) more importantly, there is a built in conservatism in the selection of  $UTS_{0.05,g}$  values for the various MSR grades in relation to the actual  $R_{0.05}$  values. The choices of  $UTS_{0.05,g}$  values for MSR grades were based on the DF species and research conducted in the early 1970's. The



Canadian SPF MSR material is modulus of elasticity governed rather strength governed; therefore, the built in conservatism in tensile strength.

First-order second-moment reliability analyses were performed for all the data cells and simulation cases, with  $\xi$  defined according Equation 5, to evaluate the robustness of the proposed length effect parameters. Here the Weibull shape parameter ( $k$ ) was needed to calculate  $\xi$  for the eight load cases. Since  $k$  depended on material variability, it was reasoned that it should take on different values for the SS, No. 2 and MSR material.

The  $k$  values were established such that the following error function was individually minimized for the SS, No. 2, and MSR material:

$$\text{Error} = \left| \sum_{j=1}^8 \sum_{i=1}^{N_{\text{CELL}}} 1 - \frac{R_{0.05i}}{R_{0.05 \text{ sim } ij}} \zeta_j \right| \quad (10)$$

where  $R_{0.05i}$  = non-parametric fifth percentile strength estimates;  $R_{0.05 \text{ sim } ij}$  = fifth percentile strength estimates from simulation;  $j$  = load case index;  $i$  = index for cell/combination; and  $N_{\text{CELL}} = 6, 6, 5$  for the SS, No.2 and MSR material, respectively.

The  $k$  values for the SS, No. 2, and MSR material were found to be 5.56, 4.42 and 8.81, respectively. Figure 2 shows example plots of  $\beta$  versus  $\phi$  relationships for SS, No. 2, and 2100f-1.8E SPF 2x4 material for Vancouver snow load with consideration of length and multiple member effects. Again these results are typical for all species, sizes and, locations. Summary results are shown in Table 7. Clearly, length effect adjustments reduced the range of  $\beta$  values for a given  $\phi$  value. Therefore, for a given  $\phi$  value of 0.9, with length and multiple member effect adjustment, the  $\beta$  values range around 2.8 for visually graded material and 3.4 for MSR material.

Table 7. Summary Results of Range of reliability indices.

Grade	S.S.			No. 2			MSR
	2x4	2x8	2x10	2x4	2x8	2x10	2x4
$\phi=0.9$							
No Adjustment							
Maximum $\beta$	2.96	3.08	3.01	2.89	2.88	2.96	3.76
Average $\beta$	2.39	3.00	2.97	2.82	2.84	2.89	3.39
Minimum $\beta$	1.60	1.71	1.82	1.53	1.56	1.58	2.46
Adjusted							
Maximum $\beta$	3.00	3.15	3.06	2.98	2.89	3.03	3.76
Average $\beta$	2.91	3.03	2.99	2.85	2.85	2.91	3.41
Minimum $\beta$	2.24	2.37	2.46	2.27	2.31	2.32	2.90

## 5 Conclusions

In this paper the background theory on length effects on the tensile strength of lumber was reviewed. Simulation and reliability studies were presented to evaluate the impact of length effect on the tensile strength of chord members in trusses. Results indicate significant length

effect can be expected for long multiple tension chord members. Based on the Weibull weakest link theory, length effect adjustment parameters were established. Simulation and reliability studies were conducted to demonstrate the robustness of the proposed length effect adjustment procedures. A procedure was developed for the design of truss chord members under tension considering Weibull weakest link based size effect and non-uniform loading along the length of bottom chord truss members such that the target reliability index can be maintained.

## 6 References

Barrett, J.D. and Lau, W. 1994. Canadian Lumber Properties Edited by E.D. Jones. Canadian Wood Council. Ottawa. Canada.

Barrett, J.D., Lam, F. and Lau, W. 1995. Size effects in visually graded softwood structural lumber. *J. of Materials in Civil Eng. ASCE*. 7(1):19-30.

Canadian Standards Association, 1994. Engineering design in wood (limit state design). CAN3-086.1-M89, Canadian Standards Association, Rexdale, Ont.

Foschi, R.O., Folz, B.R. and Yao, F.Z. 1989. Reliability-based Design of Wood Structures. Struct. Res. Ser., Rept. No. 34., Dept. Civil Eng., Univ. Brit. Col., Vancouver, Canada.

Lam, F. 1990. Short-term baseline reliability of trusses built from MSR lumber. Report prepared for Canadian Forestry Service. Forintek Canada Corp. Van., B.C., Canada. 19pp.

Lam, F. 1989. Short-term baseline reliability of trusses. Report prepared for the Canadian Forestry Service. Forintek Canada Corp. Van., B.C., Canada. 22pp.

Lam, F. and Varoglu, E. 1990. Effect of length on the tensile strength of lumber. *For. Prod. J.*, 40(5),37-42.

Madsen, B. 1992. Structural Behavior of Timber. Timber Engineering Ltd., N. Van., B.C., Canada.

Madsen, B. 1990. Length effects in 38 mm spruce-pine-fir dimension lumber. *Can. J. Civil Engr.*, 17(2), 226-237.

Showalter, K.L., Woeste, F.E. and Bendsten, B.A. 1987. Effect of length on the tensile strength of lumber. Res. Paper FPL-RP-482, USDA For. Service, For. Prod. Lab., Madison. WI.

Weibull, W. 1939. A statistical theory of the strength of materials. *Proc. Roy. Swed. Inst.*, No. 151, Stockholm.

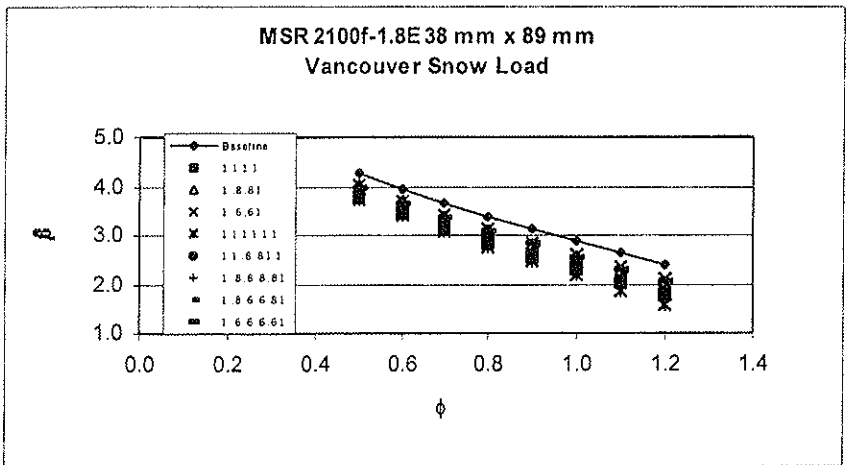
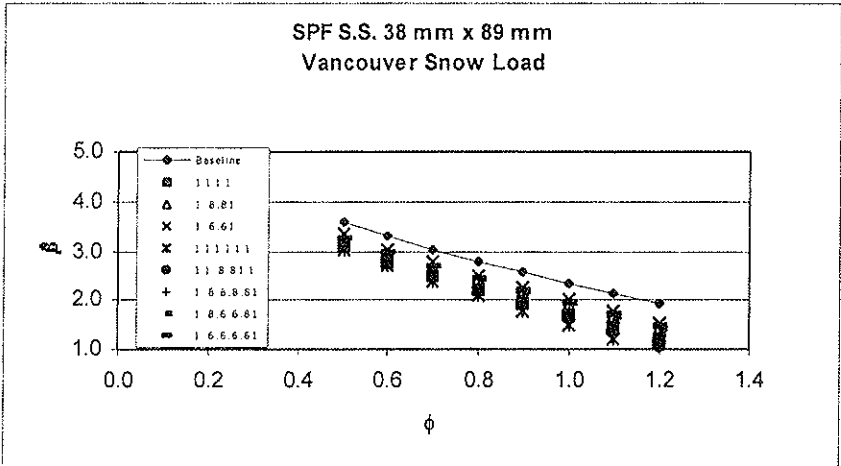
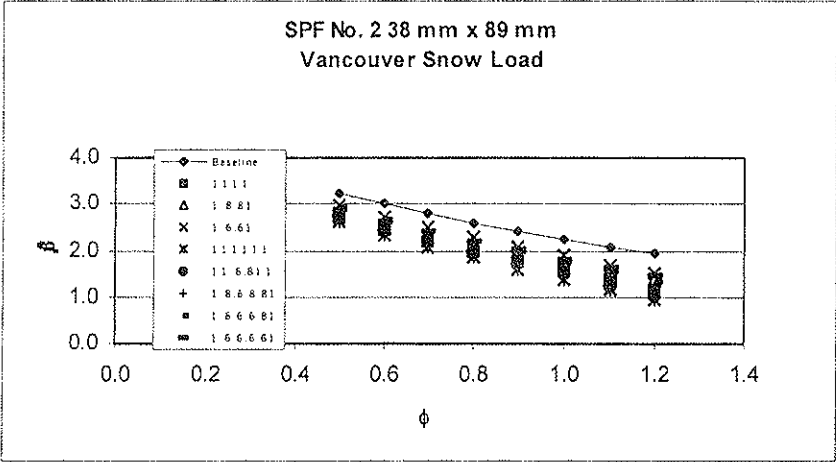


Figure 1. Reliability Index versus Performance factor relationship of the tensile strength of 2x4 SPF material (without length and multiple member effect adjustment).

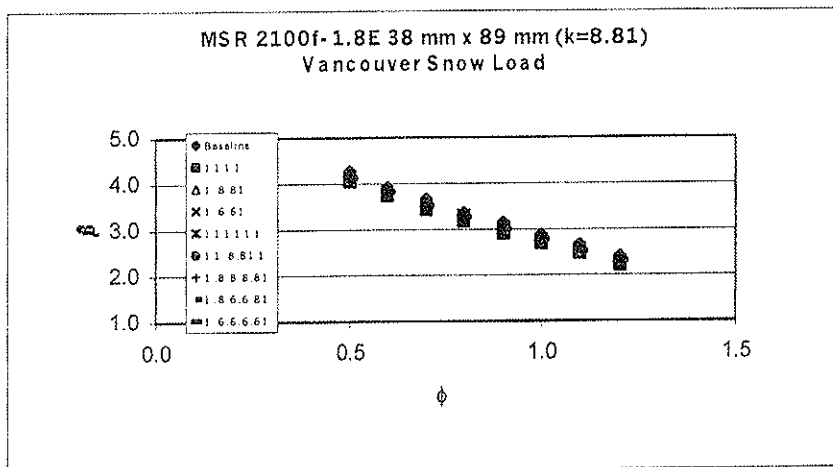
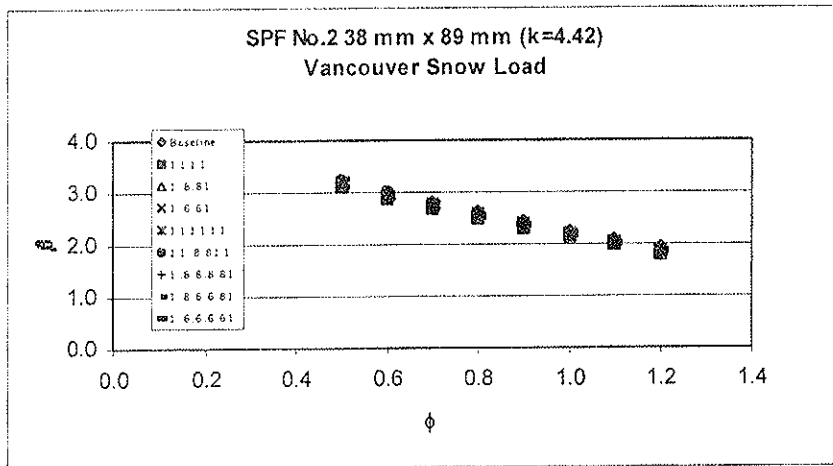
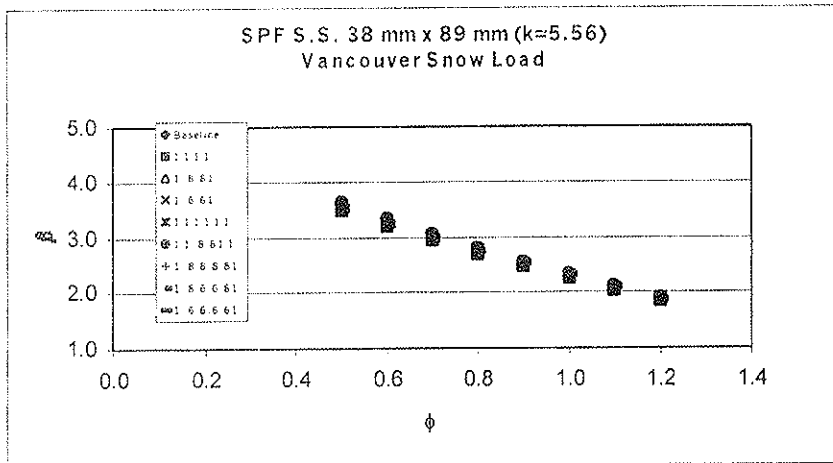


Figure 2. Reliability Index versus Performance factor relationship of the tensile strength of 2x4 SPF material (with length and multiple member effect adjustment).

**INTERNATIONAL COUNCIL FOR RESEARCH AND INNOVATION  
IN BUILDING AND CONSTRUCTION**

**WORKING COMMISSION W18 - TIMBER STRUCTURES**

**TENSILE STRENGTH PERPENDICULAR TO GRAIN OF  
GLUED LAMINATED TIMBER**

H J Blaß

M Schmid

University of Karlsruhe

GERMANY

**MEETING THIRTY-TWO**

**GRAZ**

**AUSTRIA**

**AUGUST 1999**

---

Presenter: M.Schmid

- S.Svensson questioned whether climatic treatment was considered as tension strength perpendicular to grain would be very sensitive to climatic changes.
- M.Schmid responded that the climatic condition was under normal laboratory condition and it was almost constant. The material was left in the lab for a long time.
- G.Schickhofer commented on the code applications.
- M.Schmid responded that the tension strength perpendicular to grain is strength class independent
- H.J.Blass added that the tension strength perpendicular to grain is very low and one should detail structures so that it would not depend on tension strength perpendicular to grain.
- P.Quenneville asked for an explanation of why the previous findings that tensile strength perpendicular to grain was dependent on density differ from current findings.
- H.J.Blass responded that solid database were not available before.
- A.Jorissen asked whether fracture mechanics approach was used.
- M.Schmid responded that it was not tried.
- A.Ranta-Maunus added that the past database that showed tensile strength perpendicular to grain was dependent on density was based on clear wood data.

# Tensile Strength Perpendicular to Grain of Glued Laminated Timber

H.J. Blaß, M. Schmid  
Lehrstuhl für Ingenieurholzbau und Baukonstruktionen  
Universität Karlsruhe

## 1 Introduction

The tensile strength perpendicular to grain of glued laminated timber according to the European standard EN 1194 is based on the following equation:

$$f_{t,90,g,k} = 0,2 + 0,015 f_{t,0,l,k} \quad (1)$$

where  $f_{t,90,g,k}$  is the glulam strength perpendicular to grain and  $f_{t,0,l,k}$  is the tensile strength parallel to grain of the planks. According to Eurocode 5 this characteristic strength  $f_{t,90,g,k}$  is related to a reference Volume of  $V_0 = 0,01 \text{ m}^3$ . A test method for determining the tensile strength perpendicular to grain of glulam using this reference volume  $V_0$  is given in EN 1193.

Test series according to this test procedure are reported by Aicher und Dill-Langer (1995, 1997). The material they used was especially produced for their research project. The planed planks of strength class C40 had a constant thickness of 33 mm. Planks including pith were excluded (so called 3x-log sawing, centre boards with pith were sorted out).

The aim of the project presented here was to determine the tensile strength of glued laminated timber of different strength classes commonly used in Germany. The material of the test specimens should form a representative sample taken out of numerous beams manufactured by different glulam producers.

## 2 Test Method

The test method followed EN 1193. The test set up is shown in figure 1. Two inductive measuring gauges are attached diagonally.

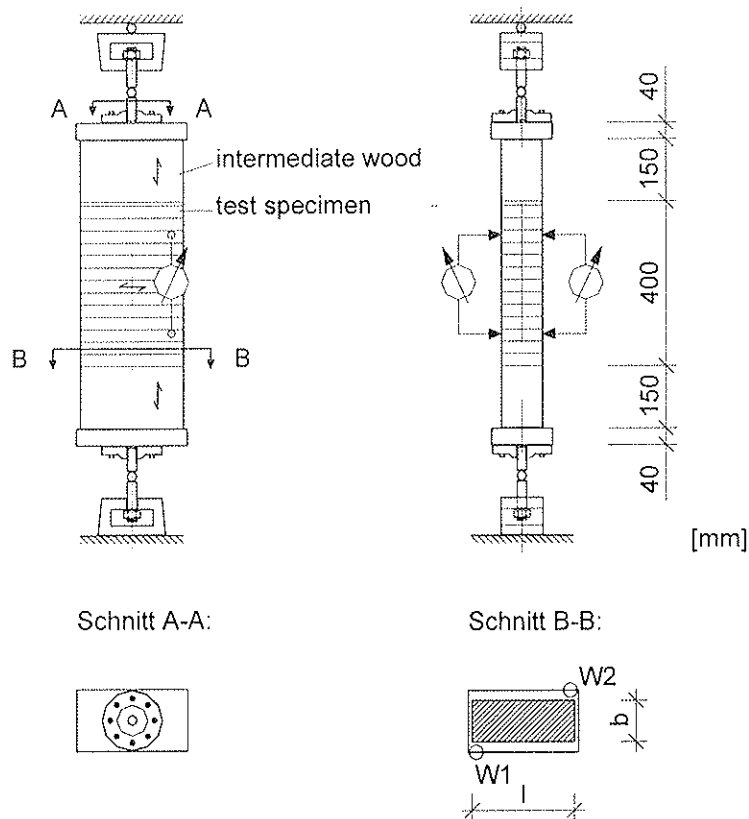


Figure 1: Test arrangement

### 3 Material

Table 1 contains the number of glulam beams of different strength classes and the respective numbers of specimens cut out of the beams. The beams of strength classes GL32 and GL36 were each delivered from two producers using the same strength grading machine. These two classes had a homogeneous cross section set-up consisting of laminations C35 or C40, respectively.

The beams of strength classes GL24 and GL28 consisted of visually graded planks. The producer of the glulam GL24 used planks C24 and better, while the beams of strength class GL28 had a combined cross section. The outer planks consisted of C30 and the inner ones of C24. Because of this similar set-up these two glulam strength classes were evaluated together.

**Table 1:** Test specimens

strength class	GL24, GL28	GL32	GL36
number of beams	54	19	24
number of specimens with the reference volume $V_0 = 0,01 \text{ m}^3$ and a height of 40 cm	79	38	36
number of test specimens with a volume $V < V_0$	46	48	61

As shown in table 1 tests were also performed with a volume smaller than the reference volume  $V_0 = 0,01 \text{ m}^3$ . These specimens had a height less than 40 cm but the same stressed area of  $250 \text{ cm}^2$  as recommended in EN 1193.

## 4 Evaluation of the tests

### 4.1 Tests with the reference volume $V_0 = 0,01 \text{ m}^3$

Figure 2 shows the frequency distribution of the tensile strength perpendicular to grain of the 153 specimens with the reference volume  $V_0$ .

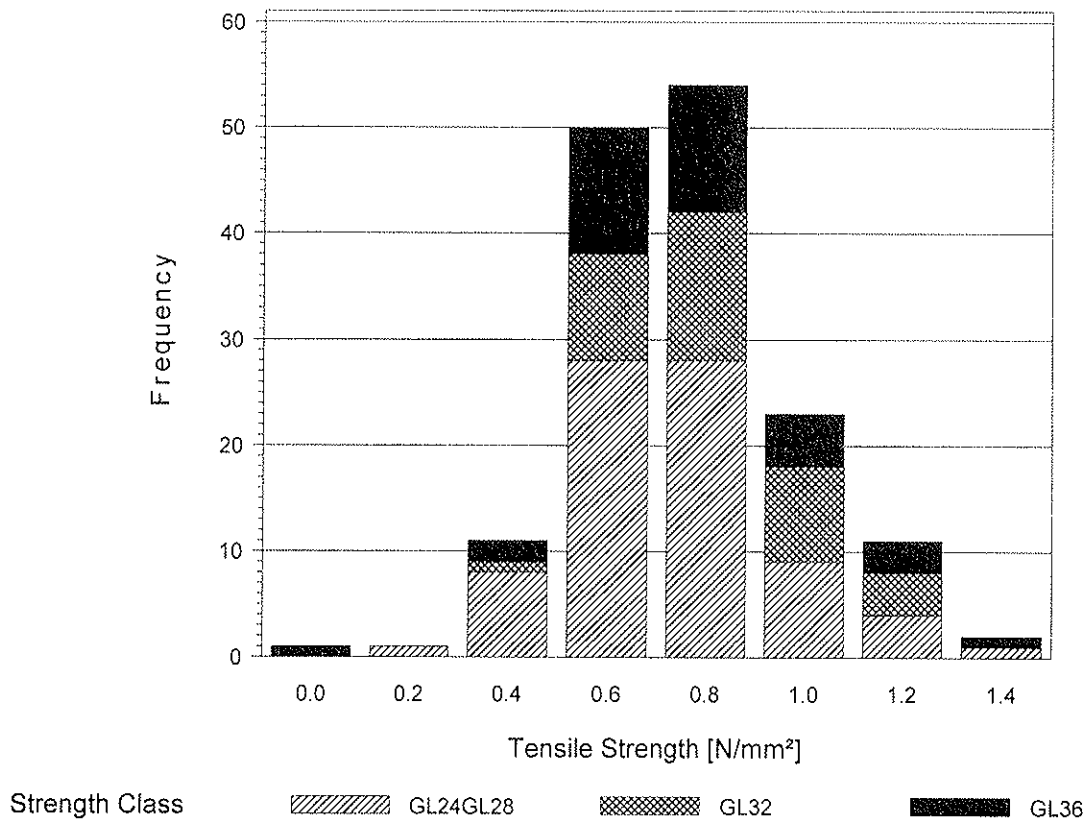


Figure 2: Frequency distribution

Table 2 summarises the results of the statistical evaluation. The 5%-percentile was determined by ranking.

**Table 2:** Statistical results for specimens with the reference volume  $V_0$

Strength Class	Number	Mean [N/mm <sup>2</sup> ]	Minimum [N/mm <sup>2</sup> ]	Maximum [N/mm <sup>2</sup> ]	5%-percentile [N/mm <sup>2</sup> ]	Standard-deviation [N/mm <sup>2</sup> ]
GL24, GL28	79	0,73	0,22	1,35	0,43	0,22
GL32	38	0,83	0,41	1,20	0,50	0,18
GL36	36	0,78	<b>0,05</b>	1,42	0,33	0,26
all	153	0,77	0,05	1,42	0,46	0,22

One specimen of strength class GL36 showed the lowest strength value of almost zero. Figure 3 shows the failed plank, figure 4 a cross section of the same plank cut from the same beam in some distance from the tested specimen shown in figure 3.



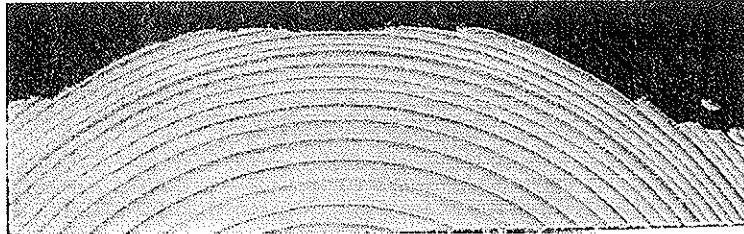


Figure 3: Failed plank of the specimen with the lowest tensile strength

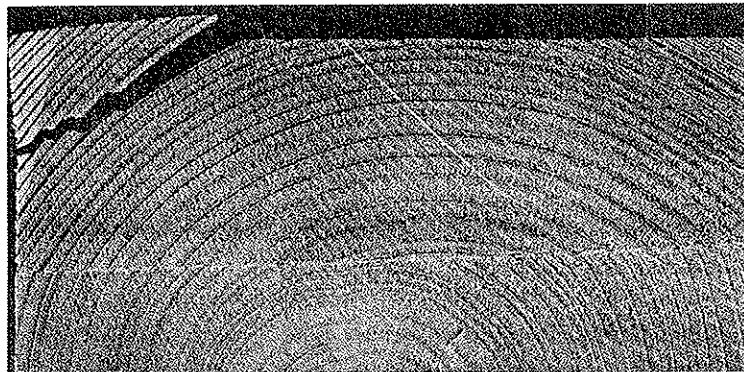


Figure 4: Untested cross section of the same plank as shown in figure 3

Figure 5 shows the load-deformation diagram of the specimen with the lowest strength.

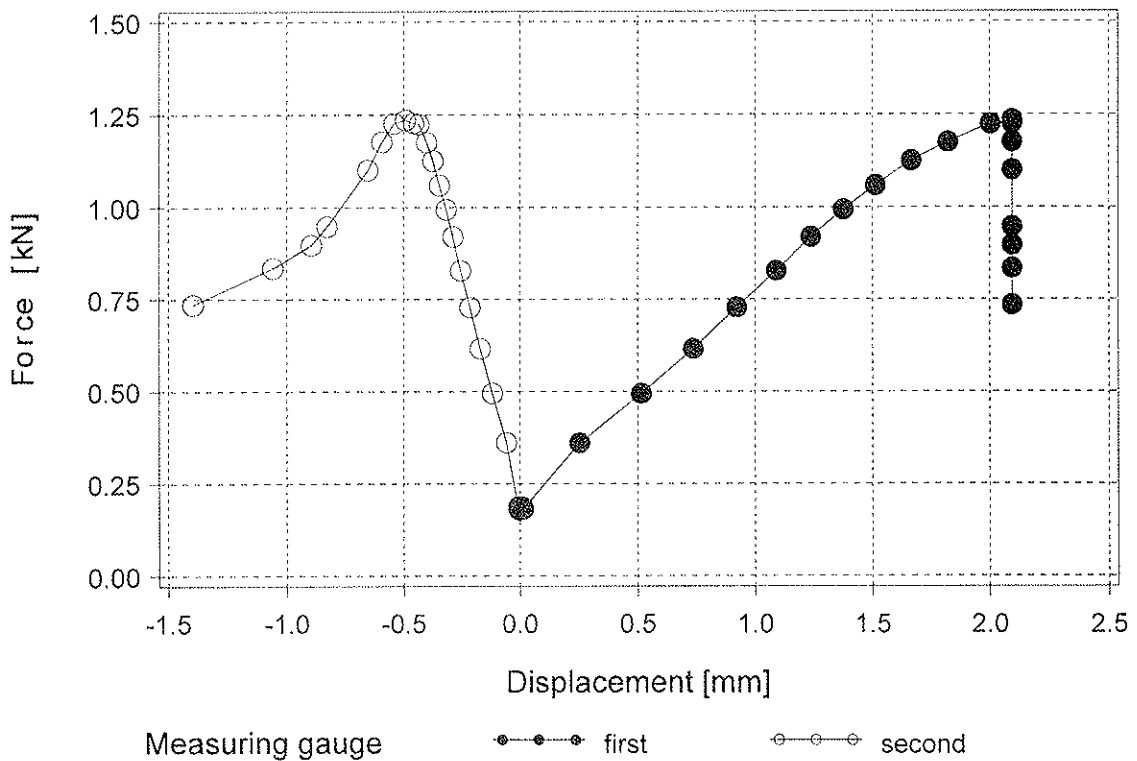


Figure 5: Load deformation of the specimen with the lowest tensile strength

Figure 6 shows a typical load-deformation diagram.

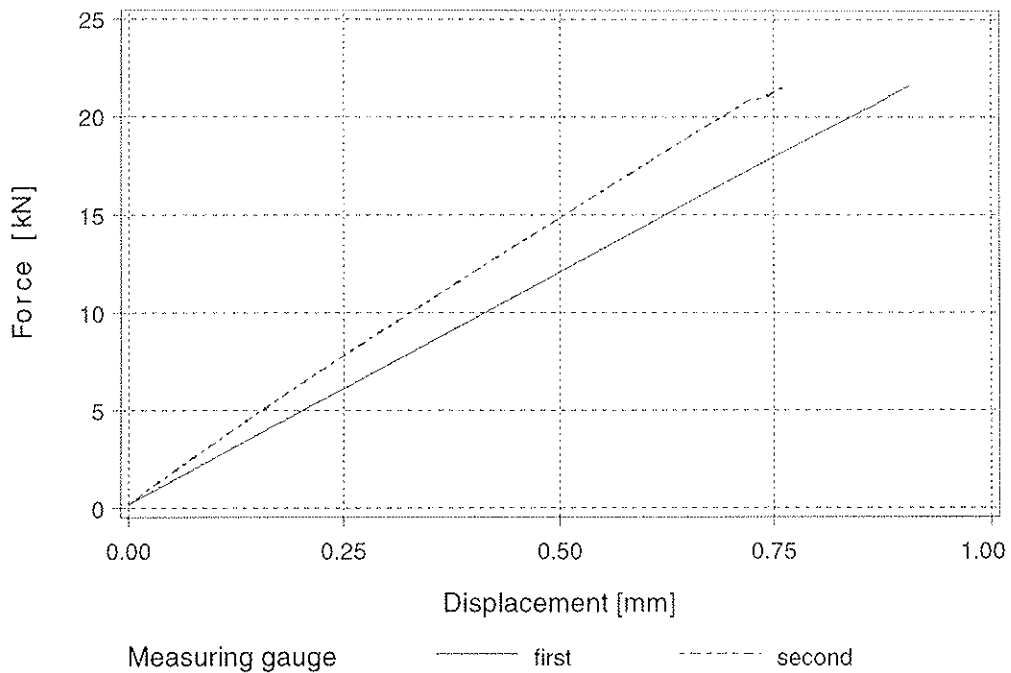


Figure 6: Example of a „normal“ load-deformation diagram

According to the diagram in figure 5 the crack seems to propagate from the side with the positive displacement while the other side even shows negative (compressive) displacements. The strength of the specimen containing a crack is limited by the start of stable crack growing while in other specimens first the formation of cracks has to take place.

One test specimen broke during the construction without loading.

Figures 7 show some typical crack shapes.

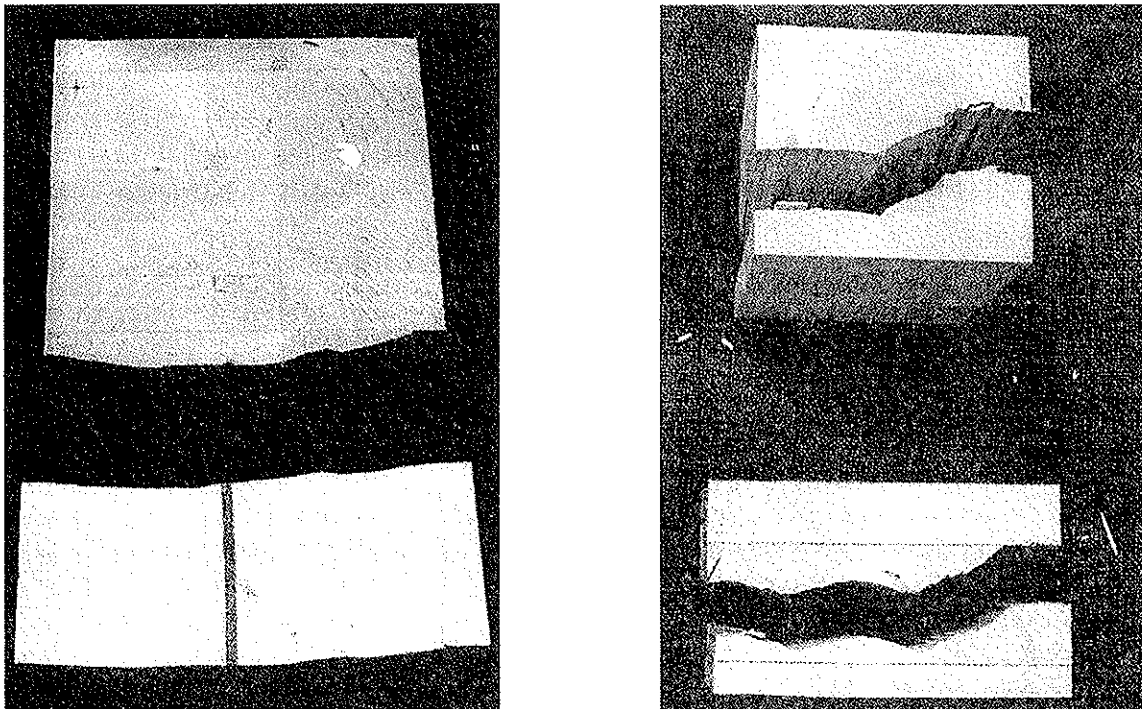


Figure 7: Typical crack shapes

If the failed plank included pith, the pith was always present in the crack (see Figure 7).

Table 3 contains the coefficients of correlation between the tensile strength and other parameters showing only a very weak correlation.

**Table 3:** Coefficients of correlation

Strength Class	Density	height of planks	width of planks
GL24GL28	-0,248	-0,159	0,171
GL32	-0,164	0,085	0,153
GL36	-0,174	0,223	0,218
all	-0,148	-0,151	0,161

The coefficient of correlation between the tensile strength and the density is even negative.

Figure 8 shows the tensile strength versus the density for all strength classes.

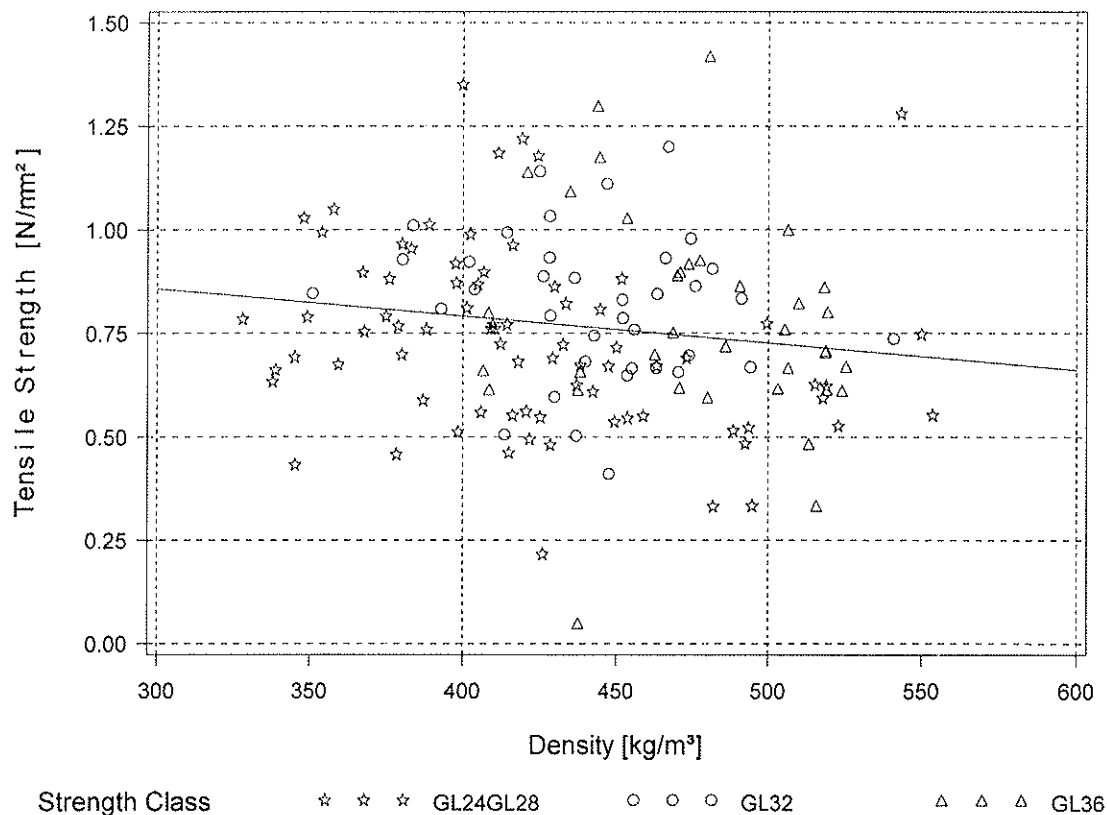


Figure 8: Tensile strength versus density

Figure 9 shows the two- and three-parameter Weibull distributions fitted to the tensile strength values of all specimens with the reference volume  $V_0$ . There is no significant difference between the two distributions.

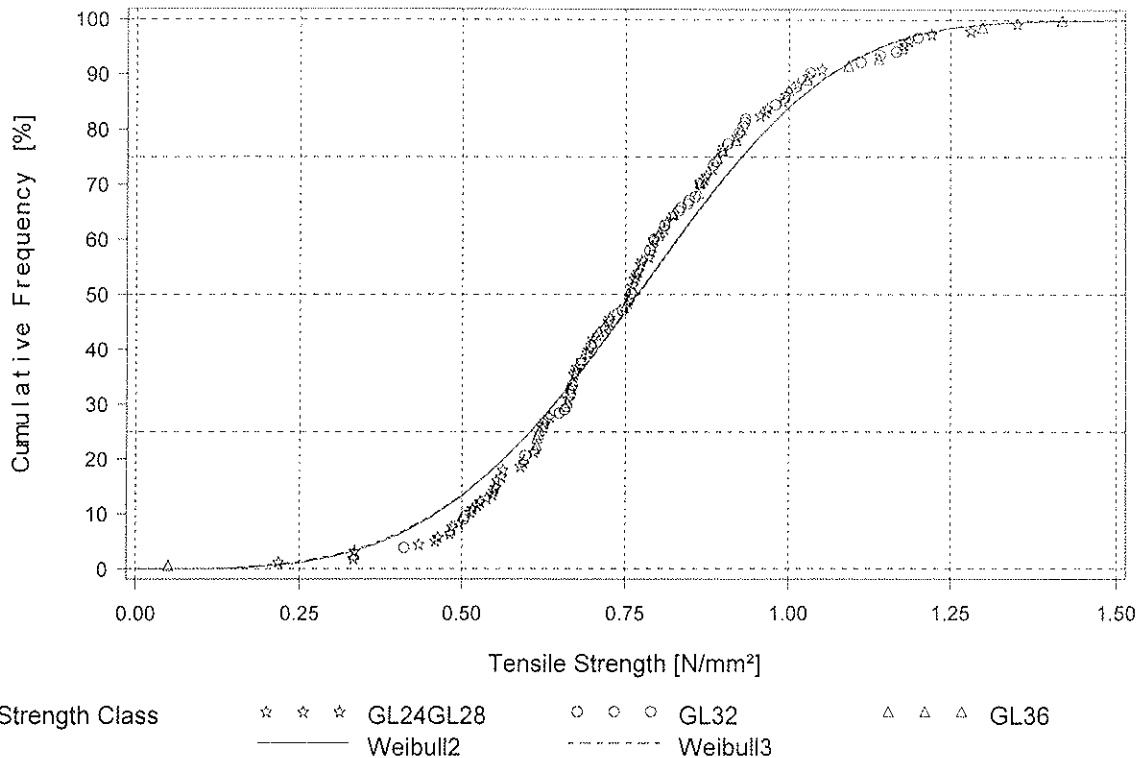


Figure 9: Weibull distribution

Table 4 contains the equations of the fitted Weibull distributions and the levels of significance based on a  $\chi$ -square test.

**Table 4:** Weibull distributions, level of significance  $\alpha$

Strength Class	2-parameter Weibull distribution	3-parameter Weibull distribution
GL24, GL28	$S = 1 - \exp - \{f_{t,90}/0,813\}^{3,591}$ $\alpha = 6,2 \%$	$S = 1 - \exp - \{(f_{t,90}-0,153)/0,651\}^{2,848}$ $\alpha = 9,2 \%$
GL32	$S = 1 - \exp - \{f_{t,90}/0,900\}^{5,092}$ $\alpha = 42,6 \%$	$S = 1 - \exp - \{(f_{t,90}-0,234)/0,659\}^{3,650}$ $\alpha = 71,5 \%$
GL36	$S = 1 - \exp - \{f_{t,90}/0,862\}^{3,172}$ $\alpha = 27,3 \%$	$S = 1 - \exp - \{(f_{t,90}+0,218)/1,093\}^{4,190}$ $\alpha = 48,1 \%$
all	$S = 1 - \exp - \{f_{t,90}/0,848\}^{3,688}$ $\alpha = 2,2 \%$	$S = 1 - \exp - \{(f_{t,90}+0,060)/0,910\}^{3,987}$ $\alpha = 5,4 \%$

#### 4.2 Tests with volumes smaller than the reference Volume $V_0 = 0,01 \text{ m}^3$

Besides the 153 tests with specimens of the reference volume, 155 tests were performed with smaller volumes with specimens consisting of one, two and three planks. Table 5 contains the evaluation of the test results.

The minimum values shown in table 5 are as high as the mean values of the specimens with the reference volume  $V_0$  as shown in table 2. This might be explained by different stress distributions in planks close to the intermediate woods compared to planks placed in the middle part of larger test specimens, further away from the intermediate wood parts.

**Table 5:** Results for specimens with a volume smaller than the reference volume  $V_0$

Strength Class	Number of Planks	Number	Mean [N/mm <sup>2</sup> ]	Minimum [N/mm <sup>2</sup> ]	Maximum [N/mm <sup>2</sup> ]	5%-percentile [N/mm <sup>2</sup> ]	Mean Volume [cm <sup>3</sup> ]
GL24, GL28	1	31	1,93	1,35	2,84	1,42	912
GL24, GL28	2	15	1,28	0,72	2,04	0,72	1822
GL32	2	17	1,48	0,82	2,15	0,82	1476
GL36	2	24	1,51	1,16	1,88	1,21	1471
GL32	3	31	1,37	0,99	1,82	1,01	2186
GL36	3	37	1,29	0,83	2,23	0,90	2195

Figure 11 shows the stress distribution calculated with a FE-Program of a plank in the centre of a specimen with the reference volume, figure 12 the stresses in the upper plank of a specimen with two planks, and figure 13 the stress distribution in the lower plank, respectively.

Figure 10 shows the model of one plank used for the calculations. Thirteen of these planks were used for the model of a specimen with the reference volume  $V_0$ . The stresses shown in figures 11 - 13 are referenced to line 1 - 1, the symmetry axis according to figure 10. The centre of the cylindrical coordinate system of each plank was positioned in the centre of the lower surface. Beside the stresses in radial and tangential direction and the shear stresses figures 11 - 13 show stresses transformed perpendicular to line 1 - 1.

The applied load would lead to an uniform stress of 0,77 N/mm<sup>2</sup>.

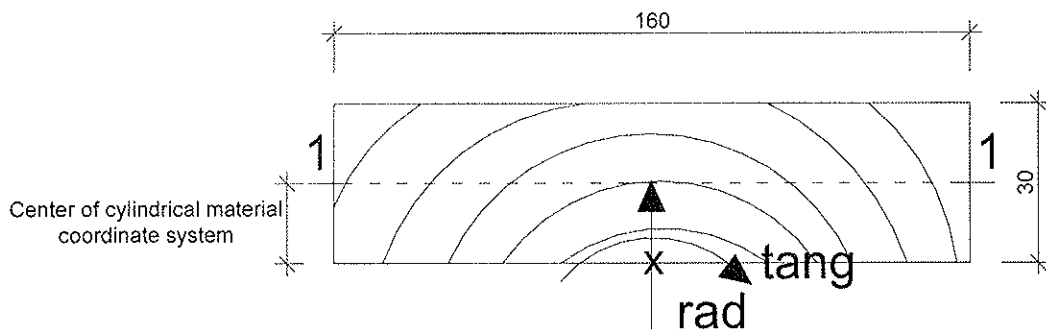


Figure 10: Model used for the FE calculation

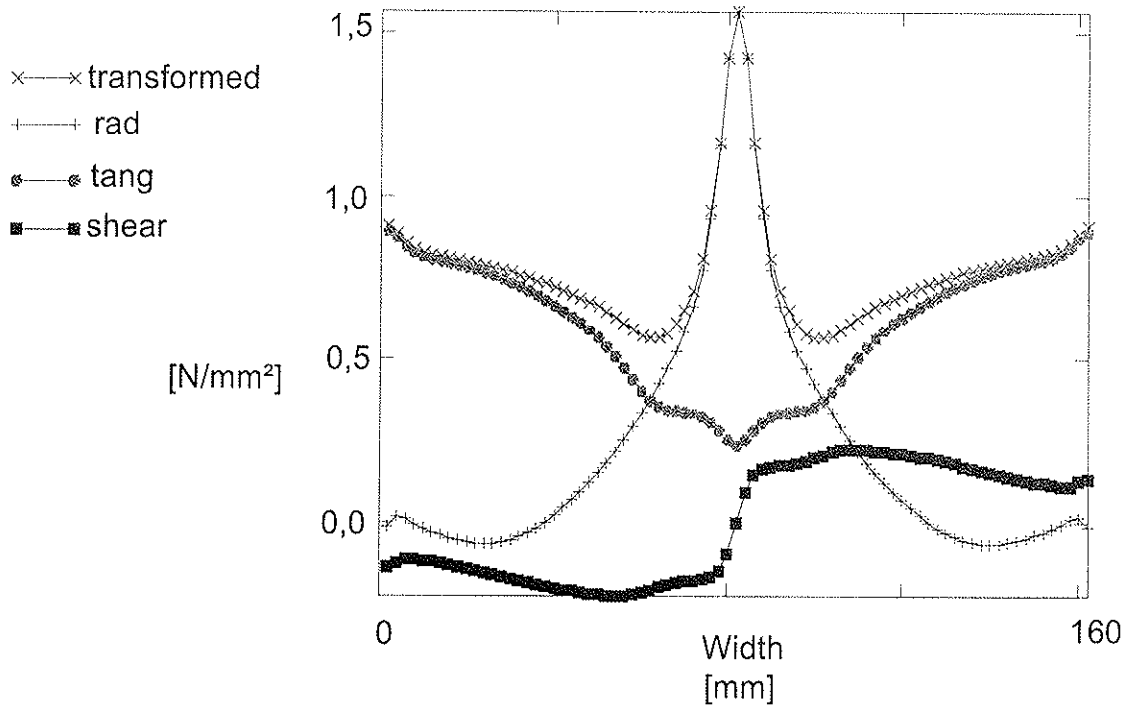


Figure 11: Stresses along line 1-1 of a plank in the midst of a specimen with the reference volume and a height of 40 cm

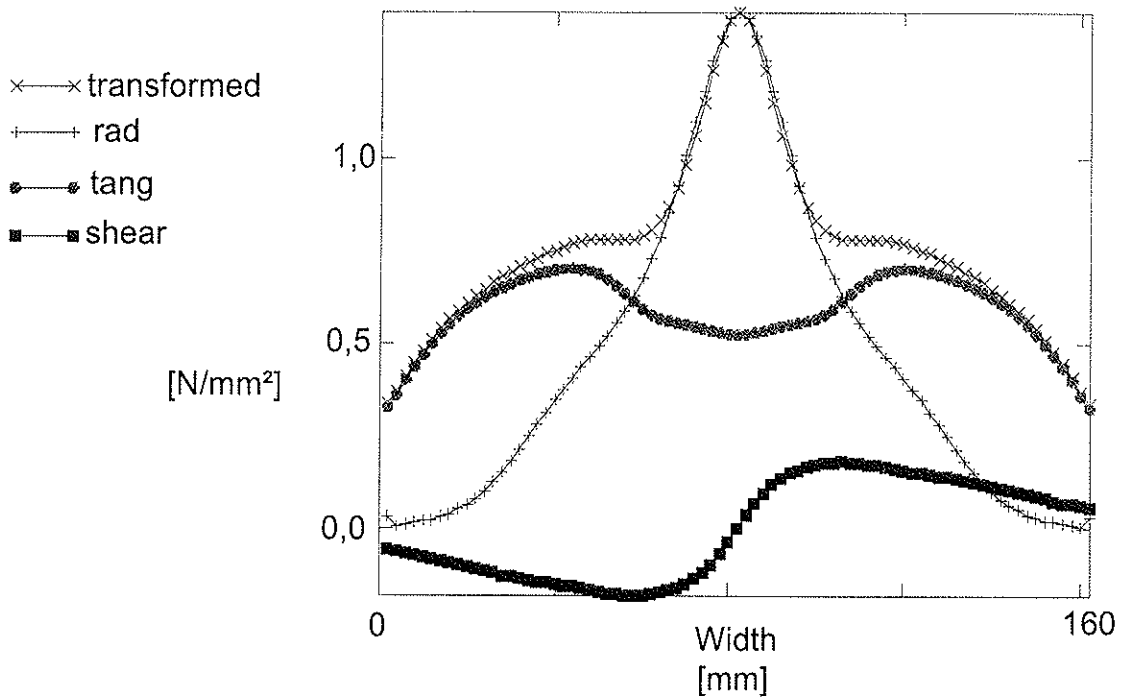


Figure 12: Stress distribution of the upper plank of a specimen of two planks

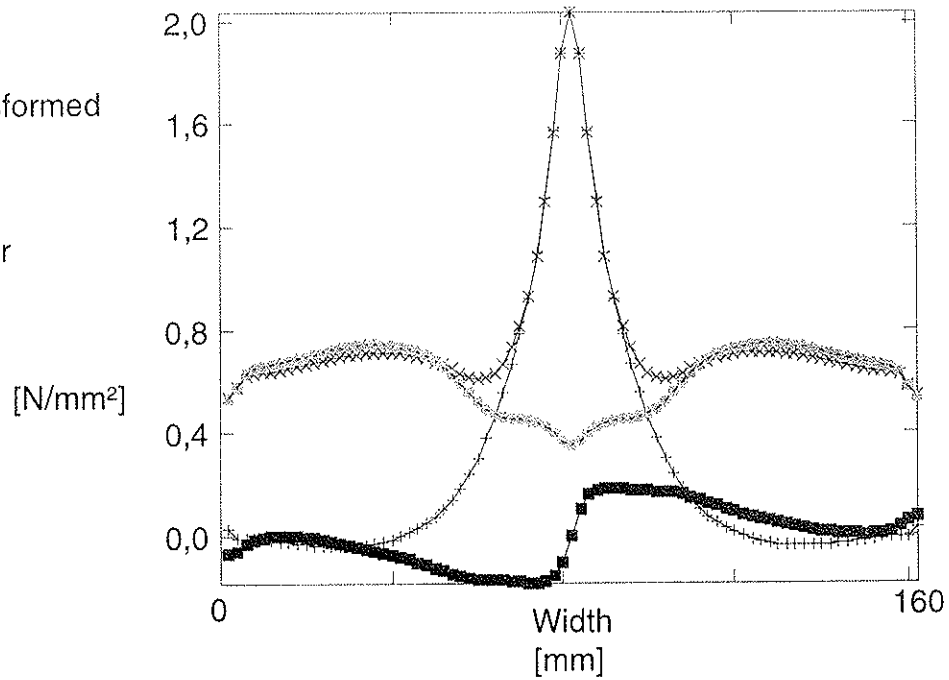


Figure 13: Stress distribution of the lower plank of a specimen of two planks

As the diagrams show, the stresses at the timber surface are lower for the planks of a specimen consisting of only two planks. According to linear elastic fracture mechanics for isotropic materials a lower load is necessary for crack growing from the surface compared to crack growing from the centre. If cracks mostly occur at the surface, this could be the reason for the higher strength of the specimens with small volumes.

## 5 Volume effect according to Weibull's theory

If the test series with two and three planks of GL32 and GL36, respectively, as shown in table 5, are evaluated as one sample, table 6 results.

**Table 6:** Combined series of specimens with a volume smaller than the reference volume  $V_0$

Number of Planks	Number	Strength Class	Mean [N/mm <sup>2</sup> ]	5% - fractile [N/mm <sup>2</sup> ]	Mean of Volume [cm <sup>3</sup> ]
1	31	GL24, GL28	1,93	1,42	932
2	15	GL24, GL28	1,28	0,72	1822
2	41	GL32, GL36	1,50	1,10	1473
3	67	GL32, GL36	1,32	0,94	2191

Using the values of table 6 and those of table 2 containing the results of specimens with the reference volume  $V_0$  the exponent  $k$  of the two-parameter Weibull distribution is calculated under the assumption of a uniform stress distribution from:

$$S = 1 - \exp - \{ \sigma / \sigma_V \}^k \quad (2)$$

Or directly by

$$\sigma_2 / \sigma_1 = (V_1 / V_2)^{1/k} \quad (3)$$

$$k = \{\ln(V_1/V_2)\} / \{\ln(\sigma_2/\sigma_1)\} \quad (4).$$

Table 7 and table 8 contain the k-values calculated with the mean-values and the 5%-percentile values, respectively, of table 2 and table 6. For comparison the k-values of the two-parameter Weibull-distribution as shown in table 4 are shown in the second column.

**Table 7:** k-values of the two-parametric Weibulldistribution calculated with the mean values of table 2 and table 6

$V_0 = 10000$ $\text{cm}^3$	Exponent k of the 2-parameter Weibull distribution as shown in table 4	GL24GL28 $V = 932$ $\text{cm}^3$	GL24GL28 $V=1822$ $\text{cm}^3$	GL32GL36 $V=1473$ $\text{cm}^3$	GL32GL36 $V=2191$ $\text{cm}^3$
GL24GL28	3,59	2,44	3,03	2,66	2,56
GL32	5,09	2,81	3,93	3,24	3,27
GL36	3,17	2,62	3,44	2,93	2,89
all	3,69	2,58	3,35	2,87	2,82

**Table 8:** k-values of the two-parametric Weibulldistribution calculated with the 5%-fractile values of table 2 and table 6

$V_0 = 10000$ $\text{cm}^3$	Exponent k of the 2-parameter Weibull distribution as shown in table 4	GL24GL28 $V = 932$ $\text{cm}^3$	GL24GL28 $V=1822$ $\text{cm}^3$	GL32GL36 $V=1473$ $\text{cm}^3$	GL32GL36 $V=2191$ $\text{cm}^3$
GL24GL28	3,59	1,99	3,30	2,04	1,94
GL32	5,09	2,27	4,67	2,43	2,41
GL36	3,17	1,63	2,18	1,59	1,45
all	3,69	2,11	3,80	2,20	2,12

The two-parameter Weibull distribution fitted to all tests with the reference volume is

$$S = 1 - \exp - \{f_{t,90}/0,848\}^{3,688} \quad (5)$$

Ranta-Maunus (1998) compares the tensile strength of specimens with the reference volume  $V_0$ , with that of larger volumes and gives for short term tests an exponent  $k = 3,33$ . Eurocode 5 assumes  $k = 5$ . Consequently the tensile strength of a stressed volume  $V_{\perp} = 0,1 \text{ m}^3$  should be reduced by

$$\begin{aligned} (V_0/V_{\perp})^{1/k} &= (0,01/0,1)^{0,2} = 0,63 \\ (V_0/V_{\perp})^{1/k} &= (0,01/0,1)^{0,3} = 0,50 \end{aligned}$$

using  $k = 5$  according to EC5  
using the exponent  $k = 3,33$ .



## 6 Conclusions

The tensile strength perpendicular to the grain shows no significant correlation with wood density and does not differ for different glulam strength classes. This contradicts EN 1194. The lowest values determined in tests are close to zero. Structural details with tensile stresses perpendicular to the grain should be avoided or the timber should be reinforced perpendicular to the grain.

More important than the volume effect according to Weibull seems to be the presence of macroscopic defects as ring shake. Macroscopic defects lead to failures governed by stable crack growth.

Based on the test results the volume effect seems to be stronger than assumed by EC5. The exponent  $k$  was determined as  $k \cong 3$  compared to  $k = 5$  given in Eurocode 5.

## 7 Literature

Aicher, S. und Dill-Langer, G. (1995). Zugfestigkeit senkrecht zur Faserrichtung von qualitativ hochwertigem Brettschichtholz gemäß CEN Festigkeitsklassen GL32 und GL36. Otto Graf Journal Vol. 6 1995, Forschungs- und Materialprüfanstalt Baden-Württemberg FMFA -Otto Graf Institut

Aicher, S. und Dill-Langer, G. (1997). DOL Effect in Tension Perpendicular to Grain of Glulam Depending on Service Classes and Volume. CIB-W18/30-9-1

Ranta-Maunus, A. (1998). Duration of Load Effect in Tension Perpendicular to Grain in Curved Glulam. CIB-W18/31-9-1

Weibull, W. (1939). The Phenomenon of Rupture in solids. Royal Swedish Institute for Engineering Research, Proceedings, Nr. 153, s.55.

**INTERNATIONAL COUNCIL FOR RESEARCH AND INNOVATION  
IN BUILDING AND CONSTRUCTION**

**WORKING COMMISSION W18 - TIMBER STRUCTURES**

**ON THE RELIABILITY-BASED STRENGTH ADJUSTMENT FACTORS  
FOR TIMBER DESIGN**

T D G Canisius  
Structural Reliability Unit  
Building Research Establishment Ltd.  
UNITED KINGDOM

**MEETING THIRTY-TWO**

**GRAZ**

**AUSTRIA**

**AUGUST 1999**

---

Presenter: T.D.G.Canisius

· No discussions.

# On the Reliability-based Strength Adjustment Factors for Timber Design

T.D.G. Canisius

*Structural Reliability and Risk Analysis Unit  
Construction Division, BRE Ltd., England*

**Key Words** beam strength, moment configuration factors, strength adjustment factors, volume effects, length effects, structural reliability

**Summary** Reliability-based moment configuration factors for timber beams were introduced in 1994. At that time, a simple strength model was used to show that reliability-based moment configuration factors were smaller, and hence 'enhance' the strength less, than the corresponding characteristic strength-based factors. This observation has been confirmed recently on the basis of an experimentally based strength model. The reason for this phenomenon and other situations where similar behaviour may be expected are presented in this paper.

## 1 Introduction

In Codes of Practice for engineering design of timber structures, strengths of various species and classes of timber are provided with respect to standard conditions and specimen dimensions. Hence, during design exercises various adjustment (or modification) factors are used to evaluate strengths under non-standard conditions.

Traditionally strength adjustment factors for timber design were based on a chosen fractile, usually the fifth percentile, of the strength probability distribution. However, as limit states design (indirectly) aims to provide predetermined levels of structural reliability, reliability-based procedures are more appropriate for the development of these factors. Reliability-based adjustment factors can be determined such that equal reliability levels are achieved under different design situations of a given member. It was Foschi *et.al.* [1989] who pioneered the development of such modification factors.

Strength adjustment factors for moment configuration effects in beams is a recent topic of interest to researchers and engineers. Moment configuration effects refer to the statistical 'strength' difference in timber beams, apparent under different bending moment configurations. This phenomenon is caused by the lengthwise variation of timber strength. For example, consider the European beam strength (MOR) test method where the strength of the (presumed) weakest cross section of each test beam is evaluated. (The strength-testing of the weakest cross section is only an ideal: it is not possible to always pre-determine and always test the weakest cross section.) When this 'minimum' test strength is used in a design exercise, it is effectively implied that the positions of maximum bending moment under all relevant design situations coincide with the weakest cross section of each and every beam. However, the coincidence of positions of weakest strength and the

maximum moment is not a certain event; but it is a probabilistic one governed by both the bending moment profile and the statistics of the lengthwise strength variation. Moment Configuration Factors (MCFs) are expected to consider this probabilistic phenomenon to evaluate the probabilistic 'strength' (maximum bending moment) of a beam under various non-standard (*i.e.* non-uniform) bending moment profiles. Figure 1 provides a schematic representation of this phenomenon with respect to a single beam.

There have been many past attempts at determining characteristic strength based MCFs, defined as the ratio between the respective (5th percentile) characteristic strength values under a given moment profile and the reference (uniform) moment profile. Most of these past works have been detailed in various previous publications such as, for example, Canisius [1992] and Canisius and Isaksson [1996], and most are available in previous CIB-W18 Proceedings. Some recent related works, including the development of strength models, are given at the end of this paper.

It was in 1994 that the concept of reliability-based moment configuration factors was introduced as a better alternative to characteristic strength-based MCFs [Canisius, 1994]. A reliability-based MCF was defined as the strength adjustment factor that provides the same reliability level under the relevant non-uniform bending moment profile and under a uniform moment, when both these loads provide the same peak bending moments. In that paper, under the considered conditions, the reliability-based strength enhancement factors were observed to be smaller (and closer to unity) than the corresponding characteristic strength-based factors. This view has now been confirmed with an experimentally based superior strength model by Isaksson [1998].

This paper explains the statistical reason for the observed differences between characteristic strength-based and reliability-based MCFs. In addition, some observations are made on strength adjustment factors that reflect other statistical and physical causes for changes in timber strength.

## **2 Reliability and Characteristic Strength-based Moment Configuration Factors**

As background material, this section presents some results obtained by Canisius [1994]. The determination of the MCFs presented did not consider phenomena such as self-weight, duration of load, load sharing and size effects, and assumed that beam failure is governed only by the bending strength.

The presented results were obtained in relation to a 3-parameter Weibull strength distribution for 47mmX95mmX4m Canadian Hem Fir under dry conditions. This strength distribution was obtained from the BRE data bank. As detailed by Canisius [1994], the test-strength distribution was manipulated to obtain an approximate statistical relation for the lengthwise variation of strength. The load distribution was assumed to be a Gumbel distribution.

Table 1 shows a comparison of characteristic strength-based and reliability-based MCFs for several simple examples. These situations correspond to a simply supported beam with a central concentrated load and a uniformly distributed load, and to a cantilever with a

concentrated load at its tip. The last column of the Table presents the MCFs determined on the basis of the (5th percentile) characteristic strength values under the respective moment configurations. The reliability-based MCFs are presented for probabilities of failure of 1E-03, 1E-04, 1E-05 and 1E-06, denoted respectively as P3, P4, P5 and P6. The considered residential and commercial loads with coefficients of variation (COV) of 0.272 and 0.133, respectively, were obtained from Foschi *et.al.* [1989].

Load Type	COV = 0.272				COV = 0.133				Characteristic strength-based
	P6	P5	P4	P3	P6	P5	P4	P3	
Conc. Ld.	1.14	1.17	1.20	1.23	1.11	1.13	1.15	1.20	1.31
UDL	1.10	1.11	1.12	1.14	1.08	1.09	1.10	1.12	1.17
Cantilever	1.19	1.22	1.25	1.29	1.15	1.17	1.20	1.26	1.38

**Table 1. Reliability-based and characteristic strength-based moment configuration factors.** (From Canisius, 1994)

As to be seen from Table 1, for each load case the MCFs decrease with the increase of reliability level considered. In each load COV case, all the reliability-based factors are smaller than the corresponding characteristic strength-based factor, and the difference increases with the increase of the target reliability level.

From the presented results it can be also seen that, for a given bending moment profile and reliability level, the reliability-based factor is smaller for the load with the lower COV. For example, the MCFs are 1.15 and 1.20 for COVs of 0.133 and 0.272, respectively, for a probability of failure of 1 in 1000 (P4 of Table 1).

### 3 A General Strength Change (Reduction)

Reliability-based and characteristic strength-based strength adjustment factors for a general strength change (in relation to a standard test strength) are considered here. These strength variations are arbitrary reductions given rise to by translations (C) and factoring (by A) according to the relation

$$X' = AX + C$$

where  $X$  is the (original) test strength and  $X'$  is the new strength under a different condition. The results presented here were obtained from an internal BRE document [Canisius, 1993].

The ratio ' $q$ ' between the reliability-based and characteristic strength-based strength adjustment factors for a load with a coefficient of variation of 0.272 are presented in Figure 2. The horizontal axis of the Figure represents the reliability levels considered in determining the reliability-based strength adjustment factors. As can be seen from the results, for strength factoring only (*i.e.* C=0) the characteristic strength and reliability-

based adjustment factors are identical (*i.e.*  $q = 1.0$ ). With the relative increase of the translational component  $C$ , the ratio  $q$  is seen to be smaller under a given  $A$  value. That is, here the strength reduction in terms of the characteristic strength is greater than what is implied by reliability-based considerations. (The opposite would have been observed under a strength enhancing phenomenon such as the moment configuration effect.) For a given  $A$  and  $C$  ( $\neq 0$ ), the difference between the two types of factors increases with the decrease of the probability of failure.

## 4 Discussion

### 4.1 The Bending Strength Distribution, and Lower and Upper Strength Bounds

Consider a beam as shown in Figure 3-a with, for example, four idealised concentrated defects. Let the unique strength of this beam when there are no defects be  $S_{\text{clear}}$ . Let the strength of the beam with defects, when under a uniform bending moment, be  $S_{\text{test}}$ . This (ideal) 'test strength' of the beam is equal to the strength of its weakest cross section (*i.e.* where the most significant defect occurs).

The strengths of the above beam when subject to two other bending moment configurations are shown in Figure 3-a. For example, when a central concentrated load and a uniformly distributed load act on the (simply supported) beam, the beam strengths are the maximum applied bending moments  $S_c$  and  $S_u$ , respectively.

Now, the defect-free strength  $S_{\text{clear}}$  of each beam in a population would be randomly distributed. Let this random distribution possess a lower limit  $S_{\text{cl-low}}$  and, possibly, also an upper limit  $S_{\text{cl-high}}$  as shown in Figure 3-b. At a cross section where there is a defect, the bending strength will be lower than the defect-free strength in relation to the relative size and location of the defect within the cross section.

Let us consider a beam with the lowest defect-free strength  $S_{\text{cl-low}}$  (Figure 3-c). This beam has been shown with the most significant defect that may be expected to occur under the relevant grading criteria. The lower bound  $S_L$  of the beam strength distribution under the uniform moment profile is equal to its strength at the cross-section with this defect. As the bending moment profile is uniform, the lower bound does not depend on the location of the defect along the beam. However, the weakest 'strength' of the beam when subject to a non-uniform bending moment profile would occur when the location of the defect coincides with the respective peak bending moment. Even then, the lowest beam strength will uniquely be  $S_L$  (see Figure 3-c). As the most significant defect is considered here, this unique strength lower bound is not affected by the presence of additional defects within the beam.

Arguments similar to the above apply with respect to the highest beam strength under various bending moment profiles. In that case, a unique upper bound will be formed by the defectless beam having the maximum strength  $S_{\text{cl-high}}$ . When there are no defectless beams a unique upper bound may not exist. However, this would not affect the following discussion which is in relation to the lower tail of the strength distribution.

## 4.2 Strength Enhancement (Modification) Factors

Consider Figure 4 where a strength enhancement is shown. Here  $X_C^T$  is the 5th percentile (characteristic) strength from the statistical distribution for test strengths (Line C1), and  $X_C^O$  is the corresponding value from the strength distribution (Line C2) under a non-uniform bending moment. Based on these, the characteristic strength-based MCF ( $MCF_C$ ) is given by

$$MCF_C = X_C^O / X_C^T .$$

During a design exercise, the use of an MCF would result in the reduction of beam section modulus such that all beam strengths (in terms of bending moment) are scaled by the factor  $1/MCF_C$ . This would result in beams with a 'test strength' distribution as denoted by Line C3 of Figure 4.

Now consider Figure 5 where the lower tail of the strength distribution and the upper tail of the action-effect (maximum bending moment) distribution are shown in detail. In the case of a structural engineering problem the overlap of load and strength curves typically occurs only slightly; for example, as shown in Figure 5. The probability of failure of a member is related to the extent of this overlap, with a higher overlap implying a relatively higher probability of failure.

In Figure 5, Line C2 for the non-uniform moment profile represents a higher reliability level than that under a uniform moment with the same maximum stress (Line C1). Line C4 is the strength distribution under the 'non-uniform moment' profile for beams with a cross-section as represented by Line C3. Now, although the expected result of the strength adjustment is that probability of failure under Line C4 be the same as that under Line C1, due to the higher level of factoring by  $MCF_C$ , this result is not achieved here. The solution for this is to use a reliability-based factor  $MCF_R$ , which is smaller than  $MCF_C$ . This would give strength distributions C5 (for uniform moment) and C6 (for non-uniform moment), resulting in identical levels of reliability under the moment profiles represented by Lines C1 and C6.

## 4.3 The Relative Size of Reliability-based MCFs

The process of determining reliability-based strength factors essentially results in a weighted average of the MCFs for fractiles within the strength region of interest, *viz.* the lower tail of the strength distribution where the overlap with the action-effect curve occurs. Now, as can be appreciated from Figure 5, when the target reliability is increased, the overlap of action-effect and strength probability distribution curves would decrease. That is, the increase of the target reliability level would result in reliability-based MCFs that are more related to the lowest portion of the strength distribution curve and less related to the MCF at the 5th percentile characteristic strength. Thus, with the MCF at the strength lower bound being unity,  $MCF_R$  also would approach unity as the target reliability level is increased. This explains the two effects observed in Section 2, *viz.*

- 'equal reliability' considerations provide strength-enhancing MCFs smaller than the corresponding characteristic strength-based MCFs, and
- as the target probability of failure decreases, the reliability-based MCFs approach unity.

It is to be noted that while the above considerations refer to the change of strength distribution curve, the numerical examples used here calculated the reliability-based factors by changing the action-effect distribution. The latter reflects the procedure for a strength check. However, any difference in MCFs due to this is not expected to be of significance for engineering purposes.

#### 4.4 Statistical Length Effect

Statistical length effect (where no fracture energy considerations are made) is a phenomenon similar to the moment configuration effect. Here, as the member length is increased, the strength distribution 'shifts to the left' to reflect a corresponding strength reduction. The lower bound of strength under any member length occurs when the most significant defect occurs in the member with the lowest defect free strength. Then, considering arguments similar to that presented with respect to MCFs, it can be shown that reliability-based strength changes are lower (*i.e.* factors to be nearer to 1) than the corresponding characteristic strength-based values. This, in fact, has been observed by Isaksson [1998].

#### 4.5 Physical Changes of Strength

In the case of physical changes of strength - *e.g.* under moisture variations - the strength lower bound itself will change. Although such changes need not be identical for all fractiles, it is plausible to assume that similar changes occur within limited ranges of fractiles, for example, within the distribution lower tail. Thus, a reliability-based factor, which is a weighted average of similar values, need not be much different from the corresponding characteristic strength-based factor. However, these considerations need not be applicable in a similar manner to damage accumulation phenomena such as the duration of load effect.

### 5 Conclusion

This paper presented some example results for reliability-based moment configuration factors (MCFs) obtained from the author's previous works. It explains the statistical reasons for the observations that reliability-based moment configuration factors (MCFs)

- are smaller than corresponding characteristic strength-based factors, and
- approach unity as the target reliability level is increased.

Although the presented numerical results are based on particular probability distributions, provided there is a (non-zero) strength lower bound and the reliability levels are not very low, the presented statistical arguments are generally applicable; including even when more than a single action is present. The paper also explains how similar arguments may be applied to other statistical strength adjustment factors and why the same need not be true for physical strength adjustment factors.

Isaksson [1998], who considered reliability-based MCFs and length effects, concluded that some strength adjustment factors may have only relatively minor effect on timber design. As explained in this paper, this is a situation aided by the presence of an invariant (non-zero) lower bound to the statistical distribution of strength.



It is seen that a study of reasons for statistical strength changes and their effect on the probability distribution can provide an initial indication of the relative size of (reliability-based) strength adjustment factors to be expected. Where the reliability-based strength adjustment factors are very low, Code developers need to weigh the benefits of possibly marginal changes in economy or safety index against the disadvantages of increasing the complexity of design and the higher possibility of human error.

## References

**Canisius, T.D.G. (1992);** *Moment Configuration Factors for Simple Beams*, Paper No. 25-6-1, Proc. CIB-W18, Meeting 25, Ahus, Sweden.

**Canisius, T.D.G. (1993);** *Changes in Material Strength and Level I Designs*, Report No. PD302/93, BRE, Watford, England.

**Canisius, T.D.G. (1994);** *Reliability-based Moment Configuration Factors for Timber Beams*, *Structural Safety*, **16**, pp. 215-226.

**Canisius T.D.G. and Isaksson T. (1996);** *Determination of Moment Configuration Factors Using Grading Machine Readings*, Paper No. 29-5-2, Proc. CIB-W18, Meeting 29, Bordeaux, France.

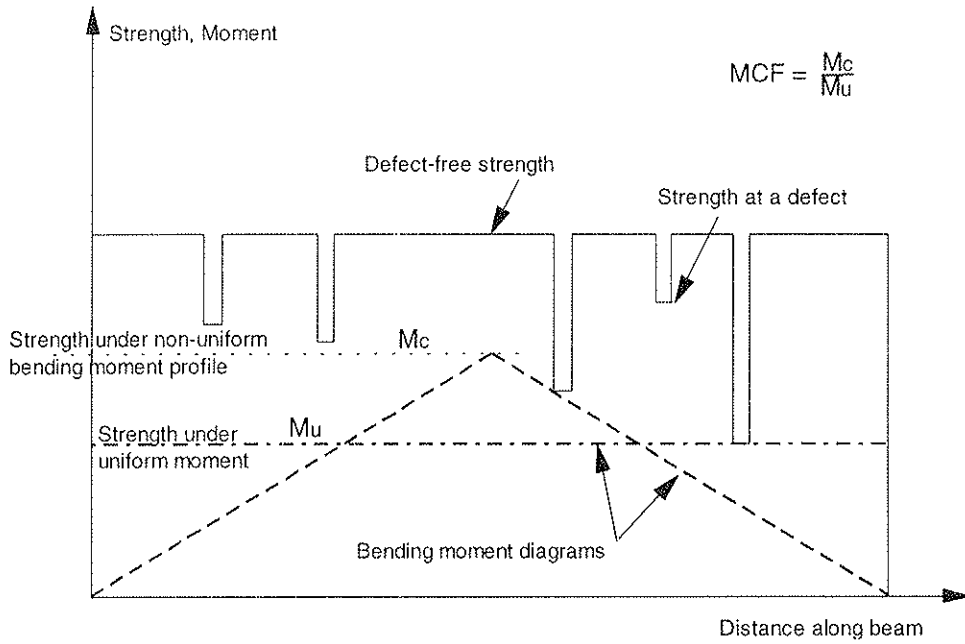
**Ditlevsen O. and Kallsner B. (1998);** *System Effects Influencing the Bending Strength of Timber Beams*, Proc. IFIP 8th WG, Working Conf. on Reliability and Optimization of Structural Systems, Krakow, Poland.

**Foschi R.O., Folz B.R., and Yao F.Z. (1989);** *Reliability-based design of wood structures*, Structural Research Series Rept. No. 34, Dept. of Civil Engineering, The University of British Columbia, Vancouver, Canada.

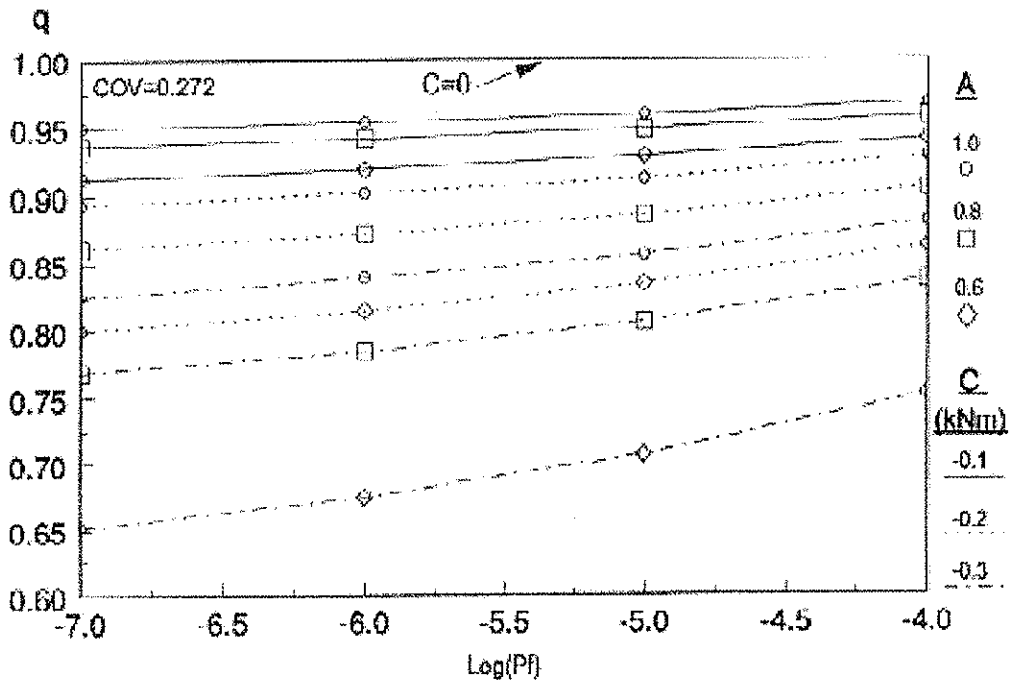
**Isaksson, T. (1998);** *Length and Moment Configuration Factors*, Paper No. 31-6-1, Proc. CIB-W18, Meeting 31, Savonlinna, Finland.

**Kallsner B., Salmela K., and Ditlevsen O. (1997);** *A Weak-Zone Model for Timber Bending*, Proc. CIB W18, Meeting 30, Vancouver, Canada.

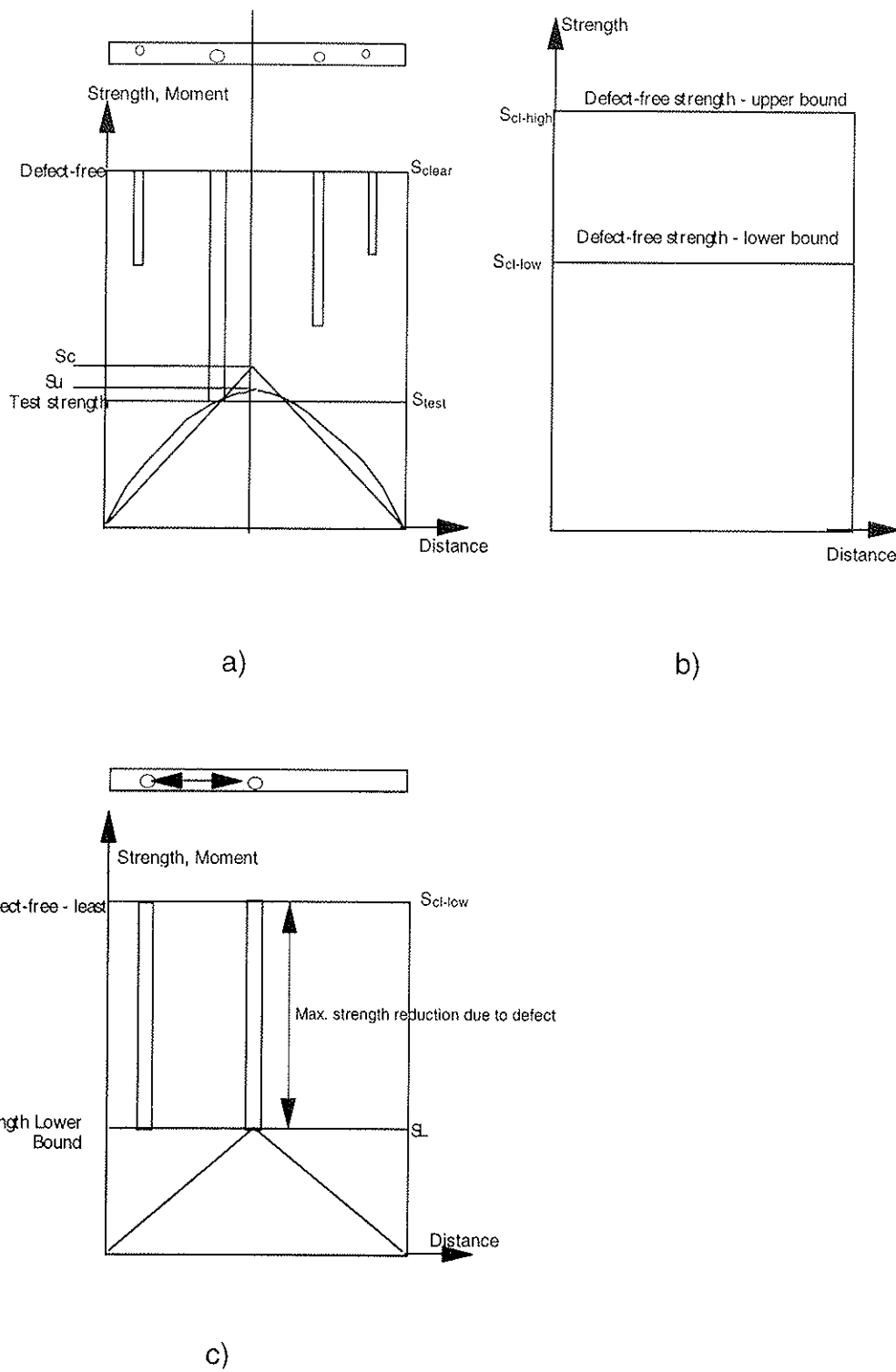
**Kallsner B. and Ditlevsen O. (1998);** *A Weak-Zone Model for the Bending Strength of Structural Timber*, Proc. World Conference in Timber Engineering, Zwitzerland.



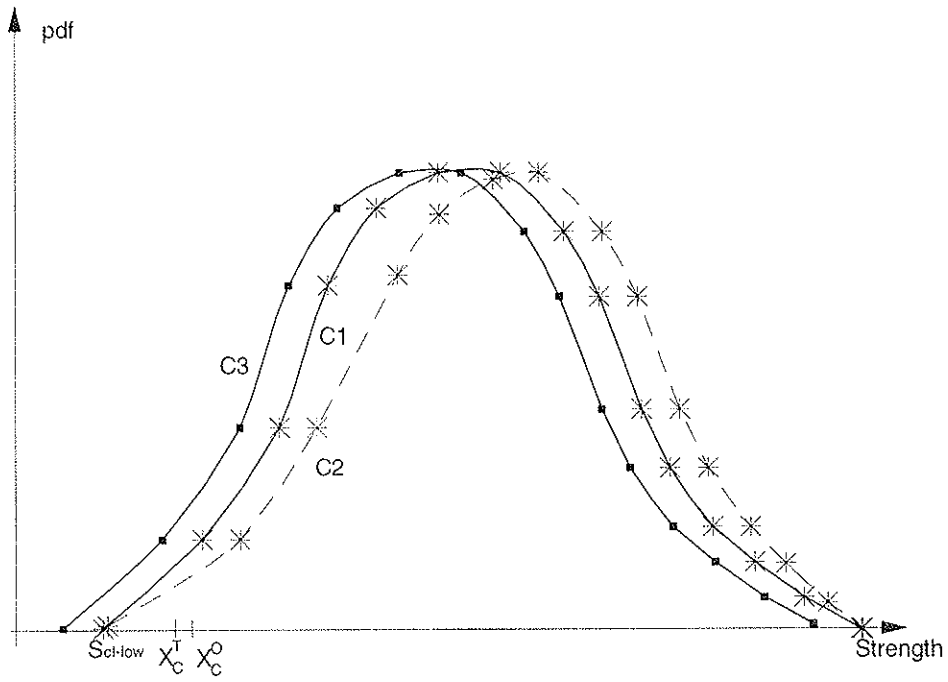
**Figure 1** Differences in bending strength due to moment configuration. (Idealised strength profile)



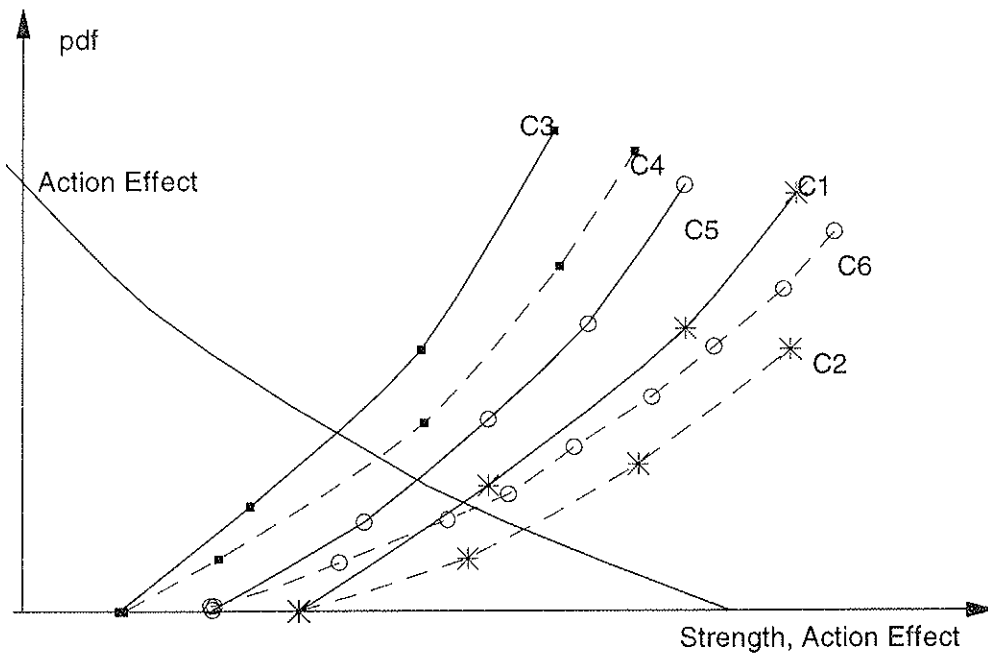
**Figure 2** The ratio  $q$  between reliability-based and characteristic strength based adjustment factors under strength reduction. (A lower ratio implies a relatively large characteristic strength based adjustment factor.)



**Figure 3** The variation of beam strength due to the presence of (idealised) defects.  
a) General beam under various moment configurations.  
b) Upper and lower bound strengths for defect-free timber.  
c) The strength lower bound.



**Figure 4** The Strength distributions and effect of using moment configuration factor.



**Figure 5** Detail of the overlap of strength and action-effect probability distributions.

**INTERNATIONAL COUNCIL FOR RESEARCH AND INNOVATION  
IN BUILDING AND CONSTRUCTION**

**WORKING COMMISSION W18 - TIMBER STRUCTURES**

**BEHAVIOUR OF WOOD-STEEL-WOOD BOLTED GLULAM CONNECTIONS**

M Mohammad

J H P Quenneville

Department of Civil Engineering

Royal Military College of Canada (RMC)

CANADA

**MEETING THIRTY-TWO**

**GRAZ**

**AUSTRIA**

**AUGUST 1999**

---

Presenter: J.H.P.Quenneville

- H.J.Larsen commented that with 6 mm displacement the failure mode should be considered as bearing (B) rather than row shear (RS) failures.
- P.Quenneville agreed that Table 2 group 2 should be identified as B/RS failures. Capacities based on RS predictions should be close to those based on B predictions. The predicted capacities of Group 2 might be increased.
- A.Jorissen questioned whether RS as a group was observed in cases with close row spacing of 5d.
- P.Quenneville responded that RS as a group was not observed in those cases as specimen thickness also would have an impact.
- A.Jorissen discussed the single fastener connection strength and the redistribution of load.
- P.Quenneville responded that some localized ductility was possible.
- H.J.Larsen cautioned that the theory and recommendations were based on test results mean values with sample size of 10 only.
- E.Karacabeyli asked whether the findings could be extrapolated to large bolt diameter cases.
- P.Quenneville responded that it would depend on the ductility or localized breaking.
- A.Jorissen pointed out that one of the equations could lead to negative shear capacity.
- P.Quenneville agreed that the equation did not have a lower bound and would look into it.
- C.Mettem discussed the issue of tension strength perpendicular to grain.
- A.Mischler questioned whether the strength of the bolts was measured.
- P.Quenneville responded that the strength of the bolts was not measured. They were Grade 2 bolts.
- A.Mischler pointed out that without measuring the strength of the bolts might lead to dangerous situation if different grades of steel were used.
- M.Ansell commented that the choice of yield stress for steel would have an impact.
- P.Quenneville responded that only mild steel would be permitted in the Canadian Code.

# Behaviour of Wood-Steel-Wood Bolted Glulam Connections

M. Mohammad and J.H.P. Quenneville

Department of Civil Engineering, Royal Military College of Canada (RMC), Canada

## Abstract

This paper details verifications tests carried out at the Royal Military College of Canada (RMC) on wood-steel-wood bolted glulam connections. Twelve groups of specimens were tested. Specimens configurations were selected in such a way to include fundamental cases. Comparisons between experimental results and predictions from proposed equations for wood-steel-wood and wood-steel bolted connections are given. Proposed design equations were found to provide better predictions of the ultimate loads than current design procedure especially for bearing. However, row shear-out predictions seem to over-estimate the shear strength. Adjustment may need to be made to the proposed equations for row shear-out by introducing the effective thickness concept instead of using the full members thickness. Better predictions for row shear-out were achieved using the effective thickness instead of the full thickness. The research program is described in this paper along with results and proposed design equations for wood-steel-wood bolted connections.

## 1 Background

### 1.1 General

The current design equations in the Canadian design code (CSA 1994), are based on work by Johansen (1949) and further modified by Larsen (1973) and were first introduced into the Canadian design code in the 1989 edition (O86-89). In this design approach, failure is assumed to be governed by bearing (crushing of wood ) and/or bending of the bolts (Mode I and Mode III according to the European Yield Model (EYM)). This assumption results in a ductile failure mode for connections as long as the minimum requirement for spacing, end distances and edge distances are met. Consequently, the failure modes that show brittle failure (which are typical in connections with multiple fasteners) were assumed not to occur.

However, when using large fastener (typical in non-residential timber structures), brittle failure modes such as splitting, row shear, tearing and a combination of tearing and shear-out (known as a group tear-out) are the norm. Test results from various sources (Yasumura *et al.* 1987, Massé *et al.* 1988, Mohammad *et al.* 1997, Quenneville 1998) confirm that for multiple fastener connections, brittle modes of failure were dominant especially for fasteners with low slenderness ratio ( $l/d$ ). These modes of failure can not be predicted by the EYM, resulting in discrepancies between design strength values and actual experimental ones.

The current design model in the Canadian code for bolted timber connections (CSA O86-94) assumes connections to fail in a ductile manner. To account for situations where the connections show a brittle behaviour (generally connections with multiple bolts), modifications factors were introduced. Test results conducted at the Royal Military College

of Canada (RMC) on double shear steel-to-wood bolted connections using 12.7 mm or 19.1 mm have shown that the current Canadian design approach leads to conservative design strength values. Connections resistances as calculated from the O86-94 design code were found to be as low as one third of the experimental values (Quenneville 1998). This leads to the connections being over-designed.

Bolted connections are a priority for the CSA O86 committee. It is recognized that there is a need for a fundamental design method for bolts. The most desirable approach would be similar to the one used for other construction materials (i.e. steel), where a two-step process is utilized. The first step would be to check yield failure in the bolt, and is calculated by multiplying the capacity of one bolt in the connection times the number of bolts. The second step consist of checking the failure around the bolt, and is calculated by determining bearing and the combined tension and shear capacity of wood. This step depends on the joint configuration, spacing, end distances, etc.

## 1.2 Proposed Design Equations by Quenneville

In an attempt to follow that concept towards developing a more rational approach to optimize connections design strength, a set of equations has been developed by Quenneville to predict the ultimate strength of connections based on the actual failure modes and mechanisms observed during tests (Quenneville 1998). Design equations were derived using specified strength values for glulam material as listed in O86-94. Failure modes covered in these design equations were row shear (RS), group tear-out (GT) and bearing (B). The connection strength ( $p_u$ ) would be the minimum of  $p_{uRS}$ ,  $p_{uGT}$  and  $p_{uB}$ . Design equations proposed by Quenneville (1998) are given below.

Row shear-out:

$$p_{uRS} = 2 n_r t_w J_r f'_v \text{MIN}(e, s_b) N \quad (1)$$

Group tear-out

$$p_{uGT} = (2t_w f'_v \text{MIN}(e, s_b) N) + (t_w (n_r - 1)(s_r - (d + 2))) f_{lg} \quad (2)$$

Bearing:

$$p_{uB1} = 0.8 f_w d t_w n_r N \quad (3)$$

$$p_{uB2} = 0.8 f_w d^2 n_s n_r N \left( \sqrt{\frac{1}{6} \frac{f_s}{f_w + f_s} \frac{f_y}{f_w}} + \frac{1}{5} \frac{t_w}{2d} \right) \quad (4)$$

$$p_{uB3} = 0.8 f_w d^2 n_s n_r N \left( \sqrt{\frac{2}{3} \frac{f_s}{f_w + f_s} \frac{f_y}{f_w}} \right) \quad (5)$$

where,

$$f'_v = f_{vO86.1} \text{MAX} \left( \left[ 1.085 - 0.085 N \left( \frac{\text{MIN}(e, s_b)}{t_w} \right) \right] \right)$$

Validation tests on steel-wood-steel bolted connections were carried out at the RMC to compare predictions from proposed equations with those of the O86.1-94 values. A reasonably good agreement was found especially for group tear-out and row shear-out.

However, proposed design equations for wood-steel-wood bolted connections were not validated and there is a pressing need to carry out some extra connection tests to ensure that the changes in bolted connection design equations are well justified and that they have been validated for practical situations. So, the main objective of this research project was to verify if the proposed design equations provide a reasonable accuracy for wood-steel-wood connections with single or multiple bolts. This will be accomplished by comparing predictions from proposed design equations with experimental tests. These tests are also required to complement the results database already available at the RMC. The configurations used were identified as the practical cases which results were not already available.

## **2 Materials and Test Procedures**

### **2.1 Specimens**

Twelve groups of 10 replicates were used in this study. Detailed groups are given in Table 1. Specimens were made of either glulam or lumber wood members. All glulam specimens consisted of a single member (130mm) or two members (80mm) with a steel plate in the middle (except for group 8). The reason for choosing the two sizes of glulam members was to compare the response of the connections, using a single wood member with a slot in the middle or when using two separate members. Specimens made with lumber (groups 9 to 12) were S-P-F, No. 1 38mm by 140mm (2 in.x 6 in.). The wood members were sampled, cut and stored in a conditioning chamber to attain a 12% equilibrium moisture content (EMC). Specimens in groups 1, 2 and 4 were made of single 130mm by 190mm Spruce glulam, grade 20f-E. A slot of 10 mm wide was made in the middle of the member for a 9.5mm (? in.) steel plate using a chain saw. One row of one or two 19.1mm ( $\frac{3}{4}$  in.) bolts was used in these groups with different end distances (depending on the specimens configuration). In groups 3 and 5 to 7, two members of 80mm x 190mm sandwiching a 9.5mm (? in.) steel plate were used (W-S-W). One or two rows of two 19.1mm ( $\frac{3}{4}$  in.) bolts were used with an end distance and a spacing of 5 times the bolt diameter. Group 8 was fabricated with a single 80mm wood member and a steel side plate (W-S). Groups 9 through 12 were fabricated using two 38mm lumber members nailed together using 90mm ( $3\frac{1}{2}$  in.) nails. Two types of bolts were used in this study, 12.7mm ( $\frac{1}{2}$  in.) and 19.1mm ( $\frac{3}{4}$  in.). Detailed connections configurations are listed in Table 1.

### **2.2 Test Set-up and Procedures**

A typical test set-up is shown in Figure 1. All bolts were finger tight to allow a self-alignment. Specimens were loaded parallel to grain and were fabricated with identical connection configurations at each end. Three set-ups were used depending on the type of specimens (W-S-W or W-S). A universal loading machine (MTS) was used to apply the load. A monotonic tension load was applied through the central steel plate (W-S-W) or through the side steel plate (W-S). Four linear variable displacement transducers (LVDTs) were used to record the slip of the wood side member(s) with reference to the steel plate (two at each end). A data logging system was used to record the machine load and slip from the four LVDTs. An initial preload of about 1.0 kN was applied to the specimens. The test was displacement driven at a rate of 0.9mm/min. (0.035in/min.) in accordance with ASTM standard D07.05.02 (ASTM 1994). Tests were stopped upon failure, when the load dropped with no recovery.



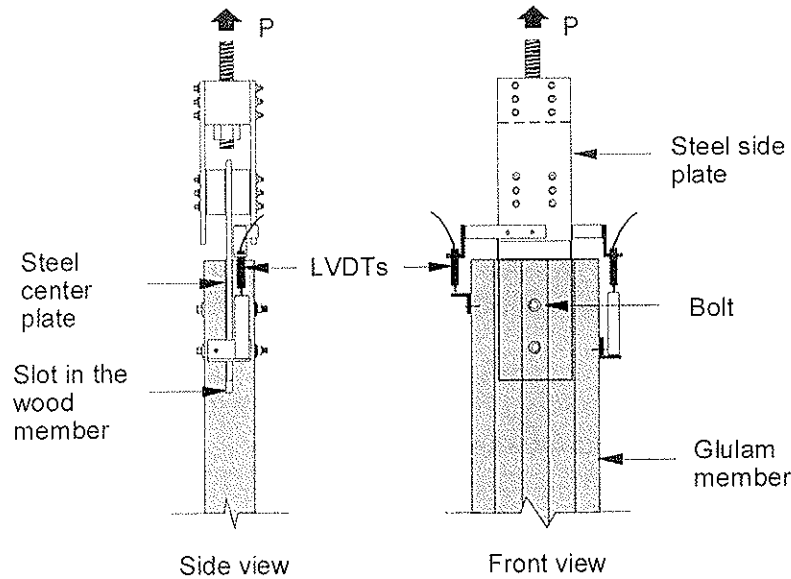


Figure 1. Typical test set-up for specimens with slots in the middle.

Table 1. Summary of specimens configurations.

Group	Wood type	Specimen size	Bolt size (d)	# of rows	# of bolts/row	Type	End distance (e)	Spacing (sb)
			(mm)				(mm)	
1	Glulam	130x190	19.1	1	1	Insert	95 (5d)	N/A
2	Glulam	130x190	19.1	1	1	Insert	191 (10d)	N/A
3	Glulam	2@80x190	19.1	1	2	W-S-W	95 (5d)	95 (5d)
4	Glulam	130x190	19.1	1	2	Insert	95 (5d)	95 (5d)
5	Glulam	2@80x190	19.1	2	2	W-S-W	95 (5d)	5d
6	Glulam	2@80x190	19.1	1	1	W-S-W	95 (5d)	N/A
7	Glulam	2@80x190	19.1	2	1	W-S-W	95 (5d)	N/A
8	Glulam	80x190	19.1	2	1	W-S	95 (5d)	N/A
9	Lumber	2@38x140	12.7	1	1	W-S	63 (5d)	N/A
10	Lumber	2@38x140	12.7	1	2	W-S	63 (5d)	63 (5d)
11	Lumber	2@38x140	19.1	1	1	W-S	95 (5d)	N/A
12	Lumber	2@38x140	19.1	1	2	W-S	95 (5d)	95 (5d)

### 3 Results and Discussion

Test results are given in Table 2. The ultimate strength values for each group was determined and the lower 5th percentile value was calculated using a two-parameter Weibull distribution based on a 75% confidence level (ASTM 1994). Tests results were adjusted for a normal duration loading by dividing by a factor of 1.25 (O86.1-94). Calculated values for connections capacities using the Canadian Standards CSA O86-94 design code are presented in Table 2 for comparison. O86.1-94 values were the lateral strength resistances as determined from O86.1-94, Clause 10.4.4 (CSA 1994). Predictions using the equations proposed by Quenneville and modes of failures observed for each group are given as well. Figure 2 shows typical load-slip relationships for all specimens in group 1 (ductile) and group 5 (brittle).

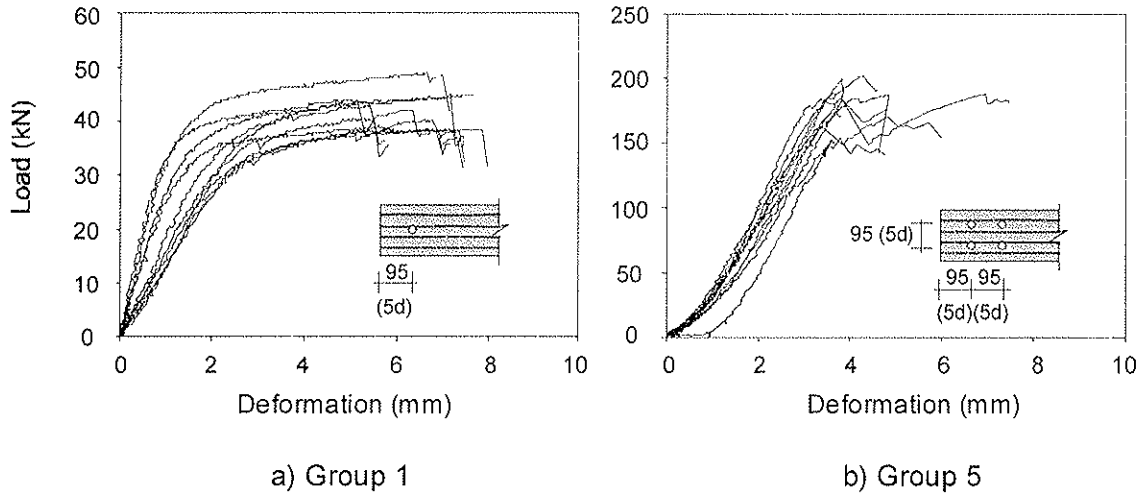


Figure 2. Typical load-slip envelopes for group 1 (ductile) and in group 5 (brittle).

### 3.1 Comparison Between Selected Groups

Connections in group 1 with an end distance of 5d has a lower 5th percentile value compared to group 2 with an end distance of 10d by a factor of 0.66. From Table 2, the 5th percentile value for groups 3 and 4 are the same. The same was found when comparing group 1 and 6 (25.7 kN compared to 28.9 kN). This indicates that for this type of connections, using two members or a single one with a steel plate in the middle does not have any significant influence on the 5th percentile strength of the connections. This is quite interesting, since the cumulative thickness of wood in group 4 is less than that of group 3 (120mm compared to 180mm). Comparing the 5th percentile value for group 7 (with two members, double shear) and group 8 (with a single member, single shear), it was found that the 5th percentile value for group 7 was almost twice as much as that for group 8, Table 2. The 5th percentile value for group 11 with a single 19.1mm bolt was found to be almost twice as much as that of 12.7mm bolts for the same end distance (5d).

### 3.2 Observations on Failure Modes

Generally, two dominant types of failures were observed in all connection specimens. These were row shear and to a lesser extent splitting. Connections specimens in group 1 with a single bolt and an end distance of 5 times the bolt diameter and with a single 130mm wood member, exhibited considerable bearing prior to failure. However, the final failure was mainly in row shear. Group 2 with a single bolt and an end distance of 10 the bolt diameter failed mostly in splitting. Bearing deformation was more obvious than in group 1. Localized row shear failures followed the major splitting failure at the ultimate load. Group 3 with two members and two bolts in a row failed in row shear as well, however, few specimens failed in splitting. Group 4, with two bolts in a row and a spacing and end distance of 5d failed mostly in row shear. Hardly any signs of bearing were observed. The failure scenario for these few specimens was as follows: splitting developed first, resulting in a sudden drop in the load, followed by failure in row shear. More bearing deformation was noticed in group 3 compared to that of group 4 which has similar configurations but made with single 130mm member and a slot in the middle. Group 5 failed mainly in row shear. Few specimens failed in splitting as well. Failure in groups 6 and 7 was mainly due to row shear. Some specimens in group 6 exhibited some bearing

deformation prior to failure. In group 8, with a single shear type of connection, failure was sudden and characterized by a row shear-out in one row followed by failure in the second. Bearing deformation was obvious in few specimens. Group 9 failed in bearing. Groups 10 and 11 failed ultimately in row shear, however, few specimens failed in bearing. Specimens in group 12 with two 19.1 mm bolts failed mainly in row shear-out.

### 3.3 Comparison Between O86 Predictions and Experimental Values

Predictions using the current design code (O86.1-94) were found to be quite conservative compared to the validation tests results (the lower 5th percentile). Validation tests showed that the ratio between O86.1-94 values and the experimental values was found to be between 0.52 to 0.85 with an average of 0.73 which is considered to be quite low. It can be seen in Figures 3-a) and b) 4 that most of O86.1-94 predicted values lie below the 45o line, thus considered to be over-designed.

Table 2. Validation tests results and predictions using O86.1-94 and proposed equations.

Group	5th %* test	O86.1 - 94	O86/ 5th %	Quenneville's Proposed Equations**							P <sub>u</sub> Min.	Observed failure mode
				P <sub>uRS</sub>	P <sub>uGT</sub>	P <sub>uB1</sub>	P <sub>uB2</sub>	P <sub>uB3</sub>	P <sub>uB4</sub>	P <sub>uB5</sub>		
..... kN .....												
1	26	21	0.81	41	41	41	28	39	--	--	28	B/RS
2	39	28	0.71	76	76	41	28	39	--	--	28	B/S
3	61	46	0.75	76	76	82	56	78	--	--	56	RS
4	61	42	0.68	105	105	110	61	78	--	--	61	RS
5	107	55	0.52	168	255	219	122	156	--	--	122	RS/S
6	29	23	0.79	55	55	55	30	39	--	--	30	RS
7	69	46	0.66	110	205	110	61	78	--	--	61	RS
8	28	23	0.83	52	101	55	30	57	48	39	30	RS
9	8	6	0.75	10	10	18	8	17	16	9	8	B
10	13	11	0.85	18	18	36	16	34	32	18	16	RS
11	15	11	0.73	14	14	25	15	28	24	19	14	RS/B
12	22	16	0.73	25	25	50	29	57	47	38	25	RS

\* Adjusted for the normal duration of loading by dividing over a factor of 1.25.

\*\* Calculated based on the following material strength values for Spruce glulam or Spruce lumber:

$f_v$ (specified strength in shear // to grain)	= 1.75 or 1.0 MPa
$f_{tg}$ (specified strength in tension // to grain)	= 12.7 or 8.6 MPa
$f_y$ (bolt yield strength)	= 310 MPa
G (mean relative density)	= 0.44 or 0.42

One reason for such discrepancies between O86 values and those of the experimental could attributed to the axial tensioning force that develops in the bolt once the plastic hinge is developed. This axial force reinforces the connection and results in the connection sustaining higher loads. In fact the axial force may even alter the mode of failure completely in some cases. The influence of the axial force was obvious especially in group 2, where almost all tested specimens exhibited that effect. This could be observed in the load-slip curve as a discontinuity in the envelope at about 55 kN followed by an increase in the capacity of the connection due to the development of a plastic hinge and the axial tensioning force in the bolt. Since the EYM is only valid for a dowel type of connections, it is not surprising that O86 predictions for bearing based on the EYM under-

estimate the failure load. The EYM does not take into consideration the axial tensioning force that develops in the bolt. That perhaps explains higher values for the experimental tests compared to O86.1-94 predictions. Other reasons could be attributed to group and loaded end distance modification factors ( $J_G$  and  $J_L$ ) used in the calculations of the O86-94 values. These factors are very restrictive resulting further in underestimating the capacity of bolted connections.  $J_L$  was estimated by extrapolation.

### 3.4 Validation of Proposed Design Equations

In order to verify if the proposed design equations provide some reasonable accuracy, strength values calculated using the proposed equations were compared with experimental values (5<sup>th</sup> %). Figures 3-a) and b) show comparisons between the experimental values (based on the validation tests conducted at RMC) and those predicted using either O86.1-94 or proposed equations. Minimum values predicted by the proposed equations were taken as the design values and were plotted against the experimental values. Predicted row shear values were also plotted since most specimens failed in row shear.

Figure 3-a) suggests a good correlation between the experimental and the minimum predicted values which are based on failure due to bearing (B) for W-S-W connections. However, predictions for row shear-out were found to be relatively high (RS). Keeping in mind that almost all groups (with the exception of group 2) failed mainly in row shear, these predictions should be closer to the experimental values than bearing predictions. Better row shear predictions were found using the proposed equations, especially for groups 9 to 12. However, row shear-out predictions for group 8 were found to be high. The following discussion describes a theory proposed by Jorissen (1998) that could explain such a discrepancy between predictions using the proposed equations for row shear-out and those obtained from tests for wood-steel-wood bolted connections.

## 4 Analysis

In the new design equations for row shear predictions of bolted wood-steel-wood connections proposed by Quenneville (1998), the row shear failure was assumed to occur over the full thickness of the wood member ( $t_w$  was taken as equal to member thickness). This assumption is usually valid for connections with rigid type fasteners, where the embedment stress is assumed to be uniform over the full timber thickness, resulting in the crack being developed over the whole thickness. This was validated with visual inspection of the failed specimens, where the shear failure plane occurred across the full timber thickness (see Figure 4-a)). Good agreements were found between predictions from Quenneville proposed equation for row shear strength and those from validation tests for steel-wood-steel connections (Quenneville 1998).

However, row shear predictions for wood-steel-wood connections calculated over the full thickness of the wood side members were found to be high, compared to the validation tests (the lower 5<sup>th</sup> percentile). Further inspection of failed wood-steel-wood connections with a middle steel plate revealed that row shear failure did not occur over the full thickness of the wood side member but over a specified thickness which was smaller than the full thickness ( $t$ ), as can be seen in Figure 4-b). Considering that similar type of fasteners ( $\frac{1}{2}$  in. or  $\frac{3}{4}$  in. bolts) were used in both types of connections and with more or less similar thickness of wood members, the influence of material properties was

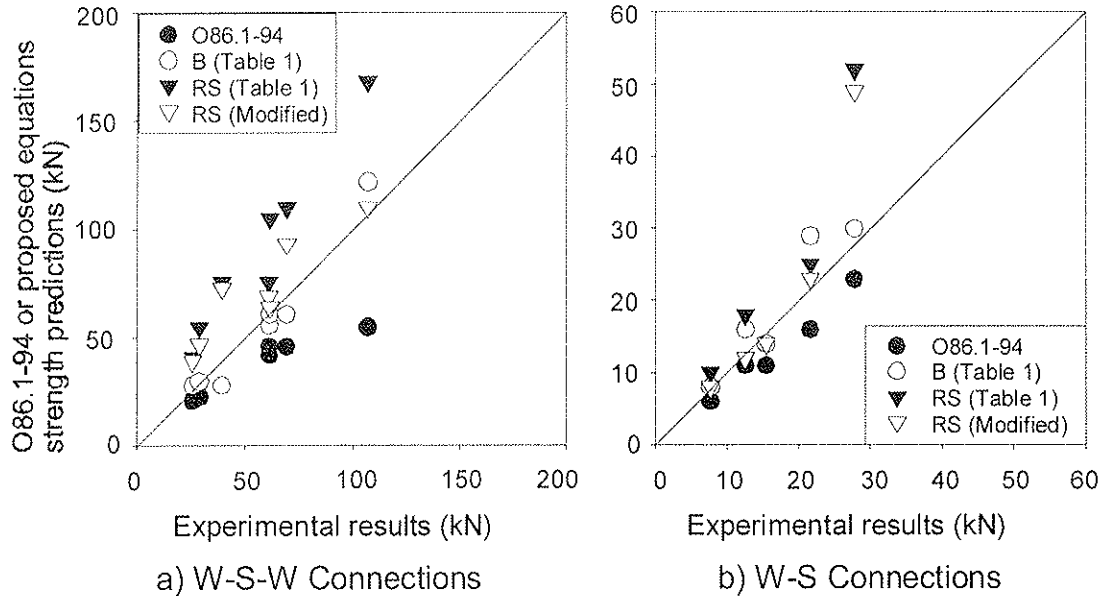


Figure 3. Comparison between experimental and predictions using either O86.1-94 code or proposed equations for: a) W-S-W connections, b) W-S connections.

eliminated (groups 1 to 8). This difference in the row shear failure pattern could be attributed to the embedment stress distribution along the fastener length. A different embedment stress distribution clearly takes place in connections with a middle steel plate, compared to those with steel side members.

Embedment stress distribution for rigid dowel type fasteners is assumed to be uniform along the fastener length, Figure 5-a), and c). However, the development of the plastic hinge in the fastener alters the embedment stress distribution along the fastener axis, and the assumption of uniform distribution over the full wood member thickness becomes no longer valid. Figure 5-b) and d) shows the embedment stress distribution along the fastener for connections with non-rigid dowel type fasteners and with steel side plates or middle steel plate. A uniform embedment stress distribution is assumed only over a specified length  $y$ . Now, for connections with a middle steel plate, this assumption results in crack propagation near the shear planes over a length  $y_e$ , which is assumed to be slightly higher than  $y$ . Let's refer to this specified thickness as the "effective thickness". This means that the shear force ( $F$ ) is acting over a reduced thickness which is less than the actual thickness of the wood side member (Jorissen 1998). The result is a lower than anticipated shear strength for the connection with a middle steel plate. This perhaps explain the high values predicted by the proposed equations if the full thickness of the wood member is used in the calculations (Table 2). The thickness across which row shear-out failure plane took place was measured for all groups and the mean value for each group is presented in column 2 (except for groups 9 to 12 where the thickness of a single lumber member was considered as being the experimental one), Table 3. These values are clearly smaller than the full thickness of connections wood members (column 2). However, for connections with steel side plates, though the embedment stress distribution is also assumed to be uniform over a length  $y$ , smaller than the full thickness, different stress distribution is associated with this type of connections, see Figure 5-b). This distribution does not seem to influence the propagation of the cracks near the shear planes. The development of infinite number of plastic hinges in the fastener (unlike the case for wood-steel-wood connections)

leads to nearly uniform stress distribution underneath the fastener. Failure usually occurs across the full thickness for the type of fasteners used in the validation study of bolted steel-wood-steel connections. This may not necessarily be the case for connections with higher slenderness ratio, where row shear failure is not dominant anyway. This may lead to the conclusion that the previous theory could be only applicable for connections with a middle steel plate. Adjustment to the wood side member thickness ( $t_w$ ) may be necessary to account for that phenomenon.

The following discussion describes how to determine the effective thickness ( $y_e$ ) across which the row shear failure takes place for wood-steel-wood connections, based on the stress distribution along the fasteners, for rigid and non-rigid dowel type fasteners.

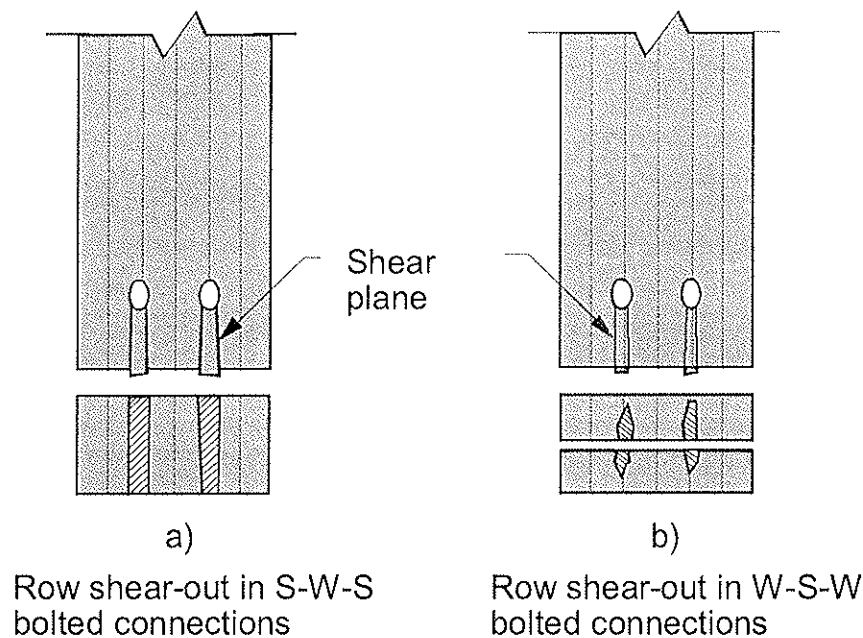


Figure 4. Typical row shear-out failure in bolted steel-wood-steel or wood-steel-wood connections.

#### 4.1 How to Determine The Effective Thickness ( $y_e$ )?

Johansen's Yield Model for double shear symmetrical connections with a single internal steel plate and assuming a rigid dowel type fastener (see Figure 5-a) and 5-c)) for failure Mode I, is given by the following equation:

$$F = d t f_w \quad (6)$$

where,

$F$  = applied load resisted by one side of the wood member, N

$d$  = bolt diameter, mm

$t$  = thickness of the side wood member, mm

$f_w$  = embedment strength of wood,  $N/mm^2$

For Mode II (Figure 5-d), the failure mode is given by the following equation:

$$F = y t f_w \quad (7)$$

where,

$y$  = the length along which the embedment stress is assumed to be uniform, mm.

Using Eq. (7), the length  $y$  can be determined as follows:

$$y = \frac{F}{d f_w} \quad (8)$$

Additional stress analysis given by Jorissen (1998) indicated that for connections with more slender dowel type fasteners, cracks propagate near the shear planes over a thickness  $y_e$ , which is assumed to be slightly bigger than  $y$ , see Figure 5-d). For connections with rigid dowel type fasteners, it can be assumed that  $y = y_e = t_w$ . The value  $y_e$  was determined using linear interpolation where  $y < y_e < t$  and was given by the following equation:

$$y_e = \left( 1 + C_y \frac{t - y}{t} \right) \quad (9)$$

where,

$C_y$  is a constant ( $0 < C_y < 1.0$ ), which was calculated based on the following equation:

$$C_y = 0.3 \frac{s_b}{e} \quad (10)$$

where,

$s_b$  = bolt spacing in a row,  
 $e$  = end distance.

For connections with a single fastener,  $C_y$  was taken as equal to 1.0. Since  $y_e = t$  for rigid dowel type of fasteners, Eq. (10) doesn't influence the calculation for rigid dowel fasteners. Eq. (10) was derived empirically using test results (Jorissen 1998).

Measured values for the effective thickness ( $y_e$ ) across which row shear-out failure took place were found to be quite comparable with those calculated using Eq. (9), except for connection made with lumber (W-S), where due to the presence of discontinuity, row shear failure occurred at the joint between the two wood members, Table 3. Substituting the value  $2y_e$  for  $t_w$  (or  $y_e$  for group 8 through 12, with a single shear) leads to better predictions for row shear-out, except for group 2, which failed mainly in splitting, see Table 2. Two sets of predictions are shown in Table 4 based on whether the length  $y$  was calculated from Eq. (7) using the mean value for  $F$  or using the 5<sup>th</sup> percentile value (from group 1). Row shear-out predictions based on the effective length, as calculated using the mean value for  $F$ , seem to agree well with the test results. Figures 3-a) and b) show comparisons between experimental results and the row shear values predicted by the proposed equations based on full wood member thickness, or the effective thickness ( $y_e$ ) (using the mean value for  $F$ , and referred to in the figure as "Modified RS"). Row shear-out predictions calculated using the effective thickness tend to agree well with the experimental values, where the row shear-out failure controlled. Substituting the 5<sup>th</sup> percentile value for  $F$  in Eq. (7) leads to lower predictions for row shear, Table 4.

Based on the above discussion, it is evident that using the full thickness in the row shear-out predictions in the proposed design equations overestimates the row shear strength of wood-steel-wood bolted connections. Better predictions for row shear-out strength could be achieved using the effective thickness approach.

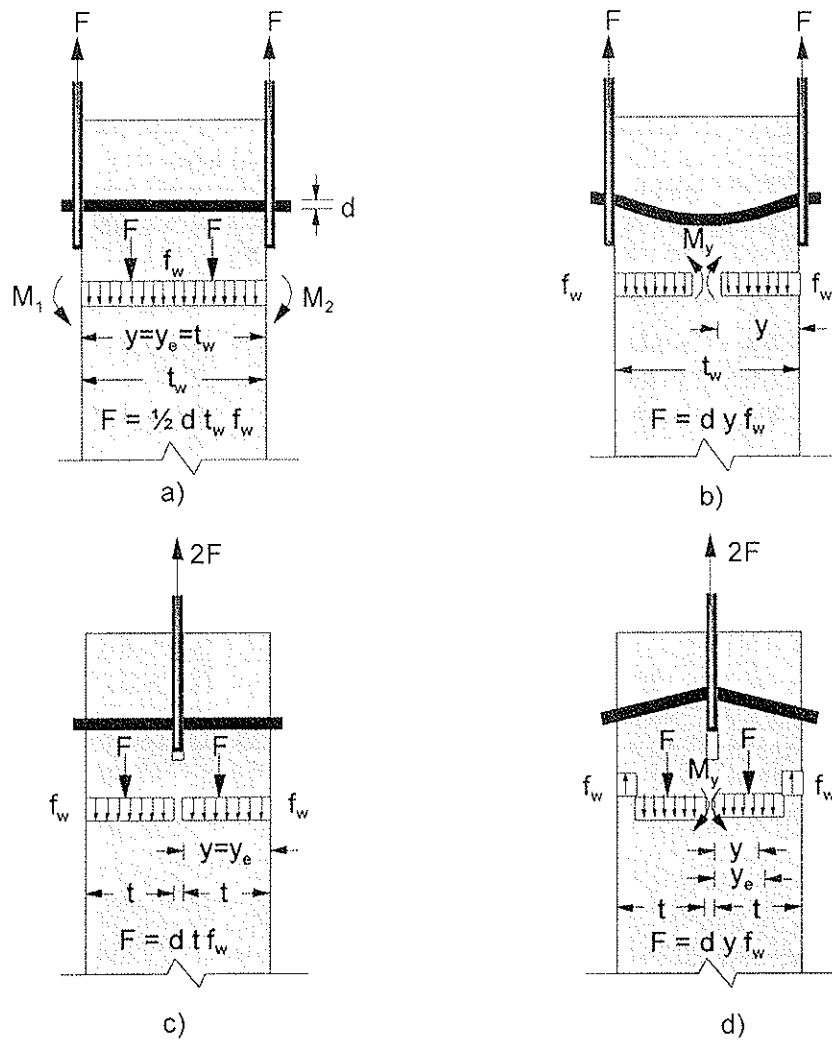


Figure 5. The embedment stress distribution ( $f_w$ ) along the fastener length for connections with steel side members and those with middle steel plate.

Table 3. Comparison between measured and calculated effective thicknesses.

Group	Wood member thickness	Effective thickness		Ratio
		Experimental	Eq. (9)	
..... (mm) .....				
1	60	48	58	0.8
2	60	57	58	1
3	80	49	55	0.9
4	60	42	52	0.8
5	80	58	55	1.1
6	80	62	68	0.9
7	80	75	68	1.1
8	80	41	58	0.7
9	76	38	66	0.7
10	76	38	54	0.7
11	76	38	76	0.5
12	76	38	71	0.5



Table 4. Test results and predictions using O86.1-94 or proposed design equations based on the effective thickness,  $y_e$  and calculated using either the mean value for  $F$  or the 5<sup>th</sup> %.

Group	5th % test	O86.1 -94	Quenneville's Proposed Equations				Bearing	
			PuRS *	PuGT *	PuRS **	PuGT **	PuB Min. *	PuB Min. **
..... kN .....								
1	26	21	39	39	35	35	27	27
2	39	28	73	73	64	64	27	27
3	61	46	69	69	52	52	54	51
4	61	42	64	64	49	49	53	49
5	107	55	110	172	83	134	108	83
6	29	23	47	47	39	39	29	27
7	69	46	93	175	78	147	58	55
8	28	23	49	96	36	71	30	27
9	8	6	8	8	7	7	8	7
10	13	11	12	12	8	8	14	12
11	15	11	14	14	12	12	14	14
12	22	16	23	23	15	15	28	26

\* Based on the mean value for "F" in Eq. (7), for connections with single fastener.

\*\* Based on the 5th percentile value for "F" in Eq. (7).

## 5 Conclusions

Based on the validation tests of the proposed design equations for wood-steel-wood bolted connections, it can be concluded that:

1. Current Canadian design code (O86.1-94) leads to over-designed wood-steel-wood bolted glulam connections, especially with multiple bolts, where it under-estimates the failure loads.
2. Proposed design equations for wood-steel-wood bolted connections provide better predictions of the ultimate loads than current design procedure, especially for bearing.
3. Better predictions for row shear-out can be achieved if the effective thickness principle is used.

## Recommendations

Findings from this project have promoted some further expansion to the project to cover bolted wood-steel-wood connections loaded parallel-to-grain with different configurations than those tested. This may include verification tests on wood-steel-wood connections with three rows with two or more bolts per row. In addition, tests are necessary to verify the proposed design equations for bolted wood-steel-wood connections loaded perpendicular-to-grain.

## Acknowledgment

Funding from the Canadian Wood Council (CWC) and the Military Engineering Research Group (MERG) is greatly appreciated.

## References

American Society for Testing and Materials (ASTM). 1988. "Standard Test Methods for Mechanical Fasteners in Wood". Standard D1761-77, ASTM, Philadelphia, PA.

American Society for Testing and Materials (ASTM). 1994. "Standard Specification for Computing the Reference Resistance of Wood-based Materials and Structural Connections for Load and Resistance Factor Design". D5457-93, ASTM, Philadelphia, PA.

Canadian Standards Association. 1989. "Engineering Design in Wood (Limit States Design)". Standard O86.1-M89. Canadian Standard Association, Rexdale, ON.

Canadian Standards Association. 1994. "Engineering Design in Wood (Limit States Design)". Standard O86.1-94. Canadian Standard Association, Rexdale, ON.

Johansen, K.W. 1949. "Theory of Timber Connectors". IABSE Journal, No. 9. pp.249-262.

Jorissen, A. 1998. "Double Shear Timber Connections with Dowel Type Fasteners". Ph.D. Thesis, Technical University of Delft, Delft, The Netherlands.

Larsen, H.. 1973. "The Yield Load of Bolted and Nailed Joints". Structural Research Laboratory, Technical University of Denmark, IUFRO Division 5, pp14.

Massé, D.I., Salinas, J.J. and Turnbull J.E. 1988. "Lateral Strength and Stiffness of Single and Multiple Bolts in Glued-laminated Timber Loaded Parallel to Grain". Engineering and Statistical Research Centre, Research Branch, Agriculture Canada, Report No. C-029, Ottawa. ON.

Mohammad, M., Smith, I. and Quenneville, J.H.P. 1997. "Bolted Timber Connections: Investigations on Failure Mechanism". Proceedings of IUFRO S5.02 Timber Engineering Conference, Copenhagen, Denmark.

Quenneville, J.H.P. 1998. "Predicting the Failure Modes and Strength of Brittle Bolted Connections". Proceeding of the 5th World Conference on Timber Engineering (WCTE), Montreux, Switzerland, 2:137-144.

Yasumura M., Murota T. and Nakai H. 1987. "Ultimate Properties of Bolted Joints in Glued-laminated Timber". Report to the Working Commission W18-Timber Structures. Dublin, Ireland.

**INTERNATIONAL COUNCIL FOR RESEARCH AND INNOVATION  
IN BUILDING AND CONSTRUCTION**

**WORKING COMMISSION W18 - TIMBER STRUCTURES**

**A NEW SET OF EXPERIMENTAL TESTS ON BEAMS LOADED  
PERPENDICULAR-TO-GRAIN BY DOWEL-TYPE JOINTS**

M Ballerini

University of Trento

Department of Mechanics & Structural Engineering

ITALY

**MEETING THIRTY-TWO**

**GRAZ**

**AUSTRIA**

**AUGUST 1999**

---

Presenter: M.Ballerini

- A.Leijten questioned whether the failure was governed by compression perpendicular to grain rather than tension perpendicular to grain. If so the Van der Put model for compression perpendicular to grain would fit the data well.
- M.Ballerini responded that the forms of the Van der Put formulae for compression and tension perpendicular to grain failures were similar. The only difference was the use of either compression or tension perpendicular to grain strength values in the respective equation.
- C.Mettem commented that modification factors for perpendicular to grain applications would also be available from TRADA.
- P.Quenneville asked where was the location of the split with respect to the bolt.
- M.Ballerini responded that the splits generally were located from mid diameter of the bolt to the compression side of the bolt.

# A new set of experimental tests on beams loaded perpendicular-to-grain by dowel-type joints

Marco Ballerini

University of Trento, Department of Mechanics & Structural Engineering, Italy

**Abstract:** The results of an experimental programme on the splitting strength of beams loaded perpendicular-to-the-grain by dowel-type joints are reported. The ultimate loads of beams failed by splitting are analysed and the types of failure are highlighted. Finally, the effectiveness of available prediction formulas from literature are compared and discussed with regard to this set of experimental data.

## 1 Introduction

Timber elements loaded over their depth by perpendicular-to-grain connections should be avoided in timber engineering. This way of loading indeed, is responsible for local perpendicular-to-grain tensile stresses, that may lead the beams to failure for splitting at load levels considerably lower than the bearing capacity of connections or of the bending strength of timber elements. Nevertheless, since in some designs this kind of loading may be fixed, the problem of the evaluation of the splitting strength of beams is still actual.

The Eurocode 5 [1] takes into consideration this problem by means of a very simple formula which doesn't take into account the effect of the joint's geometry and assumes a linear relationship between the splitting strength and the distance of the furthest row of fasteners from the loaded edge of the beam.

Some researcher think this formula unsatisfactory.

Ehlbeck, Görlacher and Werner [2-3] indeed, on the basis of the results of previous experimental researches (Mölher and Lautenschläger [4], Mölher and Siebert [5], Ehlbeck and Görlacher [6]), have developed a different formula. The formula is based on both theoretical considerations (with the support of linear elastic numerical analyses) and on the best fitting of the experimental results. Moreover, TACM van der Put [7-8], on the basis of an energetic approach in the framework of the Linear Elastic Fracture Mechanics, has developed a third prediction formula.

If the above mentioned experimental results are compared with available prediction formulas, it is possible to notice that the best fit is supplied by the formula of Ehlbeck, Görlacher and Werner, but also the one of TACM van der Put (which doesn't take into account the joint's geometry) gives reasonable results.

However, if the attention is focused on connections with few fasteners it is possible to detect how the first one is characterised by quite large scattering while the second one overestimates the splitting strengths.

Since, as stated in [2-3], the joint configuration affects considerably the strength of the beams, a new experimental programme on beams loaded by connections made with only one or two dowels (not much investigated in previous researches) has been carried out at the University of Trento. The main intent of the programme is to provide a set of tests able to

exploit the strength of beams loaded by a single connector and to evaluate, if possible, the influence on this strength of a second connector. Another characteristics of this set of tests is the slenderness of the beams which is higher than those of previous researches.

In the following the experimental programme and the test set-up will be described in detail. The experimental results will be presented, the types of failure highlighted and the influence on the strength of the main parameter exploited. Finally the effectiveness of available prediction formulas will be compared and discussed with regard to this set of experimental data.

## 2 The experimental programme and testing procedure

The experimental programme consists of two series of bending tests on simply supported glulam beams, loaded at mid-span by means of perpendicular to grain connections.

The first series, hereafter denoted S1, is characterised by connections made with only one 10 mm dowel; the second one, hereafter denoted S2, has connections made with two 10 mm dowels spaced 30 mm ( $3d$ ) on the beam height.

The glulam beams, which are made with European whitewood (*Picea abies*), have cross sections respectively of 40 by 196 mm and of 40 by 397 mm and are tested on a span length of 3400 mm. The slenderness ratios ( $L/h$ ) are then 17.3 for beams 196 mm high, and 8.6 for beams 397 mm high.

For series S1, the ratio  $\alpha$  ( $a_r/h$ ) between the distance of the fastener from the loaded edge of the beam ( $a_r$ ) and the beam's height ( $h$ ) ranges from 0.2 to 0.7 for beams 196 mm high and from 0.1 to 0.7 for beams 397 mm high. For series S2 the same ratio (computed from the furthest fastener) ranges respectively from 0.35 to 0.7 and from 0.17 to 0.7.

The tests have been carried out upside-down with the test set-up shown in figure 1. The load was applied by means of a servo-hydraulic actuator with a capacity of 100 kN controlling the displacement of actuator's head. The velocity of the head of the actuator has been fixed at 3 mm/min for beams 196 mm high, and at 1 mm/min for beams 397 mm high; consequently, the duration of tests has ranged from 8 to 20 minutes.

The load is transferred to the dowel(s) by means of two square-section steel bars which are able to prevent any rotation of the end of the dowel(s). To avoid any problem due to lateral buckling, bracings have been placed at about 1/3 of the span length at the bottom side of the beams (in compression).

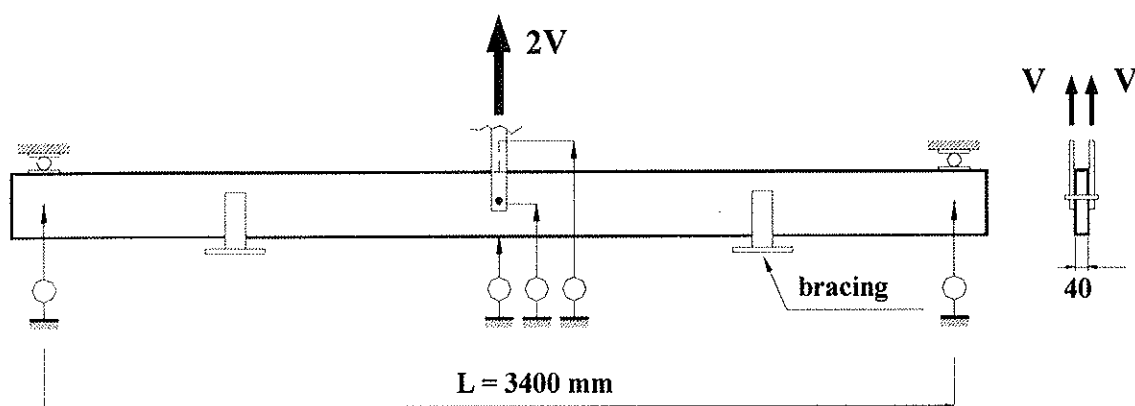


Figure 1 – Test set-up and arrangement of displacement transducers

During the tests the bottom and upper mid-span deflections of the beams, the displacement of the dowel(s) and the displacements of the beams at supports (as illustrated in figure 1) have been automatically collected.

### 3 Tests results

The results of the experimental programme are summarised in Table 1 where the main data of 49 tests are reported.

Specimen	No. of tests	d (mm)	a <sub>r</sub> (mm)	h <sub>m</sub> (mm)	$\alpha = \frac{a_r}{h}$	F <sub>u</sub> (kN)	Type of failure
S1-2020	2	10	40	0	0.20	7.6 / 7.6	total splitting
S1-2025	2	10	50	0	0.26	7.2 / 8.2	total splitting
S1-2030	2	10	60	0	0.31	8.8 / 7.8	total splitting
S1-2035	2	10	70	0	0.36	9.4 / 9.2	total splitting
S1-2040	2	10	80	0	0.41	9.9 / 10.7	total splitting
S1-2050	2	10	100	0	0.51	10.4 / 10.7	total splitting
S1-2060	2	10	120	0	0.61	14.8 / 16.3	splitt. + bending
S1-2070	2	24	140	0	0.71	13.4 / 16.0	splitt. + bending / bending
S2-2035	1	10	70	30	0.36	9.9	total splitting
S2-2040	1	10	80	30	0.41	12.2	total splitting
S2-2050	1	10	100	30	0.51	14.7	total splitting
S2-2060	1	10	120	30	0.61	14.9	splitting + bending
S2-2070	2	10	140	30	0.71	12.9 / 13.4	bending
S1-4010	3	10	40	0	0.10	6.4 / 8.1 / 7.0	limited splitting
S1-4015	2	10	60	0	0.15	8.0 / 7.5	limited splitting
S1-4020	2	10	80	0	0.20	9.2 / 9.5	limited splitting
S1-4025	2	10	100	0	0.25	10.4 / 10.4	limited splitting
S1-4030	3	10	120	0	0.30	12.9 / 12.4 / 13.4	total splitting
S1-4035	1	10	140	0	0.35	12.0	total splitting
S1-4040	2	10/24	160	0	0.40	16.5 / 18.3	total splitting
S1-4050	2	10	200	0	0.50	15.6 / 14.0	total splitting
S1-4060	2	10/24	240	0	0.60	18.9 / 20.1	total splitting
S2-4018	1	10	70	30	0.18	9.8	limited splitting
S2-4020	1	10	80	30	0.20	10.6	limited splitting
S2-4030	1	10	120	30	0.30	19.6	total splitting
S2-4040	1	10	160	30	0.40	17.1	total splitting
S2-4043	1	10	170	30	0.43	19.6	total splitting
S2-4050	1	10	200	30	0.50	18.1	total splitting
S2-4060	1	10	240	30	0.60	24.8	total splitting
S2-4070	1	24	280	70	0.71	35.6	total splitting

Table 1 – Joints' parameters, failure loads and types of failure of tested specimens.

The only data not reported in table 1 concern the properties of the wood of the beams; they can be summarised in an average density of about 430 kg/m<sup>3</sup> and a moisture content of laminations in the range of 8-12%.

Different types of failure of the beams have been observed in the experimental programme:

- the splitting failure;
- the bending failure;
- the embedding failure.

The splitting failure has been experienced by the most part of beams. In all specimens failed for splitting a stable crack propagation have been observed till the maximum load.

However, two different kinds of final collapses have been recorded:

- a total splitting of beams in two elements (sometimes with the crack propagating along the grain till the supports and sometimes with one side of the crack propagating diagonally till the upper edge of the beam);
- a limited splitting of beams but with a considerable loss of bearing capacity.

The former type of collapse (see figures 2 and 3), has been noticed in beams 196 mm high and in beams 397 mm high characterised by  $\alpha$  values greater than 0.3. The latter one (see figure 4), has been experienced only by beams 397 mm high with  $\alpha$  values lower than 0.3. These different final collapses can be ascribed essentially to the amount of internal work accumulated before failure by the more slender beams and by the less slender ones with higher  $\alpha$  values (an then higher failure loads).

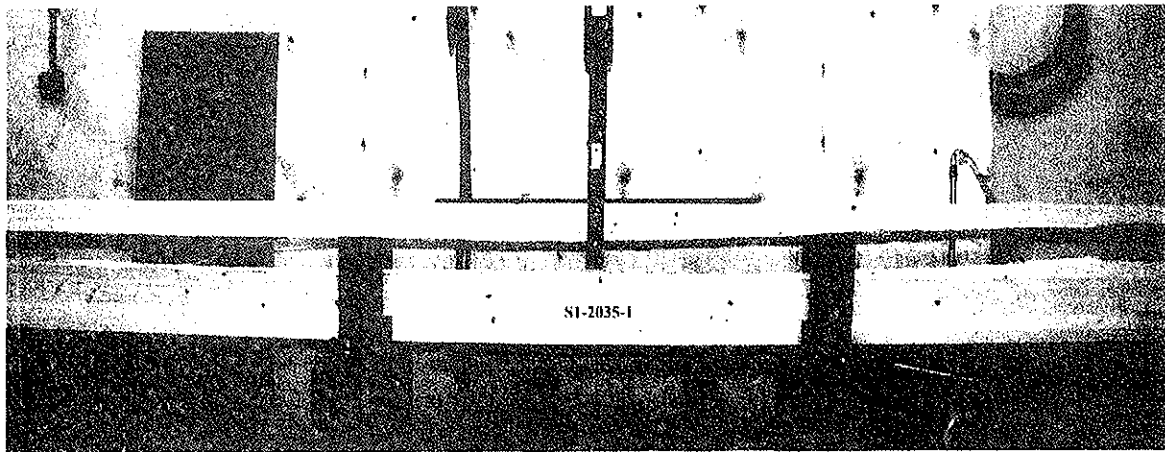


Figure 2 – The total splitting failure of specimen S1-2035-1.

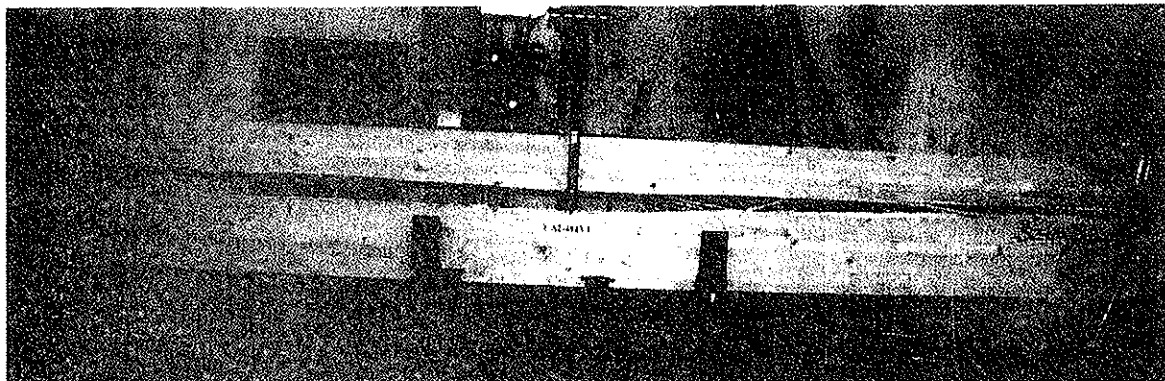


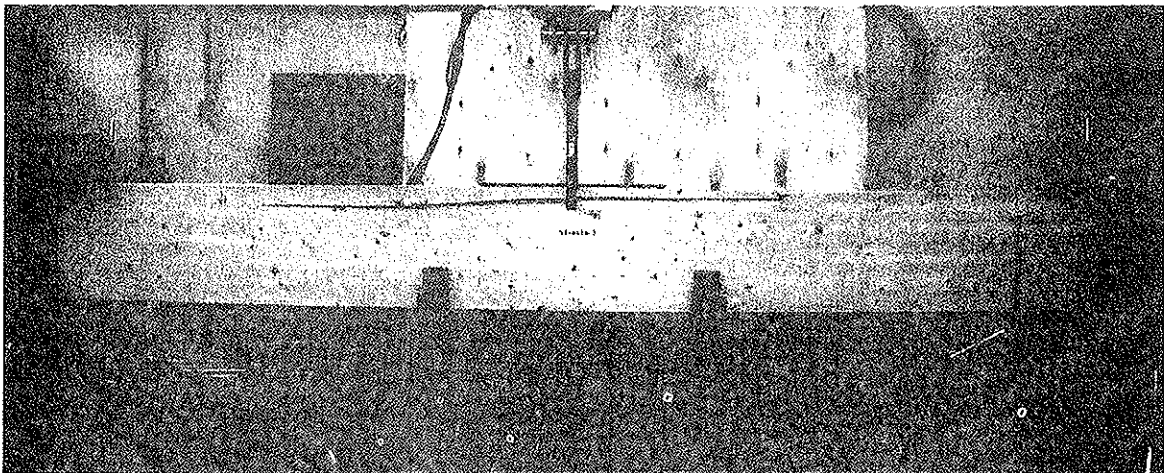
Figure 3 – The total splitting failure of specimen S2-4043-1.

The bending failure has been occurred only in the more slender beams characterised by  $\alpha$  values of about 0.6 and 0.7 (see table 1). This is due to the fact that in so slender beams failure loads of about 13-16 kN (like the ones shown by these specimens) are responsible for bending elastic stresses at the outermost fibres of about 43-53 MPa.

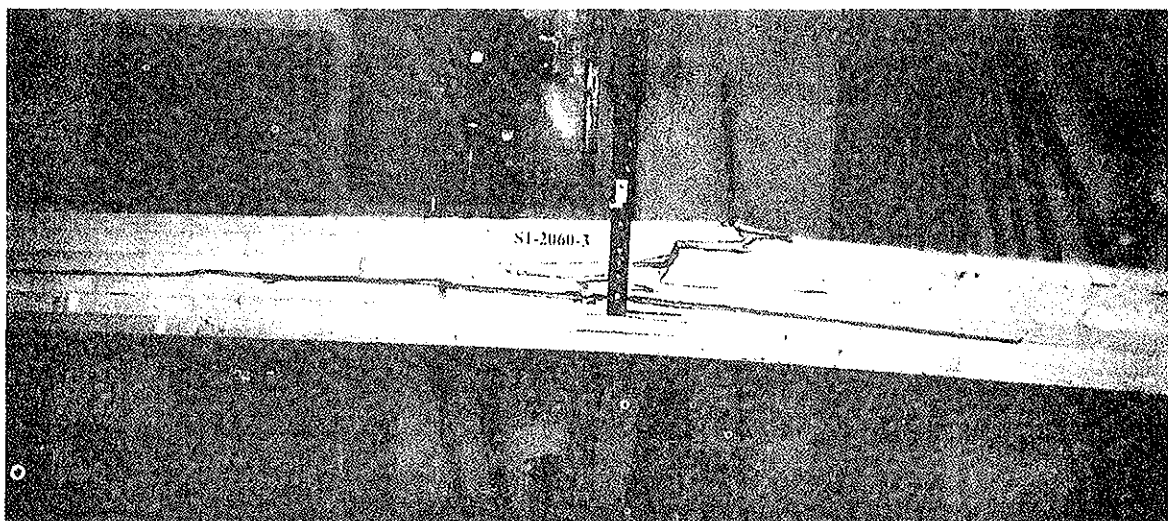
In spite of this, since the bending failure load and the splitting one are of the same order, some of these specimens have failed for splitting, suddenly followed by the bending failure of the residual section of the beam (figure 5), and not for bending.

Finally, some specimens have experienced embedding failure. The data of these tests are not reported in table 1 since are not of interest for the research. For some specimens this type of failure is a direct consequence of the small bearing area of the dowel, which gives to the connection a very limited bearing capacity. For others specimens however, it is due to the difficulty in obtaining the splitting failure when the connections are placed near the unloaded edge of the beams.

With regard to the perpendicular-to-grain plastic deformations under the dowel's contact area, it is necessary to highlight that all tests, with the only exception of those characterised by very low  $\alpha$  values, have shown more or less plastic deformations before failure.



**Figure 4** – The limited splitting failure of specimen S1-4010-2



**Figure 5** – The splitting-bending failure of specimen S1-2060-3



The typical load-deflection diagrams are reported in figure 6. From the figure it can be noticed that while the flexural behaviour of the beams is quite linear till the end of the tests, the displacements of the dowels show a change in slope well before the maximum load. Since the load at which this change happens is generally well below the bearing capacity of the dowel, probably it is the load at which the cracks start to propagate.

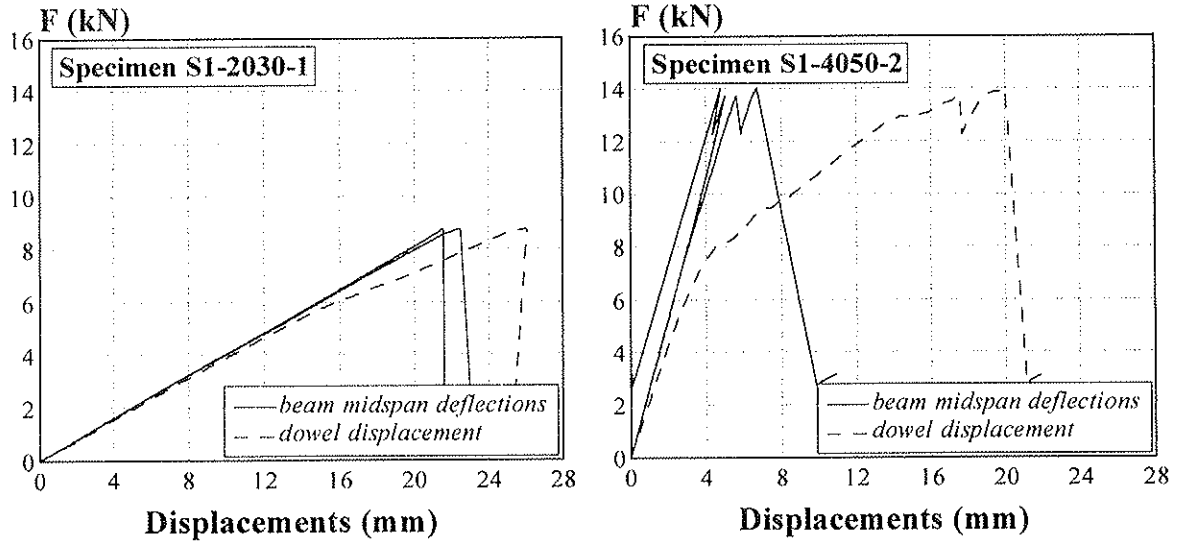


Figure 6 – Typical load-deflection (beam) and load-displacement (dowel) diagrams.

An appraisal of the influence of the fundamental parameter  $a_r$  (distance of the furthest fastener from the beam's loaded edge) on the splitting strength of tested specimens is clearly detectable in figure 7 where all the failure data are reported. In the same figure, a linear fitting has been superimposed to the data of each test series.

As is possible to see from the figure, the splitting strength of the beams grows quite linearly with  $a_r$  (the coefficients of determination -  $R^2$  - are of about 0.85 for each series) and the slope of the linear fitting is linked more to the number of rows of fastener(s) than to the size of the beams.

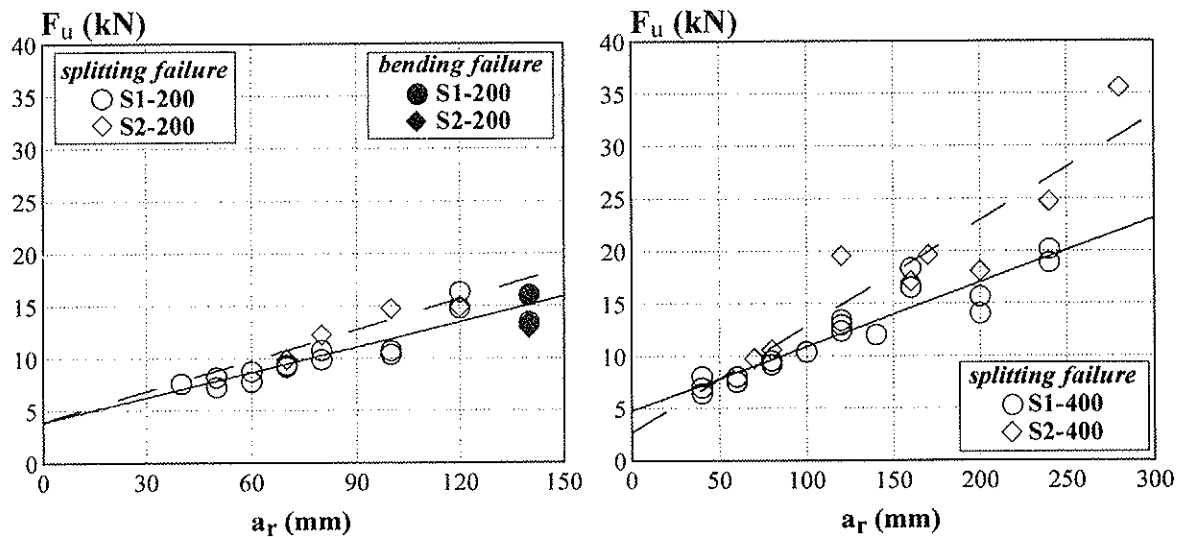


Figure 7 – Failure loads vs  $a_r$  : linear fittings.

## 4 Analysis of test results

The test results have been analysed mainly with regard to the parameter  $a_r$  because, as it is possible to see from figure 8, it is the only parameter which affects considerably the data of this set of tests.

Differently from figure 7, where the data are plotted with reference to beams' height, in figure 8 the data are plotted with reference to the connections (in the upper graph the data of joints with one fastener: S1; in the lower graph the ones of joints with two fasteners: S2).

In these graphs a power fitting has been superimposed to the data of each series and also to the data S1 and S2 independently from the height of beams.

From the figure it is possible to notice that the power fittings computed on the data S1 and S2 (independently from the height of beams) are equals to those that can be obtained from the power fitting of each series (dashed curves). This allow to say that there is not a residual influence of the height of the beams on the power fittings reported in the graphs.

As already anticipated, the main effect of the presence of a second connector in the joint is an increase in the splitting strength of the beams and, in terms of power fitting, in an increase of the exponent.

This confirms that the joints geometry has a big influence on the strength for splitting of the beams and that this effect cannot be disregarded by prediction formulas.

This effect can be taken into account in different ways. If the splitting strength of beams with joints made by more rows of fasteners is simply thought as the sum of the contribution of each row:

$$F_u = \sum_{i=1}^n k_i a_{ri}^{\beta}$$

the graph of figure 9 can be obtained from this set of data.

In the graph, the failure loads have been normalised to the failure loads of beams

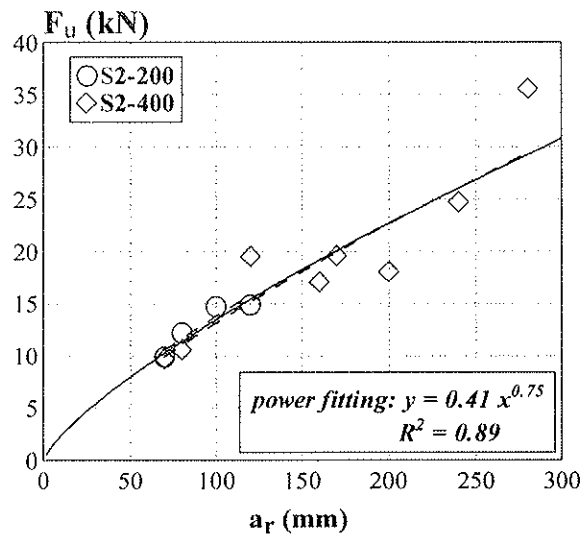
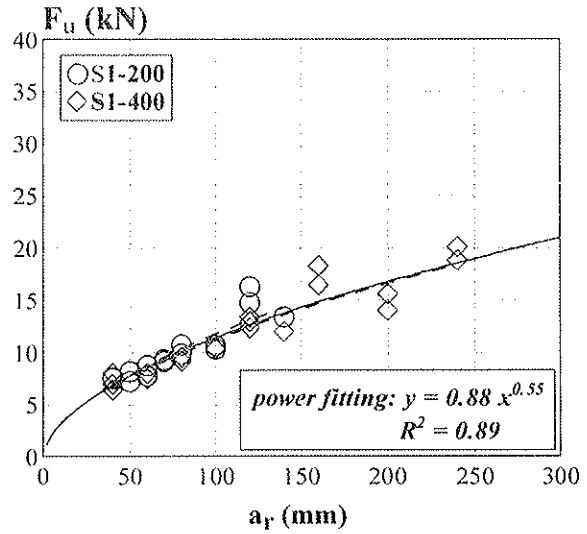


Figure 8 – Failure loads vs  $a_r$  : power fittings.

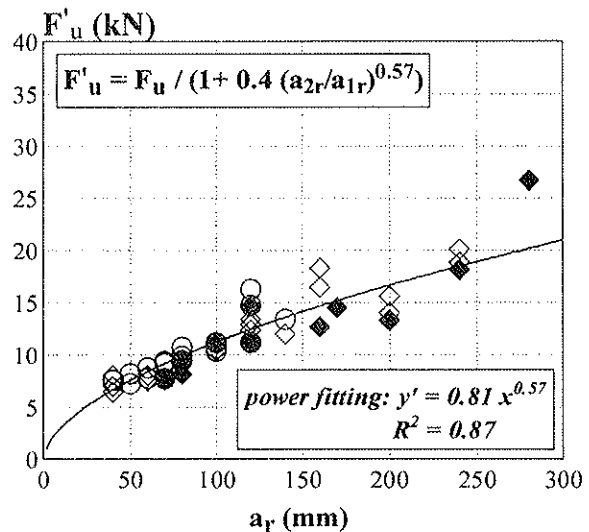


Figure 9 – Failure loads normalised to failure loads of beams with joints made by only one fastener.

with joints made by only one fastener according to the formula reported on the diagram; in the formula  $a_{ir}$  is the distance of the  $i$ -th row of fastener(s) from the loaded edge of the beam.

## 5 Comparison with prediction formulas

The failure data of this test programme have been compared with the prediction formulas of Ehlbeck, Görlacher and Werner [2-3], of TACM van der Put [7-8] and lastly with the design rule of EC5 [1].

The result of the comparisons are shown respectively in figures 10, 11 and 12 where the ratios between the predicted strengths and the experimental ones are reported versus the joint not-dimensional parameter  $\alpha$  and the height of beams.

For what concerns the first comparison (figure 10) from the left graph it is evident that the formula predicts very well the strength of beams 197 mm high (mean 1.00, stand.dev. 0.1) while it is a little less good in the case of beams 397 mm high (mean 1.25, stand.dev. 0.2). This less effectiveness of the formula is due mainly to a quite large overestimation of the beams' strength characterised by low values of the parameter  $\alpha$ . Due to this, a little average overestimation of the strength is detectable in the right graph.

For what concerns the comparison with the formula of van der Put (figure 11) from the graph it is evident a general overestimation of the strength for the beams of both sizes. This average overestimation, of about 50%, is mainly due to the high value of the "critical total energy release rate" ( $G_c$ ) proposed by the author. Moreover, from the left graph, a little influence of the parameter  $\alpha$  on the strength is detectable from the data of S1-400 series.

Finally the comparison with the EC5 design rule is reported in figure 12. The diagrams have been derived assuming for the shear strength of the wood an average value of about 3 MPa. From the graphs it is evident an influence of the parameter  $\alpha$  on the ratios of each series and also a clear bigger overestimation of the strength of the higher beams. This is due to the assumed linear relationship with the distance from the loaded edge ( $a_r = \alpha h$ ).

## 6 Conclusions

A new set of experimental results on the splitting strength of beams loaded perpendicular to the grain by dowel type connections have been illustrated and the failure modes have been reported in detail. The main features of this experimental research is the wide range of the not-dimensional parameter  $\alpha$  taken into consideration (from 0.1 to 0.7) and the slenderness ratios of the beams, well above those of previous experimental programmes.

The analysis of the results has allow to exploit the effect on the splitting strength of the distance of the furthest fastener from the loaded edge of the beam. Moreover, the comparison with the failure loads of the beams with joints made by two dowels has allow the derivation of a possible way to take into account the effect of more rows of fasteners.

Finally, the comparison with the available prediction formulas and with the design rule of EC5 has allow to derive the following drawings:

- the formula of Ehlbeck, Görlacher and Werner is the one that gives the better appraisal of the splitting strength of the beams of this experimental research;

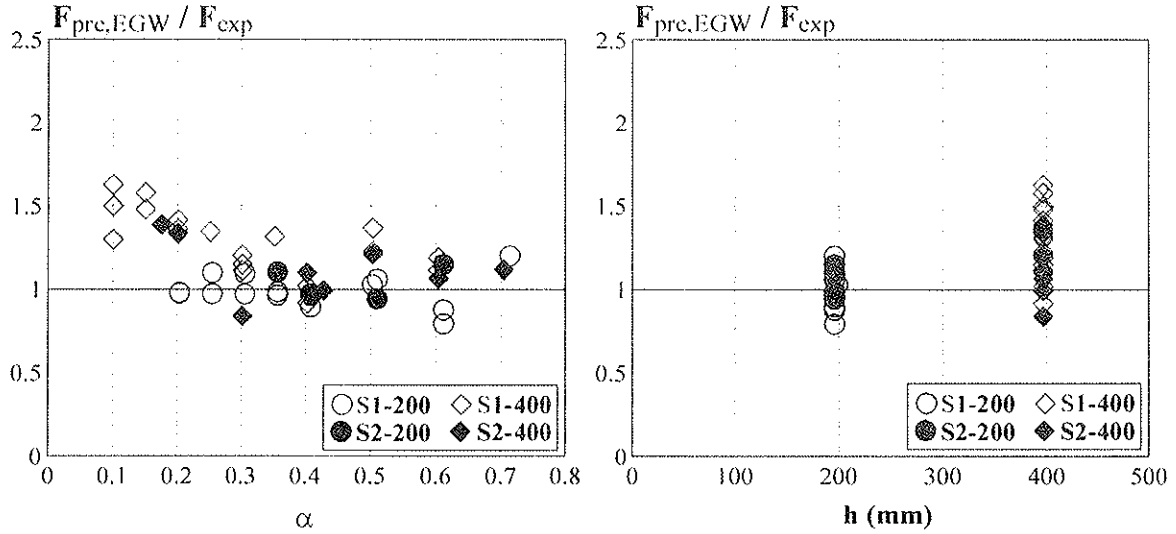


Figure 10 – Ehlbeck, Görlacher and Werner:  $F_{pre}/F_{exp}$  vs the geometrical parameter  $\alpha$  (left) and the beams' height (right).

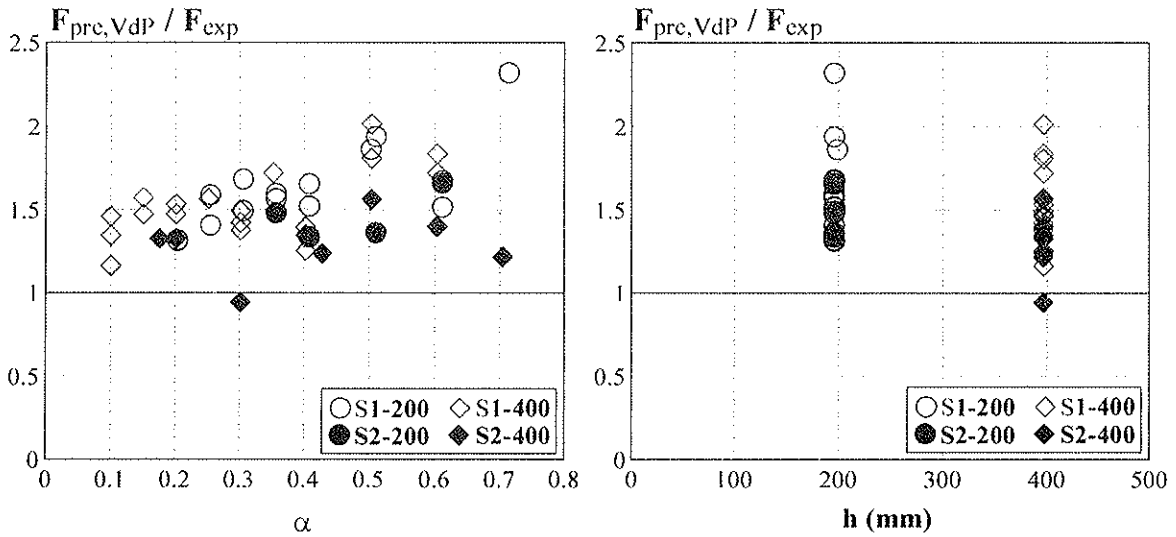


Figure 11 – TACM van der Put:  $F_{pre}/F_{exp}$  vs the geometrical parameter  $\alpha$  (left) and the beams' height (right).

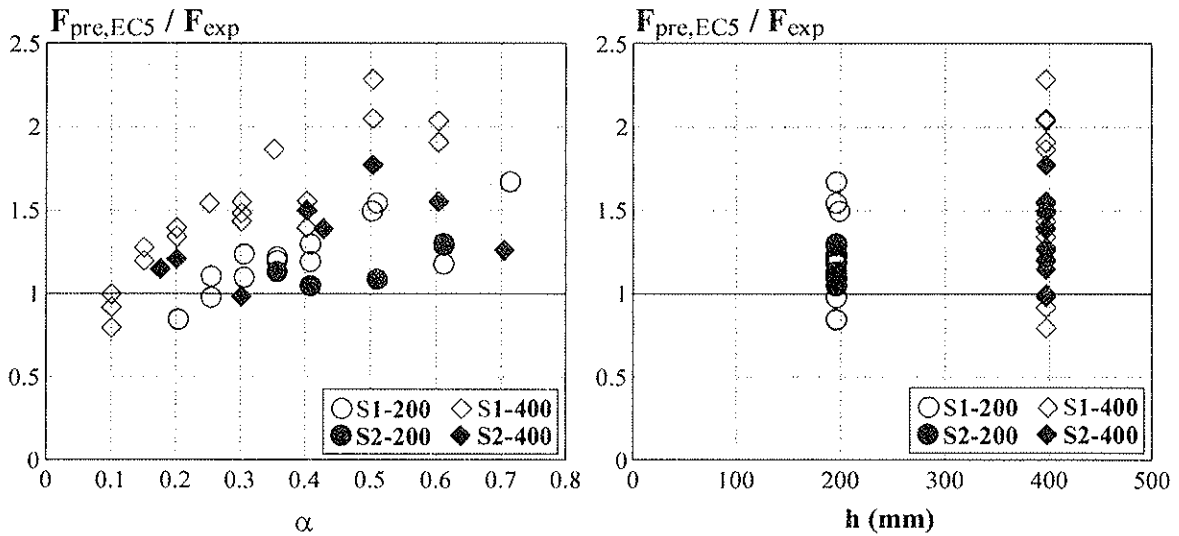


Figure 12 – EC5:  $F_{pre}/F_{exp}$  vs the geometrical parameter  $\alpha$  (left) and the beams' height (right).

- the one of TACM van der Put is globally good but overestimates the strength of the beams of about 50%;
- the design rule of EC5 is the one that shows the lower agreement with the test data (a clear influence of the parameter  $\alpha$  and an evident size effect are detectable from its figure).

## Acknowledgements

The author wish to thank the Ministry of the University and Scientific Research whose grants have allowed the development of the research. He also wish to thank Mr. Alfredo Pojer and Eng. Lucio Faccincani for their active co-operation in Laboratory tests.

## References

- [1] ENV-1995-1-1, 1993: Eurocode 5 - Design of timber structures. Part 1-1: General rules and rules for buildings. CEN.
- [2] Ehlbeck, J., Görlacher, R., Werner, H., 1989: Determination of perpendicular-to-grain tensile stresses in joints with dowel-type fasteners: a draft proposal for design rules. CIB-W18 – Timber structures. Paper 22-7-2, Berlin, German Democratic Republic.
- [3] Ehlbeck, J., Görlacher, R., 1995: Tension perpendicular to the grain in joints. Lecture C2:, STEP 1 - Timber Engineering, Centrum Hout, The Netherlands.
- [4] Möhler, K., Lautenschläger, R., 1978: Großflächige Queranschlüsse bei Brettschichtholz. Forschungsbericht des Lehrstuhls für Ingenieurholzbau und Baukonstruktionen, Universität Karlsruhe.
- [5] Möhler, K., Siebert, W., 1980: Ausbildung von Queranschlüssen bei angehängten Lasten an Brettschichtholzträger. Forschungsbericht des Lehrstuhls für Ingenieurholzbau und Baukonstruktionen, Universität Karlsruhe.
- [6] Ehlbeck, J., Görlacher, R., 1983: Tragverhalten von Queranschlüssen mittels Stahlblechformteilen, insbesondere Balkenschuhe, im Holzbau. Forschungsbericht der Versuchsanstalt für Stahl, Holz und Steine, Abt. Ingenieurholzbau, Universität Karlsruhe.
- [7] TACM van der Put, 1990: Tension perpendicular to the grain at notches and joints. CIB-W18 – Timber structures. Paper 23-10-1, Lisbon, Portugal.
- [8] TACM van der Put, 1992: Energy approach for fracture of joints loaded perpendicular to the grain. COST 508, Workshop on fracture mechanics in wooden structures, Bordeaux, France.

**INTERNATIONAL COUNCIL FOR RESEARCH AND INNOVATION  
IN BUILDING AND CONSTRUCTION**

**WORKING COMMISSION W18 - TIMBER STRUCTURES**

**DESIGN AND ANALYSIS OF BOLTED TIMBER JOINTS UNDER  
LATERAL FORCE PERPENDICULAR TO GRAIN**

M Yasumura  
Shizuoka University  
JAPAN

L Daudeville  
Laboratoire de Mécanique et Technologie  
Cachan  
FRANCE

**MEETING THIRTY-TWO**

**GRAZ**

**AUSTRIA**

**AUGUST 1999**

---

Presenter: M.Yasumura

· Brief discussion took place on the yield strength of the connection and embedment strength of the bolt.

# Design and Analysis of Bolted Timber Joints under Lateral Force Perpendicular to Grain

Motoi Yasumura  
Shizuoka University, Japan

Laurent Daudeville  
Laboratoire de Mécanique et Technologie,  
Ecole Normale Supérieure de Cachan, France

## 1. Introduction

The fracture of wood is one of the major causes of brittle failure in timber structures. It brings serious damages of timber structures under seismic action by reducing the energy dissipation. Fracture of wood occurs frequently at the joints subjected to the force perpendicular to the wood grain. This failure is not always predictable because the design of timber joints is generally based on the yield theory<sup>1-3)</sup> that does not include the failure of joints due to the fracture of wood. The fracture mechanics is one of the most effective methods to analyze the fracture of timber structures<sup>4-6)</sup>. It is particularly useful for estimating the maximum strength of the joints when the crack propagation is stable. In the previous paper<sup>4)</sup>, the fracture of a single bolted joint subjected to a lateral force perpendicular to the grain was analyzed by means of the ASM (Average Stress Method) and the LEFM (Linear Elastic Fracture Mechanics). It showed that the ASM and the LEFM were appropriate tools to predict the crack initiation and propagation of the bolted timber joints subjected to lateral force perpendicular to the grain, respectively. In this study, the load carrying capacities of a single and multiple bolted joints obtained from the lateral loading tests were compared with the results of simulation by means of the LEFM and yield strength.

The crack propagation under the coupling of Mode I and Mode II can be calculated by using either energy release rate ( $G$ ) or stress intensity factor ( $K$ ). The stress intensity factor in Mode I ( $K_I$ ) and Mode II ( $K_{II}$ ) can be calculated by the following formula;

$$K_I = \lim_{r \rightarrow 0} \sigma_{yy}(r) \sqrt{2\pi r} \quad (1)$$

$$K_{II} = \lim_{r \rightarrow 0} \sigma_{xy}(r) \sqrt{2\pi r} \quad (2)$$

where,  $\sigma_{yy}(r)$  and  $\sigma_{xy}(r)$  are the tensile stress perpendicular to the grain and the shear stress at the distance  $r$  from the crack tip. The criterion for the crack propagation is generally expressed as follows;

$$\left(\frac{K_I}{K_{IC}}\right)^m + \left(\frac{K_{II}}{K_{IIC}}\right)^n = 1 \quad (3)$$

where,  $K_{IC}$  and  $K_{IIC}$  are the critical stress intensity factors in Mode I and Mode II, respectively. The value of  $K_{IC}$  was set at  $0.439\text{MPa}\sqrt{\text{m}}$  from the previous study<sup>4)</sup> for spruce of the density of  $440\text{kg/m}^3$ . It is discussible what values should be taken for  $m$ ,  $n$  and  $K_{IIC}$ . To make the problem simple, following values were assumed from the calibration between the experimental results of a single bolted joint and the simulation.

$$m = 1 \quad ; \quad n = 2 \quad ; \quad K_{IIC} = 3 K_{IC}$$

## 2. Specimens

The outline of specimens is shown in Fig.1. Specimens consisted of spruce glued laminated wood and 12mm thick steel side plates on both sides of the wooden member, connected with bolts 16mm in diameter ( $d$ ). The glued laminated wood was made of laminae 30mm thick with an average density  $440\text{kg/m}^3$ . The quality of steel used for the side plates and bolts was JIS (Japanese Industrial Standard) SS 400. The pre-drilled holes of wooden members were equal to or slightly larger than the bolt diameters, and the diameters of the bolt holes of steel plates were 1mm larger than the bolt diameter. The thickness of the wooden member was 64mm ( $4d$ ) and 128mm ( $8d$ ).

Specimens were divided into four groups as shown in Figs.1(a) to (d). Type-T specimens had joints of a single fastener whose end and edge distances varied from 64mm( $4d$ ) to 160mm( $10d$ ) and from 64mm( $4d$ ) to 112mm( $7d$ ), respectively. Type-H specimens had joints of two fasteners aligned with the grain and spaced 64mm ( $4d$ ), 112mm ( $7d$ ) and 160mm ( $10d$ ). Type-V specimens had joints of two or three fasteners aligned perpendicular to the grain and spaced 64mm ( $4d$ ). These specimens were subjected to a tensile force perpendicular to the grain as shown in Figs.1(a) to (c). Type-B specimens had joints of single, two or three bolts aligned perpendicular to the grain spaced 64mm( $4d$ ). The height of Type-B specimens was 224mm( $14d$ ) in the case of single fastener specimen, 192mm( $12d$ ) for the specimens of two fasteners and 256mm( $16d$ ) for those of three fasteners. The end distance was 64mm( $4d$ ) and 112mm( $7d$ ) in a single fastener specimen and it was kept as 112mm( $7d$ ) for the specimens of



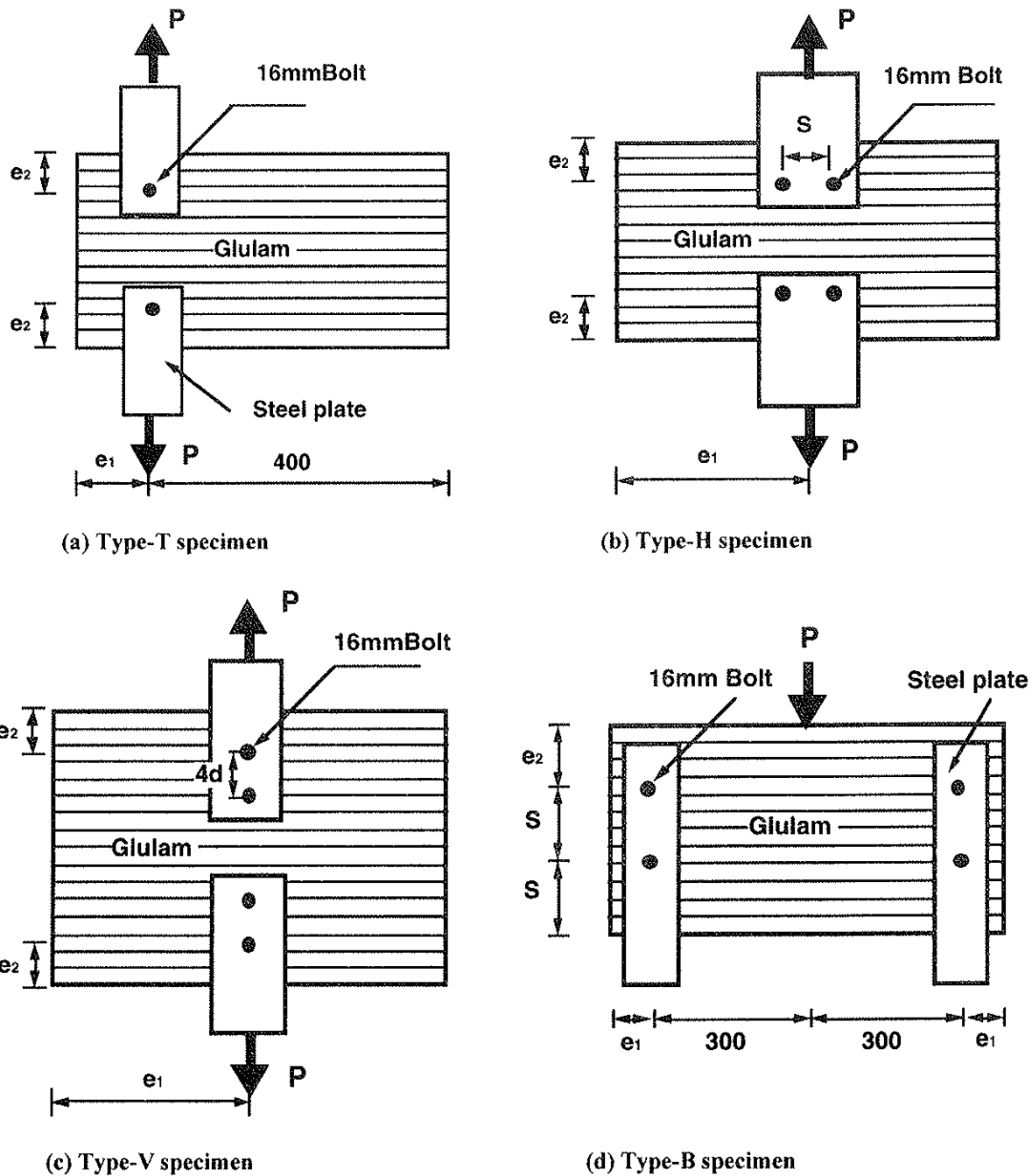


Fig.1 Outline of specimens

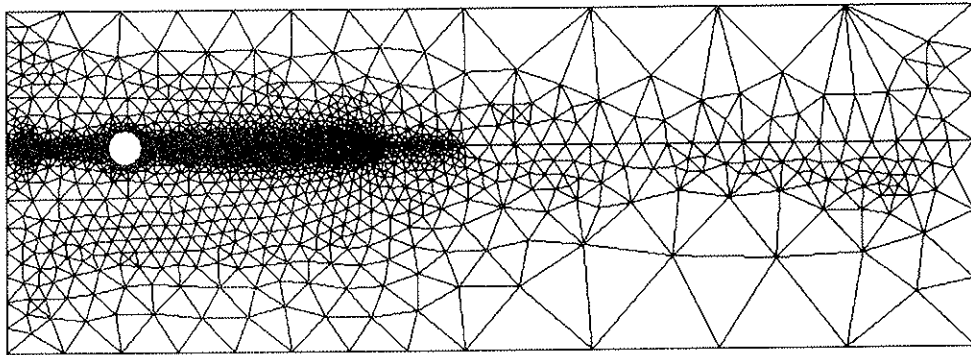
multiple fasteners. The edge distances varied from 64mm( $4d$ ), 112mm( $7d$ ), 160mm( $10d$ ) and the bolt spacing( $s$ ) was 64mm( $4d$ ). They were subjected to lateral force by bending as shown in Fig. 1(d).

### 3. Test method

Three specimens of each type were subjected to lateral loads as shown in Figs.1(a) to (d). The quasi-static tensile loads were applied to the steel side plates by a hydraulic jack in Types-T, H and V specimens, and the compressive load was applied on the center of wooden member in Type-B specimens. Relative displacement between the steel plates and wooden member was measured with four electric displacement transducers. The nuts were attached to the joints with little tightening. The lateral loads increased at a constant rate until one of the joints failed.

### 4. Modeling

Tested joints were modeled with the finite elements as shown in Fig.2. A quarter or half of the specimen was modeled considering the symmetry. The assumption for the modeling was the same as in the previous study with a single fastener<sup>4)</sup>; the contact between the wood and the bolt was complete and there was no friction on them, and the plane stress conditions were applied and there was no noticeable deformation of the bolt. Young's modulus of spruce was assumed to be 15,000 MPa in the longitudinal direction and 600 MPa in the transverse direction and the shear modulus and Poisson's ratio of 700 MPa and 0.5 were assumed, respectively.



**Fig.2 Finite element mesh for Types-T and B specimens.**

Figure 3 shows the boundary conditions of the model. The bolt hole boundary was fixed in the radial direction but only in the positive direction and free in the tangential direction. The forced displacements were applied downwards at the lower boundaries in Types-T, V and H specimens. In Type-B specimens the forced displacements were applied downwards at the right corner of the upper side. The FEM code CASTEM 2000 developed by the French

Atomic Energy Commissariat (CEA) was used for the analysis.

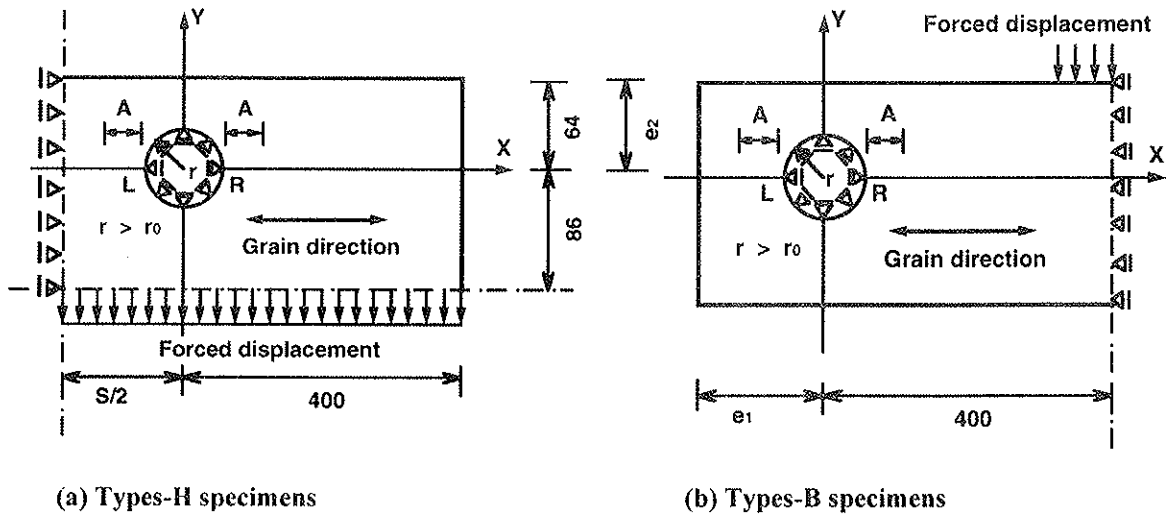


Fig.3 Boundary conditions

## 5. Results and discussion

### 5.1 Crack initiation

Figure 4 shows the tensile stress perpendicular to the grain ( $\sigma_{yy}$ ) near the bolt holes along the x-axis when the average stress perpendicular to the grain reached 4.76MPa in the Type-H specimens. This shows that the stress in the right side of the hole was slightly higher than that in the left side, and that the crack initiated at the right boundary of the hole. The stress perpendicular to the grain at the right boundary of the hole showed almost constant values

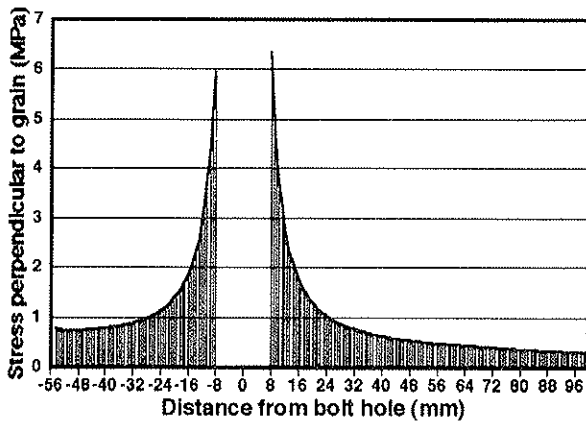


Fig. 4 Stress perpendicular to the grain in Type-H specimen (bolt spacing of  $7d$ ).

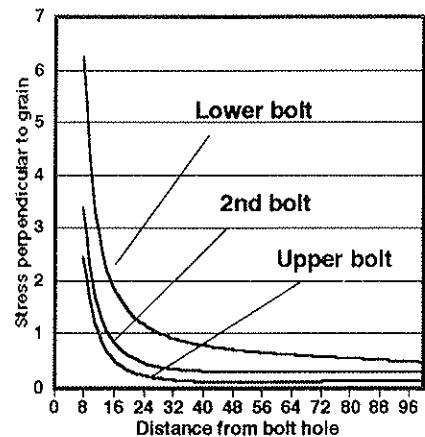
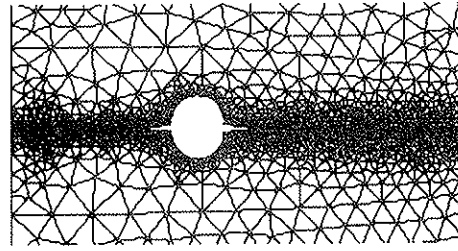


Fig. 5 Stress perpendicular to the grain in Type-V specimen (three bolts)

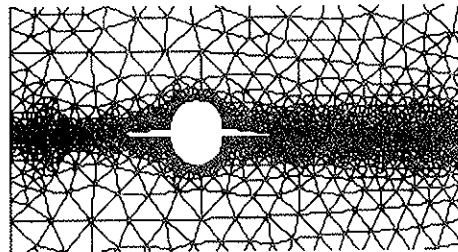
around 6.3 to 6.4 MPa regardless of the bolt spacing. The stress at the left boundary varied from 5.74, 5.92 and 6.14 MPa respectively for the bolt spacing of  $4d$ ,  $7d$  and  $10d$ . This indicates that the tensile stress perpendicular to the grain was more concentrated at the right boundary (outer side) than the left boundary (inner side) when the bolt spacing was  $4d$ , but there was little difference at the right and left boundaries when the bolt spacing was  $10d$ .

Figure 5 shows the tensile stress perpendicular to the grain ( $\sigma_{yy}$ ) near the bolt holes along the x-axis when the average stress perpendicular to the grain reached 4.76MPa in the Type-V specimens. This shows that the stress perpendicular to the grain at the bolt hole boundary of the lowest bolt was approximately 6.15 MPa regardless of the number of bolts. The stress of the second and third upper bolts was approximately 40 and 60% smaller than that of the lowest bolt, respectively. These results indicate that the stress perpendicular to the grain was concentrated mostly at the lowest bolt, and the upper bolts contributed less than the lowest bolt against the crack initiation when the multiple bolts were aligned perpendicular to the grain.

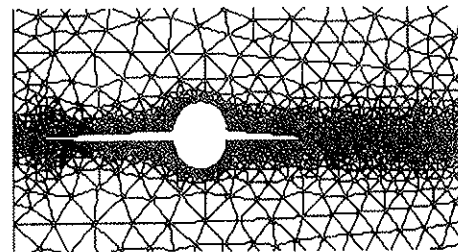
The point of stress at the crack initiation varied within the range from 6.1 to 6.4MPa for all types of joints tested in this study. This ensures that the location and the approximate force on the initiating crack can be predicted with the point of stress if the finite meshes are sufficiently fine and there is no problem of the singularity.



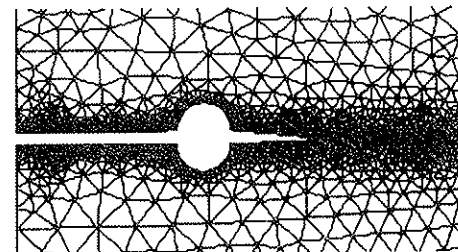
Step 20:  $P=164\text{kN/m}$  per bolt,  $A_r=0.6d$ ,  $A_l=0.5d$



Step 40:  $P=161\text{kN/m}$  per bolt,  $A_r=d$ ,  $A_l=1.1d$



Step 80:  $P=133\text{kN/m}$  per bolt,  $A_r=1.6d$ ,  $A_l=2.5d$



Failure:  $P=93\text{kN/m}$  per bolt

**Fig.6 Crack propagation in Type-H specimen (bolt spacing of  $7d$ ).**

## 5.2 Crack propagation

Figure 6 shows the process of the crack propagation in the Type-H specimens when the bolt spacing was  $7d$ . These figures show that the crack propagated at the beginning almost symmetrically to the both directions until the crack propagated up to  $1.2d$ . Then, the crack propagation on the right side had almost stopped, and the left crack continued propagating. Finally, two cracks that had propagated from both holes met at the center of the specimen. The lateral load per bolt showed almost constant value of  $160\text{N/mm}$  until the crack propagated to  $1.5d$ , and then decreased gradually as the crack propagated. The lateral load decreased suddenly to  $93\text{N/mm}$  when the crack reached the center of the specimen.

Figure 7 shows the relation between the load and the crack length in the Type-V specimens. It shows that the load increased gradually as the crack propagated up to 2 to  $2.5d$  and then decreased gradually as the crack propagated. Thus saying that the crack propagation was stable at the beginning, but became unstable when it reached up to 2 to

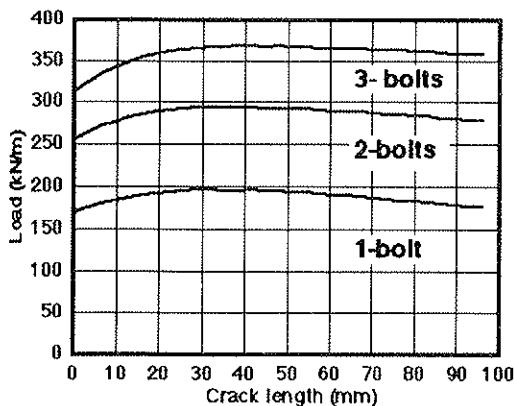


Fig. 7 Relation between lateral load and crack length in Type-V specimens

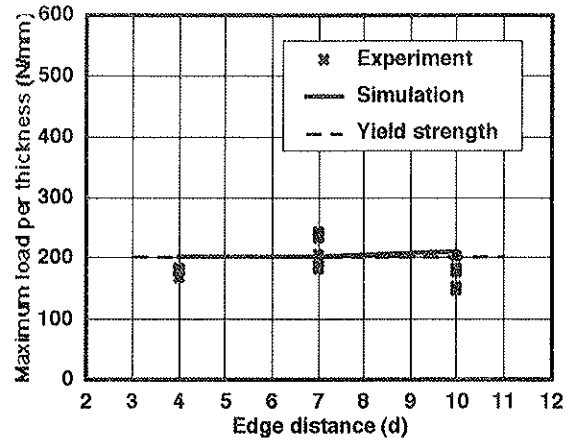


Fig. 8 Maximum load of Type-T specimens (single bolt,  $e_1=7d$ )

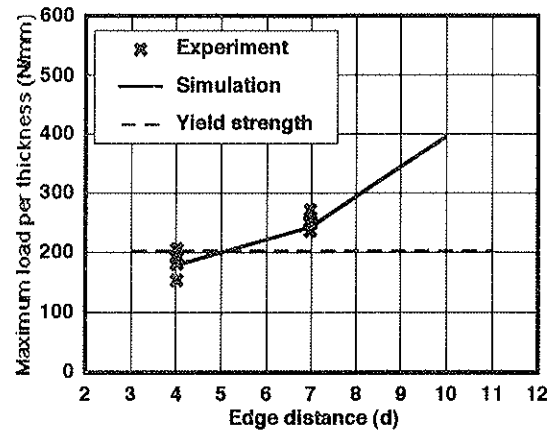


Fig. 9 Maximum load of Type-B specimens (single bolt,  $e_1=4d$ )

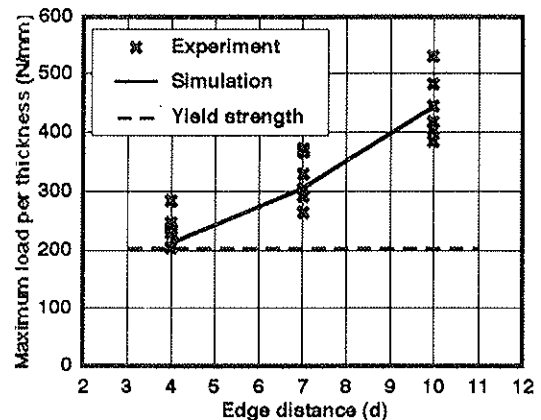


Fig. 10 Maximum load of Type-B specimens (single bolt,  $e_1=7d$ )

2.5d in the Type-V specimens.

### 5.3 Load carrying capacity

Figs. 8 shows the relationship between edge distance and the maximum load in the Type-T specimens and Figs. 9 and 10 show those of the Type-B specimens when the end distance was  $4d$  and  $7d$ , respectively. In the Type-T specimens, the maximum load from the experiment and the simulation was almost constant and close to the calculated yield strength regardless of the edge distance. The calculated yield strength of the joint that had a single bolt 16mm in diameter with steel side plating was 205N/mm when the embedding strength of the wood (obtained from 5% off-set in embedding test) and the yield moment of bolt were respectively 12.8MPa and  $218Nm^4$ ). In the Type-B specimens, the maximum load was almost the same as the yield strength when the specimen had the end distance of  $7d$ , and slightly lower than the yield strength when the edge distance was  $4d$ . However the maximum load increased as the edge distance became larger regardless of the end distance in the Type-B specimens.

Fig.11 shows the relationship between the maximum load and bolt spacing of the Type-H specimens. The maximum load was increased slightly as the bolt spacing became larger and 25 to 35% smaller than the calculated yield strength. Fig.12 shows the relationship between the maximum load per bolt and the number bolts of the Type-V specimens. The maximum load decreased remarkably as the number of bolts increased, and 35 to 41% smaller than the calculated yield strength. This indicates that all the tested joints of the Types H and V specimens with multiple fasteners failed with the fracture of the wood before the joints

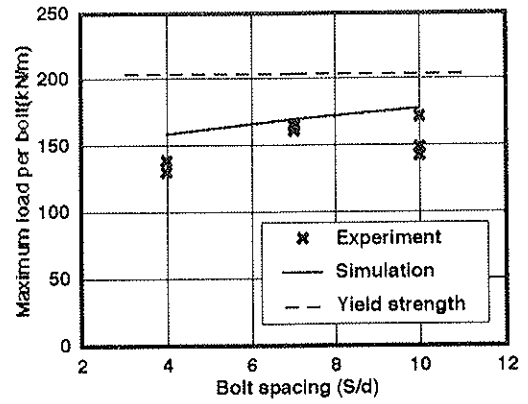


Fig. 11 Maximum load and bolt spacing in Type-H specimens.

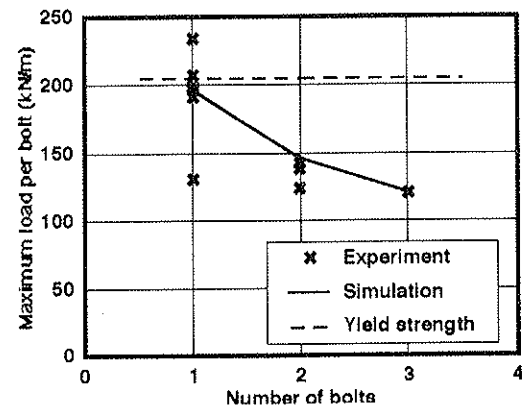


Fig. 12 Maximum load and number of bolts in Type-V specimens.

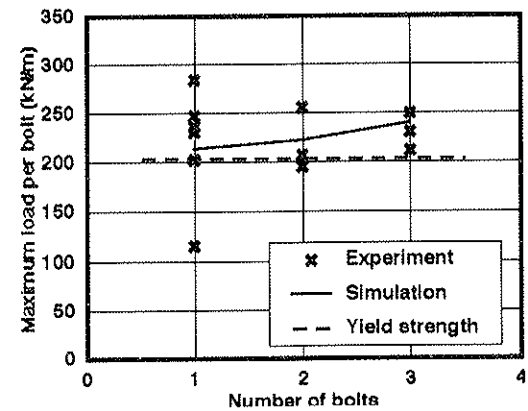


Fig. 13 Maximum load and number of bolts in Type-B specimens.

yielded. It is very important to predict the fracture of the wood before the yielding of the fasteners when the multiple joints are subjected to a force perpendicular to the grain. Fig.13 shows the relationship between the maximum load per bolt and number of bolts of the Type-B specimens. The maximum load was almost constant and slightly larger than the calculated yield strength regardless of the number of bolts when the edge distance was  $7d$ . This indicates that the joints does not fail due to the fracture of wood before the yielding of bolts if the end distance is  $7d$  and bolts are placed along the height of beam with the spacing of  $4d$ .

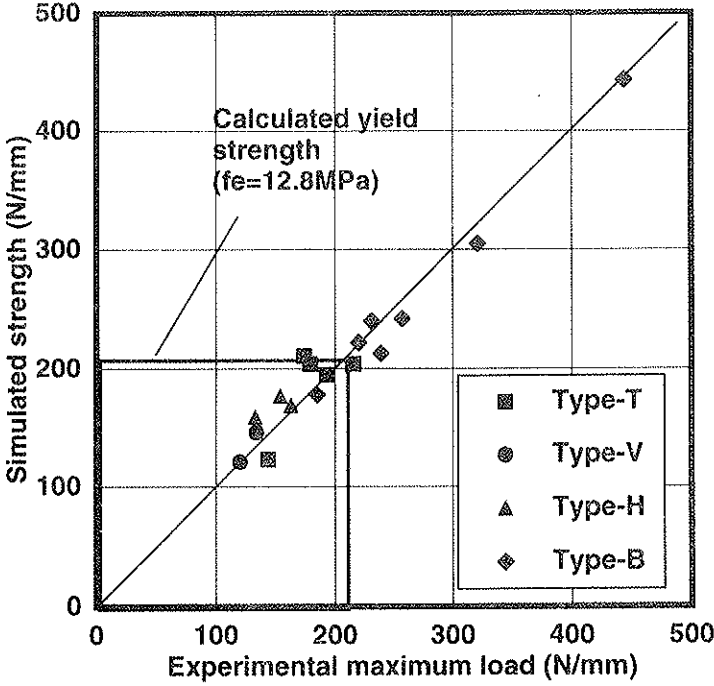


Fig.14 comparison of the experimental maximum load with the simulated values (bolt diameter 16mm)

Figure 14 shows the comparison of the experimental maximum load with the simulated values by means of the LEFM. It shows that the maximum load obtained from the simulation agreed very well with the experimental results. It also shows that the maximum load of the Types-T, H and V specimens was mostly smaller than the calculated yield strength. Special consideration should be done on the design of these joints.

### 6. Conclusions

It was found that the load carrying capacity obtained from the simulation by means of the LEFM agreed very well with the experimental results, and the LEFM was the appropriate tool to estimate the failure of bolted timber joints. It was also found that the load carrying capacity of the joints subjected to lateral force perpendicular to the grain was mostly smaller than the yield strength, and they failed due to the fracture of the wood before the yielding of bolts. Special consideration should be done on design of joints subjected to the lateral force perpendicular to the grain..

## 7. References

1. European Committee for Standardization (1993) Eurocode 5: Design of timber structures, part 1-1: General rules and rules for buildings: 72-77
2. Architectural Institute of Japan (1995) Standard for Structural Design of Timber Structures (in Japanese) : 42-45, 50-54
3. Johansen KW (1949) Theory of Timber Connections, international Association for Bridge and Structural Engineering 9: 249-262
4. Yasumura M, Daudeville L (1996) Fracture Analysis of Bolted Joints under Lateral Force Perpendicular to the Grain. *Mokuzai Gakkaishi* 42 (3): 225-233
5. Daudeville L, Davenne L, Yasumura M (1996) Experiment and Numerical Analysis of Failure in Bolted Joints, Proceedings of 1996 IWEC 1: 153-159
6. Petersson H (1995) Fracture design analysis of wooden beams with holes and notches, Proceedings of CIB-W18 meetings: 28-19-3
7. Daudeville L, Yasumura M (1996) Failure Analysis of Timber Bolted Joints by Fracture Mechanics, *Materials and Structures* 29: 418-425
8. Yasumura M (1993) Japan Overview: Design Concept and Prospect of Bolted Joints and Nailed Joints, International Workshop on Wood Connectors, Forest Products Society: 114-121
9. Valentin G.H., Bostrom L., Gustafsson P.J., Ranta-Maunus A., Gowda S. (1991) Application of Fracture Mechanics to Timber Structures RILEM State-of-the-art Report, Technical Research Center of Finland, Research Notes 1262
10. Aicher S., Bostrom L, Gierl M., Kretschmann D., Valentin G. (1997) Determination of Fracture Energy of Wood in Mode II, RILEM TC 133 Report, Swedish National Testing and Research Institute



**INTERNATIONAL COUNCIL FOR RESEARCH AND INNOVATION  
IN BUILDING AND CONSTRUCTION**

**WORKING COMMISSION W18 - TIMBER STRUCTURES**

**PREDICTING CAPACITIES OF JOINTS WITH LATERALLY LOADED NAILS**

I Smith

Faculty of Forestry and Environmental Management  
University of New Brunswick, Fredericton, NB

P Quenneville,

Department of Civil Engineering  
Royal Military College, Kingston, ON,  
CANADA

**MEETING THIRTY-TWO**

**GRAZ**

**AUSTRIA**

**AUGUST 1999**

---

Presenter: J.H.P.Quenneville

- C.N.Fouepe asked the applicability of the results to tropical hard wood.
- H.J.Blass commented that for high-density tropical hardwood pre-drilling would be needed before nailing. Also embedment strength data for high-density tropical hardwood would be needed. Otherwise the equations should still be valid.
- E.Karacabeyli asked about the applicability of the results to plywood to wood connections.
- J.H.P.Quenneville responded that the results would be valid for timber to timber connections only.

# PREDICTING CAPACITIES OF JOINTS WITH Laterally LOADED NAILS

Dr. Ian Smith, Professor of Timber Engineering  
Faculty of Forestry and Environmental Management  
University of New Brunswick, Fredericton, NB, Canada

Dr. Pierre Quenneville, Associate Professor  
Department of Civil Engineering  
Royal Military College, Kingston, ON, Canada

## Abstract

Capacities of joints with laterally loaded nails may be predicted using “European yield” type models (EYM’s) with various levels of complexity. EYM’s presume that a nail and the wood on which it bears exhibit a rigid-plastic stress-strain response. Consideration is given in this paper to the ‘original’ model published by K.W. Johansen in 1949 (and popularized by H.J. Larsen in more recent years), an empirical approximation proposed by L.R.J. Whale and coworkers in 1987, and a curtailed and ‘simplified’ model proposed by H.J. Blass and coworkers in 1999. Predictions from the various EYM’s are compared with experimentally determined ultimate capacities of single shear joints. Experiments covered a fairly broad range of combinations of ‘head-side’ and ‘point-side’ member penetrations. The impact of modeling assumptions is illustrated in the context of the Canadian timber design code. Suggestions are made regarding the necessity level of complexity for nailed joint models used in design.

## 1. Introduction

Until recently, all North American engineers designed timber structures based on the ‘working stress’ approach. Most still do so. The factor of safety is 1.3 for members loaded in bending, tension and compression [1]. For timber joints the factor of safety is inconsistent across various types of joints, and cannot actually be defined. The approach for splice joints is to take the allowable load as a fraction of the load at the ‘proportional limit’ load or an approximation to it [2]. Unadjusted allowable loads apply to a single fastener/connector subjected to normal duration loading, and a dry service condition. Deviations from reference conditions are accounted for by a sequence of modification factors. Concepts and much of the data that underpin working stress design of joints are the result of research at the US Forest Products Laboratory in the 1930’s and 1940’s [e.g 3]. It is generally accepted that the working stress method contains inconsistencies in capacities for different types of fasteners that cannot be justified [4]. For most types of mechanical joint, the ultimate load lies well above the estimated proportional limit load. The ratio of ultimate and proportional limit loads can approach 3.5 for nailed softwood joints and 7.0 for nailed hardwood joints [2]. Thus, the allowable load for a joint is commonly a small fraction of its ultimate strength. Consequently joints tend to be too stiff

and impede redistribution of forces within a system, and only limited energy dissipation can occur under cyclic loads.

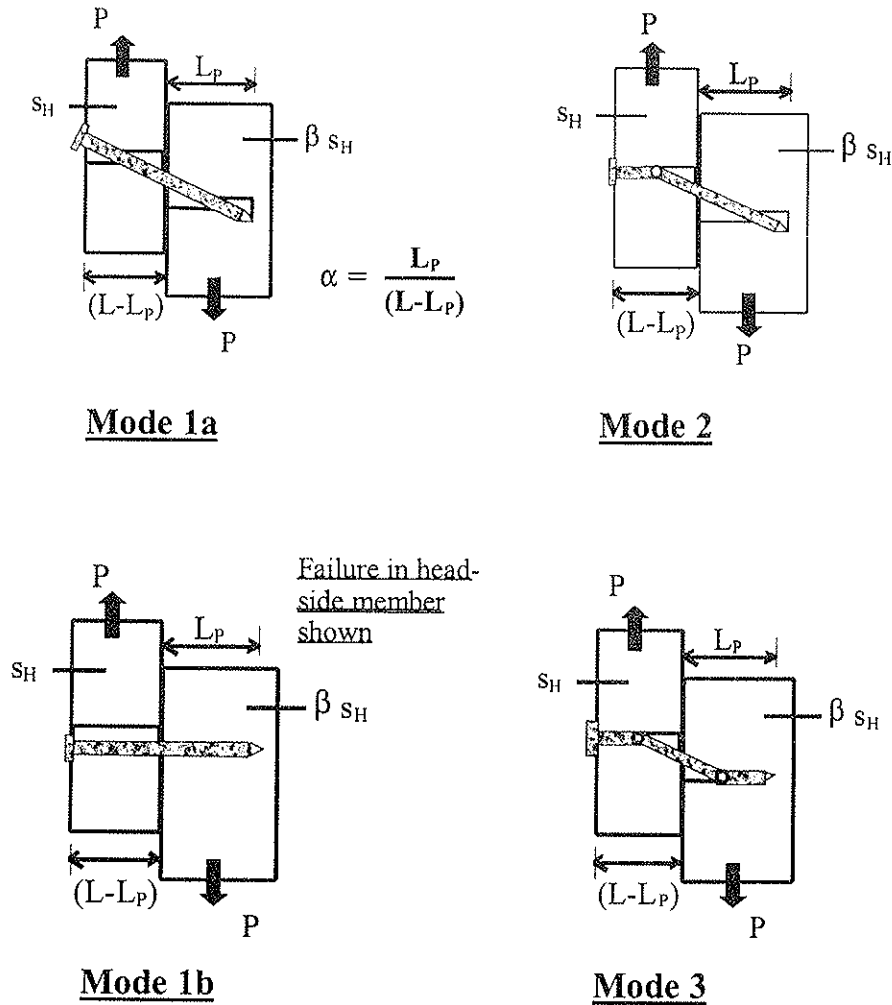
Canada introduced its first limit states design code for timber structures in 1984 [5]. For timber members this was a soft conversion from the working stress method, although account was taken of 'in-grade' test data for small dimension lumber. There was a fundamental shift with regard to joint design [6]. Data from various sources was re-analysed so that joint capacities would reflect the strength (ultimate) limit state and serviceability limit state considerations. Strength and serviceability limits were separately identified for joints made with truss plates, nails and lag screws. Only the strength limit state was considered in other cases, e.g. laterally loaded bolts, nails loaded in withdrawal. Ultimate capacities of laterally loaded bolts and nails were calculated based on Johansen's yield theory [7, 8]. The theory has become known as the European Yield Model (EYM) in North America. Its use was not transparent in 1984 as capacities were given in tabular form for different combinations of fastener diameter and commercial species group, plus member thickness and direction of loading in the case of bolts. Use of a Johansen type approach became transparent for bolted joints in the 1989 edition of the Canadian timber code. Resistance factors were assigned based on engineering judgement. A resistance factor,  $\phi$ , having a value less than one is applied to the strength,  $R$ , of a joint to account for uncertainty. Load factors,  $\alpha$  values, are applied to the unfactored load effects,  $F$  values. Conceptually an ultimate limit state design equation takes the form:  $\phi R \geq \sum \alpha F$ . Despite selective refinements, code provisions for joints remain essentially unaltered since 1984 [9, 10].

The CSA 086 Technical Committee that is responsible for the Canadian timber design code is in the process of a major overhaul of provisions pertaining to joints. Their objectives include: the elimination of inconsistencies in the approaches used to assign capacities to different types of fasteners, making the nature of the predicted failure mode transparent, and adoption of formula based methods whenever feasible. This paper considers issues related to design of laterally loaded nailed joints. Specifically, the focus is on the ability of various EYM's to predict the ultimate load capacity of a single shear timber-to-timber joint over a broad range of nail penetrations in the head-side and point-side members.

## 2. European Yield Models

EYM's presume that for joints made with metal nails the failure mode will be ductile. This is usually reasonable even for joints with multiple nails, provided that adequate end and spacing distances are employed. In Canada, like most other countries, the capacity per nail is taken to be linearly proportional to the number of nails. EYM analysis treats both the fastener and the wood foundation beneath it as being rigid-plastic materials. Thus, the 'initial yield' and fully plastic capacities for components, and therefore joints, coincide. The plastic capacity of the nail,  $M_Y$ , can be estimated from a bending test [11]. Some versions of the EYM use the nail yield stress,  $\sigma_Y$ , based on the relationship  $\sigma_Y = 6M_Y / d^3$ , where  $d$  is the nail shank diameter. The peak moment resisted by the nail is used to estimate its strength, and because nail material usually exhibits strain hardening,  $\sigma_Y$  is an apparent rather than a true yield stress. The wood foundation capacity is referred to as the embedment strength,  $s_H$ , and is obtained in a test where bending deformation of a nail is prevented [12]. Again the property is based on peak capacity. During derivation of the

capacities for nailed joints that are tabulated in CSA Standard 086.1 [5, 10] it was assumed that  $M_Y = 6.67(20-d) d^3 \text{ Nmm}$  and  $s_H = 1.1 \times$  compressive strength parallel to grain of clear wood [13], based on [7,8]. More recent information is employed later in this paper.



**Figure 1 – EYM Failure Modes: single shear arrangement**

Figure 1 shows the failure modes that are possible for a joint with a nail loaded in single shear (two-member arrangement). Comparable modes are applicable to multiple shear arrangements. Geometric variables are nail diameter,  $d$ , total nail length,  $L$ , and length of penetration into the point-side member,  $L_p$ . Joint capacity increases as thickness of the members is increased up to the point where a mode 3 failure occurs. It is assumed that the nail is driven normal to the sides of the members and that members are loaded concentrically. Neglecting force other than that normal to the axis of the nail, the yield load for a joint,  $P_Y$ , is determined for any mode from static equilibrium. The governing mode is that giving the lowest estimate of  $P_Y$ . Several forms of the EYM are in use, or have been proposed. Three forms considered here are:

- Original Model due to Johansen [7], extended by Laersen [8]. This is the basis of tabulated capacities for nailed joints in the 1984 and subsequent issues of CSA Standard 086.1 [5,10]. It was assumed that the nail penetrates two-thirds into the point-side member.

- Empirical Approximation by Whale et al [14]. This is the basis of formula based calculations of capacities for bolted and lag screwed joints within the current edition of CSA Standard 086.1 [10].
- Simplified Model proposed by Blass et al [15]. This has a curtailed set of equations that yield conservative results if members do not have adequate thickness to develop the mode 3 failure mechanism.

The appropriate formulae are summarized in the Appendix. For mode 1b it is necessary to consider the possibility of the bearing failure being in either the head-side or point-side member. Similarly, mode 2 involves the possibility of the plastic hinge forming in either member. If all modes are unconstrained, there are six equations to consider.

### 3. Joint tests: influence of head-side/ point-side penetration

Tests were made on specimens having four 3in (76mm) common wire nails loaded in single shear, Figure 2. The nails were no. 9 wire gauge, with a nominal diameter of 3.66mm [16]. The actual diameter was 3.76mm with minimal variation between nails. Thickness of the head-side member was varied between 56 and 25mm to give seven point-side penetrations that ranged from 20 to 51mm. The members were eastern Canadian grown spruce. This species belongs to the Spruce-Pine-Fir (S-P-F) commercial classification. Members were cut from 38mm thick lumber that had been conditioned to 15 percent moisture content. There were 11 test replicates per nail penetration representing matched density distributions. All members within a specimen had similar densities. The average density for joint members was  $411\text{kg/m}^3$  based on oven dry volume and mass, with a coefficient of variation 10.2 percent. The average density for S-P-F is taken to be  $420\text{kg/m}^3$  for design purposes [10]. At the time of fabrication a double layer of thin polythene sheet was placed over each joint interface to prevent inter-member friction. After fabricated specimens were returned to the conditioning chamber and tested 24 hours later. The moisture content at the time of testing was 15 percent. Load was applied to specimens using a rate of cross-head movement of 0.1in per minute (2.54mm/ min.). Joint slip was measured using two LVDT's, one mounted on each joint plane. The test method was based on that reported by Mohammad and Smith [17].

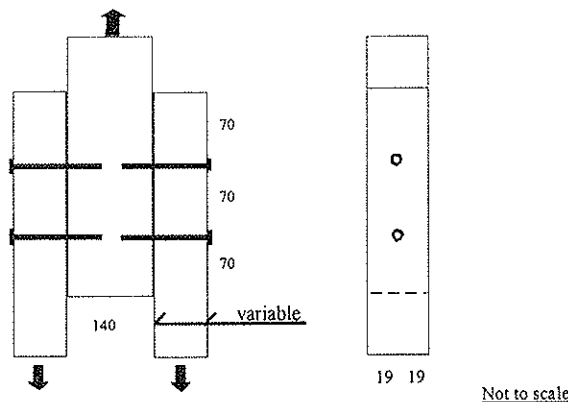


Figure 2 – Four nail test specimen (symmetric)

Two typical sets of load displacement curves are shown in Figure 3. Load is given on a per nail basis assuming each nail carries one quarter of the total load. The trend was that the maximum load capacity,  $P_{Max}$ , increased as nail penetration in the point-side was increased. The displacement at which  $P_{Max}$  was attained also increased as the penetration in the point-side was increased. Maximum loads were attained in about 10 minutes or less. Results are summarised in Figure 4. The 5, 50 and 95 percentile capacities shown were calculated assuming  $P_{Max}$  values are normally distributed.

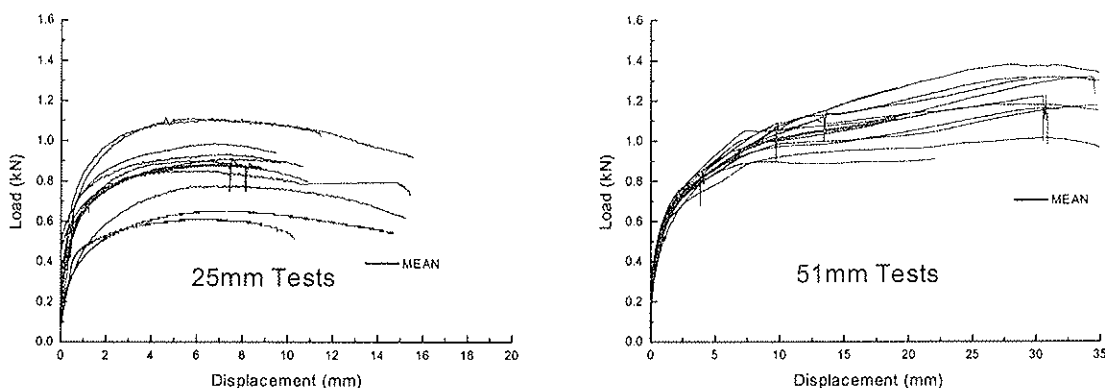


Figure 3 – Typical test results:  $L_p = 25$  and 51mm (11 replicates)

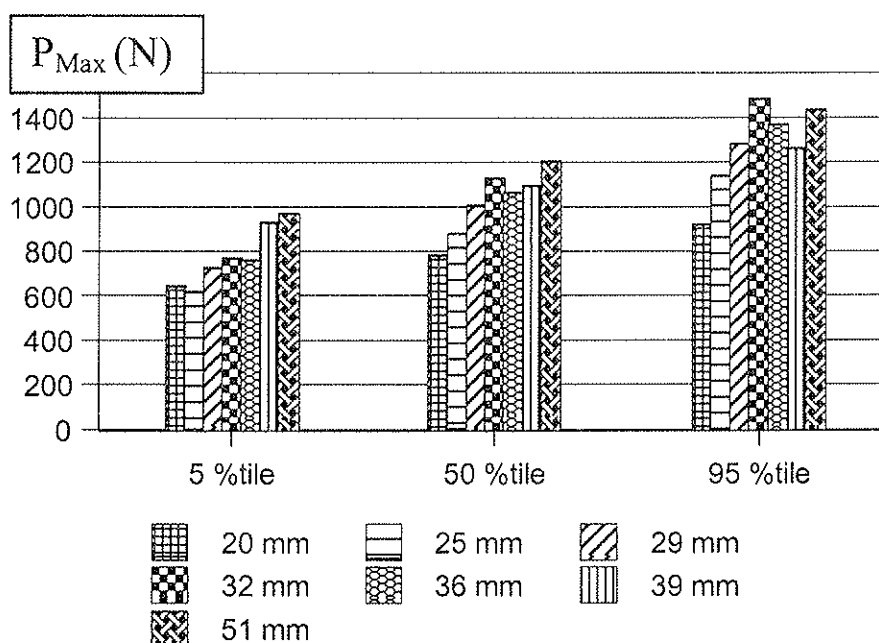


Figure 4 – Test capacity,  $P_{Max}$ , at 5, 50 and 95 percent exclusion levels (N)

#### 4. Comparison of model predictions and experimental data

Table 1 compares  $P_Y$  values predicted from the three models with average experimental  $P_{Max}$  values. All values are given on a per nail basis. The average nail moment capacity,

$M_Y$ , used in models was 7860 Nmm (coefficient of variation of 1.23 percent) as measured in three point bending tests [11]. Embedment strength was estimated from the relationship  $s_H = 0.0446 \rho_{OD} (d/6)^{-0.36}$ , where  $\rho_{OD}$  is wood density based on oven dry mass and volume. This expression is a modified form of that by Smith et al [18]. Using the mean density of  $411 \text{ kg/m}^3$ , and  $d = 3.76 \text{ mm}$ ;  $s_H = 21.8 \text{ MPa}$ .

**Table 1** – Predicted and average test capacities

Point-side penetration (mm)	Original model: $P_Y$ (N), mode	Whale et al model: $P_Y$ (N), mode	Blass et al model: $P_Y$ (N), mode	Test: $P_{Max}$ (N), mode
20	886 (2: hinge in h-s)	895 (2: hinge in h-s)	679 (interpolation)	784 (2: hinge in h-s)
25	968 (2: hinge in h-s)	977 (2: hinge in h-s)	849 (interpolation)	881 (2: hinge in h-s)
29	1043 (2: hinge in h-s)	1043 (2: hinge in h-s)	985 (interpolation)	1008 (2: hinge in h-s)
32	1105 (2: hinge in h-s)	1092 (2: hinge in h-s)	1086 (interpolation)	1130 (3 or 2: hinge in h-s)
36	1135 (3)	1135 (3)	1135 (3)	1068 (3)
39	1135 (3)	1135 (3)	1135 (3)	1097 (3)
51	968 (2: hinge in p-s)	977 (2: hinge in p-s)	849 (interpolation)	1206 (2: hinge in p-s)

Note: For a mode 2 failure, the designation h-s means the plastic hinge forms in the head-side member. Similarly, the designation p-s means the hinge forms in the point-side member.

## 5. Discussion

It can be seen from Table 1 that predictions from the original EYM and the empirical approximation by Whale et al are in close agreement for each point-side penetration. The equation for the yield load is identical for all three models in the case of penetrations where mode 3 governs. For cases where mode 2 governs and the plastic hinge forms in the head-side member (penetrations of 20 through 32mm), the simplified model by Blass et al gives a conservative estimate of  $P_Y$ . The simplified model also gives a conservative prediction for a penetration of 51mm (mode 2 with the plastic hinge in the point-side member).

Comparison of experimental with model capacities reveals that for most penetrations there is fairly good agreement whichever EYM is used. The original and empirical approximation models predict the governing failure mode correctly for every penetration. In the case of a penetration of 32mm the models predict that mode 2 governs, but the mode 3 capacity is only about 3 percent higher. Both modes 2 and 3 were observed in tests. At small point-side penetrations the original and empirical models tend to be non-conservative, while the simplified model tends to be conservative. At the largest penetration considered (51mm) all models are very conservative. Reasons for the discrepancy were apparent from observation of how specimens behaved. The experimental

failure mode was mode 2 (with a hinge in the point-side member) but the maximum load was only reached at a large slip, Figure 3. Because of large displacement effects there was an additive ‘string resistance’ due to development of tension in the nail. The string resistance could develop because the large penetration anchored the nail in the point-side member, and the nail head prevented it from pulling through the head-side member.

Experiments did not consider cases where the head-side member is very thin (smallest head-side thickness used was 26mm). This was because such a member splits while nails are being driven. Practical experience supports continued use of a current restriction in the CSA Standard 086.1 [10] that requires the thickness of the head-side member to be at 5 times the nail shank diameter. For the size of nail used in tests, this corresponds to a thickness of 19mm.

It is interesting to compare the observed 5 percentile joint capacities with those implied by CSA Standard 086.1. As seen in Figure 4, observed 5 percentile values range from 620 to 975N per nail. The 5 percentile value implied by the design code is 1250N (this incorporates an adjustment factor of 1.25 that converts from the reference ‘standard term’ loading duration to short-term test duration). The code capacity applies to all nails meeting the requirement that the nail penetrates the head-side member by at least 5d and the point-side member by at least 8d. Thus, based on the nominal nail diameter, the code permits joints made with 3in common nails that have point-side penetrations in the range 29 to 58mm. The same strength is assigned for all penetrations that are allowed. As mentioned earlier, the code capacity was calculated based on the original EYM. It was assumed that the nail penetrated two-thirds of its length (51mm) into the point-side member [13]. At this ‘calibration point’, the ratio of the 5 percentile test capacity to that implied by the code is 0.78 (975/1250). The discrepancy can be attributed in part to errors in nail and wood properties used during derivation of the code capacity. However greater influences are that the code value incorporated allowances for string resistance in the nail and inter-member friction. Comparisons of test and predicted joint capacities in Table 1 indicate that there is no justification for incorporating the string resistance. Inter-member friction is known to have a significant positive effect on the load capacity of nailed joints, but it is unreliable in practice and should therefore not be relied on. If both the string resistance and inter-member friction had been neglected the CSA Standard 086.1 capacity would have been fairly close to the test value for a point-side penetration of 51mm.

Based on foregoing discussion, it is proposed that the design of single shear nailed timber-to-timber joints be based on a reduced form of the simplified EYM proposed by Blass et al, plus a restriction on the minimum head-side member thickness, i.e.:

<b>Proposed code rules</b>		
$P_Y =$	$\frac{s_H d L_P \beta}{1 + [1 + \beta]^{1/2}}$	<p>-----</p> <p><b>Interpolation:</b> point-side penetration less than needed to develop mode 3.</p>
Min.	$s_H d [4\beta M_Y / \{(1 + \beta) s_H d\}]^{1/2}$	<p>-----</p> <p><b>Mode 3</b></p>
<p><b>The penetration in the head-side member (<math>L - L_P</math>) must not be less than 5d.</b></p>		



## 6. Conclusions

European Yield Model type calculations give accurate predictions of the maximum load capacities of nailed single shear timber-to-timber joints. A 'simplified' model based on the proposal by Blass et al is the most appropriate choice. Two model equations should be used in conjunction with a restriction on the minimum head-side member thickness. Calculations are valid across the range of head-side and point-side nail penetrations that are of interest to designers. The reference capacities for laterally loaded nailed joints that are specified in the Canadian timber design code should be revised.

## Acknowledgements

Experiments were performed at the University of New Brunswick by Mr. Jason Urquhart and Mr. Steven Craft who were Research Assistant and NSERC Undergraduate Research Award Student respectively. Financial assistance was provided by the Natural Sciences and Engineering Research Council of Canada (NSERC).

## References

- [1] Madsen, B., "Structural behaviour of timber", Timber Engineering Ltd., North Vancouver, BC, 1992.
- [2] United States Department of Agriculture, "Wood handbook: wood as an engineering material", Agriculture Handbook 72, USDA, Washington, DC, (Chapter 7 - Fastenings), 1987.
- [3] Trayer, G.W., "The bearing strength of wood under bolts", Technical Bulletin No. 332, US Department of Agriculture, Washington, DC, 1932.
- [4] McLain, T.E., "Connector code development and application in the United States: generic fasteners", In Proceedings 1992 International Workshop on Wood Connectors, Forest Products Society, Madison, WI, 52-56, 1993.
- [5] Canadian Standards Association, "Engineering design in wood (limit states design)", CSA Standard 086.1-M84, CSA, Rexdale, ON, 1984.
- [6] DeGrace, R.F., "Commentary on CSA Standard 086.1-M84 Engineering design in wood (limit states design)", Special Publication 086.1.1-M1986, Canadian Standards Association, Rexdale, ON, 1986.
- [7] Johansen, K W., "Theory of timber connectors", Publication No. 9. International Association of Bridges and Structural Engineering, Bern, Switzerland, 249-262, 1949.
- [8] Larsen, H.J., "Design of bolted joints", Proceedings International Council for Building Research Studies and Documentation: Working Commission W18 - Timber Structures, Bordeaux, France, 1979.
- [9] Lepper, M. and Smith, I., "Fastenings (commentary on chapter 10 of CSA Standard 086.1-1994)", In Wood Design Manual 1995, Canadian Wood Council, Ottawa, ON, 647-666, 1995.
- [10] Canadian Standards Association, "Engineering design in wood (limit states design)", CSA Standard 086.1-94, CSA, Rexdale, ON, 1994.
- [11] Smith, I., Whale, L.R.J., Anderson, C. and Held, L., "Influence of nail properties on nailed joint behaviour", Proceedings International Council for Building Research

- Studies and Documentation: Working Commission W18 - Timber Structures, Rapperswil, Switzerland, 1984.
- [12] Whale, L.R.J. and Smith, I., "A method for measuring the embedding characteristics of wood and wood based materials", *Materials and Structures*, 22, 403-410, 1989.
- [13] Keenan, F.J., Lepper, M.M. and Marshall, C.M., "Improved design of fastenings in timber structures based on limit states design procedures". Contract Report to Canadian Forestry Service, Hull, QB, 1982.
- [14] Whale, L.R.J., Smith, I. and Larsen, H.J., "Design of nailed and bolted joints - Proposals for the revision of existing formulae in draft Eurocode 5 and the CIB Code", *Proceedings International Council for Building Research Studies and Documentation: Working Commission W18 - Timber Structures*, Dublin, Ireland, 1987.
- [15] Blass, H.J., Ehlbeck, J. and Rouger, F., "Simplified design of joints with dowel-type fasteners", *Pacific Timber Engineering Conference*, Rotorua, New Zealand, March 14-18, Forest Research Institute Limited, Rotorua, NZ, 3.275-3.279, 1999.
- [16] Canadian Standards Association, "Wire nails, spikes and staples", *CSA Standard B111*, CSA, Rexdale, ON, 1974.
- [17] Mohammad, M.A.H. and Smith, I., "Stiffness of nailed OSB-to-lumber connections", *Forest Products Journal*, 44(11/12), 37-44, 1994.
- [18] Smith, I., Whale, L.R.J., Anderson, C., Hilson, B.O. and Rodd, P.D., "Design properties of laterally loaded nailed or bolted wood joints", *Canadian Journal of Civil Engineering*, August, 15 633-643, 1988.

## Appendix – EYM equations

### A.1 Original Model due to Johansen [7], extended by Laersen [8]

		<b>Mode</b>
$P_Y =$	$\frac{s_H d (L - L_p) \{ [\beta + 2\beta^2(1+\alpha+\alpha^2) + \beta^3\alpha^2]^{1/2} - \beta(1+\alpha) \}}{1 + \beta}$	<b>1a</b>
	$s_H d (L - L_p)$ .....	<b>1b</b>
	$s_H d \beta L_p$ .....	<b>1b</b>
	$\frac{s_H d (L-L_p) \{ [2\beta(1+\beta) + 4\beta(2+\beta) M_Y / (s_H d (L-L_p)^2)]^{1/2} - \beta \}}{2 + \beta}$	<b>2</b>
	$\frac{s_H d L_p \{ [2\beta^2(1+\beta) + 4\beta(1+2\beta) M_Y / (s_H d L_p^2)]^{1/2} - \beta \}}{2\beta + 1}$	<b>2</b>
	<b>Min.</b> $s_H d [4\beta M_Y / \{(1 + \beta) s_H d \}]^{1/2}$ .....	<b>3</b>

where:  $\alpha = L_p / (L - L_p)$

## A.2 Empirical Approximation by Whale et al [14]

		Mode
$P_Y =$	$\frac{s_{HD} [L - L_p (1 - \beta)]}{5}$ -----	1a
	$s_{HD} (L - L_p)$ -----	1b
	$s_{HD} \beta L_p$ -----	1b
	$s_{HD} \{ [\beta M_Y / \{s_{HD} (1 + \beta)\}]^{1/2} + (L - L_p) / 5 \}$ -----	2
Min.	$s_{HD} \{ [\beta M_Y / \{s_{HD} (1 + \beta)\}]^{1/2} + L_p / 5 \}$ -----	2
	$s_{HD} [4\beta M_Y / \{(1 + \beta) s_{HD}\}]^{1/2}$ -----	3

## A.3 Simplified Model proposed by Blass et al [15]

$P_Y =$	$\frac{s_{HD} (L - L_p)}{1 + [(1 + \beta) / \beta]^{1/2}}$ -----	} Interpolation: member thicknesses less than needed to develop mode 3.
	$\frac{s_{HD} L_p \beta}{1 + [1 + \beta]^{1/2}}$ -----	
Min.	$s_{HD} [4\beta M_Y / \{(1 + \beta) s_{HD}\}]^{1/2}$ -----	Mode 3

**INTERNATIONAL COUNCIL FOR RESEARCH AND INNOVATION  
IN BUILDING AND CONSTRUCTION**

**WORKING COMMISSION W18 - TIMBER STRUCTURES**

**STRENGTH REDUCTION RULES FOR MULTIPLE FASTENER JOINTS**

A Mischler

E Gehri

Chair of Wood Technology

ETH Zürich

SWITZERLAND

**MEETING THIRTY-TWO**

**GRAZ**

**AUSTRIA**

**AUGUST 1999**

---

Presenter: A.Mischler

- H.J.Blass asked for clarification of the title of the paper in relation to the conclusions.
- A.Mischler responded that the dowel slenderness ratio has a major influence on strength capacity of dowel.
- P.Quenneville asked which cases listed in Table 3 were ductile.
- A.Mischler responded that 10d/10d and 10d/7d cases were very ductile.
- A.Jorissen discussed and clarified that timber to timber joints were previously studied which differed from the current steel to timber connections. Timber to timber joints would tend to have higher ductility than steel to timber joints. In the past study sample size of 140 were used and only 2 cases were brittle failures.
- A.Jorissen asked whether the values reported in Table 1 were test results.
- A.Mischler responded that they were test results but Johansen theory fitted the results well.
- Detailed discussion took place on the difference in results between timber to timber connection and steel to timber connection with respect to the influence of the side members.
- A.Leijten questioned whether embedment tests could replace connection tests.
- H.J.Blass said that it would be end distance dependent. He also questioned whether the same level of confidence can be expected in the cases of 1 dowel in line (N=25) and 3 dowels in line (N=5).
- A.Mischler responded that this was considered by density matching of the test specimens in the single and multiple specimen groups.
- P.Quenneville asked about the use of same tolerance in the parallel and perpendicular directions
- A.Mischler clarified that in slender dowels one could balance the tolerance in the parallel and perpendicular directions. This was not the case for non-slender dowels.

# „Strength reduction rules for multiple fastener joints“

Dr. A. Mischler and Prof. Ernst Gehri

Swiss Federal Institute of Technology, Zurich, Switzerland

## 1 Introduction

The load-carrying capacity of a multiple fastener joint is often significantly lower than the strength of one fastener times the number of fasteners. Therefore, strength reduction factors for multiple fastener joints had to be introduced. But there are large discrepancies between these factors proposed in several structural codes such as the Canadian CSA 086.1 and the European ENV 1995-1-1 and ENV 1995-2.

## 2 Failure modes of multiple fastener joints

The strength reduction of multiple fastener joints are mainly caused by the failure modes which must not be the same as for the single fastener. In multiple fastener connections which are commonly used in timber structures, the failure is often caused by the timber parts and not by the fastener.

### 2.1 Failure of the timber parts

The following failure modes in the timber are possible:

- Splitting of the timber in a row of dowels
- Tensile failure of the timber in the reduced net section
- Combination of splitting, shear plug and tensile failure (Figure 1).

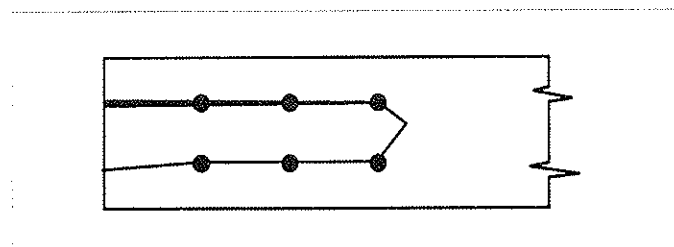


Figure 1: Typical timber failure in a multiple fastener joint as a combination of splitting, shear plug and tensile failure

## 2.2 Failure of the connection

If premature timber failure is avoided by an adequate design of the connection or by reinforcing the joint area, the failure occurs in the connection itself. The load-carrying behaviour of a dowel type connection can be described by the Johansen's theory (Figure 2).

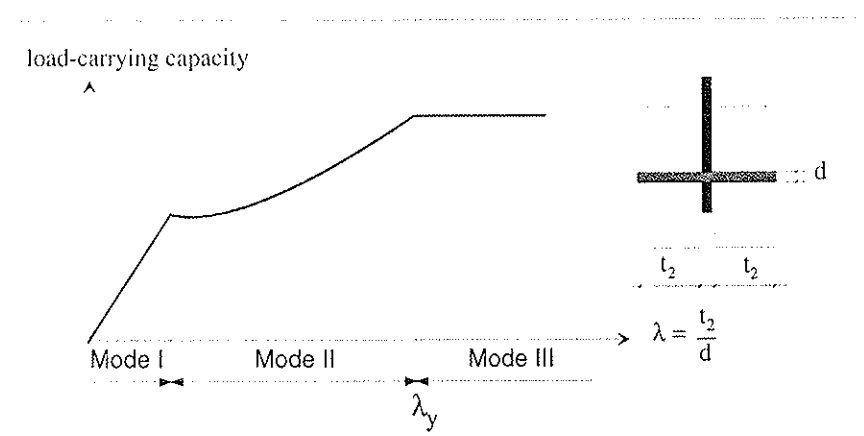


Figure 2: Failure modes according to Johansen

## 3 Importance of ductility

A very important condition in the Johansen theory is that the joint allows large ultimate deformations in order to reach the plastic failure modes. In multiple fastener connections even small fabrication tolerances lead to an uneven load distribution among the fasteners, as it is described by Wilkinson (1986). A certain amount of balancing of these unequal forces is possible by plastic deformations. Therefore the ultimate deformation capacity of a multiple fastener joint has to be even larger than the capacity of a single fastener connection.

As the timber fails in a brittle way, these deformations are typically only possible if the failure occurs after significant plastic deformations of the steel dowel. This failure mode (Type III, according to Johansen) can be reached when fasteners of effective slenderness ratio  $\lambda$  bigger than the limit slenderness ratio  $\lambda_y$  (as defined in figure 2) are used.

## 4 Research on steel-to-timber connections

In order to investigate the load-carrying behaviour of doweled steel-to-timber connections, a research project was carried out at the University of British Columbia in Vancouver Canada in 1998. The connections consisted of a timber main member in Douglas fir and steel side plates. The dowels had a diameter of 6.3 mm (1/4 "). A typical connection is shown in figure 3. The influence of the following design parameters were studied:

- Dowel slenderness ratio  $t_2/d$  (figure 3)
- Dowel bending resistance  $M_u$
- Spacing  $a_1$  and end distance  $a_{3t}$
- Fabrication tolerances

- Number of dowels in line  $n$
- Number of dowel rows  $m$

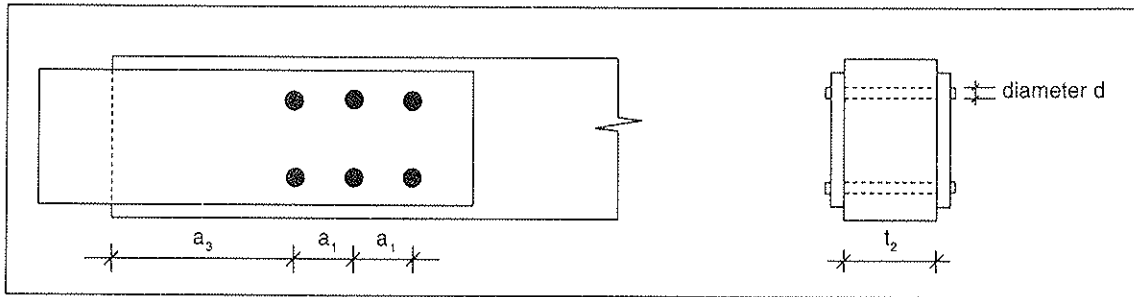


Figure 3: Configuration of the tested connections

All the specimen were density sorted in order to have the same mean density in each joint configuration.

## 4.1 Material properties

### 4.1.1 Timber

The mean density of the Douglas fir (*Pseudotsuga menziesii*) specimen was  $560 \text{ kg/m}^3$ . The embedment strength  $f_h$  was determined according EN 383 with 25 specimens:

$$f_h = 48.9 \text{ N/mm}^2$$

$$\text{Coefficient of variation} = 12 \%$$

### 4.1.2 Steel dowel

The dowels were cut from 1/4" diameter bars. Two strength classes were used: Mild steel with a mean tensile strength of  $579 \text{ N/mm}^2$  and STRESSPROOF<sup>R</sup> GP steel with a mean tensile strength of  $1020 \text{ N/mm}^2$ . The bending behaviour of the two steel strength classes is shown in figure 4.

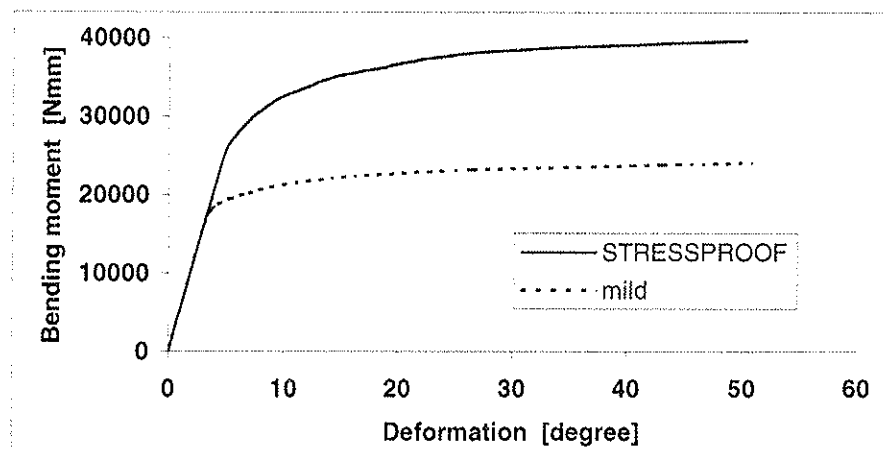


Figure 4: Bending behaviour of mild and STRESSPROOF<sup>R</sup> steel bars of 1/4" diameter

## 4.2 Fabrication of the specimen

The fabrication tolerances were a very important point in this research project. As shown by Mischler (1998), the fabrication tolerances have a strong impact on the ultimate strength of connections which fail in a brittle way. In order to achieve the same fabrication tolerances in all test series, the specimen were drilled with a CNC-machine. But the precision of this CNC-machine is not representative for connections used in practise. Therefore a defined fabrication tolerance  $\Delta$  was introduced as shown in figure 5.

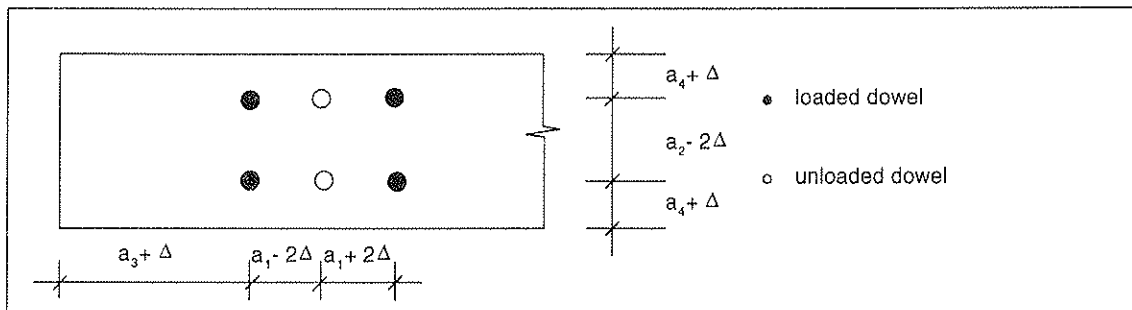


Figure 5: Drilling of the specimen with fabrication tolerances  $\Delta$

The steel plates are drilled with a high precision. Due to the tolerances in the timber parallel to the load direction the dowels are loaded uneven. The tolerances perpendicular to the load-direction lead to higher stresses perpendicular to the grain.

## 4.3 Influence of dowel slenderness ratio $\lambda$

The dowel slenderness ratio has a major impact on the load-carrying behaviour of the connection as shown in figure 2. Two different slenderness ratios were tested:

- $\lambda = 3$  : The dowel remains straight, failure mode I according Johansen
- $\lambda = 6$  : Two plastic hinges are formed in the dowel, failure mode III according to Johansen

The fabrication tolerances were 0.5 mm in both direction according to figure 5.

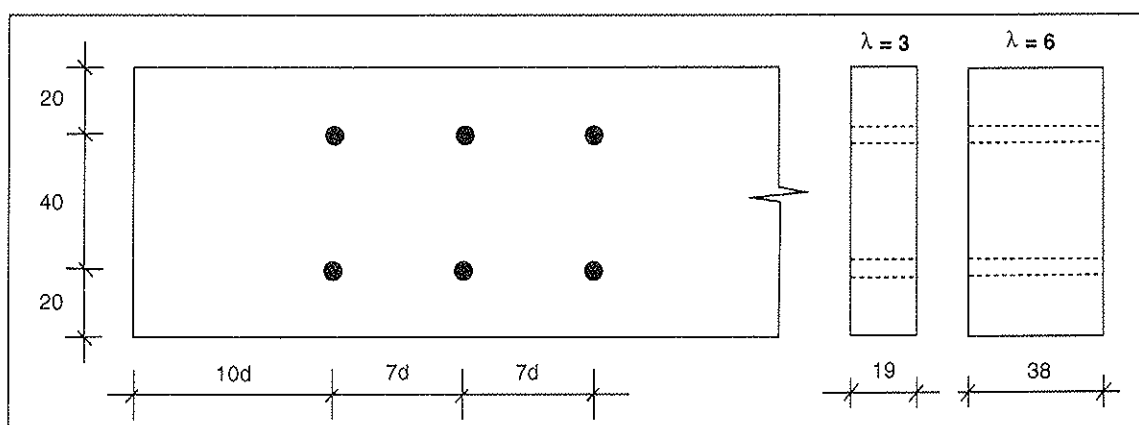


Figure 6: Specimen for connections with dowel slenderness ratio 3 and 6



The ultimate loads of the tests are represented in table 1 and typical load-slip-plots are shown in figure 7.

Ultimate load	$\lambda = 3$		$\lambda = 6$	
1 dowel in line	2.89 kN	100 %	3.33	100 %
3 dowels in line	2.08 kN	72 %	3.38	~100 %

Table 1: Comparison of the ultimate load per dowel and shear plane of connections with dowel slenderness ratio 3 respective 6 (Mean value of 25 tests with 1 dowel and 5 tests with 3 dowels in line)

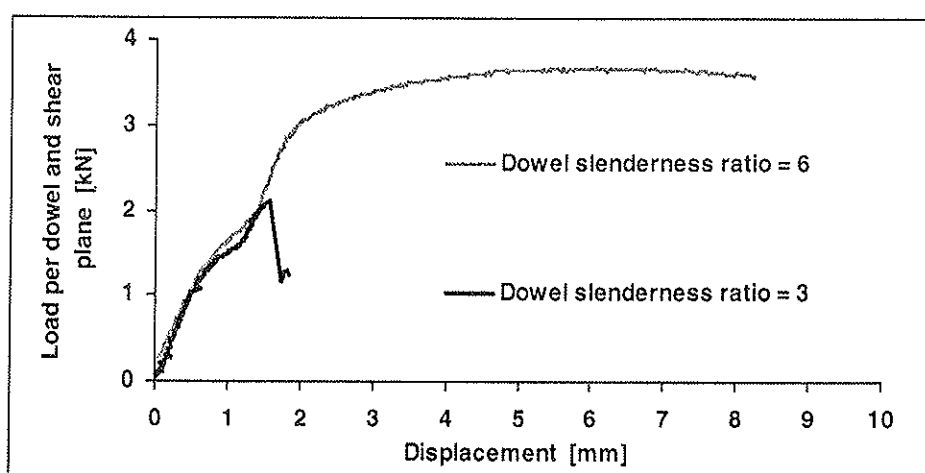


Figure 7: Typical load-slip plots of connections with 3 dowels in line, dowel slenderness ratio  $\lambda = 3$  respective  $\lambda = 6$ .

The connections with dowel slenderness  $\lambda = 3$  and 3 dowels in line fail after short deformations of only 1.5 mm in timber splitting. The ultimate deformation is too small to balance the uneven load distribution among the fasteners. Thus, the ultimate load of this connection-type is significantly lower than the sum of the single fastener strengths ( see Table 1).

On the other hand the connections with dowel slenderness  $\lambda = 6$  show a very ductile failure. The dowels are deformed plastically. Therefore, the uneven load distribution among the fasteners is balanced and the joints with 3 dowels in line reach the same ultimate load per dowel as the single fastener connection.

#### 4.4 Influence of dowel bending resistance $M_u$

For dowels with slenderness ratio  $\lambda$  exceeding  $\lambda_y$ , the load-carrying capacity is proportional to the square root of the dowel bending resistance  $M_u$ . High strength dowels cause higher stresses in the timber. Therefore, multiple fastener connections with high strength dowels tend to fail in splitting before the load-carrying capacity of the dowels is reached, even if the dowel slenderness ratio is high enough. Table 2 shows the influence of

the dowel strength on the ultimate strength of connections with 1 and 3 dowels in line and dowel slenderness ratio  $\lambda = 6$ . The connections are shown in figure 6, the moment deformation behaviour of the two steel strengths in figure 4.

Ultimate load	mild steel		STRESSPROOF steel	
1 dowel in line	3.33 kN	100 %	4.70 kN	100 %
3 dowels in line	3.38 kN	~100 %	4.19 kN	89 %

*Table 2: Ultimate load per dowel and shear plane of connections with different dowel strengths (Fabrication tolerances 0.5 mm in both directions)*

#### 4.5 Influence of spacing and end distance

In timber construction, compact joints with small steel plates are preferred to longer joints with heavy steel plates. But, if end distance and spacing among the dowels are too small, the timber fails in splitting before reaching the load-carrying capacity of the fasteners.

Table 3 shows the influence of end distance and spacing on the ultimate load of connections with 3 dowels in line. The reference value of 100 % is the ultimate load of the single fasteners. Test configuration see figure 6, fabrication tolerances = 0.5 mm in both directions.

The impact of end distance and spacing is much stronger in connections with dowels of low dowel slenderness ratio than in connections with slender dowels of mild steel.

end distance/spacing	7d / 4d	10d / 4d	7d / 7d	10d / 7d	10d / 10d
$\lambda = 3$	53 %	–	–	72 %	90 %
$\lambda = 6$ mild steel dowels	91 %	98 %	98 %	100 %	100 %

*Table 3: Influence of end distance and spacing on the ultimate load of connections with 3 dowels in line compared to the load-carrying capacity of the single fastener*

#### 4.6 Influence of fabrication tolerances

Depending on the ductility a connection is more or less sensitive to fabrication tolerances. Connections with mild steel dowels of high slenderness and large spacing among the fasteners are ductile enough to balance the uneven load distribution among the fasteners caused by the tolerances. The load-carrying capacity of connections which fail in splitting is very much affected by fabrication tolerances.

The influence of fabrication tolerances on the ultimate load of connections with 3 dowels in line according to figure 6 is shown in Table 4.

Tolerances parallel				0	0.5	0.5	0	1.0
Tolerances perpendicular				0	0.5	0	0.5	1.0
①	$\lambda = 3$	mild	10d / 7d	–	2.08	2.59	2.00	1.75
②	$\lambda = 6$	mild	10d / 7d	3.36	3.37			
③	$\lambda = 6$	mild	7d / 7d	3.42	3.27			
④	$\lambda = 6$	SP	10d / 7d	4.71	4.19			

Table 4: Ultimate load per dowel and shear plane of connections with different fabrication tolerances

Where:  $\lambda$  : dowel slenderness ratio  
mild : mild steel dowel  
SP : STRESSPROOF steel dowel  
10d / 7d : end distance/spacing

## 5 Discrepancies with the research of Jorissen

New design rules for multiple fastener joint were proposed last year by Jorissen (1998). Some of his findings have to be discussed:

### 5.1 Connections with rigid dowels

Jorissen presents a model based on fracture mechanics (Jorissen, p. 22 ff.) to predict the load carrying capacity of connections with rigid dowels (Mode I according to Johansen). In the summary of this chapter on page 28 he writes:

*„An example is presented and discussed for steel to timber connections to show the load carrying capacity according to Johansen's Yield Model, equations (2.19) and (2.20), and according to the method based on fracture mechanics, equation (2.29). In figure 2.23 the load carrying capacity is given for a wide range of diameters ( $d = 3$  to  $16$  mm) and for a timber thickness  $t = 24$  mm“.*

Jorissen compares the load carrying capacities according to the Johansen equation for rigid dowels and according to his fracture mechanics model (see figure 8):

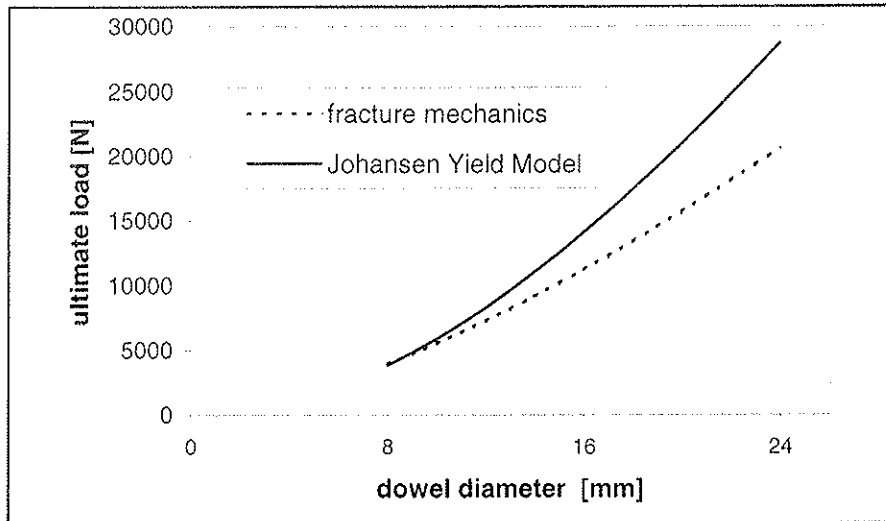


Figure 8: Load carrying capacity of a steel to timber connection according to Jorissen

He concludes: „A model based on fracture mechanics considerations may lead to a more reliable prediction of the load carrying capacity of single fastener connections with rigid dowel type fasteners than Johansen’s Yield Model“.

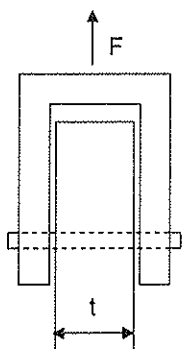
The equation for rigid dowels according Johansen’s Yield Model (Mode I) reads:

$$F = d \cdot t \cdot f_h$$

with

- d : dowel diameter
- t : timber thickness
- $f_h$  : embedment strength

The embedment strength  $f_h$  is determined according to EN 383.



$$f_h = \frac{F_{\max}}{d \cdot t}$$

The thickness should be 1.5 d to 4 d in order to comply with the principle of the test which is to avoid bending the fastener

Figure 9: Determination of embedment strength according EN 383

The Johansen equation for Mode I is not a Yield Model, but it is just the definition of the embedment strength. Therefore the line in Figure 8 which Jorissen calls Johansen Yield Model is not a result of a theoretic model but the result of 360 embedment tests (see Werner (1993), p. 2-18). Every new model has to fit this line.

The results of Jorissen are not a proof that his model based on fracture mechanics is more reliable than the Johansen equation for rigid fastener, but it shows that the values according his model do not fit with the test results.

## 5.2 Influence of the dowel slenderness ratio

Jorissen found only a small influence of the dowel slenderness ratio on the strength reduction factor for multiple fastener connections. He even proposed a simplified design rule without taking the dowel slenderness ratio into account (see Jorissen p. 156).

His consideration are based on the following test results of timber to timber joints.

(Dowel diameter  $d = 12 \text{ mm}$  , end distance  $= 7 d$  , spacing  $= 7 d$ )

$t_s$ mm	$t_m$ mm	$\lambda$ [-]	F (single) [kN]	YM [kN]	F(n = 3) [kN]	R (single) [-]	R (YM) [-]
12	24	2	7.45	9.64	19.8	0.89	0.68
24	48	4	13.1	12.4	32.8	0.83	0.88
59	72	6	15.6	14.4	44.9	0.96	1.04

Table 5: Results according to Jorissen

were  $t_s$  : timber thickness of the side member

$t_m$  : timber thickness of the middle member

$F(\text{single})$  : ultimate load of the single fastener

YM : Johansen Yield Model

$F(n = 3)$  : ultimate load of the connection with 3 dowels

$R(\text{single})$  : reduction factor based on the ultimate load of the single fastener

$R(\text{YM})$  : reduction factor based on yield Model value for single fastener

$$R = \frac{F_{\text{multiple}}}{n \cdot F_{\text{single}}}$$

Jorissen's test results show a regulation factor  $R$  of 0.89 for connections with rigid dowels (figure 10, dowel slenderness = 2). This is caused by the fact, that the test values of the single fastener connections are 30 % lower than the values according the Johansen's theory. His model based on fracture mechanics can not explain this difference, because this model gives the same values for steel-to-timber connections as for timber-to-timber connections. But single fastener steel-to-timber connections reach the higher value of the Johansen's model, as it is proved by over 360 tests.

If the yield model value is taken as basis value for the single fastener, the strength reduction factor for  $\lambda = 2$  is stronger (0.68 see Table 5). In this case figure 10 shows the same influence of the dowel slenderness ratio as the tests on steel-to-timber connections.

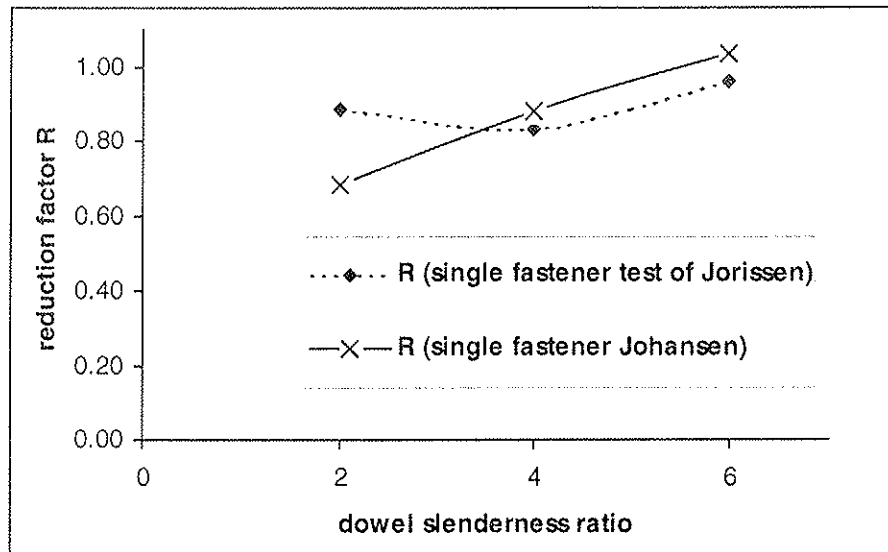


Figure 10: Influence of the dowel slenderness ratio on the strength reduction factor

## 6 Conclusion

The tests on steel-to-timber connections show the influence of

- dowel slenderness ratio
- dowel strength
- end distance and spacing
- fabrication tolerances

on the strength reduction factor of multiple fastener connections.

The only difference to the research of Jorissen is caused by the fact, that his values for the single fastener connections with rigid dowels are 30 % lower than predicted by the Johansen theory. The Johansen theory has been validated by many researchers for single fastener connections. As long as there are differences of 30% in the resistances of the single fastener connection it is not possible to establish reliable rules for multiple fastener joints.

## 7 References

- Jorissen, A. 1998: Double shear timber connections with dowel type fasteners. Delft University press, The Netherlands
- Mischler, A. 1998: Design of joints with laterally loaded dowels. CIB-W18/31-7-2, Savonlinna Finland, August 1998

- Werner, H. 1998: Tragfähigkeit von Holz-Verbindungen mit stiftförmigen Verbindungsmitteln unter Berücksichtigung streuender Einflussgrößen, 1993. Berichte der Versuchsanstalt für Stahl, Holz und Steine der Uni Karlsruhe, 4. Folge – Heft 28.
- Wilkinson, T.L. 1986: Load distribution among bolts parallel to load. Journal of Structural Engineering, Vol. 112, No. 4, April 1986.

**INTERNATIONAL COUNCIL FOR RESEARCH AND INNOVATION  
IN BUILDING AND CONSTRUCTION**

**WORKING COMMISSION W18 - TIMBER STRUCTURES**

**THE STIFFNESS OF MULTIPLE BOLTED CONNECTIONS**

A Jorissen  
ABT Consulting Engineers  
THE NETHERLANDS

**MEETING THIRTY-TWO**

**GRAZ**

**AUSTRIA**

**AUGUST 1999**

---

Presenter: A.Jorissen

- A.Ceccotti asked which density value was used in EC5 predictions and test result comparisons.
- A.Jorissen responded that an equation in EC5 was used for density adjustments.
- A.Leijten discussed the issue of serviceability versus ultimate limit state issues in bolted joints.
- A.Jorissen responded that there was no additional friction from washers.



# The stiffness of multiple bolted connections

A. Jorissen

ABT Consulting Engineers, The Netherlands

Timber Research foundation (SHR), The Netherlands

## 1 Introduction

The slip characteristics of multiple bolted connections were analysed experimentally and theoretically [1]. It was found that the stiffness values obtained by tests were considerably lower than those suggested in ENV-1-1:1993 (Eurocode 5) [2]. This can be explained by the different hole clearances of each bolt. An alternative equation for the stiffness of multiple bolted connections is proposed in this paper based on about 850 short term tests on full-scale multiple bolted connections loaded parallel to the grain and on results obtained by a load distribution model. The research was carried out at the Delft University of Technology, faculty of civil engineering, and supported by the Dutch Technology Foundation (STW) and by the industry.

## 2 Present design according to ENV-1-1:1993 (Eurocode 5)

In ENV-1-1:1993 the stiffness of connections with predrilled dowel type fasteners is calculated according to equation (1), which is used for serviceability limit states calculations.

$$k_{ser} = \frac{\rho_k^{1.5} d}{20} \text{ [N/mm]} \quad (1)$$

Where:  $k_{ser}$  = the connection stiffness per shear plane [N/mm].  
 $\rho_k$  = characteristic value of the timber density [kg/m<sup>3</sup>]. If the characteristic densities of the two jointed members are different ( $\rho_{k,1}$  and  $\rho_{k,2}$ ),  $\rho_k$  should be calculated according to equation (2).

$$\rho_k = \sqrt{\rho_{k,1} \rho_{k,2}} \quad (2)$$

$d$  = diameter of the dowel type fastener [mm].

Equation (1) was derived for connections with nails in predrilled holes. However, research carried out at the University of Karlsruhe [3] with dowelled connections in softwoods showed that equation (1) may also be used for dowelled connections.

For bolted connections the same slip modulus as for dowelled connections may be used. However, the slip values for bolted connections calculated with  $k_{ser}$  according to equation (1) should be increased by 1 mm in order to take the hole clearance into account.

### 3 Experimental research

All 850 tests were carried out according to figure 1, which was taken from EN 26891 [4].

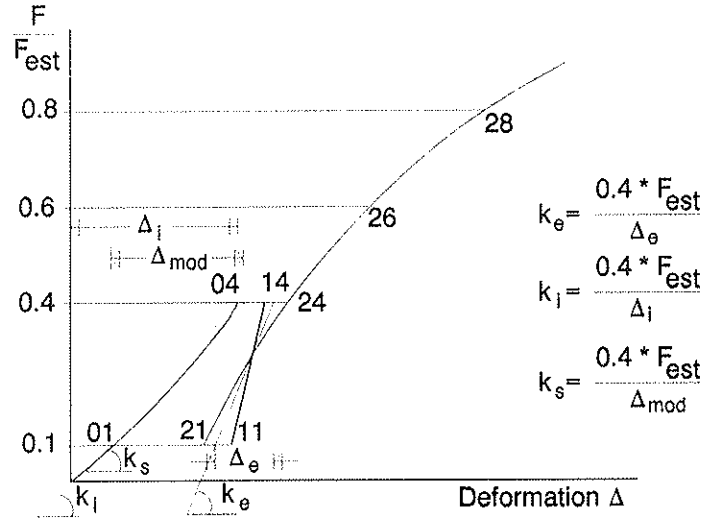


Figure 1: Load-slip curve and measurements according to EN 26891 [45].

The slip modulus  $k_{ser}$  calculated according to equation (1) is a good approximation of the slip modulus  $k_s$  defined in EN 26891 and shown in figure 1. See equation (3).

$$k_{ser} \approx k_s = \frac{0.4 F_{est}}{\Delta_{mod}} \quad (3)$$

The displacements  $\Delta_i$ ,  $\Delta_{mod}$  and  $\Delta_e$  are defined in EN 26891 as

$$\begin{aligned} \Delta_i &= \Delta_{04} \\ \Delta_{mod} &= \frac{4}{3} (\Delta_{04} - \Delta_{01}) \\ \Delta_e &= \frac{2}{3} (\Delta_{14} + \Delta_{24} - \Delta_{11} - \Delta_{21}) \end{aligned}$$

And  $F_{est}$  is the estimated maximum load.

All tests were described in [1] and are summarized in figure 2.

All tests were carried out under standardized conditions (20°C and 65% air moisture content) on symmetrical timber to timber connections and the specimens were made with European spruce. Generally M12 bolts, grade 4.6, were used (some test specimens with M16 and M20 bolts were also tested, however not shown in figure 2). Only the short term strength was determined. The slenderness ratio was varied by varying the thickness of the side members ( $t_s$ ) and middle member ( $t_m$ ). Furthermore, the number of bolts parallel to the grain ( $n$ ), the number of rows ( $m$ ), the spacing ( $a_1$ ), the end distance ( $a_3$ ) and the load direction (tension and compression) were varied.

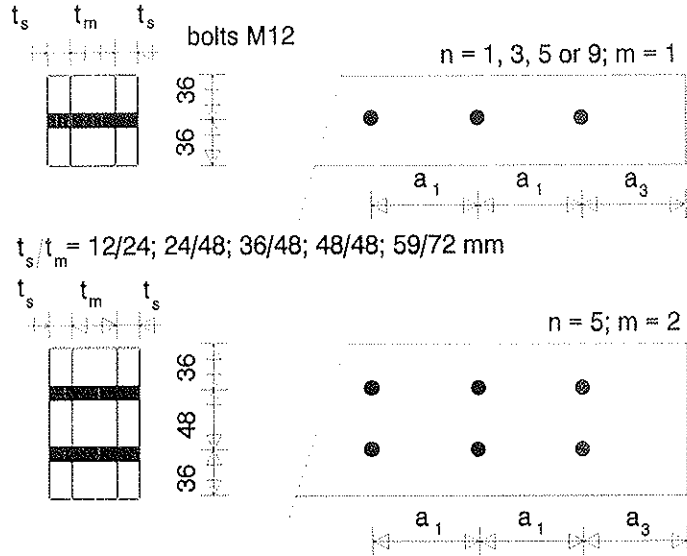


Figure 2: Connections studied.

The results for  $a_1 = a_3 = 84 \text{ mm}$  ( $\approx 7d$ ) are shown in table 1. The results are given more in detail in [1], where it can be seen that there is also some influence of the spacing  $a_1$  and the loaded end distance  $a_3$  on the stiffness parameter  $k_s$  ( $k_s$  increases if spacing  $a_1$  and/or the loaded end distance  $a_3$  increases).

#### 4 Theory: load distribution model (spring model)

A load distribution model, incorporated in a computermodel, with which the effect of the individual hole clearances of each bolt on stiffness of multiple bolted connections can be simulated, was written and used for the explanation of the reduced stiffness. This model, a spring model being a part of a strength prediction model for multiple bolted connections, was also described in [1] and is briefly summarised in this paper, see figure 3 and equations (4)

The result of equations (4) is a value for the load per fastener ( $F_i$ ).

$$\Delta_i = \Delta_{i-1} + \frac{\sum_{k=1}^{i-1} F_k}{k_{m;i-1}} = \sum_{j=2}^i \left( \frac{\sum_{k=j}^n F_k}{k_{s;j-1}} \right) + \delta_i \quad (4)$$

$$\delta_i = \frac{F_i}{k_{b;i}}$$

The axial stiffness of the timber side members between fasteners ( $i$ ) and ( $i+1$ ) is called  $k_{s,i}$ , calculated according to equation (5). In analogy, the axial stiffness of the middle member is called  $k_{m,i}$ , calculated according to equation (6).

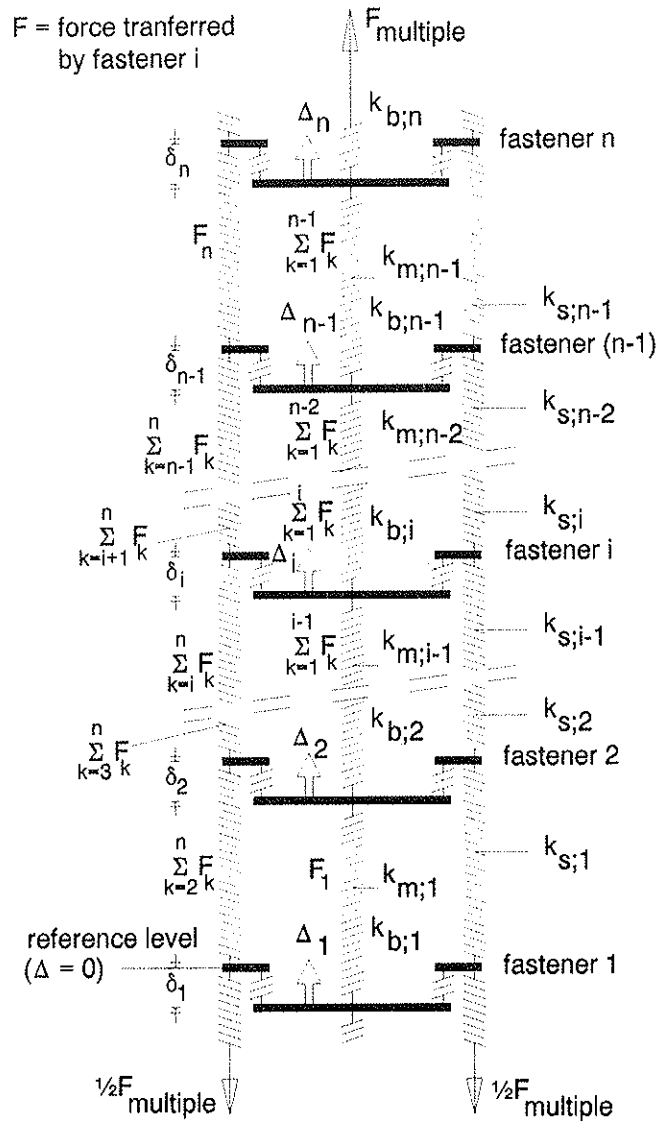


Figure 3: Spring model.

Notes:  $\Delta_i$  = the connection slip at fastener i with respect to the reference  $\Delta = 0$ .  
 $\delta_i$  = the fastener slip shown in figure 4.

$$k_{s,i} = \frac{E_{s,i} t_s A_s}{a_{1,i}} \quad (5)$$

$$k_{m,i} = \frac{E_{m,i} t_m A_m}{a_{1,i}} \quad (6)$$

Where:  $E_{si}$   $E_{m,i}$  Young's modulus for the timber side members and the middle member respectively.  
 $A_s$   $A_m$  total cross sectional area of the timber side members and the middle member respectively.  
 $a_{1,i}$  spacing between fasteners (i) and (i+1).

The stiffness parameter  $k_{b,i}$  describes the unique non-linear load-slip behaviour of the individual fasteners. To obtain this value, the load-slip curve presented by Foschi [5] and Blass [6] was extended to the curve presented by equation (7) and shown in figure 4, i.e. an initial slip  $\delta_0$  due to fabrication tolerances was introduced.

$$F = [F_0 + k_1 (\delta - \delta_0)] \left( 1 - e^{-\frac{k_0 (\delta - \delta_0)}{F_0}} \right) \leq F_{single} \quad (7)$$

Due to the different load-slip behaviour of each fastener, the load may be randomly distributed. This is different from the linear elastic results, where the load transferred by the first and last fastener is higher than the load transferred by the other fasteners.

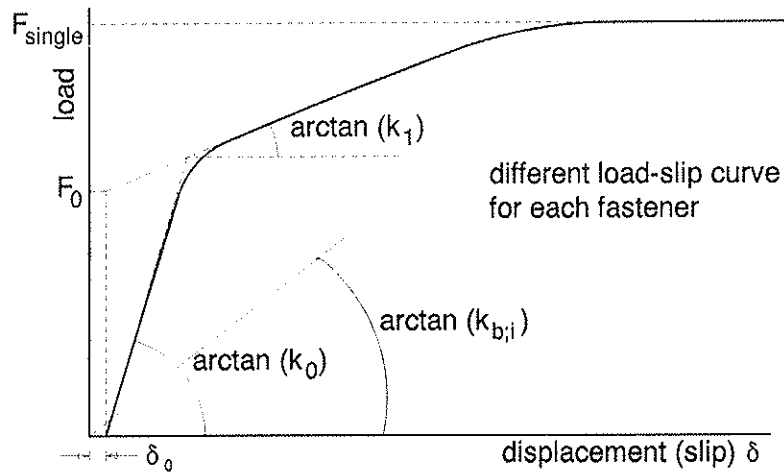


Figure 4: Load-slip curve.

Figure 5 shows an example with four fasteners, i.e.  $n = 4$ , where the initial slip  $\delta_0$  is varied ( $k_0$ ,  $k_1$ ,  $F_0$  and  $F_{single}$  are assumed to be identical for each fastener).

Figure 5 shows the influence of individual hole clearances (initial slip). In this case, the influence of the hole clearance on the load carrying capacity  $F_{multiple}$  is less than 10% if the connection slip at failure is larger than three mm ( $\Delta \geq 3$  mm). Furthermore, figure 5 shows that the maximum load carrying capacity is reached after  $\Delta = 6$  mm for zero hole clearances and  $\Delta \approx 6.3$  mm for the given hole clearances  $\delta_0$ .

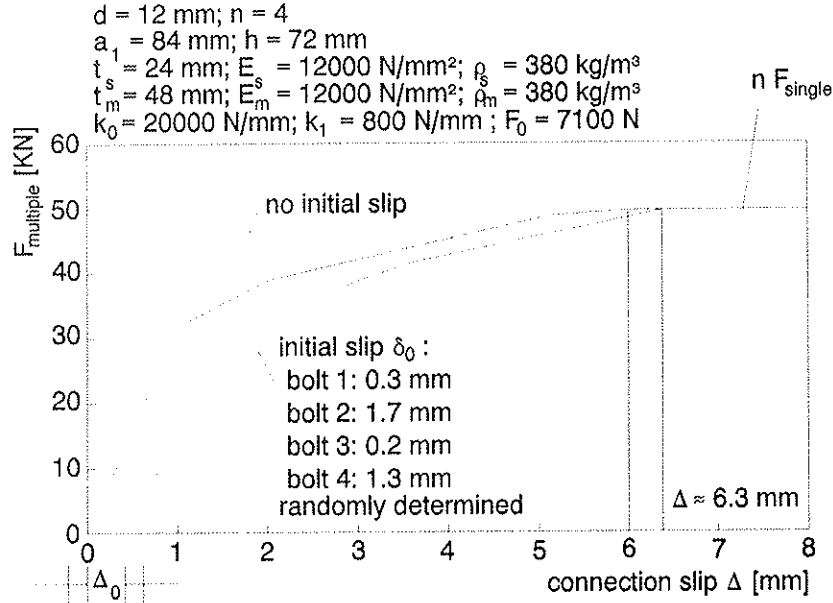


Figure 5: Calculated load-slip curves of multiple bolted connections.

The stiffness value  $k$ , which can be compared to  $k_{scr}$  (equation 1) and  $k_s$  (equation 3), was calculated according to equation (8).

$$k = \frac{F_{0.4} - F_{0.1}}{\Delta_{0.4} - \Delta_{0.1}} \quad (8)$$

Where:  $k$  = connection stiffness

$$F_{0.4} = 0.4 * n * F_{single}$$

$$F_{0.1} = 0.1 * n * F_{single}$$

$$\Delta_{0.4} = \text{slip at } F_{0.4}$$

$$\Delta_{0.1} = \text{slip at } F_{0.1}$$

Figure 5 shows that the connection stiffness  $k$  for the case without initial slip is higher than for the case with initial slip.

## 5 Results

The results according to equation 1, which is the design equation presented in ENV-1-1:1993 (Eurocode), the experimental value according to equation (3), and the theoretical values according to equation (8) are presented in table 1.

A constant characteristic density of  $378 \text{ kg/m}^3$ , determined from 2817 test specimens, was taken for substitution in equation (1). The densities measured varied between  $320 \text{ kg/m}^3$  and  $580 \text{ kg/m}^3$ . Since the differences in density between the three connected members was considerably, the characteristic value for the density determined from all tests was substituted in equation (1).

A random initial slip for each fastener between 0.0 mm and 1.5 mm was substituted in the load distribution model for the determination of the connection stiffness according to equation (8).

Table 1: Connection stiffness; results.

$t_s$ [mm]	$t_m$ [mm]	d [mm]	n	Equation			
				(1)	(3)	(8)	
				$k_{ser}$ [N/mm]	$k_s$ [N/mm]	k [N/mm]	
12	24	11.75	3	4317	1038	1810	1750 )*
		11.75	5	4317	804	1290	
		11.75	9	4317	1363	1060	
24	48	11.25	3	4133	1573	1980	2500 )*
		11.75	5	4317	1160	1610	
		11.75	9	4317	1798	1180	
36	48	10.65	5	3913	1154	1320	
48	64	15.85	5	5824	3616	4050	
60	80	19.85	5	7294	4566	5260	
59	72	10.65	3	3913	1442	1920	3400 )*
		11.75	5	4317	1582	1500	
		11.75	9	4317	1519	1440	

Notes: -  $k_{ser}$ ,  $k_s$  and k in N/mm per shear plane.

- Equation (1) was taken from the European Standard ENV-1-1:1993 (Eurocode 5).

- Equation (3) was taken from the European Standard EN 26891 (Test).

- Equation (8) was taken from [1] (Theoretical results).

)\* In reality, the initial slip varied between 0.0 and 0.5 mm for these series, which increases the value for k considerably compared to the assumed initial slip between 0.0 and 1.5 mm.

## 6 Discussion

The results for the connection stiffness presented in table 1 show a large difference between those obtained with equation (1) and those obtained with equations (3) and (8).

The values for the connection stiffness obtained with equation (8) can be expected if in all cases the initial slip is completely random for each individual bolt: the connection stiffness reduces with increasing number of fasteners. This seems not to be the case (systematic initial slip). Since the connection load for the determination of the connection stiffness is only 0.4 times the (estimated) failure load, less than half of the bolts have to carry load and have to contribute to the connection stiffness, which results in a very low connection stiffness as shown by the results obtained with equation (3). This is shown in figure 6 for two different two-bolted connections:

Connection A: the load-slip curves of both bolts are identical.

Connection B: the initial slip of bolt 2 ( $\delta_2$ ) is larger than the initial slip of bolt 1 ( $\delta_1$ ).

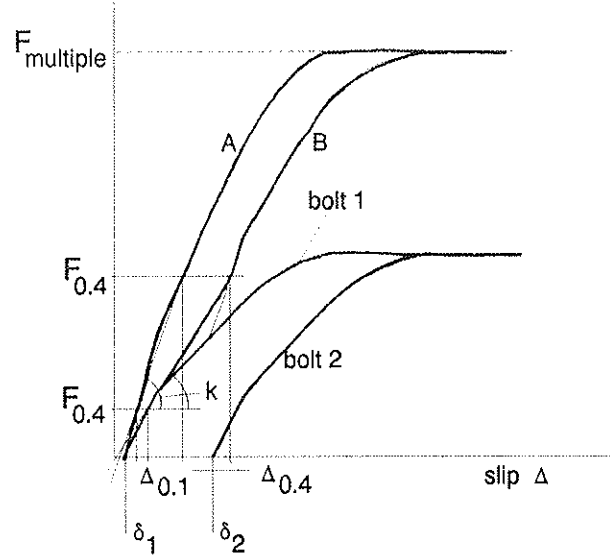


Figure 6: Stiffness of a connection with two bolts.

Figure 5 shows the large difference in connection stiffness  $k$  between the two two-bolted connections due to the difference in initial slip ( $\delta_1 = \delta_2$  for connection A;  $\delta_2 > \delta_1$  for connection B).

For connections with nine bolts in the row, the results according to equation (8), see tabel 1, also show the large influence of the initial slip.

## 7 Conclusions and recommendations

The research described in this paper show that the determination of the stiffness of multiple bolted connections according to ENV-1-1:1993 (Eurocode 5) result in too high values for this connection stiffness. On the other hand, the initial slip of the *multiple* bolted connection is neglectable, even if the initial slip of the individual bolts is not. Therefore it is recommended to change the design rules for the stiffness of *multiple* bolted connections:

- (1) the slip values should *not* be increased by 1 mm in order to take the hole clearance into account.
- (2) the connection stiffness parameter can be calculated according to equation (9).

$$k_{ser} = k_{bolt} \frac{\rho_k^{1.5}}{20} \quad (9)$$

For the determination of  $k_{bolt}$  all tests carried out for the research described in this paper were used. Minimalisation of the squares of the differences between the measured  $k_s$  (equation 3) and the calculated  $k_{ser}$  according to equation (9) results in  $k_{bolt} = 0.3$ .



## Symbols

$d$	bolt diameter
$n$	number of bolts in the load direction (parallel tot the grain)
$a_1$	bolt spacing
$a_3$	end distance
$h$	timber width
$t_s / t_m$	thickness of the timber side members / middle member
$A_s / A_m$	total cross sectional area of the timber side members / middle member
$E_s / E_m$	Young's modulus of the timber side members / middle member
$\rho_s / \rho_m$	density of the timber side members / middle member
$\rho_k$	characteristic value of the density
$k_0, k_1, F_0$	load-slip parameters (see figure 4)
$k$	connection stiffness calculated according to equation (8)
$k_b$	connection stiffness (secant modulus, see figure 4)
$k_i, k_s, k_e$	connection stiffness parameters (see figure 1)
$k_{ser}$	connection stiffness (code value)
$k_{bolt}$	suggested factor to be introduced for multiple bolted connections ( $n \geq 3$ )
$F$	load
$F_{single}$	load carrying capacity of the single bolted connection
$F_{multiple}$	load carrying capacity of the multiple bolted connection
$F_{est}$	estimated maximum load (EN 26891 [4])
$F_{0.1}$	10% of the estimated maximum load
$F_{0.4}$	40% of the estimated maximum load
$\delta$	slip of the individual bolt
$\delta_0$	initial slip
$\Delta$	connection slip
$\Delta_{0.1}$	connection slip at $F_{0.1}$
$\Delta_{0.4}$	connection slip at $F_{0.4}$

## Acknowledgements

The research described in this paper was carried out at the Delft University of Technology (TUD), faculty of civil engineering, in the Netherlands and supported by the Dutch Technology Foundation (STW). All test specimens were manufactured by the company De Groot Vroomshoop (DGV).

## References

- [1] Jorissen, A. *Double shear timber connections with dowel type fasteners*, ISBN 90-407-1783-4, Delft University Press, Delft, 1998.
- [2] ENV 1995-1:1993 (Eurocode 5). *Design of timber structures. Part 1-1: General rules and rules for buildings*. Comité Européen de Normalisation, Brussels, Belgium, 1994.

- [3] Ehlbeck, J. and Werner, H. *Design of joints with laterally loaded dowels - Proposals for improving the design rules in the CIB-Code and draft Eurocode 5*. In: Proceedings of the CIB - W18 - meeting, Parksville, Canada, Paper 21-7-4.
- [4] EN 26891. *Timber structures - Joints made with mechanical fasteners - General principles for the determination of strength and deformation characteristics*. Comité Européen de Normalisation, Brussels, Belgium, 1991.
- [5] Foschi, Ricardeo O. and Bonac Thomas. *Load-slip Characteristics for Connections with common Nails*. Wood Science, Vol. 9, No. 3, 1977.
- [6] Blaß, H.J. *Characteristic strength of nailed joints*. Forest Products Journal, Vol. 44, No. 4: 33-39, 1994.

**INTERNATIONAL COUNCIL FOR RESEARCH AND INNOVATION  
IN BUILDING AND CONSTRUCTION**

**WORKING COMMISSION W18 - TIMBER STRUCTURES**

**CONCENTRIC LOADING TESTS ON GIRDER TRUSS COMPONENTS**

T N Reynolds

V Enjily

Building Research Establishment (BRE)

CTTC - Timber Engineering

A Reffold

Gangnail Systems Ltd

L Whale

Timbersolve Ltd

UNITED KINGDOM

**MEETING THIRTY-TWO**

**GRAZ**

**AUSTRIA**

**AUGUST 1999**

---

Presenter: T.N.Reynolds

- A.Leijten raised a question on the relatively short span of 60 cm with respect to the 40 cm long metal plate and pointed out that the sample size was limited. He also questioned the use of a 2.5 factor to obtain characteristic values, which were not based on material test properties.
- T.N.Reynolds and V.Enjily responded that the study allowed the design formula to be evaluated. Furthermore additional test results on 16 girder trusses were conducted but not included in the present paper and the 2.5 factor was used to convert the girder truss results to be used in the current study.
- S.Theandersson stated that the span influence should be addressed.
- T.N.Reynolds and V.Enjily responded that the observed failure mode in this study was representative in truss applications. They tried spans of 1.6 to 1.8 m but the failure modes were found to be dominated by bending and shear failures.
- C.N.Fouepe suggested that FEM approach could be used to analyze the system.
- P.Quenneville suggested the use of Ehlbeck formula for dowel.
- T.N.Reynolds responded that the metal plate situation differ from the dowel application which would have stress concentration.
- S.Svensson stated that all test results should be shown and information on the variation of data should be provided.
- M.Ansell suggested the nail plate could be made full depth to eliminate the problem.
- T.N.Reynolds responded that similar recommendations were made to the industry.
- H.J.Blass asked why the reinforcement plate were not moved closer together in view of the failure mode of the unreinforced cases.
- T.N.Reynolds responded that the failure mode of the unreinforced cases was not known apriori and the placement of the reinforcement plates was based on industry recommendations which provided only temporary arrest of the failure.
- H.J.Blass stated that the reinforcement plates could be used in other situation such as notched beams and split area. However, design formula would be required.
- V.Enjily agreed and added that in Australia reinforcement plates were used in shear applications. The suggestion of using large plate was rejected because large presses were not available.

# Concentric Loading Tests on Girder Truss Components

by

T N Reynolds (Building Research Establishment, UK)

A Reffold (Gang-Nail Systems Ltd, UK)

V Enjily (Building Research Establishment, UK)

L Whale (Timbersolve Ltd, UK)

## 1. Synopsis

The paper describes a test method for girder truss components under concentric loading and presents the results of a programme of testing on joint types with punched metal plate connectors of varying widths and bites. The effect of reinforcing anti-split plates and their location is also evaluated.

The mode of failure in the majority of specimens was found to be of the form tension perpendicular to grain. The test results are compared with the formula for this mode given in BS 5268 part 3 (1998) which was derived from full scale girder tests. A modified formula is presented. Factors affecting the test results and further work are discussed.

## 2. Introduction

This work follows from previous investigations into the behaviour of punch metal plate connections on full-scale girder trusses (Enjily and Tarr, 1993) using a purpose-built concentric and eccentric loading test rig. A design formula was suggested by Whale (1994), re-calibrated by Reffold (1995) and incorporated into BS 5268 part 3 (1998). The objective of the test programme on components (Reynolds and Enjily, 1998) was to determine the efficacy of such tests and obtain results over a much wider variation of plate sizes and configuration than entailed in the earlier work.

## 3. Component Test Method

The components (Figure 1) consisted of an inverted "T" comprising web and chord timber elements joined together by type GN20 connectors of varying size and configuration (see Section 13). The timber was grade TR26 ER/EW (*Picea Abies*) of 35mm thickness. At the time of testing the average moisture content of the timber was 14% and did not vary significantly between specimens.

The components were suspended in the test rig using a simple hanger and yoke arrangement (Figure 2) enabling a load cell to measure the force transmitted through the specimen. The web of each test specimen was fixed into the hanger using four M12 bolts, ensuring by means of a jig that the arrangement of the component was true. The rams for the loading arms were hydraulically linked to provide equal force, applied at 600mm spacing. The test rig was set up so that the loading arms and the top of the specimen chord were level to transmit equal force across the width of the component. This system economically utilised existing parts of the full-scale girder rig.

The displacement across the connection was measured by linear sprung-loaded potentiometers fixed either side of the specimen web, with the transducer cores resting on a short length of aluminium angle fixed by a screw to the underneath of the chord. This arrangement allowed the true displacement of the chord relative to the web to be measured

without the transducers becoming damaged upon failure of the specimen. The results from the displacement transducers were averaged to take into account any rotational distortion of the specimen chord under load.

Load was applied to the specimen at a rate of approximately 0.2 kN per second (for a typical failure load of 30kN the duration of the test is therefore 150 seconds). The test data was automatically corrected for the weight of the assembly. Five replications for each joint type were performed which were then averaged. Some 40 different joint types were tested (i.e. over 200 tests in total) enabling the relationship between failure load and connector bite and width to be evaluated.

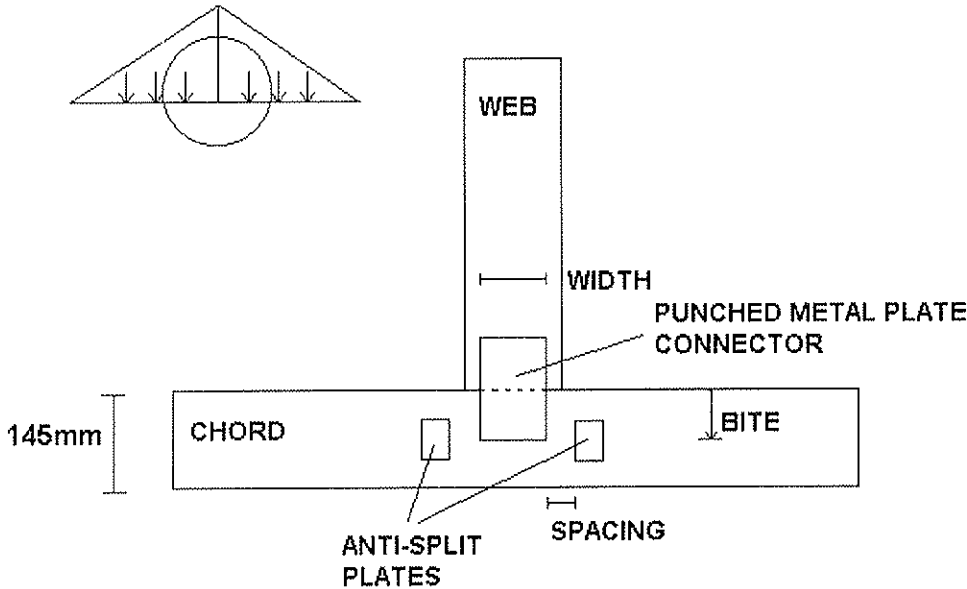


Figure 1: Test Component

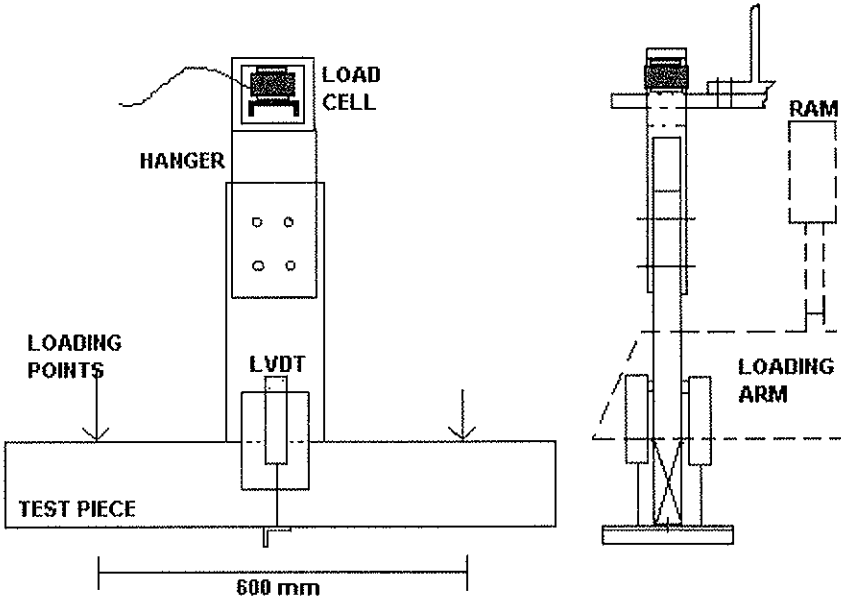


Figure 2: Test Arrangement

## 4. Results

The primary mode of failure for the majority of the test pieces was a failure in tension perpendicular to the grain of the chord element of the component which occurred at the bottom of the main connector and propagated horizontally through the specimen (see Figure 3). The nature of this failure was examined in some early tests by partly restraining the bottom of the chord and thereby arresting the fracture. Other modes of failure which occurred during the programme included tensile failure of the connector (where the joint type comprised a connector of relatively low width), anchorage to web failure (where little connector area was applied to the web) and bending failures of the chord itself. The test results from these types of failures, although useful in themselves, were naturally excluded from the following analysis.

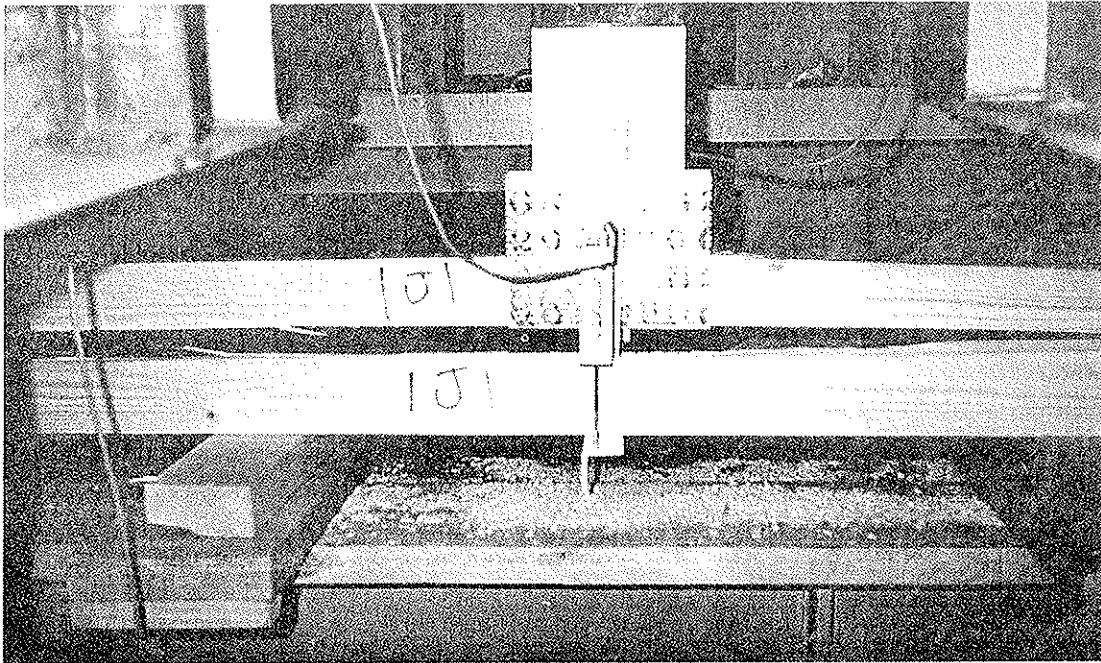


Figure 3: Component post-test

## 5. Effect of Connector Bite and Width

Figure 4 shows the approximately linear relationships between the width of directly comparable joint types, i.e. those with the same connector bite (or extent of cover over the chord) and failure load.

Figure 5 shows the relationships between connector bite and failure load for joint types of similar width. It is clear that considerable gain in the failure load can be achieved by increasing the bite of the main connector.

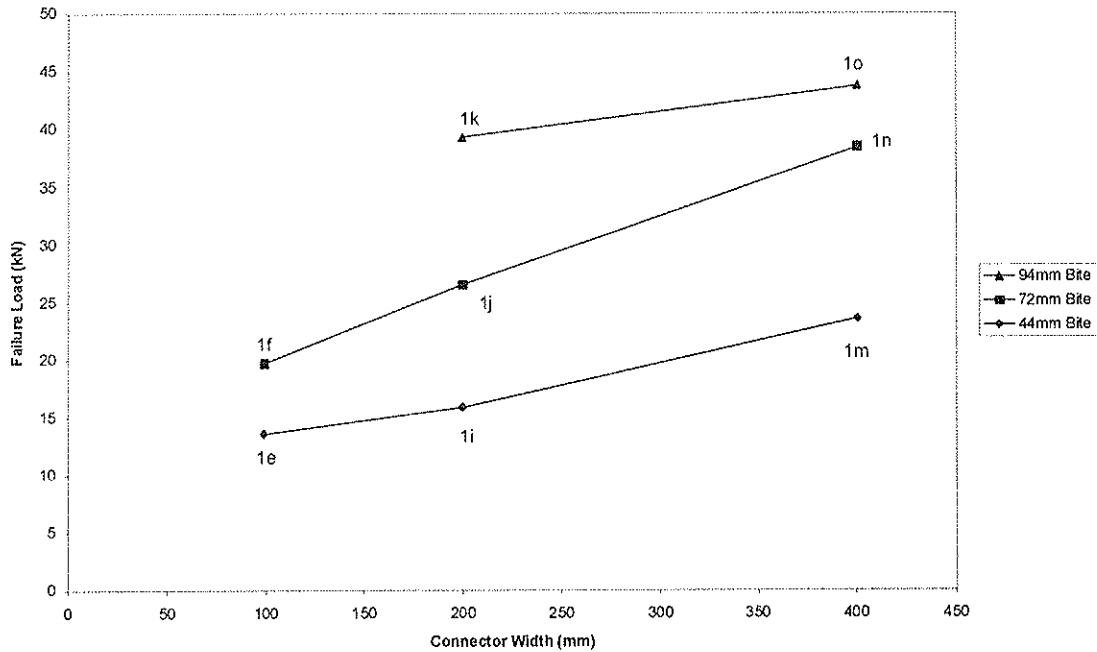


Figure 4: Effect of Connector Width on Failure Load

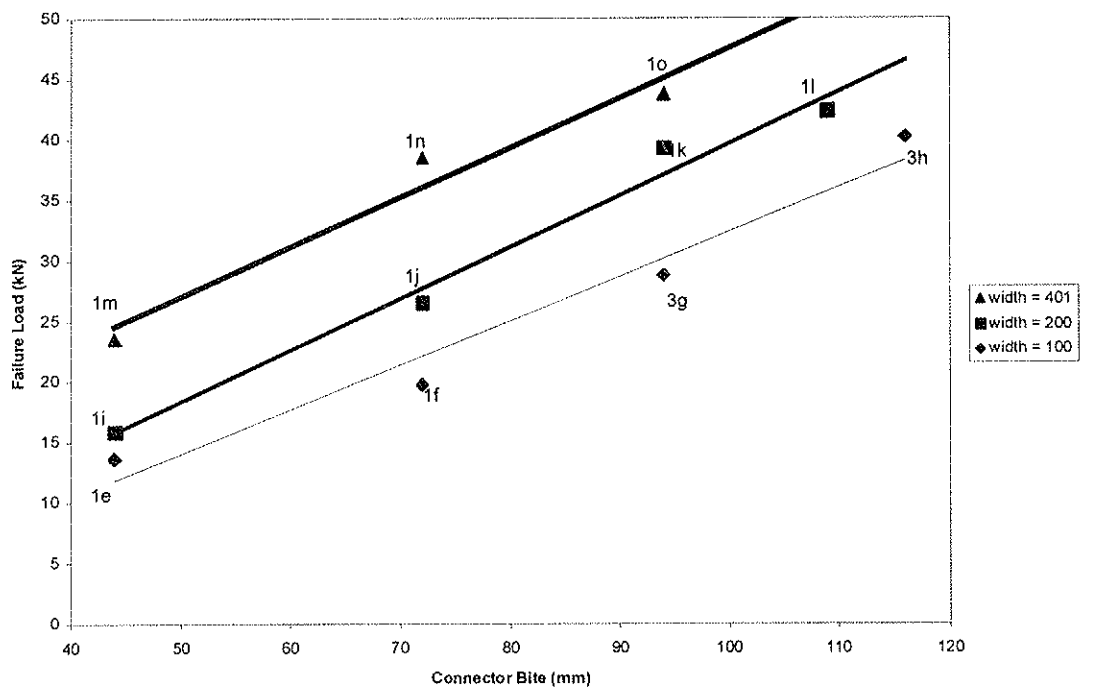


Figure 5: Effect of Connector Bite on Failure Load

Figure 6 shows the test results of all the joint types plotted as a three-dimensional surface (connector bite and width against failure load). The plot shows increasing failure loads with both increasing connector bite with width, as expected, but indicates that there are much higher gains to be made by increasing the connector bite. Increasing connector bite is at least seven times more effective that increasing connector width.

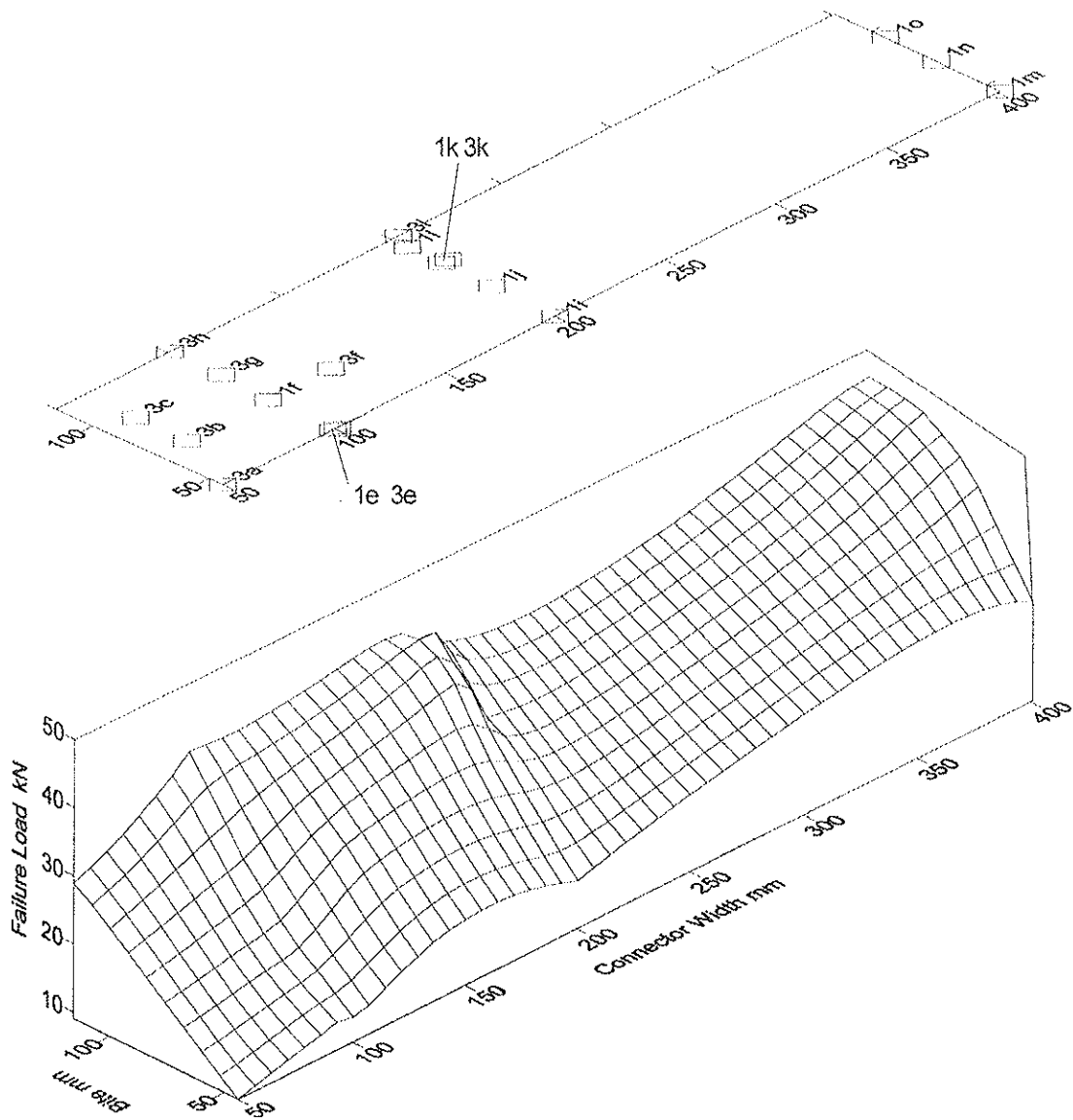


Figure 6: Relationship between Connector Bite and Width with Failure Load

## 6. Comparison with Design Formula

The design formula for failure in tension perpendicular to the grain for the chord (given in BS 5268: part 3) is:

$$\sigma_{t,90,adm} \geq K_e [ 3T / b(w + 16d) ] \quad \text{Eqn. 1}$$

where:

$\sigma_{t,90,adm}$  is the permissible tension stress perpendicular to the grain in the timber (taken as  $2.5 \times 0.44 \text{N/mm}^2$ ).



T	is the net tension force at the joint interface in the direction perpendicular to the grain (N).
$K_e$	is a tension force enhancement factor where loads are applied eccentrically to the chord member. $K_e = 1.0$ for concentrically applied loads.
w	is the width of the connector (mm).
b	is the member <u>thickness</u> (mm).
d	is the effective fastener <u>bite</u> (mm), as defined in Figure 1.

It should be noted that for type GN20 fasteners (BBA 1990) the close spacing of the nail protrusions means that there is negligible difference between the actual size of the plate and the defined terms above.

Figure 7 shows the test results for joint types of comparable width and bite which failed in tension perpendicular to the grain of the chord element, together with the results predicted by the above equation. It is clear that the equation underestimates both the effect of connector bite and width for the tests, and that the calculated results are quite conservative, particularly at high values of bite.

Figure 8 shows the same test results together with those predicted by a simple modification to the above formula (using  $2w + 20d$ ) which shows closer agreement.

Figure 9 shows the same test results together with those predicted by a further equation, the derivation of which is detailed in Reffold et al (1999):

$$\sigma_{t,90,adm} \geq T / b(w + 4.2d \times (d/45)^A] \quad \text{Eqn. 2}$$

Using a value of  $A = 0.6$ , the calculated results show a much closer agreement to the test results.

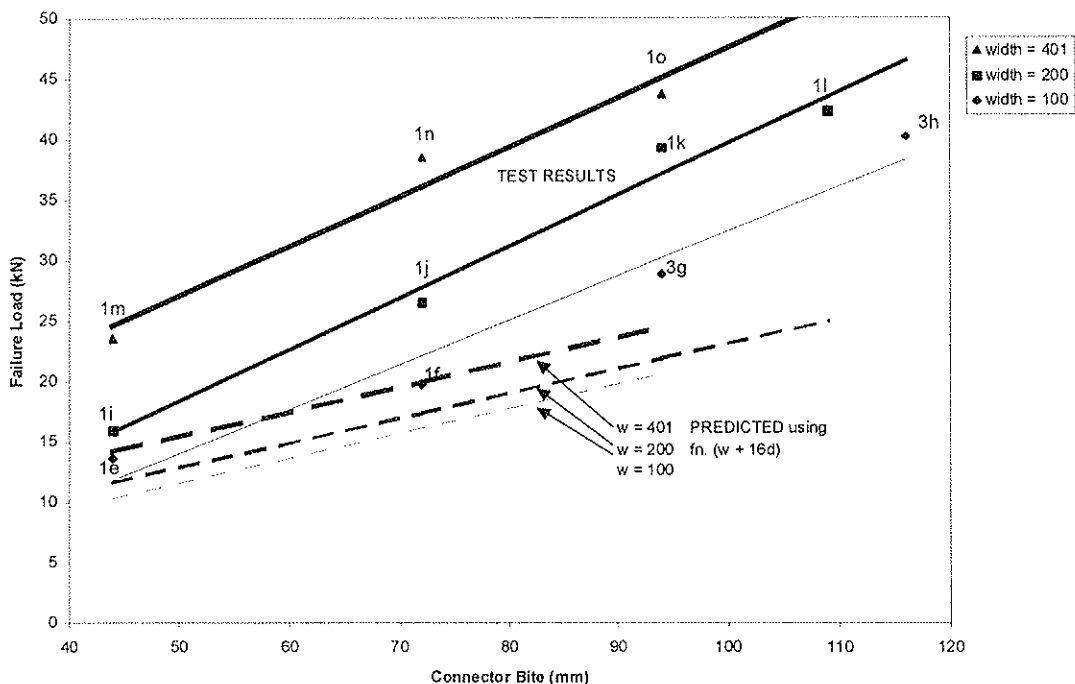


Figure 7: Test Results compared with existing formula (Eqn 1).

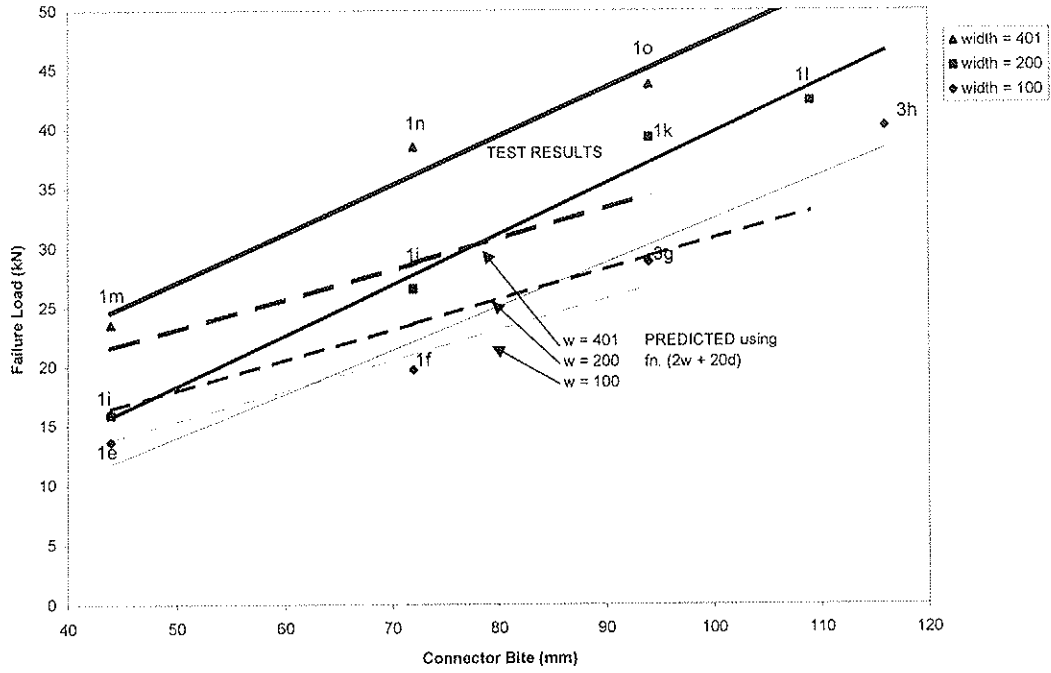


Figure 8: Test Results compared with modified formula.

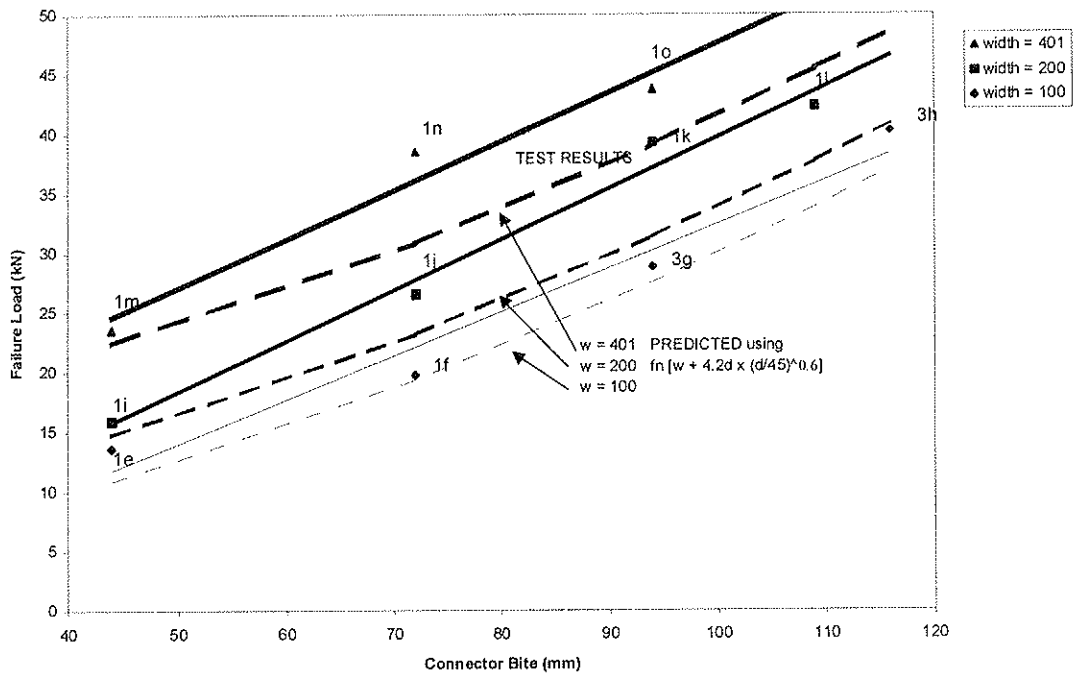


Figure 9: Test Results compared with new formula (Eqn 2).

Figure 10 shows the calculated values from Eqn 1 and 2 for all the joint types (excluding those with anti-split plates) in terms of factor of safety, with the test results as unity, plotted for convenience against the area of connector over the chord. The results (using  $\sigma_{t,90,adm} = 2.5 \times 0.44\text{N/mm}^2$ ) show that the over-conservatism present in the existing formula is greatly reduced by the new formula.

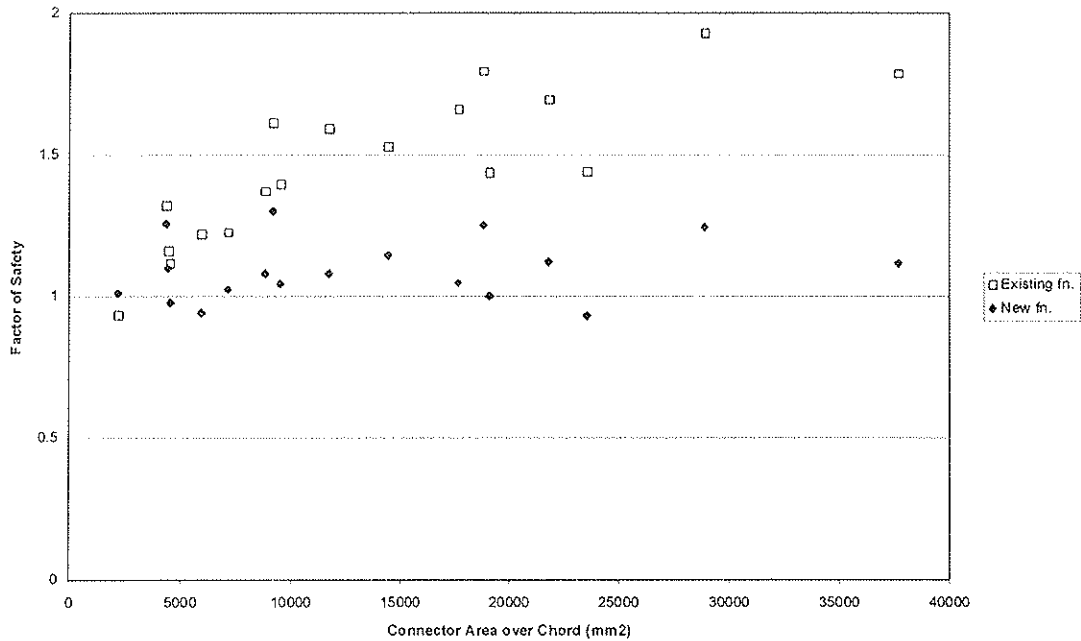


Figure 10: Comparison between Existing Formula and New Formula, with Test Results as Unity.

## 7. Effect of Timber Thickness

Initially as a check on a single joint type in 47mm thickness timber and subsequently as a short test series, results from this larger timber size on directly comparable joint types did not yield the anticipated gain in failure loads (see Table 1 below).

35mm Joint Type	Failure Load (kN)	47mm Joint Type	Failure Load (kN)
3b	17.5	4b	19.4
1e	13.6	4e	13.7
1l	41.5	4l	39.8
1o	43.6	4o	49.2
3f	26.5	4f	27.2

Table 1: Effect of Timber Thickness

The test results indicate that the tension perpendicular to grain capacity of the components was only marginally higher (on average 5%) for 47mm nominal thickness timber compared with 35mm thickness timber. The actual timber thickness' were 46mm and 34mm respectively (a difference of 30%). This suggests that there is no direct proportionality

between timber thickness and failure load, which was a fundamental assumption in the original formula.

## 8. Effect of Anti-Split Plates

The effect of anti-split plates may be illustrated by comparing the performance of joint type 1i and 1j (no anti-split plates) to joint types of series 5 which have the same width and bite of the main connector.

Joint Types	Connector Bite (mm)	Failure Load (kN)	Anti-split plates
1i	44	15.9	✘
5a,5b,5s,5m,5o,5u	44	16.8 (mean)	✓
1j	72	26.9	✘
5e,5f,5t,5n,5p,5v	72	26.6 (mean)	✓

Table 2: The Effect of Anti-split plates of Joint Capacity

Overall the test results indicate that the anti-split plates made little or no contribution to the failure loads.

In the case of series 5 joint types with low bite (44mm) the tension perpendicular to grain failure which occurs at the bottom of the main connector and propagates horizontally through the specimen merely by-passes the anti-split plates which are fixed centrally to the chord. This arrangement of reinforcement, where the overlap is small, is clearly inappropriate and was probably detailed prior to the failure mechanism becoming apparent (see Figure 11, below).

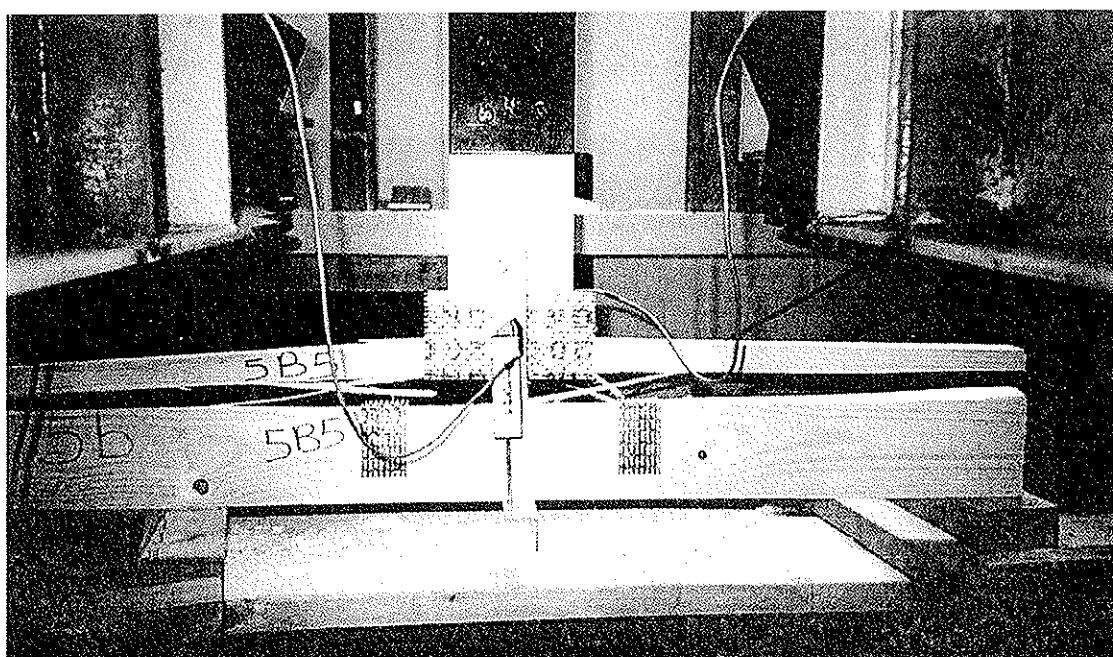


Figure 11: Joint type with little anti-split plate overlap.

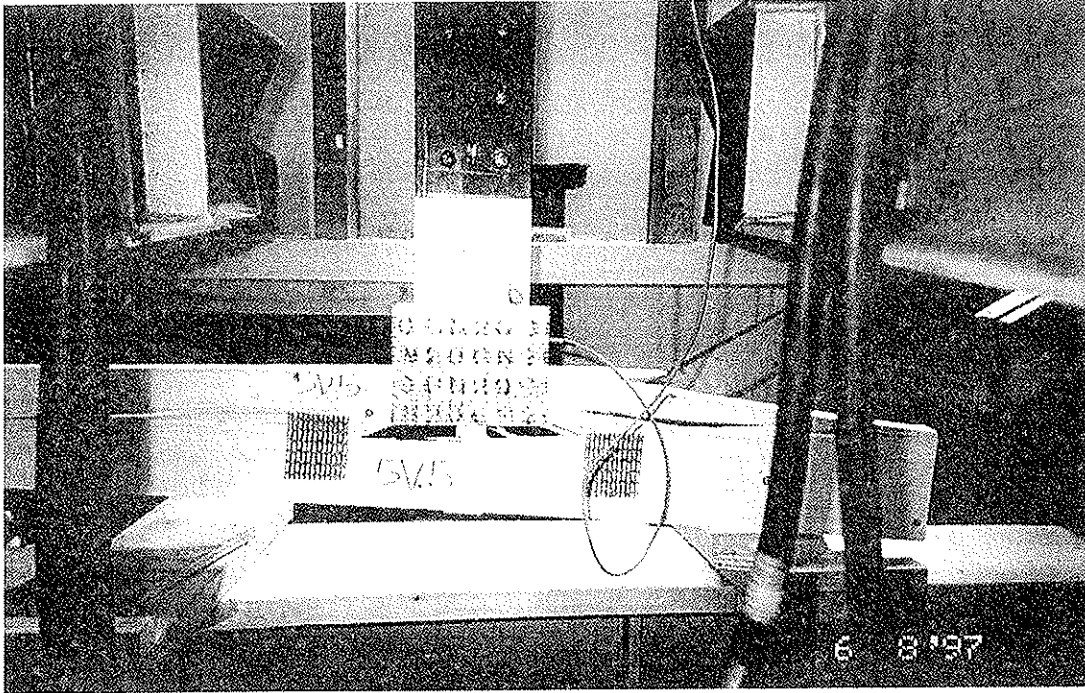


Figure 12: Joint type with 72mm bite.

Where joint types have higher bite (see Figure 12, above) the centrally placed anti-split plates are better placed to provide reinforcement since they overlap the bottom of the main connector. In a few individual tests the anti-split plates were observed to arrest temporarily a tension crack which developed at the bottom of the main connector - leading to a final peak load of a few kN higher. The failure mechanism for joint types with higher bite and anti-split plates also involves some anchorage failure and shearing of the timber around this reinforcement (the tension perpendicular to grain failure still occurs at the bottom of the main connector but tends not to propagate through the anti-split plate). This would indicate that although the anti-split plates appear to contribute to the strength of the joint by altering the failure mechanism, the failure load is principally determined by the tensile capacity of the timber directly below the main connector. It is clear, however, that the area of steelwork used in the reinforcing stitch plates would be much better utilised in increasing the bite of the main connector - allowing the tensile force in the joint to be transferred over a greater part of the chord.

## 9. Effect of Anti-Split Plate Size and Spacing

The effect of anti-split plate size (width) and spacing from the main connector may be determined by comparing the results of the following groups of tests (see Table 3 below):

Joint Type	Anti-split plate Spacing (mm)	Anti-split plate Width (mm)	Failure Load (kN)
5a	10	50	16.9
5b	25	50	15.7
5s	50	50	19.1
5m	10	76	15.2
5o	25	76	17.9
5u	50	76	15.8
5e	10	50	26.3
5f	25	50	29.6
5t	50	50	28.6
5n	10	76	25.1
5p	25	76	24.9
5v	50	76	25.1

Table 3: Effect of Anti-split Plate Size and Spacing

The results show that the anti-split plate size and spacing had negligible effect on failure loads over the range of comparable joint types tested and confirms what was detailed earlier - that anti-split plates are generally ineffective.

## 10. Discussion

A test method has been developed to determine the effectiveness of trussed rafter joint types under concentric loading. Results, although based on a relatively small number of replications for each joint type, were consistent.

Tests on truss components are highly economic compared with full scale testing and have been shown to produce useful results. They have the advantage that the forces within truss connections may be measured directly. Such tests, however, may not entirely replicate the conditions in a complete trussed rafter - such as the bending moments and tensile forces within the bottom chord (ceiling tie).

The tests are short duration compared with full-scale tests.

The tests were done using type GN20 connectors and the test results are valid only for this type of nail plate. Particular note should be made with the definition of bite with respect to this type of plate with close teeth spacing. An allowance for the position of the last row of teeth should be made in the plate position tolerance used in design.

The formulae (Eqn 1 and 2) represent design checks for the tension perpendicular to grain failure mode and not overall joint capacity, where other modes of failure may become critical. Eqn 2 is a mathematical fit for data over the test range. A simple comparison has been made between average test results and those predicted by the existing design formula.

The mode of failure for full-scale trusses is likely to be affected by nailing/bolting of multiple plies and for eccentric loading by the force transfer through the joist hanger.

The effect on eccentric loading and multiple plies has not yet been investigated for components.

## 11. Conclusions

The principal failure mode for the majority of joint types was in tension perpendicular to the grain of the component chord, which occurred at the bottom of the main connector (last row of teeth) and propagated horizontally through the specimen. This is a similar mode of failure to that observed in full scale testing.

The original design formula (Eqn 1) has been found to be quite conservative for concentric loading, particularly at high connector bites. A better fit was found between the test data for 35mm timber thickness components and a modified version of the formula (Eqn 2).

No direct proportionality was found between failure load and component timber thickness - a fundamental assumption when using the original design formula.

Anti-split plates used in the joint types were found to be ineffective, suggesting that the reinforcing material would be better utilised in increasing the main connector bite.

## 12. References

British Board of Agreement (1990) Gang-Nail 20 Gauge Punched Metal Plate Timber Fasteners. BBA Certificate No. 90/2413

British Standards Institution. *Structural use of Timber. Part 3 - Code of practice for trussed rafter roofs*. BS 5268: Part 3: 1998, B.S.I., London, U.K.

Enjily V., Tarr K. (1993) BRE Client Reports CR30/93, CR163/93, CR164/93

Reffold A. (1995) *Tension Perpendicular to Grain Failures in Joints of Girder Trussed Rafters*. Paper to ITPA.

Reffold A., Reynolds T. N., Choo B.S. (1999) *An Investigation into the Tension Strength of Nail Plate Timber Joints Loaded Perpendicular to the Grain*" (Unpublished)

Reynolds T.N., Enjily V., (1998) BRE Client Reports CR 68/97, CR 197/98

Whale, L.R.J (1994) *A Generalised Formula for Predicting Tension Perpendicular to Grain Failure at Joints*. Paper to ITPA.

### 13. General Details of Joint Types

Joint Type	Mean Failure Load (kN)	Timber Thickness (b)	Nail Plate Details	
			Width (w)	Bite (d)
1e	13.6	35	99	44
1f	19.7	35	99	72
1i	15.9	35	200	44
1j	26.6	35	200	72
1k	39.3	35	200	94
1l	41.5	35	200	109
1m	23.6	35	401	44
1n	38.5	35	401	72
1o	43.6	35	401	94
1p	46.9	35	401	109
3a	9.0	35	50	44
3b	17.5	35	63	72
3c	24.6	35	63	94
3d	28.5	35	63	116
3e	12.0	35	101	44
3f	26.5	35	127	72
3g	28.8	35	101	94
3h	40.0	35	101	116
3k	31.5	35	203	94
3l	38.1	35	203	116
4b	19.4	47	63	72
4e	13.7	47	99	44
4f	27.2	47	127	72
4l	39.8	47	200	109
4o	49.2	47	401	94

Joint Type (b = 35mm)	Mean Failure Load (kN)	Main Plate Details		Anti-split Plate Details	
		width (w)	Bite (d)	Width (w)	Spacing (s)
5a	16.9	200	44	50	10
5b	15.7	200	44	50	25
5e	26.3	200	72	50	10
5f	29.6	200	72	50	25
5h	20.7	343	44	50	25
5l	32.5	343	72	50	25
5m	15.2	200	44	76	10
5n	25.1	200	72	76	10
5o	17.9	200	44	76	25
5p	24.9	200	72	76	25
5q	25.2	343	44	76	25
5r	32.4	343	72	76	25
5s	19.1	200	44	50	50
5t	28.6	200	72	50	50
5u	15.8	200	44	76	50
5v	25.1	200	72	76	50



**INTERNATIONAL COUNCIL FOR RESEARCH AND INNOVATION  
IN BUILDING AND CONSTRUCTION**

**WORKING COMMISSION W18 - TIMBER STRUCTURES**

**DOWEL TYPE CONNECTIONS WITH SLOTTED-IN STEEL PLATES**

M U Pedersen

C O Clorius

L Damkilde

P Hoffmeyer

L Esklidsen

Department of Structural Engineering and Materials

Technical University of Denmark, Lyngby

DENMARK

**MEETING THIRTY-TWO**

**GRAZ**

**AUSTRIA**

**AUGUST 1999**

---

Presenter: M.U.Pedersen

- H.J.Blass asked how were the  $M_y$  values obtained.
- M.U.Pedersen responded that they were measured by 3 point bending of the dowel upto 35 degree.
- H.J.Blass commented that since the connection test did not reach the same level of rotation, one should consider using smaller  $M_y$  values in the model.
- A.Jorissen asked and received clarification that Johansen theory was used.
- H.J.Blass asked about the procedures used to consider oversize holes.
- M.U.Pedersen responded that the stresses in one of the direction were removed in the analysis to account for the oversized hole.

# Dowel Type Connections with Slotted-in Steel Plates

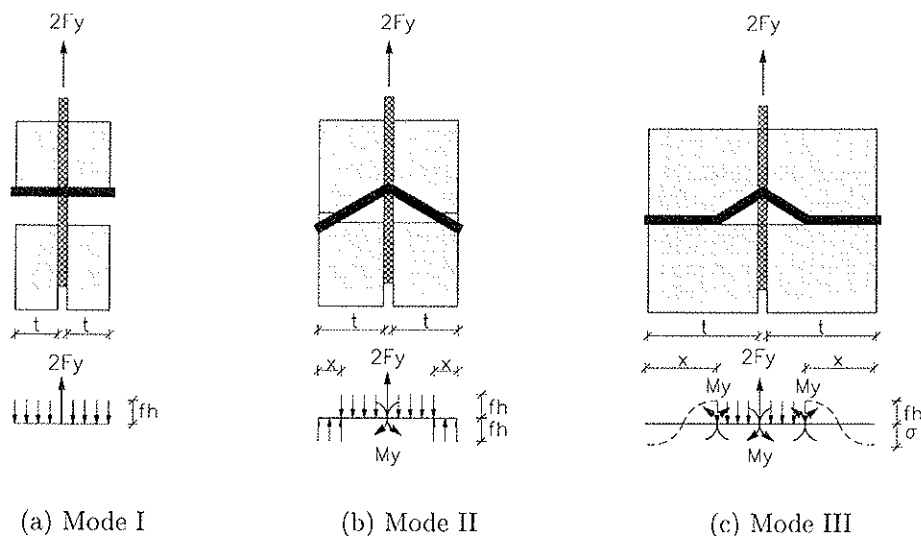
M. Uhre Pedersen, C. Odin Clorius,  
L. Damkilde, P. Hoffmeyer and L. Eskildsen  
Department of Structural Engineering and Materials,  
Technical University of Denmark. DK-2800 Lyngby

## 1 Introduction

In the Eurocode the strength of dowel type connectors is determined according to the theory of plasticity. When the loading is in the grain direction the strength is well predicted by the plasticity theory. However, when the loading is in the transverse direction splitting may supervene plastic failure, as is shown in test series on smaller specimens with slotted-in steel plates. The scope of the present investigation is to trace the effect of eccentric transverse loading of full scale connections with slotted-in steel plates primarily loaded in the grain direction.

### 1.1 Plastic failure criteria

K. W. Johansen first applied theory of plasticity to dowel type connectors in wood in (Johansen 1941). The theory is compact and simple. Perfect plasticity is assumed and the ultimate load bearing capacity of a single connector is predicted to be when either the stresses in the wood reaches the plastic failure stress level or when a combination of plastic failure in wood and dowel is attained. In Figure 1 the three possible failure



**Figure 1:** Failure modes for a double shear dowel used with a central steel plate.

modes are shown for a double shear dowel in wood with a slotted-in steel plate. The forces acting on the dowel and the plastic hinges in the dowel are schematized. The capacity of the dowel is a function of wood member thickness,  $t$ , embedding strength,  $f_h$ , diameter,  $d$ , and the plastic moment capacity,  $M_y$ , of the dowel. The failure mode

will progress from I to III as  $t$  increases, and the capacity per shear plane is determined by:

$$F_y = \min \begin{cases} t d f_h & \text{for } t < \sqrt{\frac{2M_y}{d f_h}} & \text{Mode I} \\ \left( \sqrt{2 + 4 \frac{M_y}{t^2 d f_h}} - 1 \right) t d f_h & \text{for } \sqrt{\frac{2M_y}{d f_h}} \leq t < \sqrt{\frac{16M_y}{d f_h}} & \text{Mode II} \\ \sqrt{4M_y d f_h} & \text{for } t \geq \sqrt{\frac{16M_y}{d f_h}} & \text{Mode III} \end{cases} \quad (1)$$

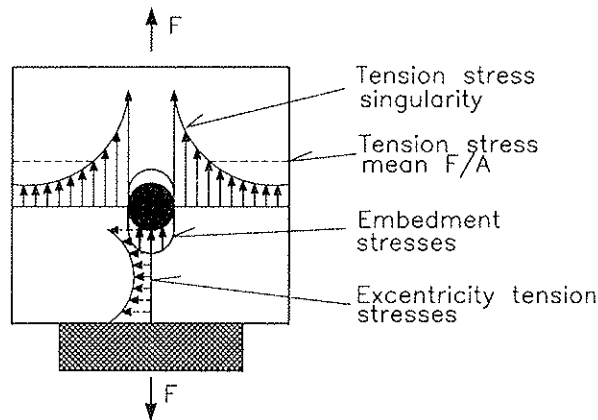
The formulas in equation (1) are similar to those given in Eurocode 5 (CEN 1995, eq. 6.2.2e-f), with the only exception that for mode II and III EC5 allows for additional 10% friction load bearing capacity.

## 1.2 Dowel spacing requirements

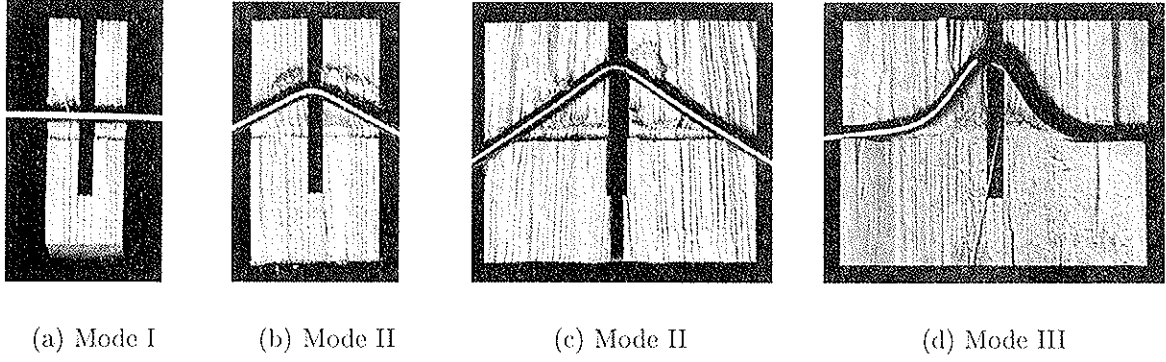
The capacity of a connector is determined by use of local strength parameters. However, the load has to be transferred from connector to the cross section of the wood, hence the plastic theory is superimposed with a set of global restrictions on the end and side distances and on the dowel inter spacing. In practice K. W. Johansen's theory for load bearing capacity of dowels consists of two steps, namely:

- The plasticity theory determining the local yield phenomena.
- A set of spacing and distance requirements to meet global non-plastic tension splitting or shear-plug failure.

Different non-plastic failures are reported in e.g. (Mohammad, Quenneville & Smith 1997). Larsen & Enquist (1996) report a test series on wood reinforcement made in order to avoid tension splitting. The underlying problem is that the way timber connections are designed, non-plastic failures are only indirectly taken into consideration. Contrary to the plastic failures, the non-plastic failures all arise due to stresses best visualized in a transverse section of the dowel in wood. Figure 2 shows a transverse section with the stress condition in the wood in dowel proximity schematized with special attention to tension and embedment stresses. The embedment stresses are of course the consequence of the dowel acting on the wood. The tension stress singularity shown is the consequence of the tension state in the wood moving towards the dowel wherein



**Figure 2:** *Schematic stress condition in a transverse section in dowel proximity, with attention to tension stresses.*



**Figure 3:** Experimentally realised of the three possible plastic failure modes for load in the grain direction.

it is concentrated and passed on. The eccentricity tension stresses are the result of the eccentricity of the distant uniform stress state in the wood member relative to the concentrated force in the dowel.

The ratio,  $\eta$ , between the embedded strength and the strength of the material where the stress singularity occurs is a mean to express the possible degree of utilization of the embedded strength. When the load is in the grain direction the tension singularity stresses shown in Figure 2 are carried by strong continuous fibres laying as tangents to the dowel hole. This of course enables high embedment stresses:

$$\eta_0 = \frac{f_{h,0}}{f_{t,0}} \approx \frac{31 \text{ MPa}}{90 \text{ MPa}} \approx 0.34, \quad (2)$$

where the value for  $f_{h,0}$  is determined experimentally for this investigation, see Section 3.2, and the value for tension parallel to the grain,  $f_{t,0}$ , is taken from (Larsen & Riberholt 1988). When the load is in the transverse direction the singularity stresses are carried in tension perpendicular to the grain – a brittle strength parameter of low value – which disables high embedment stresses:

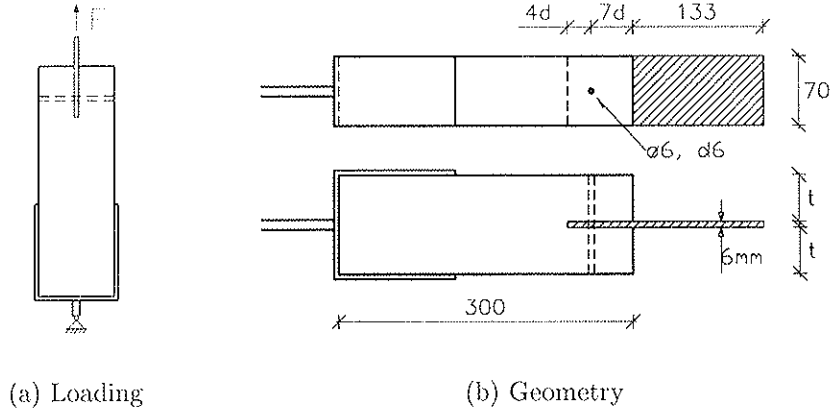
$$\eta_{90} = \frac{f_{h,90}}{f_{t,90}} \approx \frac{13 \text{ MPa}}{2.2 \text{ MPa}} \approx 5.9, \quad (3)$$

where the value for  $f_{h,90}$  is determined experimentally for this investigation, see Section 3.2. The value for  $f_{t,90}$  corresponds to the strength of small 70 x 70 x 45 mm tension test specimens. As the tension stresses in the singularity are localized the value of  $f_{t,90}$  may be higher than assumed in equation (3).

When comparing Equation (2) and (3) it is obvious that it is much more safe to utilize the full embedment strength for loading parallel to the grain than for loading in the transverse direction.

### 1.3 Loading in the grain direction

The theoretically determined failure modes shown in Figure 1 has been realized in tension parallel to the grain as shown in Figure 3. In a complete block test covering 50 specimens cut from 10 planks of pine wood (*Pinus sylvestris*) the strength of a single 6 mm dowel has been determined for 5 different wood thicknesses, (Eskildsen 1999). Table 1 lists mean strength as function of wood thickness,  $t$ . The overall geometry of the specimens is shown in Figure 4.



**Figure 4:** Test specimen geometry for tension parallel tests.

	$\rho$ [kg/m <sup>3</sup> ]	$t=12$ mm	$t=22$ mm	$t=34.5$ mm	$t=47$ mm	$t=57$ mm
Mean	580	2.68	3.94	4.48	5.06	5.13
Stdev.	53	0.36	0.50	0.52	0.39	0.46
Theoretical strength		2.68	3.76	4.37	5.18	5.18
		Mode I	Mode II	Mode II	Mode III	Mode III

**Table 1:** Ultimate strength,  $F_y$ , per shear plane [kN].

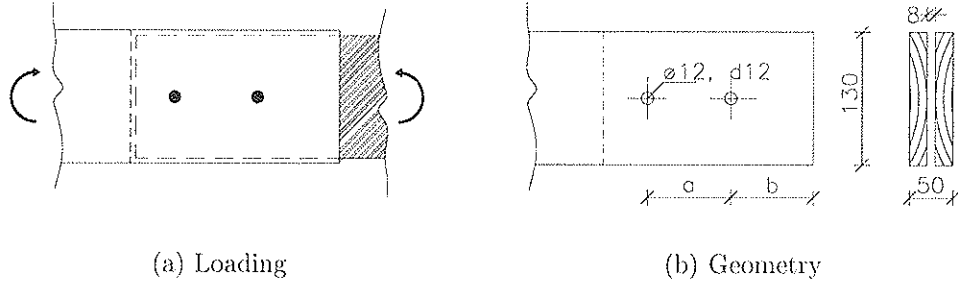
The last two rows in Table 1 gives the theoretical strength,  $F_y$ , determined according to Equation (1) and the corresponding failure mode. The embedment strength,  $f_{h,0}$ , used as input in Equation (1), is determined directly of the results for  $t = 12$  mm, and is found to be 37.3 MPa. The plastic capacity of the dowel,  $M_y$ , is determined in 3 point bending. The steel exhibits large strain hardening and a capacity of 30 Nm ( $f_y = 830$  MPa) is obtained. This yield capacity corresponds to relatively large deformations, however, the ultimate strength of the connections is also determined at relatively large deformations, see Figure 3.

The theoretical strength lies within 5% of the mean value for each geometry. The failure modes observed correspond to the theoretical, and for  $t = 47$  mm, the thickness corresponding to the transition between mode II and III, both modes are observed, the latter for the most dense specimens.

## 1.4 Loading transverse to the grain

### 1.4.1 Embedment crushing or tension splitting

When the dowel utilises the embedment strength perpendicular to the grain, the the oretically determined failure modes shown in Figure 1 may not be able to determine the ultimate strength as tension splitting may occur before the embedment strength is reached even when the joint geometry is in accordance with (CEN 1995). Joint specimens has been tested in bending as shown in Figure 5(a). The test series comprises 46 planks of Norwegian spruce (*Picea abies*) containing a joint as shown in Figure 5(b) with  $a = b = 7d$ . Table 2 lists mean value and standard deviation of the strength per shear plane,  $F_y$ , along with the density,  $\rho$ , of the wood used. No bending of dowels

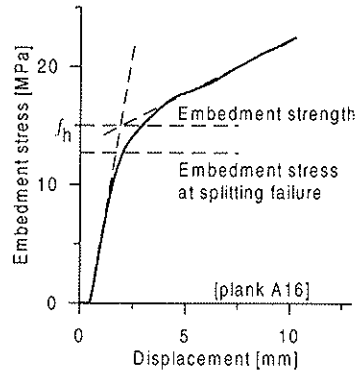


**Figure 5:** *Geometry and loading of specimens utilising  $f_{h,90}$ .*

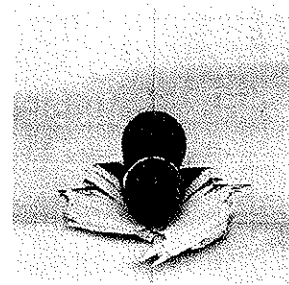
was observed. The Table also lists mean value and standard deviation of embedment strength,  $f_h$ , and density for the 19 embedment tests on wood from the sample. The embedment strength is determined as shown in Figure 6(a) as the interception of the elongation of the two linear parts of the stress-deformation curve. This estimate of the embedment strength is very conservative as hardly no plastic deformation of the wood is utilized. Figures 6(b) shows embedment failure at final crushing of the wood corresponding to plastic deformation of approx. 10 mm. By use of the conservative experimental estimate of  $f_{h,90}$ , the theoretical strength according to Equation (1) is 18% larger than the experimental strength shown in Table 2.

	Embedment tests ( $n = 19$ )		Joint bending tests ( $n = 46$ )		Theoretical
	$\rho$ [kg/m <sup>3</sup> ]	$f_h$ [MPa]	$\rho$ [kg/m <sup>3</sup> ]	$F_y$ [kN]	$F_y$ [kN]
Mean	461	17.4	473	3.70	4.38
Stdev.	25	1.8	32	0.44	Mode I

**Table 2:** *Embedment tests and 4-point bending tests with  $a=b=7d$ .*



(a) Determination of embedment strength.

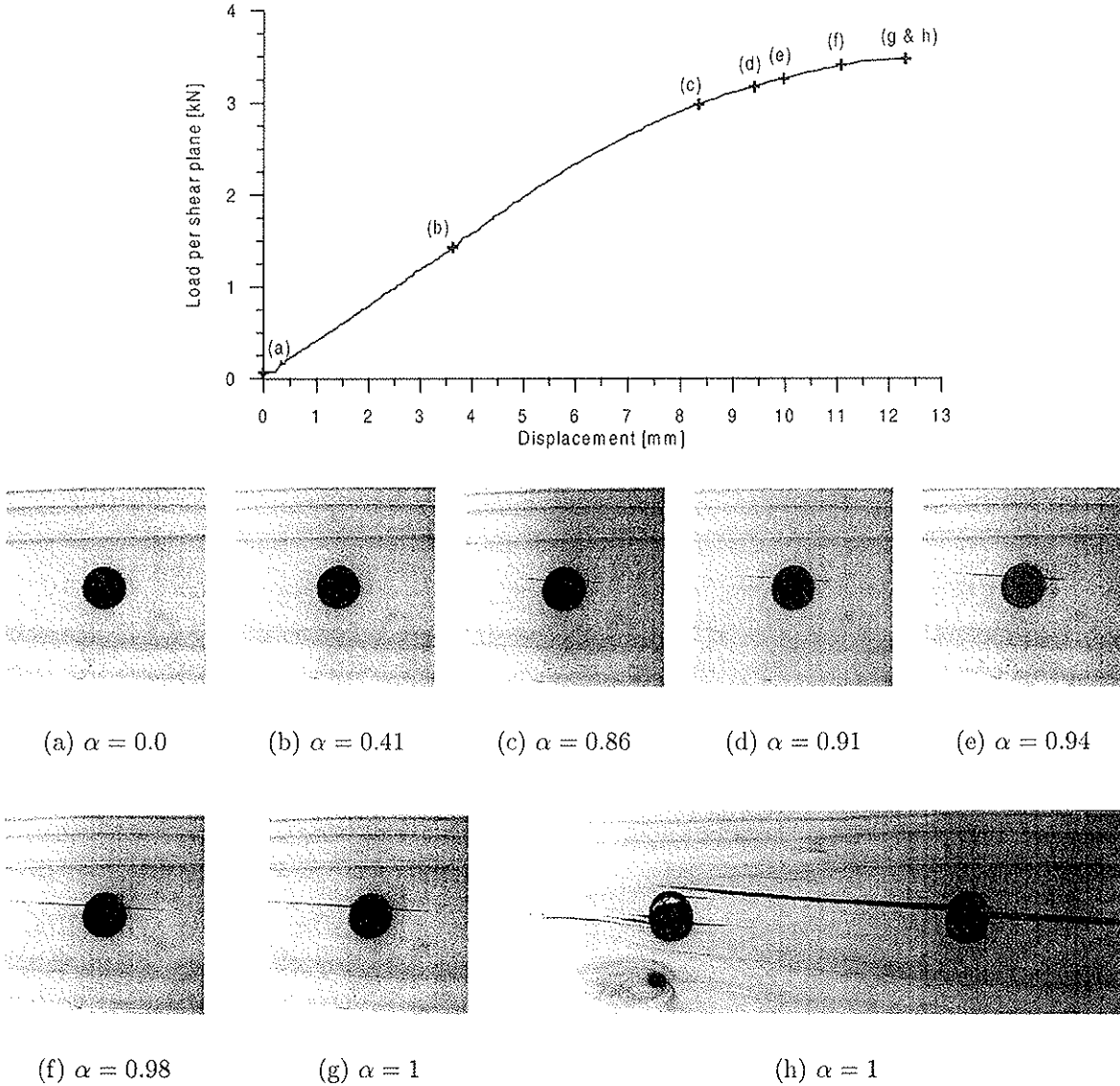


(b) Final embedment failure.

**Figure 6:** *Embedment strength tests perpendicular to the grain.*

The discrepancy arises as the connection does not fail in embedment crushing but in tension splitting. Figure 7 shows a typical load displacement curve along with photos of the dowel proximity taken at different stages of the test progression. The non-linearity

of the load displacement curve is initiated approximately in point (c) on the load-displacement curve. From the photos it is observed that this non-linear behaviour fully corresponds to the shown tension splitting crack growth. It should be observed that the embedment stress at splitting failure hardly touches the plastic regime as indicated in Figure 6(a).



**Figure 7:** Load displacement curve and tension crack development at various stages,  $\alpha = F/F_{ultimate}$ .

#### 1.4.2 Spacing and end distances

An indication test of the influence of the spacing and end distance,  $a$  and  $b$  in Figure 5(b), has been made using five specimens from each of three planks in an incomplete balanced block test. Table 3 shows the strength per shear plane. An analysis of variance shows the effect of joint geometry to be significant. Increasing the end distance,  $b$ , has no significant effect. However, the effect of increasing the dowel spacing,  $a$ , is significant at a 95% level of confidence, which is seen from the raw data in Table 3. The indication test shows that the strength per shear plane increases with increase in dowel spacing

when the loading is in the transverse direction. Hence, the strength per shear plane cannot only be governed by the local yield parameters as done in Equation (1). The strength is also a function of the global non-plastic capacity.

	$a = 7d, b = 7d$ ( $n = 3$ )	$a = 14d, b = 7d$ ( $n = 6$ )	$a = 7d, b = 14d$ ( $n = 6$ )
Mean	3.70	4.29	3.90
Stdev.	0.49	0.15	0.34

Table 3:  $F_y$ , [kN], obtained for 3 geometries using 3 planks.

## 2 Specimens and test conditions

### 2.1 Full scale tests

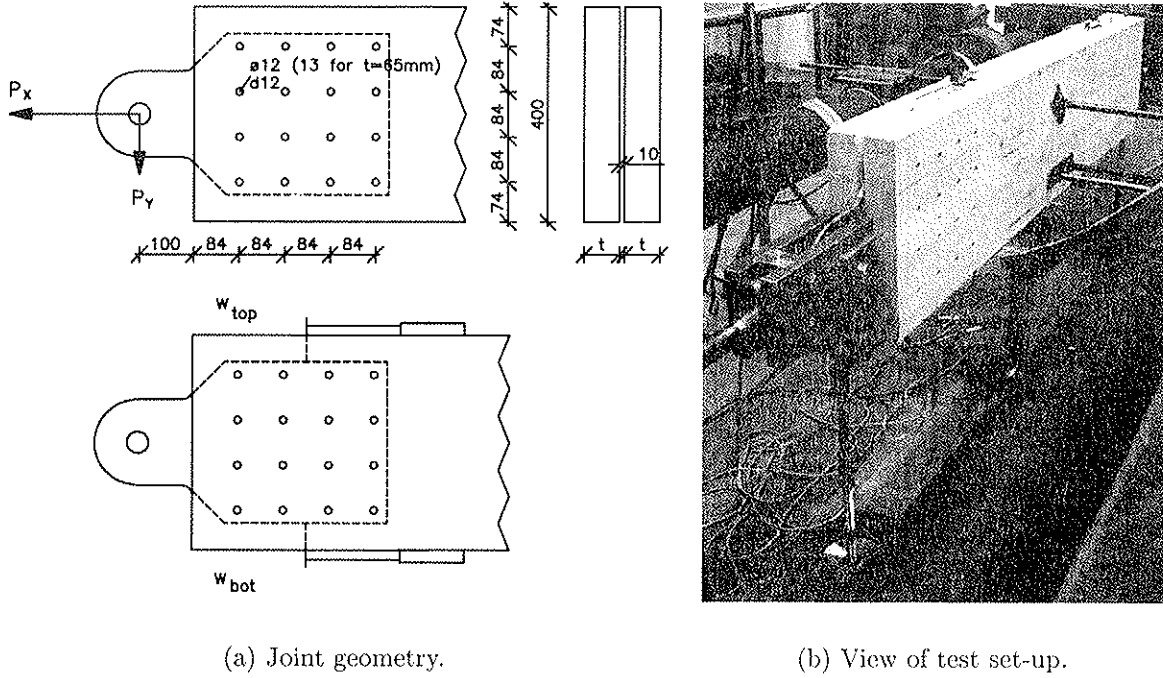


Figure 8: Full scale test specimens.

Full scale glulam specimens of spruce (*Picea abies*) has been tested in a set-up as shown in Figures 8(b) and 9. The specimens contain a full scale joint in each end consisting of 16 dowels through an 8mm steel plate in a 10mm central slot, Figure 8(a). The investigation comprises two series of 20 specimens, one series with thickness  $t = 40\text{mm}$  and one with thickness  $t = 65\text{mm}$  (total width is  $2t + 10\text{mm}$ ). The specimens were tested at a moisture content in equilibrium with  $20^\circ\text{C}$  and 65% RH in short term tests with duration between 5 and 15 min. The load conditions were either pure axial loading ( $P_y = 0$ ), eccentric pure transverse loading ( $P_x = 0$ ) or combinations of transverse and axial loading. The combined loaded specimens were firstly loaded with a fixed value of transverse load corresponding to approx. 5, 10 or 15% of the axial strength and subsequently taken to failure in a ramp of increasing axial load. During tests displacements,  $w_{top}$  and  $w_{bot}$ , were measured as shown in Figure 8(a).



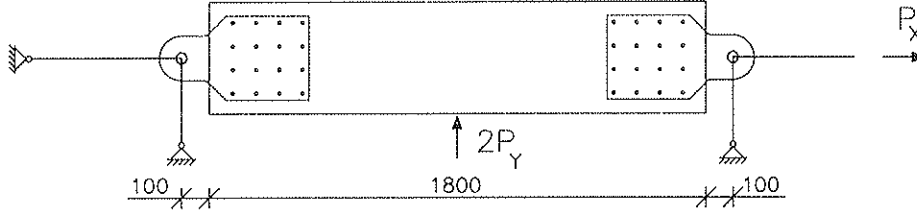


Figure 9: Overall geometry and loading condition.

## 2.2 Embedment tests

In order to implement the plastic failure criteria in Equation (1) for the loading conditions of the full scale joints shown in Figures 8 and 9, a yield surface for the single connector is established on basis of  $f_{h,0}$ ,  $f_{h,90}$  and  $M_y$ . The experimental basis for the yield surface is :

1. Embedment tests parallel to and perpendicular to the grain, a total of 19 tests.
2. Yield moment tests of dowels in 3-point bending, a total of 9 tests.
3. Connector tests, i.e. tests of the whole system of dowel in wood of full width, loaded parallel to and perpendicular to the grain, a total of 16 tests.

Embedment and connector specimens were cut from undamaged parts of the full scale specimens securing that each of the four test types were conducted on material from the same wood lamella. The load was applied to the dowel in a central 10mm slot and the width of the embedment specimens was 50mm ( $t=20$ mm). The geometry was otherwise less conservative than prescribed in (CEN 1993). The tests had duration between 5 and 10 min.

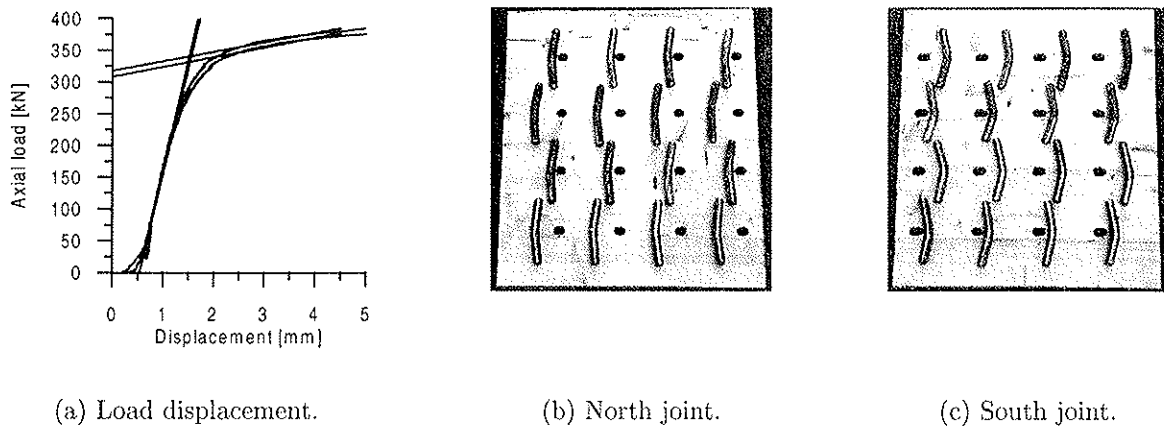
## 3 Results

### 3.1 Full scale tests

Tables 4 and 5 presents strength values for the two series of full scale tests.  $P_Y$  is the value of the eccentric transverse load per joint, Figure 8(a). For combined load  $P_Y$  is held at a constant value. In eccentric pure transverse loading,  $P_Y$  is the ultimate strength.  $P_{X,N}$  and  $P_{X,S}$  is the yield strength for the north and south joint in cases where these can be determined independently as in e.g. Figure 10(a). In cases where splitting supervenes yielding,  $P_{X,i}$  is evaluated as the load corresponding to a visible crack observed during testing and traceable on the load displacement curves, e.g. Figure 12(a). The failures corresponding to the strength values  $P_{X,N}$  and  $P_{X,S}$  are evaluated as either plastic or splitting type. The Tables also lists ultimate values of the axial load corresponding to final splitting failure. It is observed that this value approaches  $P_{X,N}$  and  $P_{X,S}$  for higher values of  $P_Y$ . Figures 10 to 14 show load displacement charts and failure modes for the five different load combinations in the  $t = 40$ mm series. In cases of dominating axial load, the mean value of  $w_{top}$  and  $w_{bot}$  is shown for each joint. In cases including substantial rotation, each of the four displacement measurements are shown.

$\rho$ [kg/m <sup>3</sup> ]	$P_Y$ [kN]	$P_{X,N}$ [kN]	$P_{X,S}$ [kN]	Mean [kN]	Stdev. [kN]	Failure type	$P_{X,ult}$ [kN]	Mean [kN]
460	-	313	312			Plastic	340	
464	-	320	325			Plastic	367	
473	-	342	334			Plastic	389	
465	-	310	302	320	13	Plastic	346	361
473	17	314	314			Plastic	347	
465	17	332	330			Plast/split	360	
472	17	323	323			Split/plast	323	
465	17	318	328	323	7	Plastic	372	351
448	33	268	264			Split/plast	302	
459	33	261	261			Splitting	261	
465	33	252	322			Splitting	322	
472	33	270	270	271	21	Splitting	270	289
473	50	204	204			Splitting	204	
465	50	207	220			Splitting	220	
461	50	234	261			Splitting	261	
467	50	151	151	204	38	Splitting	151	209
467	71	-	-			Splitting	-	
482	79	-	-			Splitting	-	
473	67	-	-			Splitting	-	
467	82	-	-	75	7	Splitting	-	

**Table 4:** Strength and density for full scale specimens with  $t = 40\text{mm}$ .



**Figure 10:** Axial testing,  $t = 40\text{mm}$ .

$\rho$ [kg/m <sup>3</sup> ]	$P_Y$ [kN]	$P_{X,N}$ [kN]	$P_{X,S}$ [kN]	Mean [kN]	Stdev. [kN]	Failure type	$P_{X,ult}$ [kN]	Mean [kN]
490	-	283	339			Plastic	393	
442	-	348	338			Plastic	395	
473	-	304	294			Plastic	377	
449	-	316	314	317	23	Plastic	370	384
468	38	300	300			Splitting	331	
471	39	250	253			Split/plast	311	
476	40	309	316			Plastic	339	
459	40	298	305			Plastic	363	
441	40	271	250			Plast/split	271	
471	40	338	353			Plastic	372	
442	44	305	230			Plast/split	305	
464	40	298	298	292	33	Splitting	298	324
505	60	146	146			Splitting	146	
459	60	169	183			Splitting	183	
469	60	204	227			Splitting	227	
474	60	197	189	183	28	Splitting	197	188
478	72	-	-			Splitting	-	
437	80	-	-			Splitting	-	
459	85	-	-			Splitting	-	
502	89	-	-	81	7	Splitting	-	

Table 5: Strength and density for full scale specimens with  $t = 65\text{mm}$ .

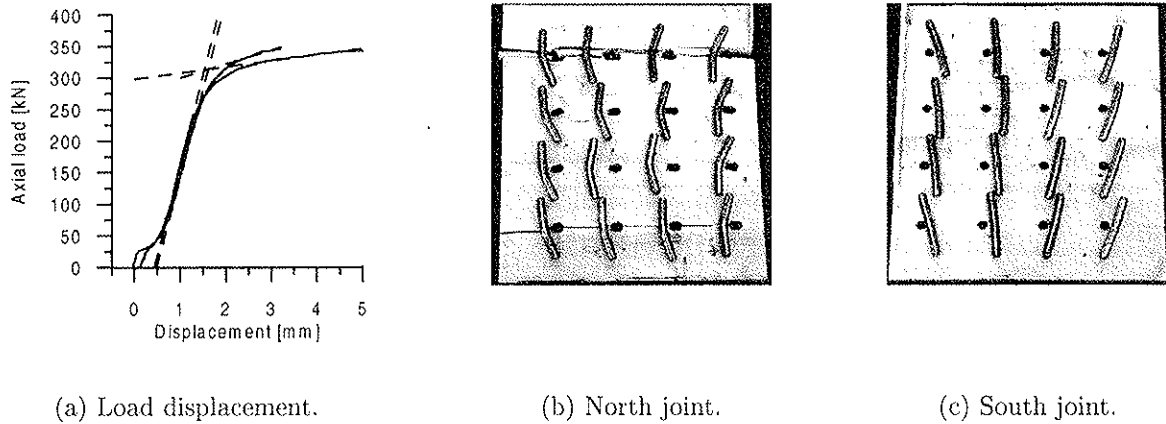
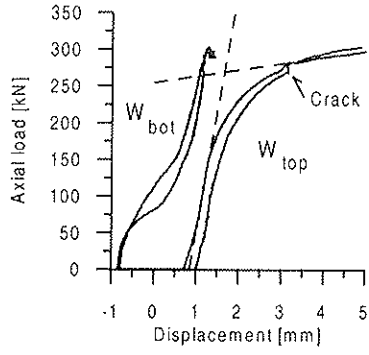
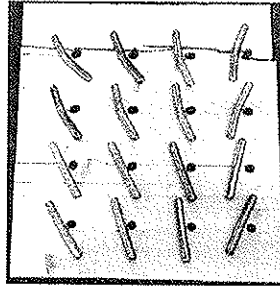


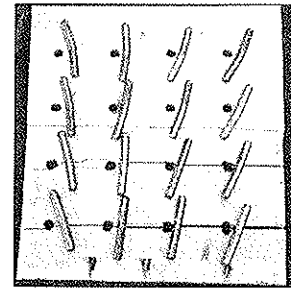
Figure 11: Axial testing combined with approx. 5% transverse load,  $t = 40\text{mm}$ .



(a) Load displacement.

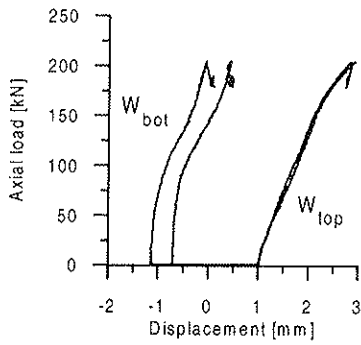


(b) North joint.

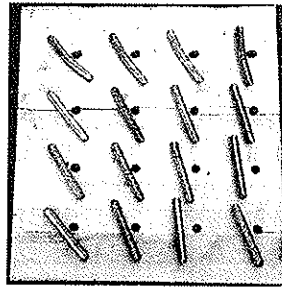


(c) South joint.

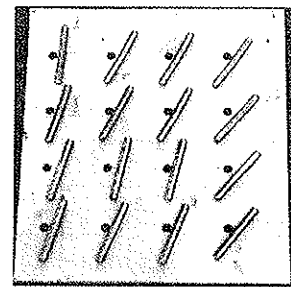
**Figure 12:** Axial testing combined with approx. 10% transverse load,  $t = 40\text{mm}$ .



(a) Load displacement.

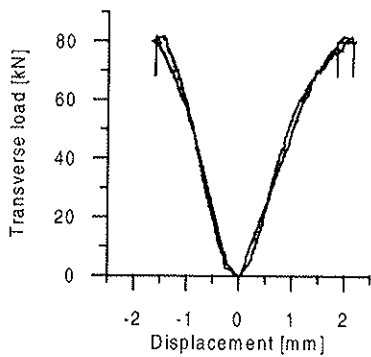


(b) North joint.

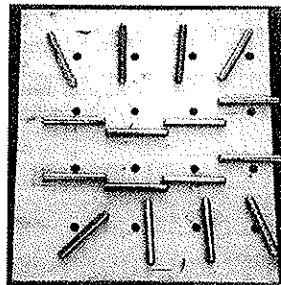


(c) South joint.

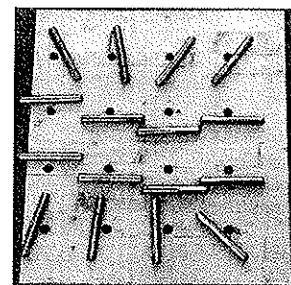
**Figure 13:** Axial testing combined with approx. 15% transverse load,  $t = 40\text{mm}$ .



(a) Load displacement.



(b) North joint.



(c) South joint.

**Figure 14:** Eccentric pure transverse testing,  $t = 40\text{mm}$ .

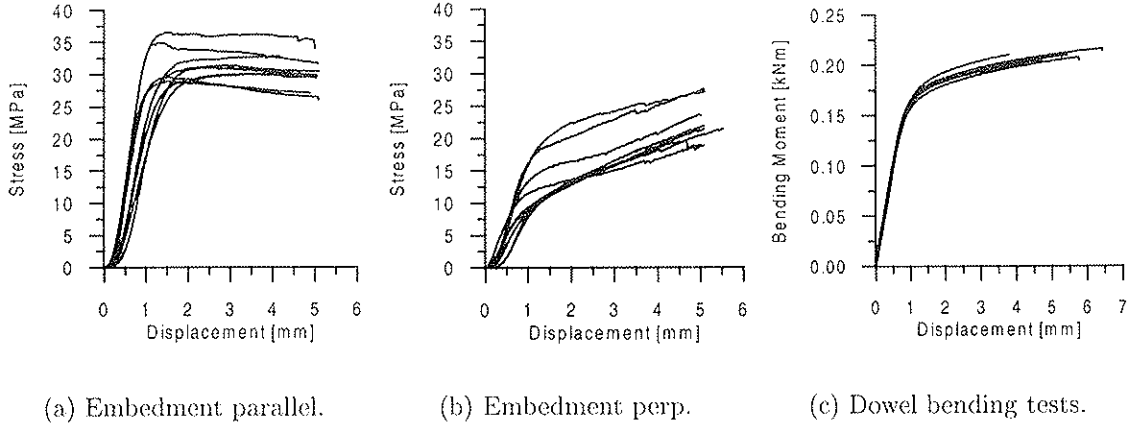


Figure 15: *Embedment and dowel bending tests.*

	$f_{h,0}$ [MPa]	$f_{h,90}$ [MPa]	$M_y$ [kNmm]	$K_{0,t=40}$ [kN/mm]	$K_{90,t=40}$ [kN/mm]	$K_{0,t=65}$ [kN/mm]	$K_{90,t=65}$ [kN/mm]
Mean	31.2	12.8	184	20.9	11.7	17.2	11.4
Stdev	2.6	3.9	-	1.6	1.5	2.4	3.2

Table 6: *Embedment and dowel strength and connector moduli.*

### 3.2 Embedment and connector tests

Figure 15 shows stress displacement charts for embedment tests parallel and perpendicular to the grain and 3-point bending tests of dowels. In loading parallel to the grain the material behaviour is fairly linear elastic–perfect plastic whereas the wood shows strain hardening for loading perpendicular to the grain. Table 6 gives mean value of embedment strength, dowel yield moment and connector stiffness. The embedment strength  $f_{h,0}$  is determined as the maximum stress whereas  $f_{h,90}$  is determined as shown in principle in Figure 6. The stiffness of the connectors,  $K$ , is determined as the slope of the linear part of the load displacement curve of tests on dowels in wood of full width.

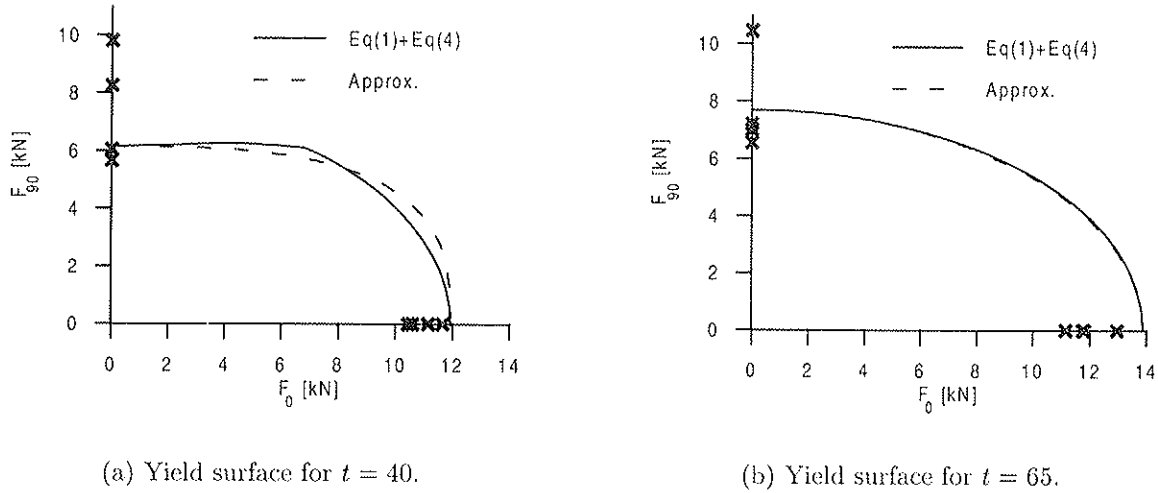
## 4 Modelling of failure

### 4.1 Yield surface

The yield surface for the connectors is established by use of the raw data given in Table 6 and by assuming linear elastic–perfect plastic behaviour. The yield strength per shear plane is determined by Equation (1) and by a Hankinson strength interpolation as given in Equation (4).

$$f_{h,\alpha} = \frac{f_{h,0} f_{h,90}}{f_{h,0} \sin^2(\alpha) + f_{h,90} \cos^2(\alpha)} \quad (4)$$

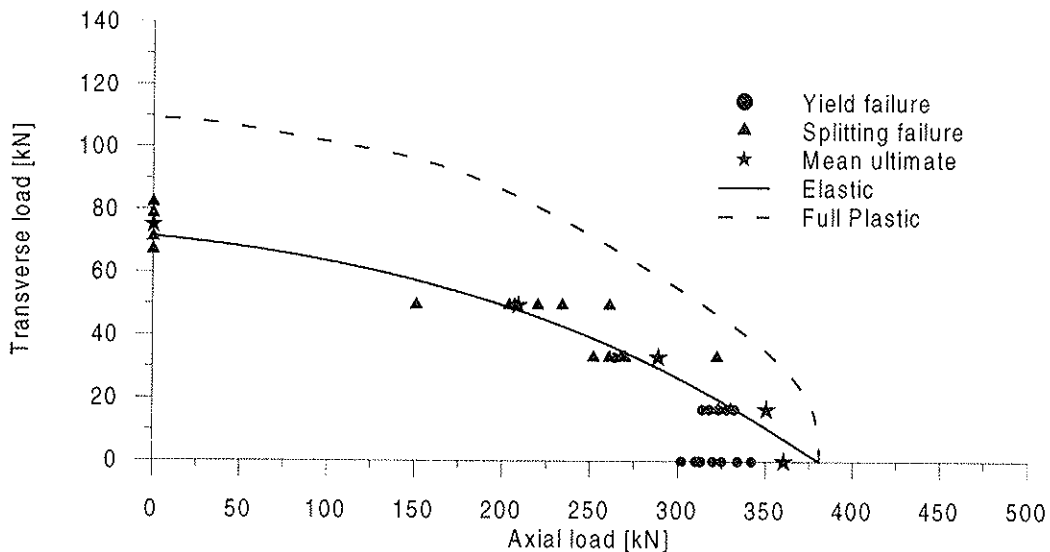
Figure 16 shows the established yield surfaces as well as the approximation used for the modelling of the full scale joint. For  $\alpha = 0^\circ$  and  $\alpha = 90^\circ$  the experimental values of  $F_y$



**Figure 16:** Yield surfaces for a single connector plotted with experimental strengths per shear plane,  $F_{y,0}$  and  $F_{y,90}$ , and the approximation used to model the full scale joints.

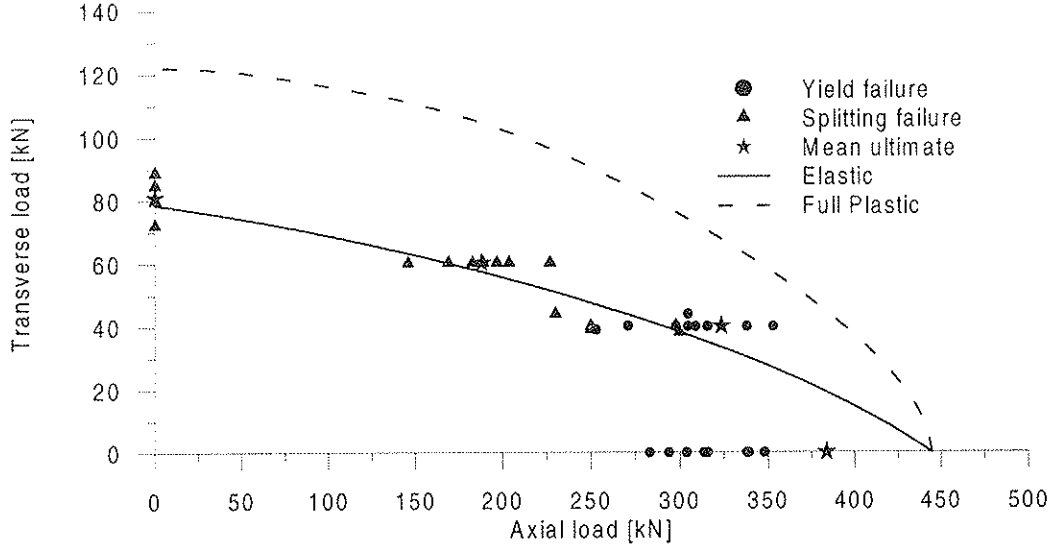
obtained in the connector tests, Section 2.2, are plotted. In the grain direction perfect plasticity may be a bit optimistic as the material exhibits some strain softening, Figure 15(a). The over-estimation of the strength  $F_{y,0}$  might be due to this stress decrease after peak. In the transverse direction the connector tests show larger scatter and the assumption of perfect plasticity is conservative as embedment strain hardening is observed, Figure 15(b); probably due to this the yield surface under-estimates the strength  $F_{y,90}$ .

## 4.2 Elastic and plastic modelling of joints



**Figure 17:** Yield surface for full scale joint,  $t=40\text{mm}$ , plotted with experimental results.

Figures 17 and 18 show experimental strength values – yield or splitting – as determined in Section 3.1, Tables 4 and 5. Mean value of ultimate strength for each load



**Figure 18:** Yield surface for full scale joint,  $t=65\text{mm}$ , plotted with experimental results.

combination is also given. The yield surfaces for the complete connection are calculated for elastic behaviour limited by a first yield criteria and for full plastic behaviour, i.e. yielding in all connectors.

## 5 Discussion

For pure axial loading the yield surfaces in Figures 17 and 18 overestimates the strength between 20 and 40%. This is also visible at connector level in Figures 16(a) and (b). Besides the strain softening already mentioned, the model in Equation (1) may be too simplified as it neglects the eccentricity due to the slot. Equation (5) gives mode II  $F_y$  with an additional eccentricity.

$$F_y = \left( \sqrt{2 + 4\frac{e^2}{t^2} + 4\frac{e}{t} + 4\frac{M_y}{t^2 d f_h}} - \left(1 + 2\frac{e}{t}\right) \right) t d f_h \quad (5)$$

In Table 7 the value of  $F_{y,eq(5)}$  is given for a 5mm eccentricity corresponding to half the width of the slot. It should be observed that the holes in the 8mm steel plate were 1mm oversized providing no rotational restraints of the dowels. It is seen that the value of  $F_{y,eq(5)}$  lies between the values of  $\bar{F}_{y,connector}$  and  $\bar{F}_{y,full\ scale}$ , i.e. approximates the strength within 5% for  $t = 40\text{mm}$ . For  $t = 65\text{mm}$  both  $F_{y,eq(1)}$  and  $F_{y,eq(5)}$  overestimates the experimental values; however, by mistake  $\text{Ø}13$  holes were used for  $d12$  dowels in this test series, Figure 8 (a). Consequently, the wood is not able to provide the full rotational restriction of the outer part of the dowel needed by mode II as shown

	$\bar{F}_{y,full\ scale}$	$\bar{F}_{ult,full\ scale}$	$\bar{F}_{y,connector}$	$F_{y,eq(1)}$	$F_{y,eq(5)}$	$F_{y,eq(6)}$
$t = 40$	10.0	11.3	11.0	11.9	10.4	-
$t = 65$	9.9	12.0	11.9	13.9	12.6	10.0

**Table 7:** Comparison of experimental and theoretical values of strength per shear plane for loading in the grain direction [kN].

	$\bar{F}_{y,connector}$	$F_{y,eq(1)}$	$F_{y,min\{eq(5),eq(1)\}}$	$F_{y,eq(6)}$
$t = 40$	7.5	6.1	6.1	-
$t = 65$	7.8	7.7	7.1	6.8

**Table 8:** Comparison of experimental and theoretical values of strength per shear plane for loading perpendicular to the grain [kN].

in Figure 1(b), hence the failure mode will as a conservative guess correspond to mode I on the limit to mode II. An indication for lack of rotation restriction of the dowels is found in the connector stiffness listed in Table 6, which show the stiffness  $K_{0,t=65}$  to be smaller than  $K_{0,t=40}$ , an effect possibly due to mode shift. Equation (6) gives  $F_y$  for mode II failure in oversized holes and a slot eccentricity as mentioned above. The value of  $F_{y,eq(6)}$  given in Table 7 is in accordance with  $\bar{F}_{y,full\ scale}$  but does fit the connector strength less well.

$$F_y = \left( \sqrt{e^2 + 2 \frac{M_y}{d f_h}} - e \right) d f_h \quad (6)$$

In this discussion it should of course be observed that the value of  $\bar{F}_{y,full\ scale}$  is by far the statistically most interesting as it corresponds to testing of 128 dowels for each thickness whereas the connector tests and the theoretical calculated strength values rests on a more limited number of tests. However, the discussion indicates that the slot-eccentricity should not totally be neglected; further the experiments show that tight fitting holes are necessary in order to obtain strengths corresponding to modes utilising rotation restriction of the outer part of the dowel.

For eccentric pure transverse loading, the full yielding model in Figures 17 and 18 overestimates the strength by approximately 50%. This is not visible at connector level in Figures 16(a) and (b). Table 8 lists mean value of the connector strength and the strength calculated according to Equations (1), (5) and (6). The connector strengths are better modelled by Equation (1) than by Equations (5) or (6). This is probably not due to lack of eccentricity and oversize effects, but because the used  $f_{h,90}$  is a conservative estimate of a parameter taking higher values for larger deformations as seen in Figure 15(b).

The comparison between experimental data and modelling in Figures 17 and 18 becomes less clear as it is obvious that the used yield model, Equation 1, has to be refined in the form of e.g. Equations 5 or 6 to model the specific geometry used. However, the central idea in the full scale experimental series, namely that the yield theory gives good strength predictions for loading in the grain direction, as shown in Section 1.3, but gives less good predictions for loading transverse to the grain, as shown in Section 1.4, is partly confirmed. The plastic plateau vanishes and splitting failure becomes more dominant for increased transverse load for the full scale tests. Generally the elastic modelling, i.e. a first yield failure criteria, fits the data best; however, besides the mentioned problems with the mechanical equations entering the yield model, the material behaviour is not adequately modelled as the pronounced strain hardening for  $f_{h,90}$  is not included. A model refined both mechanically and material wise will be implemented at a later stage.

The Eurocode allows 10% additional friction load bearing capacity for modes II and III, this could be interpreted as the additional capacity after plastic failure and before ultimate splitting failure; Tables 4 and 5 confirms these 10% for dominating axial load, but it is questionable if the friction capacity exists for dominating transverse load.



There is a move towards encouraging designers to use slender dowels, e.g. (Blass, Ehlbeck & Rouger 1999), to reduce the tendency of premature splitting. In the results here laid forward, a 6% load bearing capacity is gained on the ultimate splitting strength for pure axial loading and 8% is gained for eccentric pure transverse loading when the thickness is increased 63%. Hence, a simplification of the design rules for stout dowels will entail a relatively severe and maybe unnecessary punishment of the joints with  $t = 40\text{mm}$ .

## 6 Conclusion

In order to perform a better modelling of the results laid forward the authors would like to state and discuss the following points:

1. Plastic failure criteria can successfully be applied for dominating axial load and a 10% additional frictional load bearing capacity before final splitting is obtainable.
2. Plastic failure criteria are less successful for dominating transverse load and utilising 10% additional frictional load bearing capacity seems to be optimistic.
3. The mechanical part of the plastic model may need refinement to include eccentricity introduced in the slot in order to model plastic failure accurately.
4. The material part of the plastic model may need refinement to include strain hardening for  $f_{h,90}$ . This may explain why the severest loaded dowels in an eccentric loaded joint locally introduces splitting stresses in excess of what is expected by a perfect plastic model.
5. Dowel holes has to be tight fitting when the failure mode utilises rotational restraints of the outer part of the dowel.
6. No experimental evidence is found to substantiate the apparently sound idea of increasing the non-plastic capacity by prescribing slender dowels.

## Acknowledgement

BMF bygningsbeslag are acknowledged for providing dowels and Glulam Denmark A/S for manufacturing and delivering of the glulam specimens.

## References

- Blass, H. J., Ehlbeck, J. & Rouger, F. (1999), Simplified Design of Joints with Dowel-type Fasteners, *in* G. B. Walford & D. J. Gaunt, eds, 'Pacific Timber Engineering Conference', Vol. 3, Rotorua, New Zealand, pp. 275–279.
- CEN (1993), Timber structures – Test methods – Determination of embedding strength and foundation values for dowel type fasteners, Test Method Standard EN 383, European Committee for Standardization.
- CEN (1995), Eurocode 5 – Design of timber structures – Part 1–1: General rules and rules for buildings, Preliminary building code prENV 1995-1-1, European Committee for Standardization.

- Eskildsen, L. (1999), Samlinger i trækonstruktioner (in Danish), Final thesis, BKM, Technical University of Denmark.
- Johansen, K. W. (1941), 'Forsøg med træforbindelser (in Danish)', *Bygningsstatistiske meddelelser* **XII**(2).
- Larsen, H. J. & Enquist, B. (1996), Glass Fibre Reinforcement of Dowel-Type Joints, *in* V. K. A. Gopu, ed., 'Proceedings of the International Wood Engineering Conference, October 28–31, 1996', Vol. 1, New Orleans, Louisiana, USA, pp. 293–302.
- Larsen, H. J. & Riberholt, H. (1988), Timber constructions, Design (in Danish), SBI-anvisning 135, Statens Byggeforskningsinstitut, Hørsholm, Denmark.
- Mohammad, M. A. H., Quenneville, P. & Smith, I. (1997), Bolted Timber Connections: Investigations on Failure Mechanism, *in* P. Hoffmeyer, ed., 'Proceedings of the International Conference of IUFRO S 5.02 Timber Engineering, June 18 – 20, 1997', Copenhagen, Denmark, pp. 211–226.

**INTERNATIONAL COUNCIL FOR RESEARCH AND INNOVATION  
IN BUILDING AND CONSTRUCTION**

**WORKING COMMISSION W18 - TIMBER STRUCTURES**

**CREEP OF NAIL PLATE REINFORCED BOLT JOINTS**

J Vesa

Helsinki University of Technology

A Kevarinmäki

Technical Research Centre of Finland (VTT)

FINLAND

**MEETING THIRTY-TWO**

**GRAZ**

**AUSTRIA**

**AUGUST 1999**

---

Presenter: J.Vesa

- H.J.Blass commented that both the metal nail plate and the timber joint carried the loads. He asked whether the load sharing between the metal nail plate and the timber joint would change over time in a creep test.
- J.Vesa responded that it was not likely as the metal nail plate was much stiffer than the timber joint.

# Creep of Nail Plate Reinforced Bolt Joints

by

Janne Vesa

Helsinki University of Technology

Ari Kevarinmäki

VTT Building Technology

Finland

## 1. Introduction

The effect of nail plate reinforcement on timber joints has been researched in Helsinki University of Technology since 1992. It was found that in short duration loading the reinforcement performs well: stiffness at low load levels is high, ultimate strength is high and the joint slip in failure is large. The presented creep tests were started to verify the function of the nail plate reinforced bolted joints under varying climate conditions during long period of time.

The long-term tests started at autumn 1992. A test of 44 nail plate reinforced bolt joints was carried out. In the test series the type of nail plates, the loading direction of the nail plate as well as the direction between grain and the applied force were varied. The test series consisted of three pairs: three series were tested in a covered but unheated building (a granary) and similar series in cyclically changed humidity and temperature conditions with rapidly changing humidity. The duration of the tests in cyclically changed conditions was 200 days and the tests in the natural covered conditions are still continuing after 6.5 years loading period.

The results of the measurements between the tests series from the natural and cyclically changed conditions were compared. The joint slip after 50 years loading of the tests pieces in the natural covered conditions was estimated with a logarithmic function. These results were compared to the joint slips according to EC5. Also the joint slip from other joint types of other previous tests found from literature were compared to the nail plate reinforced bolt joints and to joint slips according to EC5.

## 2. Experimental programme

The long-term tests started before short-term results were available. Therefore, the ultimate strength of joints was estimated by multiplying the Finnish design code value for similar non-reinforced bolt joint by two. Load levels for long-term tests were chosen to be 25% and 50% from this design value. Loading was achieved with concrete blocks. The loads and average strength values from short-term strength tests are presented in table 2.1. Some of the joint types used in long-term tests were not tested in short-term tests.

The test joints consisted of one 12 mm bolt (bolt quality 8.8), reinforced timber middle member and steel side members. The reinforcement nail plates were placed symmetrically on both sides of the timber member. The bolts were tightened with handtools until the steel plates were in contact with the timber member. The test series consisted of three pairs. The

level of loading and direction between applied force varied in series. The series 1, 2, 3 and 4 were loaded parallel to grain. The series 5 and 6 were loaded perpendicular to grain. The direction between the reinforcing nail plates and loading as well as the type of the nail plates and bolts are showed in figure 2.1. The series 1, 2 and 5 were loaded in the cyclically changed conditions and the other three in the natural covered conditions. The individual test pieces are labeled with two numbers separated with a dot. First number indicates the test series and the second number the serial number of the test piece in series. The arrangements were such that measuring were conducted over two joints, i.e. joint slips are averages of two joints. This report consist of only the results of the test pieces loaded parallel to grain (Saavalainen 1993).

Table 2.1 Loadings and short-term strengths (Saavalainen 1993)

Test pieces	Short-term strength [kN]	Loading [kN]
1.1, 1.2, 4.1, 4.2	30.5	1.6
2.1, 2.2, 3.1, 3.2		3.3
1.3, 4.3	34.8	1.6
2.3, 3.3		3.3
1.4, 4.4	30.0	1.6
2.4, 3.4		3.3

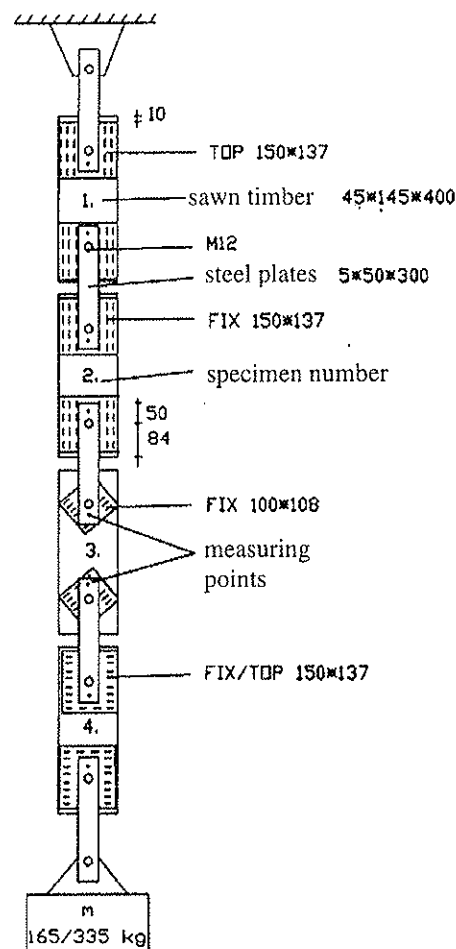


Figure 2.1 Loading arrangements

The program of humidity changes in the controlled rooms is presented in figures 2.2 and 2.3 and the climate conditions in the natural covered conditions in figure 2.4. The controlled room H023 was used because the height of the room H007 was not enough for the test series 1 and 2. Thus, the test joints 1.1 and 1.2 were loaded separately from other test pieces of those series in room H023.

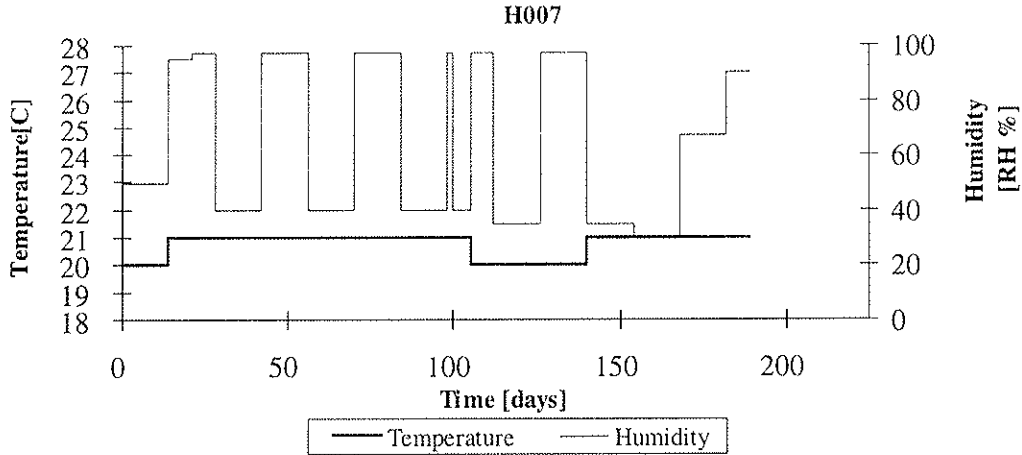


Figure 2.2 Humidity and temperature change procedure in room H007

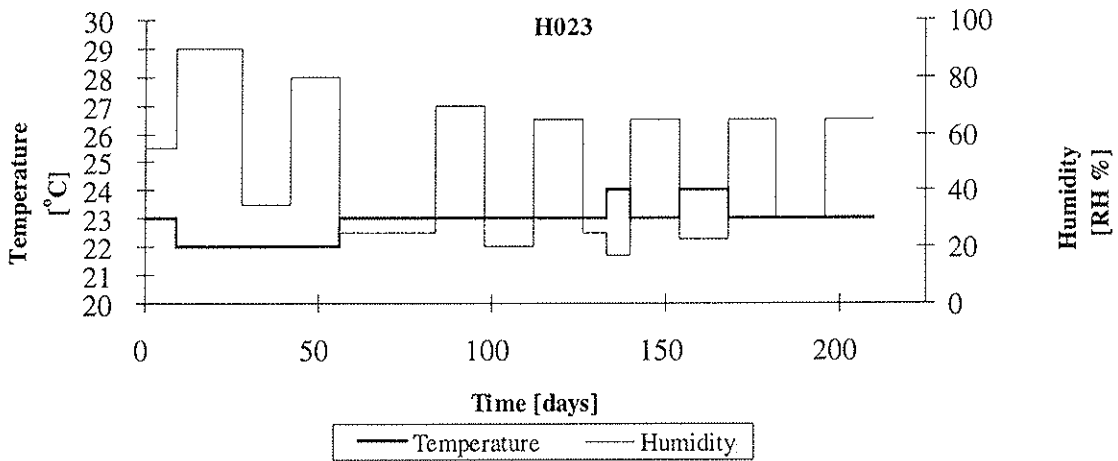


Figure 2.3 Humidity and temperature change procedure in room H023

**Relative humidity and temperature**

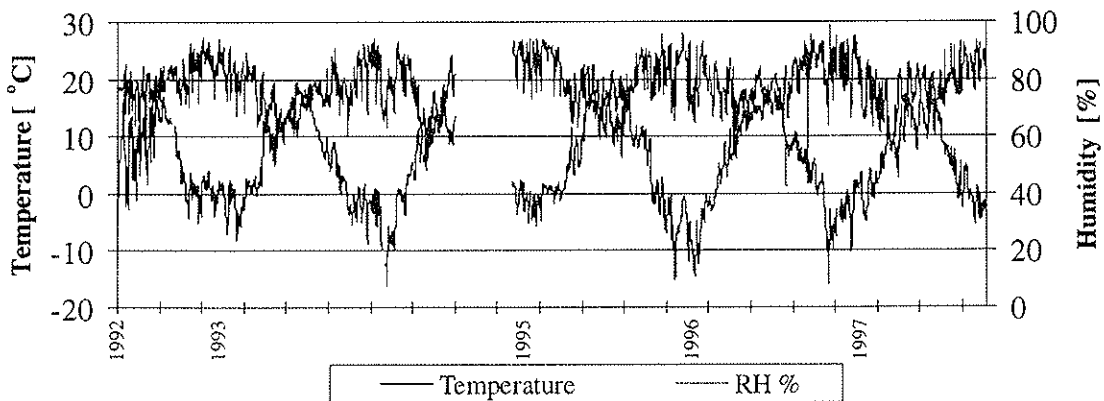


Figure 2.4 Climate conditions in the natural covered conditions measured at 13:00 o'clock

The loading time in the cyclically changed conditions was 200 days whereas loading in the natural covered conditions is still in progress. This report includes the measurements from the natural covered conditions from the first 2006 days (about 5.5 years). The initial moisture content was 14.6..15.5% of the dry weight of timber. The timber material was Finnish spruce and pine. The oven dry weight varied between 386 and 524 kg/m<sup>3</sup>.

A reference piece of timber was placed to each test location to determine the variation of moisture content. The moisture content was measured by weighing the reference timber piece (Figures 2.5 and 2.6).

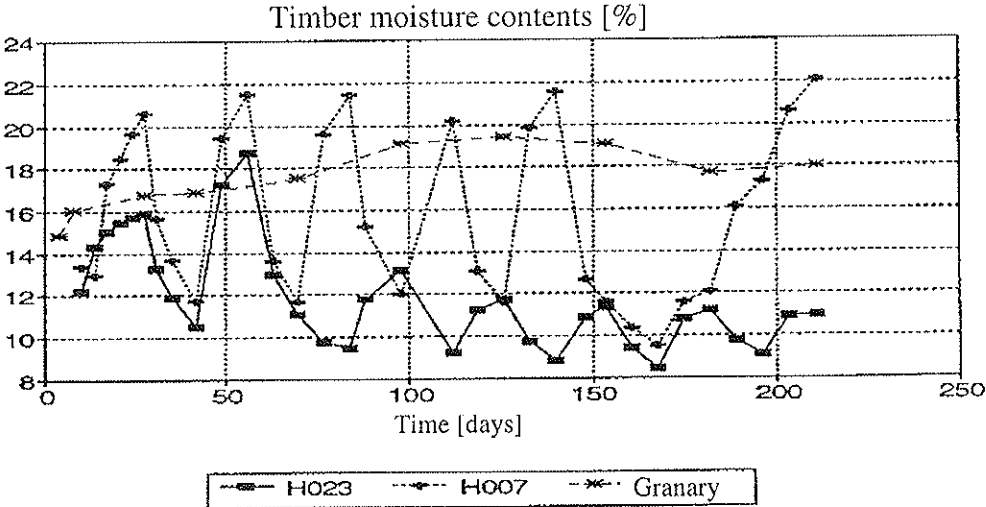


Figure 2.5 Measured timber moisture contents during first 200 days (Saavalainen 1993)

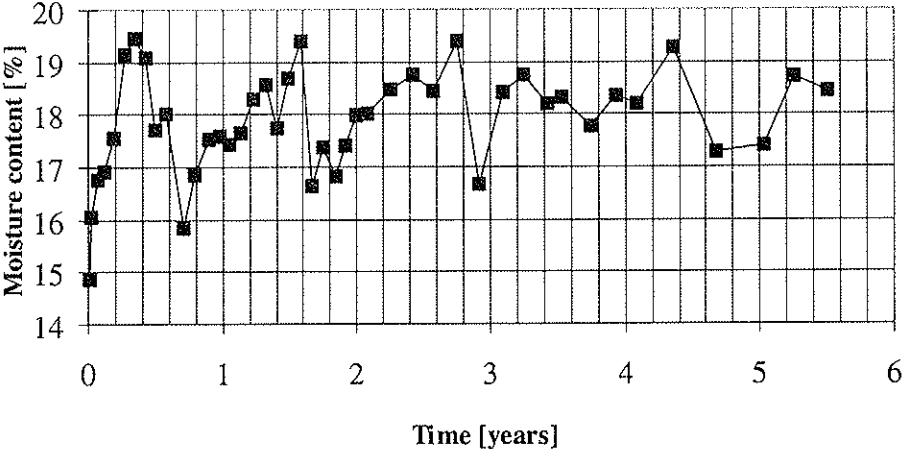


Figure 2.6 Measured timber moisture contents in the natural covered conditions during the tests

### 3. Measured joint slips

In spite of ten times longer loading period (2006 days), in most cases the joint slips of the tests pieces in the natural covered conditions did not exceed the joint slips of similar joints placed in the cyclically changed conditions. Since the situation is the same when the estimation of the joint slips after 50 years loading of the test series 3 and 4 was compared to joint slips from the series 1 and 2, the comparison of tests results is not presented here. Instead, the method of estimating future joint slips is presented in the section 3.1. In the section 3.2, the joint slips from the cyclically changed conditions after 200 days are compared to the estimated joint slips after 50 years.

#### 3.1 Estimation of the future deformations

The developing of joint slips was estimated for the test series 3 and 4. The estimation was carried out by fitting a logarithmic function to the measured results. The fitting was made separately for each measured test piece, i.e. for average results from two joints. The fitted function (3.1) was

$$C(t) = 1 + D \ln(1 + Et) \quad (3.1)$$

where  $C(t)$  is the creep factor after loading period of  $t$ ,  
 $D$  and  $E$  are constants and  
 $t$  is time in days.

The joint slip was calculated from equation (3.1) with the relation of the initial joint slip, the joint slip after certain loading time and the creep factor as shown in eq. (3.2). The values of initial joint slips and constants  $D$  and  $E$  are presented in table 3.1.

$$C(t) = \frac{\varepsilon \Delta}{\varepsilon_0 \Delta} \quad (3.2)$$

where  $\varepsilon_0$  is the initial joint slip after mounting of the load ( $t = 5$  min.),  
 $\varepsilon$  is the joint slip in time  $t$  and  
 $\Delta$  is the initial distance of the measuring points.

Table 3.1 Initial movements and constants

Test piece	$\varepsilon_0 \cdot \Delta$ [mm]	$D$ [-]	$E$ [-]	Test piece	$\varepsilon_0 \cdot \Delta$ [mm]	$D$ [-]	$E$ [-]
3.1	0.251	0.0293	27.1	4.1	0.039	0.152	3.47
3.2	0.280	0.0369	37.1	4.2	0.014	0.423	67.0
3.3	0.089	0.0608	978	4.3	0.031	0.478	11.2
3.4	0.107	0.239	0.912	4.4	0.018	0.869	27.5



The definition of the creep factor for timber joints is indistinct. For example, the method to determine the initial slip is different in almost all of the creep tests. Therefore, in this report instead of presenting the creep factor, the joint slips are presented. The fitted functions and test results for series 3 and 4 are presented in figure 3.1.

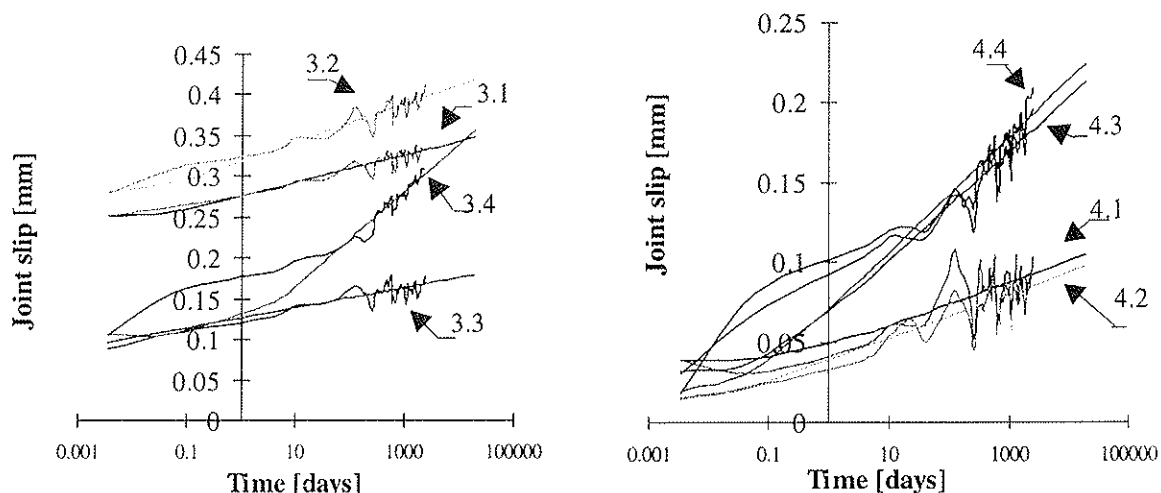


Figure 3.1 Fitted functions and the measured joint slips for the test series 3 and 4

### 3.2 Comparison of test results from cyclically changed and natural covered conditions

As mentioned before, the test series in the cyclically changed conditions were exposed to rapid humidity changes during 200 days loading period. The test series in the natural covered conditions experienced less severe humidity, and thus moisture content, changes but the loading time was about ten times longer than for the other series. In this section, the measured slips of the cyclically changed conditions test pieces are compared to the joint slips estimated according to eq. (3.1). The difference between the measured movements after 5.5 years and the estimated slips after 50 years is small as shown in table 3.2. The maximum joint slips after 200 days for the cyclically changed conditions joints and the estimated joint slips of test pieces in natural covered conditions are presented in table 3.3. The joint slips from cyclically changed conditions are larger in almost every case.

Table 3.2 The ratio between the measured joint slips after 5.5 years and the estimated joint slips after 50 years of loading

Test piece	Ratio	Test Piece	Ratio
3.1	1.03	4.1	0.97
3.2	1.04	4.2	0.94
3.3	1.00	4.3	1.12
3.4	1.16	4.4	1.26

The values in tables 3.2 and 3.3 show that deformations under severe humidity changes during relatively short period of time are larger than under the conditions comparable to the EC5's Service Class II conditions. The estimated developing of deformations after 5.5 years is slow, as expected. Some of the estimated deformations after 50 years are even smaller than the maximum value of the measured joint slips after 2006 days. This is probably caused by the moisture movements. The velocity of creep deformation and total joint slip is related to the angle between the applied force and the main direction of nail plates: larger angles induce larger creep deformations.

Table 3.3 *The largest measured joint slips in the cyclically changed conditions and the estimated joint slips after 50 years*

Test piece	Joint slip [mm]	Estimated joint slip after 50 years [mm]		Test piece	Joint slip [mm]	Estimated joint slip after 50 years [mm]	
		Series 4	Ratio			Series 3	Ratio
1.1	0.413	0.108	3.82	2.1	0.544	0.338	1.61
1.2	0.093	0.104	0.89	2.2	0.293	0.402	0.73
1.3	0.252	0.190	1.33	2.3	0.299	0.179	1.67
1.4	0.539	0.198	2.72	2.4	0.630	0.305	2.07

#### 4. Comparison to other joint types

The estimated joint slips of the nail plate reinforced bolt joints are compared to deformations of bolt, toothed plate, nailed and nail plate joints. The comparison test results are gathered from Feldborg et al. (1986), Wilkinson (1988) and Van de Kuilen (1994). These deformations and the rate of deformations are also compared to the calculated values according to EC5.

The humidity conditions in the comparison tests were either maintained constant or "continuously recorded" in which case the relative humidity varied between 40% and 80%. Thus, the conditions are less severe than in the natural covered conditions or in the latter case of same severity. All joint types were loaded in tension parallel to grain.

The test pieces in the nailed and nail plate joints consisted of two timber pieces ( $95 \times 45 \text{ mm}^2$ ) connected together with nail plates (marked here as LHy) or nailed steel (LSa) or plywood plates (LPs and LPa). The loading levels were 10 kN and 8.6 kN. The initial slip was calculated 10 min. after the mounting of the loads and the final slips was calculated after 588 or 596 days, i.e. about 1 year and 7.5 months (Feldborg et al. 1986).

The toothed plate joints consisted of three timber members whose cross sections were: middle member  $95 \times 33 \text{ mm}^2$  and side members  $95 \times 18 \text{ mm}^2$ . The fastener was assembled with a 75 mm toothed plate and a 12 mm bolt. The test programme consisted of three series with different loading levels, which were 30%, 40% and 50% of the short-term strength (= 32.6 kN). These series are marked here as HV30, HV40 and HV50 respectively. A

function was fitted to the average of measured slips of each series. The function was essentially the same as eq. (3.1) (Van De Kuilen 1994).

The bolt joints consisted of three timbers member whose cross sections were: middle member 75 x 38 mm<sup>2</sup> and side members 38 x 38 mm<sup>2</sup>. The fastener was 12.7 mm bolt. The test programme consisted of three series with the loading levels of 30% , 60% and 85% of the short-term strength (= 21.4 kN). These series are marked here as W30, W60, and W85 respectively. The loading time was one year (Wilkinson 1988).

The joint slips divided by the loading [kN] are presented in figure 4.1. The deformations from the nailed and the nail plate joints are measured values, whereas values from the toothed plate and the nail plate reinforced joints are calculated from the fitted functions. The deformations of the nail plate reinforced tests are presented from the test piece with the largest initial slip (3.2), the test piece with the largest slip after 50 years (4.4) and the test piece which showed least deformations (3.3). The measured joint slips of the bolt joints included the effect of oversized bolt holes as the joints tightened. This effect is estimated by extrapolating the initial slip values to zero force as shown in figure 4.2. The presented joint slips of the bolt joints in figure 4.1 are calculated from the given average initial slips multiplied by average creep factors reduced by the estimated bolt hole oversize effect.

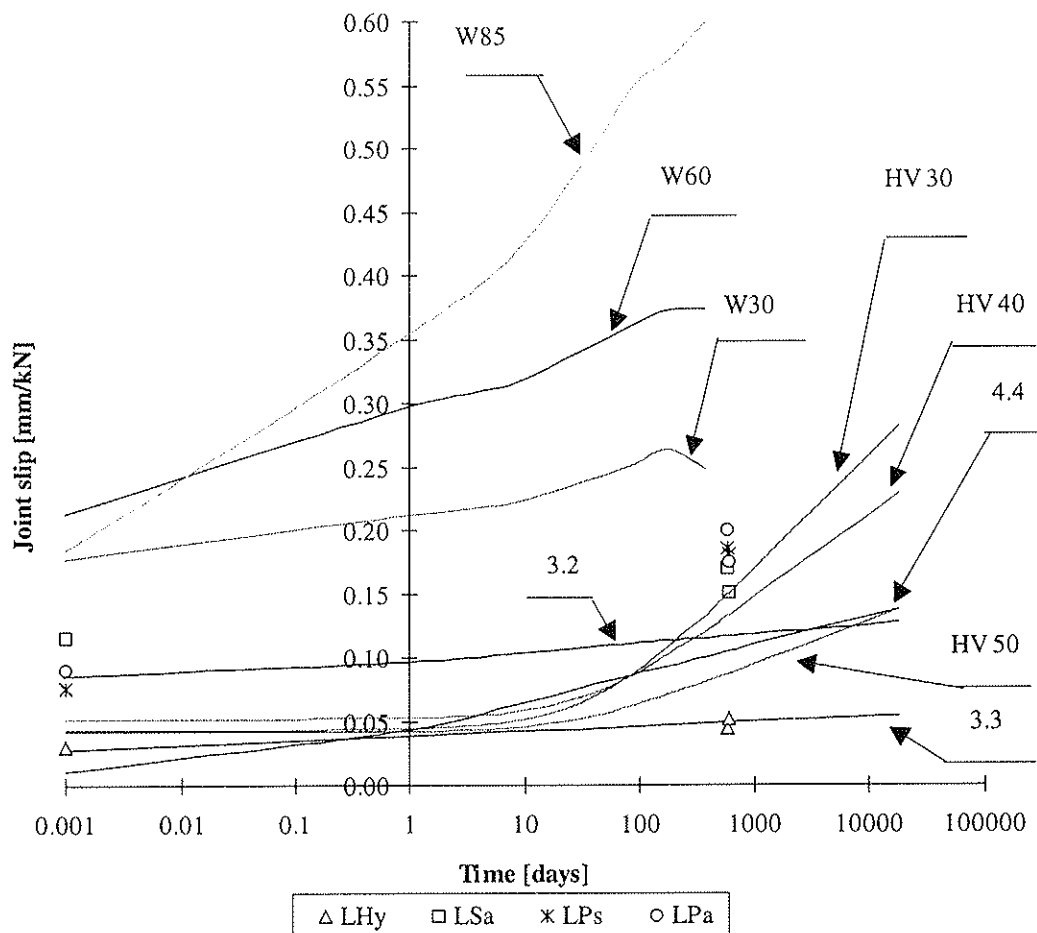


Figure 4.1 The comparison of joint slips between different joint types. Notations are explained in the text.

Figure 4.1 shows that joint slips on nail plate reinforced bolt joints are small. Only nail plate joints are stiffer than nail plate reinforced joints.

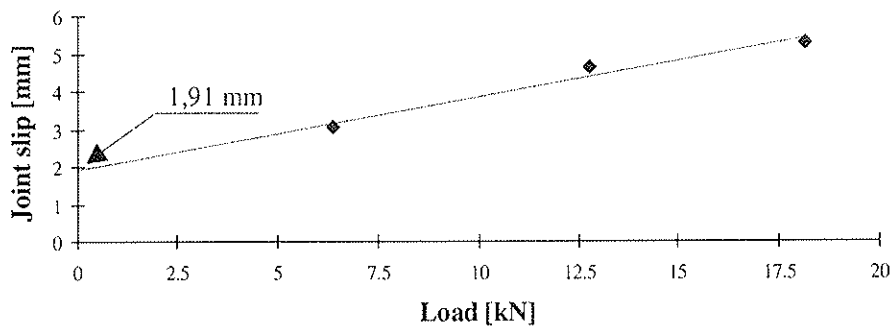


Figure 4.2 Average initial slips. The estimated effect of the oversized bolt holes is the point where the line crosses y-axis (= 1.91 mm)

#### 4.1 Comparison to EC5

The comparison between EC5 and the handled test results was done in two ways. The comparison of the bolt joints and nailed joints was made between the calculated values according to EC5 and the values calculated from the test results. The joint slips of the bolt joints are calculated in the same way as in the previous section. The comparison of the nail plate, nail plate reinforced and toothed plate joints was done only for the creep factors according to the EC5, because EC5 does not contain calculation instructions for the joint slip for these joint types. This was done by setting the initial slip to the average value of the measured initial slips, multiplying these initial slips by the EC5's creep factors and comparing these values to the joint slips of each joint type.

Figure 4.3 shows that the calculation methods in EC5 give too small values for the joint slip. The creep factors are also too small. Only the nail plate joints seem to follow the creep values in EC5. The velocity of the nail plate reinforced joints increases as the angle between the applied force and the nail plate main axis increase. Only the test piece 3.3, where the angle was 45%, makes an exception to this rule. The test pieces where the nail plate main axis is the same as the direction of load follow quite well the EC5's creep factors.

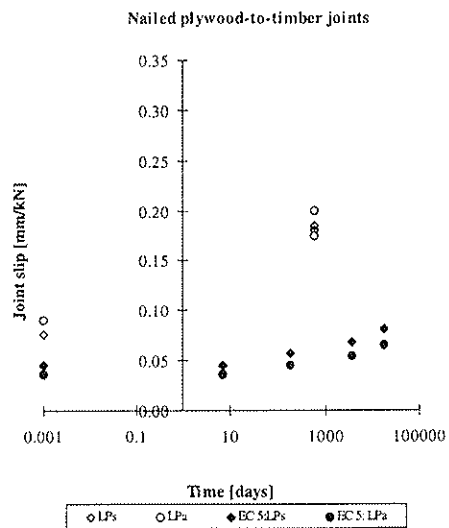
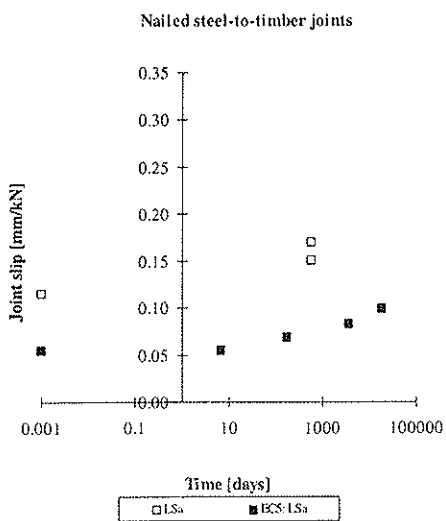
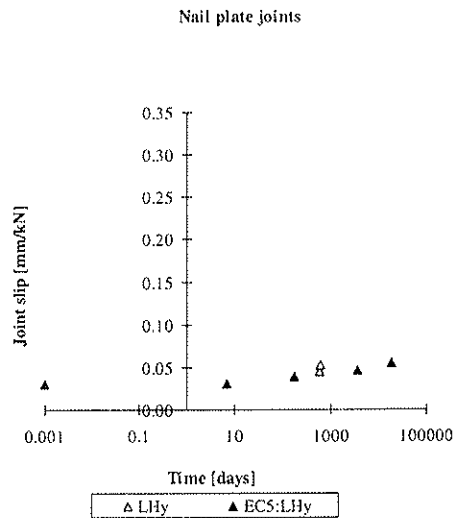
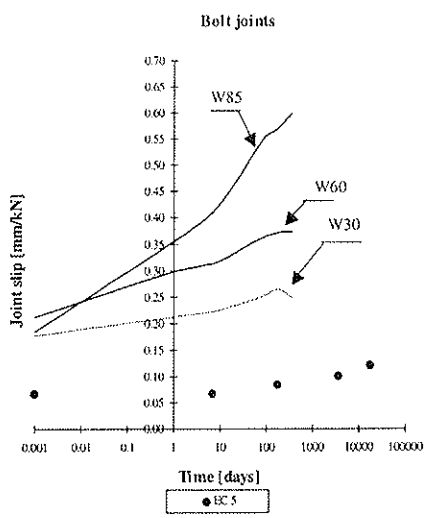
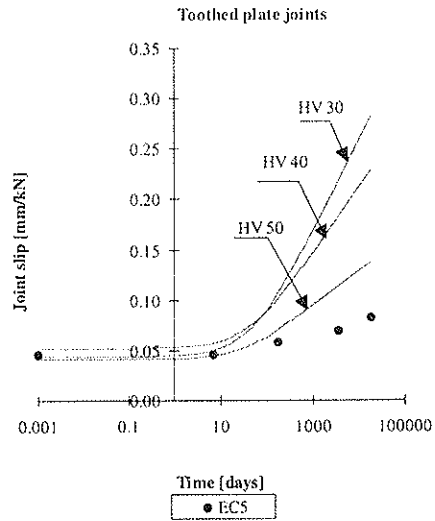
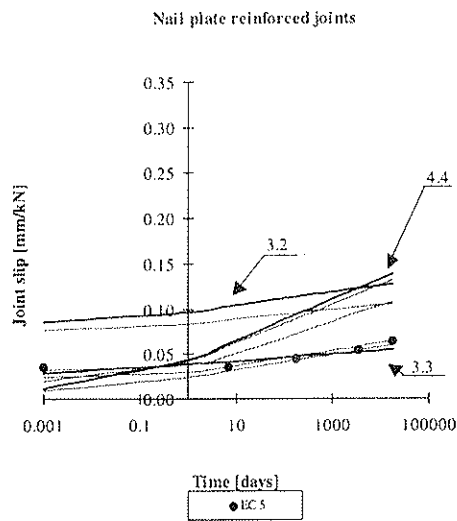


Figure 4.3 Comparison between EC5 and test results

## 5. Proposal for the calculation of the joint slip of nail plate reinforced bolt joint under service load

This proposal is based on the measurements that are made for this report and previous research in the Helsinki University of Technology.

The instantaneous slip should be taken as (Kevarinmäki 1995)

$$u_{\text{inst}} = \frac{F}{K_{\text{ser}}} + u_0 \quad (5.1)$$

where

$F$  is the load per shear plane per fastener [kN],  
 $K_{\text{ser}}$  is the slip modulus [kN/mm] and  
 $u_0$  is the initial slip [mm] due to hole clearance, etc.

The slip modulus should be calculated as (Kevarinmäki 1995)

$$K_{\text{ser}} = \rho_k^{1.5} d / 20 + K_{s,n} t_d d \quad (5.2)$$

where

$\rho_k$  is the characteristic density of the timber [ $\text{kg}/\text{m}^3$ ],  
 $d$  is the diameter of the bolt [mm],  
 $t_d$  is the design thickness of the nail plate and  
 $K_{s,n}$  is  $300 \text{ N}/\text{mm}^3$  for normal nail plates and  $450 \text{ N}/\text{mm}^3$  for special nail plates, when the yield strength  $f_y$  of the nail plates is at least  $360 \text{ N}/\text{mm}^2$ .

The initial slip  $u_0$  should be taken as (Kevarinmäki 1995)

$$u_0 = \begin{cases} 1 \text{ mm} & \text{with normal nail plates} \\ \left(1 - K_{s,n} t_d d / K_{\text{ser}}\right) & \text{with special nail plates} \end{cases} \quad (5.3)$$

The final joint slip under service load with normal nail plates should be taken as

$$u_{\text{fin}} = (u_{\text{inst}} - u_0)(1 + k'_{\text{def}}) + u_0 \quad (5.4)$$

where

$k'_{\text{def}} = k_{\text{def}}(1 + 2 \sin \alpha)$ ,  
 $\alpha$  is the angle between the applied force and the main direction of the reinforcing nail plate and  
 $k_{\text{def}}$  is the creep factor given in EC5: part 1-1: table 4.1.

## 6. Conclusions

Nail plate reinforced bolt joints are very stiff compared to other joint types that can be assembled in building site. This is emphasized in longer time periods. The creep of nail plate reinforced bolt joints increases with the angle between force and nail plate main axis.

The calculation methods in EC5 give too small joint slips. This apply both to initial deformations and deformations after given time.

Joint slips after 200 days in the tests conducted under rapidly changing humidity are generally larger than those estimated happen in naturally covered conditions after 50 years loading.

## 7. References

FELDBORG T., JOHANSEN M. 1986. Slip in joints under long-term loading. In: Proceedings of CIB W18 - Timber Structures, Florence, Italy 14 p.

KEVARINMÄKI A. 1995. Bolt Joints of Kerto-LVL Reinforced with Nail Plates. Helsinki University of Technology/LSEP, publications 49. Espoo, Finland 63 p.

VAN DE KUILEN J-W.G. 1994. Application of the theory of deformation kinetics on toothed-plate joints, In: Proceedings of COST 508 - Wood Mechanics Workshop on 'Service Life Assessment of Structures', Espoo, Finland p. 57-68.

SAAVALAINEN, I. 1993. Naulalevyillä vahvistetut pulttiliitokset. Diplomityö. Teknillinen korkeakoulu. Espoo 128 s.

WILKINSON, T.L. 1988. Duration of Load on Bolted Joints: a pilot study. Res. Pap. FPL-RP-488. Madison, WI: U.S. Department of Agriculture, Forest Service, Forest Products Laboratory. 9 p.

Eurocode 5. 1993. Design of timber structures - Part 1-1: General rules and rules for buildings. ENV 1995-1-1:1993: European Committee for Standardization. Brussels, Belgium. 110 p.

**INTERNATIONAL COUNCIL FOR RESEARCH AND INNOVATION  
IN BUILDING AND CONSTRUCTION**

**WORKING COMMISSION W18 - TIMBER STRUCTURES**

**THE BEHAVIOUR OF TIMBER JOINTS WITH RING CONNECTORS**

E Gehri

A Mischler

Chair of Wood Technology

ETH Zürich

SWITZERLAND

**MEETING THIRTY-TWO**

**GRAZ**

**AUSTRIA**

**AUGUST 1999**

---

Presenter: A.Mischler

· H.J.Blass commented that the paper content has severe deficiencies as previous work by other researchers were ignored and in some cases the interpretation of past results were incorrect. The paper in its present form would need major revisions before it would be allowed to appear in the proceedings.

· A.Mischler responded that he will discuss the issue with the first author.

· J.H.P.Quenneville also suggested that the author should examine some of the past research in UK and Canada.



# Comments to paper 32-7-10 "The behaviour of timber joints with ring connectors"

H.J. Blass and V. Krämer, Universität Karlsruhe

As already outlined after the presentation, the contribution by Gehri and Mischler contains many errors and wrong conclusions. Since the authors did not revise their paper, the major items are commented below. In the following, the original text is written in italics, the comments in roman.

## Chapter 1

*"Ring connectors were introduced into the United States in the 30ties. The most promising types were selected by the Forest Products Laboratory. Based on tests made with Douglas-fir and southern yellow pine preliminary design recommendations were published by Perkins et al (1933). The actual values are based on the work of Scholten (1944). No newer and better research is known."*

The authors ignore the research with ring connectors performed at Delft University of Technology, referenced e.g. in CIB-paper 25-7-6, where 23 research reports from Delft related to ring connectors are listed. Moreover, lecture C9 in STEP 1 references two papers by Prof. Hilson from Brighton.

## Chapter 2

*Based on the comments of Graf (1938) the german data were mainly based on compression tests; furthermore the timber specimens had only small defects. Therefore the values were reduced to...*

It is not made clear why the values were reduced. When performing compression tests with only one connector unit, the block shear failure mode cannot occur. However, in compression tests with several connectors in line the wood between the connectors may shear off.

## Chapter 3

*The above approach was used by Blass et al (1994). Blass (1995) used the same relationship for the shear block failure, but added a second condition based on the embedding strength.*

This is simply wrong (see CIB-Paper 25-7-6, 1992).

*The characteristic load-carrying capacities given in the draft of EC 5-1-1 are – compared with the actual used in Switzerland – about 40 % higher. Even if the assumptions are not quite the same, i.e. end distance of  $1,8 \cdot d_c$  instead of  $2 \cdot d_c$ , the differences seemed important. This fact alone would not justify to disagree with*

the EC5-proposal, but the possible assessment of higher loads in tension than in compression is in complete disagreement with our actual knowledge!

In the present version of the draft Eurocode 5 (Proposal of Project Team 1-1, where Prof. Gehri is a member) a rule is missing saying that for connections with only one connector unit loaded in compression the block shear failure mode is to be neglected. This proposal is already made in STEP C9 (1995). If this is taken into account, the load carrying capacity of connections loaded in compression is of course higher than for connections loaded in tension.

#### **Chapter 4**

Test conditions should reproduce the effective conditions in the structure. When testing ring connections (and also other connections) this has not been enough considered or verified. The normal case of testing only one, isolated ring under centric tension or compression forces can not represent the behaviour of a joint, above all when the joint is very sensitive to so-called secondary effects.

In the referenced research project at Karlsruhe University only test specimens were used which had been produced by timber companies. Because of this fact, a large number of "secondary effects" were included in the specimens.

Simplified tests using the unified test procedure with two connectors in line have been postulated and used by Graf (1944) and Egner (1957). It seems that their recommendations meanwhile went forgotten.

This is wrong. In the framework of the research performed at Delft University of Technology, 251 specimens containing 2 or 3 connectors in line were tested. The same applies for the research performed in Karlsruhe, where specimens with 1, 3 and 5 connector units in line were tested.

#### **Chapter 5**

Differences of behaviour of wood – in function of the load direction – are often not enough taken in consideration. Forces are not only transferred along the grain. Notches or in general, variations of the section, lead to a local deviation of the force direction, resulting locally into strains and stresses in other directions.

Here, the behaviour of notched timber specimens is compared with the behaviour of connections with mechanical fasteners. It is questionable, whether the results of Karlsen 1967, unfortunately not listed in the references, can explain the behaviour of connections.

## Chapter 6

The research made at Karlsruhe should support the strength models proposed for Eurocode 5-1-1 and given in chapter 3. Blass et al (1997) published the results of a large number of tests and compared these results with the code proposal.

The objective of the research performed in Karlsruhe was not to support the strength model forming the basis of the design rules in the present draft of Eurocode 5. The objective was to study the influence of the number of connectors in one multiple fastener connection taking into account fabrication tolerances in connections produced under real practice conditions.

The first peak load corresponds to the „shear,, failure load (first equation expressed by  $d_c^{1,5}$ ). Then the load can be increased up to the ultimate load, here expressed by the „embedding,, failure mode (second equation of EC 5-1-1, expressed by  $b_c \cdot h_e$ ).

Block shear failure already occurs at very low deformations. It is therefore very improbable, that the inner core shears off at a deformation of 2 – 3 mm as indicated in figure 6.3. Furthermore, the shear block failure in the design rules of Eurocode 5 relates to the shear failure of the wood in front of or between connectors, and not to the shear failure of the wood core within the ring connectors. Unfortunately, there is no source given for the load-slip-diagram in figure 6.3.

This would be a novelty in timber connections. The reason for that is that  $k_2$  can only for tension joints be increased to 1,25. Since  $k_2$  only appears in the first equation („shear,, failure) and the higher „embedding,, load on compression cannot be used – see foregoing remark – this is correct but not evident.

The modification factor  $k_{a3}$  takes into account the increasing shear resistance with increasing end distance. This obviously only applies for tensile connections.

In the following, several remarks containing a number of errors and misinterpretations relating to the cited Karlsruhe research project are made by the authors. Since the research report is not available to the readers, detailed comments are not made here.

## Chapter 7

Only a small number of tests should be made. Since the density of the timber may play an important role, similar densities were used for center and side members. The dimensions used for the timber members correspond to normal practice in Switzerland. The tests would be done only with 1 connector.

Without detailed information regarding the geometry of the test specimens and the density of the members the presented results cannot be used. The significance of the

results of 9 compressive and 6 tensile tests is negligible compared with the results of 908 tests used as a basis for the derivation of characteristic values.

*The small differences verified (about 5 %) between the three configurations are mainly due to more favorable supporting conditions of A. The failure mode was always the same: the core sheared away at a slip of 2 mm, followed by crushing of the timber before core.*

Without the individual test results this is an unavailing statement. Moreover, values based on three individual tests are hardly a solid data base and differences of 5 % may completely be due to variations of timber properties.

### **Chapter 8 (in paper 32-7-10: chapter 5)**

*Actual proposal in Eurocode 5-1-1 leads for tension splices to unsafe design. Furthermore no evidence could be found for the 25 % higher load-carrying capacity of a ring connector in tension (for end distance  $2,5 d_o$ ) compared to compression.*

The design models in Eurocode 5 for connectors lead to realistic and safe results since they are based on the evaluation of 908 tests. This does not mean, however, that the design of the connected members in the net cross-section can be neglected. If the design of the net cross-section is considered, this may often govern the design of the connection.

# „The behaviour of timber joints with ring connectors“

Prof. E. Gehri and Dr. A. Mischler

Swiss Federal Institute of Technology, Zurich, Switzerland

## 1 Introduction

Ring connectors have been frequently used in timber structures after 1920. Based on research made mainly in Germany and on spruce different commercial types were approved. Allowable loads were fixed and finally included in the German Timber Code.

Ring connectors were introduced into the United States in the 30ties. The most promising types were selected by the Forest Products Laboratory. Based on tests made with Douglas-fir and southern yellow pine preliminary design recommendations were published by Perkins et al (1933). The actual values are based on the work of Scholten (1944). No newer and better research is known.

## 2 Revision of the Swiss Timber Code (version 1981)

Between 1975 and 1980 the revision work went on. Formulation should be as open as possible, therefore none of the market connectors should be mentioned. Furthermore the use of the available german products should be possible. The simplest, but not at all scientific approach, was to start directly from the allowable loads given in the German Code and to search for some relationship between size and allowable load.

Shearing being the most frequent mode of rupture, the allowable loads were converted to a corresponding allowable shearing stress  $\tau_a$ . We followed the presentation given by Graf (1944). The ultimate shearing stress was presented in function of the shearing length. Tests were made with 2 connectors in line.

From the tests it could be seen (Graf/1944) the following:

- The shearing stress depends from the size of the shearing area; Graf proposed to fix the allowable shearing stress in function of the total shearing length of the joint.
- The shearing stress for the Kübler-connector (disk-connector with no core in the timber element) is – based in this assumption – higher.

Based on this – and the observation that the core shears often away before the maximum is reached – the nominal shear values were calculated without taking in account the core area.

Based on this the allowable shearing stress was fixed to:

$$\tau_{\text{allow}} = 10 \cdot A_s^{-0.25}$$

According to the Swiss Timber Code the split-ring connectors shall have a connector height  $h_c$  of at least  $d_c/4$  ( $d_c$  = outside diameter of the ring connector). Based on this relationship, we would obtain for an end distance of  $1,8 \cdot d_c$  and a spacing of  $2 \cdot d_c$  the allowable load per ring connector and shear plane to

$$F_{\text{allow}} \cong 15 \cdot d_c^{1.5} \quad d_c \text{ in mm ; } F \text{ in Newton}$$

Based on the comments of Graf (1938) the german data were mainly based on compression tests; furthermore the timber specimens had only small defects. Therefore the values were reduced to

$$F_{\text{allow}} \cong 12 \cdot d_c^{1.5} \quad d_c \text{ in mm ; } F \text{ in Newton}$$

The allowable loads are valid for one or two connectors and for tension. In case of compression an increase of about 20 % could be foreseen.

The approach given in the Swiss Timber Code is simple but also very crude.

The values are valid for an end distance of  $1,8 \cdot d_c$  and a spacing of  $2 \cdot d_c$ ; in case of compression the non-loaded end can be reduced to  $0,8 \cdot d_c$ . The members must have a thickness of at least  $1,5 \cdot h_c$  (for side members) and  $2,0 \cdot h_c$  (for the central member) as well as a width of  $4/3 \cdot d_c$ , but at least  $d_c + 40$  mm. Smaller dimensions are not allowed. When considering the strength of the connected members a so-called „notch-factor“ has to be taken in account: for ring connectors  $c_K = 0,6$  to  $0,7$ .

[Note: In the Code are not given the characteristic values; the corresponding characteristic value would be  $F_k \cong 27 \cdot d_c^{1.5}$ ]

### 3 Draft proposal for EC 5-1-1

Ehlbeck/Larsen (1993) have proposed for Eurocode 5 a similar approach: „Based on Swiss research work it can be assumed that

$$f_{v,k} = K \cdot A_s^{-0.25} \quad N/mm^2 \text{ with } A_s \text{ in } mm^2$$

*K is a constant which may depend on the timber density. It is safe to use  $K = 20$  for all European softwoods.*

The shear area  $A_s$  per connector is defined in figure 1.1.

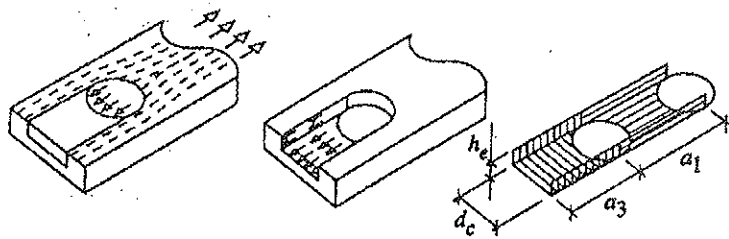


Figure 1.1: Definition of shear area (core areas are not considered)

The above approach was used by Blass et al (1994). Blass (1995) used the same relationship for the shear block failure, but added a second condition based on the embedding strength.

„However, the shear block failure occurs only if the embedding strength of the wood in front of the connector is sufficiently large. Otherwise embedding failure will govern the load-carrying capacity of the connection, as it will with larger end distances.“

The working draft for EC 5-1-1 (June 1999), section 8.9 – „Connections made with ring connectors“, is based on the above publications. It reads:

„For connections made with ring connectors of type A (timber to timber) according to prEN 912, the characteristic load-carrying capacity for a force along the grain,  $R_{o,k}$  per ring and shear plane is given by:

$$R_{o,k} = \min \begin{cases} k_1 \cdot k_2 \cdot k_3 \cdot 35 \cdot d_c^{1,5} \\ k_1 \cdot k_3 \cdot 31,5 \cdot d_c \cdot h_e \end{cases}$$

with:

- $d_c$  ring diameter, in mm (corresponds to out-side diameter)
- $h_e$  embedding ring depth, in mm ( $2 \cdot h_e = h_c =$  equal to ring depth)
- $k_i$  modification factors“

The values of

$$R_{o,k} = \begin{cases} 35 \cdot d_c^{1,5} & \text{(shear failure mode)} \\ 31,5 \cdot d_c \cdot h_e & \text{(embedding strength)} \end{cases}$$

are valid for a timber to timber connection with:

- thicknesses of members: central member =  $2,5 \cdot h_c = 5 \cdot h_e$
- thicknesses of members: side member =  $1,5 \cdot h_c = 3 \cdot h_e$
- end distance: in tension  $a_{3,t} = 2 \cdot d_c$
- end distance in compression  $a_{3,c} = 1,2 \cdot d_c$  (non-loaded end)
- spacing (with force along the grain)  $a_1 = 2 \cdot d_c$
- timber density  $\rho_k = 350 \text{ kg/m}^3$

The values are – for the above conditions – the same for forces acting in compression or in tension. With changing end distance the tension values may decrease or increase, i.e. that an increase (only in tension!) is possible, if the second condition (embedding strength) is not governing.

The characteristic load-carrying capacities given in the draft of EC 5-1-1 are – compared with the actual used in Switzerland – about 40 % higher. Even if the assumptions are not quite the same, i.e. end distance of  $1,8 \cdot d_c$  instead of  $2 \cdot d_c$ , the differences seemed important. This fact alone would not justify to disagree with the EC5-proposal, but the possible assessment of higher loads in tension than in compression is in complete disagreement with our actual knowledge!

## 4 Test conditions

Test conditions should reproduce the effective conditions in the structure. When testing ring connections (and also other connections) this has not been enough considered or verified. The normal case of testing only one, isolated ring under centric tension or compression forces can not represent the behaviour of a joint, above all when the joint is very sensitive to so-called secondary effects.

The design of connections should take into account the forces resulting from the global analysis assuming framed systems. Often a simplified analysis of the structure is done, and by code allowed, i.e. for fully triangulated trusses, where every node is assumed pin-jointed. For loads acting on the nodes, only axial forces will than be determined in the truss-members. Splice joints will therefore only be designed for axial forces, without taking into account the so-called secondary moments, which are present and would appear by using a more appropriate structural model. The problem is here that the secondary moments are not needed to achieve a static equilibrium state, but since they may have an adverse effect on the load-carrying capacity of a splice joint, they have to be taken in account for the splice joint design.

Furthermore the test procedure should take in account the standard of workmanship likely to be achieved. Misalignment of connectors and fabrication tolerances between connectors can not be considered, when testing only a single, isolated connector.

Simplified tests using the unified test procedure with two connectors in line have been postulated and used by Graf (1944) and Egner (1957). It seems that their recommendations meanwhile went forgotten.

For splices of members which are normally subjected to normal forces and small bending moments, the combined testing, using different grades of excentricity has been postulated and used by Gehri (1981/1982) in connexion with investigations on lattice trusses. Mischler (1998) made further tests with the same type of fasteners.



## 5 Types of load transfer

Differences of behaviour of wood – in function of the load direction – are often not enough taken in consideration. Forces are not only transferred along the grain. Notches or in general, variations of the section, lead to a local deviation of the force direction, resulting locally into strains and stresses in other directions.

In figure 5.1 are presented the results of tests published by Karlsen (1967), which show the effect of load direction on the load-carrying capacity of a notched specimen.

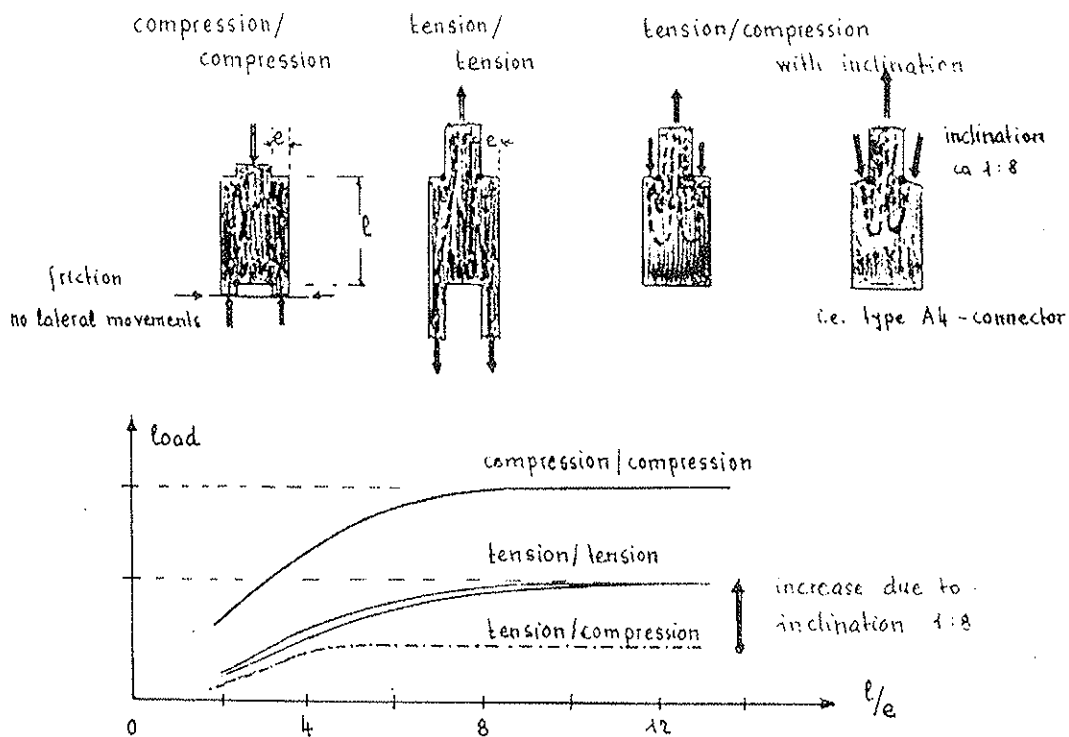


Figure 5.1: Influence of load direction on load-carrying capacity

It can easily be seen that the case of compression compared to tension leads to a much higher efficiency, or to a lower reduction. Increasing the relationship  $l/e$  above a value of 8 to 10 has quite no influence; the failure starts at a point of high local strain. In the case of compression – due to the testing procedure – friction at the support occurs, resulting in a restraint of lateral movements, creating a beneficial compression perpendicular to grain.

For ring connectors in tension load transfer is less favourable since the lines of force have to change their direction. For the case of tension/compression, the load-carrying drops therefore considerably. For optimized shapes of the ring connector the load will be introduced with an inclination of about 1:8, resulting in a higher load-carrying capacity, but still lower than for the case compression/compression.

## 6 Eurocode 5 – supporting research

### 6.1 General

The research made at Karlsruhe should support the strength models proposed for Eurocode 5-1-1 and given in chapter 3. Blass et al (1997) published the results of a large number of tests and compared these results with the code proposal.

Before going into the supporting research, three remarks should be made relative to the code proposal, remarks presented at the PT-meeting in Bordeaux ( 25th and 26th May 1999):

- The characteristic load-carrying capacity is the lower of two equations, but generally only one equation is determinant.

As can be seen from figure 6.1 the embedding capacity for timber to timber connections, for compression and for tension ( $a_{3,t} = 2 d_c$ ) leads to compare  $d_c^{0,5}$  to  $0,9 \cdot h_e$ .

<p>strength model</p> $R_o = \begin{cases} f_v \cdot A_s & \text{- shear capacity} \\ f_h \cdot d_c \cdot h_e & \text{- embedding capacity} \end{cases}$	<p>design equations</p> $R_{o,k} = \min \begin{cases} k_1 \cdot k_2 \cdot k_3 \cdot k_4 \cdot k_5 (35 \cdot d_c^{1,5}) \\ k_1 \cdot k_2 \cdot k_3 \cdot k_5 (31,5 \cdot d_c) \cdot h_e \end{cases}$ <p>[per ring and shear plane]</p>									
<p>Which case determinant? (for timber to timber <math>k_4 = 1</math>)</p> <table style="margin: auto; border-collapse: collapse;"> <tr> <td style="border: none; text-align: center; padding: 5px;">shear</td> <td style="border: none; text-align: center; padding: 5px;">embedding</td> <td style="border: none;"></td> </tr> <tr> <td style="border: none; text-align: center; padding: 5px;"><math>k_1 \cdot k_2 \cdot k_3 \cdot k_5 \cdot 35 \cdot d_c^{1,5}</math></td> <td style="border: none; text-align: center; padding: 5px;"><math>k_1 \cdot k_3 \cdot k_5 \cdot 31,5 \cdot d_c \cdot h_e</math></td> <td style="border: none;"></td> </tr> <tr> <td style="border: none; text-align: center; padding: 5px;"><div style="border: 1px solid black; display: inline-block; padding: 2px;"><math>k_2 \cdot d_c^{0,5}</math></div></td> <td style="border: none; text-align: center; padding: 5px;"><div style="border: 1px solid black; display: inline-block; padding: 2px;"><math>0,9 \cdot h_e</math></div></td> <td style="border: none; vertical-align: middle;">for <math>d_c</math> and <math>h_e</math> see prEN 912</td> </tr> </table>		shear	embedding		$k_1 \cdot k_2 \cdot k_3 \cdot k_5 \cdot 35 \cdot d_c^{1,5}$	$k_1 \cdot k_3 \cdot k_5 \cdot 31,5 \cdot d_c \cdot h_e$		<div style="border: 1px solid black; display: inline-block; padding: 2px;"><math>k_2 \cdot d_c^{0,5}</math></div>	<div style="border: 1px solid black; display: inline-block; padding: 2px;"><math>0,9 \cdot h_e</math></div>	for $d_c$ and $h_e$ see prEN 912
shear	embedding									
$k_1 \cdot k_2 \cdot k_3 \cdot k_5 \cdot 35 \cdot d_c^{1,5}$	$k_1 \cdot k_3 \cdot k_5 \cdot 31,5 \cdot d_c \cdot h_e$									
<div style="border: 1px solid black; display: inline-block; padding: 2px;"><math>k_2 \cdot d_c^{0,5}</math></div>	<div style="border: 1px solid black; display: inline-block; padding: 2px;"><math>0,9 \cdot h_e</math></div>	for $d_c$ and $h_e$ see prEN 912								
<p><math>k_2 =</math> for tension <math>\approx 0,75</math> to <math>1,25</math> <span style="margin-left: 20px;">▽</span>          for compression <math>k_2 = 1,0</math> <span style="margin-left: 20px;">○</span>      <math>k_2 = 1 \rightsquigarrow a_{3,t} = 2 d_c</math></p>										

Figure 6.1: Relationship between „shear“ and „embedding“

When introducing the values for  $d_c$  and  $h_e$  according to prEN 912 (see figure 6.2) it can be seen that shear is the governing failure mode.

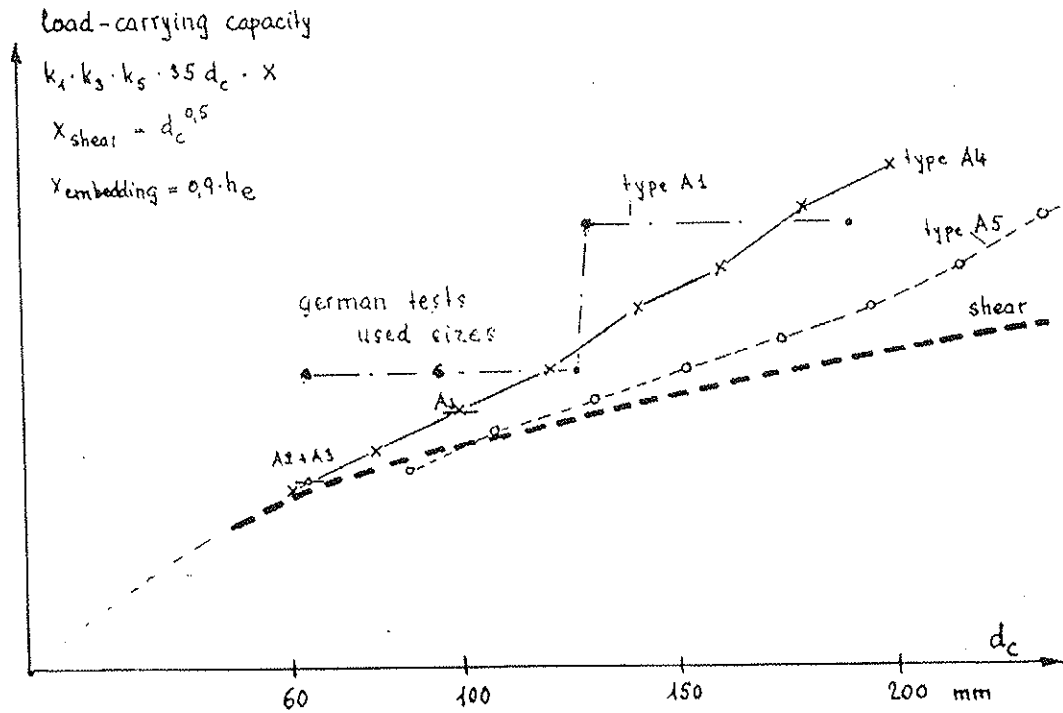


Figure 6.2: Governing failure mode for ring connectors

- To limit the capacity of connector on the „shear“ failure value, means that no use of the higher „embedding“ capacity is possible.

This can be the case above all for connectors of type A1, generally used in Germany, but normally only on compression. A typical load-displacement curve is shown in figure 6.3. A first peak appears after a displacement of about 2 to 3 mm. With the shearing away of the cores (normally 2 of the 4 cores) the load diminishes (displacement controlled test procedure) but can be increased afterwards. The maximum load may be reached after a total displacement of 10 to 15 mm.

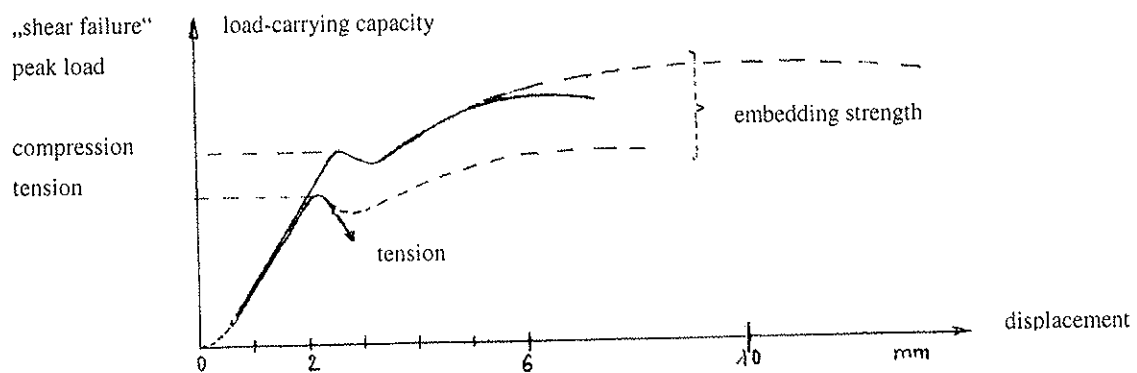


Figure 6.3: Idealized typical load-displacement curve on compression

The first peak load corresponds to the „shear“ failure load (first equation expressed by  $d_c^{1.5}$ ). Then the load can be increased up to the ultimate load, here expressed by the „embedding“ failure mode (second equation of EC 5-1-1, expressed by  $b_c \cdot h_c$ ).

Therefore not the minimum value but the higher value representing the more ductile failure mode „embedding“ should be used.

- The characteristic load-carrying capacity in tension is higher than for the same configuration in compression.

This would be a novelty in timber connections. The reason for that is that  $k_2$  can only for tension joints be increased to 1,25. Since  $k_2$  only appears in the first equation („shear“ failure) and the higher „embedding“ load on compression cannot be used – see foregoing remark – this is correct but not evident.

Based on these remarks a revision is needed. Justification will be given based on the supporting research made by Blass et al (1997), on verification tests made by Gehri (1999) and on the basic investigation made by Scholten (1944).

In the summary of Blass et al (1997) is written in relation to ring connectors:

*„In Hinblick auf die Harmonisierung der europäischen Normen werden Rechenmodelle vorgeschlagen, um die charakteristische Tragfähigkeit von Dübeln besonderer Bauart bestimmen zu können. Hierbei werden die jeweiligen Versagensmechanismen (Nachweis der Lochleibungsfestigkeit und der Scherfestigkeit des Holzes) untersucht. Bei mehr als zwei Dübeln in Krafttrichtung hintereinander wird der in DIN 1052-2 enthaltende Abminderungsfaktor vorgeschlagen.*

*Ziel des Forschungsvorhabens war es, realistische Beiwerte zur Berücksichtigung des Einflusses der Anzahl von Dübeln besonderer Bauart in einer Verbindung und der Abstände dieser Dübel insbesondere in Faserrichtung anzugeben.*

*Die Versuchsergebnisse der **Druckscherversuche** mit Einlassdübeln (Typ A1) zeigen, dass die vorgeschlagenen Bemessungsgleichungen wirklichkeitsnahe Ergebnisse liefern. Es besteht eine geringe Korrelation zwischen Rohdichte und Traglast.*

*Für die **Zugscherversuche** wurden Prüfkörper mit einem, drei und fünf Dübeln in Krafttrichtung hintereinander liegend hergestellt. Hier zeigten sich andere als die erwarteten Versagensmechanismen. Bis auf wenige Ausnahmen spalteten die Hölzer entlang der Verbindungsmittelreihe auf, oder rissen im Nettoquerschnitt ab.*

*Aufgrund der unerwarteten Versagensmechanismen und der daraus resultierenden geringen Traglasten, sind die Versuchsergebnisse der Zugscherversuche nicht für die geplante Auswertung der Ergebnisse in Hinblick auf das Zusammenwirken mehrerer Dübel in einer Verbindung zu verwenden.“*

In the following the results published will be analysed.

## 6.2 Verification of the strength model in compression (for one ring connector)

Compression tests were only made with one ring connector. Different parameters were studied: 3 dimensions of ring connectors, thickness of timber members, effect of imperfections of fabrication and effect of density within the same species.

For the analysis of the experimental data, the strength models given in STEP-C9 were used:

- shear failure mode  $R_{\text{shear}} = f_v \cdot A_s$
- embedding strength  $R_{\text{embedding}} = f_h \cdot d_c \cdot h_c$

with  $f_{v,k} = 20 \cdot A_s^{-0.25}$   
 $f_{h,k} = 0,09 \cdot \rho_k$   
 $A_s =$  shear area outside of the core

By the test configuration no real shear failure of the material between the ring connector and the steel plates (shear area outside of the core) is possible. See also footnote 15, on page 37, from Blass et al (1997), where is written: „*Der Versuchsaufbau der Druckscherversuche lässt ein Abscheren des Vorholzes nicht zu. Der Faktor  $k_{a3}$  wird deshalb zu 1 gesetzt.*“ therefore only the second equation is valid. To fix the factor  $k_{a3}$  to 1 makes no sense, since this still allows to calculate – a wrong – shear capacity!

Only the core will shear away, after a small displacement of only 2 to 3 mm. The strength model for such a test configuration is given by the higher value of the „embedding“ failure mode as shown in figure 6.3.

Based on this, the analysis should be revised. In figure 6.4 (reproduction of Bild A3-93 in the publication of Blass et al (1997) the dashed line represents the calculated shear capacity based on the shear area outside the core; this line should now be omitted, since the test method prevents this failure.

The results should therefore be covered by the full line which represents the embedding resistance case. The calculation was made with an embedding strength of  $f_{h,k} = 0,09 \cdot \rho_k$ , value also used for EC 5-1-1.

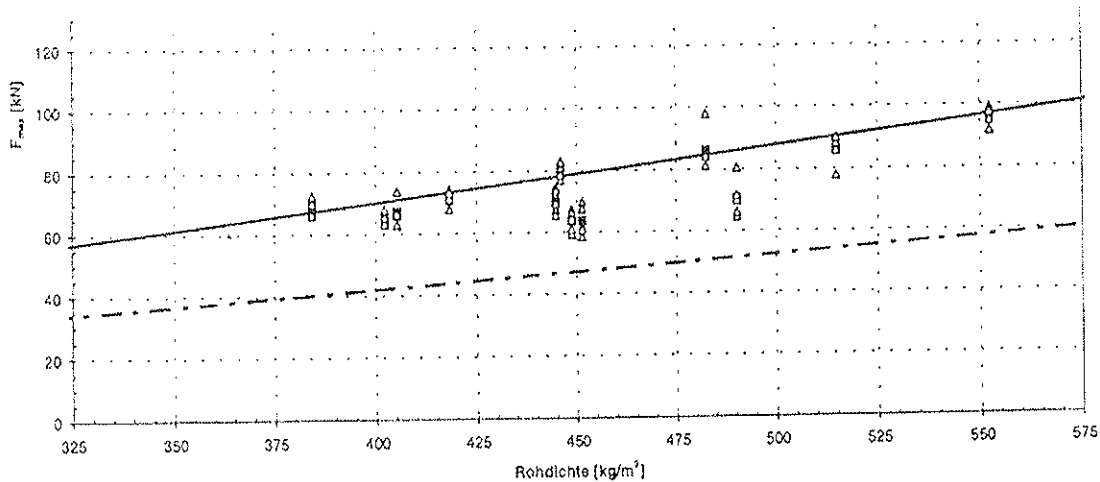


Figure 6.4: Bild A3-93; Serie A65N; from Blass et al (1997)

As can be seen from figure 6.4 the embedding strength (represented by the full line) has been overestimated by the formula of EC 5-1-1. It has to be noted here, that no allowance has been given to the contribution of the bolt.

A better approach was obtained with the test results from the serie A94 N, however the serie A128 N showed a clear overestimation.

### 6.3 Verification of the strength model in tension (for one ring connector)

The tension tests (with one ring connector) were made mainly with the smallest possible size A1-65. Only one serie was made with A1-95. The thicknesses of the members (center member  $t_2 = 75$  mm, side members  $t_1 = 45$  mm) was maintained constant through all tests.

For the size A1-65 the end distance  $a_{3,t}$  was varied from  $1,5 \cdot d_c$  up to  $3 \cdot d_c$ , for size A1-95 the end distance was taken to  $2 \cdot d_c$ .

As discussed before (see chapter 3) the same strength models as for compression are used. In case of tension the condition to consider the minimum value of both equations is normally correct. Furthermore the value of embedding strength given by the second equation is in any case too high.

The verification is to be done with the „shear“ capacity equation

$$R_{\text{shear}} = \frac{a_{3,t}}{2d_c} \cdot 35 d_c^{1,5}$$

The analysis of serie A65Z1 C is presented in figure 6.5. In this serie the end distance was  $a_{3,t} = 2,5 \cdot d_c$ ; therefore and according to the code proposal the load-carrying capacity in tension will increase by 25%! As can be seen from figure 6.5 (reproduction of Bild 4-14) the strength mode overestimates the shear capacity by about 40%. Instead of  $R_{\text{shear}} = 1,25 \cdot 35 \cdot d_c^{1,5}$  a value of  $R_{\text{shear}} = 1,25 \cdot 25 \cdot d_c^{1,5}$  seems to be adequate.

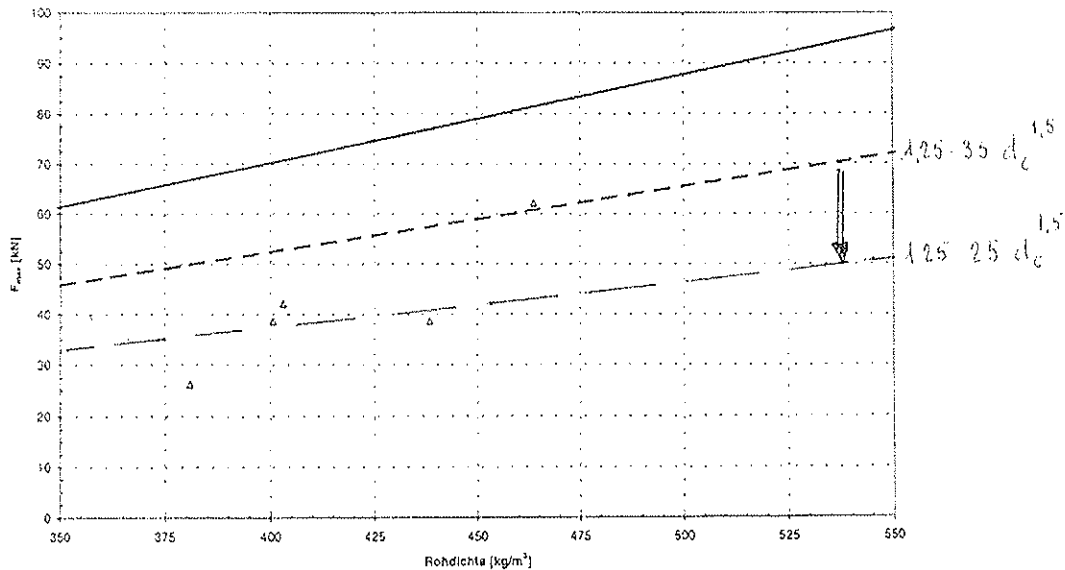


Figure 6.5: Bild 4-14 from Blass et al (1997)

The reason for such discrepancy has been found by the authors in the insufficient thickness of the side members. They showed up that the till now used practical rule „design the side members only on pure tension in the net section, but for a 50 % higher force“ gives unsafe results. Through an inappropriate strength verification (without taking in account the equilibrating effect of the bolt!) made on a side member of section 45/80 mm<sup>2</sup> for type A1-65, it could be shown that the strength was overestimated by a factor of 2,592!

The verification was based on the german allowable load of 23 kN per pair of connectors. The mean load-carrying capacity in the tests varied between 37,2 kN (serie A) and 57 kN(serie D). The dimension of the side member was in all 4 series the same. If determinant, why the large increase? According to „genauerer Nachweis“, the end distance has no effect on the verification of the section of the side member. The value of 57 kN would give a mean „safety“ value of about 2,5 regarding the allowable load of 23 kN.

## 7 Verification tests

### 7.1 Approach

Only a small number of tests should be made. Since the density of the timber may play an important role, similar densities were used for center and side members. The dimensions used for the timber members correspond to normal practice in Switzerland. The tests would be done only with 1 connector.

The idea behind these tests was to verify:

- difference in behaviour in tension and compression
- influence of test procedure in compression (direct support or adoption of a recess)
- contribution of bolt (central member with oversize hole of 25 mm for M16 bolt).

## 7.2 Compression tests

The following configurations (see figure 7.1) were used. For each configuration 3 specimens were prepared. They differed only by density. The differences were small (less than 10 %) and had a similar distribution for each configuration; therefore the middle values could be directly used for comparison.

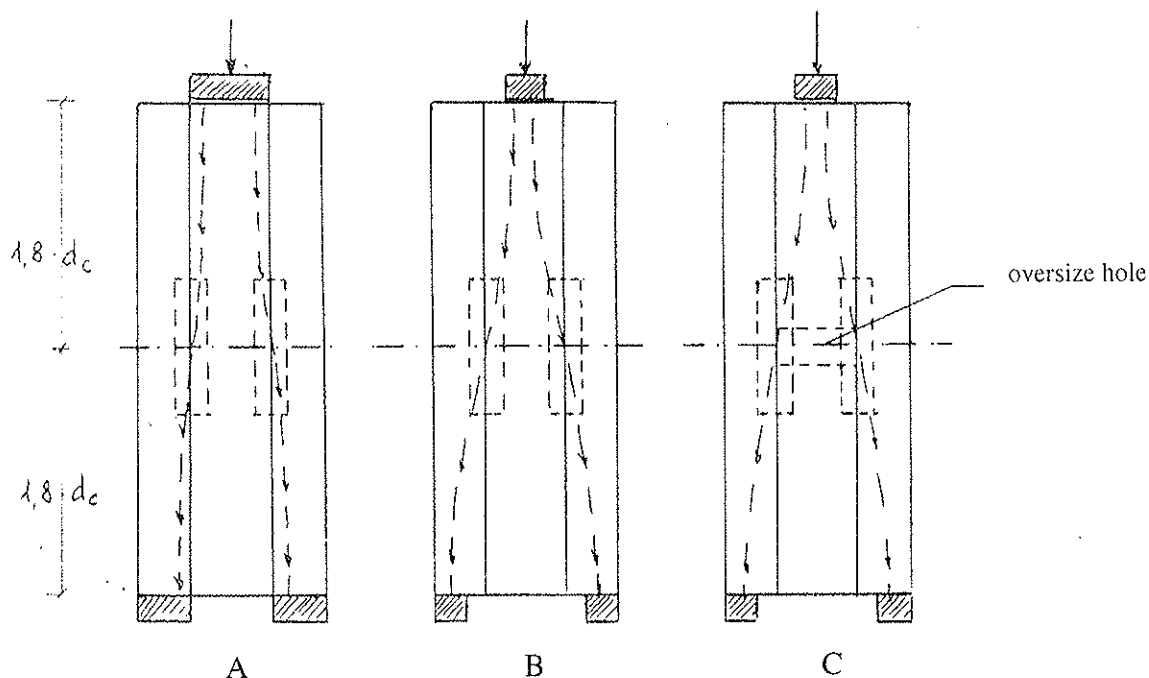


Figure 7.1: Test configuration

They show a slight difference between configuration A and B, as well as between B and C (see table 7-1).

ultimate load (in kN)	test configuration		
	A	B	C
mean of 3 tests	138	132	130

Table 7-1: Test results in compression

It has to be noted that at a slip of 2 mm the cores sheared away; afterwards the support conditions of the bolts change. For configuration C only a small action of the bolt is possible, since the maximum load corresponds to a slip of 6 to 9 mm.

The small differences verified (about 5 %) between the three configurations are mainly due to more favorable supporting conditions of A. The failure mode was always the same: the core sheared away at a slip of 2 mm, followed by crushing of the timber before core.

A direct equilibrium of the compression forces is therefore possible (see figure 7.2). The surrounding material has mainly stabilizing function. This can also be seen from the



german tests of Blass et al (1997). Using central and side members of 3/4 of the normally used, they found less than 10 % decrease in the load-carrying capacity.

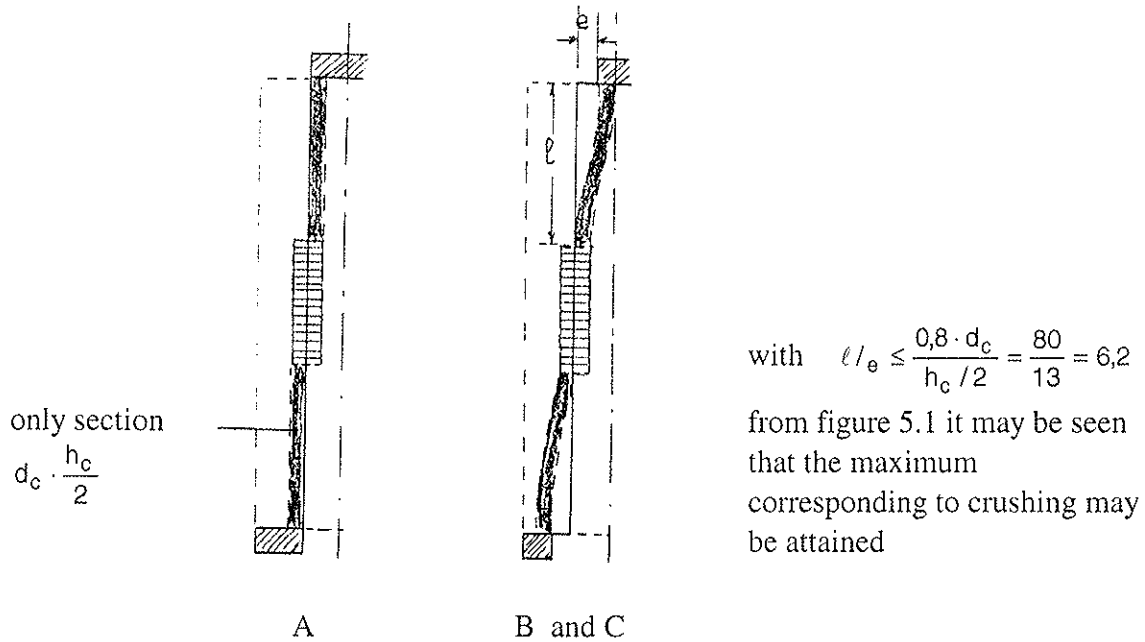


Figure 7.2: Transition of force in compression

As long as for test configurations B and C the relationship  $l/e$  is large enough (about 6 to 7 for this species of wood) only the embedding strength model should be considered.

### 7.3 Tension tests

The tests were made with a splice joint or a double joint; when comparing with the compression values, it has to be noted that in tension only the lower of two test values is known. Timber elements had the same size as used in compression. Test results are given in table 7-2.

ultimate load (in kN)	test configuration	
	B	C
mean of 3 tests	79,7	69,4

Table 7-2: Test results in tension

The reduction of more than 10 % for the configuration C is due partly to the smaller core area and partly to the smaller net section (only of the center members).

The maximum load corresponds only to a slip of less than 2 mm. Different failure modes were noticed: tension failures of center or of side members; splitting and shearing of side members.

## 5 Conclusions

The test results published by Blass et al (1997) can not sustain the proposal given in Eurocode 5-1-1.

The load-displacement curves in tension and compression show the need for differentiation (see figure 6.3):

- shear failure (corresponding to the first peak load) is about 15 % lower in tension than in compression;
- in compression an increase can be found, as long as the embedding strength has not been reached; this is the case for the smaller ring dimensions but no more for larger ring connectors;
- in tension the first peak load corresponds normally to the ultimate load; only for large end distances and small ring dimensions ( $d_c$  about 60 to 80 mm) an increase could be found.

In tension splices brittle fractures may be avoided by using:

- larger dimensions of the members (= low efficiency of the joint)
- end distance  $\geq 2,5 \cdot d_c$  ; spacing  $\geq 2,3 \cdot d_c$  ;
- the smallest connector size.

Actual proposal in Eurocode 5-1-1 leads for tension splices to unsafe design. Furthermore no evidence could be found for the 25 % higher load-carrying capacity of a ring connector in tension (for end distance  $2,5 d_c$ ) compared to compression.

## Bibliographie

- Blass H.J., Ehlbeck J., Schlager M.: Strength and stiffness of ring and shear-plate connections. Holz als Roh- und Werkstoff, 1994, p. 71-76.
- Blass, H.J.: Verbindungen mit Einlassdübeln. STEP C9, 1995
- Blass, H.J./ Ehlbeck J./Krämer V./Werner H.: Sicherheitsrelevante Untersuchungen zum Trag- und Verformungsverhalten von mehreren in Krafrichtung hintereinanderliegenden Dübeln besonderer Bauart. Versuchsanstalt für Stahl, Holz und Steine, Uni Karlsruhe, 1997.
- Egner, K.: Prüfung von Holzkonstruktionen. Handbuch der Werstoffprüfung, Dritter Band: Prüfung nichtmetallischer Baustoffe. Springer 1957.
- Gehri, E.: Fachwerkträger aus Buche und Fichte mit Stahlknotenplatten in eingeschlitzten Hölzern. Publikation Nr. 82-1, Baustatik und Stahlbau, ETH Zürich, 1982.
- Gehri, E.: Documentation for PT-meeting, May 99, Bordeaux.
- Graf, O.: Versuche über die Widerstandsfähigkeit von Knotenpunktverbindungen aus Bauholz. Der Bauingenieur, 1930, S. 277-282.
- Graf, O.: Dauerfestigkeit von Holzverbindungen. Mitteilungen des Fachausschusses für Holzfragen beim VDI und Deutschen Forstverein Nr. 22, 1938.
- Graf, O.: Vergleichende Untersuchungen mit Dübelverbindungen. Die Bautechnik, 1944, S. 23-32.

- Mischler, A.: Bedeutung der Duktilität für das Tragverhalten von Stahl-Holz-Bolzenverbindungen. Publ. Nr. 98-1, Holztechnologie, ETH Zürich, 1998.
- Perkins N.S., Landsem P., Trayer G.W.: Modern connectors for timber construction. 1933.
- Scholten, J.A.: Timber-connector joints. Their strength and design. Forest Products Laboratory. Technical Bulletin No. 865 March 1944.

**INTERNATIONAL COUNCIL FOR RESEARCH AND INNOVATION  
IN BUILDING AND CONSTRUCTION**

**WORKING COMMISSION W18 - TIMBER STRUCTURES**

**NON-METALLIC, ADHESIVELESS JOINTS FOR TIMBER STRUCTURES**

R D Drake

M P Ansell

Department of Materials Science and Engineering

University of Bath

C J Mettem

R J Bainbridge

TRADA Technology

UNITED KINGDOM

**MEETING THIRTY-TWO**

**GRAZ**

**AUSTRIA**

**AUGUST 1999**

---

Presenter: M.P.Ansell

- H.J.Blass asked how were the dowels installed.
- M.P.Ansell responded that the dowels were installed using a press.
- H.J.Larsen commented that this was an interesting test material and asked about the bending properties of the dowel.
- M.P.Ansell responded that the dowels were tested in shear mode to obtain their "bending" properties. It was felt that this mode of testing was appropriate after observing the failure mode of the dowels in a joint.
- H.J.Larsen commented that the use of Johansen theory based on shear failure might not be appropriate
- F.Lam asked whether there were plans to conduct cyclic tests.
- M.P.Ansell responded that at the moment no cyclic tests of the connection were available but there were fatigue test results in other applications.
- H.J.Blass asked about the cost of the dowels.
- M.P.Ansell responded that the cost were similar to steel.
- H.J.Blass asked about the reserved capacity in relation to the observed shear failure.
- M.P.Ansell responded that the dowel is irreversible at high loads.
- A.Jorissen asked about the post peak load response and failure mechanism.
- M.P.Ansell responded that the connection would absorb significant amount of energy at high loads based on its failure mechanism.
- E.Karacabeyli asked whether this dowel could be made into a bolt.
- M.P.Ansell responded that it would be possible.

# NON-METALLIC, ADHESIVELESS JOINTS FOR TIMBER STRUCTURES

RD Drake\*, MP Ansell\*, CJ Mettem\*\* and RJ Bainbridge\*\*

\*Department of Materials Science and Engineering, University of Bath, UK

\*\*TRADA Technology, UK

## Abstract

The construction of wide-span timber structures is strongly dependent on the effective design of joints, which are usually fabricated from steel plates, bolts and dowels. Such joints tend to be heavy, costly, prone to corrosion and vulnerable to fire with poor aesthetic qualities. This paper investigates the potential for replacing steel fasteners with non-metallic elements based on fibre-reinforced plastic pultrusions for the design of medium- to large-scale timber structures. Techniques have been developed for calculating the load bearing capacities of a range of non-metallic joints including stress analysis using finite element methods. Non-metallic joints for wood composites have been manufactured using friction-fitted, reinforced plastics in the form of dowels and plates. The reliability of these techniques has been confirmed by full scale laboratory testing of components and jointed structures under static and dynamic loads in double shear, bending, tension and moment-resisting configurations.

Non-metallic fasteners and fittings for laminated veneer lumber (LVL) joints have been found to embody significant advantages compared with standard steel fasteners. The performance of glass-reinforced plastic (GRP), pultruded dowels and steel dowels have been compared and finite element- (FE-) modelled in double shear. Failure loads for GRP pultruded dowels are marginally higher than those for steel dowels and in the former case damage occurs in the dowel and the LVL rather than in the LVL alone. Moment-resisting joints based on friction-fitted, GRP dowels are capable of absorbing more energy than joints secured by steel dowels and this ductility is a key outcome of the research. Eurocode 5 design equations for steel dowels have been modified for pultruded GRP dowels and the concept of a cross breaking strength has been developed for design purposes. The paper reviews the results of research funded by the UK Engineering and Physical Sciences Research Council.

## 1. Introduction

Structural timber composite (STC) technology based on construction with LVL (laminated veneer lumber) and glulam (glue-laminated timber) is being developed in the UK (Milner and Bainbridge, 1997 and Bainbridge and Mettem, 1997). Timber buildings that are constructed from these materials usually comprise individual, pre-fabricated members which are delivered to site and connected with metal fasteners (such as nails and bolts) and metal hardware (such as steel gusset and insert plates). These metal fasteners and hardware are expensive in both design and manufacturing time (the work is often sub-contracted to other companies) and can be difficult to fit accurately on site. Research reported in this paper concerns the joining of LVL which comprises laminae of approximately 3-4mm in thickness, pressed and bonded together to provide a STC material with very uniform properties. The length of these LVL members is limited only by transport constraints.

Following the introduction of Eurocode 5 (BSI, 1994) the timber construction industry now has an improved chance to move toward the next century by embracing new technologies and using innovative materials. The use of non-metallic joints offers a lightweight and stable alternative to metal fasteners and hardware. Unlike bolted and nailed joints, non-metallic joints are not degraded by corrosive atmospheres and their fire resistance is good. Such joints can provide a lightweight and mass producible alternative to traditional steel fastened designs. The connecting system is potentially cheap, easy to handle and can be machined in woodworking factories and on site.

The aims of the research were to design, manufacture and test non-metallic, adhesiveless joints suitable for medium- and large-scale timber structures and to develop techniques for calculating the load bearing capacities of such joints in association with finite element methods. Non-metallic joints in wood composite structures were to be manufactured using reinforced plastics in the form of dowels and plates. The reliability of the proposed techniques was to be confirmed by full-scale laboratory testing of components and jointed structures. It will be shown that dowels made from pultruded composite materials perform comparably, if not better, than steel dowels in the same situation.

## **2. Pultruded composites**

Pultruded composite materials were selected as the principal material for investigation. These materials offer all of the properties of other high quality, unidirectionally reinforced composite materials such as high specific strength and stiffness but possess the advantage of mass production. The pultrusion technique is a closed mould technique for the manufacture of fibre/matrix composites and is one of the few fully automated continuous processes used in the reinforced plastics industry (Holloway, 1989). Pultrusion involves incorporating fibres such as glass, aramid or carbon into a range of high performance resins producing a continuous product. It is a process analogous to the extrusion of plastics and non-ferrous metals in that the pultruded profile is shaped by the continuous passage of the feedstock through a forming die (Eckold, 1994). In the case of pultrusion, the reinforcing fibres themselves are used to pull the material through the die.

Glass fibre reinforcements in the form of unidirectional fibres or woven fibre mats are drawn from spools into the pultrusion die via a 'wet bath trough'. The bath 'wets out' the reinforcements with resin before they are drawn through a pultrusion die. Guide plates are generally used in front of the die to pre-form the reinforcement to the desired shape. Within the die, impregnation and consolidation occur as the resin around the reinforcements reaches the curing temperature. The rate of throughput is adjusted so that the curing of the material is essentially complete by the time the product emerges from the die. Many profiles can be produced with varying fibre and resin combinations such as phenolic resins that provide better stability at high temperatures which may occur for example in fire hazard conditions.

## **3. Research strategy**

The interaction between timber and pultruded fasteners was investigated in comparison with timber and steel fasteners in a series of embedment tests (20 tests). The performance of GRP pultrusions in double shear tests was also examined as a basis for three-dimensional FE modelling exercises. Tests were conducted to establish the effect of scale

and relative slenderness by varying the size of timber (42 tests) and the diameter of the pultruded dowel (25 tests). The effect of the arrangement of multiple dowels on strength and energy absorbing capabilities of double shear joints was established by varying the number of rows and columns of dowels (75 tests), demonstrating markedly different behaviour compared to similar arrangements of steel dowels. Following this stage of experimental work the relevant sections of Eurocode 5 were re-examined in order to make modifications to design equations reflecting the mechanical response of the new connector material in double shear timber to timber joints.

Developmental joints were manufactured starting with in-line plate and dowel type joints. Initial test results (32 tests) demonstrated that splitting of the LVL was a major shortcoming of this joint type. Discussions with TRADA Technology and Gordon Cowley of Cowley Structural Timberwork Ltd. led to the development of three-piece moment resisting joints which are commonly used in column to rafter connections. The emphasis of the final phase of the research was placed on the optimization of these full-scale moment resisting joints (40 tests) in terms of placement and number of dowels in contrast with steel-connected joints. The following sections explain how these objectives were achieved and the technological advances made.

#### **4. The basis for the design of non metallic joints**

The major thrust of the research was to develop non-metallic, adhesiveless connections for timber structures. A thorough review of the relevant timber engineering and composites literature was undertaken which indicated that glass fibre reinforced plastic (GRP) pultrusions in plate and rod form offered the most cost-effective and structurally sound solution for achieving coherent connections as a promising replacement for steel. Other materials such as carbon and Kevlar fibre-based composites possess excellent mechanical properties but in this work were ruled out on the basis of expense. Hand lay-up methods for forming composite elements were judged to be too time-consuming, imprecise and costly.

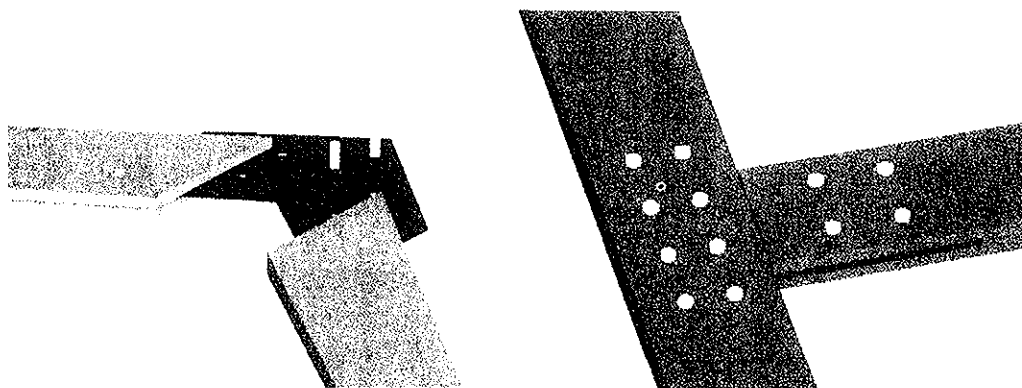


Figure 1. Proposed plate and dowel joint types, (a) knee joint, (b) T-joint.

Kerto laminated veneer lumber (LVL) was selected as the substrate timber for all tests because of its regular laminated structure and consistent mechanical properties. It was important to assess variability in the performance of the joints rather than the variability of the timber. Pultruded GRP was purchased from commercial suppliers. These pultruded dowels were examined by optical and electron microscopy after sectioning and polishing

and found to have a typical fibre volume fraction of 63%. It was envisaged that composite joints based on existing steel connected configurations would be manufactured using GRP plates slotted into the LVL and secured by friction-fitted dowels in in-line, knee and T-piece configurations, eg. Figure 1.

### 5. Calculation of load bearing capacities in non-metallic joints

In the first instance it was necessary to understand the interaction between composite dowels and LVL in simple double shear. A series of double shear tests were performed on pultruded dowels to make a direct comparison with steel dowels, Drake *et al* (1996). Three methods were used to characterise pultruded dowels, namely embedment tests, relative slenderness tests and multiple dowel tests. Embedment tests were conducted using the apparatus shown in Figure 2.

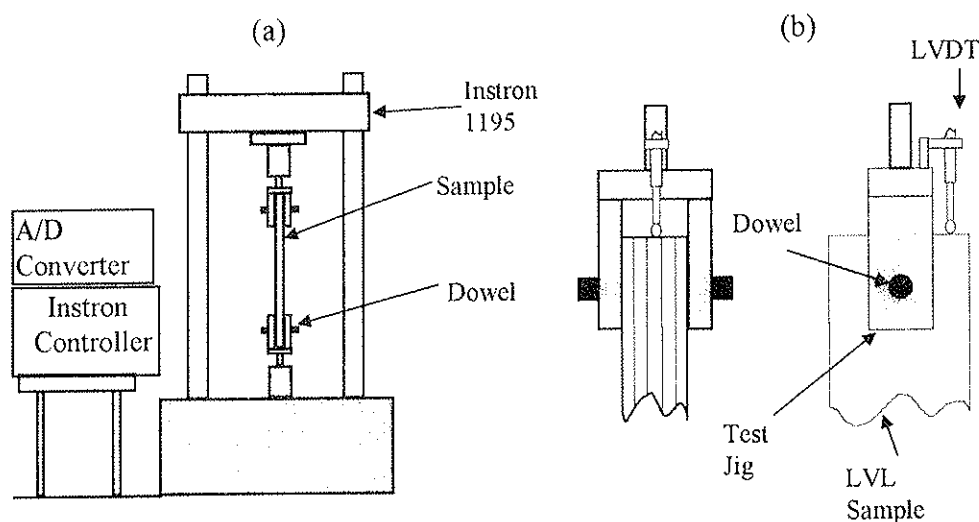


Figure 2. (a) Instron test apparatus and (b) specimen set-up.

All of the tests were carried out on a NAMAS calibrated Instron 1195 machine with a 100kN load-cell. The testing jig was constructed according to CEN (1993) and can be seen in more detail in Figure 2(b). Samples were made from Kerto LVL and dimensioned according to test piece B in CEN (704mm x 96mm x 39mm thick). The dowels were made from 16mm diameter rod and were driven through the sample centrally 112mm from the end. Dowels (pultruded and steel) of greater than 8mm in diameter were hammered into the joints using an interference type fit to improve initial load slip behaviour. Pultruded dowels of 8mm and below were pressed into place to avoid impact damage caused by hammering.

Samples manufactured with mild steel and pultruded FRP dowels were both loaded in two patterns. Pattern 1 was a straight ramp to failure. Pattern 2 consisted of an initial ramp to 40% of the specimen failure load, followed by a hold of 30 seconds, then a drop to 10% of the failure load, followed by another hold of 30 seconds and then a ramp to failure. Pattern 2, defined in CEN (1993), was used to establish the embedment characteristics of the system and also to eliminate any initial load take up. Loads were applied using the Instron 1195 and recorded every 250 milliseconds using a Marandy MR1004 Analogue to Digital converter. Sample deformation relative to the jig was measured using two LVDT



transducers at each end of the sample, which in turn was recorded by the Marandy unit. The data could then be processed using a PC.

### 5.1. Results for steel dowel in LVL, test pattern 1

Following initial compression of the LVL below the lower dowel the LVL cleaved vertically along the central plane which in turn formed a central crack downwards below the dowel. On studying the upper dowel, where the failure did not occur, crushing of the wood was observed around the top of the dowel in a uniform manner through the thickness of the sample. This suggested that the dowel did not flex extensively under loading (Figure 3). The peak forces reached for the four samples tested were 22.0kN, 21.5kN, 23.0kN and 22.5kN. The steel dowel appeared to be undamaged.

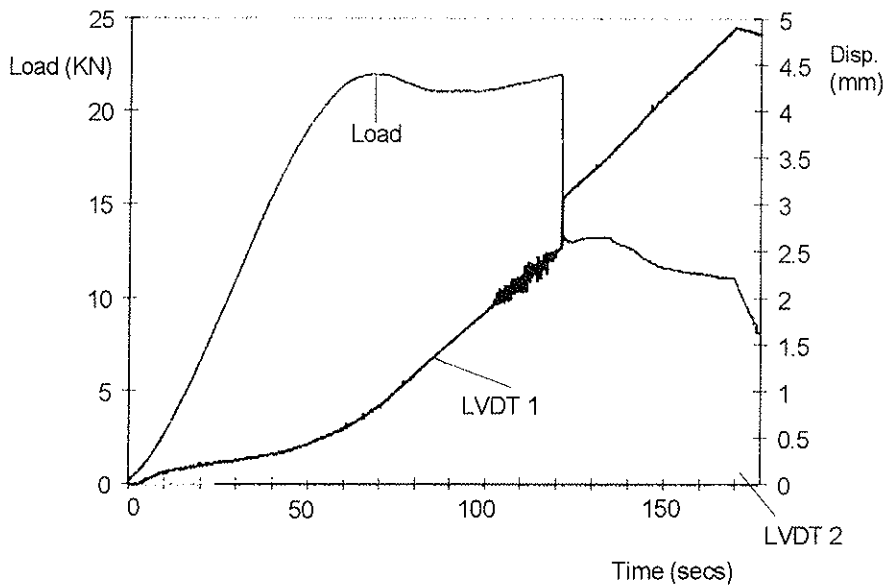


Figure 3. Double shear test for steel dowel in LVL, test pattern 1.

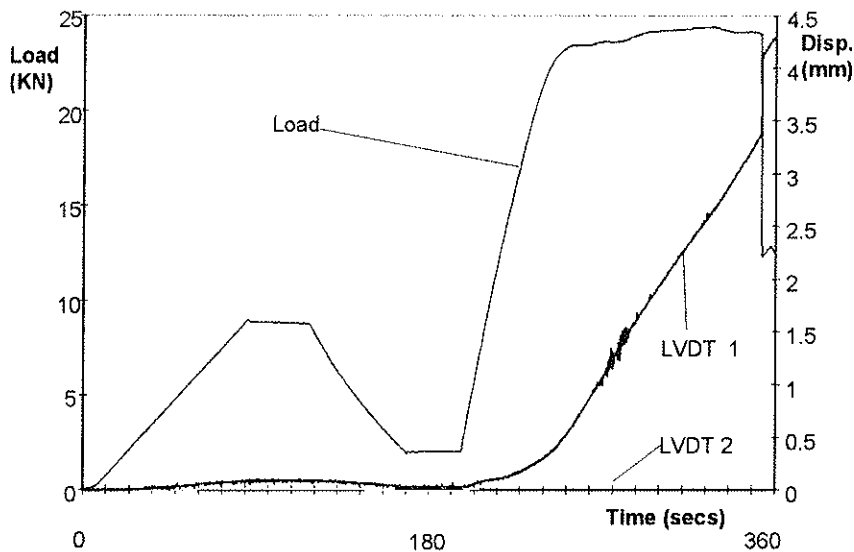


Figure 4. Double shear test for steel dowel in LVL, test pattern 2.

## 5.2. Results for steel dowel in LVL, test pattern 2

The first dwell stage of the pattern 2 test was achieved without failure although there was stress relaxation in the wood which was compensated for by adjusting the cross-head position. Very little happened in the second dwell stage (Figure 4) and the final ramp of the test culminated in a similar failure to the steel dowel in LVL, test pattern 1, but at higher load levels than before (24.8kN, 25.1kN, 25.4kN and 24.6kN).

## 5.3. Results for pultruded dowel in LVL, test pattern 1

In the case of the pultruded dowels, a similar pattern emerged to the steel dowel results, Figure 5, but the dowel was mildly damaged which initiated a different failure mode in the LVL. Instead of a centre crack forming, a central section of the LVL, approximately 10mm in width, was sheared out below the lower pultruded dowel. The LVL split longitudinally below the dowel from the edge of the dowel hole. Again, when studying the upper dowel, crushing of the wood was seen around the top of the dowel. This time however more crushing was observed near the outside edges of the sample than in the middle, suggesting that the dowel deformed under load. The peak forces reached were 24.5kN, 24.8kN, 24.1kN and 24.6kN.

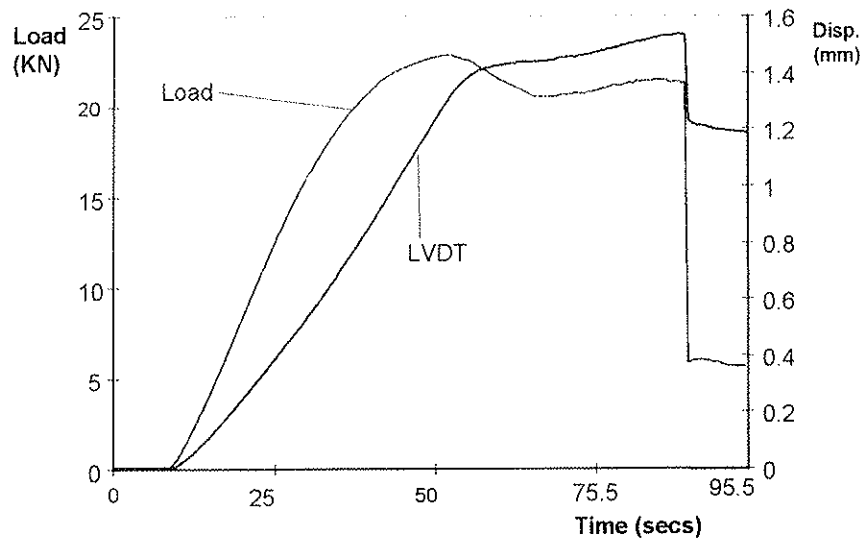


Figure 5. Double shear test for pultruded dowel in LVL, test pattern 1.

## 5.4. Results for pultruded dowel in LVL, test pattern 2

During the first three-quarters of the test (Figure 6) the pultruded dowel behaved similarly to the steel dowels in test pattern 2. In the final stage, two out of four tests behaved similarly to test pattern 1 (peak forces 25.8kN, 25.5kN) and the other two culminated in dowel failure at the interface between the steel frame and the LVL sample (peak forces of 28.5 kN, 28.1kN).

## 5.5. Dowel characterization

In order to characterize pultruded GFRP dowels and to find a modified fastener failure value for use in Eurocode 5 design prediction equations, the strength of the 16mm diameter dowels were tested in guillotine shear. The test apparatus consisted of the same test jig described previously used together with a steel central member. The specimen was loaded

to failure ensuring that the dowel was a tight fit in the hole through the test rig components. The load/time curve was again captured using an analogue to digital converter.

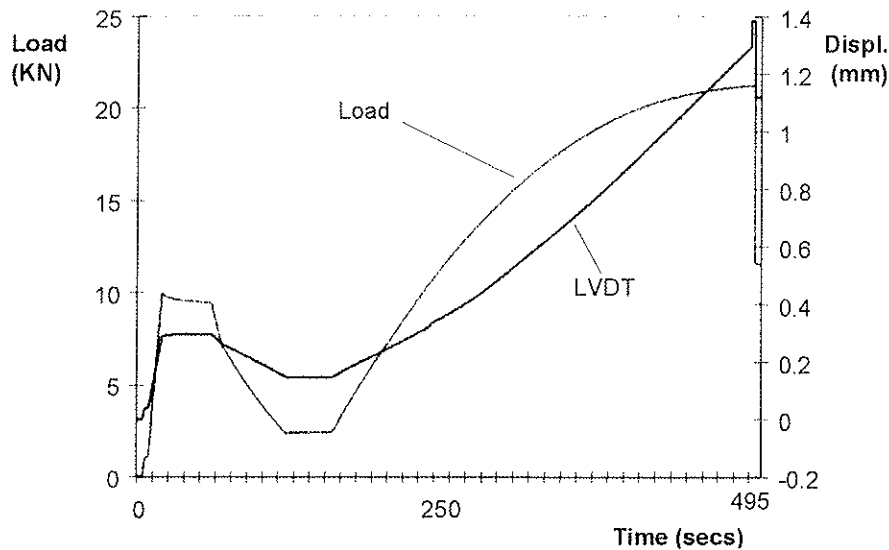


Figure 6. Double shear test for pultruded dowel in LVL, test pattern 2.

The dowels failed due to the large shearing force between the two outer members of the test piece and the central member. The steel members embedded themselves into the outer skin of the dowel causing resin failure followed by fibre shear failure. The average guillotine shear load for the dowels under test was 103MPa.

The LVL failure modes for the steel and pultruded glass fibre reinforced plastic dowels are different. In pattern 1, the steel dowels cause a large crack to propagate very quickly through the material whereas the pultruded dowels cause a lot more localized crushing near the edges of the sample. They subsequently fail by longitudinal-radial shear along ray cell planes in the adjacent veneer layers causing the central section of wood above the dowel to pull out.

For test pattern 1 the pultruded dowel samples failed at a higher load than the steel. This may relate to the difference between the flexural stiffness of the two materials. Steel, being stiffer, deflects less than the pultrusion. In what is essentially four point bend loading, the steel hardly deforms causing uniform through-thickness crushing of the wood at the top of the upper dowel and crack propagation from the bottom of the lower dowel. The pultruded dowels, however, being more compliant than the steel tend to deform under load causing localised crushing at the two outer edges of the LVL and pull out of the centre section. This is confirmed by studying Figures 5 and 6. After the specimen fails and the load drops, the dowel does not continue to pull out of the sample and increase displacement but it returns to its original shape, decreasing displacement. This is not the case with the steel dowel (Figures 3 and 4). The centre section pull out was perhaps caused by progressive damage development in the lower pultruded dowel which reduced the rate of load transfer via the LVL. The higher failure loads can be again attributed to the same phenomenon where the pultruded dowel of similar strength to steel tended to deform more, crushing the wood instead of cleaving it.

This mode of dowel deformation also explains the central member failure of the pultruded dowels in test pattern 2 at the wood/steel interface. When the pultruded dowel was studied after this type of failure annular cracks (found at the wood/steel interface position) were seen around the surface of the dowel. Smaller cracks were also seen running parallel to the fibre direction on the surface of the dowel between these two annular cracks. The appearance of the dowel suggests that failure of the joint occurred due to a partial shear failure of the dowel at the wood/steel interface.

### 5.6. Adaption of Eurocode 5 equations for pultruded dowels

The results from the embedment tests indicate that GRP dowels fail by interlaminar shear rather than the bulk plastic yield of steel dowels. So yield strength is not an applicable failure condition for GRP dowels. Furthermore the peak failure loads for pultrusions and steel are similar and the pultruded dowels are capable of absorbing significantly more energy, resulting in a more ductile joint. Accordingly it was recognised that the current failure prediction model in Eurocode 5 would not be applicable to pultruded joints. The dowel yield term in the following equation required modification.

$$M_{y,k} = 0.8 f_{u,k} d^3 / 6$$

where  $M_{y,k}$  = Characteristic yield moment of a bolt or dowel (Nmm)

$f_{u,k}$  = Mean value of the ultimate tensile and yield strength of the fastener (Nmm<sup>-2</sup>)

$d$  = Diameter of fastener (mm)

As the failure in the pultruded dowel is not a yield failure but a combination of yielding in the dowel and shear failure between the fibres and matrix, the  $f_{u,k}$  value in the previous equation was replaced with the cross breaking strength, a term based on the guillotine shear value of the material, so that the  $M_{y,k}$  expression became:

$$M_{y,k} = f_{c,b,k} d^3 / 6$$

When the failure mode predictions of this equation are compared with experimental work conducted on the effect of differing dowel size, and hence relative slenderness, on joint failure, the correlation is exceptionally good (Drake *et al*, 1998).

## 6. Behaviour of multiple pultruded dowels in double shear

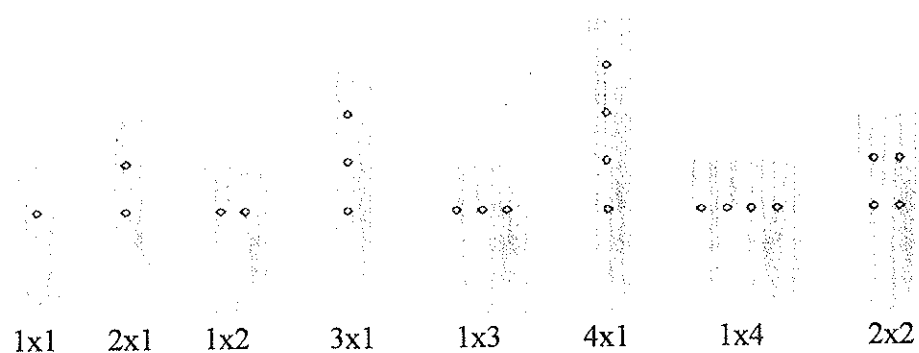


Figure 7. Dowel layout and notation for multiple pultruded dowels in double shear.

The behaviour of multiple pultruded dowels in double shear has been examined with respect to established research on group effects in multiple steel dowelled joints (Drake et al, 1999). The geometry of the dowel configurations appear in Figure 7. The test pieces comprised three elements identical to those in Figure 4, with the central element inverted, and with dowels which were pressed into pre-drilled holes with a friction fit. Load was applied to the central element in compression to impose double shear across the dowels. Typical force versus displacement characteristics are summarised in Table 1.

Joint type	Number tested	Peak force (kN)	Peak force applied per dowel (kN)	Peak shear stress (MPa)	Energy absorbed (J)
1×1	10	6.93 (±0.4)	6.93 (±0.4)	30.60 (±1.8)	115.0 (±2.8)
2×1	10	10.28 (±0.9)	5.14 (±0.4)	22.70 (±2.0)	79.7 (±4.6)
3×1	10	15.76 (±2.0)	5.35 (±0.3)	23.60 (±1.4)	64.9 (±10.3)
4×1	10	21.23 (±1.6)	5.31 (±0.4)	23.50 (±1.8)	267.7 (±35.1)
1×2	10	12.38 (±1.0)	6.19 (±0.5)	27.40 (±2.1)	240.8 (±4.0)
1×3	10	18.07 (±2.0)	6.02 (±0.7)	26.60 (±2.9)	315.9 (±9.9)
1×4	10	28.60 (±2.0)	7.15 (±0.5)	31.60 (±2.3)	541.0 (±25.7)
2×2	5	26.10 (±1.1)	6.53 (±0.4)	28.85 (±2.0)	-----

Table 1. Results of double shear tests on arrays of pultruded rods in LVL.

From this section of the research it was concluded that due to the superior ductility of pultruded dowels in joints no load reduction factor is necessary when predicting joint failure loads parallel to the grain for diameters of up to 12mm. For steel dowels above 6mm in diameter a load reduction factor is necessary. The reduced stiffness of the pultruded, dowelled joint allows even load sharing between the dowels, reducing the tendency for stresses to concentrate at the leading dowel.

## 7. Finite element modelling

During the course of the project, 3-D FE analysis was conducted to study the dowel/timber interaction. Building from a simple 2-D (with thickness) model of a plate with a loaded hole the analysis developed. A simple 3-D model with a loaded hole was considered next and this model used the orthotropic properties of the timber. The next iteration consisted of a 3-D model with a tightly fitted steel dowel 'glued' to the timber substrate material and then remotely loaded in double shear. This version was then extended to feature an orthotropic pultruded dowel. Finally contact elements were introduced to model any making or breaking of contact of the dowel with the timber substrate under load.

Results obtained from these models successfully predicted the failure modes of both steel and pultruded dowels for different dowel diameters. Figure 8 simulates stress along the grain of the LVL under load and corresponding stress levels within the deformed dowel. Plots of Von Mises stress levels and shear strains (Figure 9) also successfully predicted the areas of shear failure in the pultruded dowels that were observed experimentally. All FE images represent only one quarter of the stressed joint for reasons of symmetry.

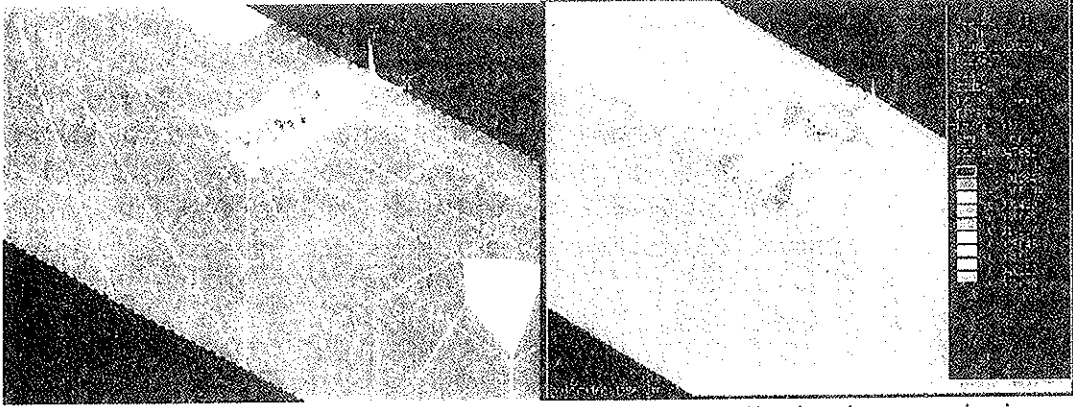


Figure 8. Longitudinal stresses at a double shear joint under tensile load.

Figure 9. Elastic shear strain in a double shear joint under tensile load

## 8. Manufacture of non-metallic joints

A wide variety of joint configurations were fabricated using simple joinery techniques and combinations of pultruded plates and dowels. Joint geometries included in-line plate and dowel type joints, single lap in-line and moment resisting joints, 3-piece moment resisting joints and simple double shear dowelled joints. The LVL was machined using circular saws, drill stands, milling machines and a home-built flitch-plate-slitter based on an electric chainsaw mounted horizontally, Figure 10. With the chainsaw blade mounted on a bed of variable height, different slot thicknesses could be achieved with the optimal thickness being 8mm enabling the slot to accommodate two 4mm thick pultruded plates.

Pultruded dowels and plates were cut and machined using the same drill bits and machine tools as for the LVL. This is an important point as this enables fabricators to manufacture joints using familiar woodworking machinery and without sub-contracting work which is often the case with steel connectors. In common with the nail plate industry it is essential to press dowels into timber, with suitable equipment, to avoid damage from hammering.

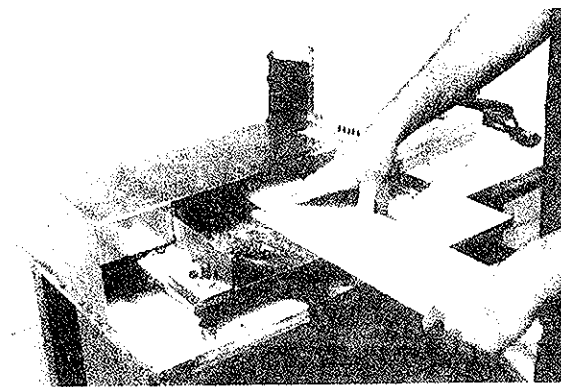


Figure 10. Chainsaw slotting jig for LVL.

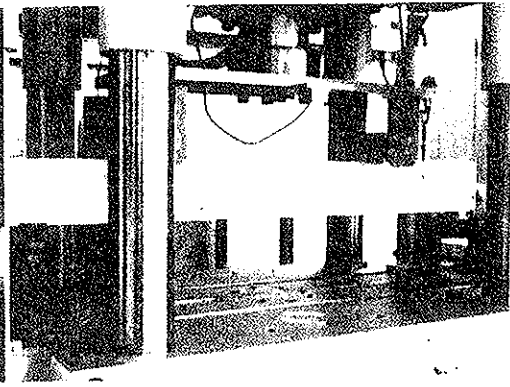


Figure 11. In-line plate and dowel joint in four point bending.

## 9. Full-scale laboratory testing

Full-scale structural static tests were conducted on the two previously selected joint types, (a) moment resisting 'knee' joints and (b) plate and dowel in-line joints. The latter joint type was tested in both tension and bending. Testing using a 4pt bending rig (Figure 11)

highlighted the problems associated with internal flitch plate type joints.

Sample type	Mean force at failure, (kN)	Mean bending strength (MPa)
Unjointed LVL	29.28	44.8
Nail-plated	20.04	30.7
6mm pultruded plate and 8 dowels	12.32	18.9
8mm pultruded plate and 8 dowels	13.28	20.3

Table 2. Bending strength of non-bonded, in-line butt joints in LVL.

Table 2 compares results for pultruded joints with dowels of 6mm and 8mm in diameter with the results of similar tests conducted on nail plated joints and also clear timber. Pultruded GRP joints do not perform as well as nail plated joints and failure was caused by splitting in the timber along the grain. Cutting a slot to install the pultruded flitch plate in such a joint reduces the section thickness, which is undesirable. Unlike nail plates which are able to constrain the faces of the LVL beam, dowel based joints are susceptible to splitting through the dowel centres which is common to failure in dowelled steel joints. These plate and dowel joints achieved higher strength under tensile loading, where failure occurred in a ductile manner in the pultruded rods with little or no deformation or damage caused to the GRP flitch plate.

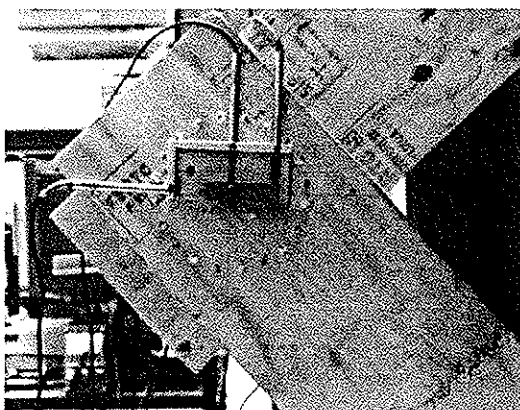


Figure 12. Instrumented moment resisting joint with ring of 8mm pultruded dowels.

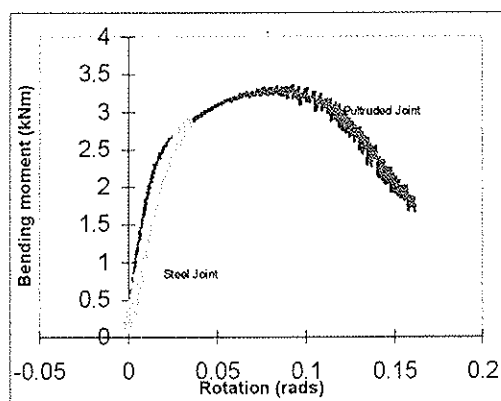


Figure 13. A comparison of 8mm dowelled 3-piece moment resisting joints using steel & pultruded dowels.

Following discussion with an industrial partner, emphasis was placed on constructing and testing various configurations of structural sized, moment resisting 'knee' type joints suitable for timber frames. These joints included dowel arrangements whose spacing were within current standards and also those outside of current codes. Two different dowel sizes were investigated and comparisons made with similar steel dowelled joints. Altogether more than 40 joints were fabricated and tested. Each joint was instrumented using LVDT transducers (Figure 12) in order to measure joint translations and rotations under load. Again, as with all pultruded joints, moment resisting knee joints were found to be more ductile and had similar failure strengths when compared to steel dowelled joints. A typical

example of this can be found in Figure 13 where a steel and a pultruded dowel joint are compared. Not only does the pultruded dowel joint achieve a superior failure load but considerably more energy is absorbed up to the point of failure due to the inherent ductility of the pultruded dowel/LVL system.

## 10. Conclusions

The research programme has made a significant contribution to the advancement of better construction techniques for timber buildings by developing jointing techniques based on non-metallic connectors. Whilst these joints offer structural integrity, high aesthetic appeal, ease of manufacture, and low weight, their key attributes are excellent ductility, low cost (similar to steel per unit length) and commercial acceptability. The research has placed these advances in a Eurocode 5 context (design modifications) and provided a foundation for current EPSRC- and EU-funded research into novel joints based on bonded-in pultruded GRP rods.

## 11. Acknowledgements

The authors would like to thank the EPSRC (The Engineering and Physical Sciences Research Council) for funding this research as part of the Built Environment programme (contract no. GR/K52065), Marti Tulkki at Finnforest Oy (Finland) for providing the Kerto LVL used in the research and Martin Strawford at Fibreline Composites Ltd for providing the pultruded composite dowels.

## 12. References

- Bainbridge R.J. and Mettem C.J.**, "A review of modern systems for producing moment resistant connections in timber structures". *Journal of the Institute of Wood Science*, 14, 3, pp.121-130, 1997.
- BSI**: DD ENV 1995-1-1:1994, "Eurocode 5- Design of Timber Structures - Part 1.1: General Rules and Rules for Building", 1994.
- CEN**, "Timber structures - test methods - determination of embedding strength and foundation values for dowel type fasteners", BS EN 383, 1993.
- Drake, R.D., Ansell, M.P., Mettem, C.J. and Bainbridge, R.J.**, "Advancement of structural connection techniques for timber buildings. Part 1: Performance of GRP pultruded dowels versus steel dowels", *Proceedings of the 1996 International Conference on Wood Mechanics (COST 508)*, Stuttgart, pp.353-364, 1996.
- Drake, R.D., Ansell, M.P., Aram, J., Mettem, C.J. and Bainbridge, R.J.**, "Non-metallic connections for timber structures" in the *Proceedings of the "5<sup>th</sup> World Conference on Timber Engineering"*, Montreux, Switzerland, ISBN 2-88074-387-7, Volume 2, pp. 577-584, August 1998.
- Drake, R.D., Aram, J.W.E. and Ansell, M.P.**, "The performance of pultruded GRP connectors in multiple dowelled double shear timber joints", *J. Inst. Wood Sci.*, 14, No.6, 1999.
- Eckold**, *Design and Manufacture of Composite Structures*, Woodhead Publishing Limited, England, 1994.
- Hollaway L.**, *Pultrusion*, RAPRA Review Report 20, Pergamon Press, 1989.
- Johansen, K.W.**, "Theory of Timber Connections", *International Association of Bridge and Structural Engineering*, Pub. No. 9, pp.249-262, 1949.
- Milner M.W. and Bainbridge R.J.**, "New opportunities for timber engineering", *The Structural Engineer*, 75, No.16, pp278-282, 1997.



INTERNATIONAL COUNCIL FOR RESEARCH AND INNOVATION  
IN BUILDING AND CONSTRUCTION

WORKING COMMISSION W18 - TIMBER STRUCTURES

EFFECT OF SPACING AND EDGE DISTANCE ON THE AXIAL STRENGTH  
OF GLUED-IN RODS

H J Blaß

B Laskewitz

University of Karlsruhe

GERMANY

MEETING THIRTY-TWO

GRAZ

AUSTRIA

AUGUST 1999

---

Presenter: B.Laskewitz

- C.N.Fouepe commented that the findings of distance  $> 5d$  would fit with theoretical results of orthotropic material.
- A.Jorissen asked how to obtain characteristic values based on regression equation.
- B.Laskewitz responded that the number of test was small but regression analysis was appropriate.
- H.J.Blass added that more test results will be available later from the European Project.
- A.Jorissen commented that  $r^2$  values were low.
- B.Laskewitz responded that density information could also be used to perform multiple regression to improve  $r^2$ .
- B.J.Yeh asked whether environmental conditions were considered.
- B.Laskewitz responded that yes there are test results.
- C.N.Fouepe asked what are the failure modes.
- B.Laskewitz responded that mixed adhesive and wood failures were observed in each failed specimen with mostly wood failure.
- E.Karacabeyli commented that improving  $r^2$  in equation would be needed.
- A.Jorissen commented that splitting of wood might be due to tension perpendicular to grain stresses.
- H.J.Blass responded that high strength steel was used to get the failure mode. Mild steel could be used to get more ductile connection.

# Effect of Spacing and Edge Distance on the Axial Strength of Glued-in Rods

H.J. Blaß, B. Laskewitz  
Lehrstuhl für Ingenieurholzbau  
Universität Karlsruhe (TH), Germany

## 1 Introduction

Glued-in rods have been used for several years in timber structures to transfer high forces from one structural element to another. In addition they are used as a reinforcement perpendicular to the grain in timber members. However, generally accepted design rules for glued-in rods are still missing.

Since 1998, the European Union supports the research project GIROD, in which design rules for glued-in rods will be drafted for inclusion in Eurocode 5. This research project is divided into several working packages carried out by different European partners. The University of Karlsruhe is responsible for working package 3 where the minimum spacing and the minimum end and edge distances of glued-in rods are determined. An overview of the project GIROD is given in annex A.

This paper presents test results with axially loaded rods glued in parallel to the grain in oversized holes in glued laminated timber members and proposes minimum rod-to-edge distances and rod spacing for timber members.

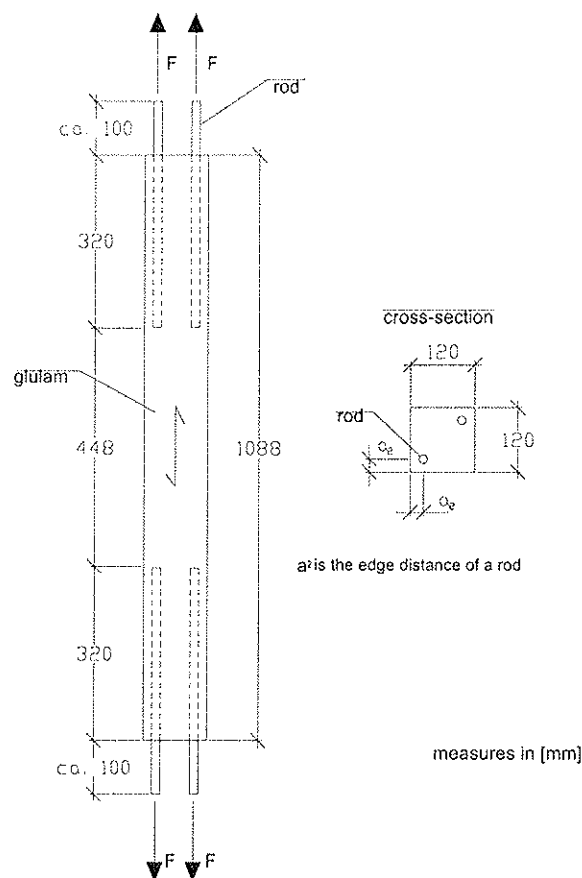
## 2 Experimental Investigations

### 2.1 Materials and Dimensions

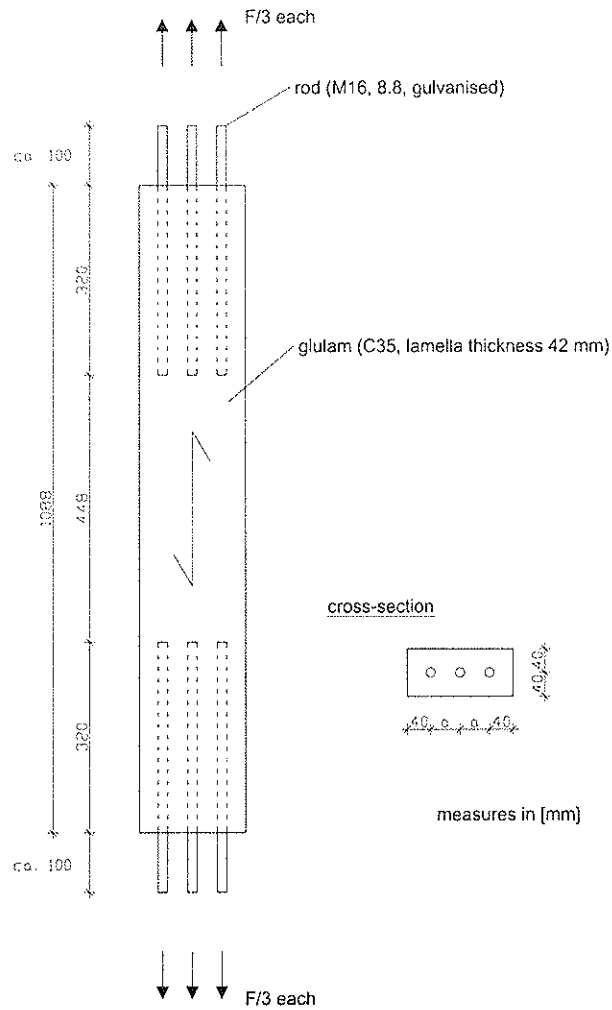
In order to be able to compare the results with those of other working packages it was agreed to use glued laminated timber made of lamellas of strength class C35. The moisture content of the timber should be 12 %. The density and moisture content of the specimens are summarised in table B1 in annex B. The threaded rods correspond to strength class 8.8 and are zinc-coated (galvanised) and not degreased. In most test specimens, the outer diameter of the rods was 16 mm. Only some comparative tests were performed with rod diameters of 12 mm and 20 mm. The threaded bars were glued-in in holes with a diameter 1 mm larger than the outer bar diameter. In most of the tests the adhesive was Casco PRF (Phenolic Resorcinol). Additionally, some tests were performed to study the influence of two different adhesives, Kleiberit Plastic-Mastic 573.8, a PUR (Polyurethane), and WEVO Spezialharz, an Epoxy.

The dimensions of the test specimens with two (one) and three rods, respectively, are shown in figures 1 and 2. Basic tests were performed with one rod in the centre of the cross-section. The specimens with two rods were used to investigate the influence of the edge distance. The requirement for the minimum edge distance was a remaining load-carrying capacity close to the value of the centrally placed rods. The specimens of these series had two rods glued-in in each end to avoid eccentric loading of the specimens. The specimens with three rods at each end were used to establish the minimum spacing also without a significant decrease of the axial strength.

The timber length between the two rod ends was chosen as 1.4 times the glued-in length. FMPA, Stuttgart, [1] has performed FEM-calculations to determine the distance and ascertain that if both ends of the two rods have a distance of 1.4 times the glued-in length, there is only a negligible influence of the distance of the rod ends on the shear stresses of the bond line. Furthermore it was agreed to use a lamella thickness of 42 mm and a cross-section of 120 x 120 mm for the tests with one or two glued-in rods. The final dimensions and design of the test specimens with three glued-in rods depend on the test results with two rods because of the minimum edge distance. This was necessary to avoid the influence of the edge distance because only the influence of the spacing between the rods should be investigated here. The dimensions can be seen in figure 2 and table 2.



**Figure 1:** Specimen for the tests to determine the minimum rod-to-edge distance with a rod diameter of 16 mm



**Figure 2:** Specimen for the tests to determine the minimum spacing

The loading arrangement consisted of a very stiff steel construction to avoid unequal loading of the rods. As far as possible pinned supports were used for the individual rods. In some cases the spacing did not allow pinned supports. The load was applied by a constant displacement of the loading rigs. The load as well as the displacement were continuously measured. Typical load-displacement curves are shown in figure B1 in annex B.

## 2.2 Testing Programme

Table 1 and 2 show the testing programme including details of the individual test series.

**Table 1:** Testing programme to determine the minimum rod-to-edge distance

Test series	Angle grain-to-rod [°]	Angle load-to-rod [°]	Glued-in length [mm]	Rod diameter [mm]	Hole diameter [mm]	Edge distance $a_2$ [mm]	Number of rods per specimen	Adhesive	Number of tests
GI-1	0	0	320	16	17	24	2 x 2	PRF	5
GI-2	0	0	320	16	17	32	2 x 2	PRF	5
GI-3	0	0	320	16	17	40	2 x 2	PRF	5
GI-4	0	0	320	16	17	48	2 x 2	PRF	5
GI-5	0	0	320	16	17	60	2 x 1	PRF	5
GI-6	0	0	320	16	17	60	2 x 1	PUR	3
GI-7	0	0	320	16	17	60	2 x 1	Epoxy	3
GI-8	0	0	400	20	22	60	2 x 1	PRF	5
GI-9	0	0	240	12	13	60	2 x 1	PRF	5

**Table 2:** Testing programme to determine the minimum rod spacing

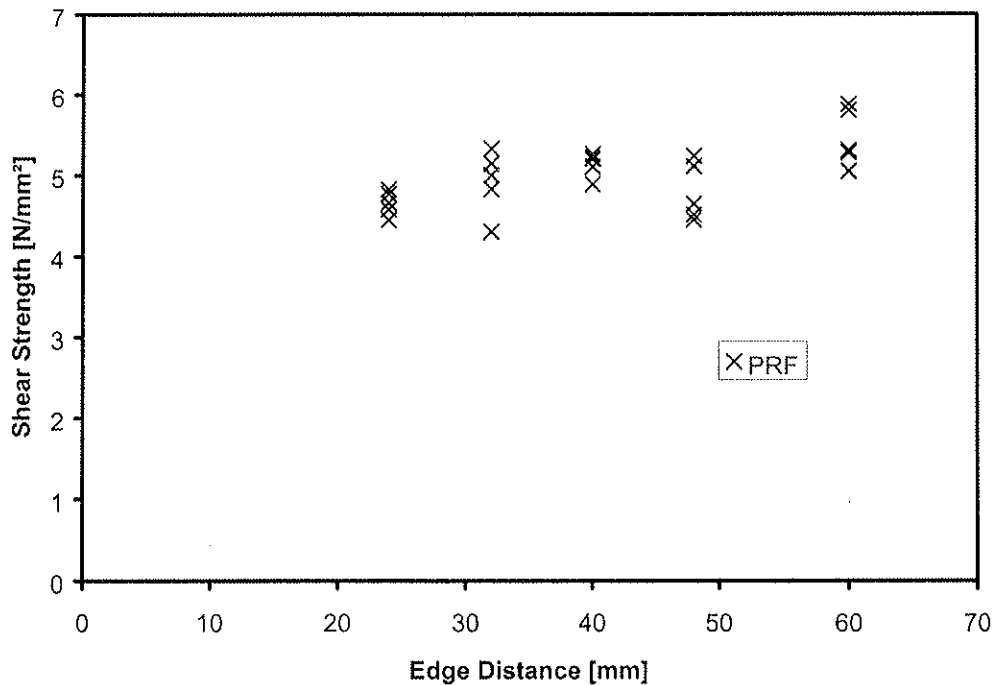
Test series	Angle grain-to-rod [°]	Angle load-to-rod [°]	Glued-in length [mm]	Rod diameter [mm]	Hole diameter [mm]	Rod-to-rod distance $a$ [mm]	Number of rods per specimen	Adhesive	Number of tests
GI3-1	0	0	320	16	17	32	2 x 3	PRF	5
GI3-2	0	0	320	16	17	40	2 x 3	PRF	5
GI3-3	0	0	320	16	17	48	2 x 3	PRF	5
GI3-4	0	0	320	16	17	60	2 x 3	PRF	3

## 2.3 Test Results

First, the results of the tests to determine the minimum rod-to-edge distance will be described. Afterwards the remaining results of the tests to study the influence of the rod spacing will be presented. Finally, these apparently different test series will be combined. Table 3 and figure 3 show the evaluated results of the tests to determine the minimum edge distance.

**Table 3:** Test results for the minimum rod-to-edge distance

Test series	Mean shear strength in bond line [N/mm <sup>2</sup> ]	Coefficient of variation [%]	Edge distance [mm]	Adhesive	Rod diameter [mm]
GI-1	4.66	3.22	24	PRF	16
GI-2	4.92	12.60	32	PRF	16
GI-3	5.13	2.88	40	PRF	16
GI-4	4.79	7.50	48	PRF	16
GI-5	5.46	6.56	60	PRF	16
GI-6	4.10	-	60	PUR	16
GI-7	4.59	-	60	Epoxy	16
GI-8	3.54	26.63	60	PRF	20
GI-9	5.26	1.48	60	PRF	12



**Figure 3:** Mean shear strength versus rod-to-edge distance

The mean shear strength shown in figure 3 is defined as the failure load divided by the surface of a cylinder with a height equal to the glued-in length and a diameter equal to the outer diameter of the rod.

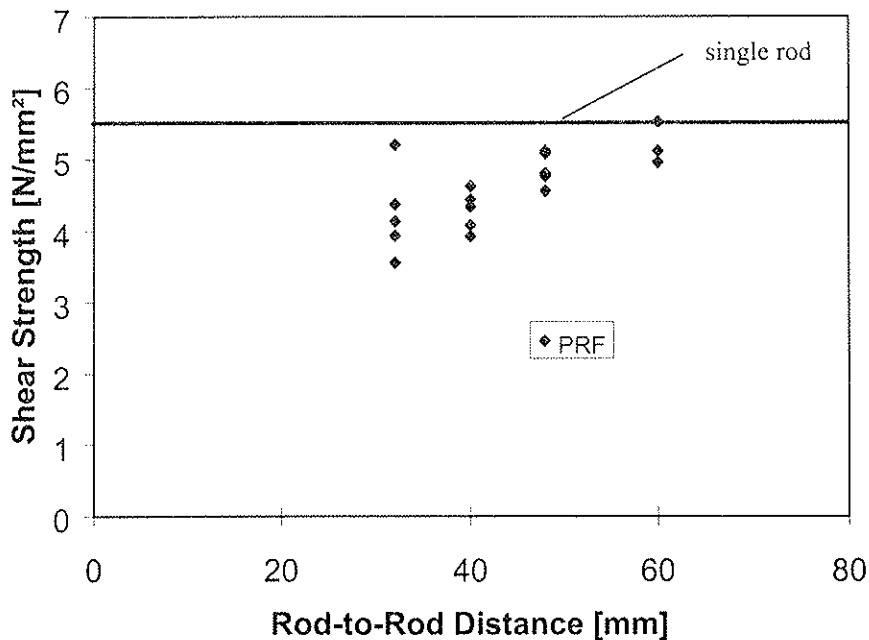
Figure 3 shows a slight increase of the mean shear strength with increasing edge distance. Even the tests with the smallest edge distance (24 mm = 1.5 d) showed a remarkable mean

shear strength in the bond line. The failure which occurred in most tests is splitting of the wood along the rod. Only the test specimens with one rod in the centre of the cross-section failed by pulling out of the rod caused by reaching the shear strength of the timber. A photograph of a failed specimen is shown in figure B2 in annex B.

Table 4 and figure 4 show the results of the tests to determine the minimum rod spacing.

**Table 4:** Test results for the minimum rod-to-rod distance

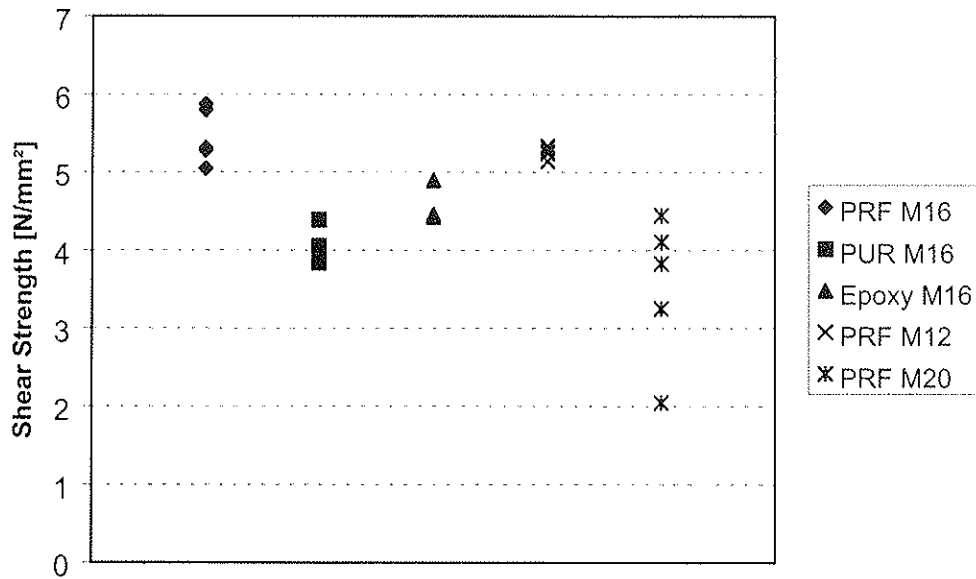
Test series	Mean shear strength in bond line [N/mm <sup>2</sup> ]	Coefficient of variation [%]	Rod-to-rod distance [mm]	Adhesive	Rod diameter [mm]
GI3-1	4.24	14.48	32	PRF	16
GI3-2	4.28	6.53	40	PRF	16
GI3-3	4.87	4.79	48	PRF	16
GI3-4	5.20	-	60	PRF	16



**Figure 4:** Mean shear strength versus rod-to-rod distance

The edge distance of the rods was 40 mm, or 2.5 times the rod diameter. Because of the very stiff test set-up a uniform load distribution between the three rods is assumed. Figure 4 shows that similar to the previous tests the load-carrying capacity increases with the rod-to-rod distance. For comparison the test results with one rod in the centre of the cross-section are shown in the diagram. The expected failure mode, namely splitting off the timber, occurred. A photograph of a failed specimen is shown in figure B3 in annex B.

Figure 5 shows the influence of different adhesives and of different rod diameters.



**Figure 5:** Mean shear strength for different adhesives and different rod diameters

The influence of the type of adhesive on the mean shear strength is significant. The specimens with PUR showed the lowest load-carrying capacity. The load-carrying capacities of the Epoxy bonded rods were slightly higher while the tests with PRF (an prototype glue) resulted in the largest strength values.

The comparative tests with different rod diameters using PRF showed a decrease of the mean shear strength and a larger variation for rods with a diameter of 20 mm although the glued-in length was always 20 times the rod diameter. The reason for this decrease is the different bond line thickness. The test specimens for the rod diameter of 20 mm were drilled with a diameter of 22 mm, while the specimens for the rod diameters of 12 mm and 16 mm had hole diameters of 13 and 17 mm, respectively. Therefore, the glue line for the 20 mm rods was thicker and caused the decrease of the load-carrying capacity.

Combining all tests where PRF was used, those to determine the minimum edge distance as well as those to establish the minimum rod spacing, leads to the diagram presented in figure 6. The distance  $a$  on the abscissa is defined as follows: for the tests to determine the the minimum edge distance, the distance  $a$  is the minimum of either half of the spacing or the edge distance. For the tests to establish the minimum rod spacing the distance  $a$  is defined as the rod spacing. A linear regression analysis leads to the following relation between mean shear strength and distance  $a$  [mm] to rod diameter  $d$  [mm] for a rod diameter of 16 mm:

$$\tau = 0.7 \cdot \frac{a}{d} + 3.7 \quad [\text{N/mm}^2]. \quad (1)$$

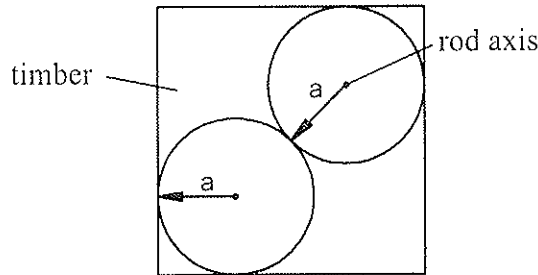
with

$$R^2 = 0.3003$$

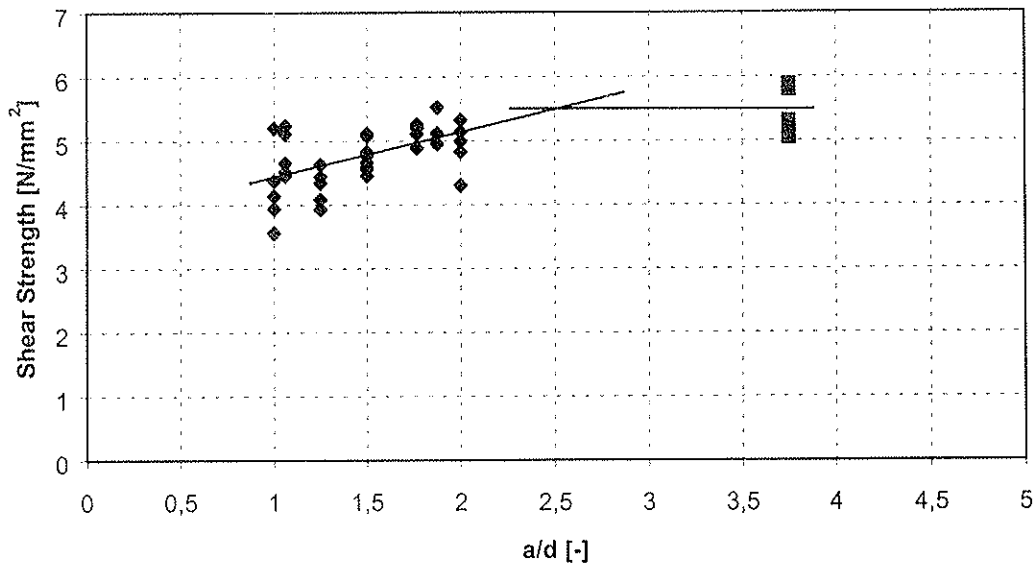


$$1 \leq \frac{a}{d} \leq 2.5$$

$$a = \min \begin{cases} \text{edge distance} \\ 1/2 \text{ spacing} \end{cases}$$



**Figure 6:** Definition of distance  $a$



**Figure 7:** Mean shear strength versus distance  $a$  to rod diameter  $d$

The horizontal straight line represents the mean value of the comparative tests with one rod in the centre of the cross-section. The point of intersection is situated close to a distance of 40 mm, or 2.5 times of the rod diameter. Consequently, a spacing of 80 mm or an edge distance of 40 mm does not cause a decrease of the load-carrying capacity compared to single rods with a diameter of 16 mm.

Additionally, a multiple linear regression was performed taking the density of the timber into account. The influence of the density was found to be not significant. However, only timber made of laminations of strength class C35 with a characteristic density of 400 kg/m<sup>3</sup> was used in the tests. In order to verify the weak influence of the density, more strength classes with different characteristic densities should be included in the study.

### **3 Conclusion**

When using glued-in rods in timber structures it is suggested to use spacings of 5 times and edge distances of 2.5 times the rod diameter. Otherwise, a decrease in load-carrying capacity, e.g. according to equation (1) should be taken into account. It is recommended not to use edge distances below two times the rod diameter because of inevitable inaccuracies when drilling the holes for glued-in rods.

### **4 References**

- [1] Aicher, S., Höfflin, L., Wolf, M. *Influence of Specimen Geometry on Stress Distributions in Pull-Out Tests of Glued-In Steel Rods in Wood*. Otto Graf Journal, Vol. 9 1998, Forschungs- und Materialprüfungsanstalt Baden-Württemberg FMPA

## Annex A

### Overview of GIROD

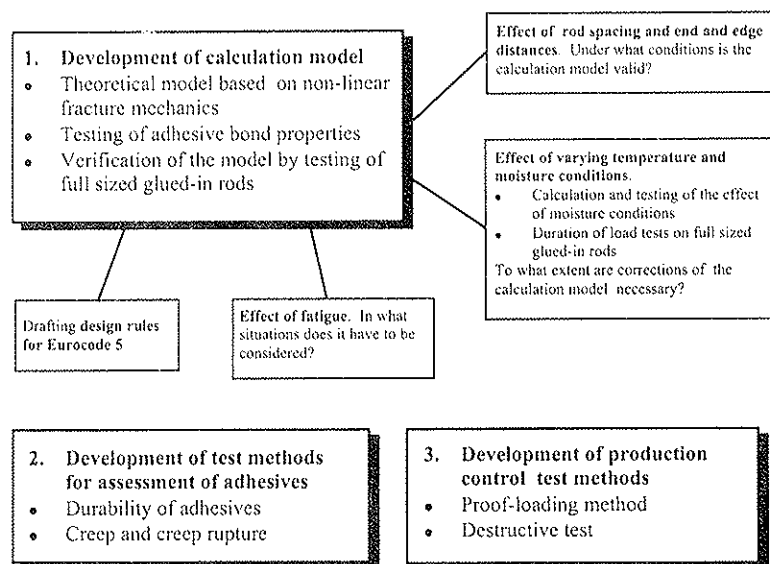
#### Objectives

The objective of this project is to provide the information required to prepare standards that will allow an increased, more advanced and more reliable use of glued-in rods in timber structures. The steps involved in reaching this objective are:

1. Perform theoretical and experimental work leading to a calculation model for axially loaded glued-in rods based on the adhesive bond properties as well as the wood and rod material properties. This must take into account the effect of varying climatic and loading conditions as well as fatigue. This step will give information required by CEN.TC250/SC5 in the preparation of Eurocode 5 - Design of Timber Structures.

2. Develop test methods for the evaluation of adhesives for glued-in rods with respect to strength, durability, creep and creep rupture behaviour under different climatic conditions. This will support the work of CEN.TC193/SC1 (Wood adhesives).

3. Derive test methods for the production control of structural glued-in rod connections. This will support the work of CEN.TC124/WG6 (Glued-in rods in timber structures).



#### Partners

Swedish National Testing and Research Institute, Sweden

Lund University, Lund Institute of Technology, Sweden

Forschungs- und Materialprüfungsanstalt, Baden-Württemberg, Germany

TRADA Technology Limited, United Kingdom

Universität Karlsruhe (TH), Lehrstuhl für Ingenieurholzbau und Baukonstruktionen

Moelven Töreboda Limträ AB, Sweden

Casco Products AB, Sweden

Studiengemeinschaft Holzleimbau, Germany

UK Glued Laminated Timber Association, United Kingdom

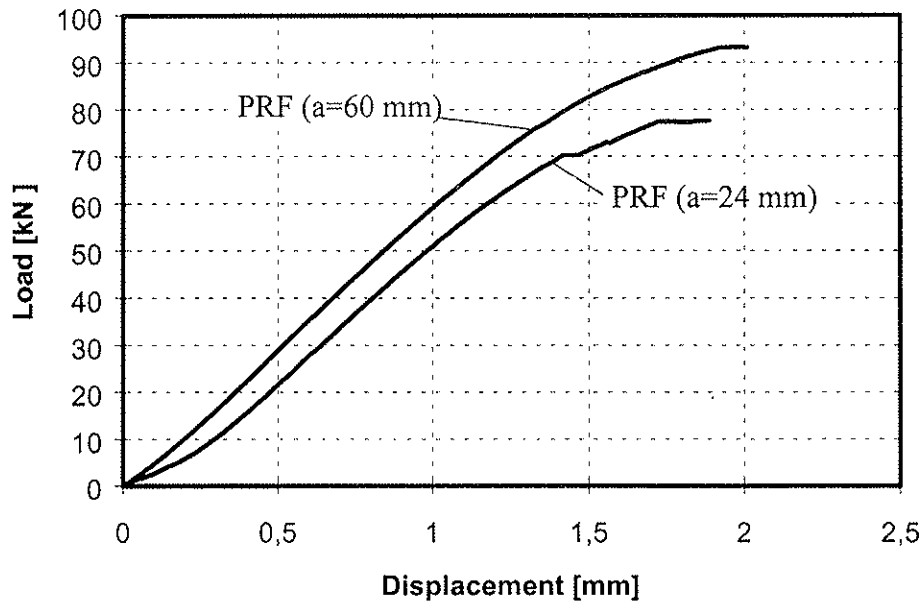
Klebchemie M.G. Becker GmbH & Co. KG, Germany

Wevo-Chemie GmbH & Co. KG, Germany

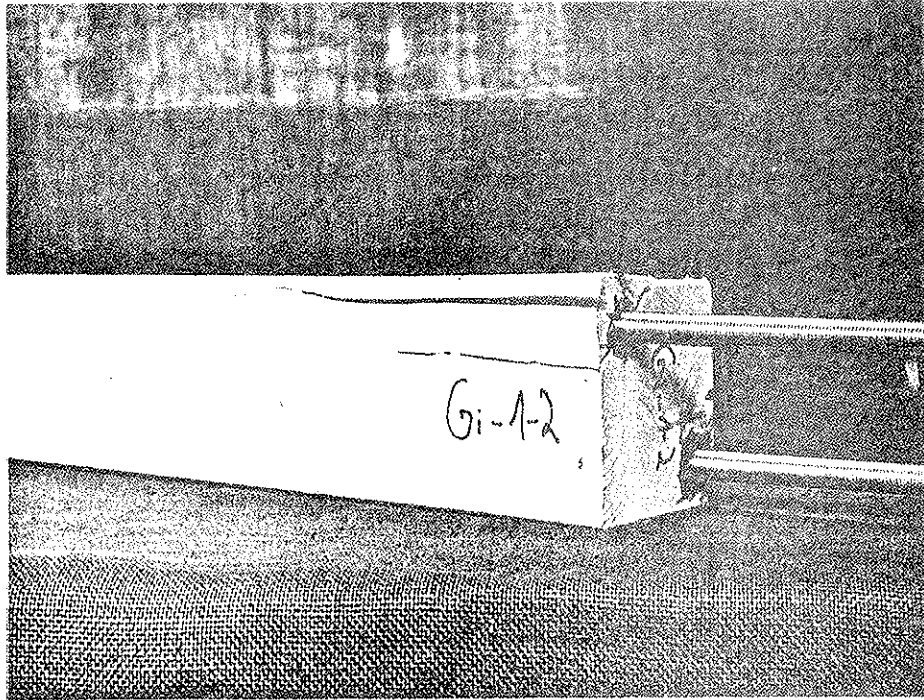
## Annex B

**Table B1:** Mean values of density and moisture content

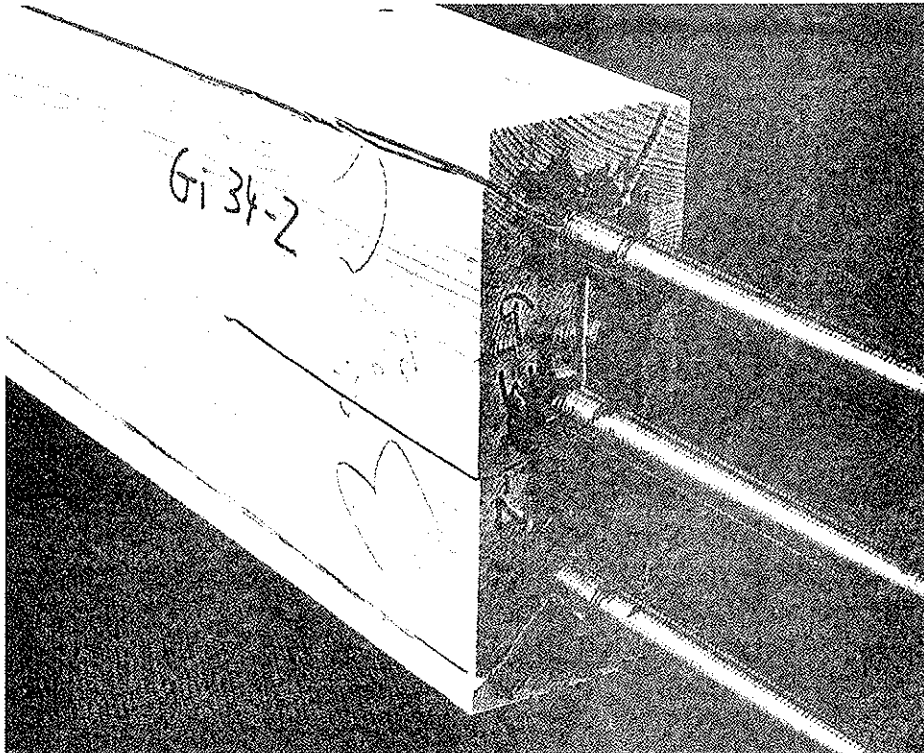
	Density [kg/m <sup>3</sup> ]	Moisture Content [%]
GI-1	466	11.9
GI-2	470	11.8
GI-3	482	11.3
GI-4	501	11.1
GI-5	508	12.0
GI-6	452	11.4
GI-7	472	10.4
GI-8	437	12.0
GI-9	445	11.6
GI-31	438	13.2
GI-32	447	13.3
GI-33	476	11.9
GI-34	475	12.9



**Figure B1:** Load-displacement curves for different edge distances



**Figure B2:** Failed specimen with an edge distance of 1.5 times the rod diameter



**Figure B2:** Failed specimen with a spacing of 3.75 times the rod diameter

**INTERNATIONAL COUNCIL FOR RESEARCH AND INNOVATION  
IN BUILDING AND CONSTRUCTION**

**WORKING COMMISSION W18 - TIMBER STRUCTURES**

**EVALUATION OF MATERIAL COMBINATIONS FOR BONDED IN RODS  
TO ACHIEVE IMPROVED TIMBER CONNECTIONS**

C J Mettem

R J Bainbridge

TRADA Technology

K Harvey

M P Ansell

University Of Bath

J G Broughton

A R Hutchinson

Oxford Brookes University

UNITED KINGDOM

**MEETING THIRTY-TWO**

**GRAZ**

**AUSTRIA**

**AUGUST 1999**

---

Presenter: C.J.Mettem

· S.Svensson received clarification from C.J.Mettem on the HDT\* values in Table 8.

# Evaluation Of Material Combinations For Bonded In Rods To Achieve Improved Timber Connections

By C J Mettem, R J Bainbridge TRADA Technology, UK  
K Harvey, M P Ansell University Of Bath, UK  
J G Broughton, A R Hutchinson Oxford Brookes University, UK

## Abstract

Well designed and executed adhesive bonded structural connections can be extremely efficient and may possess many desirable attributes in terms of manufacture, performance, aesthetics and cost. The use of bonded-in rods is an important feature of many of the methods for achieving connections using adhesives.

Bonded-in rods are now being used in several European countries, but the performance requirements and the design rules differ, which is a series obstacle to trade. A standard on design of timber (Eurocode 5 - Design of timber structures - Part 2: Bridges) has been drafted by CEN.TC250/SC5 and contains an informative Annex on the subject. There is also a 3-year European project in progress at the time of writing titled "GIROD - Glued In Rods For Timber Structures" [1], and performed through collaborative activities between partners from UK, Germany and Sweden.

This paper presents findings from studies initiated prior to the GIROD project, which focus specifically upon the influence of geometric and material variations upon strengths and modes of failure. Innovative routes explored include thick glue lines, use of various epoxy and acrylic adhesives, surface prepared ferro-reinforcement rods and FRP composite rods. These have been based upon experimentation through physical test and numerical modelling, within the context of developing information of value in aiming to derive and validate limit states design procedures.

---

## Definition Of Symbols

$X_d$	Material design property	$\gamma_M$	Partial coefficient for material properties
$X_k$	Material characteristic property	$\gamma_{Mi}$	Component partial coefficients
$L_a$	Anchorage length (bond length)	$\sigma$	Normal stress
$A_{ef}$	Effective area of rod	$\tau$	Shear stress
$t_{ad}$	Mean bondline thickness	$\lambda$	Ratio $L_a : d_{rod}$
$d_{rod}$	Nominal rod diameter	$\rho$	Density of timber
$d_{hole}$	Hole diameter	$X_{ad}$	Adhesive property or factor
FRP	Fibre reinforced plastic	$X_{FRP}$	Fibre reinforced plastic property or factor
GFRP	Glass - FRP	$f_y$	Yield strength
CFRP	Carbon - FRP	$f_{ult}$	Ultimate strength
E	Young's modulus of elasticity		

## 1. Introduction

Structural adhesives can be used to achieve efficient connections between timber components. Examples of direct timber to timber bonds can be observed in laminated timber products and finger joints. Further applications of structural adhesives in connections can be derived through bonding other materials to timber members, in the form of rods or plates. The effectiveness of such connections depends on the adequacy of the bond: if this bond is sufficient, then the strength of the joint is determined by either the strength of the host timber or the components used to achieve the connection.

Pultruded Fibre Reinforced Plastic (FRP) materials have potential application as a replacement material for steel in timber joints. This has been the subject of studies in a number of specific structural applications, for example the reinforcement of complete structural members [2], localised reinforcement [3] and strengthening of existing structures [4]. They have many advantages over steel such as higher specific stiffness and strength and they are easier to machine.

Pre-fabricated connection systems offer several potential advantages over traditional connection methods as control over quality of manufacture can be turned to advantage in terms of both the appearance and the strength of the finished item. Modern connection systems for moment resistant timber structures

which are manufactured under close supervision and with good control of quality have all the attributes of visual appeal, ease of assembly, safety and reliability.

There is a wide range of connection types within timber frame structures. From a recent review of structural timber connection systems [5], five generic types of modern concealed connection have been identified:

- Concealed bonded-in rods
- Concealed bonded-in plates;
- Adhesive bonded surface contact joints
- Timber connectors within lapped joints;
- Dowel type joints.

Some of these systems are believed to have potential application with fibre reinforced polymeric components. For example, the use of FRP bars and plates, both bonded-in and acting in dowel type joints [6,7]. This paper describes work focussed upon performance of FRP in instances where rods are bonded-in to timber and act through development of axial resistance in their longitudinal axis.

Adhesive bonded rods have potential use in both new-build and repair situations in timber structures. Figure 1 shows some of the possible configurations for new-build connections and Figure 2 shows an end repair made with bonded-in rods to connect into the "parent timber" plus a new end comprising permanent timber shuttering surrounding an epoxy resin grout core, the latter containing the continuation of the bonded-in reinforcing steel bars.

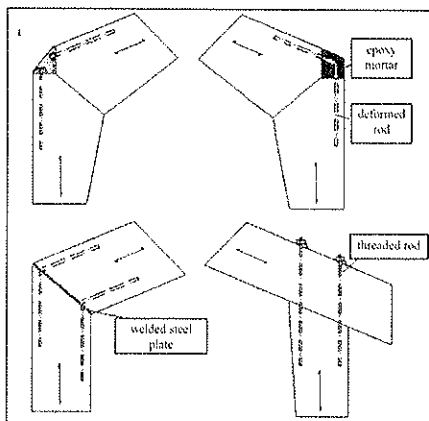


Figure 1 Examples of new build connections employing bonded-in rods

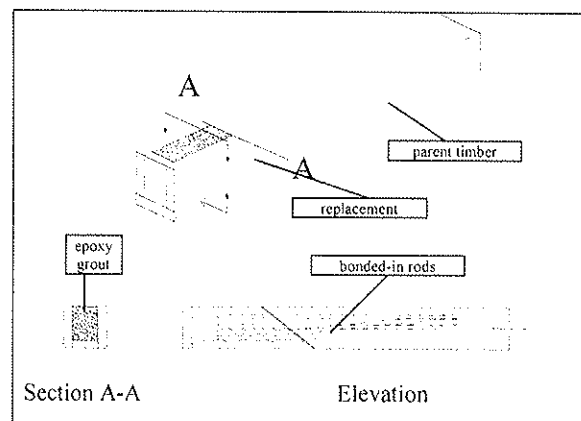


Figure 2 Example of a bonded-in rod repair detail

## 2. Adhesive Bonding

### 2.1 General Issues

Adhesive bonding techniques for timber are being supported by other structural bonding initiatives which have recently taken place in the UK [8] and elsewhere in Europe.

Common advantages achieved through using adhesive based methods instead of traditional mechanical connection methods include:

- Potential for satisfactory transfer of high localised forces
- Very stiff connections can be achieved
- Good fire properties are normally achieved, since bonded-in components are generally protected by the wood surrounding them, which will protect through charring in the case of fire.

Achievement of sufficient adhesion to a smooth surfaced component requires controlled surface preparation. Whilst this is amenable to pre-fabrication in workshop conditions, some degree of on-site bonding might be required in some projects. Therefore, unless surface preparation can realistically be relied upon, threaded, deformed or heavily textured components are preferred, in order to obtain a mechanical bond between the rod and the adhesive.

### 2.2 Structural Performance Considerations

Proper design, correct material specifications and good preparation and site practices, are all essential in ensuring good quality adhesive bonded repairs. Of course, these aspects are vital for the successful execution of all connection techniques, but specifiers always fear, possibly somewhat irrationally, that adhesive bonding may be more prone than others to bad practice or that the consequences of failure may be more severe. The retention of skilled and approved specialist contractors is essential as one of the means of ensuring reliability.

It is a common misapprehension that adhesively bonded repairs are likely to have virtually no structural fire resistance. However, fire resistance tests on certain epoxy adhesive bonded repair systems



undertaken by TRADA Technology have shown that with certain protective details, these are capable of providing more than 60 minutes of fire resistance [9].

It is essential that corrosion of bonded-in components is prevented. The risks of the bond between steel and wood being destroyed by expansion of rust have been identified [10]. Steel rods and plates must therefore be protected against corrosion, for example through galvanising or sheradising. If the components are completely concealed in a bonded connection, some adhesives, for example epoxy, also give good protection against corrosion, but this relies upon absolute encasement of the component.

It is indicated that shrinkage and swelling due to changing moisture content may cause considerable shear stress in the bond between rod and wood. Bonded-in components should therefore be used with caution in service class three, and consideration be given to the interaction of the different materials in the target service environment. The long-term performance of adhesively bonded rods connected into structural timbers is therefore an area still under investigation.

### 3. Material Combinations

A bonded-in rod connection consists of three material components:

- The adhesive
- The rod - most commonly steel, potentially FRP
- The host member - timber or timber based composite

#### 3.1 Adhesives

An overview of common structural wood adhesives and their use in timber products and structures can be found in STEP lecture A12 [11] and TRADA Wood Information Sheet 2/3-35 [12]. Further information is also available in non-timber specific publications such as the Structural Adhesives Guide produced by The Institution of Structural Engineers[8].

Bonded-in rods are normally fitted into oversized holes or slots, therefore the adhesive system used must have gap filling properties - i.e. it must retain a high proportion of its strength and stiffness when placed in 'thick' bond lines, of 1mm or more. The most common types of adhesives, include epoxy (EP), polyurethane (PUR) and phenol-resorcinol (PRF) based systems. Within these broad classifications, many different adhesives are available, the exact properties and performance of which are subject to variation between brands and products (as demonstrated later in this paper). Therefore, technical literature applicable to the actual adhesive formulation intended for use should be consulted at an early stage.

Whilst the strength of the connection depends on the strength and durability of the bond line, the final choice of adhesive formulation may also be influenced by the practicalities involved in the process of achieving the required bond, including surface preparation, quality control requirements, following manufacturers' guidance, the adhesive curing period and environment and the time requirement prior to subjecting the bond to significant load.

The performance of adhesives in these systems is achieved through:

- adhesion to the timber at the timber/adhesive interface
- mechanical resistance developed within the thickness of the adhesive layer
- adhesion to the connection components at the adhesive/component interface
- friction and mechanical interlock at the adhesive/component interface

The balance of reliance upon the adhesion to bars or plates and the mechanical interlock developed will reflect the surface texture of components (e.g. smooth or threaded rods) and will determine the surface preparation requirements to achieve sufficient reliability in the adhesion achieved.

#### 3.2 Rods

##### 3.2.1 Steel

Steel is clearly the most attractive of the metallic alloys, since it is widely available in a range of grades and stock sizes, with well established surface preparations and alloying methods that can be employed to combat potential corrosion problems.

Bonding preparations for metals is also supported by established knowledge concerning the effectiveness of surface treatments of varying complexity and sophistication. To date it has generally been considered that the requirements of adhesives in these cases are to provide anchorage to the rod or plate through combined adhesion and mechanical interlock. This is commonly taken to the extent that the pressures of economy of production process versus the low cost of materials has led to negation of specification of high levels of surface preparation and high reliance upon mechanical interlock.

### 3.2.2 *Fibre Reinforced Polymers (FRPs)*

Fibre Reinforced Polymers consist of strong fibrous materials, commonly glass, carbon or aramid, fixed in a polymeric matrix, commonly an unsaturated polyester resin, epoxy resin or vinyl ester, to achieve a stable form of composite end product, with the strength properties dictated by the behaviour of the fibres.

The properties achievable are a function of the fibre type, fibre content, orientation of fibres with respect to load and the material substructure achieved through manufacture. Guidance in this respect can be drawn from the EUROCOMP design handbook [13] and from the actual properties of specific FRP components, as provided by material suppliers and manufacturers.

The required rod form of product leads most readily to the pultrusion process of manufacture, whereby fibres are drawn through a resin bath and a forming die to produce a uniform profiled component.

Whilst these materials facilitate durable, lightweight structural solutions and provide for exacting material specifications, there are important fundamental differences between their structural behaviour and that of steel. These types of composite behave in a linear elastic fashion up to a sudden, brittle failure in tension. They do not therefore exhibit the type of yield behaviour that defines a critical failure mode in design equations for steel dowels and metallic bonded-in rods.

It is however possible to employ such materials, as in the case in reinforced concrete, where GFRP pultrusions are seeing increased use as an alternative to steel reinforcing bars. This relies upon appropriate derivation of the design capacity for the components, which in simple terms will be returned as a significantly reduced value of the ultimate capacity.

Whilst it is common for many pultruded FRP composites to have a smooth surface contaminated with die release agents, it is possible to achieve satisfactory adhesion with fairly rudimentary surface preparation. Deformed, roughened-textured and threaded FRP profiles are also available, offering considerable potential for advances in timber repair technology. Specially prepared, peel-ply surfaces are offered with some products, to provide ready-prepared bondable textures. These are used in highly safety critical repair situations, including bonded CFRP pultrusions for concrete highway bridges.

FRP materials are sensitive to temperature, but in a different way to steel. Significant creep will occur if the service temperature is close to the resin second order glass transition temperature. This is related to the heat distortion temperature. The heat distortion temperature is the temperature at which a standard beam under controlled heating conditions reaches a prescribed deflection. The glass transition temperature is the approximate midpoint of the temperature range over which glass transition takes place, below which the polymer fails in a brittle manner and above which it behaves as a rubbery solid.

### 3.3 **Timber / Timber Composite Host Material**

The host material may be either structural softwood, structural hardwood or a structural timber composite product.

As is the case with most structural applications, the moisture content will be critical in the connection. This is of particular note at the time of bonding since moisture in the host members can affect the bonding process, for example with PUR adhesives, excess moisture can lead to the production of CO<sub>2</sub> gas which forms bubbles and hence weak points within the bond.

## 4. Design Considerations

Bonded-in rods are now being used in several European countries, but the performance requirements and the design rules differ. A standard on design of timber bridges has been drafted [16] and contains an informative Annex on the subject. There is also a 3-year European project in progress at the time of writing titled "GIROD - Glued in Rods For Timber Structures" [1] performed through collaborative activities between partners from UK, Germany and Sweden.

The load-carrying capacity of connections made with bonded-in components should be verified for the following failure modes:

- Failure of the rod
- Failure of the adhesive bond, at either interface or within the bond line itself
- Localised failure of the timber adjacent to the adhesive interface
- General failure of the host timber member (e.g. pull-out failure of a whole timber block with several bonded-in rods).

The consequences of the critical failure mode should be recognised. For example, in the case of axially loaded steel rods, if the load-carrying capacity is limited by the yield strength of the rod, then abnormal loading events will most likely result in plastic deformation of the joint, rarely causing damage to a degree whereby structural safety is challenged.

In addition to the universal effects that influence connection performance, such as duration of load and service class effects, bonded-in rods respond with marked differences compared with groups of dowel-type fasteners subject to actions induced axially and laterally. Factors influencing the behaviour of axially loaded rods include:

- The strength of rods loaded in tension and compression
- The difference in stiffness between the rod, the bond and surrounding timber, which in combination with geometric factors influence the stress distributions
- The strength of the local timber
- The orientation of the rod axis with respect to the timber grain.
- Stability problems, which may become significant in rods subject to axial compression.

Actual code-checking procedures for the load-carrying capacity of laterally loaded rods are expected to be broadly analogous to those for dowel type joints. The designer will determine the critical failure mode achieved as a function of geometry, shear resistance of the rod, internal moment capacity of the rod and the embedding strength of the local timber (a function of density).

A point to note is that by bonding in the rods, an almost infinite coefficient of friction is obtained between the steel and wood surfaces, hence modes of deformation that require slippage along the length of the rod are negated. For rods perpendicular to the grain direction, it has been shown [14] that this leads to a considerable increase of both the embedding strength and the stiffness, compared with unbonded dowel-type fasteners.

Here a principal issue comes to bear, in that steel exhibits yield behaviour, whereas FRPs do not. Therefore the fundamental basis for definition of preferred failure type must be revisited.

If the design of a steel rod connection is based upon yield capacity, then exceeding the capacity will not lead to sudden collapse, but generally an SLS limit will be breached through plastic deformation of the rod. This philosophy is employed widely in reinforced concrete design where 'under-reinforcement' is targeted to avoid compression failure in concrete. Although FRPs do not exhibit plastic deformation in this way, they have been used in reinforced concrete where this has been dealt with by applying a substantial reduction factor to the ultimate capacity to derive a conservative capacity rating.

There is also an argument that this does not exploit the full potential of the timber structure and that an ideal would be achieved if the jointed structure capacity was closer to that of an unjointed equivalent. This infers that the controlling parameter should be the timber capacity and hence independent of rod behaviour.

Items within the knowledge base currently lacking in the proposed design methods include:

1. The relative effectiveness of different adhesives in these particular applications
2. The relative effectiveness of different bond thicknesses in these particular applications
3. A basis for treatment of rods other than steel

With regard to points 1 and 2, it should be noted that significantly different adhesive systems are being explored in innovative bonded-in rod technologies, compared with those traditionally accepted in timber engineering for applications such as laminating and diaphragm component manufacture.

In an effort to develop proposals for suitable content in respect of these three items, the following sections outline current research and development activities. The scope of the research covers the use of axially loaded rods bonded into oversized holes in timber using structural adhesives with recognised gap filling properties. Of the general adhesive types that could be considered and the number of commercial products available within these groups, practicalities of test resources focussed attention on those systems agreed to have highest potential on the basis of previous tests experience.

The principal aims of the research are to develop efficient, concealed, connections for timber structures using bonded-in rods; to apply adhesives and polymer composites technology in an engineering context and to disseminate guidance on the appropriate use of new materials and proposed design methods.

## 5. Potential Adhesive Types

Work involved with characterising the performance of different potential adhesives has been based on small scale pull out tests. The pull out tests were on single-ended samples as illustrated in Figure 3. In these samples, GFRP rods were bonded into blocks of LVL using different brands of epoxy and acrylic adhesive. Although this does not comprise the fullest range of possible adhesives, the sample group allowed for comparison across brands within the epoxy group (probably the most commercially important for this application), together with cross reference to two brands of a different adhesive type. An average bondline thickness of 2mm was employed in the tests (i.e.  $d_{\text{hole}} = d_{\text{rod}} + 4\text{mm}$ ). The rods were loaded in tension at a rate of 0.5mm/min until failure.

A summary of the results of the pull out test trials is also shown in Figure 3. These clearly demonstrate that the effectiveness of commercial brands within an adhesive group can vary for this application, and that there differences are also apparent between the acrylic and epoxy resin groups, the latter developing higher resistance in the test samples. This underlines the importance for close specification and the need for readily applicable data for use in design, since a design specifying 'Epoxy' adhesive may, on the evidence of these tests, draw upon data from a higher performance adhesive, and yet be executed with a product with only around 70% of that components strength.

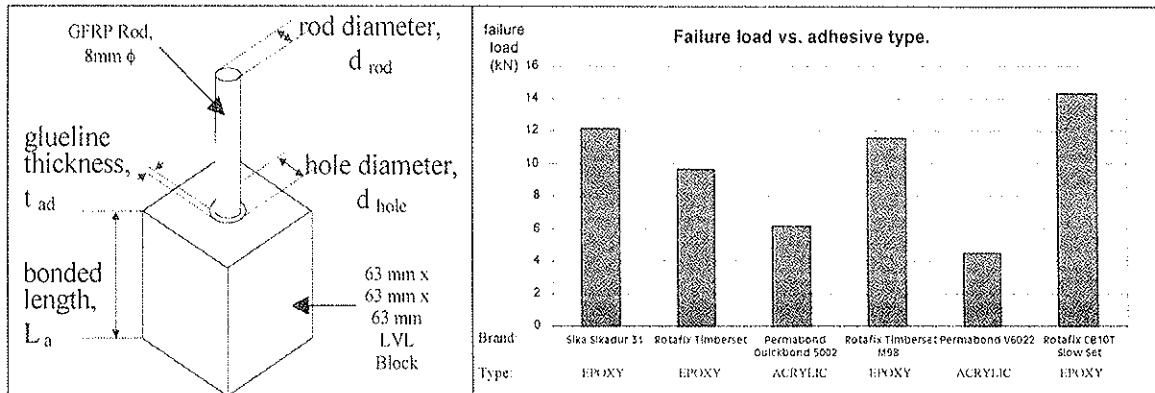


Figure 3. Single-ended pull out sample, and effect on strength through varying the adhesive type in tests

## 6. Variation of Strength with Bondline Thickness

An experimental programme was conducted upon axially loaded rods with varying thicknesses of bondline. Steel rods were bonded into LVL, using a two-part ambient-temperature cured Epoxy adhesive. The steel in this case was concrete reinforcement bar stock of 10mm diameter, gritblasted prior to bonding. The host LVL blocks measured 60 x 60 x 60mm with holes drilled perpendicular to grain through the specimen. 1mm, 3mm and 6mm bondline thicknesses were investigated, with all specimens being cured for 7 days prior to testing. Tests were conducted at 2mm/min with an Instron Tensile Testing Machine using a cage fixture. The test results of this investigation are summarised in Figure 4, in terms of the failure load and calculated mean shear stresses at failure at the interfaces through the bonded joint.

Failure of the pull-out specimens was always within the timber close to the adhesive/timber interface. The increase in failure load demonstrates the enhancements achievable with this material and geometry combination in enlargement of the hole and hence the bondline thickness. Since the rod is of a constant diameter across the test set, the rod/adhesive interface shear stress at failure follows the same trend as that observed in the ultimate load, whereas the timber/adhesive shear is reduced across the set due to the relation of stress to the bond area ( $\pi d_{\text{hole}} L_a$ ). Thus it can be seen that the limiting parameter (the strength at timber/adhesive interface) is fairly consistent across the set (6.4 - 7.6 N/mm<sup>2</sup>) whereas the adhesive/rod interface develops far higher shear stresses and increases across the set without becoming critical. Thus the adhesive retains full integrity and the overall capacity is limited by the timber substrate.

A simplified Finite Element Analysis was also performed to mirror the experimental investigation. A 2-D plane stress model using symmetry about the centre line of the rod was constructed, using COSMOS FEM. Boundary conditions were applied to represent the cage fixture employed in the tests. The LVL was modelled as isotropic with a Young's modulus (E) of 10 kN/mm<sup>2</sup>. The adhesive was given an E of 7 kN/mm<sup>2</sup> and the steel 210 kN/mm<sup>2</sup>. The analysis was linear-elastic only. The influences of bondline thickness on peel (normal) and shear stresses along embedment length as identified from the model are illustrated in Figure 5.

The FE model results indicate a further potential benefit through increased bond line thickness, namely the reduction of magnitude of peak stresses for a given load. This may be of particular importance for cases where the adhesive/timber interface is not critical.

These observations would tend to suggest that a thicker bond line will be beneficial. This is reassuring, especially in in-situ repair situations, where because of inaccuracy in the parent materials, long, tight holes are difficult to achieve. However, there are further considerations to be borne in mind. A larger hole will increase machining and require greater volumes of resin. Within larger holes, there is also more scope for the rods to bond out of alignment or in the case of multiple rods out of required spacing tolerance, and so extra care is required.

The adhesive type will also be of importance (the above tests were all based on an epoxy), since the brittleness of adhesives is known to vary between types and indeed brands, and can have an effect upon

bonded-rod performance. Furthermore, some adhesives (e.g. filled PRFs) suffer shrinkage upon curing, which has the potential to affect bond integrity at the interfaces. Thus a thicker bond line will result in greater shrinkage potential, thus the geometric stability of the adhesive requires consideration.

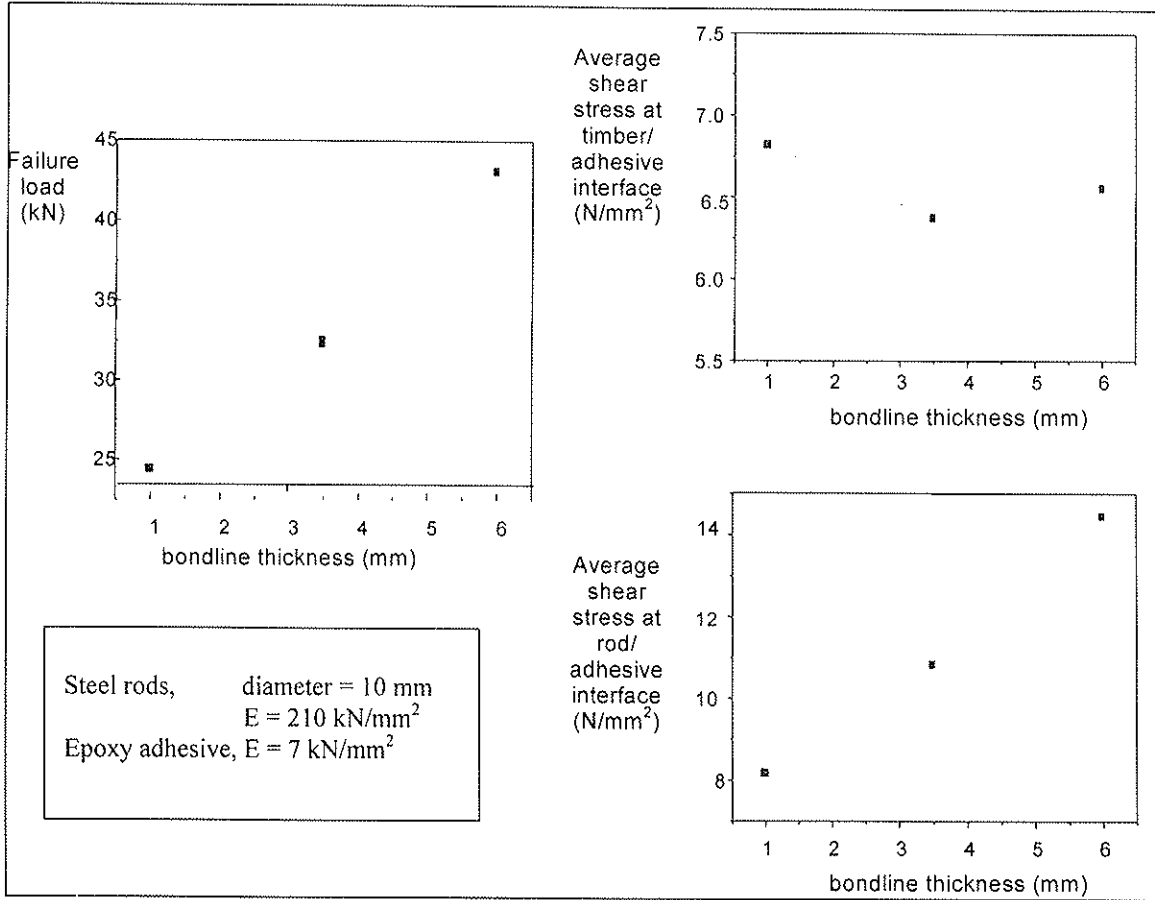


Figure 4 Influence of bondline thickness on variation of different parameters

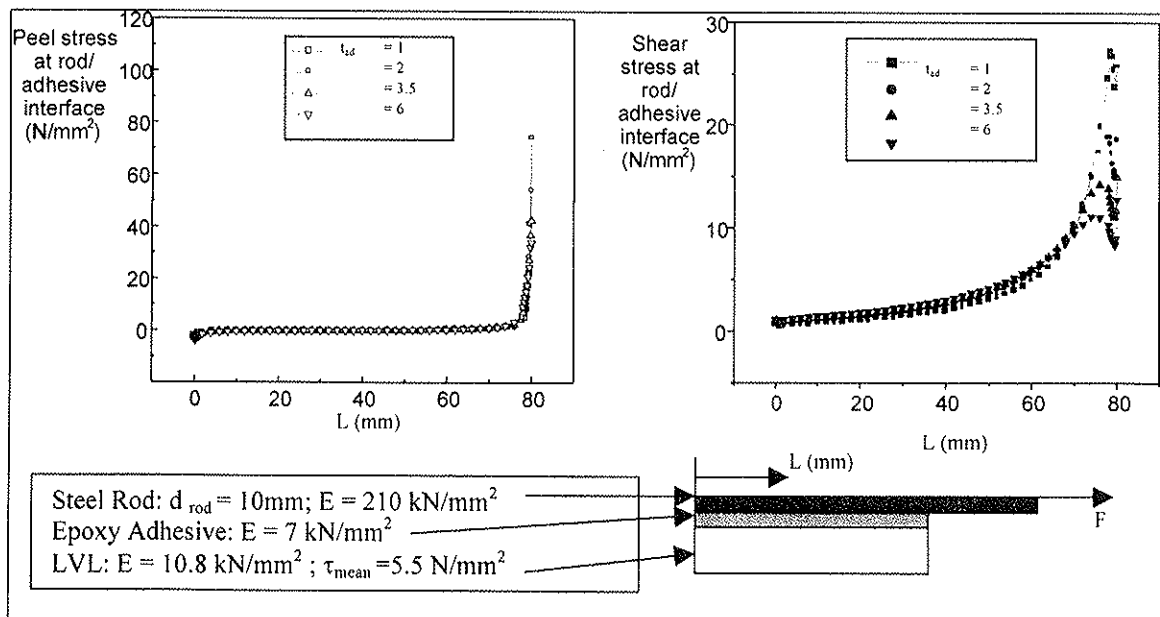


Figure 5 Influence of bondline thickness on variation of peel (normal) and shear stresses along embedment length derived through FE simulation

## 7. Effect Of Designing With FRP instead Of Steel Rods

The design implications of replacing steel rods with FRP rods can be seen to operate on two levels. First, the commonly available sections and material specifications differ between manufacturers of FRP composites, hence direct replacement may not always be possible. The second and more fundamental difference is in the codified treatment to reach a design capacity for a bonded-rod.

### 7.1 Commonly Available Rod Stocks

Theoretically, this variable can be modified to any desired value, but within a real application context there are commonly available stock sizes at defined diameters.

Since in the case of axial loading, the geometric effect is related to the cross section area resisting applied action, it is further necessary to consider the effective area of the available rods. In the case of threaded rods, this has been approached in steel construction through defined effective area, or the stress area at the root of the thread, as given in Table 1.

ISO Metric Rod	M5	M6	M8	M10	M12	M16	M20	M22	M24	M27	M30	M33	M36
Nominal Area, $A$ (mm <sup>2</sup> )	19.6	28.3	50.3	78.5	113	201	314	380	452	572	706	855	1018
Effective Area at Root of Thread, $A_{ef}$ (mm <sup>2</sup> )	14.2	20.1	36.6	58.0	84.3	157	245	303	353	459	561	694	817

\* = non-preferred sizes

**Table 1** Effective areas of steel threaded rods

Pultruded FRP rods are generally available in the range 3 - 20mm. (4,6,8,12,16) The practicalities of the pultrusion manufacturing process mean that 20mm is an approximate limit, above which manufacture becomes more complex. The FRPs considered are pultrusions which will tend to have a smooth or only mildly textured surface, relying upon actual adhesion and less on mechanical interlock of rigid adhesive and bar. Here the effective section will principally be determined by the fibre volume fraction aligned with the direction of force.

Steel rod stocks comprise a range of steels with different mechanical properties, which are commonly available in the ISO grades. The steel grade is translatable to approximate descriptions of the strength parameters, the first number being the value of the minimum ultimate tensile strength in kgf/mm<sup>2</sup> divided by 10, and the second figure being one tenth of the ratio between minimum yield stress and the minimum tensile strength, expressed as a percentage, described in Table 2.

GRADE	4.6	5.6	6.6	8.8	10.9	12.9	14.9
min ultimate tensile strength $f_{ult,k}$ (N/mm <sup>2</sup> )	392	490	588	785	981	1177	1373
min tensile yield strength $f_{y,k}$ (N/mm <sup>2</sup> )	235	294	353	628	883	1059	1236

**Table 2** Steel rod material strength

The properties of FRPs can vary massively, depending upon the precise composition and manufacture, but by way of illustration, the characteristic properties of a pultruded composite, containing a volume fraction of 65% E-glass in a polyester matrix is given in Table 3.

Property	Symbol	Characteristic Value
Longitudinal Tensile Strength	$\sigma_{x,t,k}$	690
Longitudinal Tensile Modulus	$E_{x,t,k}$	41
Longitudinal Compressive Strength	$\sigma_{x,c,k}$	414
In-plane Shear Strength	$\tau_{x,t,k}$	38
Longitudinal Failure Strain	-	2.0 %

**Table 3** Characteristic material properties for a typical pultruded FRP (EUROCOMP Data Sheet No.3)

### 7.2 Codified treatment of Bonded-in Rod Materials

In the design of structural timber connections employing bonded-in rods, work is in progress at the time of writing to develop full design rules through the GIROD project [1]. The existing model for design is presented in the informative Annex of EC5: Part2 [16], but is defined in terms of the presumption that the rod material is ferrous. Thus for design of FRP rod connections it is necessary to rethink the basis of design and

associated failure criteria, principally because the material does not yield and has no plastic residual strength beyond this recognised ultimate limit state for the bonded-in metal rod.

Thus a suitable treatment of the ultimate tensile strength is required to derive an equivalent to the bar yield failure mode and a reassessment must be made of the overall target for performance of the connection. Some aspects of the EUROCOMP design guide [13] can be employed in this respect as summarised in the following sections.

The material safety factors  $\gamma_M$  for steel and timber in this application are summarised in Table 4 [15]. For FRP materials, the definition of a suitable material factor is more complex and must take account of varying contributory factors, thus:

$$\gamma_{M,FRP} = \gamma_{M1,FRP} \gamma_{M2,FRP} \gamma_{M3,FRP} \quad (1)$$

The range of these contributory component partial factors is summarised in Table 5, with more detailed breakdown in Tables 6-8.

Ultimate limit states	
fundamental combinations	
- timber and wood-based materials	1.3
- steel used in joints	1.1
accidental combinations	1.0
Serviceability limit state	
	1.0

Table 4 Selected material safety factor coefficients  $\gamma_M$  [15]

Partial Safety Coefficient	Value	
	Max	Min
$\gamma_{M1,FRP}$	2.25	1.0*
$\gamma_{M2,FRP}$	2.7	1.1
$\gamma_{M3,FRP}$	3	1

Table 5 Partial safety factors for FRP materials [13]

\* if justified by 'detailed information or test data'

Derivation of properties		$\gamma_{M1,FRP}$
Properties of constituent materials (i.e. fibre and matrix) are derived from test specimen data		2.25
Properties from individual laminae are derived from theory		2.25
Properties of the laminae, panel or pultrusion are derived from theory		2.25
Properties of individual plies are derived from test specimen data		1.5
Properties of the laminae, panel or pultrusion are derived from theory		1.5
Properties of laminate, panel or pultrusions are derived from test specimen data		1.15

Table 6 Values for  $\gamma_{M1,FRP}$  (concerning derivation of material properties from test values)[13]

Method of manufacture	$\gamma_{M2,FRP}$	
	Fully postcured at works	Not fully postcured at works
Hand-held spray application	2.2	3.2
Machine-controlled spray application	1.4	2.0
Hand lay-up	1.4	2.0
Machine-controlled filament winding	1.1	1.7
Resin transfer moulding	1.2	1.7
Pre-peg lay-up	1.1	1.7
Pultrusion	1.1	1.7

Table 7 Values for  $\gamma_{M2,FRP}$  safety factor concerning material and production process [13]

Operating design temperature* * (°C)	HDT* (°C)	$\gamma_{M3,FRP}$	
		Short-term loading	Long-term loading
25 - 50	55 - 80	1.2	3.0
	80 - 90	1.1	2.8
	> 90	1.0	2.5
0 - 25	55 - 70	1.1	2.7
	70 - 80	1.0	2.6
	> 80	1.0	2.5

Table 8 Values for  $\gamma_{M3,FRP}$  safety factor concerning environmental effects and duration of loading [13]

\*Heat distortion temperature

\*\* For operating temperatures outside this range seek specialist advice

Factor	Range	Comment
$\gamma_{M1,FRP}$	1.15, 1.5 or 2.25	Properties may be drawn from a range of sources identified, but for this small volume usage, it is unlikely that test evidence sufficient to justify the further reduction to 1.0 will be made available in foreseeable future.
$\gamma_{M2,FRP}$	1.1	Pultrusion, fully post-cured at works have been the focus of work to date
$\gamma_{M3,FRP}$	short term load	1.0 or 1.1
	long term load	2.5 or 2.7

Table 9 Summary Of FRP partial material factors identified with potential application in bonded-in rod applications

This range of  $\gamma$  factors mean that the theoretical range of combined material safety factor (assuming that only a normal range of information and data is available) is extremely wide, ranging from 1.265 - 18.225. However this range is narrowed for building applications such that  $1.5 \geq \gamma_{M,FRP} \geq 10$ . (EUROCOMP note a 2.3.3.2. P(1)). Within the context of these studies, the range of component safety factors are as summarised in Table 9. Therefore, the calculated range of combined material safety factor for the FRP materials is 1.265 - 6.68, however, the lower limit can be raised due to the building context of the application, thus  $1.5 \geq \gamma_M \geq 6.68$ .

The effect of the safety factor reduction is illustrated as both percentage reduction and in terms of quantified material strength in Figure 6, on the basis of the general equation :

$$X_d = X_k / \gamma_M \quad (2)$$

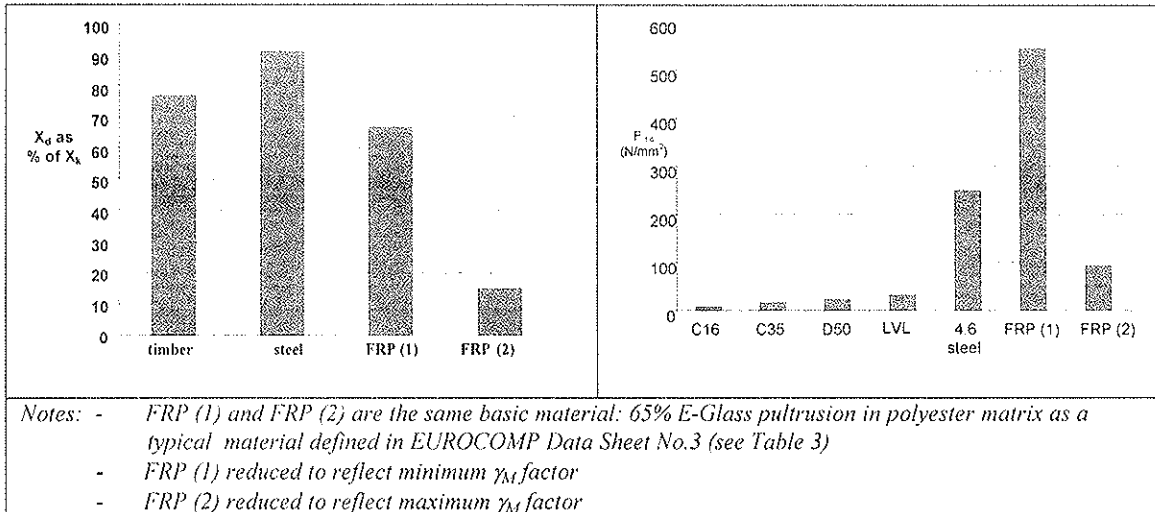


Figure 6 Comparative impact of derived design value drawn from characteristic capacities of rods and substrate timbers

There are also further implications relating to the selection of an appropriate treatment for FRP and steel rods, which can be illustrated through consideration of the design capacity compared to the characteristic ultimate capacity, as in Figure 7.

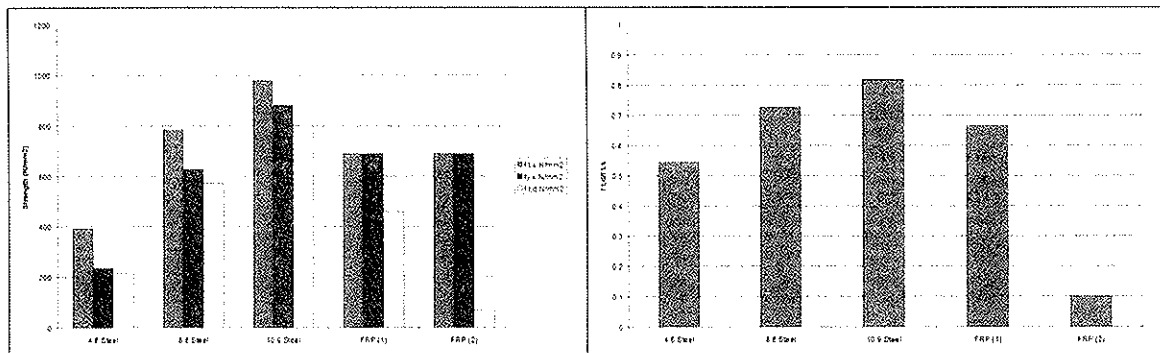


Figure 7 Comparison of design and ultimate capacities in steels of various grade and FRPs

As can be seen, and by definition, the higher grade steels have a yield (i.e. design basis) which is closer to the characteristic ultimate strength. This is important, since considering steel and FRP in relation to ultimate capacity places them on a level footing in terms of strength consideration. The second of the graphs in Figure 7 illustrates the ratio of design strength to ultimate strength, or in other words the portion of characteristic capacity being exploited through design. As illustrated, through application of the  $\gamma_{M,FRP}$  factors described above, the end result is further from the ultimate capacity than in its steel counterpart, even though the steel is based upon a reduced characteristic relating to yield.

This also brings into question the validity of employing a universal material partial factor for steel across all grades, since the higher grades have an enhanced design point as reference for calculation of the capacity of bonded-in rods. This is of particular importance when considering that in general, higher strength metals are more brittle, and hence exhibit less of the gradual failure features that are the target for yield-based



design. Also because in instances where fatigue may be of prime significance the design point at yield will be a higher fraction of the ultimate strength, which has a logarithmic impact upon the fatigue life (number of cycles to failure).

The differential treatment of steels of varying grade also finds precedence in the limit states steel design code BS 5950 [19], whereby  $\gamma_{M,steel}$  is taken as 1.0 across the range, tabulated design solutions for Grade 4.6 and 8.8 being given, whilst alternative derivations for other grades being presented as:

$$\text{Shear Strength} \quad \tau_d = 0.48 f_{ult,t,k}, \text{ but } \leq 0.69 f_{y,k} \quad (3)$$

$$\text{Tensile strength} \quad f_{t,d} = 0.58 f_{ult,t,k}, \text{ but } \leq 0.83 f_{y,k} \quad (4)$$

Values and decisive parameters are identified in Table 10.

Grade	4.6	5.6	6.6	8.8	10.9	12.9
Shear Strength	160	202	243	375	471	565
Based on $f_{ult}$				✓	✓	✓
Based on $f_y$	✓	✓	✓			
Tension Strength	195	244	293	450	569	682
Based on $f_{ult}$				✓	✓	✓
Based on $f_y$	✓	✓	✓			

**Table 10 Values for safe capacities of bolts / threaded rods from BS 5950 Table 32**

There is also potential to draw upon EUROCOMP approach to adopt a similar format to that employed for derivation of FRP material partial safety coefficients in order to derive adhesive material safety factors, as follows :

$$\gamma_M = \gamma_{M1,ad} \gamma_{M2,ad} \gamma_{M3,ad} \gamma_{M4,ad} \quad (5)$$

Factor		Classification	Value
$\gamma_{M1,ad}$	Source of Adhesive Properties	Typical or textbook values for appropriate adherends	1.5
		Values obtained by testing	1.25
$\gamma_{M2,ad}$	Method Of Adhesive Application	Manual application, no adhesive thickness control	1.5
		Manual application, adhesive thickness controlled	1.25
		Established application procedure with repeatable and controlled process parameters	1.0
$\gamma_{M3,ad}$	Type of Loading	Long term	1.5
		Short term	1.0
$\gamma_{M4,ad}$	Environmental conditions	Service conditions outside the adhesive test conditions	2.0
		Adhesive properties determined for the service conditions	1.0

**Table 11 Summary of adhesive partial material factors identified with potential application in bonded-in rod applications [13]**

The significance of brittleness in adhesives is also recognised in an application note to Table 11, such that in cases whereby the failure strain < 3%,  $\gamma_M$  should not be less than 1.5 [13].

## 8. Material Parameter Study In A Typical Joint Configuration

The following section looks at design implications of introduction of FRPs into a single bonded rod connection, and compares resultant design capacities for steel of different grades and FRP reduced to cover the range of  $\gamma_{M,FRP}$  factors identified previously. The calculations have been performed following the current basis in EC5:Part 2, and do not incorporate resolution of all items discussed in previous sections of this paper( i.e. all calculation followed through based on yield of steel grades).

For simplification in this particular study, the influence of bond thickness has not been explored. It has also been taken that bond capacity is adequate and that the timber section is sufficient to transfer the developed forces. Hence focus shifts to the possibility of either failure in the rod or failure in the timber surrounding the bond. The study has been performed assuming a nominal bond thickness of 1 mm where the nominal bond thickness is assumed to be half the difference between hole diameter and nominal rod diameter.

The equations for design employed are given in Table 12. And the resultant capacities over a range of rod diameters are given in Figures 8-13.

Mode Of Failure	Steel Rod	FRP Rod
Rod	$\frac{f_{y,k} A_{ef}}{\gamma_{M,Steel}}$	$\frac{f_{l,o,k} A}{\gamma_{M,FRP}}$
Adhesive	Assumed Adequate	Assumed Adequate
Local Timber	$\frac{1.2 \times 10^{-3} d_{hole}^{-0.2} \rho_k^{1.5} (\pi d_{hole} L_a)}{\gamma_{M,Timber}}$	$\frac{1.2 \times 10^{-3} d_{hole}^{-0.2} \rho_k^{1.5} (\pi d_{hole} L_a)}{\gamma_{M,Timber}}$

Table 12 Basis of calculations to illustrate design solutions

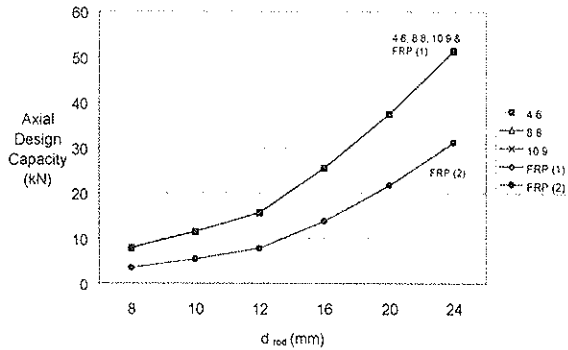


Figure 8 Design capacity for rods in C16, λ = 10

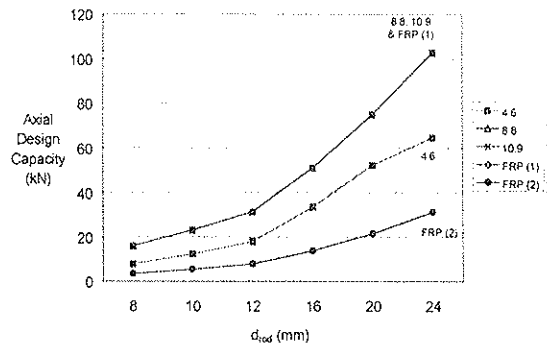


Figure 9 Design capacity for rods in C16, λ = 20

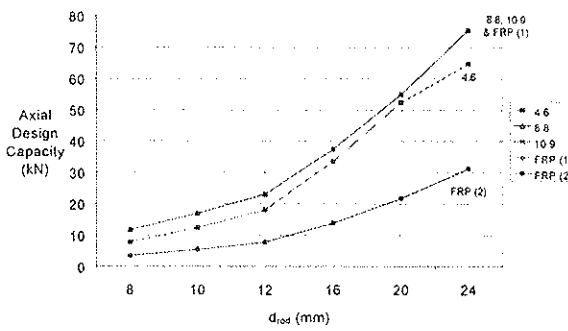


Figure 10 Design capacity for rods in C35, λ = 10

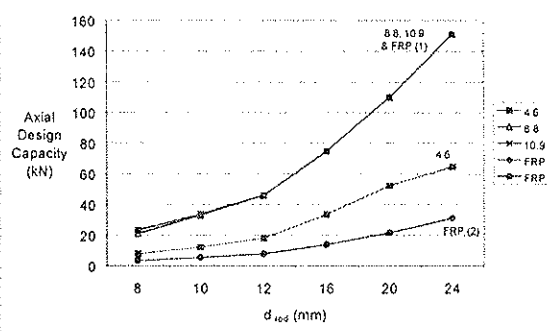


Figure 11 Design capacity for rods in C35, λ = 20

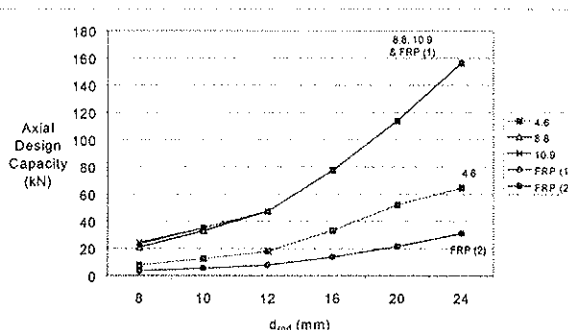


Figure 12 Design capacity for rods in D50, λ = 10

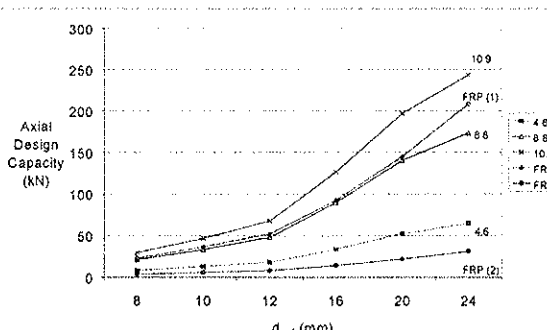


Figure 13 Design capacity for rods in D50, λ = 20

From these parameter studies it is clear that on the existing basis of design, within the range of common parameters considered, the bonded-in rod capacity might be defined either by the rod or the timber. The general trends confirm that the lower strength the host timber, the less of a difference the rod type makes upon the design capacity (e.g. Figure 8). The ratio of bond length to rod diameter also has a clear impact, with larger ratios leading to more pronounced definition of the rod type across the set of design capacities.

Thus, on the existing basis of design, there may be little advantage in utilising higher strength rods in some real design situations, since the capacity of the host timber has an impact such that the benefits of the higher grades might only be realised to benefit in higher grade timber with large λ ratios. The issues of thicker

bond line, hence larger adhesion areas at the timber/adhesive interface coupled with the variation of adequacy of the range of potential adhesives will impact upon this, as will any revision to the basis for treatment of higher grade steels whereby capacity might be defined by a more severe reduction of ultimate capacity than that employed as a reduction on yield strength via  $\gamma_M$  alone.

## 9. Conclusions

FRP materials appear to have a useful role for execution of bonded-in rod type connections. However they require different design considerations and should not necessarily be considered as direct substitutes for steel rods.

Different adhesive types have different behaviours, but there are also noticeable differences between brands within a generic type. Therefore specific data should be employed relevant to a resin system deployed in accordance with manufacturer guidance.

Extremely thick bondlines have been investigated in this research, and pull-out strengths increased linearly with bondline thickness, consistent with the increase in bonded area of timber at large hole diameters. FEA results clearly exhibit a fall in peak shear and peel stress at the adhesive/timber interface with increasing bondline thickness.

These studies have highlighted some of the potential problems with the current design basis centred upon yield capacity of rods when employing a wider range of materials. Employment of high performance adhesives in thick bond lines together with a re-assessment of rod design capacity could provide design benefit utilising the fuller range of available materials.

The geometric configuration will combine with the material properties of rod, adhesive and host timber to define the failure mechanism. The implications for design vary. As far as ULS behaviour is concerned, the interaction of material combinations and implications of selection reflect the chosen basis of design and the way in which the material behaviour to failure is tackled with a view to establishing satisfactory reliability in the end solution.

Lightness and ease of bondability (especially through peel ply techniques) mean that FRP solutions may provide a valuable alternative in new-build and in renovation and repair work. In either case, the combination of bonding technology and appreciation of design concepts in a fundamentally different material may pose challenges to the full implementation across construction.

Process issues are of importance, and design needs to be attuned to specific materials of known quality, reliance upon workmanship and low visual inspection opportunity. Therefore the communication, monitoring, feedback and overall skill levels are paramount in achieving low defect levels and suggest that these systems are better suited to pre-fabrication in preference to site manufacture solutions. There is, however clearly scope for partial prefabrication with site processes focussed upon mechanical connection of adhesive bonded rods.

There is a clear need for quality control type test configurations to be developed, especially bearing in mind simple, easily operable procedures suited to SME manufacturers who dominate timber engineering operations throughout Europe.

## Acknowledgements

This paper is in part the result of work supported by the EPSRC (The Engineering and Physical Sciences Research Council) as part of the Materials for Better Construction Programme. The authors wish to acknowledge this and would also like to thank the Industrial Collaborators- Brecon Beacons National Park, Buro Happold Ltd., Coed Cymru, Ove Arup & Partners, Permabond, Rotafix and Sika Ltd.

## References

- [1] GIROD Project Website: <http://www.sp.se/building/wood/girod.htm>
- [2] TINGLEY, D.A. and GAI, C. (1998). FRP reinforced Glulam Performance: A case Study of The Lighthouse Bridge. WCTE'98 - The Fifth World Conference on Timber Engineering, Lausanne, Switzerland, August 17-20, 1998.
- [3] LARSEN, H.J. and ENQUIST, B. (1996). Glass Fibre Reinforcement of Dowel Type Joints . International Wood Engineering Conference '96, New Orleans, USA.
- [4] WALSER, R. and STEINER, W. (1997). Strengthening A Bridge With Advanced Materials. Structural Engineering International, 1997, 2/97, IABSE.

- [5] BAINBRIDGE, R.J. and METTEM, C.J. (1998). Moment Resistant Connections in Timber Structures: A Review of Existing and Innovative Systems. *Paper 11590*, Structures and Buildings Journal, The Institution of Civil Engineers, Thomas Telford Publishing Ltd., London.
- [6] DRAKE, R.D., ANSELL, M.P., ARAM, J.W.E., METTEM, C.J. and BAINBRIDGE, R.J. (1998). Non-Metallic Connections For Timber Structures. WCTE'98 - The Fifth World Conference on Timber Engineering, Lausanne, Switzerland, August 17-20, 1998, 2-577.
- [7] DRAKE, R.D., ANSELL, M.P., METTEM, C.J. and BAINBRIDGE, R.J. (1999). Non-Metallic, Adhesiveless Joints For Timber Structures. CIB-W18/32-7, CIB-W18 Meeting Thirty-Two, Graz Austria, August 1999.
- [8] INSTITUTION OF STRUCTURAL ENGINEERS, (1999). Guide To the Structural Use Of Adhesives. IStructE, London, UK.
- [9] METTEM, C.J., PAGE, A.V. and ROBINSON, G.C. (1993). Repair of Structural Timbers - Part 1 Fire Resistant Repairs. Research Report RR 1/93 Pt2, TRADA, High Wycombe, UK.
- [10] RIBERHOLT, H. (1988). Glued Bolts in Glulam - Proposals For CIB Code. CIB-W18/21-7-2, Proceedings of CIB-W18, Meeting Twenty One, Parksville, Vancouver Island, Canada
- [11] RAKNES, E. (1995). Adhesives. STEP Lecture A12, Timber Engineering STEP 1, STEP, EUROFORTECH, Centrum Hout, Almere
- [12] TRADA (1993). Adhesives For Wood and Wood Products - VBS EN Standards. WIS 2/3-35, TRADA, High Wycombe, UK.
- [13] CLARKE, J.L. (Editor) , (1996). Structural Design of Polymer Composites - EUROCOMP Design Code and Handbook. E & F N Spon, London.
- [14] RODD, P.D., HILSON, B.O. and SPRIGGS, R.A. (1989). Resin Injected Mechanically Fastened Timber Joints. Second Pacific Timber Engineering Conference, Auckland, New Zealand.
- [15] DD ENV 1995-1-1 (1994). Eurocode 5 Design of Timber Structures - Part 1.1: General Rules And Rules For Buildings.
- [16] DD ENV 1995-2 (1997). Eurocode 5 Design of Timber Structures - Part 2: Bridges.
- [17] HARVEY, K., ANSELL, M. HUTCHINSON, A., and BROUGHTON, J. (1998). Improved Timber Connections Using Bonded-In Rods. WCTE'98 - The Fifth World Conference on Timber Engineering, Lausanne, Switzerland, August 17-20, 1998.
- [18] HUTCHINSON, A., and BROUGHTON, J. (1998). Pull-out Behaviour Of Reinforcement Bonded Into Timber. Structural Adhesives in Engineering V, Institute of Materials, Fifth International Conference, Bristol, UK, April, 1998.
- [19] BSI (1985). BS5950:Part1:1985. Structural Use of Steelwork in Building:Part1. Code of Practice For Design in Simple and Continuous Construction: Hot Rolled Sections. BSI, London, UK.
- [20] JOHANSSON, C. J., (1995). Glued -in Bolts. Step Lecture C14, Timber Engineering STEP 1, STEP, EUROFORTECH, Centrum Hout, Almere
- [21] HUTCHINSON A R and BROUGHTON J G (1998), Resins in timber repairs, Proc. of the Construction and Building Research Conference, COBRA, Oxford, Sept. 2-3<sup>rd</sup>, Vol.2, pp73-86, 1998.
- [22] HUTCHINSON A R and BROUGHTON J G (1999), Bonded Connections in Timber Structures, Poster Presentation, Swiss Bonding '99, 13<sup>th</sup> Int. Sym., HSR Rapperswil am Zurichsee, Switzerland, 4-6<sup>th</sup> May.
- [23] HARVEY, K., and ANSELL, M. (1999) "Improved Timber Connections Using Bonded-in Rods," Poster Presentation, Workshop Damage in Wood, COST Action E8, Bordeaux, France, 17th-28th May 1999.
- [24] RIBERHOLT, H. and SPOER, P. (1983) Design of the Inbonded Rods That Are Used For the Windblade Root Section on Nibemolle - B, Report No 167, Series R, Department of Structural Engineering, Technical University of Denmark.
- [25] DD ENV 1991-1 (1994). Eurocode 1 Basis of Design And Actions On Structures - Part 1: Basis Of Design.

**INTERNATIONAL COUNCIL FOR RESEARCH AND INNOVATION  
IN BUILDING AND CONSTRUCTION**

**WORKING COMMISSION W18 - TIMBER STRUCTURES**

**BENDING-STRESS-REDISTRIBUTION CAUSED BY DIFFERENT CREEP  
IN TENSION AND COMPRESSION AND RESULTING DOL-EFFECT**

P Becker  
K Rautenstrauch  
Bauhaus-University Weimar  
GERMANY

**MEETING THIRTY-TWO  
GRAZ  
AUSTRIA  
AUGUST 1999**

---

Presenter: P.Becker

- H.J.Larsen severely questioned the basic assumptions made in the paper.
- S.Thelandersson agreed with H.J.Larsen that the principle of linear viscoelasticity theory would not be appropriate in this case.
- H.J.Larsen stated that the results may be acceptable only if limitations were put on the approach based on the assumed stress strain relationship and not generalised to application to timber.
- A.Ranta-Maunus commented that non-linear creep model was used in VTT. Results were presented a few years ago in Copenhagen. The results also showed minor influence on DOL.
- M.Ansell agreed with the point that initial damage was compression and ultimate failure was in tension.
- F.Rouger also pointed out that since the influence on DOL was insignificant; therefore, the title of the paper was inappropriate.

# Bending-stress-redistribution caused by different creep in tension and compression and resulting DOL-effect

Peter Becker, Karl Rautenstrauch  
Bauhaus-University Weimar, Germany

## 1 Introduction

Creep is generally assumed to be larger for compression than for tension to some degree. This results in a change of stress-distribution. The stress for the tension edge will increase and decrease for the compression edge. An analytical solution of this behaviour can be easily derived with the assumption of creep limits for both impacts.

The resulting stress-distribution will lead to a decreasing computational bending strength value, because the stress for the tension edge, which will be finally responsible for failure, has already increased during lifetime of a structural element. The exact difference can be determined by simulation. For initial and resulting stress-distribution load increments are applied until tension strength is reached for the tension edge. Plasticating ability of wood subjected to compression is considered.

## 2 Background, Observations and Assumptions

To compute a resulting stress distribution creep laws have to be applied, which result in a final creep deformation state. This comes with the use of creep factors, which indicate the magnitude of additional time-dependent deformation in relation to the initial elastic one.

In many experiments, done in bending, tension and compression, it has been found out, that creep is larger in compression than in tension (i.e. Gressel 1984, Glos et al 1987, Rautenstrauch 1989, Bengtsson et al 1997, Hunt 1997). Researchers do not agree with the quantity of the difference, but the quotient of the creep factors in compression and tension  $\varphi_c/\varphi_t$  should be somewhere between 1 and 4. It probably strongly depends on stress level, moisture content and quality of wood. The reason for this is that creep in compression becomes nonlinear for increasing stress and moisture levels (Keith 1972). The proportional limit is reached earlier for low quality material. The stress-threshold for non-linearity in tension is assumed to be much higher, so it is hardly obtained during the lifetime of a structural element.

For analytical reasons the Bernoulli hypothesis of a plane remaining cross-section is adopted. The moisture distribution over the cross-section is taken as uniform, so the climatic conditions are assumed to be more or less constant. For stationary behaviour the same E-modulus for tension and compression is taken.

If the observations and assumptions are used to simulate the long-term behaviour of a bending element under constant load the following phenomena are registered:

- The neutral axis is moving towards the tension edge. The compression zone becomes larger.
- The stress for the compression edge decreases and increases for the tension edge.

- In the final deformation state the overall strain becomes the  $(1+\varphi)$ -multiple of the elastic strain at any cross-section point.

The last observation is very essential to the stress-strain analysis. It can be proven by solving the time-dependent material law, taken from linear viscoelasticity theory, analytically.

### 3 Stress and strain analysis

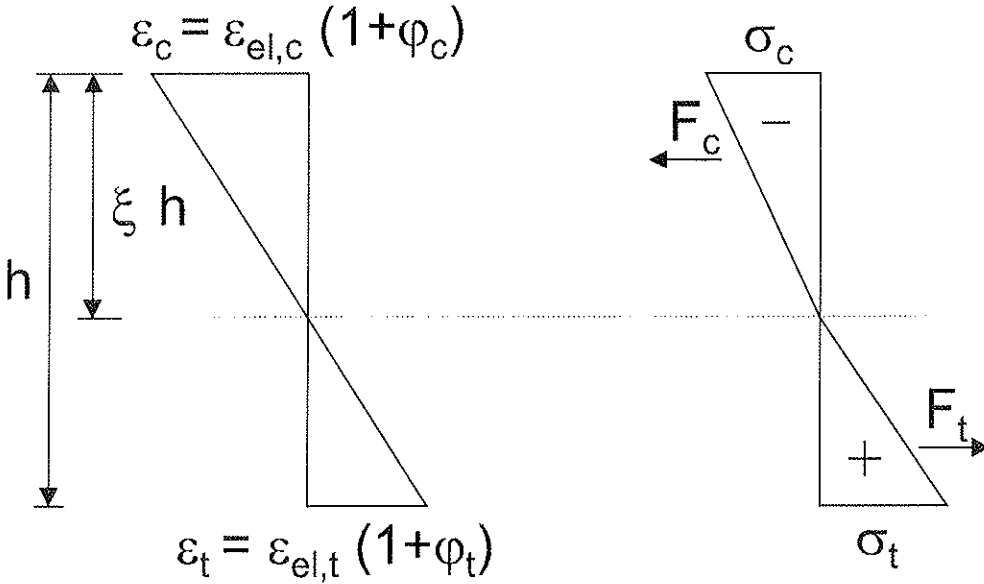


Fig. 1 Strain and stress distribution after long-term loading

The assumed strain-distribution after long-term loading results in a bilinear stress-distribution (figure 1). The edge-stresses are related to the elastic strain by Hooke's law:

$$\sigma_{c,t} = E \cdot \varepsilon_{el,c,t} \quad (1)$$

It is very important to recognize though, that the elastic edge strains  $\varepsilon_{el,c}$  and  $\varepsilon_{el,t}$  in figure 1 and equation (1) are not identical to the initial ones. It is the elastic deformation establishing in the final deformation state after long-term loading.

The resulting forces of compression and tension zone can be obtained by assuming the location of the neutral axis as it is done in figure 1. If the width of the cross-section is notified by  $b$ , they can be simply expressed:

$$F_c = \frac{1}{2} \cdot \sigma_c \cdot b \cdot \xi \cdot h \quad \text{and} \quad F_t = \frac{1}{2} \cdot \sigma_t \cdot b \cdot (1 - \xi) \cdot h \quad (2)$$

The conditions of equilibrium yield two equations. In the first one the bending moment resulting from the stress distribution has to reflect the given one:

$$\frac{2}{3} F_c \cdot \xi \cdot h + \frac{2}{3} F_t \cdot (1 - \xi) \cdot h = M \quad (3)$$

In the second one the sum of horizontal forces has to remain zero assuming pure bending.

$$F_c + F_t = 0 \quad (4)$$

$F_c$  and  $F_t$  can be expressed by  $\varepsilon_{el,c}$  and  $\varepsilon_{el,t}$  using equations (1) and (2). So equations (3) and (4) contain three unknowns, which are  $\varepsilon_{el,c}$ ,  $\varepsilon_{el,t}$  and the location of the neutral axis, defined by  $\xi$ , respectively, so one further condition is needed for solving the problem. It is obtained with a compatibility condition, which is gained by applying the intercept theorem to the strain distribution of figure 1.

$$\frac{(1 + \varphi_c) \varepsilon_{el,c}}{\xi \cdot h} = \frac{(1 + \varphi_t) \varepsilon_{el,t}}{(1 - \xi) \cdot h} \quad (5)$$

Now a complete solution is possible. All variables can be expressed by the known parameters (bending moment  $M$ , creep factors  $\varphi_c$  and  $\varphi_t$ , cross-section  $b/h$ ). Introducing the section modulus  $W$  the result for the edge stresses then is

$$\sigma_c = \frac{M}{W} \cdot \frac{1}{2} \left[ 1 + \sqrt{\frac{1 + \varphi_t}{1 + \varphi_c}} \right] \quad (6a)$$

$$\sigma_t = \frac{M}{W} \cdot \frac{1}{2} \left[ 1 + \sqrt{\frac{1 + \varphi_c}{1 + \varphi_t}} \right] \quad (6b)$$

The location of neutral axis becomes

$$\xi = \frac{1}{1 + \sqrt{\frac{1 + \varphi_t}{1 + \varphi_c}}} \quad (7)$$

Example:

A beam is stressed by a load, which causes nominal edge stresses of 10 MPa. If the creep factors are assumed as  $\varphi_c = 1,5$  and  $\varphi_t = 0,5$ , for long-term loading the edge stresses will then become

$$\sigma_{c,t=\infty} = 10 \cdot \frac{1}{2} \cdot \left[ 1 + \sqrt{\frac{1 + 0,5}{1 + 1,5}} \right] = 8,87 \text{ MPa}$$

$$\sigma_{t,t=\infty} = 10 \cdot \frac{1}{2} \cdot \left[ 1 + \sqrt{\frac{1 + 1,5}{1 + 0,5}} \right] = 11,45 \text{ MPa}$$

So in the long run the stress for the tension edge will actually be about 14,5% higher than it is dimensioned for.



## 4 Determining bending creep factor

If the creep factors in tension and compression are assumed to be equal, it is obvious, that the creep factor in bending is the same also, presuming the shear proportion of deflection is neglected. The situation is different, if tension and compression creep factors are unequal. It can be expected that the bending creep factor is placed somewhere in between. Neglecting the shear deformation the relation of bending moment  $M$  and curvature  $w''$  can be taken for quantifying the bending creep factor.

$$w'' = -\frac{M}{EI} \quad (8)$$

Assuming linear viscoelasticity curvature and bending moment can be taken proportional along the beam. The curvature or the second derivative of deflection may be expressed by the strains of tension and compression edge (figure 1).

$$w'' = \frac{\varepsilon_t - \varepsilon_c}{h} \quad (9)$$

Using the solution of section 3 and putting it into equation (9) it becomes

$$w'' = \frac{1}{4} \cdot \frac{M}{EI} \cdot [\sqrt{1 + \varphi_c} + \sqrt{1 + \varphi_t}]^2 \quad (10)$$

Integrating twice and applying existing boundary conditions the final overall long-term deflection may be determined for any location on a beam. Subtracting the initial elastic deflection and dividing the remaining creep deflection by the elastic deflection results in the bending creep factor, which for the given assumptions only depends on the tension and compression creep factors.

$$\varphi_b = \frac{1}{4} \cdot [\sqrt{1 + \varphi_c} + \sqrt{1 + \varphi_t}]^2 - 1 \quad (11)$$

### Example

Creep factors in compression and tension are assumed as  $\varphi_c = 1,5$  and  $\varphi_t = 0,5$  respectively. The creep factor in bending then becomes

$$\varphi_b = \frac{1}{4} \cdot [\sqrt{1 + 1,5} + \sqrt{1 + 0,5}]^2 - 1 = 0,97$$

Obviously the bending creep factor is slightly less than the mean of creep in tension and compression. This does not reflect the observations of Gressel (1984), who observed bending creep being almost as high as compression creep. The difference might be explained by the influence of shear deformation (elastic and creep) being neglected in this analytical study.

The creep factors given in codes have to be understood as bending creep factors. Taking a bending creep factor  $\varphi_b$  and assuming a certain value of the quotient  $\varphi_c/\varphi_t$ , the creep factors for tension and compression can be determined by using equation (11).

Figure 2 now reflects the influence of the quotient  $\varphi_c/\varphi_t$  on the long-term resulting edge stresses of a bending element. The nominal initial edge stresses were 10 MPa. As expected a strong dependency to the quotient is obtained.

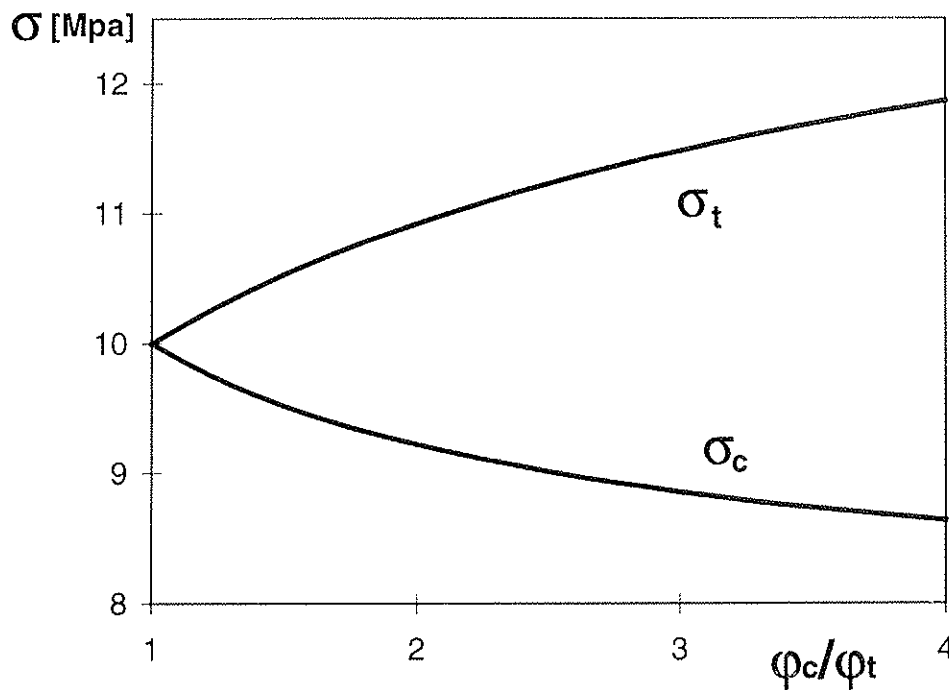


Fig. 2 Stresses for tension and compression edge depending on the quotient  $\varphi_c/\varphi_t$ ,  $\varphi_b = 1,0$

## 5 Effect on DOL-behaviour of a beam

After concluding a certain effect of the different creep behaviour in tension and compression to the edge stresses of a bending element and quantifying this phenomenon, the question comes up, if the increase of tension stress leads to an earlier failure and can therefore be made responsible to a certain part of the duration of load phenomenon.

To find out about this a layer model was chosen to simulate the DOL-effect in the following way:

- The initial bending strength is checked by raising the load until a certain failure criterion, which will be described later, is reached.
- The second step consists of long-term loading of the beam under service conditions until a final deformation and stress state as indicated in figure 1 is obtained.
- After this the load is continuously increased again until the defined failure criterion is reached.
- Finally the initial bending strength and the bending strength after long-term loading are compared to check the pure effect of different creep in tension and compression on the duration of load phenomenon.

As stationary material law in tension linear-elastic brittle behaviour is assumed. For compression the material law invented by Glos (1978) is taken. As can be seen in figure 3 the plasticating ability of the material for compression loading is taken into account by the material law of Glos. Failure is always obtained at the tension edge as soon as the tension strength is exceeded. So deformation ability in compression is assumed to be infinite. This corresponds to behaviour observed in bending experiments, where specimens usually fail at the tension side.

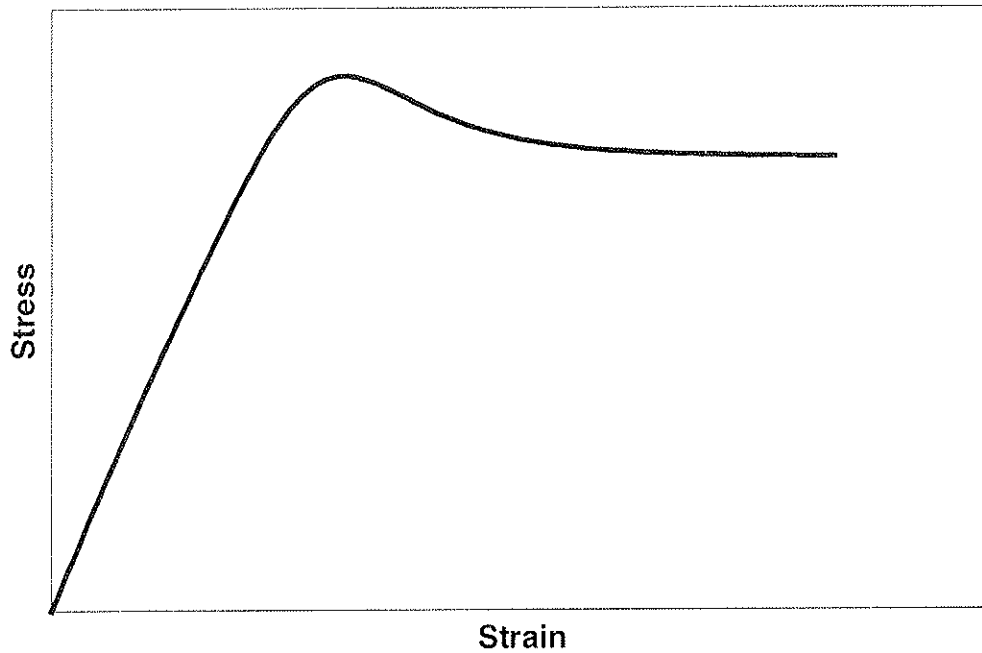


Fig. 3 Material law in compression according to Glos (1978)

In the simulation material properties of European spruce were chosen. It was distinguished between the quality of the simulated timber. Therefore material properties of high, average and low quality spruce were arbitrary chosen (Table 1). The usage of different E-modulus values was also possible in the simulation as can be seen in table 1.

	$E_t$ [Mpa]	$E_c$ [Mpa]	$f_t$ [Mpa]	$f_c$ [Mpa]
High quality material	15350	14720	70	48
Normal quality material	12450	12450	50	40
Low quality material	9000	9800	25	32

Table 1 Arbitrary chosen mechanical parameters for simulation of high, normal and low quality timber

The computational resulting bending strengths, initial and long-term after finalized stress-redistribution, can be taken from table 2. They are obtained by dividing the applied moment  $M$  through section modulus  $W$ . The bending creep factor is assumed to be  $\varphi_b = 1,0$ .

The influence of different creep in tension and compression turns out to be low as can be shown in table 2. The plasticating ability of wood in compression is mainly responsible that the bending strength does not decrease by more than two percent for material of normal and high quality although tension stress may increase by more than 20% ( $\varphi_c/\varphi_t = 4$ ) in service state.

The difference becomes larger for low quality material. The reason for this is that it is not taken benefit of the plasticating ability in compression this time, because tension strength is reached much earlier. Low quality material is usually based on a low raw density and especially by a high “knot area ratio“-value (KAR). Because material properties for tension are much more affected by knots than the ones for compression, the stress in the tension zone has to be absorbed by less area, which leads to higher stresses and therefore to larger creep on the tension side also. This is the reason why high quotients of  $\varphi_c/\varphi_t$  can rather be not expected for low quality material and the influence on the DOL-effect can be expected to be relatively low also.

	$\varphi_c / \varphi_t$	1	2	3	4
High quality material	$f_{b,t=0}$ [MPa]	64,70	64,70	64,70	64,70
	$f_{b,t=\infty}$ [MPa]	64,70	64,38	64,20	64,01
	$\Delta f_b$ [%]	-	0,5	0,8	1,1
Normal quality material	$f_{b,t=0}$ [MPa]	48,51	48,51	48,51	48,51
	$f_{b,t=\infty}$ [MPa]	48,51	47,93	47,54	47,30
	$\Delta f_b$ [%]	-	1,2	2,0	2,5
Low quality material	$f_{b,t=0}$ [MPa]	25,64	25,64	25,64	25,64
	$f_{b,t=\infty}$ [MPa]	25,64	24,76	24,21	23,83
	$\Delta f_b$ [%]	-	3,4	5,6	7,1

Table 2 Comparison of short- and long-term bending strength for different quotients  $\varphi_c/\varphi_t$

## Conclusion

Different creep in tension and compression was observed by many researchers. The exact difference can hardly be quantified because it strongly depends on climatic and loading conditions and also on the quality of the material.

It generally leads to changing edge stresses, which under the assumption of linear viscoelasticity can be easily determined by equation (6) using creep factors. If certain factors are given for compression and tension creep a bending creep factor, which is slightly lower than the mean of tension and compression creep, can be determined also (11).

Because of the strong ability of the material to plasticate under compression, the influence of an increasing tension stress on the duration-of-load phenomenon turns out to be quite low, almost negligible for normal and high quality material. Taking timber of low quality

the influence becomes larger, a big difference in tension and compression creep can rather be not expected for this kind of material though.

## References

- Bengtsson, C., Kliger, R., Johansson, G. (1997) - Creep in bending, tension and compression - experiments and speculations. Int. Conf. of IUFRO S5.02, Copenhagen, Denmark.
- Glos, P. (1978) - Zur Bestimmung des Festigkeitsverhaltens von Brettschichtholz bei Druckbeanspruchung aus Werkstoff- und Einwirkungskenngrößen (Determining strength behaviour of glulam in compression from basic material and impact properties, in German). PhD-Thesis, University of Munich, Germany.
- Glos, P., Heimeshoff, B., Kelletshofer, W. (1987) - Einfluß der Belastungsdauer auf die Zug- und Druckfestigkeit von Fichten-Brettlamellen (Influence of load duration on the tension- and compression-strength of spruce, in German). Holz als Roh- und Werkstoff 45, 243-249.
- Gressel, P. (1984) - Kriechen von Holz und Holzwerkstoffen (Creep of wood and wood-based materials, in German). Bauen mit Holz 86, 216-223.
- Hunt, D.G. (1997) - Dimensional changes and creep of spruce, and consequent model requirements. Wood Science and Technology 31, 3-16.
- Keith, C.T. (1972) - The mechanical behaviour of wood in longitudinal compression. Wood Science 4, 235-245.
- Rautenstrauch, K. (1989) - Untersuchungen zur Beurteilung des Kriechverhaltens bei Holzbiegeträgern (Experiments and investigations to the creep behaviour of timber beams, in German). PhD-Thesis, University of Hannover.

**INTERNATIONAL COUNCIL FOR RESEARCH AND INNOVATION  
IN BUILDING AND CONSTRUCTION**

**WORKING COMMISSION W18 - TIMBER STRUCTURES**

**THE LONG TERM PERFORMANCE OF PLY-WEB BEAMS**

R Grantham

V Enjily

Building Research Establishment (BRE)

CTTC - Timber Engineering

UNITED KINGDOM

**MEETING THIRTY-TWO**

**GRAZ**

**AUSTRIA**

**AUGUST 1999**

---

Presenter: R.Grantham

- P.Becker commented that the creep recovery period was too short.
- R.Grantham agreed but pointed out that there were funding limitations.
- H.J.Larsen stated that comments and reference to EC5 should be revised to reflect design values issue.
- S.Svensson questioned about the influence on climatic data to results.
- R.Grantham and V.Enjily responded that there was insufficient detailed climatic data to allow comparisons; therefore, the formula only accounted for time effects and did not account for climate.
- S.Svensson commented that the results would be highly dependent on climatic conditions.
- V.Enjily responded that additional results were available from a different study.
- A.Ranta-Maunus stated that shear creep is much more significant than bending creep in panel material; therefore, I-beam would be especially susceptible to creep under permanent loads.
- V.Enjily stated that creep in I-beam rather than creep of individual elements was measured.
- M.U.Pedersen commented that the change in deformation resulted from drying shrinkage on the compression side.
- C.Mettem discussed issues on web buckling and depth of web member. He also commented that report on component-based properties rather than material properties might cause difficulties for application to design.
- R.Grantham responded that lateral web buckling was not observed.
- F.Rouger asked and received clarification on the calculation of design load.

# The long term performance of ply-web beams

R. Grantham and V. Enjily  
Timber Engineering, CTTC,  
Building Research Establishment Ltd., UK

## Abstract

Ply-web beams have been used for a number of years in floor and flat roof constructions, such as swimming pools, that require medium-span structural beams. Many of the advantages associated with ply-web beams stem from their structural efficiency, utilising structural timber flanges and plywood webs. This produces lightweight components that are easily installed on site and reduce the dead weight of construction when compared to solid timber beams. The design of ply-web beams has been thoroughly investigated with the exception of their long-term performance. Very few studies have covered this aspect of design, which may be critical in service conditions producing fluctuating moisture contents in the beam.

This paper reports the results of long-term performance tests on Ply-web 'I' beams over a period of 6 years when loaded to a variety of utilisation ratios in uncontrolled conditions. Both Finish Birch and Canadian Douglas-fir plywood were used for the web of beams, which were monitored for relative creep under conditions of naturally fluctuating relative humidity and moisture content. Comparisons made with the guidance given in EC5 at both the Serviceability and Ultimate Limit State have highlighted some significant differences between design predictions and the actual performance. Firstly, strength tests conducted on ply-web beams with Finnish Birch webs showed an insufficient factor of safety for EC5 designs. At the Serviceability Limit State, the deflection of ply-web beams with both web types was in excess of EC5 predictions. Recommendations have been made for  $k_{def}$  factors to control the creep deflection of ply-web beams.

## 1 Introduction

Ply-web beams have been used to construct flat, low pitched and other roofs for many years during which time there have been some incidences of excessive deflections, often resulting in ponding and leaks<sup>(1,2)</sup>, and sometimes leading to collapse of a substantial part of the roof structure<sup>(3)</sup>. Excessive deflections have usually been due to either inadequate design procedures or inadequate methods of manufacture or quality control as well as a number of cases where it appears that the excessive deflections were due to changes in the moisture content of the beams. This may have been due to drying out or in some cases where the deflections gradually increased over a long period, due to lack of provision for creep in the design.

Records of temperature and humidity in house roofs and in sheltered locations open to outdoor air flow in the UK, indicate that the moisture content of timber in these situations can be expected to vary by 3% during a 12 month period. Some



small scale beam tests carried out at the Polytechnic of Central London,<sup>(2)</sup> indicated that fluctuating relative humidity can cause excessive creep deflections.

This paper describes an extended study conducted at the Building Research Establishment into the creep of ply-web beams. The results of long-term creep tests conducted over a period of 6 years are presented, along with a series of tests to identify the strength degradation of loaded beams. Current design methods for ply-web beams are reviewed herein, with additional assessment of the creep deflection factors from experimental results.

## 2 Previous studies of creep in ply-web beams

Studies of creep effects in the constituent elements of ply-web beams, both solid wood and wood based panels, have been numerous<sup>(4,5,6,7)</sup> and these studies contribute toward the wealth of knowledge presently available<sup>(8,9)</sup>. Specific research into the creep deformation of ply-web beams is more limited<sup>(10,11,12)</sup>. However, by considering the knowledge gained, both from whole component tests of composite I beams and tests on the constituent elements, some important considerations may be made on the long term performance of ply-web beams:

- *Relative humidity*: creep in solid timber, wood based panels and composite I beams occurs mainly because of changes in the moisture content due to environmental relative humidity. The effect is more marked in naturally varying conditions in the long-term<sup>(8)</sup> as opposed to artificial cyclic variation of conditions. Even moderate fluctuations in humidity might have a significant effect<sup>(13)</sup> but the greatest increase in creep rate is observed during drying periods<sup>(14)</sup> due to the mechano-sorptive behaviour of timber and panel products.
- *Temperature*: creep rates for wood based panels have been shown to increase in conditions with higher temperature, and in a non-linear manner toward the higher end of the temperature scale. The influence of temperature on creep is less significant than that of relative humidity but follows the same trend of increased effect under cyclic conditions<sup>(8)</sup>.
- *Utilisation ratio*: the proportion of dead loading to the design load (stress level or utilisation ratio) affects both the creep rate and ultimate creep deflection<sup>(8)</sup>. The relationship between utilisation ratio and creep is thought to be linear for the majority of component materials generally adopted in ply-web beams, although a study of birch plywood<sup>(7)</sup> concluded that the relationship was non-linear above ratios of 0.3 to 0.5. A previous series of long term creep tests on ply-web beams at BRE<sup>(11)</sup> showed that a linear relationship was a good approximation for the combined materials in a component system.

## 3 Long-term creep tests

### 3.1 Specimen design and construction

The ply-web beams used for testing were designed in 1991 using the most recent version of BS5268: Part 2: 1988<sup>(15)</sup>. Since then the design standard has undergone a couple of revisions in 1991 and 1996 to include both textual and

technical amendments. The design included recommendations for load sharing, flange and web permissible stresses and deflection limits provided in the 1988 version of this code. Bending stresses were assessed using the *composite material method* in the Timber Designers' Manual<sup>(16)</sup>. This reference also provide formulae for determining the panel and rolling shear stress and the shear deflection, which was based on the shear form factor first proposed by Roark<sup>(16)</sup>:

$$K_{form} = \frac{Ah^2}{10I_x} \left[ 1 + \frac{3(h^2 - h_w^2)h_w}{2h^3} \left( \frac{b}{t} \right) \right]$$

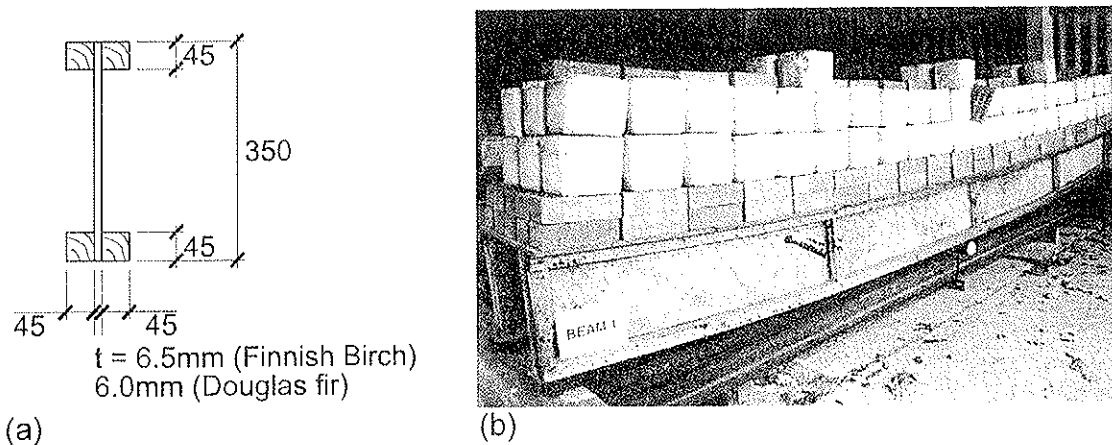
All of the beams were 4.8m long, 350mm deep, I sections with full depth plywood webs. Each flange was constructed from two pieces of 45x45mm SS grade (C24 equivalent) European Whitewood. These were continuous along the whole length without finger jointing. Composite action between the flanges and plywood web was achieved using resorcinol-formaldehyde glue and nailing to achieve sufficient gluing pressure. A similar construction was also adopted for the stiffeners at the beams ends, quarter points and mid-span. Figure 1a shows a cross-section of the beam construction with glued flanges where nails provided the clamping force. In total, 20 beams were constructed in this manner, half of which adopted 6.5mm thick (five ply), sanded Finish Birch plywood for the web while the others used 6mm thick (three ply), good one side, sanded Canadian Douglas fir plywood.

### 3.2 Loading regime and environmental conditions

Of the sixteen beams constructed two Finnish Birch ply-web beams and two Canadian Douglas fir ply-web beams were used as controls to monitor the effects of natural ageing. These were left in an unloaded state in the same conditions as loaded beams. The load levels adopted for the remaining beams were 40%, 70% and 100% of the design load for long-term duration (equivalent to permanent in EC5) using the 1988 version of BS 5268: Part 2<sup>(15)</sup>. This equates to the following loads over the 4.775m span of the beams:

• Canadian Douglas fir ply-web beams	100% design load	-	1.41kN/m
	70% design load	-	0.98kN/m
	40% design load	-	0.56kN/m
• Finnish Birch ply-web beams	100% design load	-	2.45kN/m
	70% design load	-	1.71kN/m
	40% design load	-	0.98kN/m

All of the loaded beams were simply supported at their ends using captive round bar as shown in figures 1b and 2a. For stability, beams of the same web type were paired and lightly connected along their top flanges with plywood boarding to provide a platform for loading. Each pair of beams was loaded in succession using a combination of bricks and concrete blocks to achieve the required load level.



**Figure 1: (a) Test specimen dimensions  
(b) Ply-web beam with 100% of the design load**

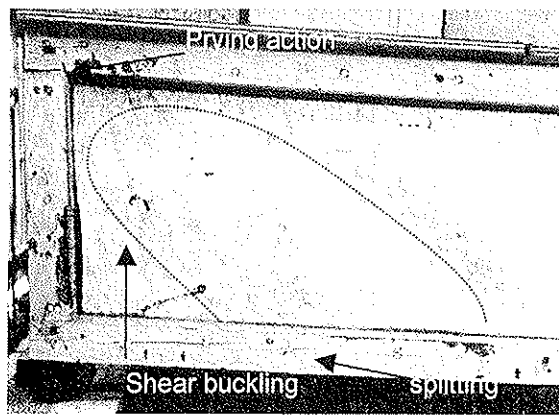
They remained in a loaded state for about 6-years after which time the loads were removed to monitor any recovery of the beams, both elastic and creep recovery deflections.

The beams were placed in a sheltered environment for the long-term creep tests which was open to atmospheric changes in temperature and humidity whilst being protected from direct sunlight and rain. These are realistic conditions that beams in a ventilated flat roof space would endure. The mean temperature over the 6-year test period was about  $12^{\circ}\text{C}$ , with 90% of recorded temperatures falling between  $2^{\circ}\text{C}$  and  $21^{\circ}\text{C}$ . Over the same period, the relative humidity varied between 42% and 96%, with an average reading of about 70%.

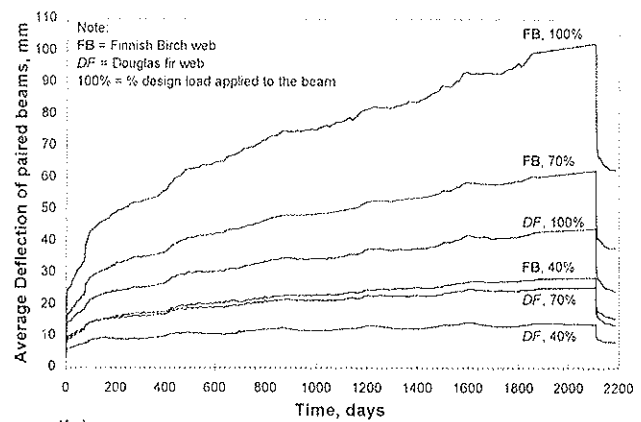
These conditions produced fluctuating moisture contents in the ply-web beams. However, the flange moisture content did not vary much on average from the readings of 14% to 14.5% taken when they were first loaded.

### 3.3 Test results and modelling of relative creep

Shortly after the beams had been loaded, measurements of the mid-span deflection provided a comparison for the predicted elastic deflection using BS5268. Reasonable agreement between the design and experimental readings of instantaneous deflection verified codified values for the elastic shear and bending moduli. During the first month of load duration, three pairs of ply-web beams had exceeded the BS 5268 deflection limit of  $14.27\text{mm}$  ( $\text{span} \times 0.003$ ). Deflections increased over the project duration at varying rates with the most heavily loaded Finnish Birch ply-web beam reaching a maximum deflection of over  $100\text{mm}$  (see figure 2b). At this level of deformation, the beams exhibited typical signs of distress such as; shear buckling of the webs, slight splitting of the flange members and prying action at the connection between the flange and stiffeners due to large deflections (see figure 2a).



(a)



(b)

**Figure 2: (a) Typical signs of distress shown at the ply-web beam support (Finnish Birch ply-web beam with 100% design load)  
(b) Deflection of the ply-web beams**

After 2109 days from loading the beams, the dead weights were removed. Recovery of deflected profile of beams was monitored until no significant further recovery was observed. Using information gained during the recovery period, such as the value of instantaneous recovery and creep recovery, the deformations of beams under sustained load can be described using three main components:

- Elastic
- Visco-elastic (recoverable creep)
- Flow (irrecoverable creep and plastic deformation)

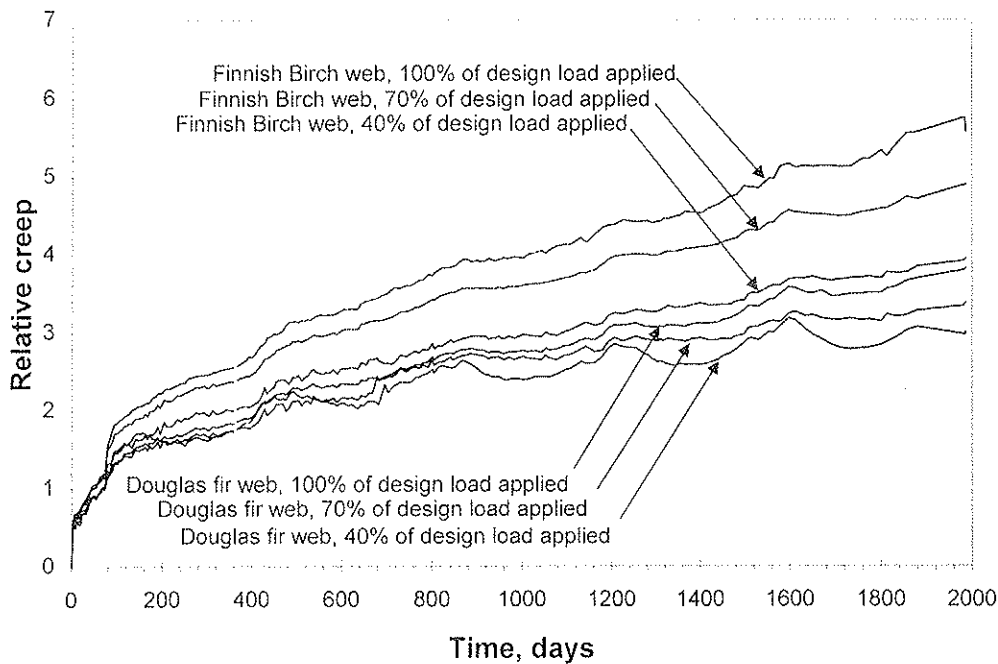
Comparison of deflection readings during the loaded and unloaded periods showed that the instantaneous elastic deflection was equal to the instantaneous recovery deflection. For this study, the creep recovery was shown to equal the 80-day deflection, after which point there was a sudden increase in the creep rate as shown in figure 2b. Previous studies conducted at the BRE observed a different comparable timescale for the visco-elastic creep, which indicates that this phenomenon may be dependent on the prevailing environmental conditions. Without additional experimental study, it was not possible to separate the two constituents of creep deflection in this project.

The usual method for describing the overall creep deflection and that employed in EC5<sup>(17)</sup> ( $k_{def}$  factors), is to express it in terms of the initial elastic deflection:

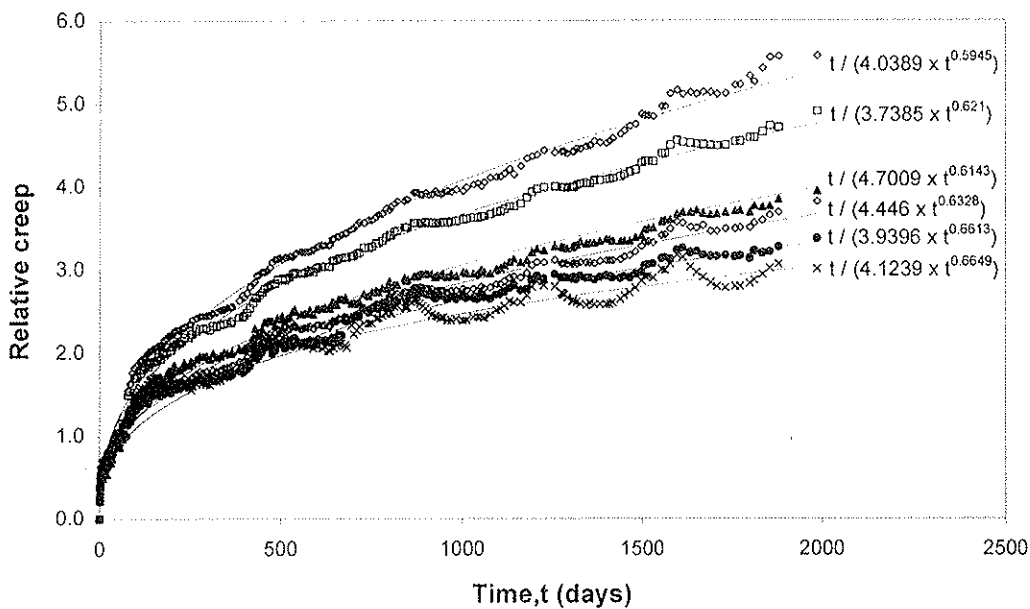
$$\text{Relative creep} = \frac{\delta_t - \delta_i}{\delta_i} \quad \text{where } \delta_i \text{ is the initial elastic deflection}$$

and  $\delta_t$  is the deflection after duration t

Figure 3 shows the relative creep for the beams monitored in this study. It should be noted that the large values of relative creep shown in this figure are not a direct indication of the  $k_{def}$  factors for ply-web beams. Since creep is dependent on the level of stressing, this must also be considered in deriving suitable  $k_{def}$  factors.



**Figure 3: Relative creep of the ply-web beams tested**



**Figure 4: Curve fitting of relative creep data**

For the extrapolation of data beyond the six year test period, two types of creep model were considered: a 5-parameter rheological model and a power law model. Both types have been used previously for creep predictions of solid timber and panel products and demonstrated a good fit with this creep data ( $R^2$  values of 0.994 or better). The greatest efficacy of prediction was obtained with a power model of the form:

$$\text{Relative creep} = \frac{t}{(A \times t^B)}$$

where A and B are constants

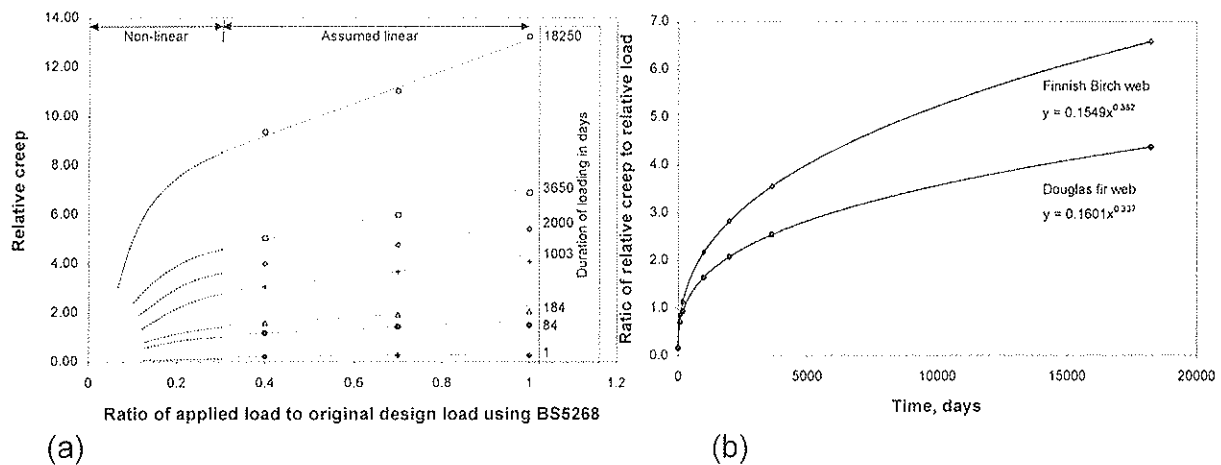
and t is the load duration in days

The predicted creep using this model is shown in figure 4 for the test duration.

## 4 Assessment of $k_{def}$ factors in EC5

Since designs using EC5 predict a different load capacity than designs to BS5268, the code used for the original test load predictions, a relationship was required between supported load, creep deflections and load duration. This would enable the 6-year creep data to be used for assessing  $k_{def}$  factors in EC5.

The power model predictions of relative creep were used to determine a relationship between relative creep and relative load, defined as the ratio of supported load to the original design load. Several samples of the relative creep for all the beams were plotted against the relative load in figure 5a. If linear regression analysis of discrete sets of data was weighted around the 40% and 70% relative load, extrapolation of the lines passed through the point (-1,0). This was observed for both Douglas fir and Finnish birch ply-web beams. The gradients of each line determined in figure 5a were plotted against the load duration in figure 5b, which shows a power relationship supported by the data. This chart may be used as a predictive tool to determine the deflection of ply-web beams tested as part of this study when subjected to a variety of load duration's and utilisation ratios.



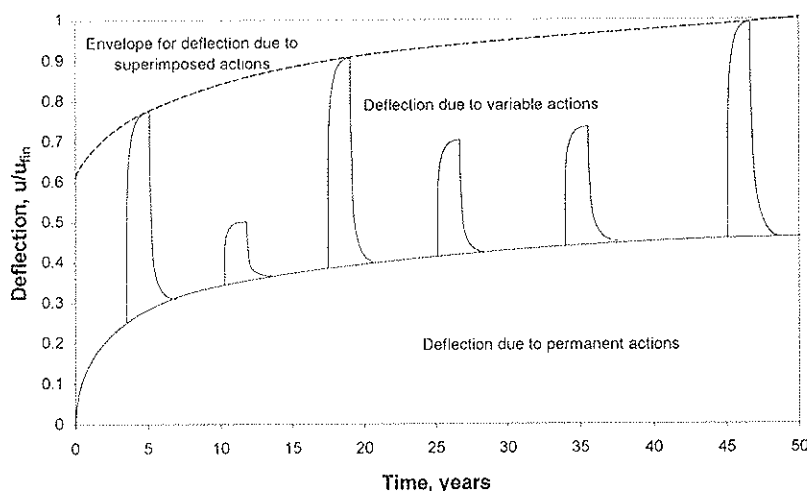
**Figure 5: (a) Relationship between Relative Creep and Relative Load for Finnish Birch ply-web beams subjected to different duration's of load.  
(b) Chart used for predicting Relative Creep of ply-web beams**

To assess the  $k_{def}$  factors in EC5, designs were produced using this code and the material properties in pr EN 12369: 1996 and BS EN 338: 1995. Deflection due to creep was generally the governing design criteria, which was limited to  $L/300$ ; the most onerous deflection limit expected to be adopted by designers. All current modification factors for load duration, material properties and creep deflection were included in the designs to determine the limiting load capacities of beams within the scope of this study. These load capacities were used as initial values for predicting the relative creep of beams using the relationship in figure 5a for a variety of loads and load durations. Re-iteration of the load capacity produced convergent values of relative creep. These are provided for different load durations in table 1.

Load Duration	① Predicted $k_{def}$ factors for ply-web beams in EC5 designs		②	③	④=(①+②)/2	④/③
	Finnish Birch web	Canadian Douglas fir web	Current $k_{def}$ factors for ply-web beams using EC5	Average $k_{def}$ factor from predictions	Comparison Index	
Medium-term	1.27	1.13	0.25	1.20	4.8	
Long-term	3.66	2.63	0.51	3.15	6.2	
Permanent	6.71	4.40	0.81	5.56	6.9	

**Table 1: Predicted and current  $k_{def}$  factors in EC5 for Service Class 2**

To check the validity of predicted  $k_{def}$  factors, the deflection of beams subjected to different types of action was considered, where these actions are generally superimposed<sup>(18)</sup> as shown in figure 6 below.



**Figure 6: Superposition of deflections due to different types of action**

The test data suggests that any creep deflection for medium-term actions such as snow loading will be fully recoverable, as shown in the above figure. For greater duration's of loading, a proportion of irrecoverable creep deflection will occur. This amounts to almost 50% of the elastic plus inelastic deflection for actions supported over long-term durations and has been considered in determining  $k_{def}$  factors in table 1.

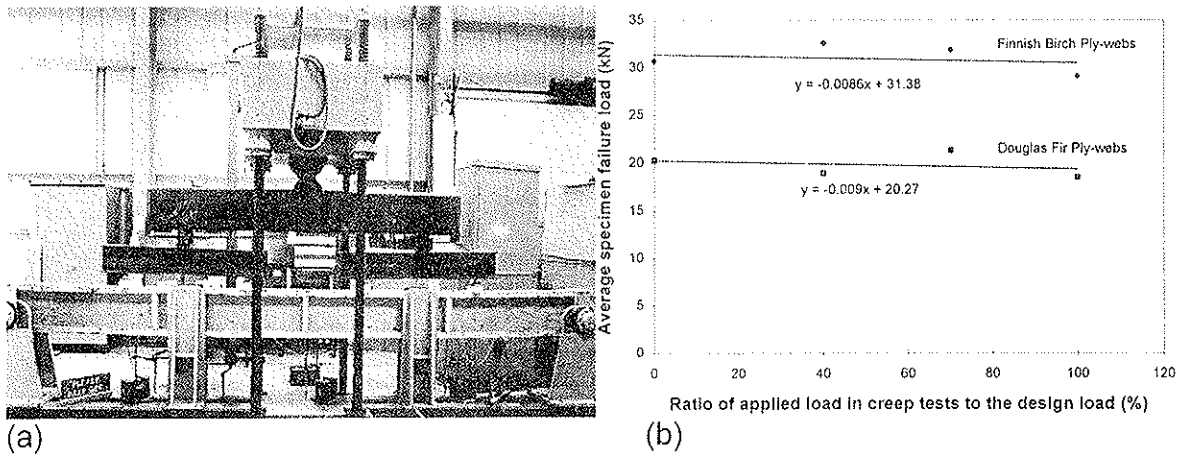
The following figure 7 shows the predicted deflection of Finnish Birch ply-web beams subjected to both permanent and variable actions; Douglas fir ply-web





supported end supports with full lateral restraint and intermediate full lateral restraints at third points along the beam length.

Although some of the beams displayed signs of distress from the long-term creep tests, loading of the beams to failure did not indicate any serious degradation of component strength. This is indicated in figure 8b, which compares the strength test results for both Finnish Birch and Canadian Douglas fir ply-web beams. There is a slight negative slope to the linear regression of strength for both beam types indicating that load history may affect the ply-web beam strength, but not significantly. Adoption of this relationship for strength degradation would only affect the factor of safety for these beams by a maximum of 3%.



**Figure 8: (a) View of ply-web beam and loading test rig  
(b) Results of ply-web beam strength tests**

Control beams that had not been loaded during the 6 year creep tests were not significantly stronger on average than the loaded beams and in some cases failed at lower load levels.

All of the beams tested exhibited a factor of safety of 2.76 to 3.96 when failure loads were compared to the most onerous design load (method 5) using BS 5268. Section 8 of BS 5268 recommends that the safety factor should be greater than or equal to 2.3 for the long-term load duration and a sample size of two. The factors of safety in table 2 are clearly adequate for both beam types using this design code.

At the ultimate limit state using EC5, the Canadian Douglas fir ply-web beams exhibited similar factors of safety which were greater than the required factors of safety in Table 5 of the UK NAD to EC5. None of the designs for Finnish Birch ply-web beams produced sufficient factors of safety according to the UK NAD. From inspection of the design values for deflection the factors of safety at the serviceability limit state are expected to be sufficient for both beam types.

Ply-web beam type	Applied load in creep tests, % of design load	Design Load, kN/m			Failure load, kN/m	Factor of safety		
		<sup>1</sup> EC 5		<sup>2</sup> BS 5268		EC 5		BS 5268
		Medium-term	Long-term			Medium-term	Long-term	
Finnish Birch	0	4.90	4.29	2.59	7.69	1.57	1.79	2.97
	40	4.90	4.29	2.59	8.16	1.67	1.90	3.15
	70	4.90	4.29	2.59	7.98	1.63	1.86	3.08
	100	4.90	4.29	2.59	7.28	1.49	1.70	2.81
Canadian Douglas fir	0	1.49	1.30	1.41	5.08	3.41	3.91	3.60
	40	1.49	1.30	1.41	4.74	3.18	3.65	3.36
	70	1.49	1.30	1.41	5.34	3.58	4.11	3.79
	100	1.49	1.30	1.41	4.64	3.11	3.57	3.29

NOTES:

1. Determined without the use of load safety factors or combination factors. Material properties from EN 338 and prEN12369.
2. Using the 1991 version of BS 5268: Part 2 for long-term duration only.

**Table 2: The results of strength tests carried out on the ply-web beams**

## 6 Conclusions

The indications from the strength tests are that:

- The strength of ply-web beams is not adversely affected by prolonged loading or large deflections.
- Safety factors of more than 2.5 exist between failure loads and permissible design loads using BS5268. Additional pond loading due to creep deflections may erode this safety factor in practice.
- Similar safety factors have been determined for designs using EC5 for Canadian Douglas fir ply-web beams.
- Beams designed to EC5 using Finnish Birch ply-webs had reduced factors of safety beyond that recommended in the UK NAD to EC5.
- Material and construction quality, have a more marked effect than load history on the failure load of ply-web beams.

The following may be concluded from creep test measurements, creep modelling and the derivation of creep deflection factors:

- The continued creep of all the ply-web beams tested, indicated that cessation of creep was not expected within the long-term duration category of EC5.
- Power models used to predict relative creep proved a good prediction for the long-term creep but may overestimate  $k_{def}$  factors for permanent load duration.
- Test data showed that a non-linear relationship exists between the load duration, utilisation ratio and relative creep of ply-web beams. The relationship was markedly different for beams constructed with different types of plywood web.
- The current  $k_{def}$  factors in EC5 grossly underestimate the creep of ply-web beams exposed to fluctuating environmental conditions for all load duration categories.
- The proposed  $k_{def}$  factors control creep deflections within limiting values for a variety load combinations and durations.

## 7 Acknowledgement

The authors wish to acknowledge the long-term commitment and financial support of the Construction Directorate, DETR without which the findings of this project would not have been possible.

## 8 References

1. Haussler R. W., 'Roof deflection caused by rainwater pools'; Civil Engineering, pp. 58-59, October 1962.
2. Tyne J. R., 'The effect of humidity changes on the deflections of ply-web beams'; Polytechnic of Central London, Occasional Paper No.3, December 1978.
3. Mayo A. P., 'An investigation of the collapse of a swimming pool roof constructed with plywood box beams'; Building Research Establishment Current Paper, CP 44/75, April 1975.
4. Armstrong L. D. and Kingston R. S. T., 'The effect of moisture content changes on the deformation of wood under stress'; Australian Journal of Applied Science, 13(4), pp. 257-276, 1962.
5. Hearman R. E. S. and Paton J. M., 'Moisture content changes and creep of wood'; Forest Products Journal, pp. 457-359, August 1964.
6. Pierce C. B., Dinwoodie J. M. and Paxton B. H., 'Creep in chipboard – Part 5: An improved model for prediction of creep deflection'; Journal of Wood Science and Technology, Vol. 19, No. 83(91), 1985.
7. Ranta-Maunas A., 'A study of creep of plywood'; Structural Mechanics Lab., Technical Research Centre of Finland, Report No. 5, pp. 92, 1976.
8. Dinwoodie J. M. and Bonfield P. W., 'Recent European research on the rheological behaviour of wood based panels'; Proc. of COST Action 508 wood mechanics workshop, BRE, UK, pp. 3-38, March 1995.
9. Leichti R. J., Falk R. H. and Laufenberg T. L., 'Prefabricated wood composite I-beams: a literature review'; Wood and Fibre Science, 22(1), pp. 62-79, 1990.

10. Bocquet J. F., Bouchair A., Faugeras J. C. and Racher P., 'Creep behaviour of glued thin-webbed I beams'; Proc. of COST Action 508 wood mechanics workshop, BRE, UK, pp. 70-82, March 1995.
11. Enjily V., 'Long-term performance of ply-web beams'; Building Research Establishment Note, N95/89, August 1989.
12. Dutko P. and Bulko P., 'Performance of girders of homogeneous and non-homogeneous cross-section under long term load'; Proc. of International Timber Engineering Conference, London, Vol. 3, pp. 204-211, 1991.
13. Taylor G. D. and Pope D. J., 'Creep allowances for glued laminated timber used in structural frames for buildings'; Journal of the Institute of wood science, Vol. 13, No. 4 (Issue 76), 1994.
14. Szabo T. and Ifju G., 'Influence of stress on creep and moisture distribution in wooden beams in sorption conditions'; Wood Science, 2(3), pp. 159-167, January 1970.
15. British Standards Institution, Structural use of timber: Part 2. Code of practice for the permissible stress design, materials and workmanship', BS 5268: Part 2: 1988, BSI, London, 1988.
16. Baird J. A. and Ozelton E. C., 'Timber Designers' Manual' – 2<sup>nd</sup> edition; Granada Technical Books, London, 1984.
17. British Standards Institution, 'Eurocode 5: Design of timber structures, Part 1.1: General rules and rules for buildings', DD ENV 1995-1-1: 1994, BSI, London, 1994.
18. Martensson A. and Thelandersson A., 'Design principles for deflection control in timber structures'; Proc. of Pacific Timber Engineering Conference, Australia, Vol 2, pp. 213-221, 1994.

**INTERNATIONAL COUNCIL FOR RESEARCH AND INNOVATION  
IN BUILDING AND CONSTRUCTION**

**WORKING COMMISSION W18 - TIMBER STRUCTURES**

**THE BENDING STIFFNESS OF NAIL-LAMINATED TIMBER ELEMENTS  
IN TRANSVERSE DIRECTION**

T Wolf

O Schäfer

Darmstadt Technical University

GERMANY

**MEETING THIRTY-TWO**

**GRAZ**

**AUSTRIA**

**AUGUST 1999**

---

Presenter: T.Wolf

- H.J.Blass asked and received clarification that the withdrawal information of nails was based on measurements conducted in another institution.
- H.J.Blass commented that the deformation of 2 to 3 mm was high and head side deformation should also be considered.
- P.Quenneville asked and received clarification that repeated loading was not considered.
- G.Schickhofer disagreed with the use of concrete model analogy.
- B.Mohr stated permanent load should not be applied to nails.
- H.J.Blass clarified that permanent load should not be applied to smooth shank nail only.
- G.Schickhofer further stated that these members should be considered as one span elements without plate action.

# The bending stiffness of nail-laminated timber elements in transverse direction

Thomas Wolf, Oliver Schäfer  
Darmstadt University of Technology, Germany

## 1 Introduction

The load bearing behaviour of nail-laminated timber elements is not adequately researched yet. In the design process of nail-laminated timber elements analogies to ruled structural parts in timber work are searched to transfer familiar proves.

The transverse bending stiffness is a characteristic value, which is required at different points.

Existing approaches for the determination of the transverse bending stiffness found in literature do not reflect the real conditions.

In this paper a new analytical approach for the determination of the transverse bending stiffness is derived. In a parameter study the resulting values of bending stiffness are examined for plausibility and the influence of the important parameters is presented. A final example shows the significance of this characteristic value in the design of nail-laminated timber elements.

## 2 Computational model

This model is based on theoretical considerations. Due to missing experimental results the method could not be verified yet.

In the new approach – in accordance to the well-known model of a reinforced concrete beam at cracked state – the occurring state of strain is derived by the equilibrium of the compressive force in the wood and the tensile force of the nails. The knowledge of the neutral axis location and the height of the compression zone respectively, enables the determination of an equivalent bending stiffness. Thereby only the effective parts of the cross section are taken into consideration. These are the stiffness of the wood in the compression zone and the axial tensile nail compliance in the tension zone.

The value of the bending stiffness is mainly influenced by the defined withdrawal stiffness of the applied nails. This characteristic value cannot be accessed directly for a special nail. It has to be deduced by the load-withdrawal relationship of a nail, which may be determined by withdrawal tests in accordance to the german code DIN 1052-2. Usually in these tests the ultimate axial withdrawal resistance is determined without recording the load-displacement data. In [6] the load-displacement curves of a test series for an annularly threaded nail are provided.

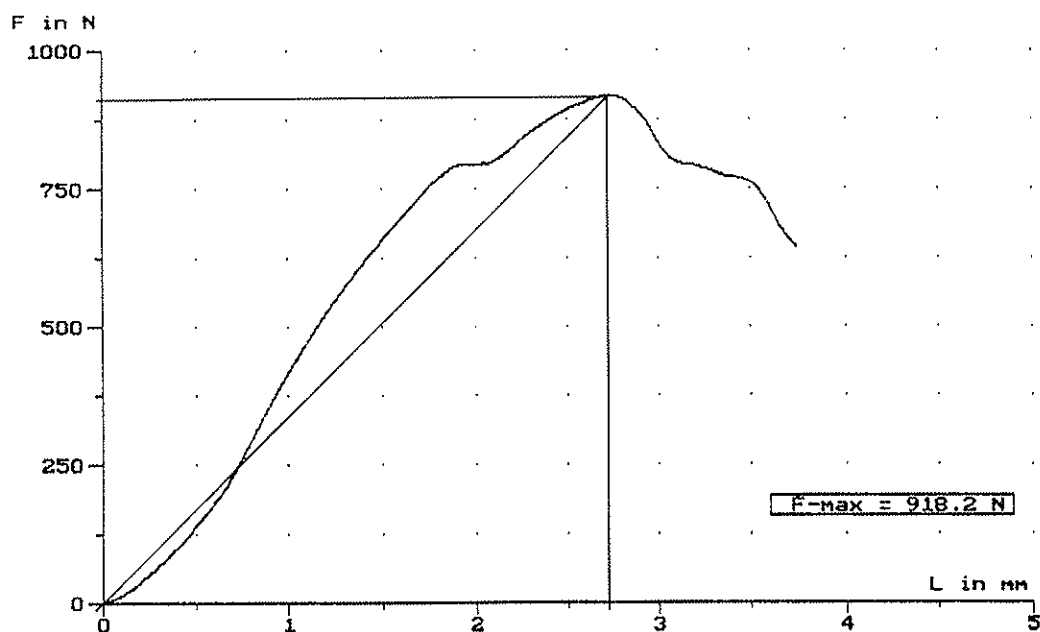


Figure 1 Load-withdrawal displacement relationship of an annularly threaded nail [6]

For the calculation model the withdrawal stiffness is assumed to be constant. It is defined by the quotient of the maximum withdrawal force and the respective displacement. (figure 1)

$$C_m = \frac{F_u}{s_u} \quad (1)$$

- $C_m$  average withdrawal stiffness of a nail in N/mm
- $F_u$  ultimate withdrawal resistance in N
- $s_u$  respective withdrawal-displacement in mm

In a good approximation the joints between the boards can be neglected at the compression side. So the modulus of elasticity perpendicular to grain  $E_{\perp}$  of the boards is applied for the calculation of the material behaviour similar to a homogenous structure.

At the tension side, the compound of timber and nails determines the performance of the cross-section. The real load bearing behaviour can hardly be estimated and is approached by an elastic material-law. The appropriate modulus of elasticity is evaluated in a way, which reflects the load-deformation behaviour of a basic element (board + nail).

Equilibrium of forces, the compression force of the wood and the tensile force of the nail connection leads to the following formula concerning the height of the compression zone:

$$h_D = -2 \cdot K_1 + \sqrt{4 \cdot K_1^2 + 2 \cdot K_1 \cdot (h_{N1} + h_{N2})} \quad (2)$$

$$K_1 = \frac{n \cdot t_B \cdot C_m}{E_{\perp}} \quad (3)$$

- $h_D$  Compression zone height in mm
- $h_{N1}$  Distance of the lower nail row from the top edge of the nail-laminated timber element in mm
- $h_{N2}$  Distance of the upper nail row from the top edge of the nail-laminated timber element in mm
- $n$  Number of nails per meter and nail row, which satisfy the minimum driving depth according to DIN 1052 Part 2
- $t_B$  Thickness of single laminated member in mm
- $E_{\perp}$  Modulus of elasticity perpendicular to grain according to DIN 1052 Part 1 in  $\text{N/mm}^2$

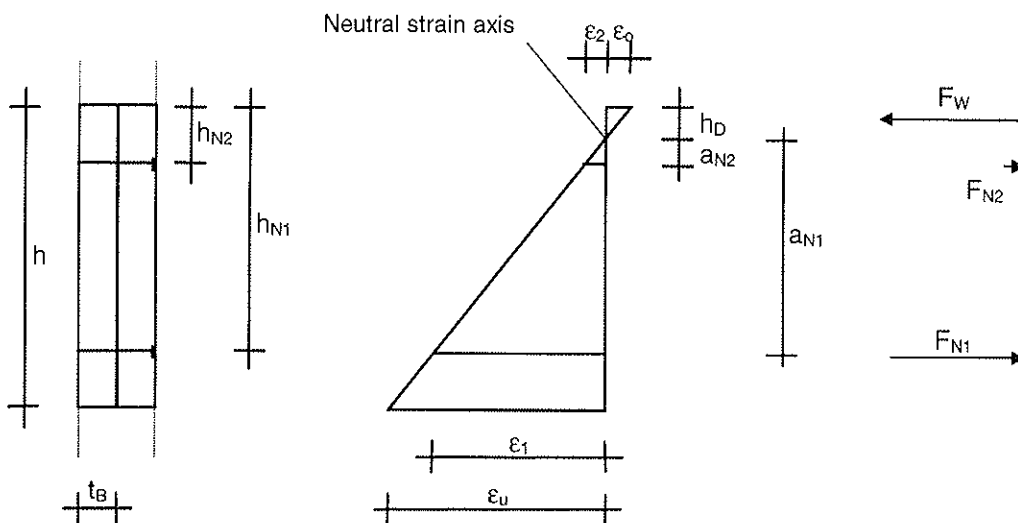


Figure 2 Geometry of cross-section, strain distribution, internal forces



The transverse bending stiffness relative to the neutral axis can be specified in dependence of the compression zone height:

$$(EI)_b = n \cdot E_s \cdot \frac{\pi \cdot d_n^4}{32} + n \cdot C_m \cdot t_B \cdot (a_{N1}^2 + a_{N2}^2) + E_{\perp} \cdot \frac{b \cdot h_D^3}{3} \quad (4)$$

$$a_{Ni} = h_{Ni} - h_D \quad (5)$$

$(EI)_b$  Equivalent bending stiffness transverse to the board direction Nmm<sup>2</sup>/m

$E_s$  Modulus of elasticity of steel in N/mm<sup>2</sup>

$d_n$  Nail diameter in mm

$a_{N1}$  Distance of lower nail row to neutral axis in mm

$a_{N2}$  Distance of upper nail row to neutral axis in mm

$b = 1000$  mm width of the reference section

### 3 Parameter study

In this investigation the withdrawal test data of the annularly threaded nail RNa 31x65 [6] is applied. The results of a test series according to DIN 1052-2 Appendix A are listed in table 1

	Ultimate withdrawal resistance $F_u$	Withdrawal displacement for $F_u$ $s_u$
Mean value	1067,3 N	2,5 mm
Standard deviation	109 N	0,4 mm

Table 1 Results of a test series for determination of withdrawal resistance according to DIN 1052-2 Appendix A

As average value of withdrawal stiffness  $C_m = F_u/s_u = 426,9$  N/mm is obtained

Here the withdrawal stiffness is kept constant. Its influence to the bending stiffness can be included by modifying the number of nails.

The following objects should be examined by the parameter study:

- Influence of the element's height to the element's bending stiffness
- Influence of the number of nails respective the withdrawal stiffness of a nail to the bending stiffness

- Ratio of different parts of bending stiffness
- Value of the allowable bending moment transverse to the span
- Influence of the board thickness to the bending stiffness.

The following parameters are given as fixed values.

Modulus of elasticity of boards (NH S10)	$E_L$	[N/mm <sup>2</sup> ]	300
allowable compression stress of boards	$\sigma_{DL}$	[N/mm <sup>2</sup> ]	2,0
Modulus of elasticity of nail-wire	$E_{NA}$	[N/mm <sup>2</sup> ]	210000
Withdrawal stiffness of nail	$C_m$	[N/mm]	426,9
allowable withdrawal force of nail	$F_R$	[N]	782,7
Withdrawal displacement of nail respective the allowable withdrawal force of nail	$s_R$	[mm]	1,8
Distance of the lower nail row to the bottom edge	$(h-h_{N1})$	[mm]	25
Distance of the upper nail row to the top edge	$h_{N2}$	[mm]	25

Table 2 Constant parameters

The range of the parameters, which are analysed, is specified in table 3.

Board height	$h$	60...240mm
Nail distance	$e_{NA}$	40...400 mm
Board thickness	$t_B$	24...80 mm

Table 3 Ranges of analysed parameters

In the following diagrams, the results of the parameter study are presented graphically.

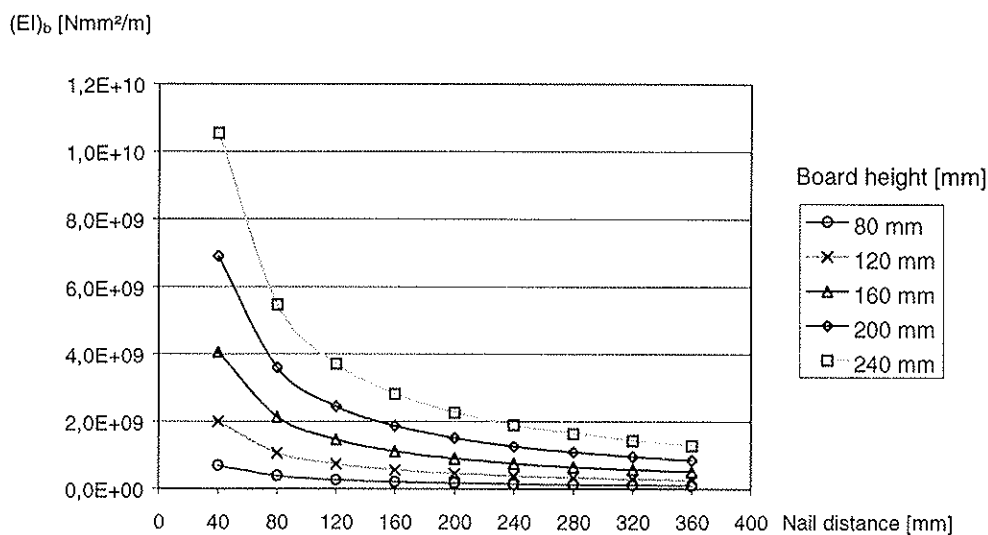


Figure 3 Bending stiffness  $EI_b$  depending on number of nails and board height (Board thickness = 24mm)

In Figure 4 the different parts of transverse bending stiffness and the bending stiffness in span direction for a nail-laminated timber element of 240 mm height are presented.

The part of transverse bending stiffness concerning the lower nail row is more than 90 %, so the parts of the wood and the upper nail row can be neglected in a good approximation. The real value of the equivalent modulus of elasticity for the compression zone, due to the joints between the boards is of minor importance.

Altogether the transverse bending stiffness reaches roughly 0,01 % to 0,1 % of the bending stiffness in span direction.

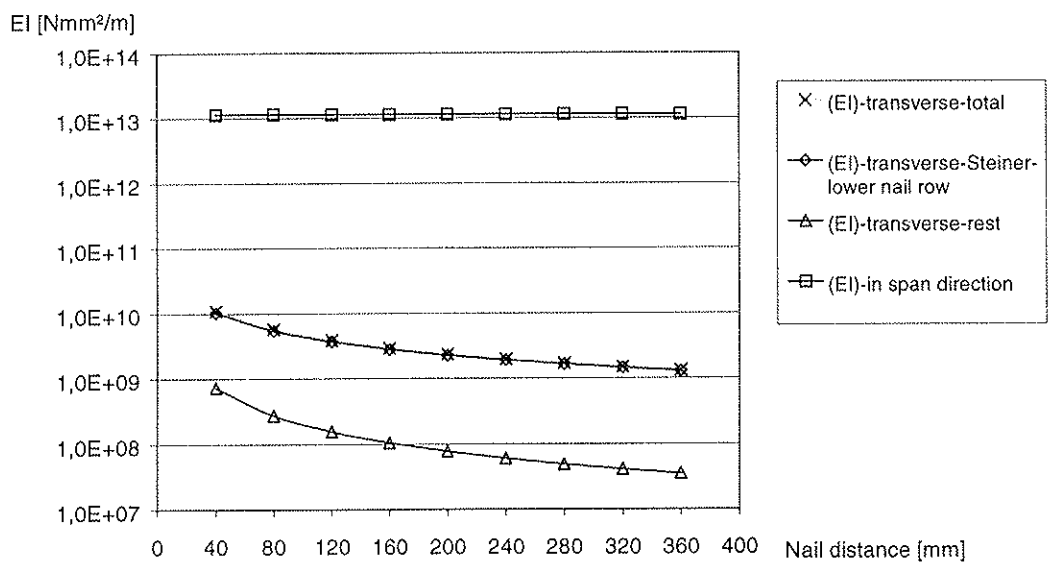


Figure 4 The different parts of bending stiffness  $EI_b$  and the bending stiffness in span direction  $EI_s$ . (Board height = 240mm)

In Figure 5 the allowable bending moment of a nail-laminated timber element transverse to the span is shown.

As failure criteria the achievement of the allowable withdrawal force of the nails respective the allowable compression stress of the wood is defined.

The limitation line separates the different modes of failure. Below the line it is the strength of the wood and above the line it is the strength of the nail connection, which is decisive for the allowable bending moment.

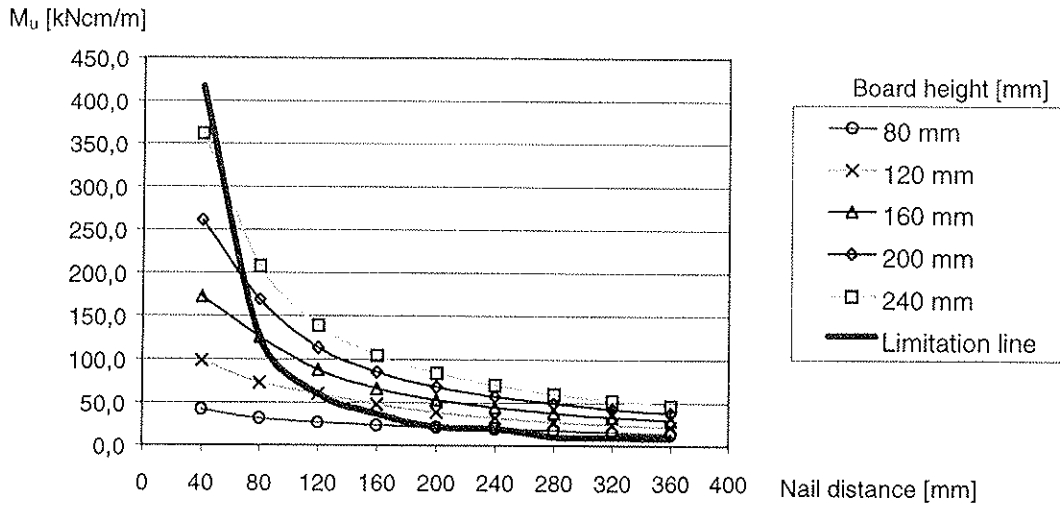


Figure 5 Allowable bending moment transverse to the span

The relationship of bending stiffness and board thickness is presented in figure 6. There is nearly a linear correlation between board thickness and bending stiffness by the developed approach.

Thereby it is assumed, that the withdrawal stiffness of the nails remains constant for the considered value of board thickness. In a comparative test the according properties of the connection have to be ensured.

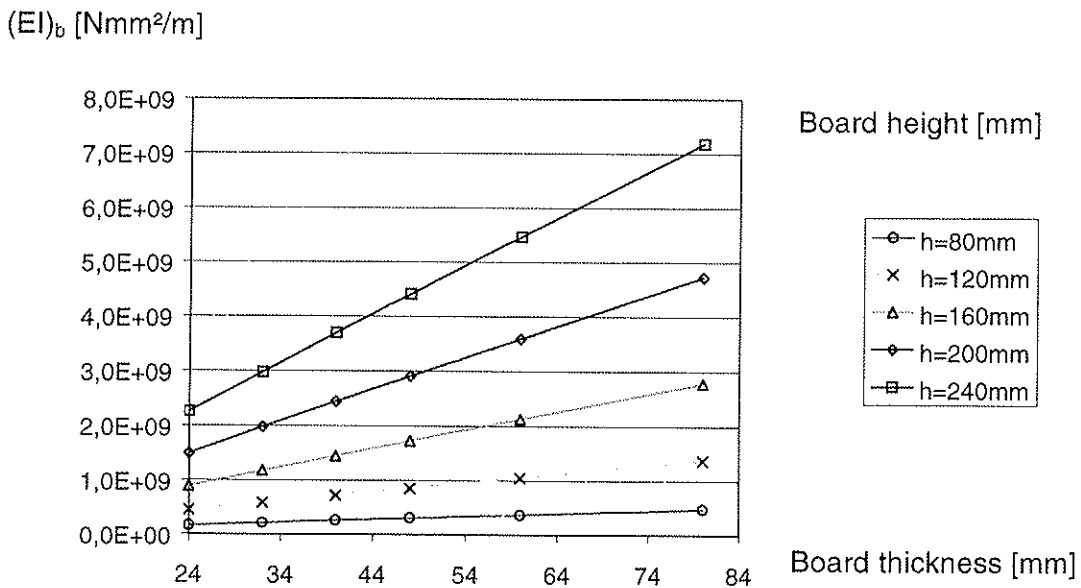


Figure 6 Bending stiffness depending on board thickness (nail distance = 200 mm)

## 4 Application example

### Determination of the transverse bending stiffness:

The following geometrical variables are given:

Height of the nail-laminated timber slab	140 mm
Single board thickness	30 mm
Edge distance of the nail rows	25 mm
Nail distances within one nail row	300 mm

This results in:

$$h_{N1} = 140 - 25 = 115 \text{ mm}$$

$$h_{N2} = 25 \text{ mm}$$

$$n = 1/0,3 = 3,33 \text{ m}^{-1}$$

Moduli of elasticity according to german codes:

$$E_{\perp} = 300 \text{ N/mm}^2$$

$$E_S = 210000 \text{ N/mm}^2$$

As fasteners the annularly threaded nails of Chapter 3 (RNa 31x65) are chosen:

$$C_m = 426,9 \text{ N/mm}$$

Determination of compression zone height according to equation (2) and (3):

$$K_1 = \frac{3,33 \cdot 30 \cdot 426,9}{1000 \cdot 300} = 0,1422 \text{ mm}$$

$$h_D = -2 \cdot 0,1422 + \sqrt{4 \cdot 0,1422^2 + 2 \cdot 0,1422 \cdot (115 + 25)} = 6,0 \text{ mm}$$

Nail row distances to neutral axis (eq.(5)):

$$a_{N1} = 115 - 6,0 = 109 \text{ mm}$$

$$a_{N2} = 25 - 6,0 = 19 \text{ mm}$$

Equivalent transverse bending stiffness (eq.(4))

$$(EI)_b = 3,33 \cdot 210000 \cdot \frac{\pi \cdot 3,1^4}{32} + 3,33 \cdot 426,9 \cdot 30 \cdot (109^2 + 19^2) + 300 \cdot \frac{1000 \cdot 6,0^3}{3}$$

$$\Rightarrow (EI)_b = 5,500 \cdot 10^8 \text{ Nmm}^2/m = 5500 \text{ kNcm}^2/m$$

#### Limiting vibrations according to EC 5:

According to EC 5/4.4.3 the maximum velocity has to be limited. It depends on the value of transverse bending stiffness  $(EI)_b$ . The following specifications of geometry and load of the nail-laminated timber floor are assumed:

Length of the nail-laminated timber floor in span direction	4,0 m
width of the nail-laminated timber floor transverse to the span direction	5,0 m
Dead load of the nail-laminated timber element	5,0 kN/m <sup>3</sup>
Dead load of the floor layers	0,2 kN/m <sup>2</sup>

The mass per square unit results in:

$$m = (5 \cdot 0,14 + 0,2) \cdot 100 = 90 \text{ kg/m}^2$$

The natural frequency is determined with the help of equation (4.4.3c) from EC 5:

$$f_1 = \frac{\pi}{2 \cdot 4^2} \cdot \sqrt{\frac{2,52 \cdot 10^6}{90}} = 16,4 \text{ Hz}$$

Using equation (4.4.3e) in EC 5 the number of first-order vibrations with a resonance frequency below 40 Hz can be determined:

$$n_{40} = \left( \left[ \left( \frac{40}{16,4} \right)^2 - 1 \right] \cdot \left( \frac{5}{4} \right)^4 \cdot \frac{2,52 \cdot 10^6}{550,0} \right)^{0,25} = 15,3$$

Velocity in cause of an ideal unit impulse EC5/(4.4.3d):

$$v = \frac{4 \cdot (0,4 + 0,6 \cdot 15,3)}{90 \cdot 5 \cdot 4 + 200} = 0,01916 \frac{\text{m}}{\text{Ns}^2}$$

Limitation of the velocity EC5/(4.4.3b):

$$v \leq 100^{(f_1 \zeta^{-1})} \frac{m}{Ns^2}$$

$$\Rightarrow 100^{(16,40,01^{-1})} = 0,02129 > 0,01916$$

The prove turns out to be close to the limit. It has to be considered, that the proves of EC 5 were developed for timber joist floors and reflect the properties of the nail-laminated timber floors only approximately.

## 5 Conclusion

The developed computational model enables the calculation of an analytically detectable value for the transverse bending stiffness. The knowledge of the “withdrawal stiffness” of the applied nails is necessary. This characteristic value has to be determined by withdrawal tests.

The new approach results in a lower value for the bending stiffness than estimated in former publications. The transverse bending stiffness is very low and reaches only 0,01 to 0,1 % of the bending stiffness in span direction.

It is obvious, that a sufficient transverse load distribution can not be based on the transverse bending stiffness. A sufficient transverse load distribution can only be guaranteed by the shear stiffness of the nail connection. Further investigations ([1], [7]) lead to the conclusion, that the assumption of sufficient transverse distribution concerning nail-laminated timber floors is not correct.

Assuming this conclusion an additional prove with a point load of 1 kN in worst loading position, according to german code DIN 1055, is necessary. In this case the transverse distribution of a point load has to be known. This is why the importance of the transverse bending stiffness and the described computational model may overlap the shown prove of limiting vibration.

## 6 References

- [1] Haller, P., Pannke, K.: Structural and Physical Behaviour of Nailed Laminated Timber Elements, World Conference on Timber Engineering 1998
- [2] Wolf, T., Tichelmann, K., Pfau, J.: Brettstapelbauweise: Konstruktionsübersichten, Bemessung, Bauphysik, Details; Informationsschrift herausgegeben von: Bund Deutscher Zimmermeister im ZDB, Bonn; Vereinigung Deutscher Sägewerksverbände e.V., Wiesbaden; Versuchsanstalt für Holz- und Trockenbau, Darmstadt 1998
- [3] Werner, H.: Brettstapelbauweise, Informationsdienst Holz, Holzbau Handbuch, Reihe 1, Teil 17, Folge 1, München 1998
- [4] United States Department of Agriculture, Forest Service (Editor): Timber Bridges - Design, Construction and Maintenance. Engineering Staff. Washington DC. June 1990
- [5] Kreuzinger, H., Mohr, B.: QS-Holzplattenbrücken, Informationsdienst Holz, Holzbau Handbuch, Reihe 2, Teil 3, Folge 1, München 1995
- [6] VHT, Forschungs-, Entwicklungs- und Materialprüfungsanstalt: Prüfbericht, Eignungsprüfung und Einstufung in Tragfähigkeitsklasse des Rillennagels RNa 31x65, Darmstadt 1998
- [7] Gabriel, S.: Statische Untersuchungen an Brettstapelwänden unter horizontaler und vertikaler Beanspruchung, Diplomarbeit, TU Dresden 1996
- [8] Ohlsson, S.: Springiness and human-induced floor vibrations, A Design Guide, Swedish Council for Building Research, Stockholm, Sweden 1988
- [9] Kreuzinger, H., Mohr, B.: Schwingungsprobleme nach Eurocode 5 bei Wohnungsdecken, Forschungsbericht für die DGfH, München 1994
- [10] Colling, F., Wagner, G., Winter, S.: Tragwerksplanung, Eurocode 5 - Holzbauwerke, Bemessungsgrundlagen und Beispiele, Informationsdienst Holz, Holzbau Handbuch, Reihe 2, Teil 1, Folge 1, München 5/95



**INTERNATIONAL COUNCIL FOR RESEARCH AND INNOVATION  
IN BUILDING AND CONSTRUCTION**

**WORKING COMMISSION W18 - TIMBER STRUCTURES**

**ANALYSIS OF TIMBER REINFORCED WITH  
PUNCHED METAL PLATE FASTENERS**

J Nielsen

Department of Building Technology and Structural Engineering  
Aalborg University  
DENMARK

**MEETING THIRTY-TWO**

**GRAZ**

**AUSTRIA**

**AUGUST 1999**

---

Presenter: J. Nielsen

- H.J.Blass asked whether the installation of nail plates would have a weakening effect from the nails cutting the wood fibers.
- J.Nielsen stated that this would be an issue with thick nail plates.
- S.Thelandersson asked about the use of grading method.
- J.Nielsen responded that the material was visually graded
- S.Thelandersson further commented that machine grading could be used to develop matched sample group.
- J.Nielsen responded that the material was density/weight matched.
- F.Lam asked about the compression failure mode and stated that reinforcement on the tension side would not help the situation.
- P.Quenneville stated that 4 point bending should be used to eliminate the compression problem.
- J.Nielsen agreed.
- S.Svensson questioned and received clarification on load deformation curves.
- P.Quenneville suggested that characteristic strength might be increased by reinforcing defects rather the entire section.
- E.Karacabeyli asked if the use of a bigger plate would affect results.
- J.Nielsen responded that moment capacity would be different.
- A.Jorissen stated that the linear model could not predict large deformation due to compression failure.
- J.Nielsen agreed and this would be a research topic in the future.

# Analysis of Timber Reinforced with Punched Metal Plate Fasteners

Jacob Nielsen

Department of Building Technology and Structural Engineering,  
Aalborg University, Sohngaardsholmsvej 57, DK-9000 Aalborg, Denmark  
E-mail: i6jn@civil.auc.dk

## 1 Introduction

The controlling sections of chords in a truss are often influenced by a moment peak, see figure 1. At triangular trusses the maximum peak moment and maximum axial compression force in the top chord often appear at the heel joint.

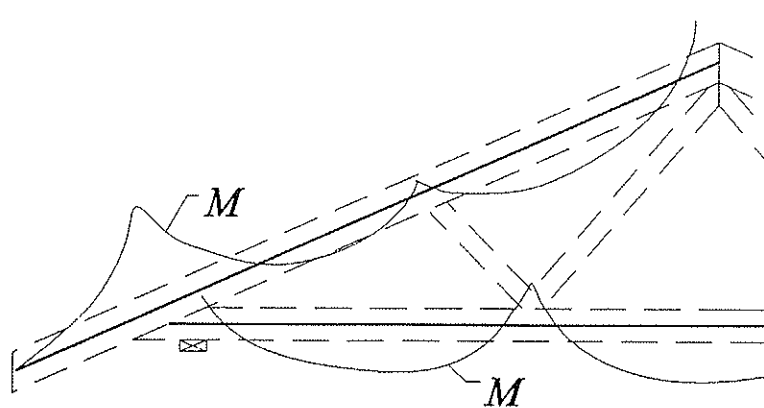


Figure 1: Variation of the moment,  $M$ , in the chords of a W-truss.

In order to obtain optimal truss designs different statistical analyses of the wood strength parameters have been made to obtain increased capacity of the sections with moment peak. Another method of increasing the moment capacity is to reinforce the dimension controlling areas with a punched metal plate of same type as used in the joints of the truss, see figure 2. An advantage of this method is that the price of the reinforcement material and the production of the reinforcement are very limited compared to the total costs of a truss. By introducing the reinforcement it may be possible to reduce the cross-sectional depths of the chords.

The reinforcing effect of punched metal plate fasteners in areas with a moment peak is analysed by tests. According to DS/EN 408 the bending capacity (bending strength) of timber shall be determined for beams loaded in 4-point bending. However, the

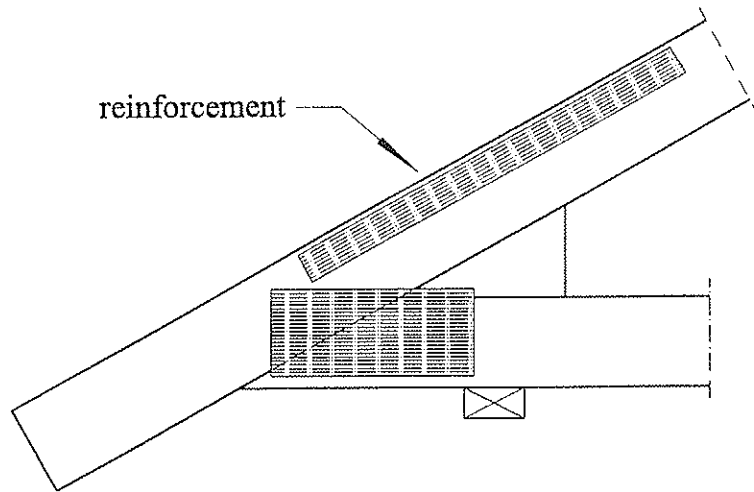


Figure 2: Heel joint with a wedge and a reinforcement.

present work is limited to analysis of the reinforcing effect in areas with moment peaks only. Therefore, the test specimens are made with beams loaded in 3-point bending, as shown in figure 3.

The tests and the test results are described in this paper. The failure types are given and some load-displacement curves are shown. Further, the tests are compared to a numerical model.

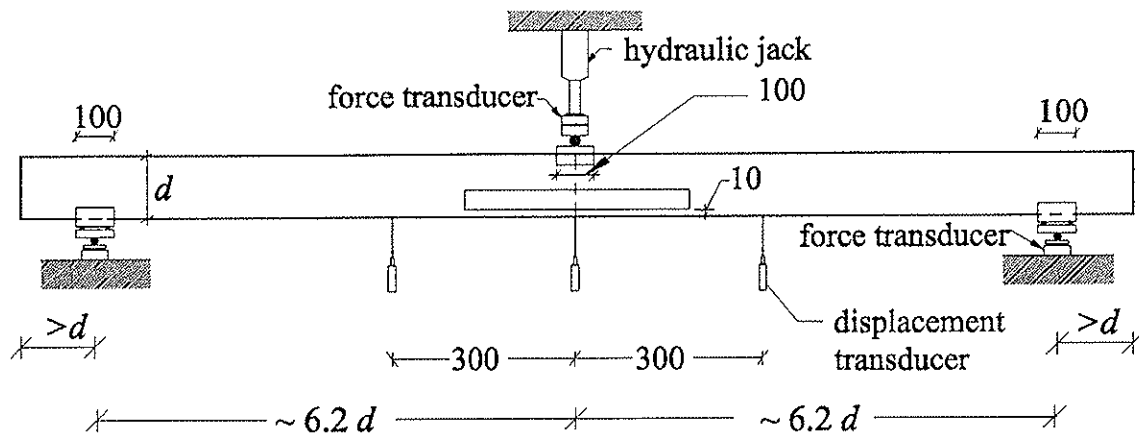


Figure 3: Test arrangement for beams in 3-point bending. Dimensions in mm.

## 2 Test series

The test programme is shown in table 1. The applied timber is Swedish spruce with 45 mm thickness. The timber was selected and graded<sup>1</sup> by a truss plant.

Series no.	No. of tests	Timber			Plate	
		grade <sup>1</sup>	$d$ mm	span mm	width $w$ mm	length $l$ mm
RS1	10	K18	120	1500	-	-
RS3	20	"	170	2100	-	-
RS5	10	K24	170	"	-	-
RS6	10	K18	120	1500	34	776
RS7	10	"	120	"	76	516
RS8	10	"	120	"	34	516
RS9	10	"	170	2100	76	516
RS10	10	"	170	"	34	776
RS12	10	"	170	"	34	516
RS14	10	K24	170	"	34	776
RS15	10	"	170	"	34	516

Table 1: Test program with 11 different series.

The reinforcement is made by GNA 20 S plates from Gang-Nail Systems. The thickness of the plate is 1 mm and the tooth length is about 8 mm. Different widths and lengths of the plates are used. All plates are located at the centre of the beams 10 mm from the tensile edge, see figure 3. The test specimens have been conditioned and manufactured according to prEN 1075. During the test period the moisture content of the timber was about 10-12%.

To obtain a section with a moment peak all samples are loaded in 3-point bending, see figure 3. The distance between the mid load and the reactions is  $\sim 6.2d$ , where  $d$  is the cross-sectional depth of the beam.

According to DS/EN 408 the load is applied at constant loading head movement (deformation controlled) so the maximum load is reached within 300s ( $\pm 120$ s). The loading heads have a width of 100 mm.

In figure 4 the scaled test specimens with a reinforcement are shown.

---

<sup>1</sup>Strength classes K18 and K24 can be transmitted to S8 and S10, according to ECE Timber Committee.

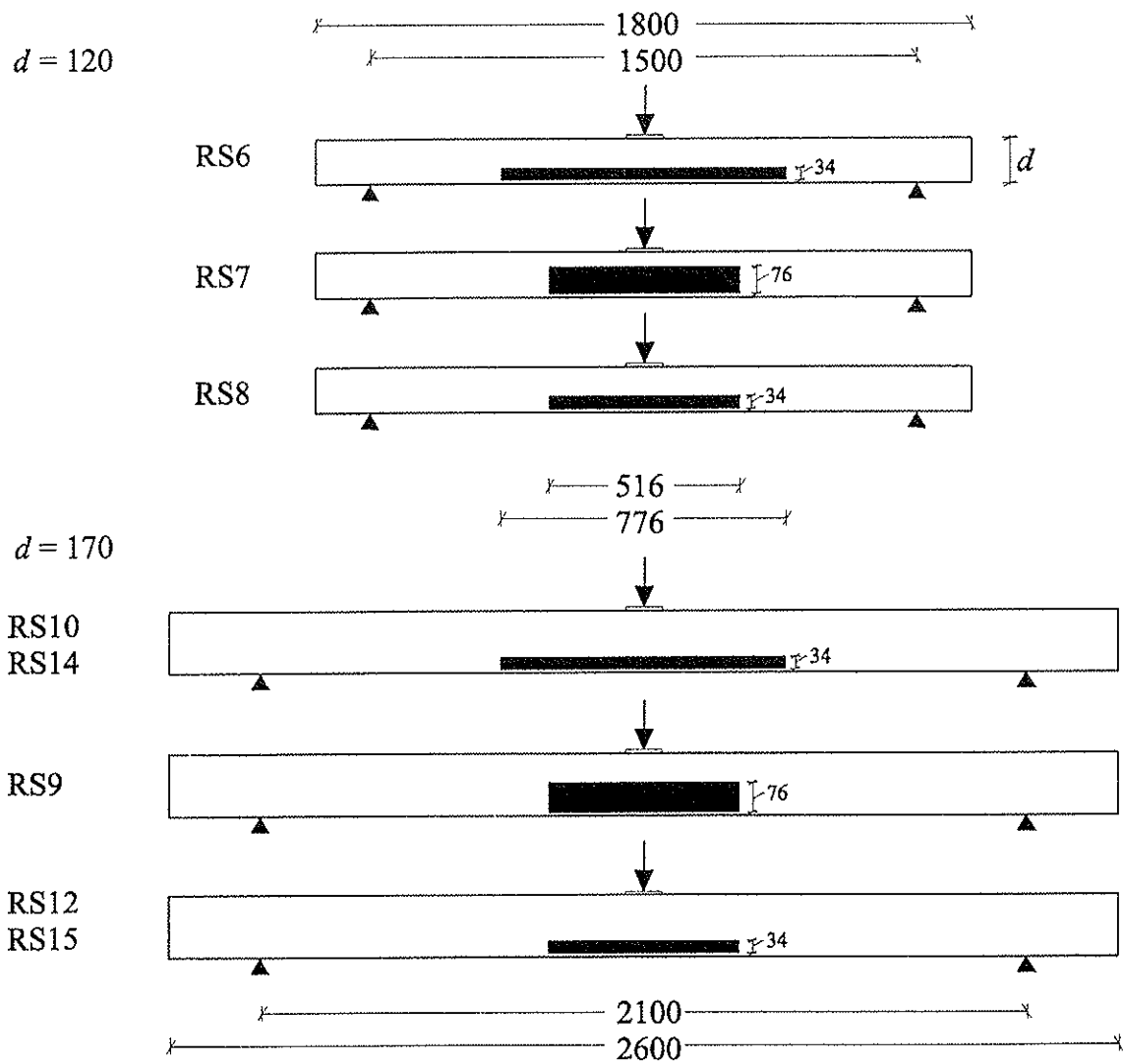


Figure 4: Test specimens with plate reinforcement. Dimensions in mm.

### 3 Results and discussion

In table 2 the failure loads, failure types and location of failure in each series are given. The mean value  $m$ , the standard deviation  $s$ , and the coefficient of variation  $\delta$  are calculated according to DS/EN 1058.

The average wood density is found between 448 - 507 kg/m<sup>3</sup>.

#### 3.1 Failure

In general the failure for all beams with or without reinforcement is very sensitive to the appearance and the size of the knots in the tensile side in the area of the load supply.

Series no.	No. of tests	Timber grade	Reinforc. plate		Failure								
			$w$	$l$	load			type			location		
					$m$	$s$	$\delta$	T	K	S	I	O	
$d = 120\text{mm}$					kN	kN	%						
RS1	10	K18	-	-	12.41	2.94	24	1	9		8	2	
RS6	10	K18	34	776	16.42	3.04	19	3	7		9	1	
RS7	10	K18	76	516	15.32	2.46	16	5	5		8	2	
RS8	10	K18	34	516	15.02	2.80	19	4	6		5	5	
$d = 170\text{mm}$													
RS3*	20	K18	-	-	21.15	3.68	17	9	8		12	5	
RS5	10	K24	-	-	20.17	4.32	21	6	3	1	9	1	
RS9	10	K18	76	516	19.94	3.67	18	5	5		6	4	
RS10	10	K18	34	776	20.23	2.97	15	3	5	2	9	1	
RS12	10	K18	34	516	21.80	5.62	26	2	5	3	7	3	
RS14	10	K24	34	776	22.78	1.69	7	6	2	2	8	2	
RS15	10	K24	34	516	22.66	3.44	12	4	3	3	8	2	

T: Tensile failure of the fibres. No knot observed at failure.

K: Tensile failure started at a knot.

S: Shear failure in the timber. A crack starts at or below the reinforcement and runs to the beam end parallel to the fibre.

I: Failure started *within* the reinforcing area. In series with no reinforcing, failure started close ( $\pm 0.2$  m) to the force.

O: Failure started *outside* the reinforcing area or  $> 0.2$  m from the load.

\* Some failures not observed.

Table 2: Failure load, number of failure types and location of failure in each series.

In table 2 it is seen that the failure loads for the reinforced series with  $d=120$  mm are increased between 20 to 30% compared to the series without plate (RS1). The reinforcing effect is most distinct with long reinforcement plates. In the series with 776 mm reinforcement (RS6) most of the failure occurred within the area of the reinforcement. In series RS7 and RS8 almost half of the failures occurred outside the reinforcement area. The tests with failure outside the reinforcement are caused by

the "flat" variation of the moment, see figure 5. In general the moment outside the reinforcing area should be low compared to the moment within the reinforcing area.

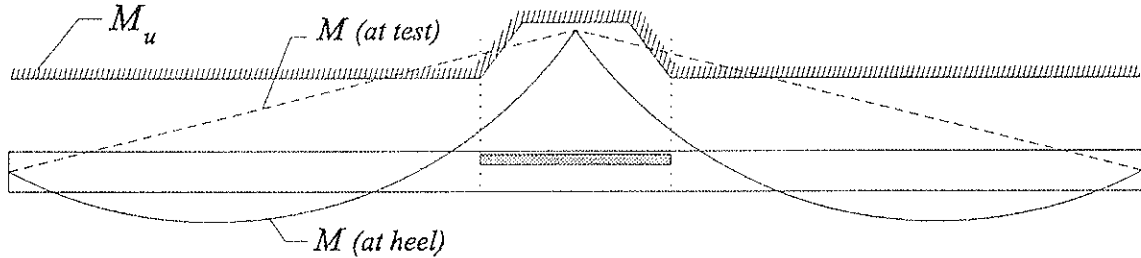


Figure 5: Variation of sectional moment with peaks ( $M$ ) in relation to the moment capacity ( $M_u$ ) of a reinforced beam.

Tests with a failure location outside the reinforced area may distort the effect of the reinforcement and they should not be included in the calculation of the average failure load. However, the average failure load of the tests with failure located within the reinforced zone only varies between  $\pm 1\%$  of the values given in table 2. In series RS7 and RS9 the average failure values are increased by  $\sim 5\%$ .

In a few cases total tensile failure in the plates occurred, see figure 7, and in other cases local tensile failure was observed. The decreased coefficient of variation in tests with a reinforcement shows that the failure load is less sensitive to weak sections.

The increasing effect of the reinforcement on the failure load in the series with  $d=170$  mm did not take place. In series with long plates (RS10), where the effect is assumed to be most distinct, the failure loads are even less than the failure loads of the beams without a reinforcement. The coefficient of variation in the series is almost the same. Failure within the reinforcing area causes full tensile failure in the steel or in very few cases withdrawal of the teeth.

An examination of the failure types in the tests with a low failure load compared to the mean value of each series shows that the failure in many cases occurred at knots within the reinforcing area. As it was expected that the reinforcement would have an effect in exactly these cases this indicates that the tensile strength of the plate is too low for a cross-sectional depth of 170 mm. A plate with an increased tensile capacity compared to the GNA 20 S may have a larger effect on the moment capacity of the beam. However, if the reinforced beams shall be an option for practical truss manufacturing it is required that the reinforcement is made by rather small strips ( $w < 40-50$  mm) of plate as the area of a large reinforcing plate may conflict with a beam connector plate, see figure 6.

Visually some of the beams in series planned for K18 may be graded in K24. This assumption is supported by the results from series RS3 and RS5. The mean value of the series with K18 (RS3) are found to be lower than the same value in series with K24 (RS5).

In some tests in RS10, RS12, RS13 and RS15 the failure was caused by shear failure in the wood. This failure type is most distinct in tests with a reinforcement. A crack stated just below the plate and extended to the end of the beam. The size of the

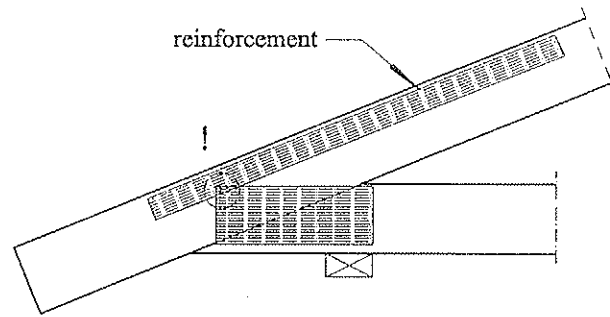


Figure 6: A reinforcement plate in conflict with a beam connecting plate.

failure load for this failure type is found to be rather high (between 20.5kN and 30kN,  $m=25,3\text{kN}$ ).

### 3.1.1 Embedding at the loading area

In many specimens the 100 mm loading head at the centre of the beam was more or less embedded in the beam. In a few cases the indentation into the wood was more than 10 mm. The embedding is caused by the force perpendicular to the grain. Some failure lines were observed at the load head, see figure 7. The crushing of the wood is most distinct in areas with no knots at the loading head. Crushing perpendicular to

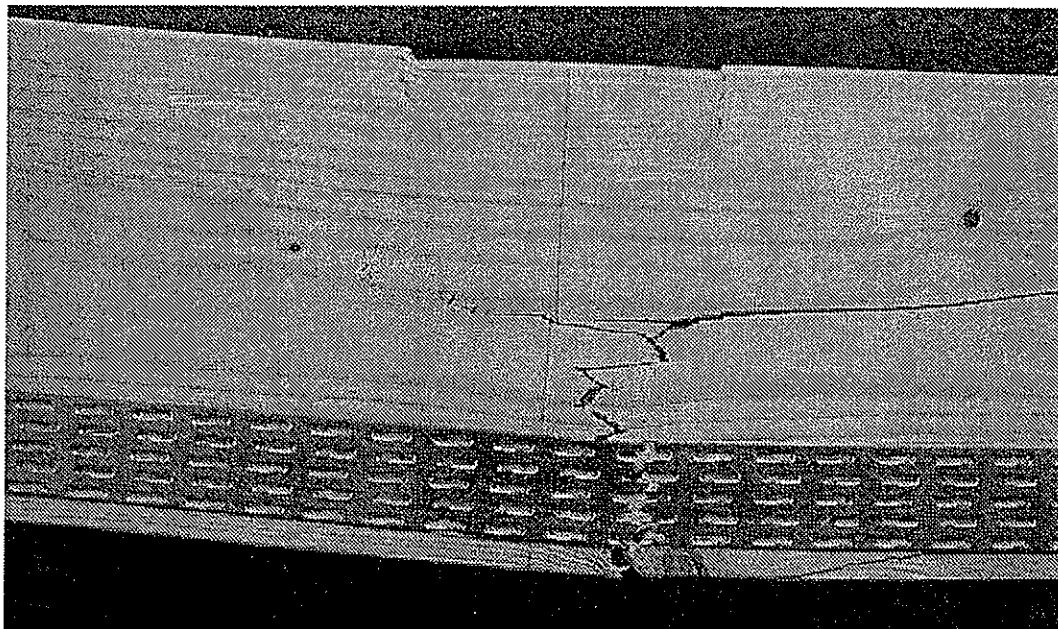


Figure 7: Lines with compression at the loading head and full tensile failure in plate.

the grain can be avoided by increasing the width of the loading head, however, this will cause the moment variation and the moment peak to be less distinct.

The appearance of the moment peak in top chord sections at heel joints will be affected by the size of the contact zone between the top chord and the wedge/ bottom chord,



see figure 2. The extent of the contact zone parallel to the chord is hardly bigger than 100 mm. Therefore, it is believed that crushing perpendicular to the grain also appears in chords with moment peaks close to the failure moment. Some analyses on the contact zone are given in Nielsen 1996.

The crushing at the loading head can also be avoided by increasing the span, however this will also cause the moment peak to be less distinct.

### 3.2 Load-displacement curves

In figure 8 the load-displacements curves for the tests in series RS1 and RS6 are shown. The "O" and "X" denote the maximum load in series RS1 and RS6, respectively.

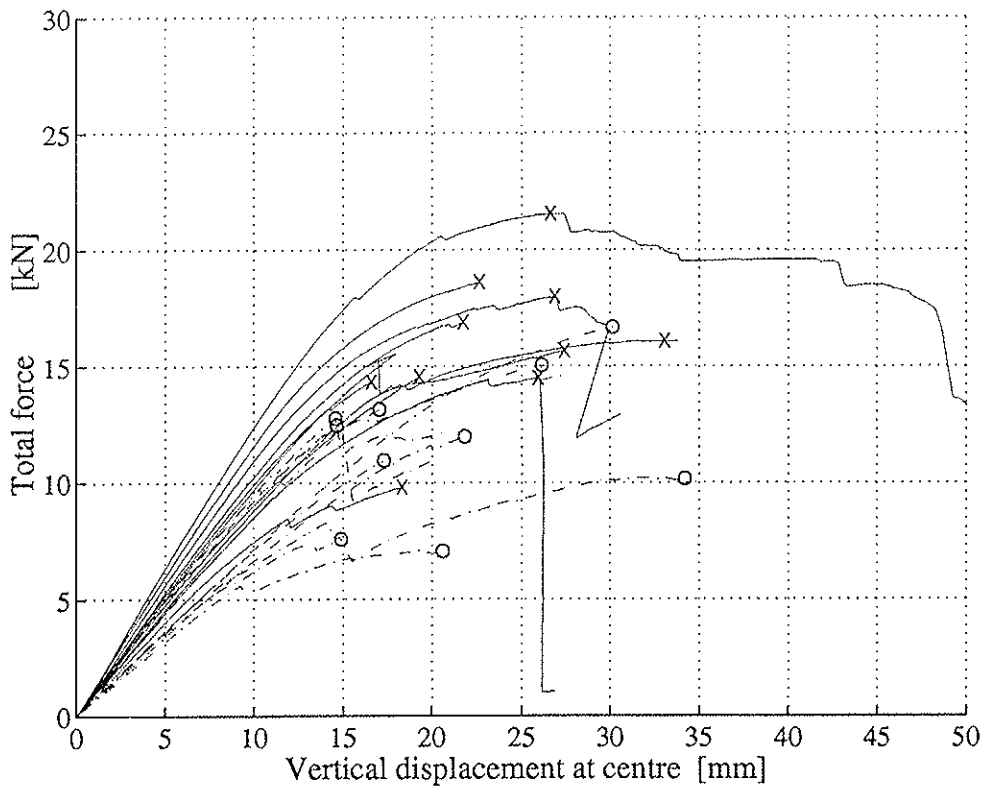


Figure 8: Load-displacement curves of RS1(dash,O) and RS6(solid,X).

In figure 8 it is seen that the initial stiffness of the reinforced beams is increased compared to the non-reinforced beams. The reinforcement changes the properties of the failure from a brittle failure to be slightly more ductile. The displacements at maximum load are almost unchanged.

In a few tests a negative increment of the displacement is observed. This is caused by fact that the displacement measuring pins "jump" out of the measuring points when a sudden crack arise.

In general the effect on the stiffness is very much the same as found for the strength. The stiffness is increased by 20% to 30% for reinforced series with  $d=120\text{mm}$  and the effect is vanishing for the reinforced series with  $d=170\text{mm}$ .

## 4 Comparison with numerical model

Since 1992 a numerical beam model for trusses with punched metal fasteners has been developed and implemented in the MATLAB environment. The programme is called TRUSSLAB. The theory behind the model is given in Foschi(1977), Nielsen(1996) and Ellegaard et al.(1999). TRUSSLAB is in still progress by calibrating the model to fit experimental test results for several different types of tests. So far the model has been compared with tests on splices in tension and bending, Nielsen (1996). The model is able to predict the load-displacement curve even with contact between the timber members and/or plastic conditions in the nail plate. The intention is to develop a model which can estimate the stiffness and the failure in arbitrary joints with punched metal plate fasteners.

### 4.1 The model

In figure 9 a model of the tests in series RS6 is shown.

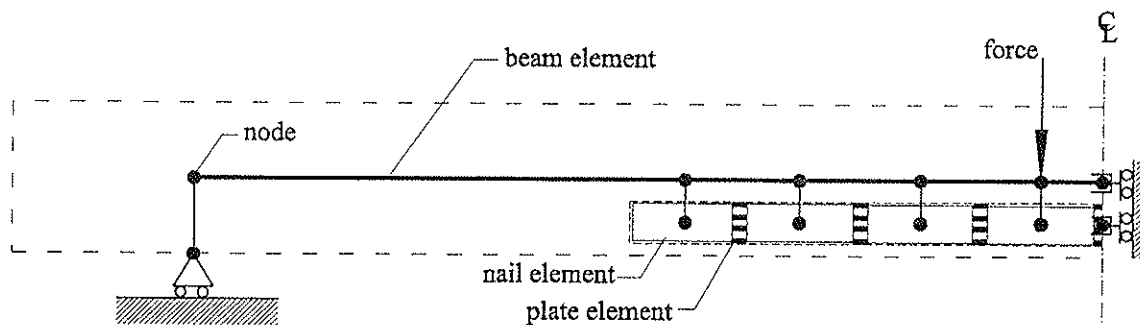


Figure 9: Model of the tests in series RS6.

As the problem is symmetric, only the left half is modelled. For the timber beam Timoshenko beam elements are used and the reinforcement is divided into 4 nail elements connected by 4 plate elements. By dividing the plate into several elements the extent of the plastic zones can be followed. Small auxiliary elements are used to transfer the forces between the beam elements and nail elements. Further description of the the model and the properties of plate and nail elements is given in Nielsen(1996) and Ellegaard et al.(1999).

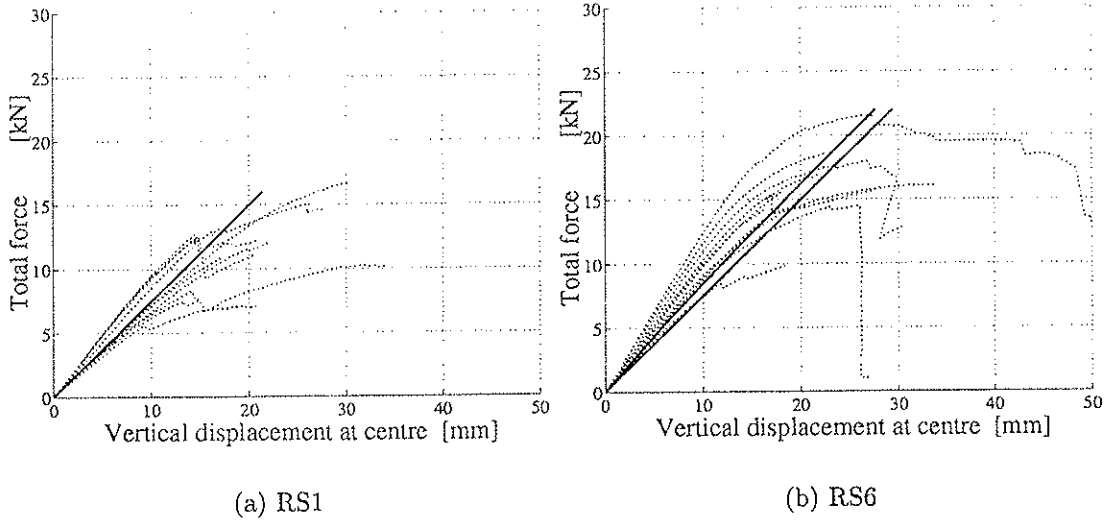


Figure 10: Numerical and experimental load-displacement curves.

## 4.2 Results and discussion

In figure 10 the numerical load-displacements curves are compared with the experimental results.

In figure 10(a) it is seen that the load-displacement curve of the numerical model with average wood properties according to DS413 ( $E=9000\text{MPa}$ ,  $G=600\text{MPa}$ ) estimates the load-displacement curves of tests. It is assumed that the same stiffness properties can be used to estimate the load-displacement curves of series RS6.

In figure 10(b) it is seen that the load-displacement curve of the numerical model overestimates the displacements. The stiffness of the model is not very sensitive to a variation of the plate location or the plate stiffness. An explanation of the overestimation may be that the wood stiffness of the tests specimens in series RS6 is larger than expected.

According to the model there is a plastic state in the all plate elements. In the two plate elements close to the centre the whole plate is plastic. The plate becomes plastic from 6 kN.

## 5 Conclusion

Based on the tests the following conclusions can be made:

- The failure load and the stiffness of 120 mm beams with reinforcement are increased by 20 to 30%.
- The reinforcement has no effect on 170 mm beams.

In further analyses it is recommended to:

- use a plate with high tensile capacity (thickness  $> 1$  mm) in beams with a cross-sectional depth of 170mm.
- locate the reinforcement closer to the tensile edge of the timber ( $< 10$  mm).
- limit the width of the reinforcement ( $< 40 - 50$  mm)
- test beams with other cross-section depths and load conditions.

## 6 References

1. DS/EN 408 Timber structures - Structural timber and glued laminated timber - Determination of some physical and mechanical properties. European Standard, CEN January 1995.
2. prEN1075 Timber structures - Test methods - Joints made of punched metal plate fasteners. European Standard, CEN April 1993.
3. DS/EN 1058 Wood-based panels - Determination of characteristic values of mechanical properties and density. European Standard, CEN July 1995.
4. Foschi, Ricardo O., 'Analysis of wood diaphragms and trusses. Part II: Truss-plate connections', Can. J. Civ. Eng. Vol. 4, pp 353-362, 1977.
5. Nielsen J. (1996), 'Stiffness Analysis of Nail-Plate Joints Subjected to Short-Term Loads', Ph.D.-thesis, Structural Design Paper No. 2, Aalborg University.
6. Ellegaard P., Nielsen J. (1999), 'Advanced Modelling of Trusses with Punched Metal Plates', Symposium Proceedings, RILEM Symposium on Timber Engineering 1999, Stockholm, Sweden.
7. DS413:1998 (5.1), 'Code of Practice for the Structural Use of Timber', (in Danish), Danish Standard Association, 1998.

**INTERNATIONAL COUNCIL FOR RESEARCH AND INNOVATION  
IN BUILDING AND CONSTRUCTION**

**WORKING COMMISSION W18 - TIMBER STRUCTURES**

**THREE-DIMENSIONAL INTERACTION IN STABILISATION OF  
MULTI-STOREY TIMBER FRAME BUILDINGS**

S Andreasson

Department of Structural Engineering

Lund University

SWEDEN

**MEETING THIRTY-TWO**

**GRAZ**

**AUSTRIA**

**AUGUST 1999**

---

Presenter: S.Andreasson

- B.Källsner questioned the procedure that calibrated the model directly to full scale wall tests rather than fastener load slip information. He pointed out that the calibrated model would be specific to the full scale wall tests because the stiffness of the structure is sensitive to the location and distribution of fasteners within a system and the application of dead load during testing.
- A.Andreasson responded that the smear action of fastener was considered and single fastener based model calibration was difficult.
- F.Lam agreed that although single fastener based model calibration procedures were more difficult, past work at UBC are successful examples.

# Three-dimensional interaction in stabilisation of multi-storey timber frame buildings

Sverker Andreasson<sup>1</sup>

Department of Structural Engineering, Lund University, Sweden

## Summary

A study has been performed with a finite element model in order to investigate the distribution of forces in multi-storey timber frame buildings under combined lateral and vertical loading. The model has been calibrated and verified against full-scale tests, performed on separate shear walls. During the tests, the vertical support forces have been monitored as well as the load and top displacement. The calibrated model has been used primarily to investigate the distribution of dead load when combined with lateral loads on shear walls and transverse walls with gypsum sheathing. The results indicate that the in-plane stiffness of diaphragms in a lateral-force-resisting system is considerable, and imply that a great portion of the dead load can be utilised to counteract uplift forces caused by lateral loading. The conclusion is that the designers have great possibilities to take advantage of dead load when stabilising the system by properly connecting the different diaphragms in order to achieve interaction in three dimensions. This is not always the practice in the current two-dimensional design approach.

## 1 Introduction

A growing interest in multi-storey timber frame buildings in the Nordic countries has increased the need to understand the overall structural performance of the system. Current design principles fail to take interaction between components into account. The overall performance of a structural system exposed to horizontal loading is simplified into two-dimensional analyses, where only the shear walls are assumed to be active. This approach leads to the practice of all structural components, such as shear walls and diaphragms, being designed separately, with no consideration given to load sharing in the three-dimensional structure. Current design principles further presuppose rigid frame members that are hinged to each other [5]. Flexibility of the joints is not considered. Such methods of analysis are consequently unable to predict the effect of more flexible joint conditions and changed anchorage configurations. The aim of the present study is to investigate effects of the interaction between diaphragms concerning the distribution of dead load in a system of diaphragms.

---

<sup>1</sup> Also Structural Engineer, NCC AB, SE-205 47 Malmö, Sweden

In order to investigate the force transfer in multi-storey timber frame buildings, a static non-linear finite element model has been developed in the general analysis program ANSYS5.4. The multi-storey structure is idealised as horizontal and vertical diaphragms connected by springs. The finite element model has been calibrated and verified against full-scale tests performed on shear wall units with different configurations. In order to study the distribution of reaction forces, a test rig that allows monitoring of support forces has been developed.

## **2 Limitations**

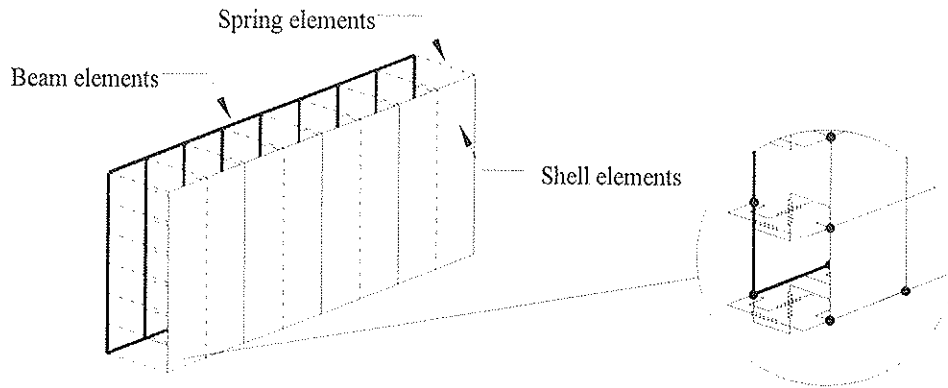
This study covers structural systems exposed to static loading. No dynamic effects are included since the design methods in the Nordic countries do not take seismic loads into consideration. The collection of basic design data, such as material properties, is outside the scope of this study. The properties of materials, such as the stiffness of connectors and E-modulus of sheathing and framing, are estimated from non-statistical experiments performed within the study, and results found in literature, e. g. [4]. Non-linearity is not considered for the framing and sheathing, only for fasteners and connectors. The framing and the sheathing elements are assumed to be homogenous and isotropic. Out-of-plane buckling is not taken into account in the finite element model. Nor is the asymmetry due to the fact that sheathing panels may be attached only to one side of the diaphragms considered. Strength design, such as timber and joint-failure design, is also outside the scope of this study.

## **3 Description of the finite element model**

The non-linear finite element model is developed in the general finite element program ANSYS 5.4. The model is created in 3D-space with beam, shell and spring elements. These elements are assembled to vertical and horizontal diaphragms with the use of macro scripts written in ANSYS Parametric Design Language. The diaphragms can be oriented in two perpendicular directions, located arbitrarily in relation to each other and built up in several storeys. The diaphragms can be connected both in vertical and horizontal directions with spring elements representing nails, screws, connectors and hold-downs. The connections can be made between vertical diaphragms or between horizontal and vertical diaphragms.

### **3.1 Vertical diaphragms**

A vertical diaphragm, i. e. a shear wall, is built up by beam, shell and spring elements representing the framing, the sheathing and the fasteners respectively. The beam elements at the joints between the studs and plates are connected to each other by three perpendicular uncoupled spring elements in order to model the flexibility of the joints satisfactorily. The vertical springs in the framing joints are non-linear, with different load-deformation properties in tension and compression. The shell elements are attached to the beam elements with two perpendicular uncoupled non-linear springs in the plane of the diaphragm, and one linear spring in the out-of-plane direction (Fig. 1). Each sheathing panel is separately attached to the framing. The fastener spacing can be varied arbitrarily, and can also be different at centre and edge of the sheathing. Bearing effects between adjacent sheathing panels are incorporated in the model. Thus, the sheathing elements are prevented from numerically overlapping one another.

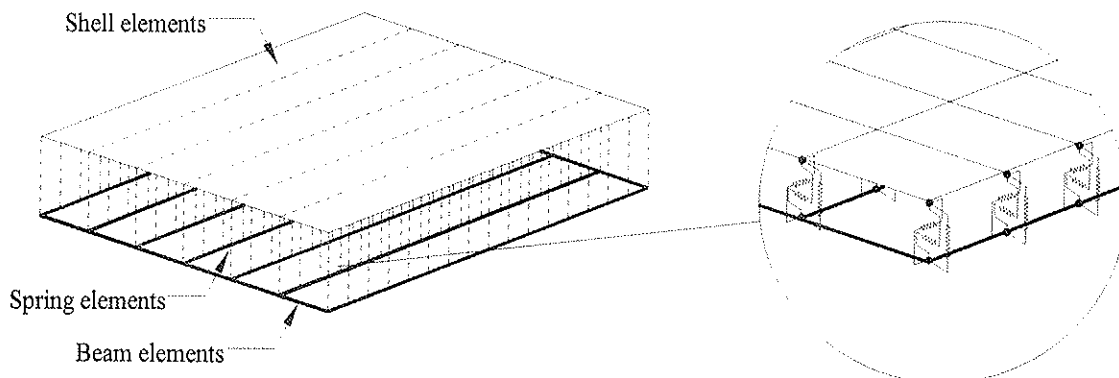


**Fig. 1:** Composition of vertical diaphragm

Window and door openings can be implemented in the vertical diaphragms. The openings can be of varied dimensions and located arbitrarily.

### 3.2 Horizontal diaphragms

Horizontal diaphragms are composed of beam, shell and spring elements. The floor framing is built up by beam elements, representing the joists, chords and struts. The beam elements are connected to each other in the same way as in the vertical diaphragms, except that all springs are linear. The floor sheathing is idealised as a single sheathing panel.



**Fig. 2:** Composition of horizontal diaphragm

This is a simplification, but an acceptable one since the flooring panels are often glued to the truss framing and to each other. This creates a very stiff component in comparison with the vertical diaphragms. The panel is composed of shell elements that are attached to the beam elements with non-linear spring elements (Fig. 2). The fastener spacing can be varied arbitrarily.

### 3.3 Anchorage assemblies

Two shear walls on different storeys can be attached to each other by vertical, non-linear springs, representing hold-downs. The anchorage springs connect either a stud in the bottom storey to the foundation or the studs in two adjacent storeys. The stud on the lower storey must be located directly below the stud in the upper storey. The hold-downs can be installed at all stud locations.

The connections between diaphragms within the model are further described in a paper [1] presented previously.



## 4 Experimental studies and model calibration

In order to investigate the overall performance of a timber frame structure, it is essential to obtain knowledge about the behaviour of an individual diaphragm exposed to lateral and vertical loading.

### 4.1 Test method

Most shear wall experiments performed do not give any information of the vertical support forces due to lateral loads, e. g. test prEN594 [3] prescribed by Eurocode [2]. In order to get this information, a test rig which allows monitoring of vertical support forces has been developed (Fig. 3). The wall specimens are mounted with compression load cells at the bottom plate directly under each stud, except at the location closest to the horizontal load. Here, a tension load cell is connected to the anchorage at the joint between the stud and the bottom plate. An end stop at the bottom plate prevents the wall from sliding.

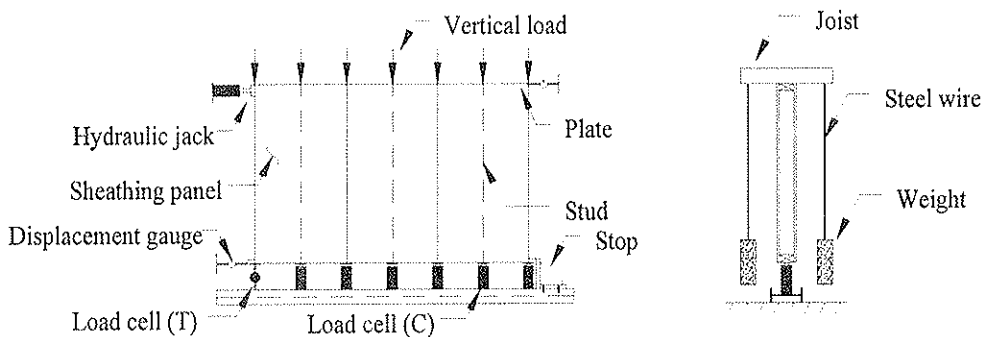


Fig 3: Test rig developed in the study for monitoring of load, displacement and vertical support forces

Vertical load is applied at the top plate directly above each stud via wood joists carrying pairs of concrete weights in steel wires. During the tests, the horizontal load, the vertical support forces and the top displacements are monitored.

### 4.2 Configuration of test specimens

The test walls were assembled by 45 x 90 mm ungraded timber as framing members and 13 mm gypsum boards (DANOGIPS) as sheathing. The gypsum boards were attached to the framing with drywall screws for wooden joists, 3.9 x 41 mm (ESSVE). The screw spacing was 100 mm on the perimeter and 200 mm in the interior of the sheathing. Anchorage brackets of steel, 65 x 55 x 3 mm, were attached rigidly to the foundation and with eight screws 4.2 x 35 mm to the end studs.

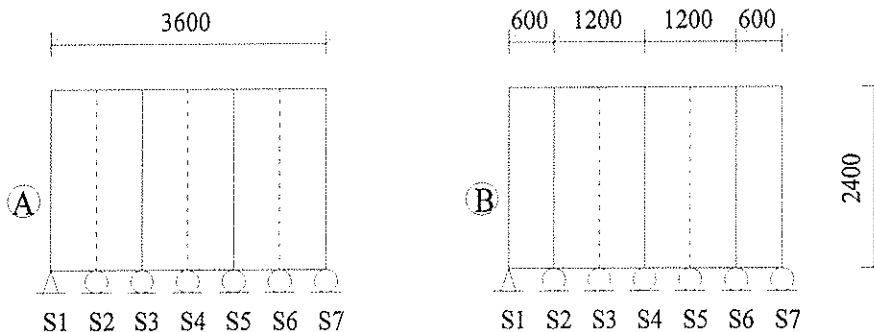


Fig 4: Alternative configurations of sheathing panels in test shear walls

Tests were performed with two wall specimens, each with the height of 2.4 m and the length of 3.6 m. The length corresponds to the width of three standard gypsum panels. In the first shear wall, only one side was sheathed with three full-size gypsum panels (Fig. 4 configuration A). In the second test, a shear wall with sheathing on both sides was used. One side was sheathed with three full-size panels (Fig 4, configuration A). On the other side, the sheathing panels were staggered in relation to the first side, i. e. two full-size panels and two halves were used (Fig. 4 configuration B). The choice of this panel configuration was made in order to investigate if the stiffness is influenced advantageously if the panel joints for the different sides of the wall are staggered. A vertical load of 2.4 kN was applied at each stud.

### 4.3 Calibration of the finite element model

The fastener properties were determined by calibrating the finite element model against the first full-scale test, i. e. a kind of an inverse modelling procedure. This is, of course, a simplification that would be rather harsh if the aim of the analyses was to determine the behaviour of separate fasteners. The objective of this study was, however, to investigate the overall performance of a diaphragm and the behaviour of a system composed of several diaphragms. In view of this and the fact that the number of fasteners was large, an approach with smeared fastener properties should work satisfactorily.

The fastener properties were calibrated so that the finite element model gave the same load-displacement curve as achieved in the first test (Fig. 5, to the left).

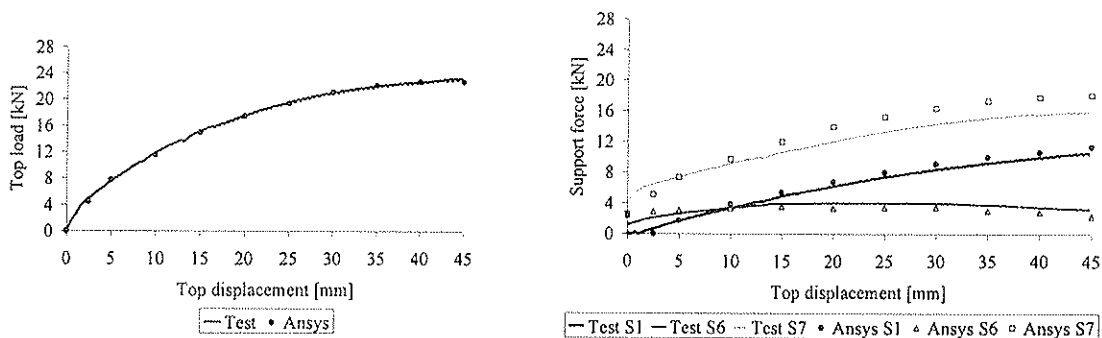


Fig. 5: Results for first test wall and corresponding results from Ansys analysis

In order to determine the quality of the calibration, the results for the vertical support forces were compared as well (Fig. 5, to the right). The numbering of the supports is given in figure 4. It can be seen that the finite element model gives reasonable results for the support forces when only calibrated after the force-displacement curve.

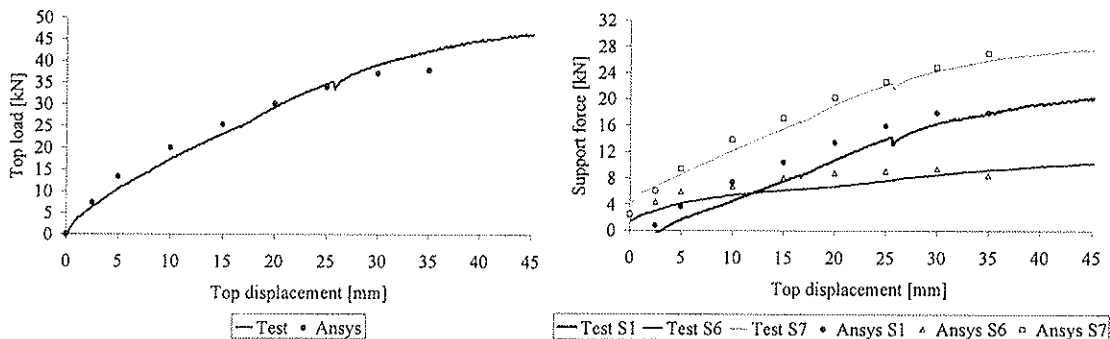


Fig. 6: Results for second test wall and corresponding results from Ansys analysis

The model was also compared with the second test wall, without any further adjustments of the model properties. The match between the Ansys model and the second test is quite good (Fig. 6). Bearing in mind the complicated structure with staggered panels, the results show a reasonable fitting for the purpose of this study. The main reason for the mismatch with the tests might be linked to the difficulty of determining the correct properties for, and the effect of, the semi-rigid anchorage and the bearing between panels.

It can be noted that the model is not able to reliably predict the failure load. This is probably due to various phenomena connected with the brittle cracking of the gypsum panels in the tests, which is too complicated to simulate numerically. The aim of the model is, however, to predict the behaviour of a system exposed to loading within the structure's capacity, why this will not pose a problem.

## 5 Numerical experiments

As mentioned previously, the analysis of the interaction between diaphragms has been oversimplified due to lack of understanding of their joint performance. This is evident when it comes to the question of how to deal with the distribution of dead load for shear walls supporting floor diaphragms, or the dimensioning of anchorage detailing and diaphragm connections. In order to investigate this closer, several finite element analyses have been made. Primarily structures with gypsum-sheathed diaphragms have been analysed in this study. The interest in this area is due to the fact that diaphragms sheathed with gypsum are used very frequently in lateral-force-resisting design in the Nordic countries. It is only when the capacity of the gypsum is too low that plywood panels are used, e. g. in the lower storeys of multi-storey buildings.

### 5.1 Distribution of dead load along shear walls

No distinct guidelines for the distribution of dead loads in lateral-force-resisting systems are provided in the codes. This is due to poor knowledge of how great part of the dead load that will be transferred to the location of the uplift force. The consequence is that some designers hesitate to use the dead load to counteract the uplift force, while others tend to use it uncritically.

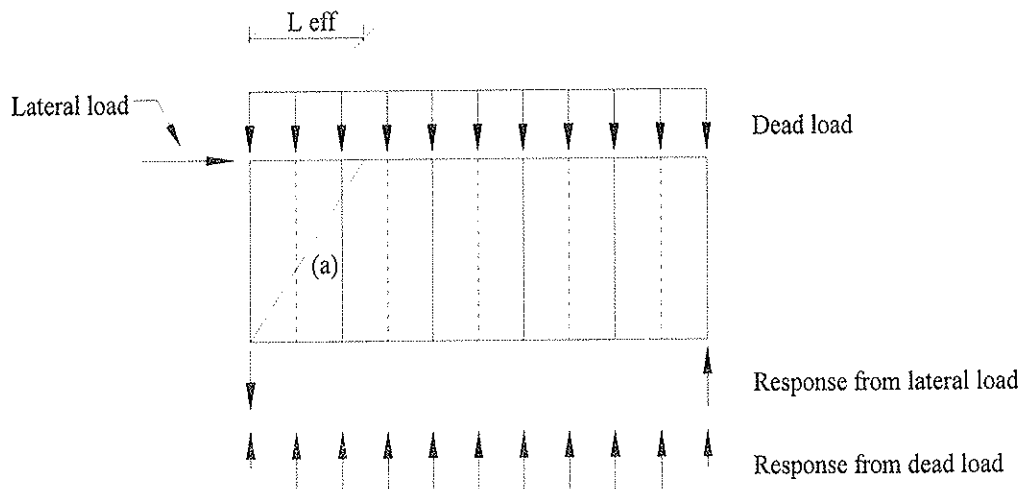


Fig 7: Possible distributions of dead load for a horizontally loaded shear wall

A safe approach is to assume that the uplift force is counteracted only by the dead load corresponding to the actual stud affected by uplift. In that case, the effective length over which the dead load is calculated would be half a stud spacing. This assumed distribution is indicated with the reaction forces in figure 7 above. The in-plane stiffness of the diaphragms will probably transfer a larger part of the dead load along the wall to the point of uplift (Fig. 7, curve a). If the shear wall was considered to be very stiff in plane, the dead load counteracting the uplift force would be the load over half the length of the wall. Hence the length over which the dead load should be calculated ( $L_{eff}$  in Fig. 7) is somewhere between half the stud spacing and half of the wall length. Which of the extremes that is the most representative is determined by parameters such as number of sheathing layers, panel distribution, wall height and length ratio, et cetera.

It is also of great interest to investigate how these forces are transferred over the storey boundaries. Can a multi-storey structure be seen as one continuous diaphragm over all storeys (Fig. 8 b and 8 c) or will it act as several separate diaphragms (Fig 8 a)?

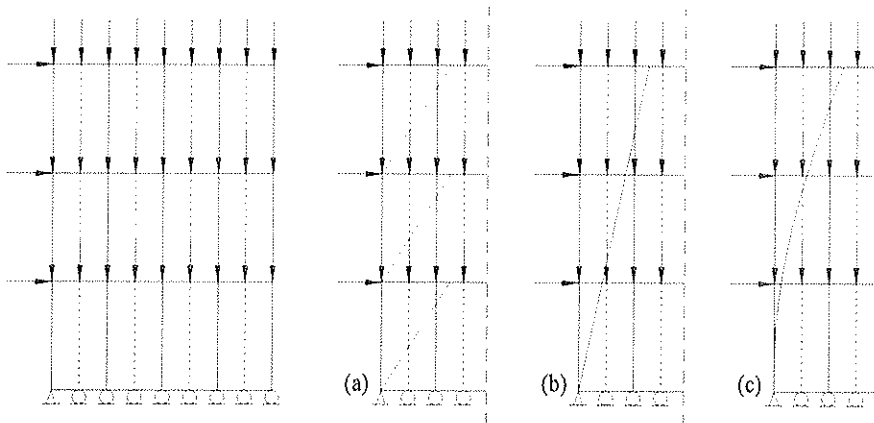


Fig 8: Possible distributions of dead load for horizontally loaded shear walls in multi-storey structures

In order to investigate the influence of these parameters, a number of finite element analyses has been performed using the previously described model.

## 5.2 Transfer of dead load via transverse walls

In the current design practice for lateral-force-resisting systems, only the shear walls are assumed to be active. Due to this fact, shear walls and diaphragms are being designed separately with no consideration given to load sharing in the three-dimensional structure. Structural engineers often hesitate to take advantage of adjacent walls in order to counteract uplift forces or to transfer the uplift forces to anchorage assemblies in the transverse walls.

Another issue of great interest within this field is the possibility to counteract uplift action with the dead load affecting the transverse walls, e. g. when the joists in the flooring are supported on the transverse walls. The question is how stiff the walls are concerning in plane bending, and also how great shear forces can be transferred between the different parts of the walls. Additionally, how far away from the connection to the shear wall will the dead load on the transverse walls help to counteract the uplift force (Fig. 9)? Will the effective length for the dead load differ significantly depending on wall length, magnitude of load, number of storeys, et cetera? Efforts have been made in the study in order to find an idealised effective length (Fig. 9, curve b) that converts the load distribution to a rectangular one, which is easier to use.

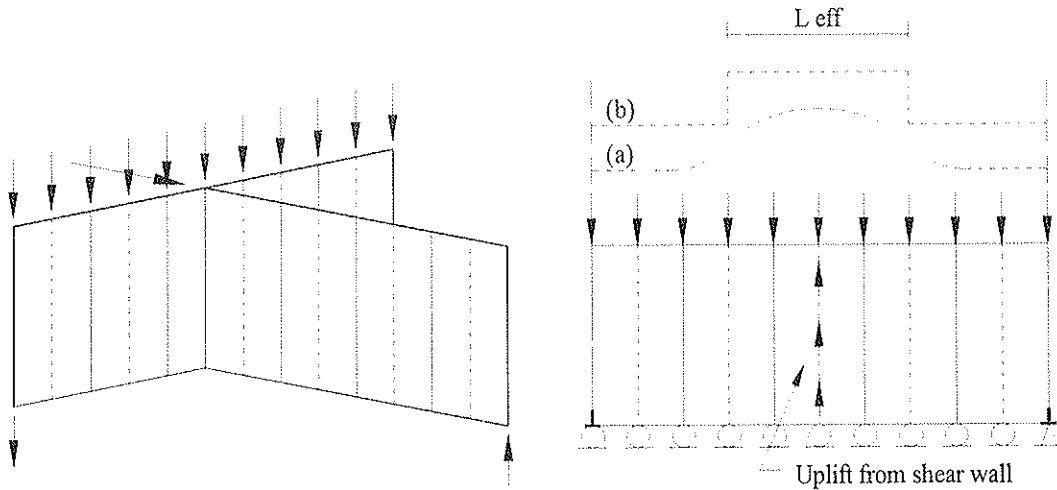


Fig 9: Distribution of dead load for horizontally loaded shear wall

Finite element analyses have also been performed in order to investigate the possibility to take advantage of anchorage bolts in a transverse wall in order to counteract uplift action in an adjacent shear wall.

## 6 Results and discussion

The results of the study are presented briefly in the following sections. The amount of dead load that can be utilised in different design situations is presented as a ratio, here called effective length ratio ( $L_{eff}$ ) since it is a question of a tributary length. This ratio gives the quotient of the vertical load transferred to the location of the uplift and the dead load applied at each stud (Fig 7).

### 6.1 Investigation of dead load on shear wall

A shear wall with the length of four standard sheathing panels, i. e. 4.8 m, is chosen as the base configuration in the numerical analyses (Fig. 10). The height is 2.4 m and the fastener spacing is 100 mm on the perimeter and 200 mm in the interior of the sheathing.

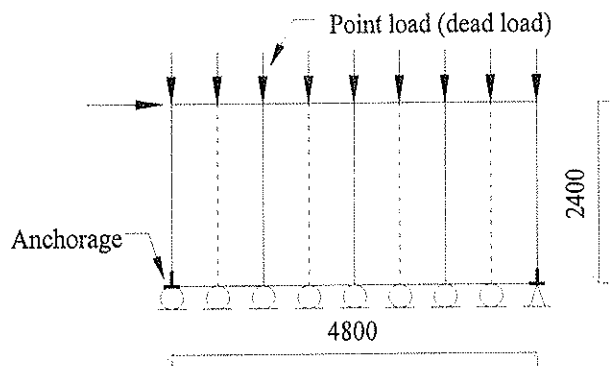


Fig. 10: Base configuration of shear wall in Ansys analyses

The walls are gypsum-sheathed on one or both sides. A dead load is introduced as point loads with the magnitude of 2.5 kN applied on the top plate directly above each stud. The horizontal load is applied as a point load at the windward end of the top plate. The wall is

anchored to the ground at the windward end and supported at the bottom plate directly under each stud. The anchorage bracket is semi-rigid.

In the results below, the effective length ratio is given for different wall configurations. In this case, the ratio is equal to the number of studs which loads are transferred to the uplift position. The results are also given as a percentage of the total applied dead load.

### 6.1.1 Effect of sheathing configuration and wall length

In order to investigate the effect of the sheathing configuration and wall length on the force distribution, analyses were made with three different configurations and four different lengths. The results (Table 1) indicate that there is a significant difference between walls sheathed on one and two sides respectively. The difference between a staggered configuration and an equal configuration for walls sheathed on two sides seems to be of minor importance.

**Table 1:** Effective length ratio for different lengths and configurations

<b>L<sub>eff</sub> ratio</b>	Single Sheathed	Double (Equal)	Double (Staggered)
3.6 m (3 panels)	<b>1.95 (28 %)</b>	-	<b>2.70 (39 %)</b>
4.8 m (4 panels)	<b>2.05 (23 %)</b>	<b>3.20 (36 %)</b>	<b>3.20 (36 %)</b>
6.0 m (5 panels)	<b>2.10 (19 %)</b>	-	<b>3.50 (32 %)</b>
9.6 m (8 panels)	<b>2.10 (12 %)</b>	-	<b>3.65 (21 %)</b>

It can be seen that the effective length over which the dead load is transferred to the uplift stud increases with the wall length up to about 8 panels. The relative length, though, decreases with the wall length.

### 6.1.2 Effect of panel width

The influence of the size of the sheathing panels is investigated in further analyses where the panel width is decreased from 1.2 m to 0.8 m. The total wall length is 4.8 m.

**Table 2:** Effective length ratio for different panel widths

<b>L<sub>eff</sub> ratio</b>	Single Sheathed	Double Sheathed
Standard (1.2 m)	<b>2.05 (23 %)</b>	<b>3.20 (36 %)</b>
Narrow (0.8 m)	<b>2.50 (19 %)</b>	<b>4.15 (32 %)</b>

The effective length ratio increases when using narrow sheathing panels (Table 2), but regarding the difference in stud spacing, the wall stiffness actually decreases. The absolute effective length is reduced by approximately 15 percent in spite of the increased numbers of studs and fasteners in the wall with narrow panels.

### 6.1.3 Effect of anchorage stiffness

The anchorage stiffness has a great influence on the distribution of the dead load.

**Table 3:** Effective length ratio for different anchorage stiffness

<b>L<sub>eff</sub> ratio</b>	Single Sheathed	Double Sheathed
No anchorage	<b>3.40 (38 %)</b>	<b>4.45 (49 %)</b>
Semi-rigid	<b>2.05 (23 %)</b>	<b>3.20 (36 %)</b>
Rigid	<b>0.85 (10 %)</b>	<b>1.75 (19 %)</b>

A very stiff anchorage will not allow for the deformations necessary to redistribute the dead load along the shear wall (Table 3). In practice, it is impossible to achieve a completely rigid anchorage. Some vertical deformation will always be present, why the dead load counteracting the uplift force probably always will exceed the vertical load applied at the end stud ( $L_{eff} > 1.0$ ).

#### 6.1.4 Effect of magnitude of dead load

The magnitude of dead load influences the distribution. A very large load will not be transferred to the same extent as a small load, due to the relation of the wall stiffness and the magnitude of the load (Table 4).

**Table 4:** Effective length ratio for different levels of dead load

$L_{eff}$ ratio	Single Sheathed	Double Sheathed
1.25 kN/stud	2.65 (30 %)	3.60 (40 %)
2.50 kN/stud	2.05 (23 %)	3.20 (36 %)
5.00 kN/stud	1.40 (18 %)	2.50 (31 %)

#### 6.1.5 Effect of number of storeys

The distribution of dead load in a laterally loaded multi-storey structure was studied by adding one storey at a time on top of the previously analysed structure (Fig. 10). A horizontal diaphragm on top of each shear wall separated the storeys. Dead load of equal magnitude is applied at each storey. The distribution is studied for each floor (Table 5).

**Table 5:** Effective length ratio for different numbers of storeys at each floor (ground/first/second)

$L_{eff}$ ratio	Single Sheathed	Double Sheathed
1 Storey	2.05 (23 %)	3.20 (36 %)
2 Storeys	2.35/2.70 (26/30 %)	3.25/3.30 (36/37 %)
3 Storeys	2.45/2.70/2.85 (27/30/32 %)	3.30/3.35/3.40 (37/37/38 %)

The results imply that the distribution of dead load over the structure is governed by the distribution at each floor, as indicated in figure 8 a. The effective length ratio for a separate shear wall decreases with the magnitude of the dead load. This also applies for a multi-storey structure. The effective length ratio for a multi-storey structure as a whole seems to be greater than for a separate shear wall with the same magnitude of dead load at each storey.

These findings imply that the effective length over which the dead load will be transferred to the location of the uplift can be estimated from the stiffness of a separate shear wall. This approach seems to be on the safe side.

One interesting finding, not accounted for in the previous results, is that the total support force at the compression side of a shear wall always is below the sum of the compression force due to the lateral load and the dead load applied at that very stud.

## 6.2 Dead load applied on transverse walls

The possibility to transfer dead load applied on transverse walls to the uplift end of a shear wall is dependent on the length of the transverse wall, the number of storeys, and, of course, the sheathing configuration. The behaviour is similar to the transfer of loads along a shear wall. The length is of minor importance. A wall sheathed on both sides is so stiff in

its plane that it should have the capacity to transfer the load over all its length to the uplift location. This is at least true for the wall lengths considered in conventionally designed structures. The parameter governing the effective length for the load transfer is the tolerable vertical deformation at the uplift location.

**Table 6:** Deformation and effective length ratio for different wall lengths and different number of storeys

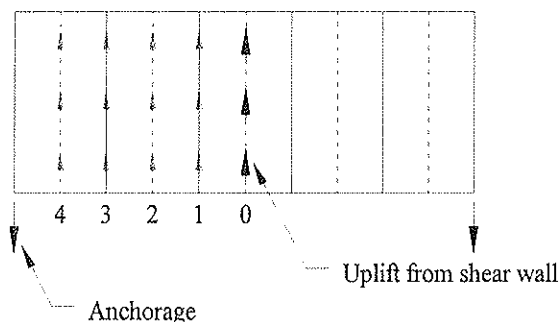
	Vertical deformation	$L_{eff}$ ratio
4.8 m, 1 Storey	3.4 mm	9.0 (100 %)
7.2 m, 1 Storey	5.9 mm	11.0 (100%)
9.6 m, 1 Storey	16.7 mm	17.0 (100 %)
9.6 m, 2 Storey	16.7 mm	14.4 (84 %)
9.6 m, 3 Storey	16.7 mm	9.7 (57 %)

In order to transfer all dead load along the wall to the point of the uplift, it is enough to allow for a deformation of only 3.5 mm for the 4.8 m wall, 6 mm for the 7.2 m wall, and 17 mm for the 9.6 m wall (Table 6).

For a multi-storey structure with dead load of the same magnitude at each floor, the stiffness will actually decrease with the number of storeys. For a fixed deformation, the effective length for the total structure will decrease with the number of storeys (Table 6). This is, of course, due to the fact that the total load over the structure increases with the number of storeys. This indicates that the multi-storey wall structure acts as one diaphragm over all storeys, not as separate diaphragms that would have given the result for one storey multiplied with the number of storeys (Fig. 8 a).

### 6.3 Interaction with adjacent anchorage mountings

The possibility to use anchorage bolts in an adjacent wall for counteracting uplift forces in shear walls is dependent on the configuration of the transverse wall. Analyses, where the uplift force from the shear wall action was applied at various stud locations along a transverse wall (Fig. 11, position 0-4), showed that there is a significant difference in force transfer capacity between walls sheathed on one side and two sides respectively. For walls sheathed on both sides with staggered sheathing, the choice of location of the connection to the shear wall is of no importance. For the walls sheathed on only one side, it is crucial if a perimeter or centre stud is chosen as the connection stud. This is, of course, mostly due to the fact that a centre stud has greater fastener spacing.



**Fig. 11:** Uplift force from shear wall transferred to anchorage in transverse wall

The results imply that transverse walls sheathed on two sides are capable of transferring uplift forces large enough to anchorage most gypsum sheathed shear walls occurring in conventionally designed structures.



## 7 Conclusions

The compression force at the end of a shear wall will always be below the sum of the dead load applied at the stud and the resultant vertical force caused by the horizontal load. On the uplift side of a shear wall, the dead load counteracting the uplift force is always greater than the dead load on that actual stud. The tributary area for the dead load counteracting the uplift force increases slightly with the number of storeys and the wall length (within reasonable limits), and more obviously with the number of sheathing layers. An increase in the anchorage stiffness gives a decreased tributary area for the dead load transferred to the point of uplift.

The possibility to take advantage of hold-downs in adjacent walls in order to counteract uplift forces in a shear wall is mainly governed by the stiffness of the connection between the walls. The capacity of the transverse walls necessary in order to transfer the uplift force from the uplift point to the anchorage is rarely a restriction in a conventionally designed system.

Dead load applied along a transverse wall can be effectively transferred to an adjacent shear wall if the shear wall is properly connected to the transverse wall and not anchored to the foundation. Hence, there is a possibility to use dead load to counteract uplift forces also when the flooring joists are supported on the transverse walls and not on the shear wall.

## 8 Further Work

Further efforts will be made in order to analyse structures with plywood sheathed diaphragms and diaphragms with mixed sheathing materials. Structures with both gypsum sheathed and plywood sheathed shear walls in the same floor will also be analysed in order to find out more about their joint performance. In such a study, parameters like wall length, eccentricities and openings will be investigated.

## 9 Acknowledgements

The author appreciates Mr Leif Tolle, undergraduate student in wood science and technology at University of Hamburg, and Mr Per-Olof Rosenkvist, Research Engineer at Structural Engineering, Lund University, for conducting the tests of the shear walls.

## 10 References

- [1] Andreasson, S., System aspects of stabilisation of multi-storey timber framed buildings, Proceedings of PTEC 99, Rotorua, 1999, Vol. 1, pp 33-40
- [2] European Committee for Standardisation, Eurocode 5, Brussels, 1993
- [3] European Committee for Standardisation, European Standard prEN 594:1991, Brussels, 1991
- [4] Gyproc Handbok 1991:3, Malmö, 1991
- [5] Källsner, B. and Lam, F., *Diaphragms and shear walls*, In STEP 3. Holzbauwerke, Grundlagen, Entwicklungen, Ergänzungen. Fachverlag Holz, Düsseldorf 1995, pp 15/1-15/19.

**INTERNATIONAL COUNCIL FOR RESEARCH AND INNOVATION  
IN BUILDING AND CONSTRUCTION**

**WORKING COMMISSION W18 - TIMBER STRUCTURES**

**APPLICATION OF CAPACITY SPECTRUM METHOD TO TIMBER HOUSES**

N Kawai  
Building Research Institute  
JAPAN

**MEETING THIRTY-TWO**

**GRAZ**

**AUSTRIA**

**AUGUST 1999**

---

Presenter: N.Kawai

· M.Yasumura asked and received clarification of the procedures used to establish heq values and suggested that higher cycles rather than the first cycle in the load deformation curves of cyclic tests could be used to establish heq values.

# Application of Capacity Spectrum Method to Timber Houses

Naohito Kawai

Building Research Institute, JAPAN

## 1 Summary

Capacity spectrum method (CSM) is known as a convenient prediction method for earthquake response of buildings, and is now discussed in Japan as one of the procedures to confirm the seismic performance of buildings in a technical standard under the revised Building Standard Law of Japan. In this paper, the results of CSM are compared with the results of time history analyses (THA), using one mass system models and two mass system models with the load-displacement hysteresis model based on the results of static cyclic loading tests on shear walls. The comparison of the results for one mass system models shows that equivalent linear response tends to give a smaller prediction the time history analysis when the equivalent viscous damping ratio,  $h_{eq}$ , of first loop of cyclic loading protocol proposed in ISO/TC165 is used. When  $h_{eq}$  is reduced to 80% of the original in CSM, the prediction gives better agreement for one mass system models in maximum response displacement. Also for two mass system models, the results of CSM with 80% of  $h_{eq}$  agreed well with those of THA in maximum response displacement. However, there was a case that CSM gives smaller prediction of relative story displacement, which is 64% of a result of THA.

## 2 Introduction

In the seismic design or the evaluation of seismic performance of buildings, the prediction of maximum response displacement against strong ground motion is one of the most important problems. Time history analysis (THA) is, of course, one of the prediction methods. However, as it needs high techniques and the results vary according to the characteristics of the input waves, it is not suitable for a general seismic design procedure. While, as convenient prediction methods of non-linear response based on a linear response analysis, two methods are known, one is the application of property of energy conservation and another is the method called equivalent linear response analysis or capacity spectrum method (CSM). Veletsos and Newmark first proposed the former in 1960 [1]. The latter was proposed by Shibata and Sozen in 1976 [2] and a sophisticated procedure was established by Freeman in 1978 [3]. However, the applicability of these convenient methods to wooden buildings has not been discussed enough.

In this paper, the prediction results of earthquake response by CSM are compared with the results of time history analysis, using one mass system models and two mass system models with the load-displacement hysteresis curves based on the results of static cyclic loading tests on shear walls, and the applicability of these convenient methods is discussed.

In the application of CSM, it is necessary to calculate the load-displacement skeleton curve of each story. When a timber house is designed to prevent any preceding failure in joints of frames or in horizontal diaphragms and the eccentricity of the structure is small enough, the load-displacement curve of a story is calculated as the summation of those of shear walls, and the application of CSM can be easy as described in this paper. While, if there is a possibility that the failure at joints in frames or at horizontal frames precedes the failure in shear walls, It is necessary to calculate the load-displacement curve for the application of CSM by some appropriate method, such as step by step analysis.

### 3 Application to one mass system models

#### 3.1 Load-displacement hysteresis model

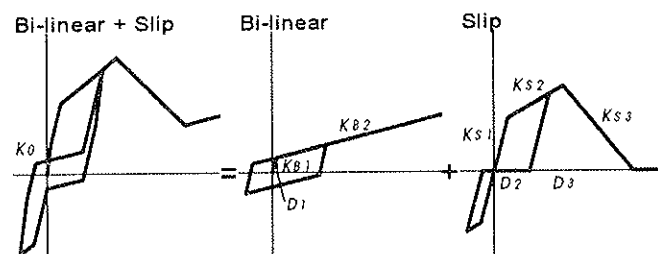
One mass system models with load-displacement hysteresis models of three types of shear walls were employed in the analysis. The types of shear walls assumed are a plywood sheathed shear wall (PW1) and a braced frame (BF) used in Japanese conventional construction and a plywood sheathed shear wall (PW2) used in Japanese wood frame construction. Table 1 shows the types of shear walls assumed.

As the load-displacement hysteresis model of each shear wall, a combination model of bi-linear model and slip model was applied, and the parameters were determined based on the static cyclic loading tests on the shear wall. Figure 1 shows the combination model and Table 2 shows the parameters used in the analysis. It has been confirmed that the results of time history analysis using these models agreed well with the results of pseudo-dynamic tests or shaking table tests [4][5].

For each type of shear walls, models with maximum 16 values of initial period, from 0.2 to 0.5 sec every 0.02 sec, were analysed as long as applicable.

**Table 1** Types of shear walls assumed in the models

Wall type	Resisting element	Thickness or cross section	Fastener
PW1	Hardwood Plywood	t=9mm	JIS N50 @150mm
BF	Brace	30mm × 105mm	Steel plate (BP)
PW2	Conifer Plywood	t=9.5mm	JIS CN50 @100mm



**Figure 1** The combination model of bi-linear and slip

**Table 2** Parameters used in the models

Wall Type	$K_{B1}/K_0$	$K_{B2}/K_0$	$K_{S1}/K_0$	$K_{S2}/K_0$	$K_{S3}/K_0$	$D_1(\text{mm})$	$D_2(\text{mm})$	$D_3(\text{mm})$
PW1	0.53	0.03	0.47	0.07	-0.11	4.5	18	90
BF	0.55	0.03	0.45	0.14	-0.17	3.75	22.5	56.25
PW2	0.58	0.02	0.42	0.04	-0.06	4	20	70

### 3.2 Input waves

Ten artificial earthquake waves, which have same target response spectrum and same duration time of 120 sec, were used as the input waves. The target response acceleration spectrum at the damping ratio ( $h$ ) of 5% ( $S_{a,5}$  (cm/sec<sup>2</sup>)) is given by Equation (1).

$$S_{a,5} = \begin{cases} 480 & (T \leq 0.04) \\ 7250T + 190 & (0.04 < T \leq 0.14) \\ 1205 & (0.14 \leq T < 0.573) \\ 691/T & (T \geq 0.573) \end{cases} \quad (1)$$

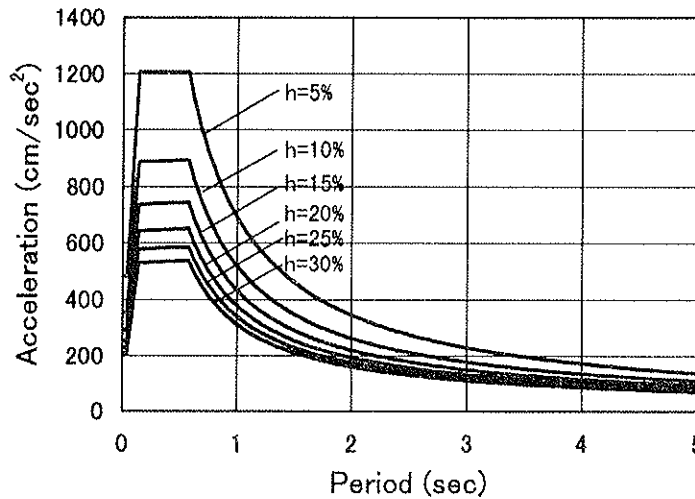
where,  $T$  = Natural period of one mass system (sec).

For the other values of  $h$ , response acceleration spectrum ( $S_{a,h}$ ) was assumed to be a product of  $S_{a,5}$  and a factor ( $F_h$ ) given by Equation (2) [6].

$$F_h = \frac{1}{\sqrt{1 + 17(h - 0.05) \exp(-2.5T/T_e)}} \quad (2)$$

where,  $T_e$  = Effective duration time. In this case,  $T_e = 30$  sec.

Figure 2 shows the target response acceleration spectrum at  $h=5\%$  and the spectra at some values of  $h$ , obtained using  $F_h$ .



**Figure 2** Target response acceleration spectrum of input waves and spectra at some values of  $h$

### 3.3 Time history analysis

Linear acceleration method was applied to one mass system models using hysteresis models of three types of shear walls with 16 values of initial period for each, against 10 artificial earthquake waves. The value of viscous damping ratio ( $h$ ) was assumed to be 2% of critical damping calculated with the initial stiffness. For the wall types PW1 and PW2, the influence of the damage at nailed joints in one side to the strength in the opposite side was taken into account with using the same experienced maximum displacement in both sides if the displacement is over the displacement at maximum strength [4][5].

### 3.4 Capacity spectrum method

The procedure to predict the maximum response displacement by CSM is as follows.

First, demand spectrum is drawn using spectral acceleration ( $S_a$ ) and spectral displacement ( $S_d$ ) at any values of period ( $T$ ), as shown in Figure 3 (a).

In this study,  $S_d$  is calculated by Equation (3).

$$S_d = \frac{S_a}{\omega^2} \quad (3)$$

where,  $\omega$  = circular frequency ( $= 2 \pi / T$ ).

Next, capacity spectrum is drawn by static non-linear analysis of the structure. For a one mass system model, capacity spectrum is just same as the load-displacement skeleton curve of the model with a unit mass and the initial stiffness corresponding to the initial period.

The prediction point of the non-linear response is given as the intersection of the demand spectrum and the capacity spectrum, if the damping assumed in the demand spectrum is same as the damping of equivalent linear response at the prediction point. If the damping is given as a function of displacement, as shown in Figure 3(b), we can draw a transition curve which connects the points on the demand spectrum of the proper damping corresponding to the displacement, as shown in Figure 3(c).

Thus, the prediction is given as the intersection of the transition curve and the capacity spectrum, as shown in Figure 3(d).

In this study, the values of equivalent viscous damping for three shear walls were calculated with using the first loop of the models under the cyclic loading protocol proposed in the document of ISO/TC165[7], and the approximate equations were derived. Figures 3(b) and 4 show the approximate equations of equivalent viscous damping for three types of shear walls.

And the damping ratio used to draw the transition curve ( $h_{e1}$ ) was calculated by Equation (4), considering the difference of the stiffness used to calculate the equivalent viscous damping ratio.

$$h_{e1} = h_{eq} + \frac{T_e}{T_0} h_v \quad (4)$$

where,  $h_{eq}$  = Equivalent viscous damping ratio,  $h_v$  = Viscous damping ratio (=2%),  $T_0$  = Initial period and  $T_e$  = Period of equivalent linear response.

In addition, the values of predicted displacement using 80% of  $h_{eq}$ , as Equation (5) shows, were also calculated to discuss the proper value of  $h$ , which gives better prediction in this convenient prediction method.

$$h_{e2} = 0.8h_{eq} + \frac{T_e}{T_0}h_v \quad (5)$$

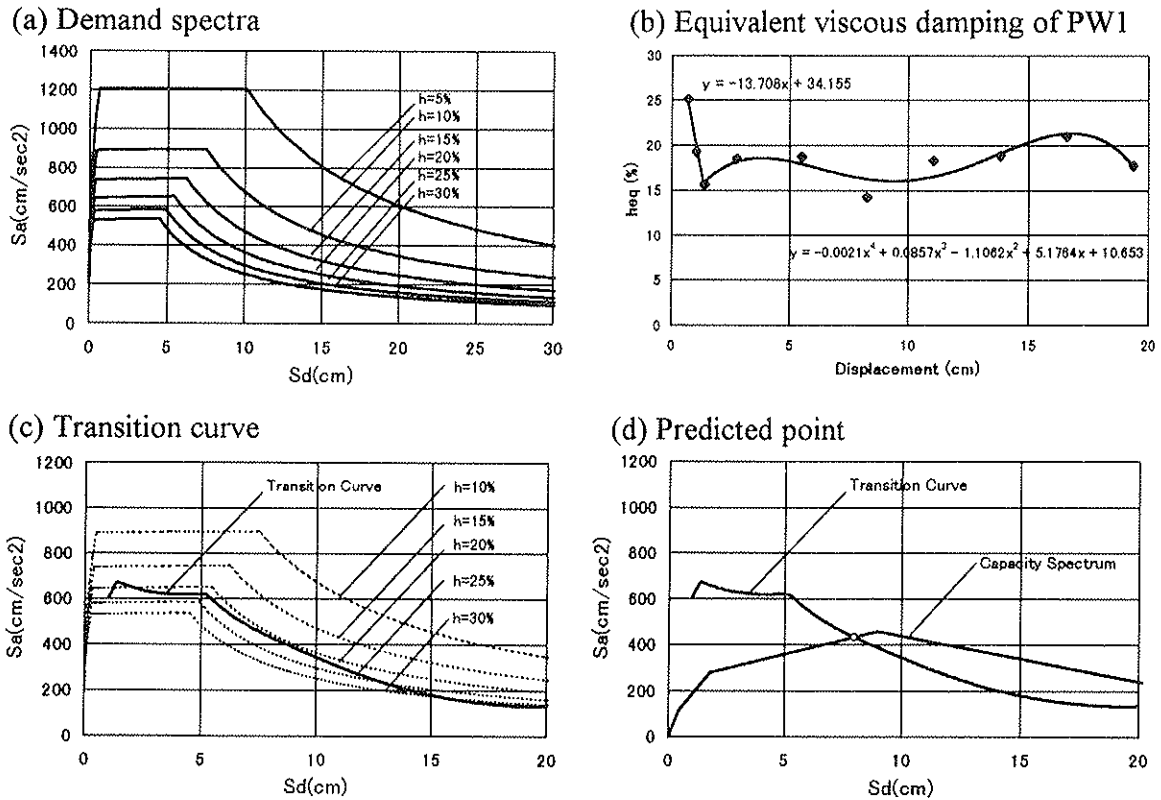


Figure 3 Procedure to obtain the prediction by Capacity spectrum method

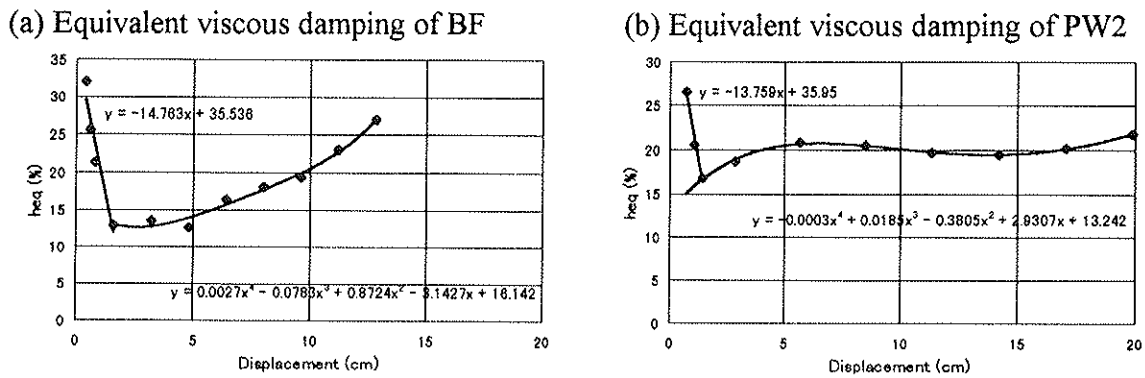


Figure 4 Equivalent viscous damping of BF and PW2

### 3.5 Results

Figure 5 shows the comparison of maximum response displacement and the comparison of damping ratio between the prediction by CSM and the results THA. On figure 5, values of damping by THA were calculated as  $h_s$  by Equation (6)[8].

$$h_s = \frac{-\int_0^t \ddot{y}_0 y dt}{2\omega_e \int_0^t \dot{y}^2 dt} \quad (6)$$

where,  $y$  = relative displacement,  $\dot{y}$  = relative velocity,  $\ddot{y}_0$  = ground acceleration and  $\omega_e$  = circular frequency of equivalent linear response.

$h_s$  is the value of average equivalent damping which is derived from the assumption that the work by ground motion,  $\int_0^t (-m\ddot{y}_0)y dt$ , equals the work by equivalent dash pot,  $\int_0^t c_e \dot{y}^2 dt$ .

According to the calculation results, in case the damping ratio  $h_{e1}$  by Equation (4) is used, the prediction by CSM gives smaller values of maximum response displacement than the results of THA, which are 74%, 76% and 80% of the THA in average for PW1, BF and PW2, respectively.

In case  $h_{e2}$  calculated with 80 % of  $h_{eq}$  by Equation (5) is used, the prediction agreed better than the case  $h_{e1}$  is used. The ratios of the prediction of CSM to the THA results are 88%, 94% and 100% in average for PW1, BF and PW2, respectively. However the prediction is still smaller especially in the areas of small response displacement when the response displacement is near the displacement at the maximum strength.

Concerning the damping,  $h_{e2}$  is still larger than  $h_s$ , as Figure 5 shows. It suggests that smaller reduction factor than 80% or some other assumption of damping, such as equivalent viscous damping ratio calculated from the hysteresis loop of stabilised (second or third) cycle, is required for better agreement.

## 4 Application to two mass system models

### 4.1 Structural models

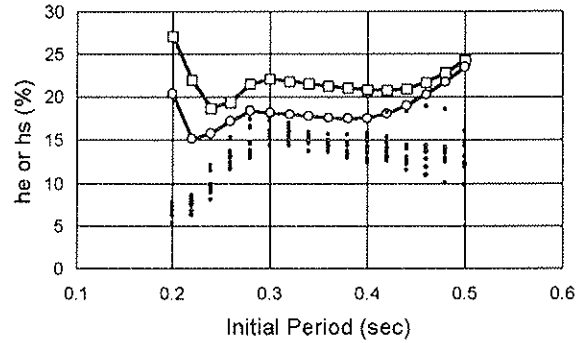
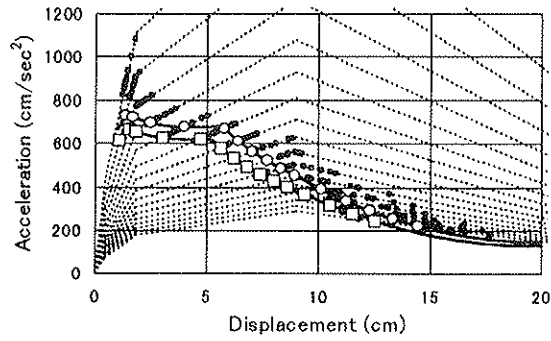
Models used in this study are two mass system models with load-displacement hysteresis model of PW1. The masses of first and second story are assumed to be equal. For total 6 cases with natural frequency of 0.4 sec and 0.5 sec, and with stiffness distribution factor,  $R_s$ , given by Equation (7) of 0.5, 0.75 and 1, were examined by comparing the prediction of CSM and the results of THA.

$$R_s = \frac{\alpha_i}{\bar{\alpha}_i} \quad (7)$$

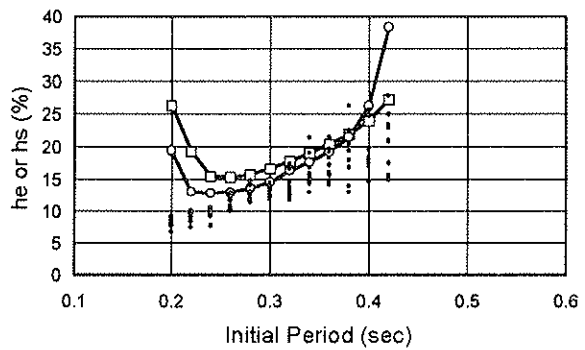
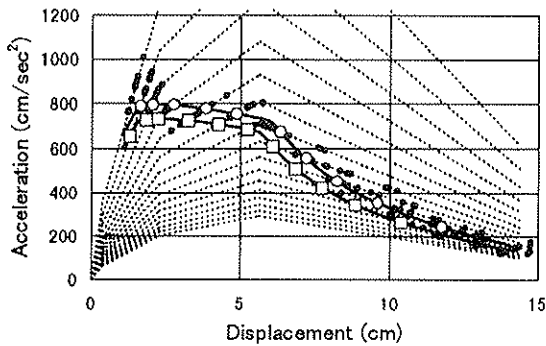
where,  $\alpha_i$  = reciprocal of slope by relative story displacement of each story calculated as static elastic response and  $\bar{\alpha}_i$  = average of  $\alpha_i$ .



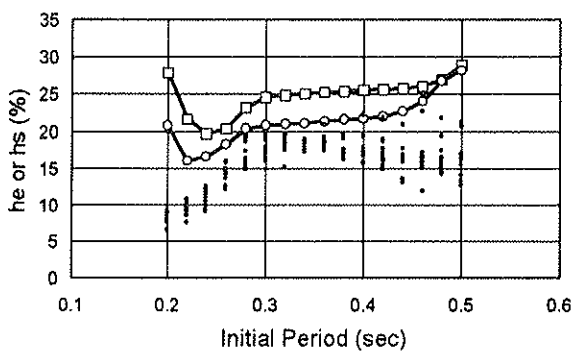
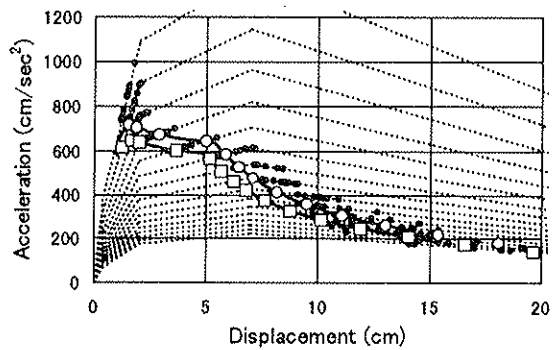
(a) PW1



(b) BF



(c) PW2



- = Prediction by CSM with  $h_{e1}$  (with original  $h_{eq}$ ),
- = Prediction by CSM with  $h_{e2}$  (with 80% of  $h_{eq}$ ) and
- = Results of THA.

**Figure 5** Comparison between the prediction by equivalent linear response and time history analyses.

## 4.2 Input waves

Three of ten artificial earthquake waves used for one mass system models, which have same target response spectrum, were used as input waves.

### 4.3 Time history analysis

Linear acceleration method was applied to two mass system models with viscous damping of 2% which is assumed to be proportional to initial stiffness.

### 4.4 Capacity spectrum method

Capacity spectrum for a two mass system model can be obtained with assuming one type of distribution of seismic force,  $A_i$ , given by Equation (8) which is used in current technical standard in Japan, and by calculating the acceleration and the displacement of an equivalent single-degree-of-freedom model for each step in step by step method, using Equations (9) and (10).

$$A_i = 1 + \left( \frac{1}{\sqrt{\alpha_i}} - \alpha_i \right) \frac{2T}{1+3T} \quad (8)$$

where,  $\alpha_i$  = ratio of mass over  $i$ th story to total mass and  $T$  = primary natural period.

$$S_a = \frac{\sum m_i \delta_i^2}{(\sum m_i \delta_i)^2} \cdot \sum P_i \quad (9)$$

$$\Delta = \frac{\sum m_i \delta_i^2}{\sum P_i \delta_i} \cdot S_a \quad (10)$$

where,  $S_a$  = acceleration of capacity spectrum,  $m_i$  = mass of each story,  $\delta_i$  = displacement of each story,  $P_i$  = seismic force applied to each story and  $\Delta$  = displacement of capacity spectrum.

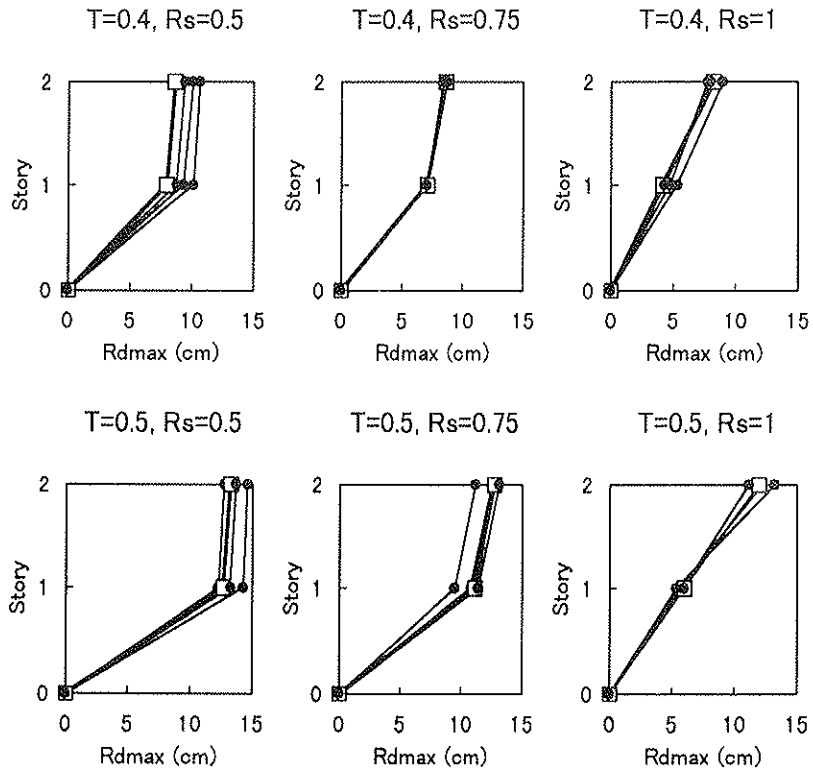
Also in this case, damping ratio of  $h_{e2}$  calculated by Equation (5) was used for CSM, using equivalent viscous damping as the weighted mean of each story weighted by the product of story shear force and relative story displacement.

### 4.5 Results

Figure 6 shows the comparison of maximum story displacement and Figure 7 maximum relative story displacement between CSM and THA.

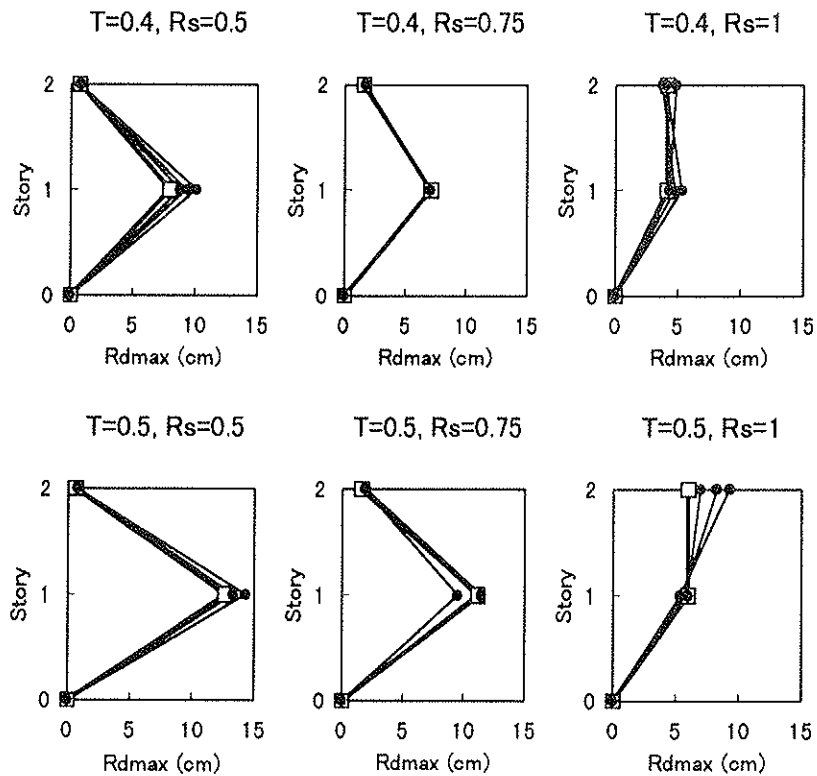
Predictions of maximum story displacement by CSM agreed well with those of THA. The ratio of the values by CSM to those by THA is from 78% to 117%.

Predictions of maximum relative story displacement also agreed well as a whole. However, there was a case that CSM gives smaller prediction of relative story displacement, which is 64% of a result of THA. It seems to be risky to use the result of CSM directly for the evaluation of maximum relative story displacement.



□ = Prediction by CSM with  $h_{e2}$  and · = Results of THA.

**Figure 6** Comparison of maximum story displacement



□ = Prediction by CSM with  $h_{e2}$  and · = Results of THA.

**Figure 7** Comparison of maximum relative story displacement

## 5 Conclusions

The earthquake response predictions by capacity spectrum method were compared with the results of time history analyses using one mass system models and two mass system models, load-displacement relationships of which are determined by those of shear wall(s). The results are summarized as follows.

- According to the results of the examination using one mass system models, capacity spectrum method gives good prediction compared with the results of time history analyses in maximum displacement, when the equivalent viscous damping ratio reduced to 80% of the original is used.
- Also for two mass system models, capacity spectrum method gave good agreement in maximum story displacement with reduced values of equivalent viscous damping to 80%.
- However, it seems to be risky to use the result of capacity spectrum method directly for the evaluation of maximum relative story displacement, as there was a case that gives smaller prediction, which is 64% of a result of time history analysis.

## 6 Acknowledgement

The author thanks Dr. I. Okawa, Building Research Institute, for his kindness to provide the artificial earthquake waves for this study.

## 7 References

1. Veletsos, A. S. and Newmark, N.M., Effect of inelastic behaviour on the response of simple systems to earthquake motions, *Proceedings of the Second World Conference on Earthquake Engineering, Vol. 2*, 1960, pp895-912
2. Shibata, A. and Sozen, M. A., Substitute-structure method for seismic design in R/C, *Proceedings of the ASCE, Journal of the Structural Division, Vol. 102*, ST 1-3, 1976, pp1-18
3. Freeman, S. A., Prediction of response of concrete buildings to severe earthquake motion, Douglas McHenry International Symposium on Concrete and Concrete Structures, SP-55, American Concrete Institute, 1978, pp589-605
4. Kawai, N., Pseudo-dynamic test on shear walls, *5th World Conference on Timber Engineering, Proceedings Volume 1*, 1998, pp412-419.
5. Kawai, N., Seismic performance testing on wood framed shear wall, *CIB-W18 Proceedings Meeting Thirty-one*, 1998, 31-15-1, pp1-10
6. Architectural Institute of Japan, *Recommendations for Loads on Buildings*, 3rd Edition, Architectural Institute of Japan, 1993
7. ISO/TC165/WG7, Timber structures – Joints made with mechanical fasteners – Quasi-static reversed-cyclic test method, 1998
8. Shibata, A., *Seismic Structural Analysis*, Morikita Co. Ltd., 1981

**INTERNATIONAL COUNCIL FOR RESEARCH AND INNOVATION  
IN BUILDING AND CONSTRUCTION**

**WORKING COMMISSION W18 - TIMBER STRUCTURES**

**DESIGN METHODS FOR SHEAR WALLS WITH OPENINGS**

C Ni

E Karacabeyli

Forintek Canada Corp.

CANADA

A Ceccotti

Department of Civil Engineering

University of Florence,

ITALY

**MEETING THIRTY-TWO**

**GRAZ**

**AUSTRIA**

**AUGUST 1999**

---

Presenter: E.Karacabeyli

- V.Enjily received clarification of the term vd.
- M.Yasamura asked about the applicability of the procedures to multi-story systems.
- E.Karacabeyli responded that the design procedures could be applied to multi-story system based on a story to story approach.
- H.J.Larsen received clarification of the formula J with respect to both loading directions.
- S.Thelandersson asked about the applicability of the procedures to serviceability rather than capacity.
- E.Karacabeyli and A.Ceccotti responded that stiffness and displacement work was not considered here. More analyses would be needed.

# Design Methods For Shear Walls With Openings

Chun Ni and Erol Karacabeyli  
Forintek Canada Corp., 2665 East Mall, Vancouver, BC, Canada V6T 1W5

Ario Ceccotti  
Department of Civil Engineering, University of Florence, Italy

## Abstract

Nailed shear wall systems provide the lateral load resistance for most wood-frame buildings. When designing shear walls containing openings, hold-down connections are normally required at the ends of each wall segment between openings. The shear wall containing openings is then designed as multiple shear wall segments. The design capacity of such a shear wall is generally determined by summing the capacities of all the shear wall segments. For applications where shear walls do not have hold down connections at the boundary of the openings, a method for determining the capacity is needed. The empirical "perforated shear wall" approach developed in Japan has been shown by number of researchers to predict conservatively the capacity of such shear walls. In this study, an alternative design method for the design of shear walls with openings is developed, and verified against available test data obtained on full-size shear walls. The predicted capacities from this method are found to be in reasonable agreement with the test results. A simplified version of this method is proposed for code implementation.

## 1 Introduction

Nailed shear wall systems, with their excellent energy dissipation and ductility characteristics, provide the lateral load resistance for most wood-frame buildings. Structural engineers, when designing shear walls containing openings, normally specify hold-down (or tie-down) connections at the ends of each wall segment between openings, and design the shear wall containing openings as multiple shear wall segments. The design capacity of the shear walls is generally assumed to be the sum of the capacities of each shear wall segment. In practice, the capacity computed using this approach often exceeds the capacity required. When this occurs, the engineer attempts to reduce the cost of the wall by reducing the number of hold-downs while maintaining the wall-opening configuration. This is where the engineer encounters difficulty because there is no standard procedure for assessing the capacity of such walls.

Sugiyama (1981) proposed an empirical equation to calculate the lateral load carrying capacity and the stiffness of shear walls without hold-downs around openings. His empirical equation forms the basis of the perforated shear wall (shear walls with openings) design method which appears in the Standard Building Code 1994 Revised Edition (1994) and the Wood Frame Construction Manual for One- and Two- Family Dwellings - 1995 High Wind Edition (1996).

Sugiyama's empirical equation was verified using results from tests on one-third scale shear walls conducted by Yasumura and Sugiyama (1984). Johnson and Dolan (1996) tested ten 2.4m × 12.2m shear walls, and they found that Sugiyama's equation predicted

conservatively the load carrying capacity of the shear walls. This approach, however, has only been verified against test data obtained on shear walls tested without vertical loads. For perforated shear walls, vertical loads help to reduce the effect of uplift forces around openings; consequently, the structural demand on nailed joints due to uplift forces perpendicular to bottom plate are minimized. As a result, the perforated shear walls with vertical load may have higher lateral load carrying capacity compared to those without vertical loads.

In this study, an alternate design method (Method A) for the perforated shear walls was developed. Shear walls with openings were tested simultaneously under vertical and lateral loads. The predicted capacities from this method were in reasonable agreement with test results. A simplified version (Method B) of this method is proposed for code implementation.

## 2 Design Methods

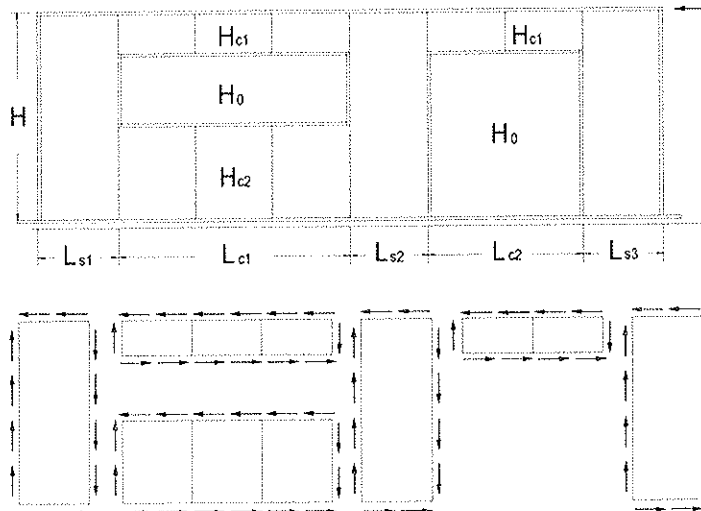
### 2.1 Method A

In Method A, the design capacity of a shear wall with openings is assumed to be equal to the sum of the capacities of all shear wall segments and components above and below openings (Figure 1). The lateral load capacity of shear wall with openings is calculated by

$$V = \sum_{i=1}^n J_{hd}^i v_d^i L_s^i + \sum_{j=1}^m J_c^j v_d^j L_c^j \quad (1)$$

where

- V lateral load capacity of the shear wall.
- $v_d$  unit length lateral load capacity of the shear wall.
- $L_s$  length of shear wall segment.
- $L_c$  length of wall component above or below openings.
- $J_{hd}$  hold-down effect factor for shear wall segment.
- $J_c$  modification factor for wall component.



Note: Nailed joint forces applied around the perimeter of the panels

Figure 1 – Method A.

In Equation (1), the first and second term represent respectively the contribution of wall segments, and wall components above or below the openings.

Based on the test results from Forintek's Seismic Research Program,  $J_{hd}$  was found to be

$$J_{hd} = \frac{1}{1 + \frac{H}{L_s} \left(1 - \frac{P_u}{v_d H}\right)^3} \quad (2)$$

where

H height of shear wall.

$P_u$  resistance to uplift force on the end stud of a shear wall segment due to hold-downs, vertical load, and wall components above or below openings.  $P_u$  is equal to  $v_d H$  if resistance is sufficient to prevent end stud uplift at wall capacity.

Wall components above and below the openings are also treated as walls with the edges adjacent to wall segments representing the top and bottom plates. The modification factor

of a wall component  $J_c$  is equal to  $J_c = \frac{1}{1 + \frac{L_c}{H_c}}$  for wall component above opening, and

$J_c = 1.0$  for wall component below opening.

## 2.2 Method B

Method B is a simplified version of method A, and is proposed for code implementation. In method B, the contribution of the sheathings above and below the openings to the overall performance of the wall is not considered. Method B is compatible with the traditional approach to calculate the load carrying capacities of shear walls with openings. The design capacity of a shear wall with openings is assumed to be equal to the sum of the capacities of all shear wall segments, as shown in Figure 2. The lateral load capacity of a shear wall with openings is

$$V = \sum_{i=1}^n J_{hd}^i v_d^i L_s^i \quad (3)$$

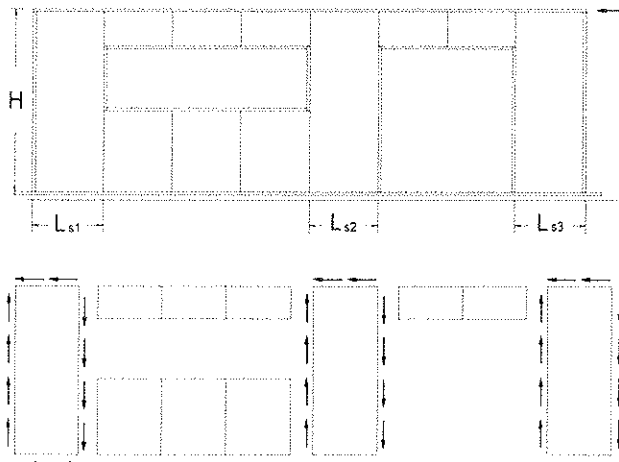
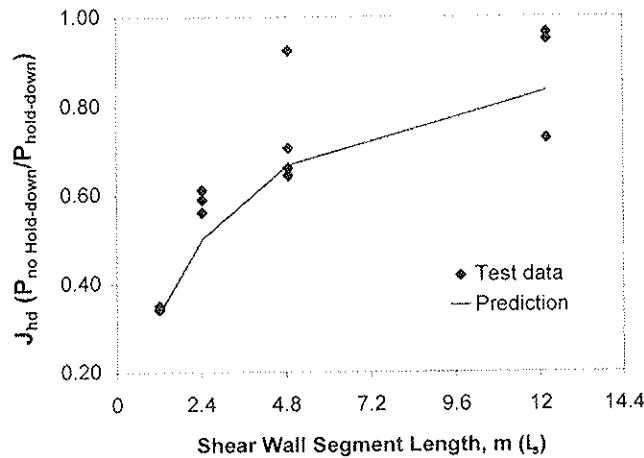


Figure 2 – Method B.



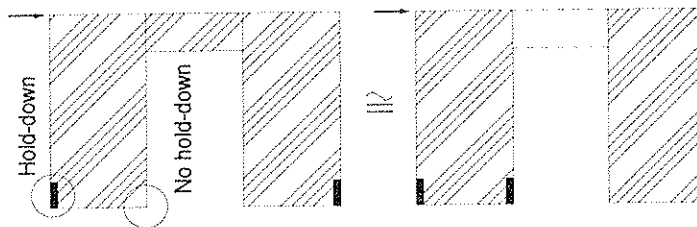
The hold-down effect factor  $J_{hd} = 1.0$  with hold down connectors designed to resist uplift forces at both ends of the shear wall segment, and  $J_{hd} = \frac{1}{1 + \frac{H}{L_s}}$  without hold down

connectors at both ends of the shear wall segment. This empirical relationship was based on test data obtained on shear wall segment tested with and without hold down connectors at the two ends. The predictions versus test data are shown in Figure 3.



**Figure 3** – Load capacities of shear walls without hold down connectors at both ends.

When shear wall segment has only one hold-down at one end, the wall segment can be treated as given in Figure 4.



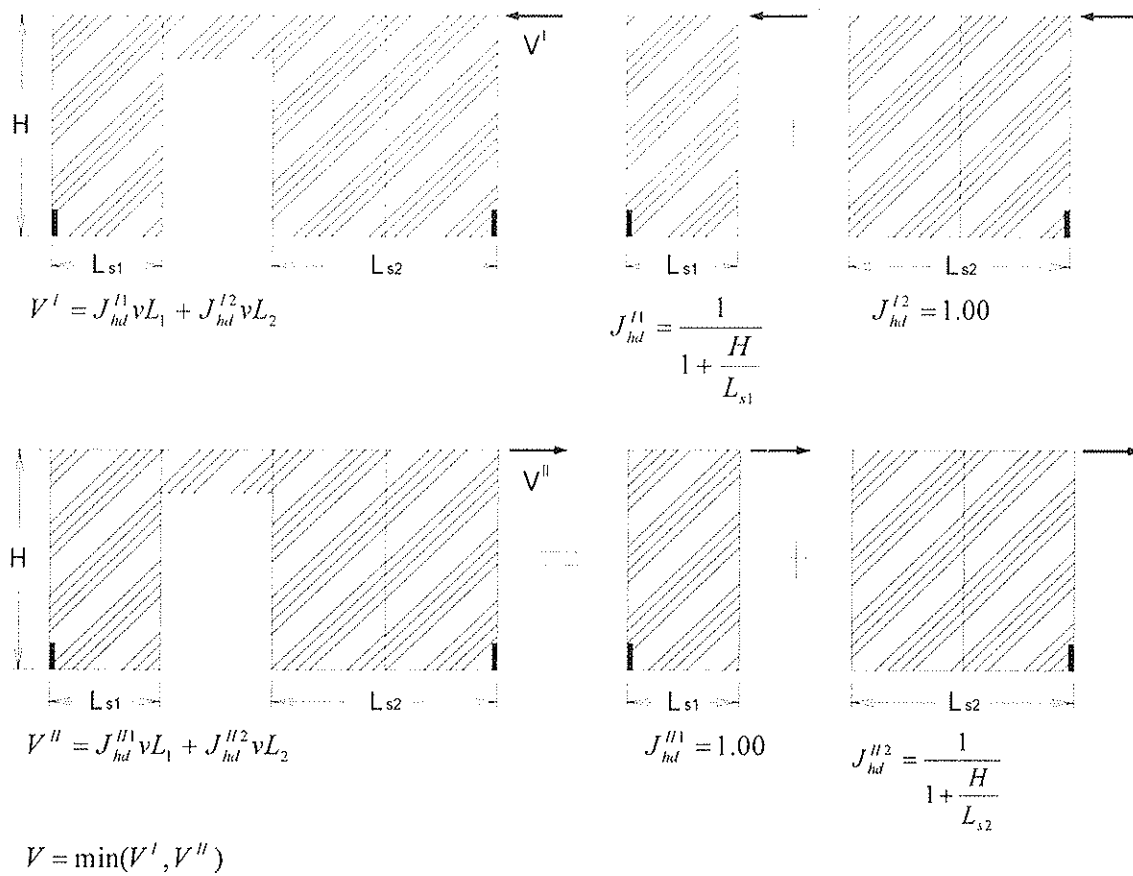
**Figure 4** - Guidance for shear wall segments with one hold-down.

Because the shear walls may be subjected to lateral loads in both directions, the lateral load carrying capacity is the lesser of the predicted loads from Methods A or B. An example is given in Figure 5 to demonstrate the application of Method B.

### 3 Wall Tests

A total of ten walls were tested under monotonic and reversed cyclic loads. The shear wall specimens were constructed using No. 2 and better grades of Spruce-Pine-Fir 38mm × 89mm lumber for the wall studs, and the top and bottom plates. Stud members were spaced 400mm on center. The top plate, the end studs and studs at the door consisted of

double members, while the bottom plate and the interior studs consisted of single members. Canadian Softwood Plywood (CSP), 9.5mm thick, was used to sheath the walls.



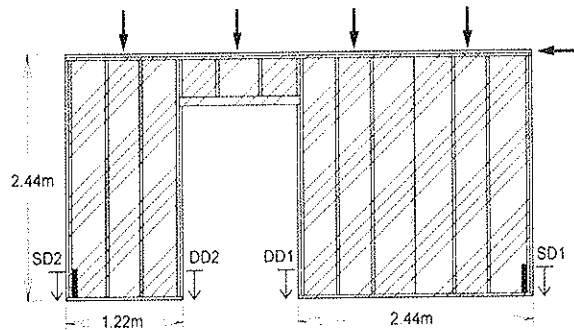
**Figure 5** – Application of Forintek’s method B.

The sheathing panels were connected to the framing members with power nails, which were 3.05mm in diameter and 63mm in length. Table 1 lists the tested shear walls without hold-downs around openings. Figure 6 shows the shear wall test setup.

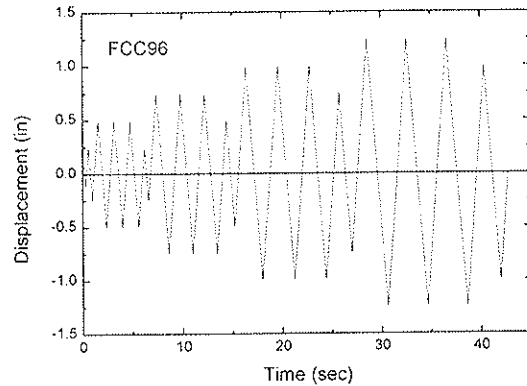
**Table 1** - Shear wall test matrix.

Shear wall	Wall length (m)	Wall height (m)	Size of Opening	Vertical load (kN/m)	Load protocol
30-05	4.88	2.44	No openings	0	Monotonic
30-07	4.88	2.44	No openings	0	Monotonic
48-24	2.44	2.44	No openings	0	FCC96
48-26	2.44	2.44	No openings	0	FCC96
50-03	4.88	2.44	1.22 m × 2 m	0	Monotonic
50-04	4.88	2.44	1.22 m × 2 m	0	FCC96
50-05	4.88	2.44	1.22 m × 2 m	4.6	Monotonic
50-06	4.88	2.44	1.22 m × 2 m	9.1	Monotonic
50-01	4.88	2.44	1.22 m × 2 m	18.2	Monotonic
50-02a	4.88	2.44	1.22 m × 2 m	18.2	FCC96

Monotonic and reversed cyclic displacement schedules were used. The displacement rate for the monotonic test was 7.6mm/min. The reversed cyclic loading (FCC96) was one of the cyclic schedules developed at Forintek under the Seismic Research Program (1996). FCC96 uses a constant displacement rate of 31.75mm/min. A typical displacement schedule of FCC96 is shown in Figure 7.



**Figure 6** - Schematic diagram of the shear wall test setup.



**Figure 7** - Load protocol of FCC96.

## 4 Test Results And Analysis

The test results are summarized in Table 2. It was found that the maximum displacements were similar for shear walls with and without vertical loads. The ultimate lateral load capacity, however, was increased by about 15% when vertical load was applied. The load capacities were similar for walls with different vertical loads.

**Table 2** - Summary of test results.

Specimens	$P_{max}$	$D_u$ <sup>1</sup>	SK <sup>2</sup>	Maximum vertical displacement			
				SD1	SD2	DD1	DD2
	kN	mm	kN/mm	mm	mm	mm	mm
30 <sup>5</sup> Monotonic	36.1	81.6	2996	15.2	3.8	-	-
48 <sup>6</sup> Cycle/1 <sup>st</sup> 3	19.9	52.4	956	8.9	11.4	-	-
48 <sup>6</sup> Cycle/3 <sup>rd</sup> 4	16.3	42.9	820				
50-03 Monotonic	34.0	76.2	1779	10.2	1.5	4.1	16.5
50-04 Cycle/1 <sup>st</sup> 3	30.5	61.1	2347	8.9	8.4	20.1	18.8
50-04 Cycle/3 <sup>rd</sup> 4	25.6	56.7	2383				
50-05 Monotonic	39.0	76.6	1892	10.9	3.0	2.3	8.4
50-06 Monotonic	39.9	84.3	2078	12.2	3.0	2.3	9.1
50-01 Monotonic	39.6	70.9	2166	7.9	1.8	2.3	3.6
50-02a Cycle/1 <sup>st</sup> 3	39.1	50.2	2992	8.1	5.6	3.0	2.0
50-02a Cycle/3 <sup>rd</sup> 4	32.5	43.8	3090				

<sup>1</sup>  $D_u$  displacement at 80% of maximum load.

<sup>2</sup> SK secant stiffness between 10% and 40% maximum load.

<sup>3</sup> Cycle/1<sup>st</sup> average (+/-) first envelope curve in cyclic test.

<sup>4</sup> Cycle/3<sup>rd</sup> average (+/-) third envelope curve in cyclic test.

<sup>5</sup> 30 average test results of specimens 30-05 and 30-06.

<sup>6</sup> 48 average test results of specimens 48-24 and 48-26.

Maximum vertical displacements at end studs for walls with or without vertical loads were similar. This may be due to the similar restraints at end studs because the same type of hold-downs was used for walls. The vertical displacements around openings, however, were much larger for walls without vertical loads. The vertical load significantly reduced stud uplifts around openings. In terms of preventing uplift, the vertical load works as a hold-down. This may explain why walls tested with vertical loads have greater lateral load capacity than walls tested without vertical loads.

## 5 Comparison

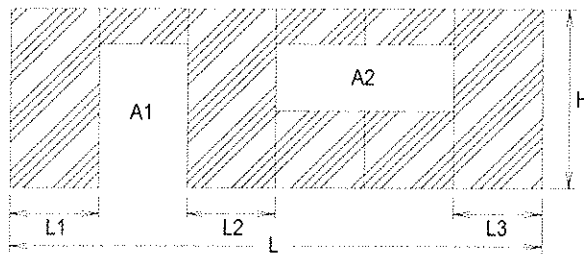
Sugiyama (1981) proposed an empirical equation to calculate the lateral load capacity of shear walls without hold-downs around openings. The total load capacity of shear walls with openings equals the load capacity of a traditional shear wall of equal length times the lateral load ratio,  $R$ . The lateral load ratio,  $R$ , is given as

$$R = \frac{r}{3 - 2r} \quad (4)$$

Variable  $r$  is the sheathing area ratio. The sheathing area ratio,  $r$ , is defined as

$$r = \frac{1}{1 + \frac{\sum A_i}{H \sum L_i}} \quad (5)$$

where  $\sum A_i$  is the sum of the area of the openings,  $H$  is the height of the wall, and  $\sum L_i$  is the length of full height sheathed wall segments. These variables are illustrated in Figure 8.



**Figure 8** - Variables used to calculate sheathing area ratio.

The test and predicted lateral load carrying capacities under monotonic and reversed cyclic loads are summarized in Table 3. Lateral load ratios for walls with different vertical loads were the same based on Sugiyama's method and Method B; consequently both methods resulted in conservative predictions. On the other hand, Method A accounts for the contribution of vertical loads. Compared to test results, Method A offers better prediction than the other two methods.

**Table 3 - Test and predicted monotonic lateral load carrying capacities.**

Shear wall		Forintek's method A			Forintek's method B			Sugiyama's method			
Wall type	$P_{max}$ (kN)	$R^1$	$P^2$ (kN)	$P/P_{max}$	$R^1$	$P^2$ (kN)	$P/P_{max}$	$R^1$	$P^2$ (kN)	$P/P_{max}$	
30 <sup>5</sup>	Monotonic	36.1	1.000	36.1	1.00	1.000	36.1	1.00	1.000	36.1	1.00
48 <sup>6</sup>	Cyclic/1 <sup>st</sup> <sup>3</sup>	39.8	1.000	39.8	1.00	1.000	39.8	1.00	1.000	39.8	1.00
	Cyclic/3 <sup>rd</sup> <sup>4</sup>	32.6	1.000	32.6	1.00	1.000	32.6	1.00	1.000	32.6	1.00
50-03	Monotonic	34.0	0.572	20.7	0.61	0.500	18.1	0.53	0.550	19.8	0.58
50-04	Cyclic/1 <sup>st</sup> <sup>3</sup>	30.5	0.572	22.8	0.75	0.500	19.9	0.65	0.550	21.9	0.72
	Cyclic/3 <sup>rd</sup> <sup>4</sup>	25.6	0.572	18.7	0.73	0.500	16.3	0.64	0.550	17.9	0.70
50-05	Monotonic	39.0	0.657	23.7	0.61	0.500	18.1	0.46	0.550	19.8	0.51
50-06	Monotonic	39.9	0.718	25.9	0.65	0.500	18.1	0.45	0.550	19.8	0.50
50-01	Monotonic	39.6	0.750	27.1	0.68	0.500	18.1	0.46	0.550	19.8	0.50
50-02a	Cyclic/1 <sup>st</sup> <sup>3</sup>	39.1	0.750	29.9	0.76	0.500	19.9	0.51	0.550	21.9	0.56
	Cyclic/3 <sup>rd</sup> <sup>4</sup>	32.5	0.750	24.5	0.75	0.500	16.3	0.50	0.550	17.9	0.55

<sup>1</sup> Shear wall lateral load ratio.

<sup>2</sup> Predicted wall capacity.

<sup>3</sup> Cycle/1<sup>st</sup> average (+/-) first envelope curve in cyclic test.

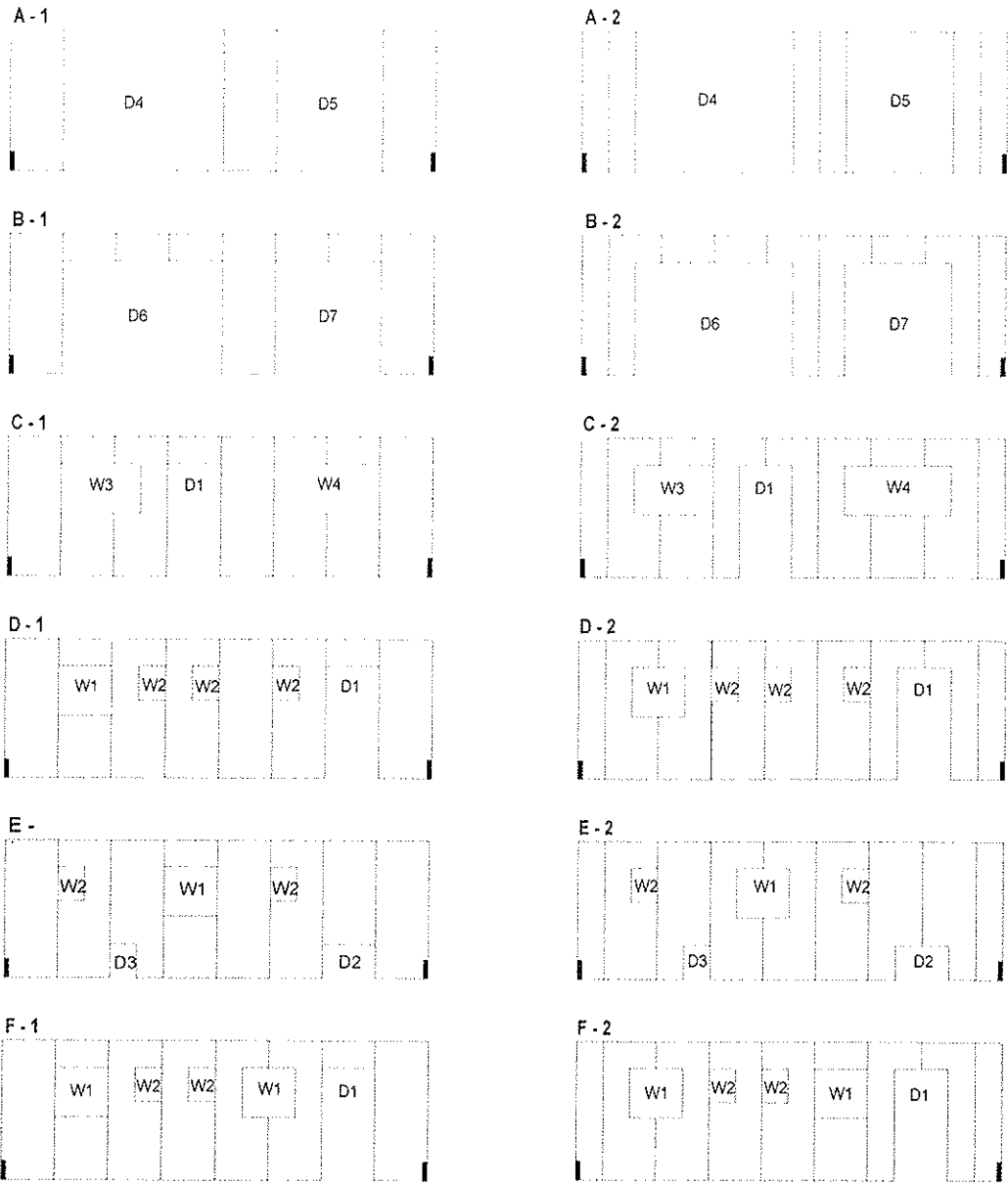
<sup>4</sup> Cycle/3<sup>rd</sup> average (+/-) third envelope curve in cyclic test.

<sup>5</sup> Average test results of specimens 30-05 and 30-06.

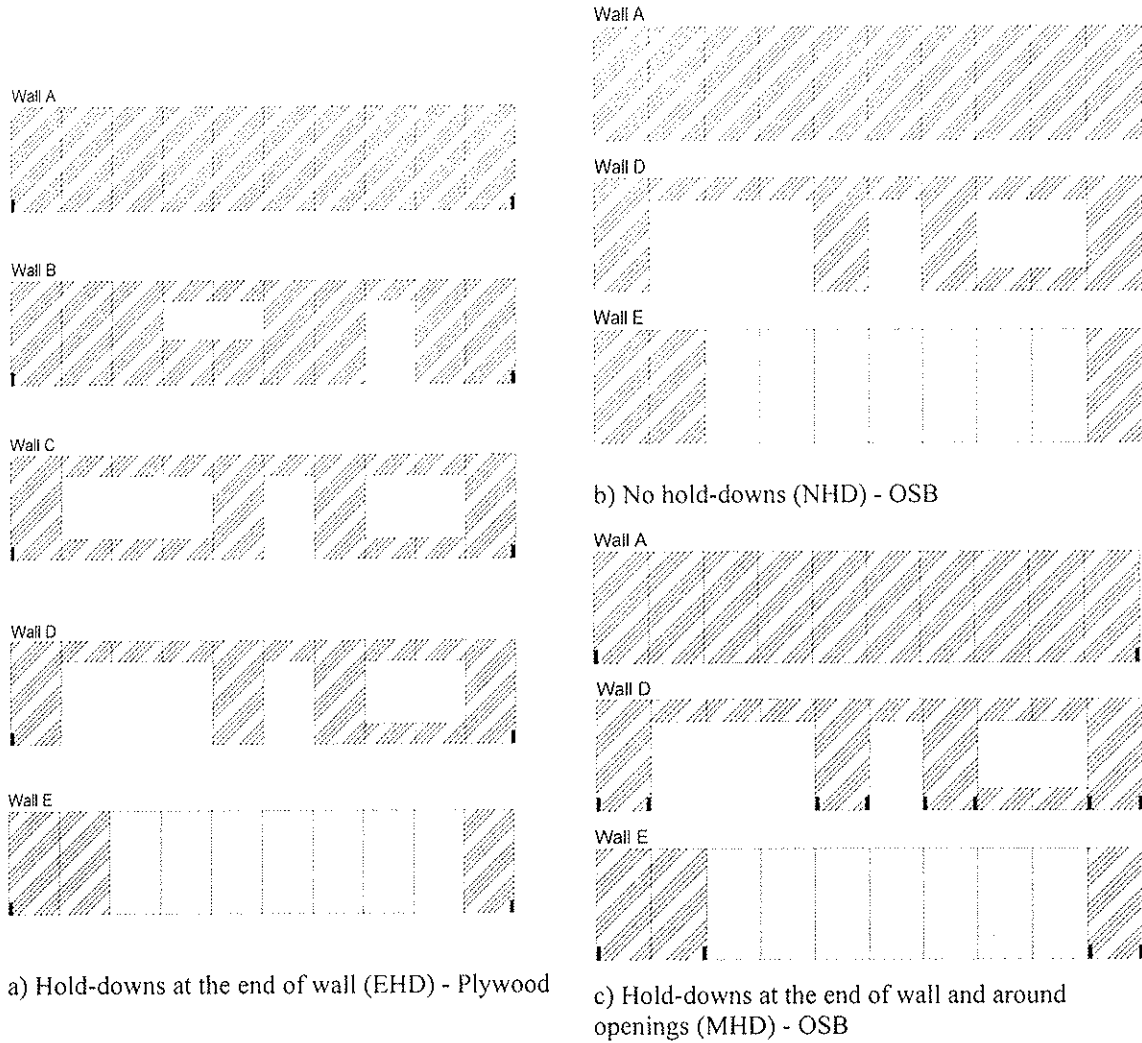
<sup>6</sup> Average test results of specimens 48-24 and 48-26 multiplied by two to take into account wall length.

Method A, Method B and Sugiyama's method were also compared to the test data reported by Yasumura (1986) and Dolan and Heine (1997a, 1997b). Yasumura (1986) tested twelve 2.44 m × 7.28 m shear walls with various openings, as shown in Figure 9. The walls were constructed with 38 mm × 89 mm Spruce-pine-fir as framing members and 9.5 mm Douglas fir plywood as sheathings. The studs were spaced at 450 mm on center. The plywood panels were fastened to the frame with CN50 wire nails spaced at 100 mm on center around the perimeter of the panels and 200 mm on center along the intermediate studs.

Dolan and Heine tested ten shear walls 2.4m high and 12m long, with and without openings. The walls were constructed following common United States construction practices, framed with 38 x 89-mm lumber, and sheathed with 12-mm (15/32 inch) plywood or OSB on one side and 12.7-mm (1/2 inch) drywall on the other side. Figure 10 illustrates the five different wall configurations studied. Lateral load tests were performed without vertical loads applied.



**Figure 9** - The shear wall configurations tested by Yasumura (1986).



**Figure 10** - The shear wall configurations tested by Dolan and Heine (1997a, 1997b).

The results are shown in Tables 4, 5, and 6. Again, it was found that Method A gave a closer prediction than Sugiyama’s method and Method B. On the other hand, the latter two methods are perhaps more practical and result in conservative load capacities.

**Table 4** – Comparison of Yasumura’s test results and predicted lateral load capacities.

Shear wall Wall type	$P_{max}^3$ (kN)	Forintek’s method A			Forintek’s method B			Sugiyama’s method		
		$R^1$	$P^2$ (kN)	$P/P_{max}$	$R^1$	$P^2$ (kN)	$P/P_{max}$	$R^1$	$P^2$ (kN)	$P/P_{max}$
A Monotonic	20.7	0.193	20.7	1.00	0.193	20.7	1.00	0.167	17.9	0.86
B Monotonic	33.2	0.229	24.5	0.74	0.193	20.7	0.62	0.199	21.3	0.64
C Monotonic	64.5	0.438	47.0	0.73	0.203	21.7	0.34	0.362	38.8	0.60
D Monotonic	71.3	0.601	64.5	0.90	0.222	23.9	0.33	0.495	53.0	0.74
E Monotonic	74.9	0.636	68.3	0.91	0.222	23.9	0.32	0.607	65.1	0.87
F Monotonic	72.5	0.542	58.1	0.80	0.198	21.3	0.29	0.430	46.1	0.64

<sup>1</sup> Shear wall lateral load ratio.

<sup>2</sup> Predicted wall capacity.

<sup>3</sup> Average of wall configurations 1 and 2.

**Table 5** - Comparison of Dolan's test results and predicted lateral load capacities – plywood.

Shear wall Wall type	P <sub>max</sub> (kN)	Forintek's method A			Forintek's method B			Sugiyama's method			
		R <sup>1</sup>	P <sup>2</sup> (kN)	P/P <sub>max</sub>	R <sup>1</sup>	P <sup>2</sup> (kN)	P/P <sub>max</sub>	R <sup>1</sup>	P <sup>2</sup> (kN)	P/P <sub>max</sub>	
EHD - A	Monotonic	172.6	1.000	172.6	1.00	1.000	172.6	1.00	1.000	172.6	1.00
	Cyclic/1 <sup>st.5</sup>	142.3	1.000	142.3	1.00	1.000	142.3	1.00	1.000	142.3	1.00
	Cyclic/4 <sup>th.4</sup>	122.3	1.000	122.3	1.00	1.000	122.3	1.00	1.000	122.3	1.00
EHD - B	Monotonic	102.8	0.598	103.2	1.00	0.480	82.8	0.81	0.509	87.9	0.85
	Cyclic/1 <sup>st.5</sup>	90.3	0.598	85.1	0.94	0.480	68.3	0.76	0.509	72.4	0.80
	Cyclic/4 <sup>th.3</sup>	77.4	0.598	73.1	0.94	0.480	58.7	0.76	0.509	62.3	0.80
EHD - C	Monotonic	61.4	0.365	63.0	1.03	0.200	34.5	0.56	0.286	49.3	0.80
	Cyclic/1 <sup>st.5</sup>	60.5	0.365	51.9	0.86	0.200	28.5	0.47	0.286	40.7	0.67
	Cyclic/4 <sup>th.4</sup>	52.5	0.365	44.6	0.85	0.200	24.5	0.47	0.286	34.9	0.67
EHD - D	Monotonic	53.8	0.301	52.0	0.97	0.200	34.5	0.64	0.235	40.6	0.75
	Cyclic/1 <sup>st.5</sup>	51.2	0.301	42.9	0.84	0.200	28.5	0.56	0.235	33.5	0.65
	Cyclic/4 <sup>th.4</sup>	44.0	0.301	36.8	0.84	0.200	24.5	0.56	0.235	28.8	0.65
EHD - E	Monotonic	36.5	0.200	34.5	0.95	0.200	34.5	0.95	0.125	21.6	0.59
	Cyclic/1 <sup>st.5</sup>	33.4	0.200	28.5	0.85	0.200	28.5	0.85	0.125	17.8	0.53
	Cyclic/4 <sup>th.4</sup>	29.4	0.200	24.5	0.83	0.200	24.5	0.83	0.125	15.3	0.52

<sup>1</sup> Shear wall lateral load ratio.

<sup>2</sup> Predicted wall capacity.

<sup>3</sup> Cycle/1<sup>st</sup> average (+/-) first envelope curve in cyclic test.

<sup>4</sup> Cycle/4<sup>th</sup> average (+/-) third envelope curve in cyclic test.

**Table 6** - Comparison of Dolan's test results and predicted lateral load capacities - OSB.

Shear wall Wall type	P <sub>max</sub> (kN)	Forintek's method A			Forintek's method B			Sugiyama's method			
		R <sup>1</sup>	P <sup>2</sup> (kN)	P/P <sub>max</sub>	R <sup>1</sup>	P <sup>2</sup> (kN)	P/P <sub>max</sub>	R <sup>1</sup>	P <sup>2</sup> (kN)	P/P <sub>max</sub>	
MHD - A	Monotonic	153.9	1.000	153.9	1.00	1.000	153.9	1.00	1.000	153.9	1.00
	Cyclic/1 <sup>st.5</sup>	123.2	1.000	123.2	1.00	1.000	123.2	1.00	1.000	123.2	1.00
	Cyclic/4 <sup>th.4</sup>	105.4	1.000	105.4	1.00	1.000	105.4	1.00	1.000	105.4	1.00
MHD - D	Monotonic	68.9	0.429	66.0	0.96	0.400	61.6	0.89	0.235	36.2	0.53
	Cyclic/1 <sup>st.5</sup>	59.6	0.429	52.8	0.89	0.400	49.3	0.83	0.235	29.0	0.49
	Cyclic/4 <sup>th.4</sup>	52.0	0.429	45.2	0.87	0.400	42.2	0.81	0.235	24.8	0.48
MHD - E	Monotonic	48.0	0.300	46.2	0.96	0.300	46.2	0.96	0.125	19.2	0.40
	Cyclic/1 <sup>st.5</sup>	37.4	0.300	37.0	0.99	0.300	37.0	0.99	0.125	15.4	0.41
	Cyclic/4 <sup>th.4</sup>	31.6	0.300	31.6	1.00	0.300	31.6	1.00	0.125	13.2	0.42
NHD - A	Monotonic	111.7	0.833	128.3	1.15	0.833	128.3	1.15	1.000	111.7	1.00
	Cyclic/1 <sup>st.5</sup>	118.8	0.833	102.7	0.86	0.833	102.7	0.86	1.000	118.8	1.00
	Cyclic/4 <sup>th.4</sup>	100.1	0.833	87.8	0.88	0.833	87.8	0.88	1.000	100.1	1.00
NHD - D	Monotonic	43.6	0.235	36.1	0.83	0.133	20.5	0.47	0.235	26.3	0.60
	Cyclic/1 <sup>st.5</sup>	44.9	0.235	28.9	0.64	0.133	16.4	0.37	0.235	28.0	0.62
	Cyclic/4 <sup>th.4</sup>	38.7	0.235	24.7	0.64	0.133	14.1	0.36	0.235	23.6	0.61
NHD - E	Monotonic	19.6	0.133	20.5	1.05	0.133	20.5	1.05	0.125	14.0	0.71
	Cyclic/1 <sup>st.5</sup>	21.4	0.133	16.4	0.77	0.133	16.4	0.77	0.125	14.9	0.69
	Cyclic/4 <sup>th.4</sup>	18.2	0.133	14.1	0.77	0.133	14.1	0.77	0.125	12.5	0.69

<sup>1</sup> Shear wall lateral load ratio.

<sup>2</sup> Predicted wall capacity.

<sup>3</sup> Cycle/1<sup>st</sup> average (+/-) first envelope curve in cyclic test.

<sup>4</sup> Cycle/4<sup>th</sup> average (+/-) third envelope curve in cyclic test.



## 6 Conclusion

A method for the design of shear walls with openings is presented. The predicted capacities from this method are found to be in reasonable agreement with the test results. A simplified version of the method is proposed for code implementation.

## Reference

Dolan, J.D., Heine, C.P., 1997a. *Monotonic tests of wood-frame shear walls with various openings and base restraint configurations*, VPI&SU Report No. TE-1997-001, Department of Wood Science and Forests Products, Virginia Polytechnic Institute and State University, Blacksburg, Virginia.

Dolan, J.D., Heine, C.P., 1997b. Sequential phased displacement cyclic tests of wood-frame shear walls with various openings and base restraint configurations, VPI&SU Report No. TE-1997-002, Department of Wood Science and Forests Products, Virginia Polytechnic Institute and State University, Blacksburg, Virginia.

Johnson, A.C., Dolan, J.D., 1996. Performance of long shear walls with openings, International Wood Engineering Conference, New Orleans, Vol.2, p.337-344.

Karacabeyli, E., Ceccotti, A., 1996. Test results on the lateral resistance of nailed shear walls, Proceedings of the International Wood Engineering Conference, New Orleans, Louisiana.

SBC, 1994. Standard Building Code - Revised Edition, Southern Building Code Congress International, Birmingham, AL.

Sugiyama, H., 1981. The evaluation of shear strength of plywood-sheathed walls with openings, *Mokuzai Kogyo (Wood Industry)*, Vol.36, Vol.7.

WECM, 1996. Wood Frame Construction Manual for One- and Two- Family Dwellings – SBC High Wind Edition, American Forest and Paper Association, Washington, D.C.

Yasumura, M., Sugiyama, H., 1984. Shear properties of plywood-sheathed wall panels with opening, *Transaction of the Architectural Institute of Japan*, No.338, p.88-98.

Yasumura, M., 1986. Racking resistance of wooden frame walls with various openings. CIB-W18/19-15-3, International Council for Building Research and Documentation, Working Commission W18 – Timber Structures, Meeting Nineteen, Florence, Italy.

**INTERNATIONAL COUNCIL FOR RESEARCH AND INNOVATION  
IN BUILDING AND CONSTRUCTION**

**WORKING COMMISSION W18 - TIMBER STRUCTURES**

**STATIC CYCLIC LATERAL LOADING TESTS ON NAILED  
PLYWOOD SHEAR WALLS**

K Komatsu

K H Hwang

Wood Research Institute

Kyoto University

Y Itou

New Constructor's Network, Gifu

JAPAN

**MEETING THIRTY-TWO**

**GRAZ**

**AUSTRIA**

**AUGUST 1999**

---

Presenter: K.Komatsu

- A.Cecotti asked about the procedures to get ductility-based force reduction factor based on a static analysis.
- K.Komatsu responded that the Japanese system would only require static cyclic results and would not need ductility-based force reduction factor.
- F.Lam asked and received clarification that only envelope curves from static cyclic test results were shown.

# Static Cyclic Lateral Loading Tests on Nailed Plywood Shear Walls

**Dr. Kohei Komatsu**

Associate Professor, Laboratory of Structural Function  
Wood Research Institute, Kyoto University, Uji, Kyoto, Japan

**Mr. Kweon-Hwan Hwang**

Doctor Course Student, Laboratory of Structural Function  
Wood Research Institute, Kyoto University, Uji, Kyoto, Japan

**Mr. Yoji Ito**

Engineer, R&D Division, New Constructor's Network, Gifu, Japan

## Abstract

Simplified calculation method for predicting shear deformation of the model shear resistance system composed of semi-rigid jointed glulam portal frame with nailed plywood shear wall panel was proposed in this report. Load - slip relationship of nail joint, moment - rotation relationship of column leg joints and beam-column joints were all expressed in the form of 3-parameters exponential function to make nonlinear calculation possible. Coincident between observed behavior with calculated ones were good with a few exceptions. As a whole, proposed calculation method was thought to be usable for practical design purposes.

## 1. Introduction

Nailed plywood shear wall is one of the most important lateral resistance component for modern wooden structures. Especially, since the fatal damages of many wooden houses partly due to insufficient strength capacity of wooden bracing system in 1995' Kobe Earthquake had been reported, needs for nailed plywood shear wall system are increasing year by year.

We also started a cooperative research work after the Kobe Earthquake for developing stiffer, stronger and more ductile shear wall system than the existing wooden bracing system in order to realize a three story wooden residential house system.

In this report, a simplified calculation method for predicting stiffness and yielding capacity of wooden lateral shear resistance system in which nailed plywood panel(s) are involved partly is presented and the proposal is to be verified by various types of experimental result.

## 2. Simplified Calculation Method

### 2.1 Model Shear Resistance System and Assumptions

Fig.1 shows a model shear resistance system whose frame system is composed of glulam beam and columns with non-linear semi-rigid connections and nailed plywood panel(s) partly .

In order to make a design calculation procedure be as practical as possible, the following simplifications were assumed :

1. Joint rigidity  $R_{ji}$ , are small enough compared with those of glulam members, thus

deformations due to glulam members can be neglected.

2. Rotational angle  $\theta$  of column-leg joints (Point-A, Point-D) and those of column-girder joints (Point-B, Point-C) are the same respectively.
3. Shear deformation angle  $\gamma$  of whole glulam frame (A-B-C-D) is the same as that of the nailed plywood panel.

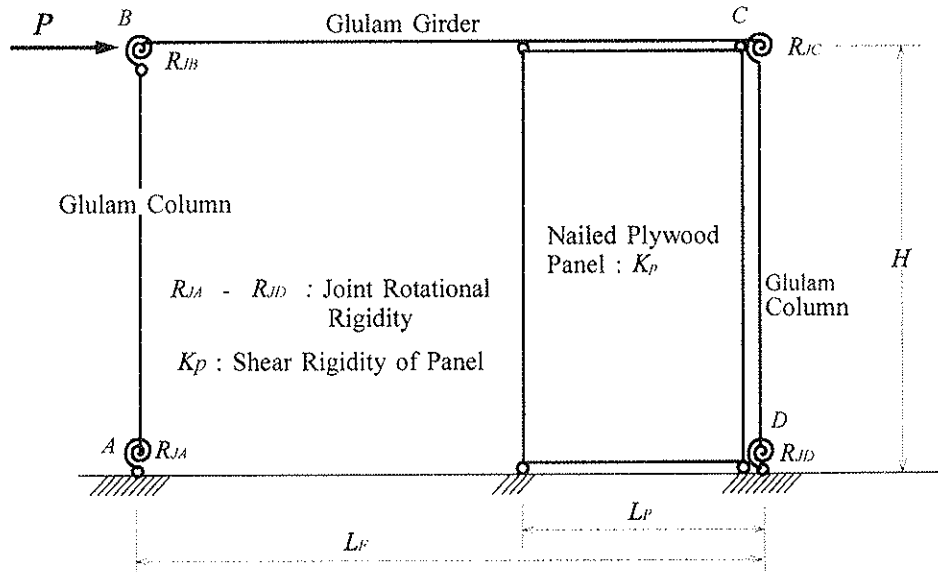


Fig.1 Model Shear Resistance System.

By taking three assumptions mentioned above into consideration, deformed shape of the model shear resisting system will be illustrated as Fig.2.

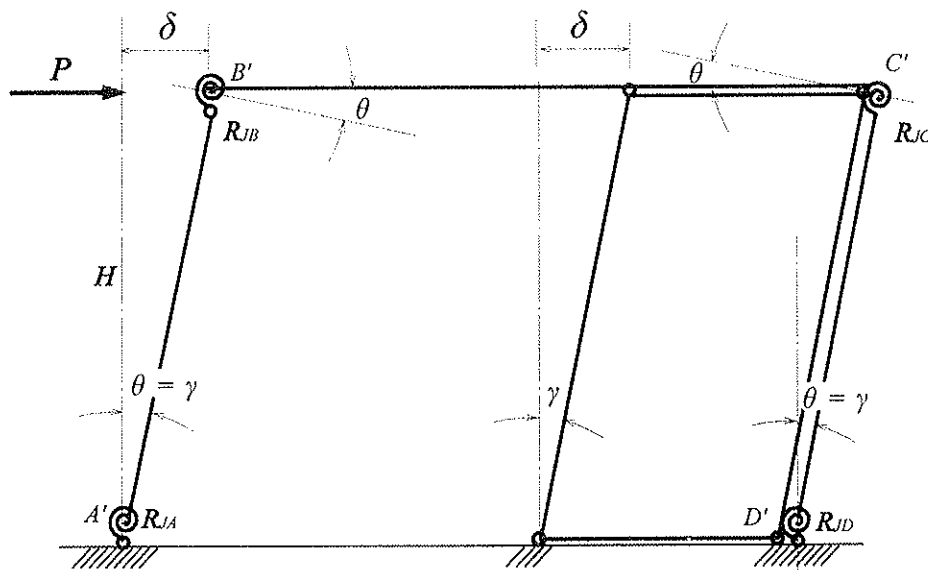


Fig.2 Deformed shape of the model shear resisting system.

## 2.2 Shear Deformation of Nailed Plywood Panel

There have been reported a lot of papers on the shear deformation of nailed plywood panels. Among those previous approaches, Professor Sugiyama's assumption [Sugiyama 1993] is

seemed to be the simplest but the most practical and useful. In this report, Professor Sugiyama's assumption was used to evaluate shear deformation of nailed plywood panel as well as shear force acting on a single nail. Fig.3 illustrates assumptions of force acting on nails and slip of nail.

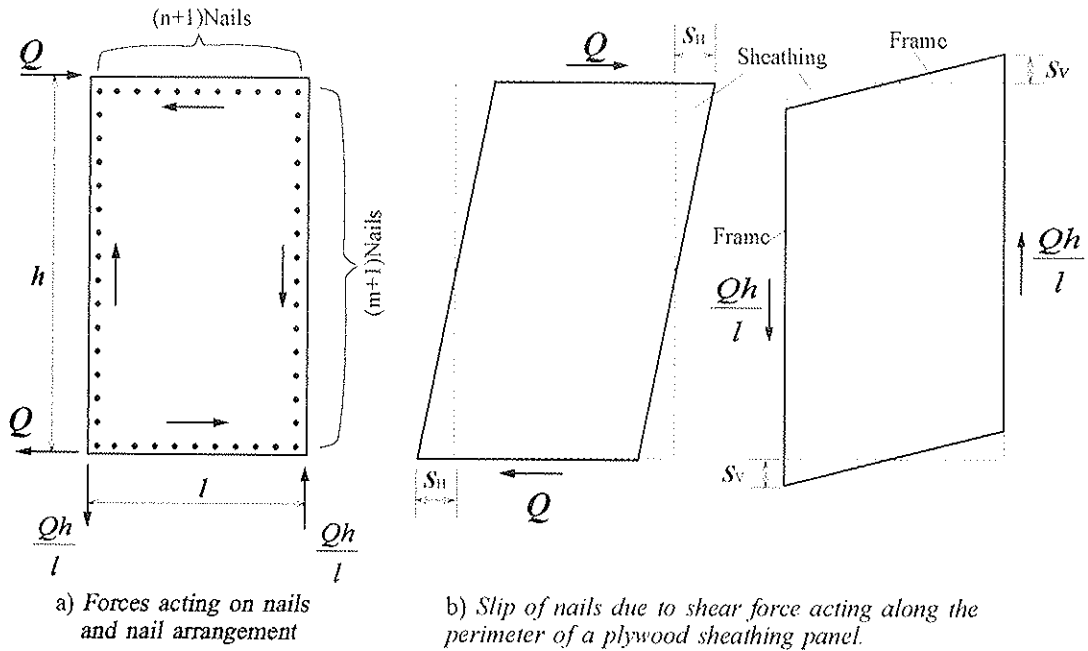


Fig.3 Assumptions of force acting on nails and slip of nails (Sugiyama 1993).

At first, the shear force  $q$  acting on a nail is given by any function of nail slip  $S$ .

$$q = f(S) \dots (1)$$

In this report, we use a secant slip modulus  $K_s$  for making mathematical expression be more explicit, namely.

$$q = K_s \cdot S \dots (2)$$

Shear force acting on the nails along the horizontal upper or/and lower perimeter is ;

$$q_H = \frac{Q}{(n+1)} \dots (3)$$

From equations (2), (3), horizontal slip of nail  $S_H$  is;

$$S_H = \frac{Q}{K_{sH}(n+1)} \dots (4)$$

Shear force acting on the nails along the vertical perimeter is ;

$$q_V = \frac{Qh}{l(m+1)} \dots (5)$$

From equations (2), (5), vertical slip of nail  $S_V$  is;

$$S_v = \frac{Qh}{K_{sv}(m+1)} \dots (6)$$

Energy principle gives the following equation;

$$W_{\text{external}} = U_{\text{plywood}} + U_{\text{nail}} \\ \Rightarrow \frac{1}{2}Q\delta = \frac{1}{2}\tau\gamma V + \frac{1}{2}\{2q_{uh}S_{H(n+1)} + 2q_vS_v(m+1)\} \dots (7)$$

Substituting equations (3), (4), (5), (6) into equation (7) and by assuming constant shear stress and strain distribution in the plywood sheet, shear deformation of nailed plywood panel can be expressed as;

$$\delta = \left[ \frac{h}{Gt} + \left[ \frac{2}{(n+1)K_{SH}} + \frac{2}{(m+1)K_{SV}} \left( \frac{h}{l} \right)^2 \right] \right] Q \dots (8)$$

or by expressing apparent shear rigidity of nailed plywood panel as  $K_p$ , equation (8) is written as ;

$$Q = K_p \delta, \quad \frac{1}{K_p} = \left[ \frac{h}{Gt} + \left[ \frac{2}{(n+1)K_{SH}} + \frac{2}{(m+1)K_{SV}} \left( \frac{h}{l} \right)^2 \right] \right] \dots (9)$$

where

- $G$  : shear rigidity of plywood.
- $(n+1)$  : number of nails along horizontal perimeter
- $t$  : thickness of plywood
- $(m+1)$  : number of nails along vertical perimeter.
- $h$  : height of plywood panel
- $l$  : length of plywood panel
- $K_{SH}$  : secant slip modulus of nail along horizontal perimeter
- $K_{SV}$  : secant slip modulus of nail along vertical perimeter

### 2.3 Shear Deformation of Semi-Rigid Jointed Glulam Frame

From the assumptions- 1 and -2, the shear deformation of semi-rigid jointed glulam frame without nailed plywood panel and subjected to a horizontal shear force  $Q$  might be estimated by taking strain energy only from joint's rotations into account;

$$\frac{1}{2}Q\delta = \frac{1}{2}\{M_A\theta + M_B\theta + M_C\theta + M_D\theta\} \dots (10)$$

Relationship between moment and rotational angle is;

$$M_i = R_{J_i}\theta = R_{J_i} \frac{\delta}{H} \quad (i=A,B,C,D) \dots (11)$$

Thus, shear deformation of glulam frame without nailed plywood panel is ;

$$\delta = \frac{Q}{K_F}, \quad K_F = \frac{\sum R_{J_i}}{H^2} \dots (12)$$

### 2.4 Total Deformation of Model Shear Resistance System - A Parallel Model

From the 3rd assumption in clause 2.1, we might be able to consider the model shear resistance

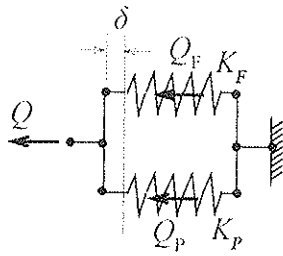


Fig.4 A parallel springs model

Shear force to be held by the semi-rigid jointed frame :  $Q_F = K_F \delta \dots (13)$

Shear force to be held by the nailed plywood panel :  $Q_P = K_P \delta \dots (14)$

Total shear force to be held by the whole system :  $Q = Q_F + Q_P \dots (15)$

system as a parallel spring model which is composed of a frame spring whose shear rigidity of  $K_F$  and panel spring whose shear rigidity of  $K_P$  as shown in Fig.4.

Each spring has different shear force corresponding to each shear rigidity when they are forced to deform by  $\delta$ . Namely;

### 3. Experiments for Evaluating Material Parameters

#### 3.1 Load - Slip Relationship of Nailed Plywood

Fig.5 and Table 1 show shear test set-up and specification for determining the load- slip relationship of nailed plywood joints.

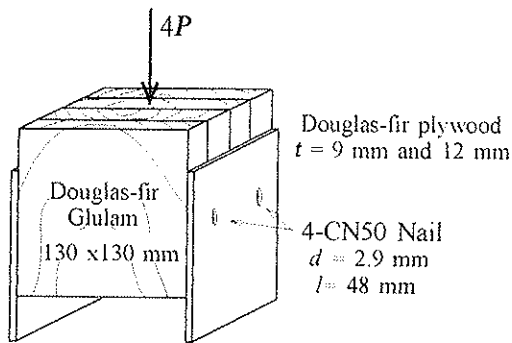
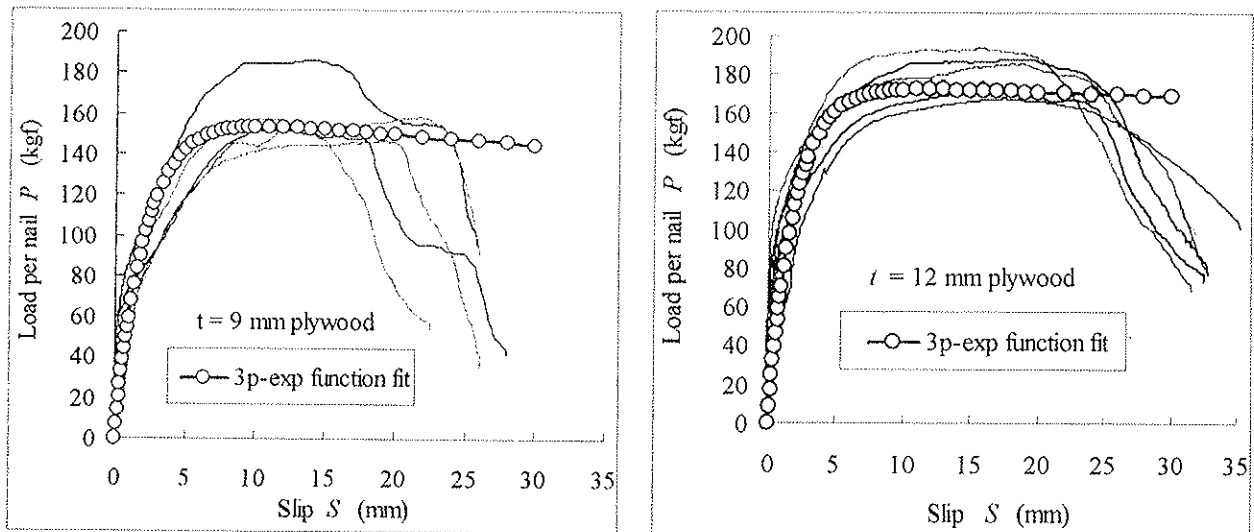


Table 1 Specification of nail shear test

Part	Species	Dimension	Specification
Plywood	Douglas-fir	$t = 9 \text{ mm}$	$r_u = 0.62$
		$t = 12 \text{ mm}$	$r_u = 0.66$
Main member	Douglas-fir	$b \times h = 130 \times 130$	$MOE = 110000 \text{ kgf/cm}^2$
Nail	CN50	$d = 2.9 \text{ mm}$	$l = 48 \text{ mm}$

Fig.5 Nail shear test set-up

Fig.6 shows test result and fitted regression curve by the 3-parameter exponential function introduced by Professor Foschi (Foschi 1974).



Figs.6 Results of nail shear tests and fitted regression curve by 3p-exponential function.

All parameters obtained by curve fitting are tabulated in Table 2.

Table 2 Three parameters exponential function for the nailed plywood joints

Type of plywood	$P_u$ (kgf)	$K_u$ (kgf/cm)	$K_s$ (kgf/cm)
9 mm	160	-5	744
12 mm	175	-2	902

\* 3-parameter exponential function : 
$$P = (P_u + K_u S) \left\{ 1 - \exp\left(\frac{-K_s}{P_u} S\right) \right\}$$

### 3.2 Beam-Column Moment-Rotation Relationship

This experiment was done quite independently by another researcher (Sakata 1997) for the 3rd author of this paper, and here only the test results and curve fit results are shown in Fig.7 without expressing details about experiments. All parameters obtained by curve fitting on the experimental data as well as deduced ones are tabulated in Table 3.

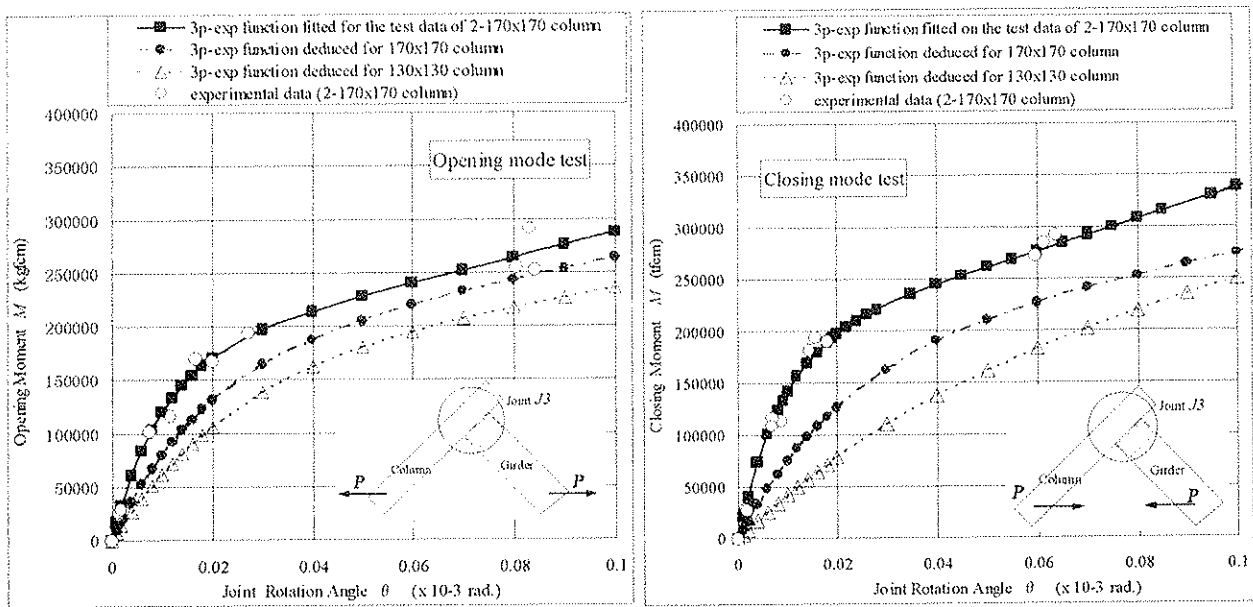


Fig.7 Moment-Rotation Relationship for Beam-Column Joints (data from Sakata 1997)

Table 3 Three parameters exponential functions for the beam-column joint J3

Column Size	Type of Loading	$M_u$ (kgfcm)	$R_{Ju}$ (kgfcm/rad.)	$R_{Jo}$ (kgfcm/rad.)
2-170 x 170	Opening mode	170000	1179000	18430000
	Closing mode	185000	1532000	22705000
170 x 170*	Opening mode	170000	943000	10135000
	Closing mode	185000	919000	9082000
130 x 130*	Opening mode	170000	684000	7371000
	Closing mode	185000	888000	4541000

\*: no experimental data were existed, thus 3 parameters were deduced so as to fit with  $P - \delta$  data observed on M1 and M4 specimens.

3-parameters exponential function : 
$$M = (M_u + R_{Ju}\theta) \left\{ 1 - \exp\left(\frac{-R_{Jo}}{M_u} \theta\right) \right\}$$



### 3.3 Moment-Rotation Relationship of Column Leg Joints

This experiment was taken by the authors preliminary and here only the test results are briefly introduced. Fig.8 shows column type variation tested and loading test set-up for determining the moment-rotation relationship of the column leg joints.

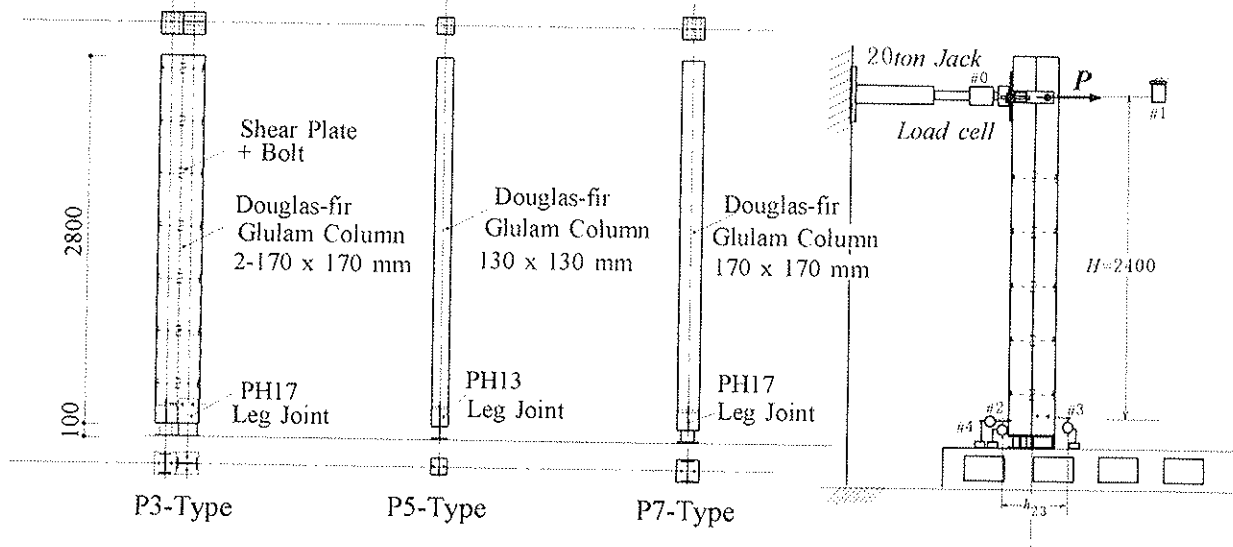
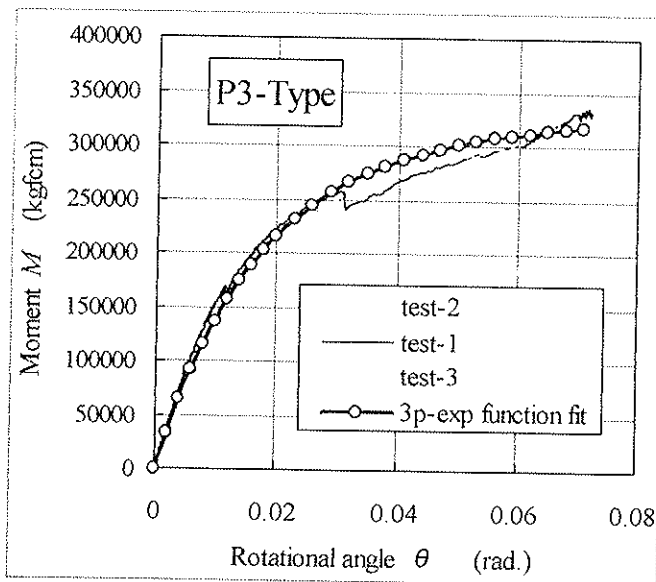


Fig.8 Column variation and loading set-up for column leg joints



An example of curve fitting on the experimental  $M-\theta$  data by a 3 parameters exponential function is shown in Fig.9. All parameters obtained by curve fitting are tabulated in Table 4 .

Fig.9

An example of curve fitting on the experimental  $M-\theta$  data taken from the P3-type leg joint using a 3-parameters exponential function.

Table4 Three parameters exponential function for the column leg joints

Column Size	Type of leg	$M_u$ (kgfcm)	$R_{Ju}$ (kgfcm/ad.)	$R_{Jo}$ (kgfcm/ad.)
2-170 x 170	P3-Type	310000	170000	18000000
130 x 130	P5-Type	5500	4000	140000
170 x 170	P7-Type	40000	100000	690000

$$3\text{-parameters exponential function : } M = (M_u + R_{Ju}\theta) \left[ 1 - \exp\left(\frac{-R_{Jo}}{M_u}\theta\right) \right]$$

# 4. Experiments on Model Shear Resistance System

## 4.1 Test Specimens

Table 5, Figs.10 , 11 and 12 show specification and configurations of test specimens.

Table 5 Specification of Test Specimens for Model Shear Resistance System

Specimen	Sheathing material	Nail & pitch	Main column (mm)	Main column leg joint	Span L (mm)	Number of replication
M1	none		130 x 130	PH-13	1820	1
M2	D.f plywood, $t = 9$ mm	CN50, @150 mm	130 x 130	PH-13	1820	3
M3	D.f plywood, $t = 9$ mm	CN50, @50 mm	130 x 130	PH-13	1820	3
M4	none		170 x 170	PH-17	1820	1
M5	D.f plywood, $t = 12$ mm	CN50, @50 mm	170 x 170	PH-17	1820	3
M6	none		2-170 x 170	PH-17	3640	1
M7	D.f plywood, $t = 12$ mm	CN50, @50 mm	2-170 x 170	PH-17	3640	3
Common Spec.	Girder : 130 x 390 mm, Douglas fir glulam ( $r_u=0.6$ )					
	Column : 89 x 130, 130 x 130, 170 x 170 mm, Douglas fir glulam ( $r_u=0.6$ )					
	Sill : 130 x 105 mm, American cypress glulam (Scientific name was unknown)					
	Beam-column joint : J3 type (Specially developed) D.f: Douglas fir					

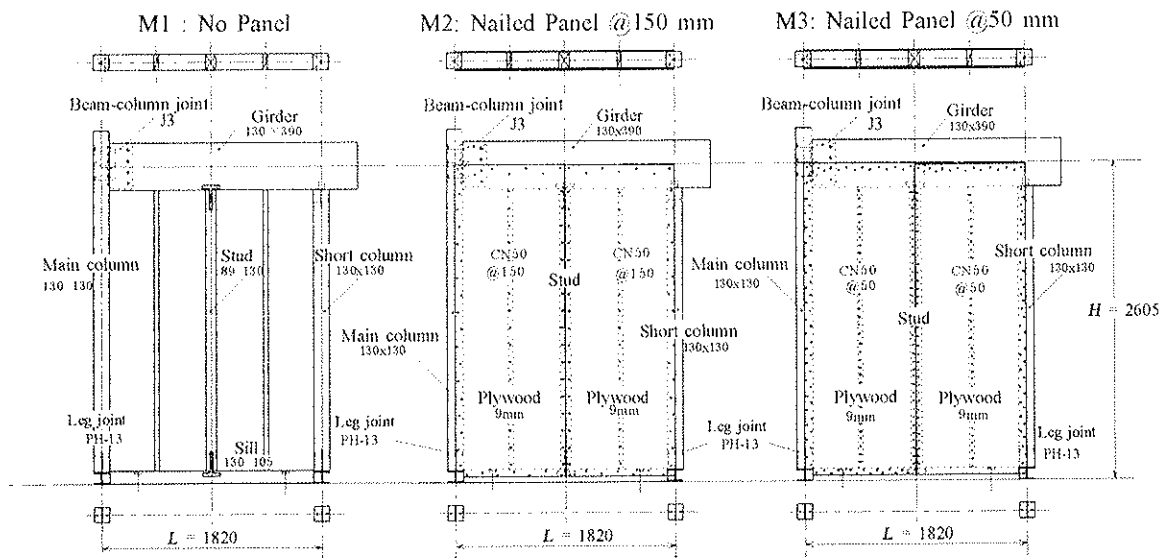


Fig.10 Details of test specimens ( $L = 1820$  mm, main column's cross section is 130 x 130 mm).

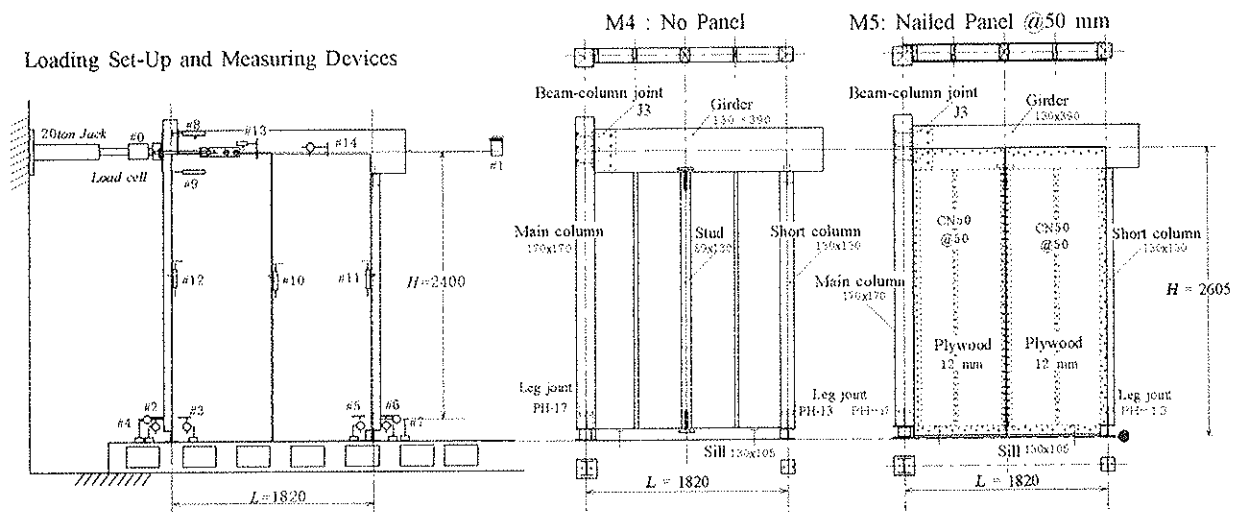


Fig.11 Test set-up and location of deflection measuring devices common to most specimens as well as details of test specimens ( $L = 1820$  mm, main column's cross section is 170 x 170 mm)

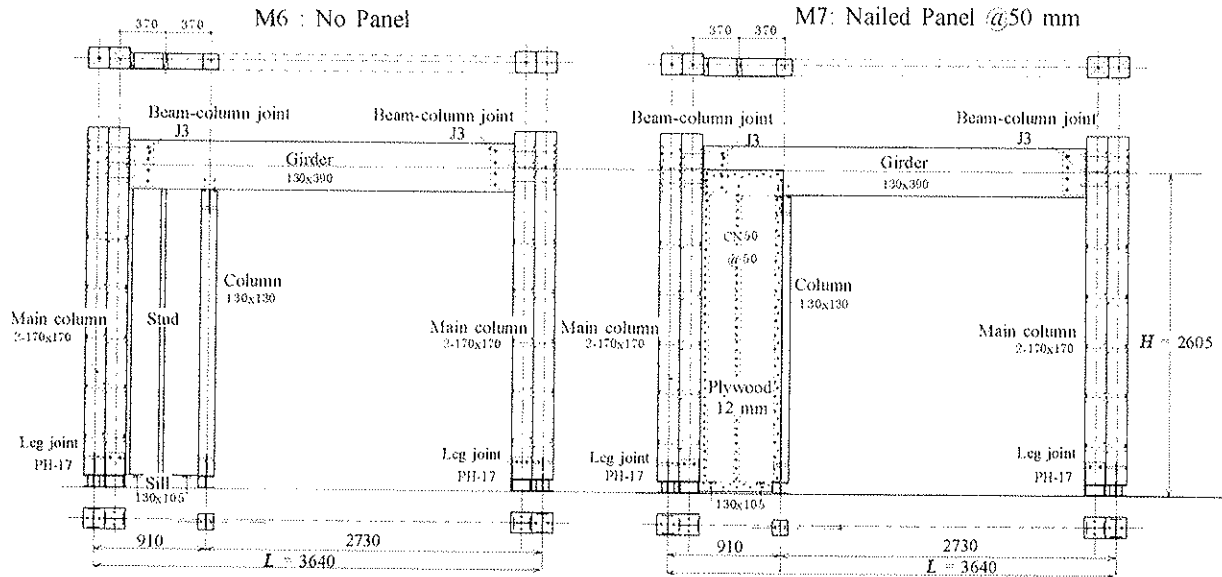


Fig.12 Details of test specimens ( $L = 3640$  mm, columns are double-170 x 170 mm)

## 4.2 Loading Schedule

All test specimens were loaded statically by controlling apparent shear deformation angle subjected to the following loading schedule;

First cycle	:	0	→	+1/300 rad.	→	0	→	-1/300 rad.	→	0
Second cycle	:	0	→	+1/120 rad.	→	0	→	-1/120 rad.	→	0
Third cycle	:	0	→	+1/60 rad.	→	0	→	-1/60 rad.	→	0
Fourth cycle	:	0	→	+1/30 rad.	→	0	→	-1/30 rad.	→	0
Final cycle	:	0	→	Push $P_{max}$						

## 5. Results and Discussion

Figs. 13, 14, 15, 16, 17, 18, and 19 show comparisons between observed shear force ( $Q$ )- shear deflection angle( $\gamma$ ) relationships (envelope curve) and calculated ones based on the simple assumption mentioned in the clause 2.0.

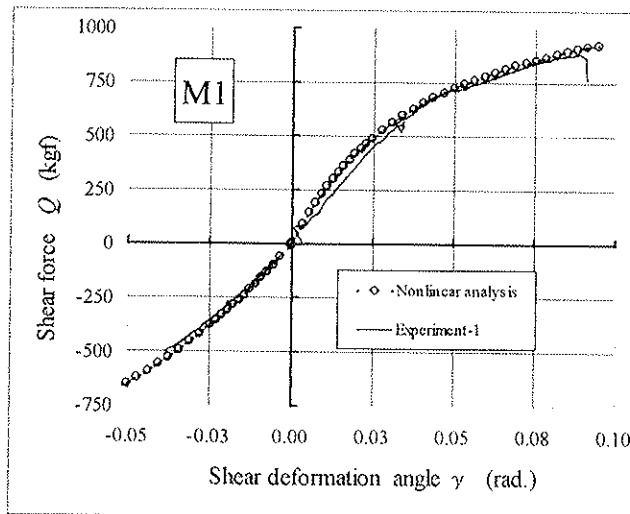


Fig.13 Comparisons between observed envelope curve vs. model calculation for M1.

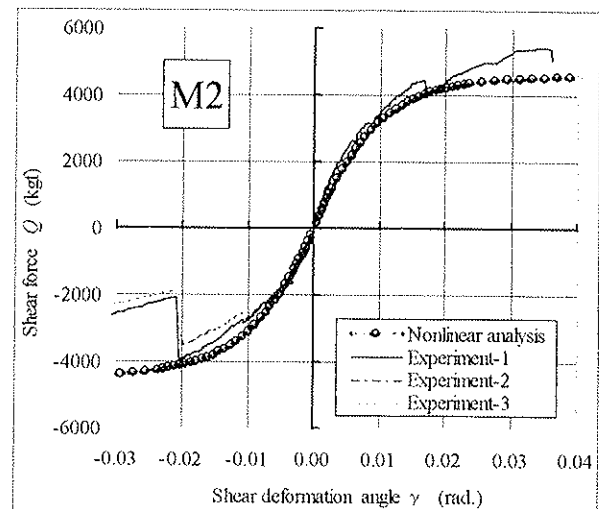


Fig.14 Comparisons between observed envelope curve vs. model calculation for M2.

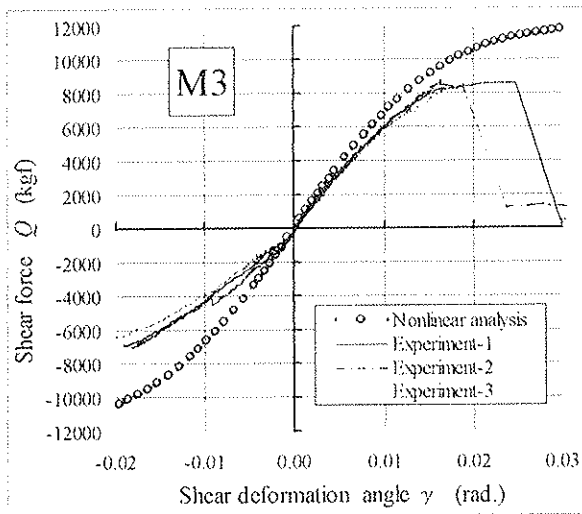


Fig.15 Comparisons between observed envelope curve vs. model calculation for M3.

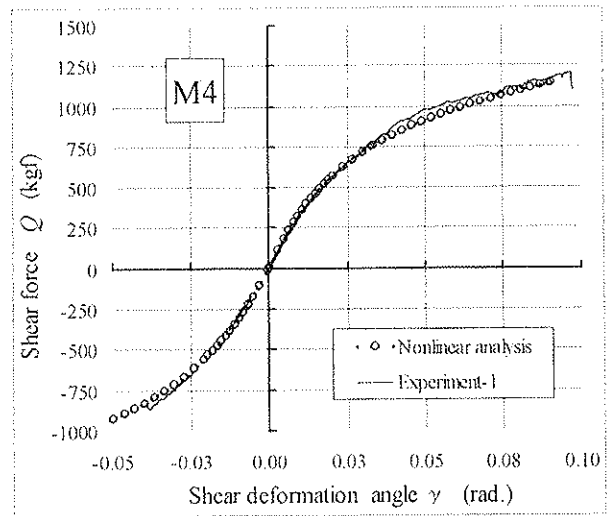


Fig.16 Comparisons between observed envelope curve vs. model calculation for M4.

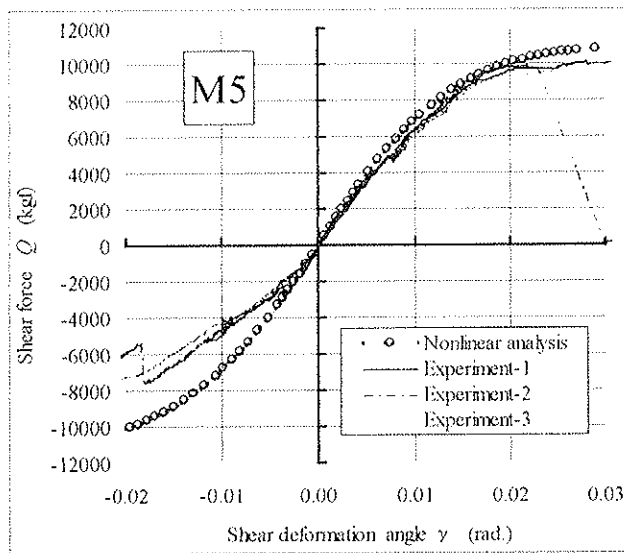


Fig.17 Comparisons between observed envelope curve vs. model calculation for M5.

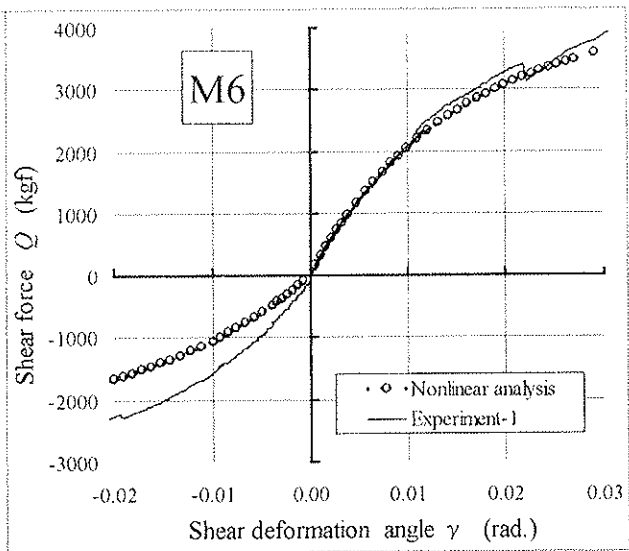


Fig.18 Comparisons between observed envelope curve vs. model calculation for M6.

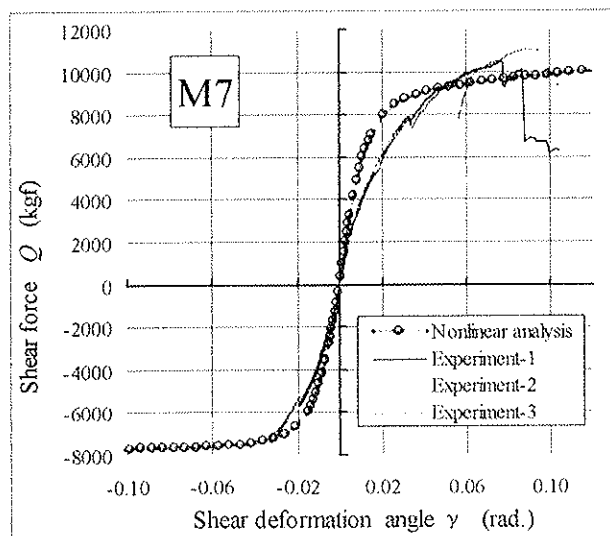


Fig.19 Comparisons between observed envelope curve vs. model calculation for M7.

In the cases of M1 and M4, 3-parameters of beam-column J3 joint were intentionally selected so as to fit the calculated result on the observed data, because no experiment were done for the case of 130x130 mm column as well as for 170x170 mm column.

In the case of M2, as nail pitch was relatively wide, calculated result well coincided with observation. While, in the case of M5 in which 3 times nails were driven, panel was so strong compared with column leg joint sustaining pull-out force, thus deformation of leg joint was dominant from relatively low loading level.

For M3 specimen, this exceed deformation (not rotational but pull-out) at leg joint was thought to be the main cause for the discrepancy between calculation and observation. In most test specimens except M6, observed pull side stiffnesses were much lower than those predicted by the calculation. This trend was thought to be caused by pull-out at the joint between girder and short column, although this joint was assumed to be a perfect pinned joint without any deformation. As a whole, however, simplified calculation method proposed in this report was thought to be usable for practical design purposes.

Failure phenomena of all specimens were tabulated in Table 6 with several photographs for showing in details.

Table 6 Failure phenomena of test specimens.

Specimen	Description of failure phenomena	Remark
M1	Large deformation remained, but no failure	
M2-1 to M2-3	Punching shear failure at nail heads along vertical perimeters	Photo.1
M3-1 to M3-3	Tensile fracture at the anchor bolt by pull-out force in the main column	Photo.2
M4	Large deformation remained, but no failure	
M5-1 to M5-3	Tensile fracture at the anchor bolt by pull-out force in the main column	
M6	Large deformation remained, but no failure	
M7-1 to M7-3	Punching shear failure at nail heads, faulure at J3 joint,	Photo.3



Photo.1 Punching shear failure at nail

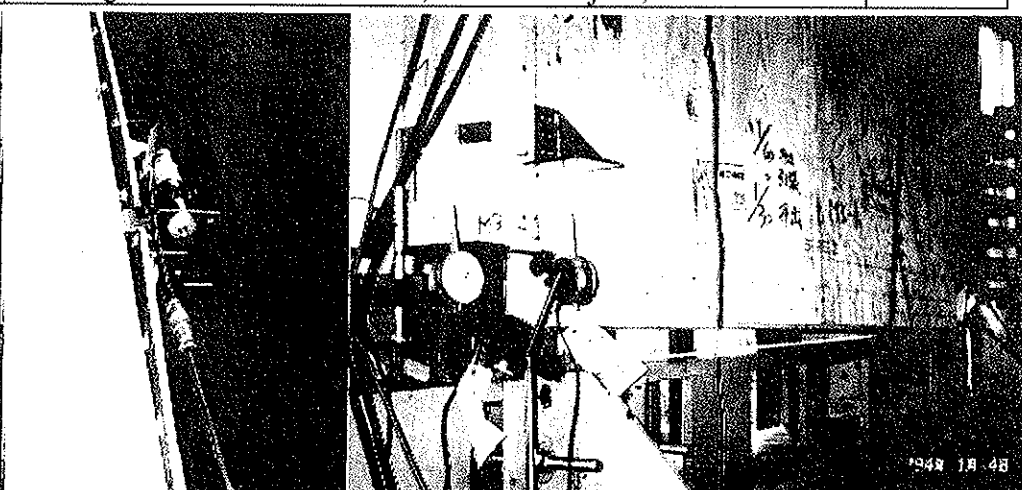


Photo.2 Anchor bolt failure



Photo.3 Large deformation of glulam portal frame with nailed plywood panel.

## 6. Conclusions

Simplified calculation method for predicting shear deformation of the model shear resistance system in which semi-rigid jointed glulam portal frame with nailed plywood shear wall panel was proposed in this report. Load - slip relationship of nail joint, moment - rotation relationship of column leg joints and beam-column joints were all expressed in the form of 3-parameters exponential function to make nonlinear calculation possible. Coincident between observed behavior with calculated ones were good with

a few exceptions. As a whole, proposed calculation method was thought to be usable for practical design purposes.

## References

- Hideo Sugiyama and Tadashi Matsumoto : "A Simplified Method of Calculating the Shear Strength of a Plywood-Sheathed Shear Wall with Openings 1 - Evaluation of the racking load of a shear wall without openings", Journal of the Japan Wood Research Society, 39(1), 75-79, (1993).  
 R.O.Foschi : "Load-slip Characteristics of Nails", Wood Science, 7(1), 69-76, (1974).  
 Sakata : "Experimental Report on Beam-Column L-Shape Joint", Unpublished (1997).

## Appendix : Numerical calculation procedures

Step 1. Give initial nail slip, say  $S_v = 0.01$  cm .

Step 2. Calculate nail shear force using 3-p exp function

$$q_v = (q_u + K_u \cdot S_v) \left\{ 1 - \exp\left[ \frac{K_o}{q_u} S_v \right] \right\}$$

Step 3. Calculate shear force for panel  $Q_p$  using eq. (5)

$$Q_p = q_v(m+1) \left( \frac{l}{h} \right)$$

Step 4. Calculate nail slip  $S_H$  from eqs. (4) and (6) by assuming  $K_{sv} = K_{sh}$  as the first guess

$$S_H = S_v \left( \frac{K_{sv}}{K_{sh}} \right) \left( \frac{m+1}{n+1} \right) \left( \frac{l}{h} \right)$$

Step 5. Calculate nail shear force  $q_H$  using 3-p exp function

$$q_H = (q_u + K_u \cdot S_H) \left\{ 1 - \exp\left[ \frac{K_o}{q_u} S_H \right] \right\}$$

Step 6. Calculate secant slip modulus  $K_{sh} = q_H/S_H$  and substitute  $K_{sh}$  to the Step 4 again until estimation of  $S_H$  become conversion. This operations were enough by 2cycles in usual.

Step 7. Calculate shear deformation of panel  $\delta$  by substituting  $K_{sh}$ ,  $K_{sv}$ , and  $Q_p$  into eq. (8)

$$\delta = \left[ \frac{h}{GIt} + \left\{ \frac{2}{(n+1)K_{sh}} + \frac{2}{(m+1)K_{sv}} \left( \frac{h}{l} \right)^2 \right\} \right] Q_p$$

Step 8. Calculate joint moment  $M_i$  using 3-p exp function by considering rotational angle  $\theta$  is equivalent shear deformation angle  $\gamma = \delta/H$

$$M_i = (M_u + R_{jv}\theta) \left\{ 1 - \exp\left[ \frac{-R_{jo}\theta}{M_u} \right] \right\}$$

Step 9. Calculate secant rotational rigidity of joint-i as  $R_{ji} = M_i/\theta$  and estimate shear rigidity of glulam portal frame  $K_F$

Step 10. Calculate shear force  $Q_F$  for glulam portal frame as  $Q_F = K_F \delta$

Step 11. Calculate the total shear force of the whole system as  $Q = Q_p + Q_F$

Step 12. Go to next nail slip stage. (Buck to the Step 1)

**INTERNATIONAL COUNCIL FOR RESEARCH AND INNOVATION  
IN BUILDING AND CONSTRUCTION**

**WORKING COMMISSION W18 - TIMBER STRUCTURES**

**FLOOR VIBRATIONS**

B Mohr

Technical University of Munich

GERMANY

**MEETING THIRTY-TWO**

**GRAZ**

**AUSTRIA**

**AUGUST 1999**

---

Presenter: B.Mohr

- T.D.G.Canisius asked whether experiment data were used to calibrate simplified model.
- B.Mohr responded that the simplified model was compared to FEM results.

# Floor Vibrations

Bernhard Mohr

Technical University of Munich, Germany

## 1 Introduction

The serviceability becomes more decisive nowadays because of the use of high strength materials, plain timber construction elements (e.g. nail laminated timber decks) and longer spans. Beside the deflection requirements the dynamic aspects must be considered.

Eurocode 5 /EC5-1/ requires for residential floors having a fundamental frequency below 8 Hz "a special investigation" which is not described there. Usual wooden floors having beams and boardings may be modelled as grill girders. Such a computation of the deflection because of a concentrated static force for wooden floors is not contained in standard tables and requires a lot of time. A research project on this score was done in 1998 at the Technical University of Munich by Kreuzinger and Mohr /Kre17/.

## 2 Bibliographical Research

### 2.1 Sensibility of the human body for vibrations

The human perceptibility to vibration

- is dependent on the vibration *acceleration* in case of frequencies lower than about 8 Hz,
- is dependent on the vibration *velocity* in case of frequencies above about 8 Hz,
- increases with the duration of the vibration
- increases with an increasing number of impulses
- decreases with the relationship to and the awareness of the vibration cause
- decreases with human activity
- decreases by increasing damping
- has logarithmic character like the sensibility to sound
- is strongly subjective.



## Design values for human sensibility

The following design values are proposed for wooden residential floors and damped vibrations. The values result from bibliographical research (specially /Wis2/) and in situ tests with a questioning of users. There is a difference between

- the possibility of transferability to adjoining rooms: single span or more spans with one continuous girder
- the number of impulses: one or repeated
- the demands of the user: low or high

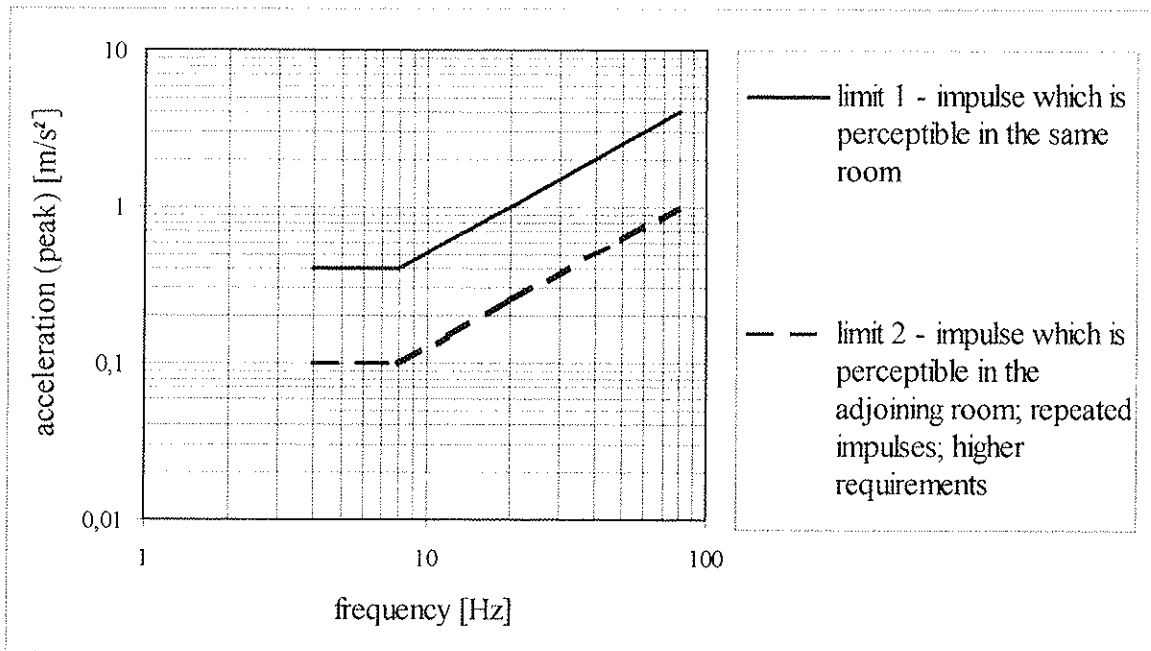


figure 1 : Dependence of the acceleration on the fundamental frequency

## Damping Ratio

The following modal damping ratios  $D$  are seemed to be suitable to characterize different timber floor constructions for design. They result of the literature and in situ tests.

$D=0,01$  for timber floors without any additional boarding for sound isolation

$D=0,02$  for plain glued laminated timber floors with additional boarding for sound isolation

$D=0,03$  for girder floors and nail laminated timber floors with additional boarding for sound isolation

The values of figure 1 correspond to  $D=0,01$  and may be increased with the factor

$k_D = 1,15$  for  $D = 0,02$  and

$k_D = 1,25$  for  $D = 0,03$ . /Kre17/

## 2.2 Design Standards

The design standards found in literature have the following targets:

1. There are repeated cyclic actions which cause resonance with floors having a low fundamental frequency. In this case either the fundamental frequency should have a minimum value or the resulting acceleration should be limited (/Bac6/, /Ohl1/, /Mur3/, /Gru1/).
2. Impulses of a longer duration (e.g. foot fall) require a minimum of stiffness (/EC5-1/, /EII5/, /Fos6/, /Mur3/, /Ohl4/).
3. Impulses of a shorter duration (e.g. heel drop) should be considered by a requirement to the mass of the floor (/EC5-1/, /Ohl4/, /EII5/).

## 3 Investigation of Timber Floors

### 3.1 Theoretical Investigations

#### 3.1.1 Frequency Requirement

A dynamic computation was done with usual floor configurations. Following values were used:

- dynamic (generalized) mass of 300 kg
- maximum animation frequency of 6,9 Hz for the 3. harmonic
- the fourier coefficient  $\alpha_3 = 0,06$  for the 3. harmonic (see /ISO 10137/)
- the weight force of the person  $P_0 = 700$  N
- damping ratio  $D = 0,03$

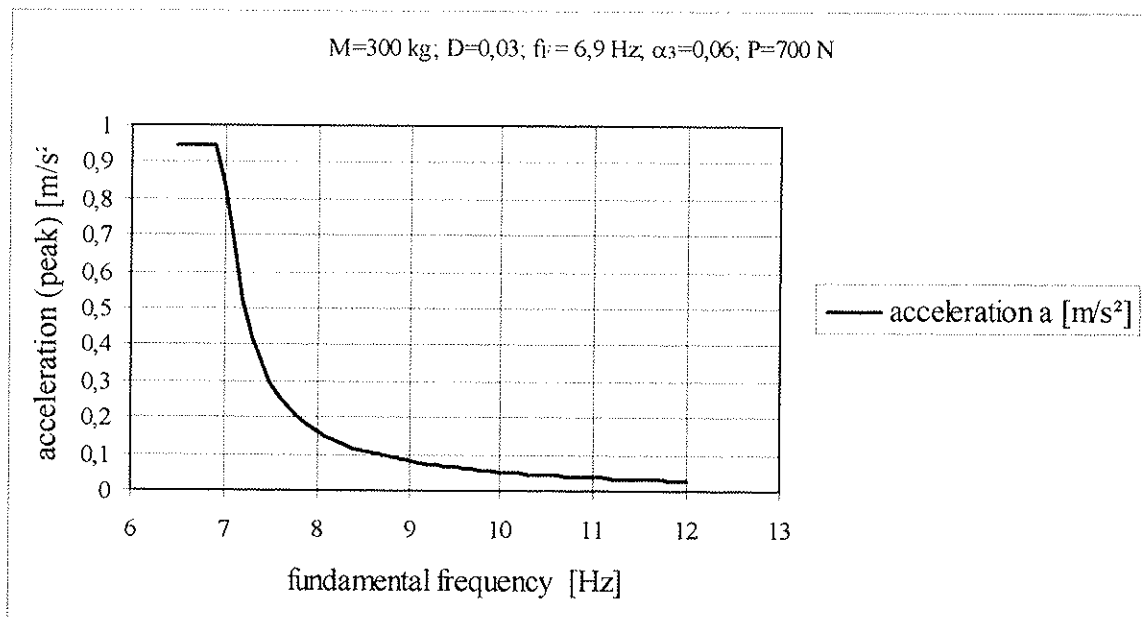


figure 2: Dependence of the acceleration on the fundamental frequency

As a result the acceleration for floors having fundamental frequencies below 8 Hz increases strongly (figure 2). Therefore the fundamental frequency should be limited. Otherwise a dynamic computation (see chapter 4.2) must be done.

### 3.1.2 Stiffness Requirement

#### Finite-element-model and the action "footfall"

Many wooden floors with different spans, widths, masses and stiffness were modelled by finite-elements. They were loaded not only by a single concentrated force but also by the force-time-progress of a real footfall in the middle of the floor. All results of the single computations led to the following formula by solving the multiple regression problem:

$$w_{\text{stat}} = \frac{1}{47,36} * \frac{P * \ell^{2.07}}{(EI)_\ell^{0.75} * (EI)_b^{0.21}} \quad (R^2 = 0,962) \quad (1)$$

The differences between the results of the finite-elements computation and the regression analysis were small. Only floors having lower widths and high equivalent plate bending stiffness perpendicular to the span showed a little bit greater differences.

#### Analytical results

The timber floor was modelled by a girder on elastic bedding (figure 3):

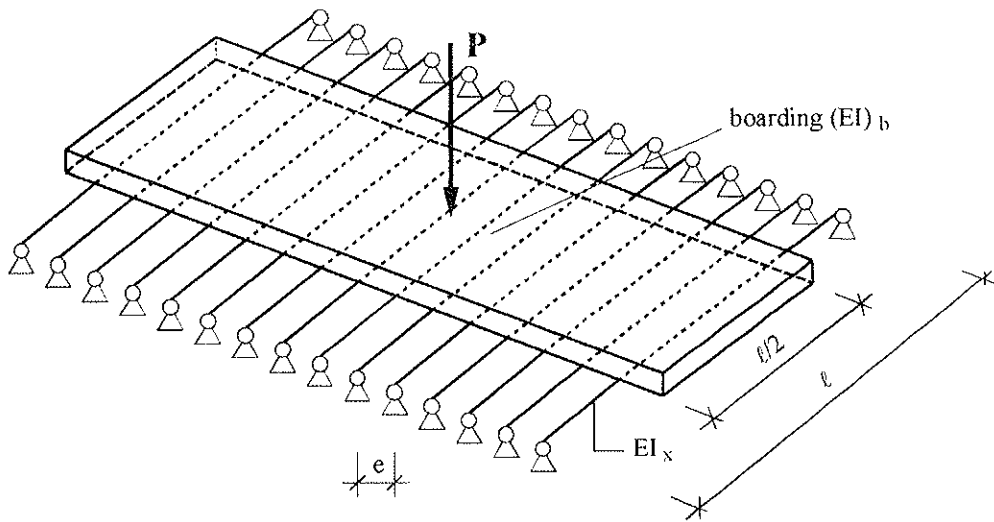


figure 3: Modelled timber floor

The deflection in case of a single load was computed to:

$$w = \frac{1}{43,37} * \frac{P * \ell^2}{(EI)_\ell^{0.75} (EI)_b^{0.25}} \quad (2)$$

There was only a little difference from the result of the finite-elements computation. An effective static width could also be computed:

$$\Leftrightarrow b_m \approx \frac{1}{1,1} * \sqrt[4]{\frac{(EI)_b}{(EI)_\ell}} * \ell \quad (3)$$

### Dependence acceleration - deflection caused by a concentrated single load

There was a very good correlation between the quotient acceleration in cause of a foot fall and the maximum acceleration due to figure 1 and the deflection in cause of a concentrated force of 1 kN. This is shown in figure 4.

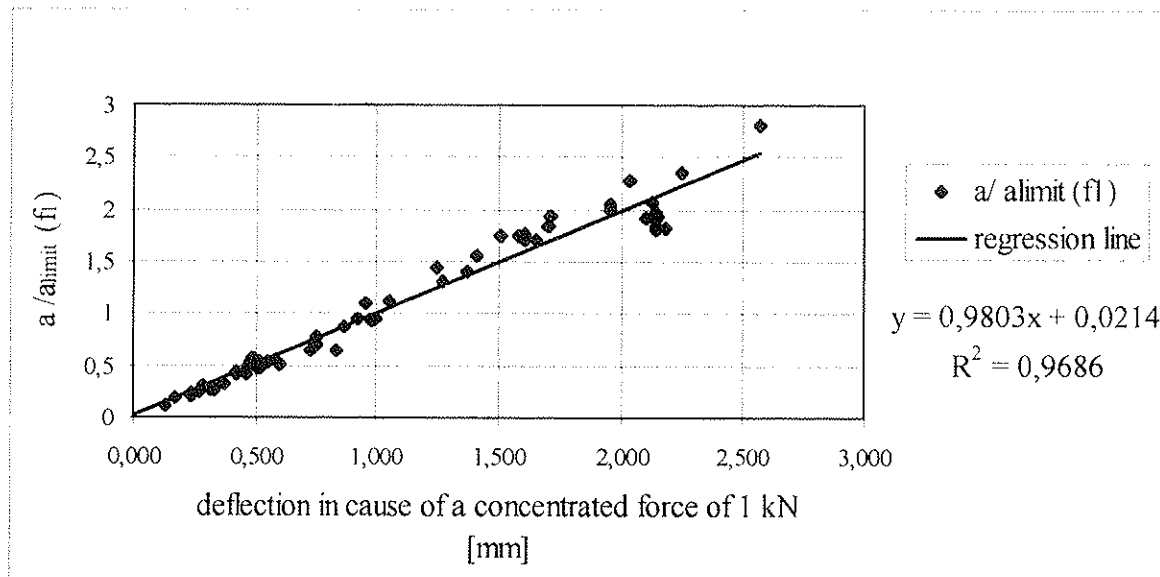


figure 4: Correlation between the acceleration and deflection

As a result the design values for the acceleration (figure 1) will be kept, if the static deflection in cause of a concentrated force of 1 kN is not greater than 1 mm:

$$\frac{w}{P} \leq 1,0 \frac{\text{mm}}{\text{kN}} \quad (4)$$

### 3.1.3 Mass Requirement

#### Finite-element-model and the action "heel drop"

The same procedure as in 3.1.2 was used for the short term action of a "heel drop". (A person is standing on his toes and lets himself fall to the heels.) The result was:

$$v_{\text{heel drop}} = \frac{0,573}{\left[ \text{m}^{-0,5} (EI)_{\ell}^{0,25} (EI)_b^{0,25} \right]^{0,9891}} \approx \frac{0,6}{\text{m}^{-0,5} (EI)_{\ell}^{0,25} (EI)_b^{0,25}} \quad [\text{m/s}] \quad (5)$$

for  $[\text{kg/m}^2; \text{MNm}^2/\text{m}]$

#### Vibration velocity approximately to Eurocode 5

The formulas of Eurocode 5 were modified. All additive terms were neglected and that led to the following formula:

$$v = 0,4 \frac{1}{(EI)_b^{0,25} * \ell * \text{m}^{-0,75}} \quad \left[ \frac{\text{m/s}}{1 \text{Ns}} \right] \quad (6)$$

(for units:  $\text{MNm}^2/\text{m}$ , m,  $\text{kg/m}^2$ )

### 3.2 In situ tests

Twenty residential timber floors were measured in Germany and Switzerland and characterized with the rate 1 (no vibration problem) to 4 (heavy vibration problem) by the user and the examiner.

#### Frequency Requirement

Most of the floors are having fundamental frequencies above 8 Hz. Floors with fundamental frequencies between 8 and 10 Hz showed a small increase of the measured acceleration, if they were loaded with repeated actions by human beings. These repeated actions were designed in dependence of the fundamental frequency of the floor for the in situ tests. But these actions are unusual in case of a normal use of the floor and therefore Kreuzinger und Mohr /Kre17/ proposed the requirement

$$f_1 \geq 8 \text{ Hz} \quad (7)$$

to limit the acceleration in cause of repeated actions (namely walking).

#### Stiffness Requirement

The characterizations of the floors and the computed deflections in cause of a concentrated force are shown in figure 5.

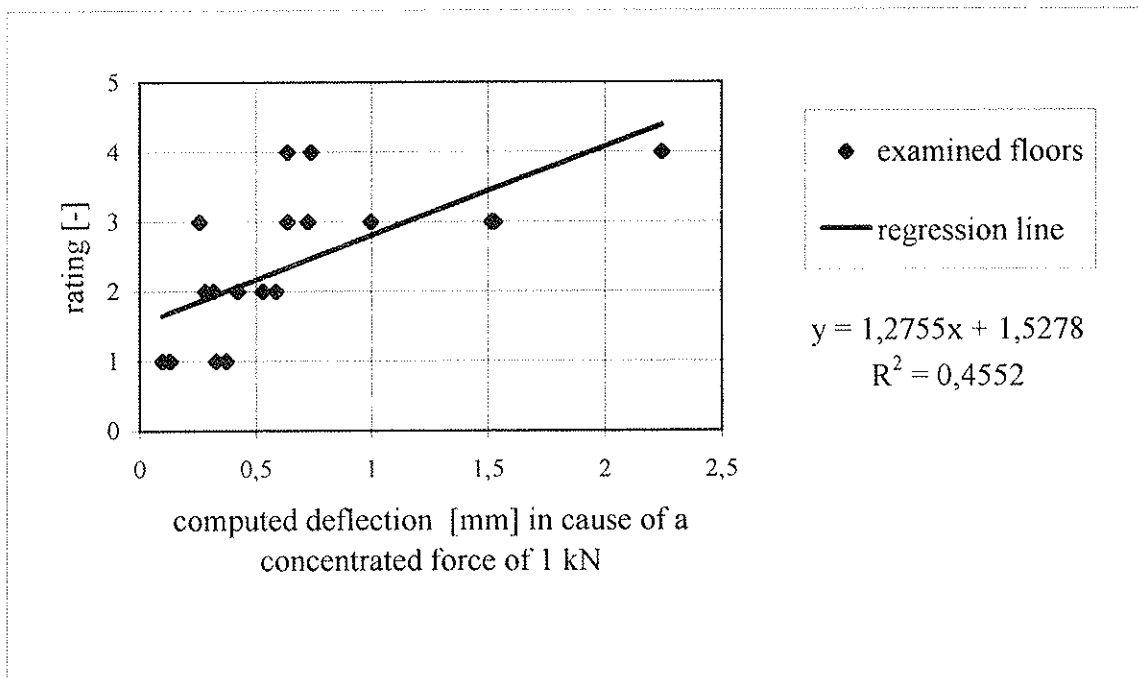


figure 5: Discussion of the stiffness requirement

There is a moderate correlation between characterization and deflection. The quantitative rating shows that a computed deflection of

- 1,0 mm / 1 kN results in a vibration problem and
- 0,5 mm / 1 kN results in a small vibration problem and
- 0,25mm / 1 kN results in no vibration problem.

## Mass Requirement

The rating of the floors and the quotient between computed velocity and the limit velocity according to Eurocode 5 is shown in figure 6.

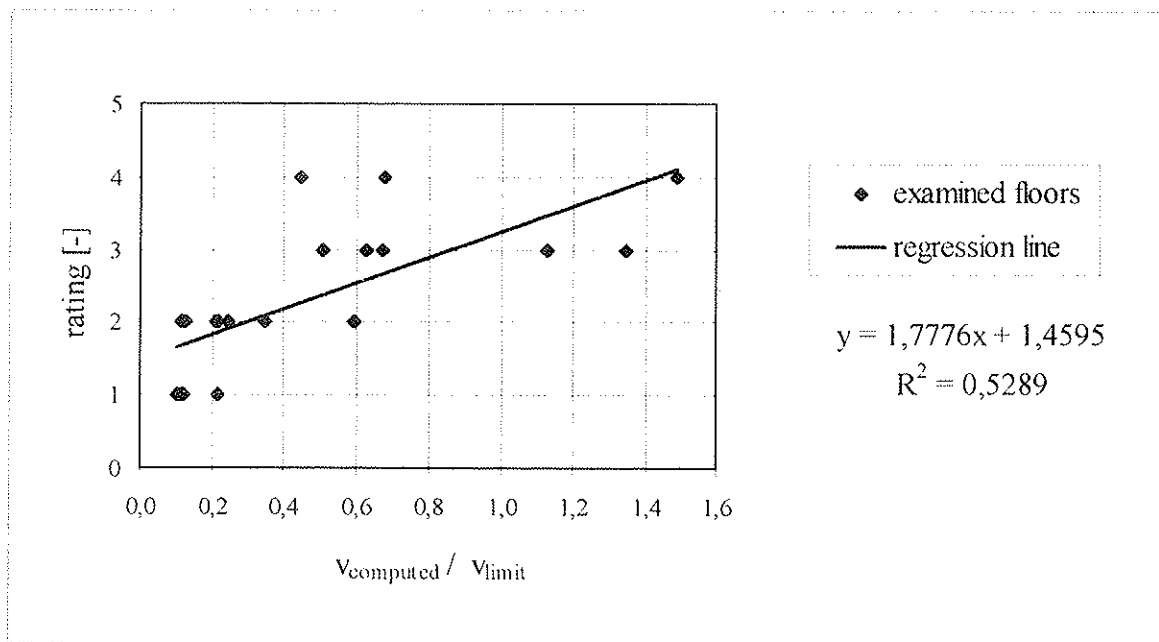


figure 6: Discussion of the mass requirement of Eurocode 5

There is a good correlation between this quotient and the characterization. But the existing limit of Eurocode 5 should be lowered. The factor 3 is proposed.

$$\Rightarrow v_{\text{limit}} = \frac{100^{(f_i * D - 1)}}{3} \quad (8)$$

## Alternative Proposal

The quotient velocity in cause of a "heel drop" (see 3.1.3) and the maximum velocity of Eurocode 5 and the characterization were compared. This resulted in a better correlation than the requirement of Eurocode 5. In cause of the higher impulse of a "heel drop" the velocity limit must be increased:

$$v_{\text{heeldrop, limit}} = 6 * v_{\text{max, ECS-1}} \quad (9)$$

The resulting formula is:

$$v_{\text{heeldrop}} = \frac{0,6}{m^{0,5} (EI)_\ell^{0,25} (EI)_b^{0,25}} \leq v_{\text{heeldrop, limit}} = 6 * 100^{(f_i * D - 1)} \quad (10)$$

(for units: m/s, kg/m<sup>2</sup>, MNm<sup>2</sup>/m)

## 4 Design Proposal

### 4.1 Common

The effect of different actions must be considered by corresponding design requirements (see 2.2):

1. Frequency requirement
2. Stiffness requirement
3. Mass requirement

These requirements should be recommended, because there are some users, that want to have a "soft" floor. These should be permissible in exceptional cases.

### 4.2 Repeated Cyclic Actions - Frequency Requirement

#### Simplified design

The fundamental frequency of residential timber floor should be limited:

$$f_1 \geq 8 \text{ Hz} \quad (7)$$

The mass  $\bar{m}$  is the sum of the self-weight  $q_g$  and the quasi-permanent loads  $\psi_2 q_p$  (e.g. furniture):

$$\bar{m} = \frac{q_d}{g} \quad \text{e.g. } 1 \text{ kN/m}^2 = 100 \text{ kg/m}^2 \quad (11)$$

$$\text{and: } q_d = q_g + \psi_2 q_p \quad (12)$$

#### Design for floors having lower fundamental frequencies $f_1 < 8,0 \text{ Hz}$

The acceleration in cause of repeated actions should be limited:

$$a \approx 0,4 \frac{P_0 * \alpha_i(f_1)}{M_{gen}} * \frac{1}{\sqrt{\left[ \left( \frac{f_1}{f_F} \right)^2 - 1 \right]^2 + \left( 2D \frac{f_1}{f_F} \right)^2}} \quad (13)$$

$P_0$  : weight force of a person ( $P_0 = 700 \text{ N}$ )

$f_F$  : forcing frequency according to table 1

$\alpha_i(f_1)$  : fourier coefficient in dependence of the fundamental frequency of the floor.

table 1: fourier coefficient in dependence of the fundamental frequency of the floor

fundamental frequency	Fourier coefficient	Forcing frequency $f_F$	Comments
$3,4 < f_1 \leq 4,6$	$\alpha_2 = 0,2$	$F_F = f_1$	/ISO 10137/
$4,6 < f_1 \leq 5,1 \text{ Hz}$	$\alpha_2 = 0,2$	$F_F = f_1$	Simplification
$5,1 < f_1 \leq 6,9 \text{ Hz}$	$\alpha_3 = 0,06$	$F_F = f_1$	/ISO 10137/
$f_1 > 6,9 \text{ Hz}$	$\alpha_3 = 0,06$	6,9 Hz	/ISO 10137/

The generalized mass may be computed by:

$$M_{\text{gen}} = m * \frac{\ell}{2} * b_{\text{m,stat}} \quad (14)$$

The effective width  $b_{\text{m,stat}}$  is the same as in formula 3.

The maximum acceleration for repeated actions should be limited to

$$a_{\text{limit}} = 0,10 \text{ m/s}^2 \quad (\text{see 2.2, limit 2})$$

### 4.3 Impulses with longer duration - stiffness requirement

The deflection in cause of a concentrated force should be limited for floors with a single span to:

$$\frac{w}{P} \leq 1,0 \frac{\text{mm}}{\text{kN}} \quad (4)$$

These limits may be reduced to a half or to a quarter to consider higher demands. The deflection in cause of a concentrated load may be computed by:

$$w = \frac{1}{43,37} * \frac{P * \ell^2}{(EI)_\ell^{0,75} (EI)_b^{0,25}} \quad (2)$$

Floors that have higher damping ratios may be designed with multiplication factors:

$$k_D = 1,15 \text{ for } D = 0,02, \quad k_D = 1,25 \text{ for } D = 0,03$$

The possibility of a vibration transfer must be considered for floor constructions that have two or more spans.

### 4.4 Impulses with shorter duration - mass requirement

There are two proposals for the mass requirement.

1) Modified formula of Eurocode 5:

The maximum velocity should not extend the value:

$$v_{\text{limit}} = \frac{100^{(f_1 D - 1)}}{3} \quad (8)$$

The velocity in cause of an ideal unit impulse may be computed to:

$$v = 0,4 \frac{1}{(EI)_b^{0,25} * \ell * m^{0,75}} \left[ \frac{\text{m/s}}{\text{INs}} \right] \quad (\text{for units: MNm}^2/\text{m, m, und kg/m}^2) \quad (6)$$

2) The alternative design proposal is:

$$v_{\text{heeldrop}} = \frac{0,6}{m^{0,5} (EI)_\ell^{0,25} (EI)_b^{0,25}} \leq v_{\text{heeldrop,limit}} = 6 * 100^{(f_1 D - 1)} \quad (10)$$

(for units: m/s, kg/m<sup>2</sup>, MNm<sup>2</sup>/m, Hz)



## 5 References

- /Bac6/ Bachmann et al.: *Vibration Problems in Structures*. Birkhäuser Verlag, Basel Boston Berlin. 1995.
- /Ell5/ Ellingwood, B.; Tallin, A.: *Structural Serviceability: Floor Vibration*. In: *Journal of the Structural Engineering* 110 (1984), Nr. 2, p. 401-418.
- /EC 5-1/ENV 1995-1: *Eurocode 5: Entwurf, Berechnung und Bemessung von Holztragwerken. Teil 1: Allgemeine Bemessungsregeln, Bemessungsregeln für den Hochbau*. Deutsche Fassung Oktober 1993.
- /Fos6/ Foschi, R. ; Gupta, A. : *Reliability of floors under impact vibration*. In: *Canadian Journal of Civil Engineering* 14 (1987), S. 683-689.
- /Gru1/ Grundmann, H.; Kreuzinger, H.; Schneider, M. : *Schwingungsuntersuchungen für Fußgängerbrücken*. In: *Bauingenieur* 68 (1993), p. 215-225.
- /ISO 10137/ ISO 10137: *Bases for design of structures; serviceability of buildings against vibration*. 1992-04.
- /Kre17/ Kreuzinger, H.; Mohr, B. : *Gebrauchstauglichkeit von Wohnungsdecken aus Holz*. München, Technische Universität, Fachgebiet Holzbau. Forschungsbericht Januar 1999.
- /Mur3/ Murray, T. M.; Allen, D. E.: *Floor vibrations - A new design approach*. In: *Report of the International Colloquium Goeteborg 1993: Structural Serviceability of Buildings*. S. 119-124, IABSE Report 69.
- /Ohl1/ Ohlsson, S.: *Springiness and human-induced floor vibrations floor vibrations - A Design Guide*. Swedish Council for Building Research. Stockholm, Sweden 1988.
- /Ohl4/ Ohlsson, S.: *Grenzzustände der Gebrauchstauglichkeit - Schwingungen*. In: *Arge Holz e.V. (Hrsg.): Holzbauwerke, STEP1: Bemessung und Baustoffe nach Eurocode 5*. (1995), Fachverlag Holz Düsseldorf 1995.
- /Wis2/ Wiss, J. F.; Parmlee, R. A.: *Human Perception of Transient Vibrations*. In: *Journal of the Structural Division* 100 (1974), ST4, p. 773-787.

### List of symbols

$a$	: acceleration	[m/s <sup>2</sup> ]
$a_{\text{limit}}$	: tolerable acceleration	[m/s <sup>2</sup> ]
$b_m$	: effective width	[m]
$D$	: damping ratio	[-]
$e$	: distance between the floor girders	[m]
$(EI)_x$	: stiffness of the floor girder	[MNm <sup>2</sup> ]
$(EI)_r$	: equivalent plate bending rigidity in span direction	[MNm <sup>2</sup> /m]
$(EI)_B$	: equivalent plate bending rigidity perpendicular of the span direction	[MNm <sup>2</sup> /m]
$f$	: frequency	[Hz]
$f_1$	: fundamental frequency	[Hz]
$f_F$	: forcing frequency	[Hz]
$g$	: acceleration due to gravity $g = 9,81 \text{ m/s}^2$	
$k_D$	: multiplication factor for higher damping ratios	[-]
$\ell$	: span	[m]
$m$	: mass per unit area	[kg/m <sup>2</sup> ]
$M$	: mass	[kg]
$P$	: force	[kN]
$P_0$	: force of a person	
$R$	: correlation coefficient	[-]
$v$	: velocity	[m/s]
$v_{\text{limit}}$	: tolerable velocity	[m/s]
$w$	: deflection	[mm]
$\alpha_i$	: fourier coefficient of the $i$ . Harmonic	[-]
$\psi_2$	: factor for quasi-permanent values	[-]